Foundations of Mathematical Neuroscience

Bard Ermentrout
Department of Mathematics
University of Pittsburgh

David Terman
Department of Mathematics
Ohio State University

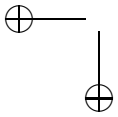
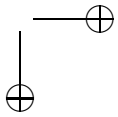

Contents

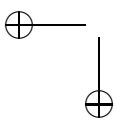

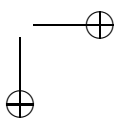

List of Figures

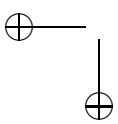

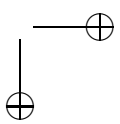

Preface

One can say that the field of computational neuroscience started with the 1952 paper of Hodgkin and Huxley in which they describe, through nonlinear partial differential equations, the genesis of the action potential in the axon of the giant squid. These equations and the methods that arose from this combination of modeling and experiments have since formed the basis for every subsequent model for active cells. The Hodgkin-Huxley model and a host of simplified equations that are derived from them have inspired the development of new and beautiful mathematics. Dynamical systems and computational methods are now being used to study activity patterns in a variety of neuronal systems. It is becoming increasingly recognized, by both experimentalists and theoreticians, that issues raised in neuroscience and the mathematical analysis of neuronal models provides unique interdisciplinary collaborative research and educational opportunities.

This book is motivated by a perceived need for an overview of how dynamical systems and computational analysis have been used in understanding the types of models that come out of neuroscience. Our hope is that this will help to stimulate an increasing number of collaborations between mathematicians, looking for classes of interesting and relevant problems in applied mathematics and dynamical systems, and neuroscientists, looking for new ways to think about the biological mechanisms underlying experimentally observed firing patterns.

The book arose out of several courses that the authors have taught. One of these is a graduate course in computational neuroscience that has students from psychology, mathematics, computer science, physics and neuroscience. Of course, teaching a course to students with such diverse backgrounds presents many challenges. However, the course provides many opportunities to encourage students, who may not normally interact with each other, to collaborate on exercises and projects. Throughout the book are many exercises that involve both computation and analysis. All of the exercises are motivated by issues that arise from the biology.

We have attempted to provide a comprehensive introduction to the vocabulary of neuroscience for mathematicians who are just getting interested in the field but who have struggled with the biological details. Anyone who wants to work in computational neuroscience should learn these details as this is the only way one can be sure that the analysis and modeling is actually saying something useful to the biologists. We have also tried to provide background material on dynamical systems theory, including phase plane methods, oscillations, singular perturbations and bifurcation analysis. An excellent way to learn this material is by using it,

together with computer simulations, to analyze interesting, concrete examples. The only prerequisite is a basic calculus course; however, it is very useful if students are comfortable with the basic theory of ordinary differential equations as well as linear algebra. Much of the mathematics is at the level of the book by Strogatz.

The book is organized from the bottom up. That is, we start with the biophysics of the cell membrane and from this introduce compartmental models, continuum limits and cable theory. We then add active ion channels. Prior to the work on active channels, all equations are linear and in theory completely solvable in closed form. Here we introduce a number of interesting approaches toward quantifying the responses of passive membranes to inputs. ...

There are several recent books that cover some of the same material in the present volume. *Theoretical Neuroscience* by Dayan and Abbott has a broader range of topics than our book. However, it does not go very deeply into the mathematical analysis of neurons and networks, nor does it emphasize the dynamical systems approach. A much closer book is *Dynamical Systems in Neuroscience* by Eugene Izhikevich. This book emphasizes the same approach as we take here. However, the main emphasis of DSN is in single neuron behavior. We cover a good deal of single neuron biophysics, but include a much larger proportion of theory on systems neuroscience and applications to networks.

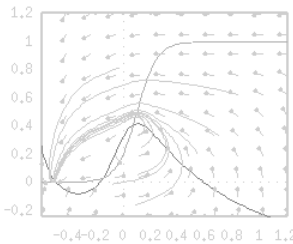

Chapter 1

Some basic biology

Neuroscience is the study of the brain. Brain function underlies all behavior including simple motor activity such as walking and smiling and higher order cognitive behavior such as thinking, learning and memory. The brain consists of *neurons* and *glial cells*. Neurons are the basic signaling units of the nervous system. The majority of this book is devoted to the mathematical analysis of models that describe the behavior of these cells. Glial cells are important in maintaining the health of neurons and how they behave and interact. Neurons communicate with each other at *synapses*. It has been estimated that there are approximately 10^{11} neurons and 10^{15} synapses in the human brain. Hence, neurons typically receive inputs from a very large number of other cells.

In the remainder of this chapter, we describe some basic properties of the brain, neurons and synapses. We will only touch on material that is absolutely essential for anyone interested in computational neuroscience. We highly recommend that the reader study this material in more detail by consulting one of the many excellent books devoted to neuroscience. Such books include Kandel/Schwartz/Jessell, Johnston/Wu, ... In fact, much of the following discussion is based on material from those books.

1.1 The brain

The brain is highly organized both anatomically and functionally. The central nervous system (CNS) consists of two main parts: the spinal cord and the brain. The brain itself is partitioned in several areas. These are: the medulla oblongata, the pons, the cerebellum, the midbrain, the diencephalon, and cerebral hemispheres. Each of these consists of many parts or nuclei. For example, the diencephalon contains the thalamus and the hypothalamus. The cerebral hemispheres consist of the cerebral cortex and deep-lying structures that include the basal ganglia, the hippocampus and the amygdaloid nucleus. The cortex consists of four lobes; these are the frontal, parietal, occipital and temporal lobes.

Different brain structures are responsible for different functions. For example,

the brainstem is responsible for maintaining many of the functions necessary for life such as breathing and heart rate. The basal ganglia participate in regulating motor performance and the thalamus processes most of the information reaching the cerebral cortex from the rest of the CNS. The cerebral cortex is the large region (large in mammals, notably humans, but nonexistent in many other vertebrates) that is directly beneath the skull. The cortex is responsible for our sensory, cognitive, and voluntary motor behaviors. The different lobes of the cortex have specialized functions: the frontal lobe is largely concerned with the planning and organization of future actions; the occipital lobe is concerned with vision; the pariental lobe receives sensory information; and the temporal lobe is involved with hearing and other aspects of language and memory.

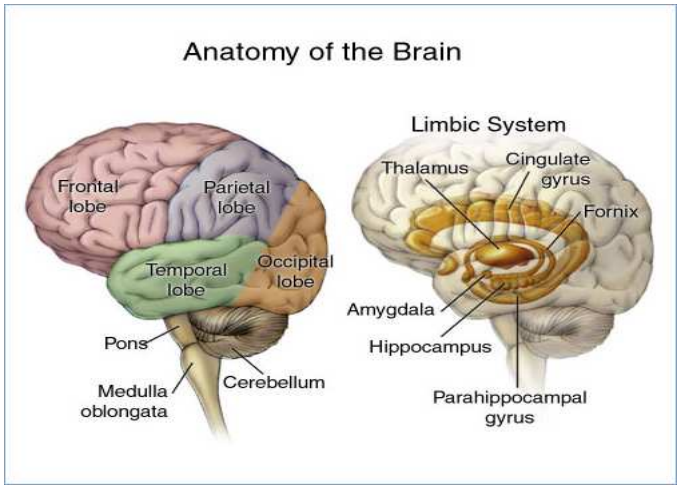

Figure 1.1.

We note that each hemisphere is concerned primarily with sensory and motor processes on the contralateral side of the body. That is, sensory information that enters the spinal cord from the left side of the body crosses over to the right side of the nervous system, while motor areas in one hemisphere exert control over the movements of the opposite half of the body.

Cognitive and motor activities may be highly localized within the cerebral cortex. There are, in fact, sensory maps in which sensory information such as touch is organized topographically in the brain. Each part of the body is represented separately in a specific location in the somatosensory cortex. Sensitive regions, such as the fingers and mouth, take up the most space. This is shown in Figure 1.2.

As one further example of how cognitive activities are localized within the brain, consider language. Different aspects of language are processed in different areas of the cortex. One area, called *Wernicke's area*, is important to the understanding of spoken language, while another area, called *Broca's area*, is concerned

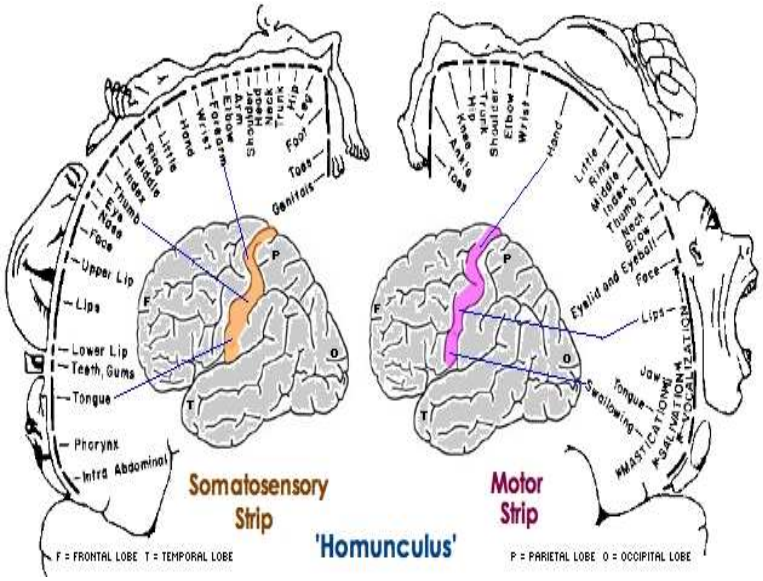

Figure 1.2.

with issuing specific commands that cause the mouth and tongue to form words. Hence, damage to Wernicke's area makes it impossible for a person to understand speech, while damage to Broca's area makes it impossible for a person to speak.

While cognitive and motor activities are localized within the brain, it is important to realize that complex mental activities, such as learning or memory, typically involve interconnections between many brain regions. We have seen, for example, that language involves both Wernicke's and Broca's area, which lie in different parts of the left cerebral hemisphere. Interrelated mental activities are processed by many neural pathways that are distributed in parallel. For this reason, damage to one single area often does not necessarily lead to the loss of a specific function.

1.2 The neuron

Neurons are specialized cells that like all other cells contain the usual organelles necessary for staying alive. These include the mitochondria, responsible for fueling the cells, and the nucleus, which holds the genetic material that gets passed on when the cell divides.

The structure of a neuron can be divided into three parts: (i) the *dendrites*; (ii) the *soma*; and (iii) the *axon*. The soma or cell body is the site of the nucleus and all the normal cellular machinery. Functionally the soma plays the role of integrating all of the inputs of the cell to produce some output. The dendrites and axon are processes that emanate from the soma. Neurons usually have several dendrites; these form the "input lines" of the cell. The dendrites often branch out

in a tree-like fashion that can be very large. In many cases, the majority of the surface area of the cell is taken up by the dendrites. Neurons usually have some sort of general orientation. Dendrites that lie at the top of the neuron are called *apical dendrites* and those that lie at the base are called *basal dendrites*. Figure 1.2 shows the variety of possible shapes that neurons can take; the main differences are in the shapes of the dendritic trees. Although neurons share many common features, it has been estimated that there are as many as 10,000 different types.

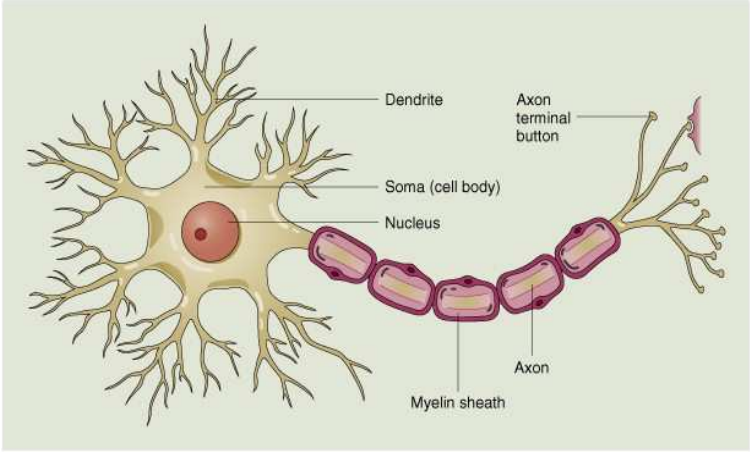

Figure 1.3.

The axon typically leaves the soma as a single thin process but then branches out in order to connect to other cells. The diameter of an axon may range from .2 to 20 μm and may extend for up to one meter. The axon is the major conducting unit of the neuron; it can convey information great distances by propagating a transient electrical signal called the *action potential*. The action potential is initiated at a specialized region of the soma called the *axon hillock*. Large axons are surrounded by a fatty insulating sheath called *myelin*. This is essential for high-speed conduction of action potentials. The sheath is interrupted at regular intervals by *nodes of Ranvier*.

The action potential represents a change in the neuron's *membrane potential*. Neurons, like all other cells, maintain a potential difference of about 65 mV across their external membrane. What distinguishes neurons and other excitable cells from most cells in the body is that this resting membrane potential can be altered and can, therefore, serve as a signaling mechanism. The action potential corresponds to a change in resting potential that propagates along the axon. The action potential is initiated when the membrane potential at the axon hillock reaches some threshold potential; once this threshold is reached, the signal propagates in a all-or-none fashion. That is, the amplitude and duration of the signal is always the same no matter how it is generated. Action potentials may last as short as 1 ms and

may travel at rates that vary between about 1 and 100 meters per second. After each action potential, there is a period during which a second impulse cannot be initiated. The is referred to as the *refractory period.*

Stronger stimuli often produce higher frequencies of impulse firing. Since the shape and speed of each action potential does not depend on the stimulus, information about the stimulus is often carried in the frequency of firing. The frequency is limited by the refractory period. Some neurons are capable of continuously generating action potentials, even without inputs. The temporal pattern of firing may be quite complicated. A neuron may generate a single spike in a periodic fashion, or may generates *bursting activity* in which there are episodes of high frequency firing separated by periods of quiescent behavior. More complicated firing patterns are possible and these will be described later in the text.

In the following sections, we shall give much more details of the mechanisms underlying the generation of action potentials. This, in turn, will lead to the famous Hodgkin-Huxley model for the propagation of action potentials along the nerve axon.

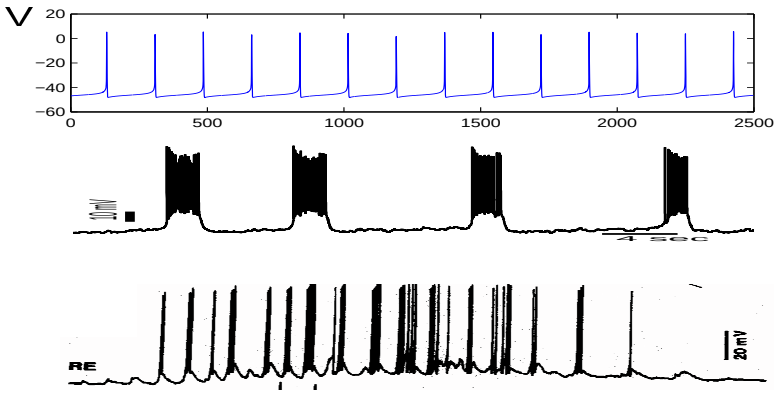

Figure 1.4.

1.3 The synapse

Neurons communicate with each other at synapses. The cell that is sending the signal is called the *presynaptic neuron* and the cell that is receiving the signal is called the *postsynaptic neuron.* Synapses can be either electrical or chemical. In electrical synapses, there is a direct connection from one neuron to another by way of a channel or gap junction. This type of synapse is rare among the principal cell types in the mammalian brain; for this reason, we will concentrate primarily on chemical synapses.

In chemical synaptic signaling, there is a space, called the *synaptic cleft*, separating the presynaptic from the postsynaptic cell. Most presynaptic neurons terminate near the dendrites of the postsynaptic cell; however, communication may occur with the cell body or, less often, with portions of the axon.

Signals from the presynaptic neurons result in the release of chemicals, called *neurotransmitters*. Neurotransmitters diffuse across the synaptic cleft and bind to receptors on the postsynaptic cell causing changes in the membrane potential. The membrane potential of the postsynaptic cell may either increase or decrease relative to its resting potential. This depends on the nature of the neurotransmitter and the type of receptor it binds to. A reduction of membrane potential (that is, the inside of the cell becomes less negative with respect to the outside) is called *depolarization* and the synapse is said to be *excitatory*. An increase of membrane potential (the inside becomes more negative) is called *hyperpolarization*. In this case, the synapse is said to be *inhibitory*.

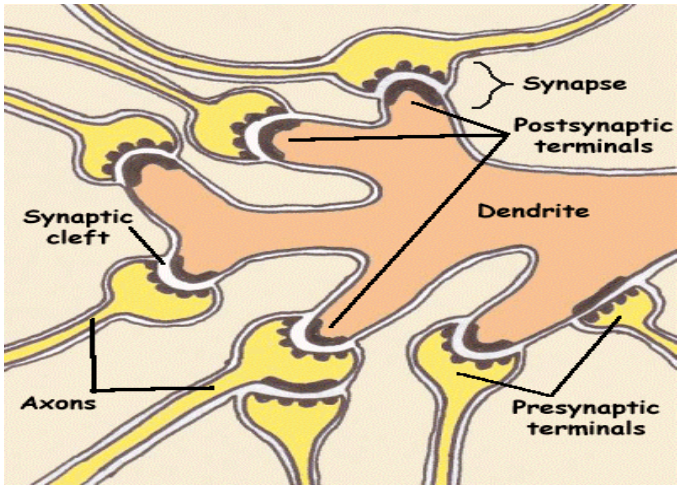

Figure 1.5.

We have seen that chemical synapses can be either excitatory or inhibitory. They can also be classified as *direct* or *indirect*. In a direct synapse, the postsynaptic receptor contains both the transmitter binding site and the ion channel opened by the transmitter as part of the same receptor. In an indirect synapse, the transmitter binds to receptors that are not themselves ion channels. Direct synapses are typically much faster than indirect synapses. In fact, direct synapses are often referred to as *fast* synapses, while indirect synapses are referred to as *slow* synapses.

Electrical synapses have the advantage that they are fast; there is not the time delay associated with chemical synapses. However, chemical synapses, which are much more abundant in the human brain, have many advantages. They are able to

amplify signals; a single action potential from the postsynaptic cell may result in a much more powerful, longer lasting response in the postsynaptic cell. Moreover, indirect synapses can be modified, through a process called *neuromodulation*, so that the efficacy of the synaptic response may change (through learning, for example).

The architecture of synaptic connections may be quite complicated. Each neuron in the human brain receives, on average, inputs from about 10000 other neurons. Neurons may communicate with other cells close by, while neurons with long axons may make synapses up to a meter away. Synaptic communication need not be in one direction; that is, neurons may make reciprocal synapses onto their presynaptic cells. Since most neurons have similar electrical properties, different functions carried out by different parts of the brain may be due to differences in the synaptic connections.

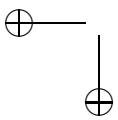

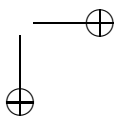

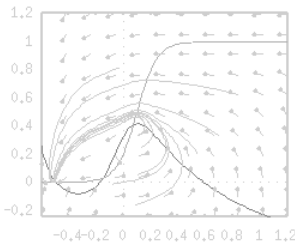

Chapter 2

The Hodgkin-Huxley equations

2.1 The resting potential

All living cells have an electrical voltage, or potential difference, between their inside and outside. Since the cell's membrane is what separates the inside from the outside, this potential difference is referred to as the *membrane potential*. In mathematical terms, the membrane potential V_M is defined as

$$V_M \;=\; V_{in} - V_{out}$$

where V_{in} is the potential on the inside of the cell and V_{out} is the potential on the outside. This will change during an action potential, for example.

The *resting potential* refers to the potential across the membrane when the cell is at rest. A typical neuron has a resting potential of about -70 millivolts. An *inward current* corresponds to a positively charged ion, such as Na^+, entering the cell. This raises the membrane potential; that is, it brings the membrane potential closer to zero. In this case, the cell is said to be *depolarized*. An *outward* current corresponds to a positively charged ion, such as K^+, leaving the cell or a negatively charged ion, such as Cl^-, entering the cell. In this case, the cell becomes *hyperpolarized*.

The potential difference arises from differences in the concentrations of various ions within and outside the cell. The maintenance of the potential difference also involves the transport of ions across the cell membrane and the selective permeability of the membrane to these ions. The principal ions found on either side of the cell membrane are Na^+, K^+, and Cl^-. The concentration of K^+ ions inside a cell is about 10 times that in the extracellular fluid, whereas the concentrations of Na^+ and Cl^- are much higher outside the cell than inside.

The lipid bilayer of the cell membrane is a poor conductor of ionic current because it is not permeable to ions. However, the membrane does contain channel proteins that allow for the ions to move through it. There are two types of ion channels in the membrane: gated and nongated. Nongated channels are always open, while gated channels can open and close and the probability of opening often depends on the membrane potential; these are referred to as *voltage-gated chan-*

nels. Gated channels are typically selective to a single ion. The *permeability* of the membrane to a particular ion depends on the number of open channels selective to that ion. Most gated channels are closed at rest. Hence, the nongated ion channels are primarily responsible for establishing the resting potential. An action potential is generated when gated channels open allowing for the flux of ions across the cell membrane.

Because of concentration differences, when the appropriate channels are open, sodium and chloride ions tend to diffuse into the cell, while potassium ions tend to diffuse outwards. Note that ions do not simply diffuse in or out of an open channel until the concentrations of that ion on either side of the cell is zero. This is because of the electric field created by separation of positive and negative charges across the cell membrane.

Suppose, for example, that the cell is permeable only to K^+. The concentration gradient of K^+ moves K^+ ions out of the cell. However, the continued efflux of K^+ builds up an excess of positive charge on the outside of the cell and leaves behind an excess of negative charge on the inside. The negative charge consists mostly of impermeable organic anions A^-. This buildup of charge acts to impede the further efflux of K^+, so that eventually an equilibrium is reached. At this equilibrium, the electrical and chemical driving forces are equal and opposite. The membrane potential at which K^+ ions are in equilibrium across the membrane is called the *K^+ Nernst*, *equilibrium* or *reversal potential*.

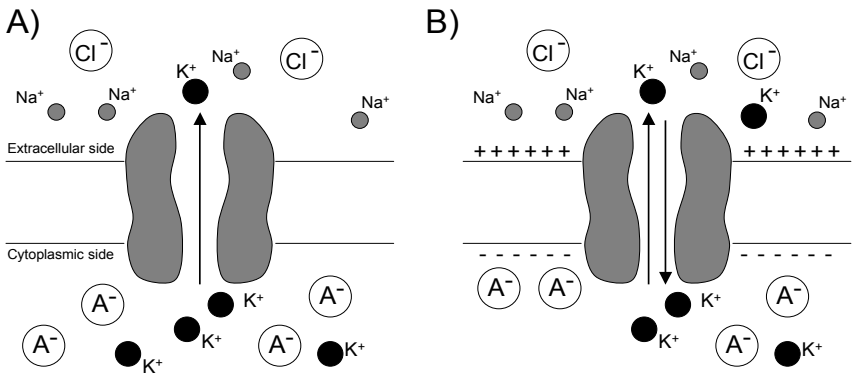

Figure 2.1. *The K^+ flux is determined by both the K^+ concentration gradient and the electrical potential across the membrane. A) For a cell that is permeable only to K^+, the concentration gradient of K^+ moves K^+ ions out of the cell. B) The continued efflux of K^+ builds up an excess of positive charge on the outside and negative charge on the inside. At equilibrium, the electrical and chemical driving forces are equal and opposite.*

In the next section, we shall derive the following expression for the K^+ Nernst

potential:

$$E_K = \frac{RT}{zF} \ln \frac{[K^+]_{out}}{[K^+]_{in}}. \tag{2.1}$$

Here, E_K is the K^+ Nernst potential, R is the gas constant, T is the temperature in degrees Kelvin, z is the valence of K^+, F is Faraday constant and $[K^+]_{out}$ and $[K^+]_{in}$ are the concentrations of K^+ ions outside and inside of the cell. A similar formula holds for the Na^+ and Cl^- Nernst potentials.

Neurons at rest are permeable to Na^+ and Cl^- in addition to K^+. Because of their concentration differences, Na^+ and Cl^- ions move into the cell and K^+ ions move outwards. The influx of Na^+ ions tends to depolarize the cell, while the efflux of K^+ and the influx of Cl^- have the opposite effect. The resting potential of the cell is the potential at which there is a balance between these fluxes. It depends on the concentrations of the ions both inside and outside of the cell, as well as the permeability of the cell membrane to each of the ions. We note that at rest, there are many more K^+ and Cl^- channels than Na^+ that are open. Hence, the cell's resting potential is determined primarily by the K^+ and Cl^- Nernst potentials. In the following sections, we shall derive the *Goldman-Hodgkin-Katz equation*, which gives an explicit expression for how the resting potential depends on the concentrations, both inside and outside, of ions and the permeabilities of the membrane to the ions.

In order for a cell to maintain a constant resting potential, the efflux of K^+ ions must balance the influx of Na^+ ions. (Here we are ignoring Cl^- ions.) That is, the charge separation across the membrane must be constant. If these steady ion leaks continue unopposed, then potassium ions within the cell would become depleted, while the concentration of sodium ions inside the cell would increase. This would eventually result in a loss of the ionic gradients, necessary for maintaining the resting potential. The dissipation of ionic gradients is prevented by active pumps the extrudes Na^+ ions from the cell while taking in K^+. The Na^+-K^+ pump is an integral membrane protein that exchanges three Na^+ ions for two K^+ ions. This is probably the most important ion transporter in biological membranes; however, there are many other proteins in the membrane that are capable of pumping ions from one side of the membrane to the other.

2.2 The Nernst equation

Here we derive the Nernst equation and in the next section, we derive the Goldman-Hodgkin-Katz (GHK) equation. Recall that if the membrane is permeable to only one ion, then that ion's Nernst potential is the resting potential at which the electrical and chemical driving forces balance. The GHK equation is, in some sense, a generalization of the Nernst equation in which we assume that the membrane is permeable to more than just one ion. The GHK equation determines the resting potential at which the electrical and chemical forces, generated by each of these ions, balance with each other. The first step in deriving these equations is to derive the *Nernst-Plank* equation.

In what follows, let $[C](x)$ be the concentration of some ion and $V(x)$ be the potential at the point x across the membrane. Then Fick's law of diffusion says

that the diffusive flux, J_{diff}, is given by:

$$J_{diff} = -D\frac{\partial[C]}{\partial x}.$$

The diffusion constant, D has units of cm^2/sec and the concentration is in molecules per cubic centimeter so that the diffusive flux has units of molecules/sec-cm^2. (Think of the flux as movement across the two-dimensional cell surface.) The direction of movement is from high concentrations to low concentrations. The diffusion constant (empirically measured) depends on the size of the molecule and the medium in which it is diffusing. A typical value for ions like potassium, chloride, and sodium is $2.5 \times 10^{-6}\text{cm}^2/\text{sec}$. Calcium has a diffusion constant about an order of magnitude less.

The other physical force that is responsible for the passive movement of ions is the electrical drift described by the microscopic version of Ohm's law:

$$J_{drift} = -\mu z[C]\frac{\partial V}{\partial x}.$$

The electric field, $E \equiv -\frac{\partial V}{\partial x}$, is the gradient of the potential V (measured in volts) and thus has units of volt/cm. z is the valence of the ion ($\pm 1, \pm 2$, etc). The parameter μ is mobility and has dimensions of cm^2/V-sec and $[C]$ is the concentration. The higher the concentration, the greater the drift. Note that drift has the same dimensions as the diffusive flux.

The total flux across the membrane is given by the sum of these two:

$$J_{total} = -D\frac{\partial[C]}{\partial x} - \mu z[C]\frac{\partial V}{\partial x}.$$

Einstein's relation connects the mobility with the diffusion coefficient:

$$D = \frac{kT}{q}\mu$$

where k is Boltzmann's constant (joule/°K), T is the absolute temperature, and q is the charge (measured in coulombs). Thus, we can write the total flux as:

$$J_{total} = -\frac{\mu kT}{q}\frac{\partial[C]}{\partial x} - \mu z[C]\frac{\partial V}{\partial x}.$$

It is convenient to convert this equation, which is in terms of the number of individual molecules into its molar equivalent, by dividing by Avogadro's number. It is also convenient to replace kT/q with RT/F where R is the ideal gas constant and F is the Faraday constant. (A list of these constants is given at the end of this section.) This will yield the flux per mole. Multiplying this flux by the valence and Faraday's constant yields a current flux:

$$I = -\left(uzRT\frac{\partial[C]}{\partial x} + uz^2F[C]\frac{\partial V}{\partial x}\right)$$

measured in amperes/cm^2. The quantity u is the molar mobility, μ/N_A. This equation is the *Nernst-Planck Equation*.

The Nernst equation is obtained by setting the current to zero. That is, for a given ion species, at equilibrium, the diffusion and electric effects balance:

$$I = -\left(uzRT\frac{\partial[C]}{\partial x} + uz^2F[C]\frac{\partial V}{\partial x}\right) = 0.$$

As an exercise, it is left to the reader to prove that this implies the *Nernst equation*:

$$V_{eq} \equiv V_{in} - V_{out} = -\frac{RT}{zF}\ln\frac{[C]_{in}}{[C]_{out}}. \tag{2.2}$$

That is, the equilibrium, or Nernst, potential, occurring when all the fluxes balance, depends on the logarithm of the ratio of the concentrations of the ions inside and outside of the cell.

To illustrate how to use the Nernst equation to compute an equilibrium potential, note that in a typical mammalian cell, there is 140 mM of potassium inside the cell and 5 mM outside. At room temperature $37°C$, $RT/F = 62$ mV. This means the equilibrium potential of potassium is

$$-62\log\frac{140}{5} = -89.7\text{mV}.$$

As above, we will leave the details of this calculation the reader.

2.3 The Goldman-Hodgkin-Katz equation

The Nernst-Planck equation describes the movement of charged ions in aqueous media. However, the cell membrane has thickness and there may be energy barriers or blocking sites within the channel. In this case, the ions flowing through the open channel may not obey the Nernst-Planck equation and we must model the complex behavior within this membrane to get a true picture of the flux across the cell. This type of biophysics is beyond the details that are needed for this book, but the resulting equation does play a role in later parts. Thus, we will present a shortened derivation of a simplification of what happens within the membrane. Goldman, Hodgkin, and Katz came up with this simplified model called the *constant field equation* (CFE). They assume that (i) the electric field across the lipid membrane is constant, (ii) the Nernst-Planck equation holds within the membrane, and (iii) the ions all move independently.

Let V_M be the total potential across a membrane of width l and let $V(x)$ be the potential at the point x across the membrane. Since the electric field is constant, $E = -V_M/l$. This implies that $dV/dx = V_M/l$. The mobility of ions within the membrane will be different than in the aqueous solution; denote this mobility by u^*. Finally, let β be the ratio of the ion solubility within the membrane to the solubility in the aqueous solution. Thus, if $[C]$ is the aqueous concentration, then $\beta[C]$ is the membrane concentration. With these assumptions the Nernst-Planck

equation for current across the membrane is:

$$I = -u^* z^2 F\beta[C]\frac{V_M}{l} - u^* zRT\beta\frac{d[C]}{dx}, \qquad 0 < x < l.$$

This is just a first order linear ordinary differential equation for $[C]$ subject to the *two* boundary conditions

$$[C](0) = [C]_{in}, \qquad [C](l) = [C]_{out}.$$

One cannot, in general, solve a first order equation with two boundary conditions. However, the current I is unknown, so that choosing this correctly will allow us to find a solution that satisfies both boundary conditions. We leave this elementary exercise to the reader. The result is:

$$I = \frac{u^* z^2 F V_M \beta}{l}\left[\frac{[C]_{out}e^{-\xi} - [C]_{in}}{e^{-\xi} - 1}\right]$$

where

$$\xi = \frac{zV_M F}{RT}.$$

This expression is often written in terms of the permeability,

$$P \equiv \frac{\beta u^* RT}{lF};$$

that is,

$$I = PzF\xi\left(\frac{[C]_{out}e^{-\xi} - [C]_{in}}{e^{-\xi} - 1}\right). \tag{2.3}$$

The permeability has dimensions of cm/sec. Thus, the dimensions are in terms of current per unit area.

This is the current due to a single ionic species. The current vanishes at the equilibrium or Nernst potential of the ionic species. A common quantity to plot is the current-voltage $(I - V)$ plot. If the inside and outside concentrations are identical, then the $I - V$ plot is linear. For $[C]_{out} > [C]_{in}$ (resp. $[C]_{out} < [C]_{in}$) the $I - V$ plot is concave down (resp. concave up). The reader is encouraged to plot the current as a function of the voltage for different concentration ratios. If the concentrations are quite different on the inside and outside, then the $I - V$ curve is *strongly rectifying*. That means that the magnitude of the current depends strongly on whether or not the potential is above or below the equilibrium.

Given several ionic species, the total current is just a sum of the individual currents. This is a consequence of assumption (iii) which says that the ions do not interact. Suppose that there are three permeant ions: K^+, Na^+ and Cl^- with corresponding currents, I_K, I_{Na} and I_{Cl}. At equilibrium the total current, $I = I_K + I_{Na} + I_{Cl}$ vanishes; that is, $I = 0$. The potential at which this occurs is:

$$V_M = \frac{RT}{F}\ln\frac{P_K[K^+]_{out} + P_{Na}[Na^+]_{out} + P_{Cl}[Cl^-]_{in}}{P_K[K^+]_{in} + P_{Na}[Na^+]_{in} + P_{Cl}[Cl^-]_{out}} \tag{2.4}$$

Table 2.1. *Typical ion concentrations in cells. (From Johnstonand Wu).*

Ion	**Inside (mM)**	**Outside (mM)**	**Equilibrium Potential** $E_i = \frac{RT}{zF} \ln \frac{[C]_{out}}{[C]_{in}}$
Frog Muscle			$T = 20°C$
K^+	124	2.25	$58 \log \frac{2.25}{1.24} = -101mV$
Na^+	10.4	109	$58 \log \frac{109}{10.4} = +59mV$
Cl^-	1.5	77.5	$-58 \log \frac{77.5}{1.5} = -99mV$
Ca^{2+}	10^{-4}	2.1	$29 \log \frac{2.1}{10^{-4}} = +125mV$
Squid Axon			$T = 20°C$
K^+	400	20	$58 \log \frac{20}{400} = -75mV$
Na^+	50	440	$58 \log \frac{440}{50} = +55mV$
Cl^-	40-150	560	$-58 \log \frac{560}{40-150} = -66$ to $-33mV$
Ca^{2+}	10^{-4}	10	$29 \log \frac{10}{10^{-4}} = +145mV$
Mammalian cell			$T = 37°C$
K^+	140	5	$62 \log \frac{5}{140} = -89.4mV$
Na^+	5-15	145	$62 \log \frac{145}{5-15} = +90 - (+61)mV$
Cl^-	4	110	$-62 \log \frac{110}{4} = -89mV$
Ca^{2+}	10^{-4}	2.5-5	$31 \log \frac{2.5-5}{10^{-4}} = +136 - (+145)mV$

where the P_j's are the permeabilities of each of the three ionic species. This is a generalization of the Nernst equilibrium discussed above and is called the Goldman-Hodgkin-Katz equation (GHK). With one species, the equation reduces to the Nernst potential. For example, in the squid axon, the ratios of the permeabilities, at rest, are $P_K : P_{Na} : P_{Cl} = 1 : 0.03 : 0.1$. The ion concentrations inside the cell are, respectively, for K, Na and Cl, 400 mM, 50 mM, and 40 mM; while outside the cell they are 10 mM, 460 mM, and 540 mM. Thus, at room temperature, the equilibrium or resting potential is -70 mV.

Table 2.2. *Elementary constants*

$$
\begin{aligned}
N_A &= 6.022 \cdot 10^{23}\ /mol \quad \text{Avogadros number} \\
k &= 1.380658 \cdot 10^{-23} j/K \quad \text{Boltzmanns constant} \\
R &= 8.31451\ j/(mol - K) \quad \text{Ideal gas constant} \\
e &= 1.602177 \cdot 10^{-19}\ C \quad \text{electron charge} \\
F &= 96485.3\ C/mol \quad \text{Faraday's constant} \\
\epsilon_0 &= 8.85 \cdot 10^{-12}\ F/m \quad \text{permittivity constant} \\
\text{Kelvin} &= \text{ Centigrade } + 273.16 \\
1\ j &= .238845\ cal
\end{aligned}
$$

$$
\begin{aligned}
L &= \text{liter} \\
nt &= \text{newton} \\
j &= \text{joule (nt-sec)} \\
V &= \text{volt} = 1 joule/coulomb \\
C &= \text{coulomb} \\
A &= \text{ampere (C/sec)} \\
\Omega &= \text{Ohm (V/A)} \\
S &= 1/\Omega = \text{siemens (A/V)} \\
F &= \text{farad (sec-A/V)} = \text{(C/V)}
\end{aligned}
$$

2.4 Exercises

1. Suppose the external potassium in a mammalian cell is increased by a factor of 10. What is the new value of E_K?

2. At $10°C$ a cell contains 80 mM sodium inside and has only 100 mM sodium outside. What is the equilibrium potential for sodium?

3. Using the same permeabilities for the mammalian cell as were used for the squid axon, compute V_{rest}, V_m using the table of ion concentrations.

4. Derive the Nernst equation from the Nernst-Planck equation by setting the current to 0 and integrating with respect to x across the membrane.

5. Using the elementary constants defined in Table 2.3, obtain the two simplified versions of the Nernst equation. Compute the calcium equilibrium potential for a mammalian cell assuming that the extracellular concentration is 5 mM and the intracellular is $10^{-4} mM$.

6. Derive the constant field equation from the linear Nernst-Planck equation.

7. Derive the GHK equation from the constant field equation.

8. Consider the GHK equation and plot the $I - V$ relation for different values of the inside and outside concentrations. Show that for $[C]_{out} > [C]_{in}$ (resp. $[C]_{out} < [C]_{in}$) the $I - V$ plot is concave down (resp. up)

2.5 Equivalent circuits: the electrical analogue

We have seen in the previous section that the electrical properties of cells are determined by the ionic species that move through the membrane. Currents flow according to the permeabilities of ion channels and concentration gradients across the cell membrane. However, all of our discussion so far has been in a steady-state environment. The Goldman-Hodgkin-Katz equation does not determine how the membrane potential changes in response to changes in the permeabilities. For this reason, it cannot be used to understand how these changes in permeabilities may generate an action potential. A very useful way to describe the behavior of the membrane potential is in terms of electrical circuits; this is commonly called the *equivalent circuit model*. The circuit consists of three components: (1) conductors or resistors, representing the ion channels; (2) batteries, representing the concentration gradients of the ions; and (3) capacitors, representing the ability of the membrane to store charge. The equivalent circuit model leads to both an intuitive and quantitative understanding of how the movement of ions generate electrical signals in the nerve cell.

We first consider a membrane that is only permeable to potassium. The equivalent circuit is shown in Figure 2.2. The lipid bilayer that comprises the cell membrane has dielectric properties and as such behaves in much the same manner as a capacitor. Recall that capacitors store charge and then release it in the form of currents. The relationship between the charge stored and the potential is given by:

$$q \;=\; C_M V_M; \tag{2.5}$$

that is, the total charge q is proportional to the potential V_M with a proportionality constant C_M called the membrane capacitance. Note that the total capacitance depends on the total area of the dielectric; thus larger neurons have a larger total capacitance than smaller ones. The capacitance per square centimeter is called the *specific membrane capacitance* and will be denoted as c_M. Hence, the total membrane capacitance C_M is the membrane specific capacitance c_M times the total surface area of the cell. In general, the specific membrane capacitance may depend on the potential; however, for most cell membranes, the specific membrane capacitance is very close to 1 μ F/cm^2.

Since current is the time derivative of charge, we can differentiate (2.5) and obtain an expression for the specific capacitance current:

$$i_{cap} \;=\; c_M \frac{dV_M}{dt}. \tag{2.6}$$

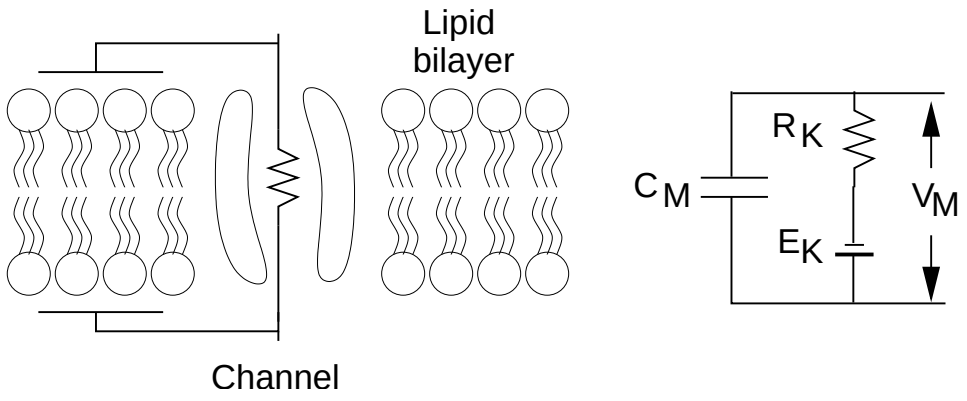

Figure 2.2. *Cartoon of the cell membrane showing the insulating lipid bilayer and a K^+ channel which allows current to flow. The equivalent electrical circuit is shown on the right*

This gives the capacitance current per unit area. We will denote the total capacitance current as I_{cap}.

In the equivalent circuit, K^+ channels are represented as a conductor in series with a battery. If $\hat{g}_K$ is the conductance of a single K^+ channel, then, using Ohm's law, the ionic current through this channel is

$$\hat{I}_K \;=\; \hat{g}_K(V_M - E_K). \tag{2.7}$$

Here E_K is the potential generated by the battery; this is given by the K^+ Nernst potential. The *driving force* is $V_M - E_K$. Now suppose there are N_K potassium channels in a unit area of membrane. These can all be combined into the single equivalent circuit shown in Figure 2.2. The conductance per unit area, or specific membrane conductance (S/cm^2) is given by $g_K = N_K \times \hat{g}_K$ and the specific membrane resistance (Ω-cm^2) is $r_K \equiv 1/g_K$. Since the Nernst potential depends only on the concentration gradient of K^+, and not on the number of K^+ channels, it follows that the K^+ current, per unit area, is given by

$$I_K \;=\; g_K(V_M - E_K) \;=\; \frac{V_M - E_K}{r_K}. \tag{2.8}$$

Kirchhoff's current law states that the total current into the cell must sum to zero. Together with the equivalent circuit representation, this leads to a differential equation for the membrane potential:

$$0 \;=\; i_{cap} + I_K \;=\; c_M \frac{dV_M}{dt} \;+\; \frac{V_M - E_K}{r_K} \tag{2.9}$$

or

$$c_M \frac{dV_M}{dt} \;=\; -\,\frac{V_M - E_K}{r_K} \;=\; -\,g_K(V_M - E_K). \tag{2.10}$$

Figure 2.3 shows an equivalent circuit with three parallel conductances and a current source, $I(t)$. Here the capacitance current must be equal to the sum of the ionic currents and the current source. As before, the capacitance current, per unit area, is given by (2.6) and the ionic current, per unit area, is given by

$$i_{ion} = g_{Cl}(V_M - E_{Cl}) - g_K(V_M - E_K) - g_{Na}(V_M - E_{Na}). \tag{2.11}$$

The current source is not typically expressed as current per unit area, so we must divide $I(t)$ by the total surface area of the neuron, A. It then follows that

$$c_M \frac{dV_M}{dt} = -g_{Cl}(V_M - E_{Cl}) - g_K(V_M - E_K) - g_{Na}(V_M - E_{Na}) + I(t)/A. \tag{2.12}$$

Note that we can rewrite this equation as

$$c_M \frac{dV_M}{dt} = -\frac{(V_M - E_R)}{r_M} + I(t)/A \tag{2.13}$$

where

$$E_R = g_{Cl}E_{Cl} + g_K E_K + g_{Na}E_{Na}$$

is the cell's resting potential and

$$r_M = \frac{1}{g_{Cl} + g_K + g_{Na}}$$

is the specific membrane resistance.

For a passive membrane in which the conductances and currents are all constant, then V_M will reach a steady state:

$$V_{ss} = \frac{g_{Cl}E_{Cl} + g_K E_K + g_{Na}E_{Na} + I/A}{g_{Cl} + g_k + g_{Na}}.$$

In absence of the applied current, the steady state potential is a weighted sum of the equilibrium potentials of the three currents. This is similar to the Goldman-Hodgkin-Katz equation (2.4) in which the contribution to the resting potential by each ion is weighted in proportion to the permeability of the membrane for that particular ion. Note, however, that in the equivalent circuit model, the equilibrium is a linear weighted sum of the equilibrium potentials, while in the GHK equation, the sum is nonlinear.

We remark that membrane conductance and permeability are related concepts; however, they are not the same. The permeability depends on the state of the membrane, while conductance depends on both the state of the membrane and the concentration of the ions. The permeability to K^+, for example, may be high if there are a large number of open K^+ channels. However, if the concentration of K^+ ions is low on both sides of the membrane, then the K^+ conductance would be low.

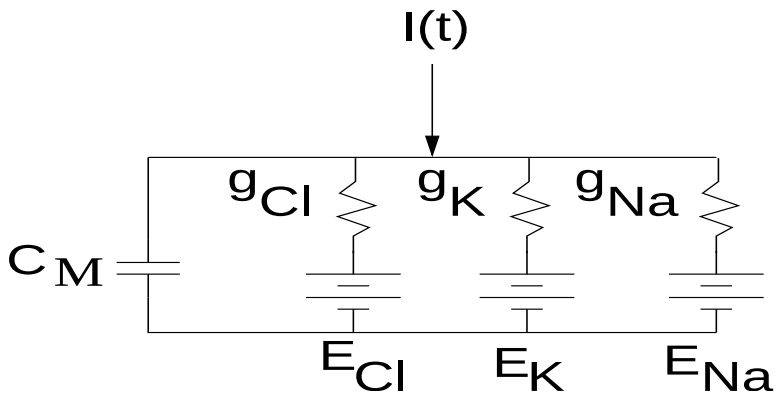

Figure 2.3. *Equivalent circuit for a membrane with three channels.*

2.6 The membrane time constant

In this section, we consider how a passive, isopotential cell responds to an applied current. This will help explain how each component of the electrical circuit contributes to changes in the membrane potential. The cell is said to be *passive* if its electrical properties do not change during signaling. Such a cell cannot generate an action potential; however, it is important to understand how a cell's passive, or constant, properties influence changes in the membrane potential before considering active signaling. Moreover, many dendrites do not have gated channels so their behavior is influenced primarily by their passive properties. The cell is said to be *isopotential* if the membrane potential is uniform at all points of the cell; that is, the membrane potential depends only on time. To simplify the analysis, we will consider a spherical cell with radius ρ.

Suppose that this cell is injected with an applied current, $I(t)$, that is turned on at $t = 0$ to some constant value, I_0, and turned off at $t = T$. Here, we assume that $I_0 > 0$; however, this is really not necessary. Note that for an isopotential cell, the injected current distributes uniformly across the surface. It follows that for a spherical cell, the current flowing across a unit area of the membrane is

$$I_M(t) = \frac{I(t)}{4\pi\rho^2} = \begin{cases} \frac{I_0}{4\pi\rho^2} & \text{if} \quad 0 < t < T \\ 0 & \text{otherwise} \end{cases} \tag{2.14}$$

As before, suppose that c_M is the specific membrane capacitance, r_M is the specific membrane resistance and E_R is the cell's resting potential. To simplify things, we take $E_R = 0$ so that V_M measures deviation of the membrane potential from rest. From 2.13, the membrane potential satisfies the ordinary differential equation

$$c_M \frac{dV_M}{dt} = -\frac{V_M}{r_M} + I_M(t). \tag{2.15}$$

If the cell starts at rest, then the solution of this linear equation satisfies

$$V_M(t) = \frac{r_M I_0}{4\pi\rho^2}\left(1 - e^{-\frac{t}{\tau_M}}\right) \quad \text{for} \;\; 0 < t < T \tag{2.16}$$

where $\tau_M \equiv \frac{1}{c_M r_M}$ is the *membrane time constant* and

$$V_M(t) = V_M(T)e^{-\frac{t}{\tau_M}} \quad \text{for} \;\; t > T. \tag{2.17}$$

The solution is shown in Figure 2.4. Once the current is turned on, the membrane potential asymptotically approaches the steady state value $r_M I_0/(4\pi\rho^2)$. The approach is exponential with the time constant τ_M. The membrane time constant also determines the rate at which the membrane potential decays back to rest after the current is turned off. The steady state membrane potential satisfies

$$I_0 \frac{r_M}{4\pi\rho^2} \equiv I_0 R_{INP} \tag{2.18}$$

where R_{INP} is the *input resistance* of the cell. Note that if the input current changes by ΔI, then the steady state membrane potential changes by $R_{INP} \times \Delta I$; that is, the input resistance is the slope of the $I - V$ curve obtained by plotting the steady state voltage against the injected current.

The initial rise in membrane potential is determined primarily by the membrane capacitance. Initially the voltage across the resistor and capacitor are both equal to 0. From Ohm's law, it follows that initially no current flows through the resistor and all the current is due to the capacitor. Because of the capacitive current, the potential across the capacitor and hence the membrane potential, will become more positive. As V_M increases, the membrane potential difference begins to drive current across the membrane resistance resulting in less current across the capacitor. Eventually, the membrane potential reaches a value where all the membrane current flows through the resistor. This value is given by $V_M = I_0 R_{INP}$.

Figure 2.4 also shows responses in which there are purely resistive or purely capacitive elements. If there is no membrane capacitance, then V_M satisfies

$$V_M(t) = r_M I_M(t). \tag{2.19}$$

That is, V_M jumps to the steady state potential, $R_{INP} I_0$, as soon as the injected current is turned on and it jumps back to rest as soon as the current is turned off. If there is only a capacitive element, then the membrane potential changes linearly as long as there is an applied current.

2.7 The cable equation

We have, so far, considered the passive properties of an isopotential cell. This analysis may be used to describe signaling within the cell body, which can be approximated by a sphere. However, it is clearly not appropriate for studying electrical properties of the axon or dendrites. These are better approximated by cylinders that are not isopotential. A subthreshold voltage signal that is initiated at one

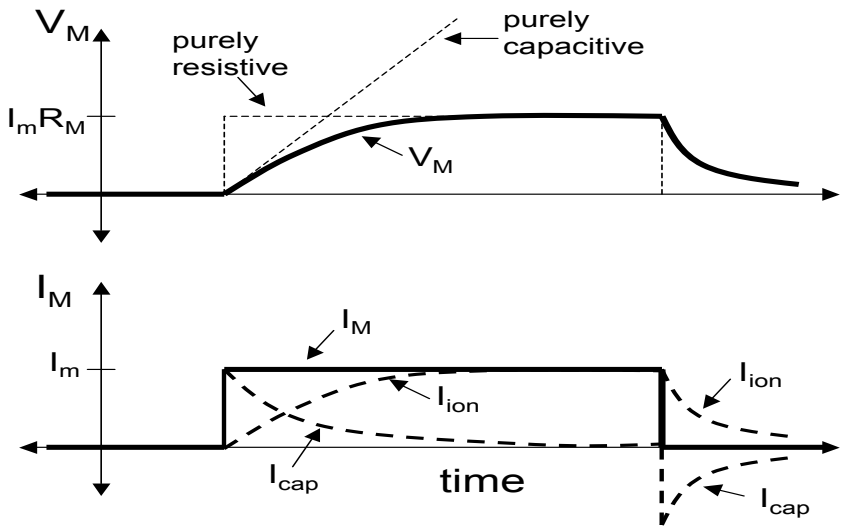

Figure 2.4. *The change of membrane potential in response to a step of current. The membrane potential is shown with a solid line. The dashed lines show the time courses of the purely capacitive and resistive elements. The bottom panel shows the time course of the total membrane current, the ionic current and the capacitive current.*

point along the axon or dendrite will decrease in amplitude with distance from the point of initiation. It is important to understand how the geometry of the cell affects the spread of the signal. The signal may, for example, correspond to synaptic input from another neuron. Understanding how geometry affects the spread of the signal will help determine whether the synaptic input will cause the cell to fire an action potential. Here we assume that the membrane is passive, so the analysis is more applicable to dendrites than to axons. However, as we shall describe later, the passive spread of current flow helps determine the velocity of propagating action potentials in the axon.

We consider a cell that is shaped as a long cylinder, or cable, of radius a. We assume that the current flow is along a single spatial dimension, x, the distance along the cable. In particular, membrane potential depends only on the x-variable, not on the radial or angular components. The cable equation is a partial differential equation that describes how the membrane potential $V_M(x,t)$ depends on currents entering, leaving and flowing within the neuron. The equivalent circuit is shown in Figure 2.5 where I_{long} is the current along the inside of the cable, I_M is the current across the membrane, R_L is the resistance of the cytoplasm, R_e is the resistance of the extracellular space, R_M is the membrane resistance and C_M is the membrane capacitance. In what follows, we will assume that $R_e = 0$, so that the extracellular

space is isopotential. This assumption is justified if the cable is in a bath with large cross-sectional area.

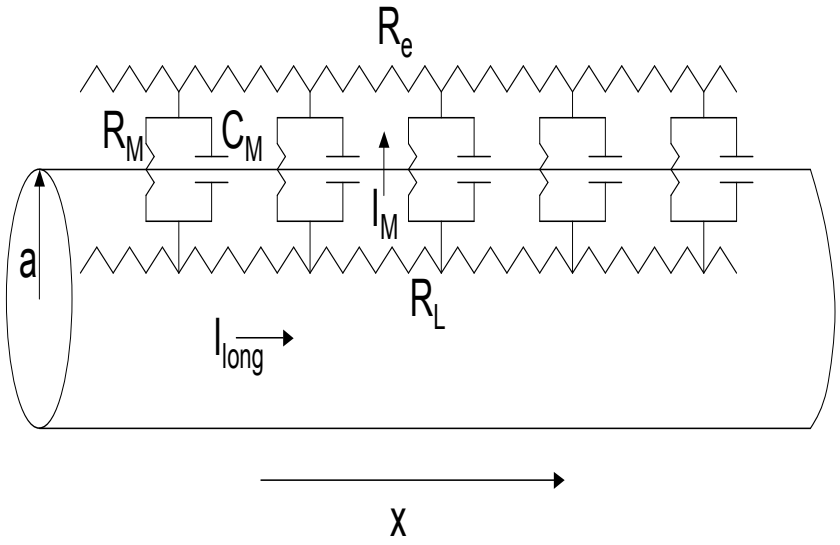

Figure 2.5. *Equivalent circuit for a uniform passive cable.*

We first consider the axial current flowing along the neuron due to voltage gradients. Note that the total resistance of the cytoplasm grows in proportion to the length of the cable and is inversely proportional to the cross-sectional area of the cable. The specific intracellular resistivity, which we denote as r_L, is the constant of proportionality. Hence, a cable of radius a and length Δx has a total resistance of $R_L = r_L \Delta x/(\pi a^2)$ It follows from Ohm's law that at any point x, the decrease in V_M with distance is equal to the current times the resistance. That is,

$$V_M(x + \Delta x, t) - V_M(x, t) = -I_{long}(x, t) R_L = -I_{long}(x, t) \frac{\Delta x}{\pi a^2} r_L. \tag{2.20}$$

There is a minus sign because of the convention that positive current is a flow of positive charges from left to right. If voltage decreases with increasing x, then the current is positive. In the limit $\Delta x \to 0$,

$$I_{long}(x, t) = -\frac{\pi a^2}{r_L} \frac{\partial V_M}{\partial x}(x, t). \tag{2.21}$$

Let i_{ion} be the current per unit area due to ions flowing into and out of the cell. Then the total ionic current that flows across a membrane of radius a and length Δx is given by $I_{ion} = (2\pi a \Delta x) i_{ion}$.

Recall that the rate of change of the membrane potential is determined by the capacitance. The total capacitance of a membrane is equal to the specific

membrance capacitance c_M multiplied by the total surface area of the membrane. Hence, for a cable of radius a and length Δx, the total capacitance is given by $C_M = (2\pi a \Delta x) c_M$ and the amount of current needed to change the membrane potential at a rate $\partial V_M / \partial t$ is

$$I_{cap} = (2\pi a \Delta x) c_M \frac{\partial V_M}{\partial t}. \tag{2.22}$$

From Kirchhoff's law, the change in intracellular axial current is equal to the amount of current that flows across the membrane. Hence,

$$I_{cap}(x,t) + I_{ion}(x,t) = I_{long}(x + \Delta x, t) - I_{long}(x,t) \tag{2.23}$$

from it which it follows that

$$(2\pi a \Delta x) c_M \frac{\partial V_M}{\partial t} + (2\pi a \Delta x) i_{ion} = \frac{\pi a^2}{r_L} \frac{\partial V_M}{\partial x}(x + \Delta x, t) - \frac{\pi a^2}{r_L} \frac{\partial V_M}{\partial x}(x,t)$$

We divide both sides of this equation by $2\pi a \Delta x$ and let $\Delta x \to 0$ to obtain the cable equation:

$$c_M \frac{\partial V_M}{\partial t} = \frac{a}{2 r_L} \frac{\partial^2 V_M}{\partial x^2} - i_{ion} \tag{2.24}$$

For a passive cable, in which the resting potential is assumed to be zero,

$$i_{ion} = V_M(x,t)/r_M \tag{2.25}$$

where r_M is the specific membrane resistance. Then (2.24) becomes

$$c_M \frac{\partial V_M}{\partial t} = \frac{a}{2 r_L} \frac{\partial^2 V_M}{\partial x^2} - \frac{V_M}{r_M}. \tag{2.26}$$

We can rewrite this equation as

$$\tau_M \frac{\partial V_M}{\partial t} = \lambda^2 \frac{\partial^2 V_M}{\partial x^2} - V_M \tag{2.27}$$

where

$$\lambda = \sqrt{\frac{a r_M}{2 r_L}} \quad \text{and} \quad \tau_M = c_M r_M \tag{2.28}$$

are the *space* or *length constant* and the *membrane time constant*, respectively. Note that the space constant depends on the geometry of the cable, that is the cable's diameter; however, the time constant does not.

Later, we shall give a detailed analysis of solutions to the cable equation and properties of passive dendrites. For now, it is instructive to consider steady state solutions. Suppose, for example, we consider a semi-infinite cable (defined for $x > 0$) and we inject a step of current, I_0, at $x = 0$. As $t \to \infty$, the solution

$V_M(x,t)$ approaches a steady-state solution $V_{ss}(x)$ that does not depend on time. Setting $\frac{\partial V_M}{\partial t} = 0$ in (2.27), we find that V_{ss} satisfies

$$\lambda^2 \frac{d^2 V_{ss}}{dx^2} - V_{ss} = 0. \tag{2.29}$$

In order to solve this equation, we need boundary conditions. Recall from (2.21) that

$$I_L = -\frac{\pi a^2}{r_L} \frac{\partial V_M}{\partial x}.$$

It follows that V_{ss} must satisfy the boundary condition

$$\frac{dV_{ss}}{dx}(0) = -\frac{r_L}{\pi a^2} I_0. \tag{2.30}$$

The solution of (2.29), (2.30) is

$$V_{ss}(x) = \frac{\lambda r_L}{\pi a^2} I_0 e^{-x/\lambda}. \tag{2.31}$$

Note that the membrane potential decays exponentially. The distance at which the potential has decayed to $1/e$ is the space constant λ. Since the space constant is proportional to the square root of the cable's radius, we conclude that thicker axons or dendrites have longer space constants than narrower processes. That is, thicker processes transmit signals for greater distances. As we discuss later, this is important because it influences the ability of the neuron to spatially summate incoming synaptic potentials. Moreover, the electrotonic, or passive, conduction plays an important role in the propagation of the action potential. Thicker cells with a longer space constant are more easily excited and are able to generate faster action potentials.

The input resistance is defined to be the steady-state membrane potential, evaluated at $x = 0$, divided by the injected current. That is,

$$R_{inp} = V_{ss}(0)/I_0 = r_L \lambda = \frac{1}{\pi a^{3/2}} \sqrt{r_M r_L / 2}. \tag{2.32}$$

Note that the input resistance of the cable varies with the -3/2 power of the cable radius. Therefore, the input conductance is directly proportional to the 3/2 power of the cable radius. The input resistance is important because it is something that can be measured experimentally. Since it is also possible to measure the space constant λ, one can compute r_M and r_L from experimental data.

2.8 The squid action potential

We have so far viewed the membrane as a passive cable. However, linear cables cannot transmit information over long distances unless the cable has an enormous diameter. For example, the squid axon is more than 5 centimeters long, has a diameter of about a half a millimeter, a resting membrane resistance of r_M=700

Ω cm^2 and a transmembrane resistance of r_L=30 Ω cm. Thus, the space constant for the squid axon is $\lambda = 5.4$ mm. This is an order of magnitude smaller than the length. If the potential at one end of the axon is held at 120 mV above rest, then the potential at the other end is about 10 μV above rest, a 10000-fold decrement. In order for neural signals to reach any distance, there must be another way to carry them so that they do not degrade.

Nature has solved this problem by inserting *voltage-gated* channels into the membranes of many cell types. These channels are proteins which selectively let different ion species into the cell. Furthermore, the permeability of the channels depends on the local environment near the channel. In particular, for voltage gated channels, whether the channel is open or closed depends on the local potential near the channel. It is the opening and closing of voltage-gated channels that is responsible for the generation of the action potential that propagates along the axon.

Hodgkin and Huxley (1952) were the first to provide a comprehensive, quantitative description of the regenerative currents generating the action potential. The choice of the squid axon was fortuitous since the electrical properties rely primarily on sodium and potassium ions. Consider the equivalent circuit shown in Figure 2.6 and assume that the cell is isopotential. Then the membrane potential satisfies

$$c_M \frac{dV}{dt} = -g_{Na}(V - E_{Na}) - g_K(V - E_K) - g_L(V - E_L).$$

Here, we write V instead of V_M. $I_L \equiv g_L(V - E_L)$ is called the *leak current*. It corresponds to passive flow of ions through nongated channels. The leak conductance, g_L, is constant. Since most nongated channels are permeable to K^+ ions, E_L is close to E_K. The conductances g_{Na} and g_K may change with time since these correspond to the opening and closing of Na^+ and K^+ channels, respectively. At rest, g_K is about 30-fold bigger than g_{Na} so that the resting state is near E_K at about -65 mV. Suppose that we could increase the conductance of g_{Na} 100-fold. Then the resting potential would be much closer to the Nernst potential of sodium, which is about +55 mV. Thus the amplification of the potential, such as during an action potential, involves changes in the relative conductances of the dominant ionic species. Hodgkin and Huxley's insight was that voltage-gated channels provide the substrate for this dynamic regulation of the conductances.

The basic mechanisms underlying action potentials are the following. At rest, most of the sodium channels are closed so the membrane potential is determined primarily by the K^+ Nernst potential. If the cell is depolarized above some threshold, then sodium channels open and this further depolarizes the cell. This allows even more sodium channels to open, allowing for more sodium ions to enter the cell and forcing the cell towards the sodium Nernst potential. This is the up-stroke of the action potential. The sodium channel is transient so that even when depolarized, the Na^+ channels eventually shut down. In the meantime, the depolarization opens potassium channels and potassium ions exit the cell. This hyperpolarizes the cell as the membrane potential moves toward the potassium equilibrium potential. Until the voltage-gated potassium channels close up again, the membrane is refractory. During this time, pumps exchange excess sodium ions inside the cell with excess

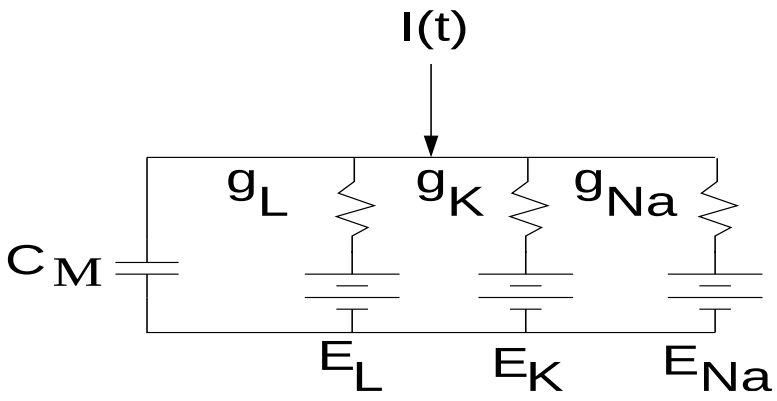

Figure 2.6. *Equivalent circuit underlying the Hodgkin-Huxley equations.*

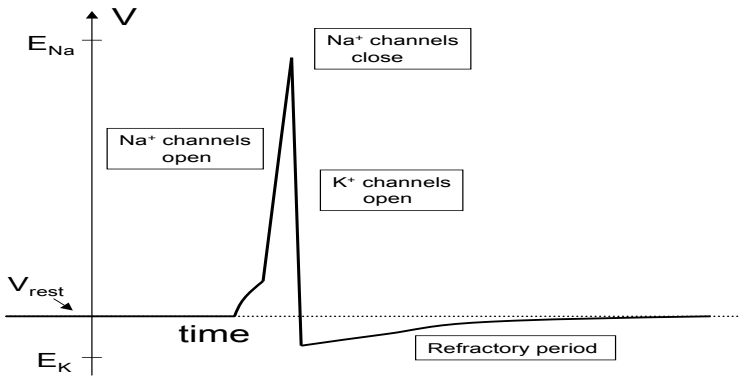

Figure 2.7. *The action potential. During the upstroke, sodium channels open and the membrane potential approaches the sodium Nernst potential. During the downstroke, sodium channels are closed, potassium channels are open and the membrane potential approaches the potassium Nernst potential.*

potassium ions outside of the cell.

Only a very small change in the percentage of the concentration of Na^+ ions is needed to generate an action potential. From the exercises, we find that approximately 53 million Na^+ ions must diffuse across the membrane to depolarize it from -60 to +50 mV. This influx in Na^+ ions represents only a .012% change in the internal Na^+ concentration which is typically around 12 mM. Hence, changes in local charge separation, not in concentration, are required for an action potential.

2.9 Voltage-gated channels

In the Hodgkin-Huxley model, each channel is viewed as a transmembrane protein that forms a pore through which ions can diffuse down their concentration gradients. The pores have gates that can be either open or closed; the probability that a gate is open or closed depends on the membrane potential. The gate model can be summarized by the diagram:

$$C \underset{\alpha(V)}{\overset{\beta(V)}{\rightleftharpoons}} O \tag{2.33}$$

where C and O correspond to the closed and open states, respectively, and $\alpha(V)$ and $\beta(V)$ are the voltage-dependent rate constants at which a gate goes from the open to closed and closed to open states, respectively. If we let m be the fraction of open gates, then $1-m$ is the fraction of closed gates, and, from the law of mass action,

$$\frac{dm}{dt} = \alpha(V)(1-m) - \beta(V)m = (m_\infty(V) - m)/\tau(V) \tag{2.34}$$

where

$$m_\infty(V) = \frac{\alpha(V)}{\alpha(V)+\beta(V)} \quad \text{and} \quad \tau(V) = \frac{1}{\alpha(V)+\beta(V)}. \tag{2.35}$$

It is easy to solve this equation if V is constant. The solution starting at $m(0)$ is

$$m(t) = m_\infty(V) + (m(0) - m_\infty(V))e^{-t/\tau(V)}.$$

Note that the solution approaches the steady-state $m_\infty(V)$ at a rate determined by the time-constant $\tau(V)$.

One must obtain expressions for the voltage-dependent rate constants α and β. In the Hodgkin-Huxley model, these functions were derived by fitting the data. Borg-Graham and others have suggested a simple formulation based on thermodynamics. The idea is that the probability of opening or closing a channel depends exponentially on the potential. Thus,

$$\alpha(V) = A_\alpha \exp(-B_\alpha V) \quad \text{and} \quad \beta(V) = A_\beta \exp(-B_\beta V). \tag{2.36}$$

From this, we find that

$$m_\infty(V) = \frac{1}{1+\exp(-(V-V_h)/V_s)}$$

where V_h, V_s are constants. We leave as an exercise the calculation of these constants in terms of the constants A and B. The time constant, $\tau(V)$ will generally be a skewed bell-shaped function of V. If $B_\beta = -B_\alpha$, then $\tau(V)$ is a hyperbolic secant.

2.10 Hodgkin-Huxley model

We are now ready to derive the Hodgkin-Huxley model for the propagation of an action potential along the squid's giant axon. As in Section 2.7, we view the axon as a cylinder of fixed radius, a, so the membrane potential depends on the spatial

variable x and time t. Here we assume that there are voltage-gated K^+ and Na^+ channels and a leak current. Then balancing currents, as in (2.23), we have

$$I_L = I_{cap} + I_{ion} \tag{2.37}$$

or, using (2.6) and (2.24),

$$\frac{a}{2r_L}\frac{\partial^2 V_M}{\partial x^2} = c_M \frac{\partial V_M}{\partial t} + I_K + I_{Na} + I_L. \tag{2.38}$$

If each ionic current is Ohmic, then this can be written as

$$c_M \frac{\partial V_M}{\partial t} = \frac{a}{2r_L}\frac{\partial^2 V_M}{\partial x^2} - g_K(V_M - E_K) - g_{Na}(V_M - E_{Na}) - g_L(V_M - E_L). \tag{2.39}$$

To complete the model, we need to describe how one computes the membrane conductances g_K, g_{Na} and g_L. Note that the voltage-gated conductances g_K and g_{Na} change with time during an action potential.

Hodgkin and Huxley used two experimental methods in order to separate the ionic currents and compute how the K^+ and Na^+ conductances depend on voltage. The first was a simple feedback circuit called the *voltage-clamp* that allows the experimenter to hold the membrane potential at a constant or holding level V_C. The voltage clamp does so by injecting a current into the axon that is equal and opposite to the current flowing through the voltage-gated channels. Electrical details can be found in Johnston and Wu. Note that the voltage-clamp separates the total membrane current into its ionic and capacitive components. Recall that the capacitive current satisfies $I_{cap} = C_M dV_M/dt$. If the membrane potential is fixed at some constant, then the capacitive current must be zero. Moreover, the total current can be made spatially uniform by inserting a highly conductive axial wire inside the fiber; the axon is then said to be *space-clamped*. In this case, $\frac{\partial^2 V_M}{\partial x^2} = 0$. It then follows that any changes in current must be due either to the leak or to the opening and closing of voltage-gated membrane channels.

We first consider how the voltage-clamp can be used to determine the leak-conductance, g_L. Note that most of the voltage-gated channels are closed at rest. Moreover, if we hyperpolarize the cell, then we may assume that all of the voltage-gated channels are closed. It follows that if the membrane potential is clamped at some sufficiently strong hyperpolarized level, then the total current is given by the leak; that is,

$$I_M \approx g_L(V_C - E_L).$$

From this equation, we can easily solve for g_L.

Figure 2.8 shows the results of a voltage-clamp experiment when the membrane potential is clamped at 0 mV. Note that there is an inward current followed by an outward current. This result suggests that the depolarizing voltage step turns on two voltage-gated channels. The inward current is due to the influx of Na^+ ions, while the outward current is due to the outward flow of K^+ ions. It is not clear, however, how these two separate ions contribute to the total membrane current. For this it is necessary to isolate the two voltage-gated currents.

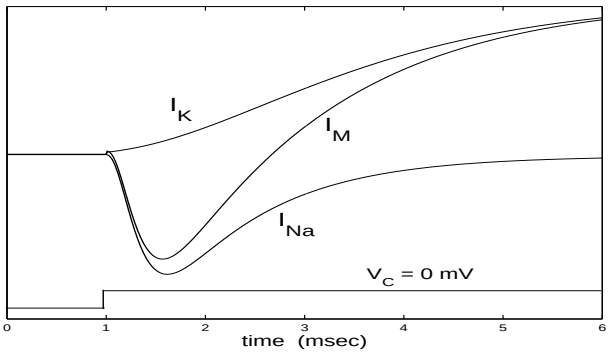

Figure 2.8. *Numerically computed voltage-clamp experiment. The membrane potential is stepped from rest to 0 mV. This results in an inward current followed by an outward current. The separate potassium and sodium currents are also shown.*

Hodgkin and Huxley were able to isolate the K^+ current by replacing Na^+ ions in the external bathing solution with a larger, impermeant cation. This eliminated the inward Na^+ current. Now there are dozens of compounds that selectively block different currents, many derived from natural toxins. (For example, the compound tetrodotoxin, which blocks sodium channels, comes from the Pacific pufferfish, a tasty, if slightly dangerous, Japanese delicacy called fugu.) Once Na^+ is removed, the voltage-clamp can be used to determine how I_K depends on the membrane potential. That is, one holds the membrane potential at various levels and determines the time-course of the total membrane current I_M. If Na^+ is removed, then the potassium current is computed by subtracting the leak current from I_M.

It is also now possible to block K^+ channels using the drug tetraethylammonium. However, this was not available to Hodgkin and Huxley. However, if I_K and I_L are known, then one computes I_{Na} simply by subtracting I_K and I_L from I_M. Once these currents are determined, we can calculate the I_K and I_{Na} conductances using Ohm's law. That is,

$$g_K(t) = \frac{I_K(t)}{(V_M - E_K)} \quad \text{and} \quad g_{Na}(t) = \frac{I_{Na}(t)}{(V_M - E_{Na})}. \tag{2.40}$$

Figure 2.9 shows the I_K and I_{Na} conductances for different levels of the holding potential. Note than g_{Na} turns on more rapidly that g_K. Moreover, the Na^+ channels begin to close before the depolarization is turned off, while the K^+ channels remain open as long as the membrane is depolarized. This suggests that the Na^+ channel can exist in three states: resting, activated and inactivated. When the cell is depolarized, the Na^+ channels switch from the resting (closed) to the activated (open) state. If the depolarization is maintained, then the channel switches to the inactivated (closed) state.

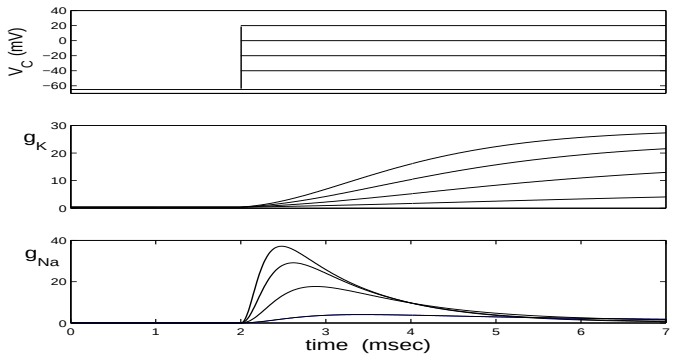

Figure 2.9. *Numerically computed voltage-clamp experiment. The membrane potential is stepped to different values and the resulting potassium and sodium conductances are computed.*

A physical interpretation of the Na^+ channel is shown in Figure 2.10. There are two gates in the sodium channel: a fast one (the activation gate) represented by the line and a slow one (the inactivation gate) represented by the ball. Both gates must be open for the channel to conduct Na^+ ions. At rest, the activation gate is closed and the inactivation gate is open. When the membrane is depolarized, the activation gate opens which allows sodium into the cell. The inactivation gate (ball) closes at the higher potential so that the flow of sodium is transient. Hodgkin and Huxley used a more complicated voltage clamp protocol, first stepping to a fixed voltage and then apply brief voltage steps to probe the fast activation and slow inactivation gates. Details can be found in Kandel/Schwartz/Jessell.

Using the voltage-clamp data, Hodgkin and Huxley derived expressions for the K^+ and Na^+ conductances. They proposed that

$$g_K = \bar{g}_K n^4 \quad \text{and} \quad g_{Na} = \bar{g}_{Na} m^3 h \tag{2.41}$$

where $\bar{g}_K$ and $\bar{g}_{Na}$ are maximum conductances and n, m and h are gating variables that take values between 0 and 1. Hence, n^4 represents the probability that a potassium channel is open: the potassium channel has 4 independent components each of which are identical. The probability that the sodium activation gate is open is m^3 and the probability that the sodium inactivation gate is open is $1 - h$. Each of the gating variables satisfies a first order differential equation of the form (2.34). That is, they satisfy equations of the form:

$$\begin{aligned}
\frac{dn}{dt} &= \alpha_n(V)(1-n) - \beta_n(V)n \;=\; (n_\infty(V) - n)/\tau_n(V) \\
\frac{dm}{dt} &= \alpha_m(V)(1-m) - \beta_m(V)m \;=\; (m_\infty(V) - m)/\tau_m(V) \\
\frac{dh}{dt} &= \alpha_h(V)(1-h) - \beta_h(V)h \;=\; (h_\infty(V) - h)/\tau_h(V).
\end{aligned}$$

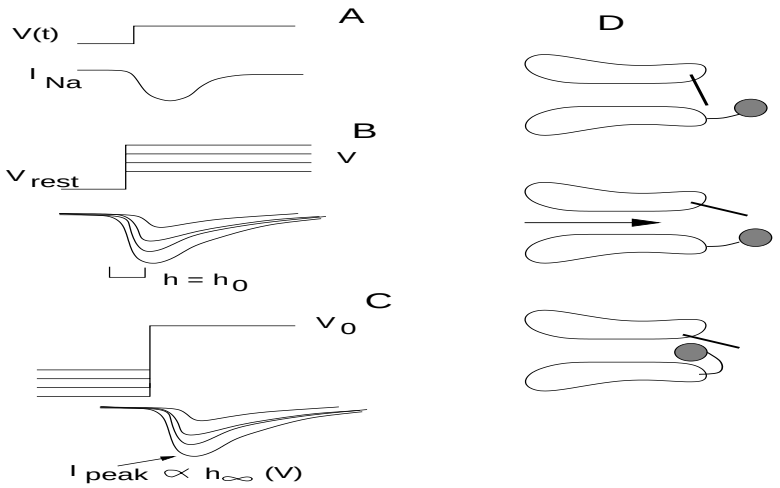

Figure 2.10. *The Hodgkin-Huxley sodium channel. (A-C) Voltage clamp dynamics. (D) Physical model of the channel. If the voltage step is small (A), then the Na-channel's activation gate (line) is closed but the inactivation gate (ball) is open. At intermediate steps (B), both gates are partially open. For large steps (C), the activation gate is open and the inactivation gate is closed.*

If $X = n, m$ or h, then

$$X_\infty(V) = \frac{\alpha_X(V)}{\alpha_X(V) + \beta_X(V)} \quad \text{and} \quad \tau_X(V) = \frac{1}{\alpha_X(V) + \beta_X(V)}. \tag{2.42}$$

To match the data, Hodgkin and Huxley chose the following parameters and gating functions: $\bar{g}_{Na} = 120$ mS/cm^3, $\bar{g}_K = 36$ mS/cm^3, $\bar{g}_L = 0.3$ mS/cm^3, $E_{Na} = 50$ mV, $E_K =$ -77 mV, $E_L =$ -54.4 mV,

$$\begin{aligned}
\alpha_n(V) &= 0.01(V+55)/(1-\exp(-(V+55)/10)) \\
\beta_n(V) &= 0.125\exp(-(V+65)/80) \\
\alpha_m(V) &= 0.1(V+40)/(1-\exp(-(V+40)/10)) \\
\beta_m(V) &= 4\exp(-(V+65)/18) \\
\alpha_h(V) &= 0.07\exp(-(V+65)/20) \\
\beta_h(V) &= 1/(1+\exp(-(V+35)/10)).
\end{aligned}$$

In Figure 2.11, we plot the *activation curves* $n_\infty(V), m_\infty(V)$ and $h_\infty(V)$ along with $\tau_n(V), \tau_m(V)$ and $\tau_h(V)$. Note that n_∞ and m_∞ are increasing functions that approach 0 for hyperpolarizing currents and approach 1 for depolarizing currents. Hence, n and m become activated when the membrane is depolarized. On the other hand, $h_\infty(V)$ is a decreasing function so the sodium channels inactivate when the membrane is depolarized. It is also important to note that $\tau_m(V)$ is considerably

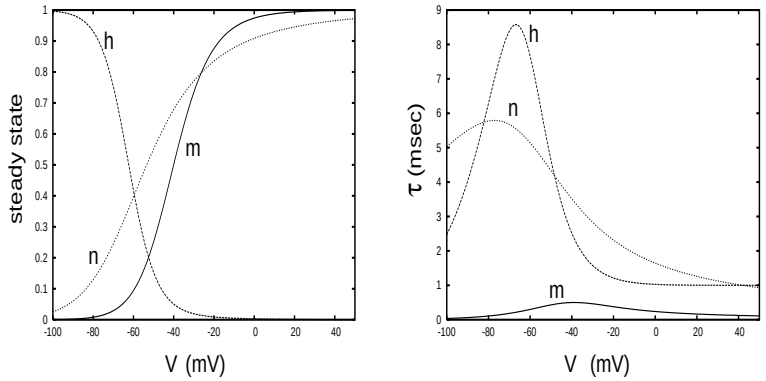

Figure 2.11. *HH functions. Left shows the steady state opening of the gates and right shows the time constants.*

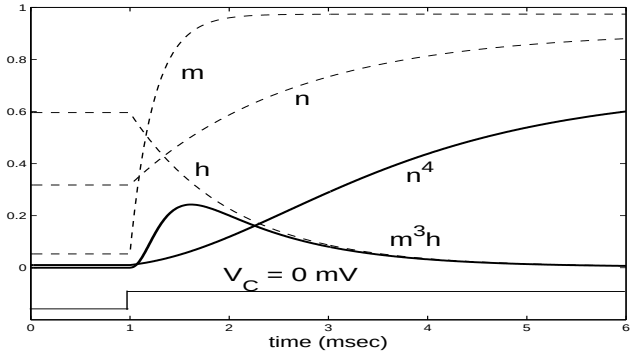

Figure 2.12. *Response of the activation and inactivation variables* $m, h,$ and n *to a step in voltage.*

smaller than τ_n or τ_h. Hence, sodium channels activate much faster than they inactivate or potassium channels open. In Figure 2.12, we show the response of $m, h,$ and n to a step in voltage.

2.11 The action potential revisited

In summary, the Hodgkin-Huxley model is a system of four differential equations; there is one equation for the membrane potential and three equations for channel gating variables. In the case of a spaced-clamped squid axon, we write these

equations as:

$$\begin{aligned} c_M \frac{dV}{dt} &= -\bar{g}_{Na} m^3 h (V - E_{Na}) - \bar{g}_K n^4 (V - E_K) - \bar{g}_L (V - E_L) \\ \frac{dn}{dt} &= \phi[\alpha_n(V)(1-n) - \beta_n(V) n] \\ \frac{dm}{dt} &= \phi[\alpha_m(V)(1-m) - \beta_m(V) m] \\ \frac{dh}{dt} &= \phi[\alpha_h(V)(1-h) - \beta_h(V) h] \end{aligned} \tag{2.43}$$

Here we added a parameter ϕ; this is the *temperature factor.* It is important to realize that the temperature at which an experiment is done can be very important. Since channels are stochastic in nature, they are sensitive to the temperature so that the rates of switching states depend exponentially on the temperature. Higher temperatures cause faster switching. Thus, there is a factor:

$$\phi = Q_{10}^{(T - T_{base})/10}. \tag{2.44}$$

Q_{10} is the ratio of the rates for an increase in temperature by 10° C. For the squid, $T_{base} = 6.3°$ C and $Q_{10} = 3$.

Figure 2.13 shows solutions of these equations in response to different levels of steps in currents. Note that there is "all-or-none" behavior: When the applied current is below some threshold, the membrane potential returns quickly to rest; when the current is above some threshold, there is an action potential. If the applied current is sufficiently large and held for a sufficiently long time, then the model generates a periodic response.

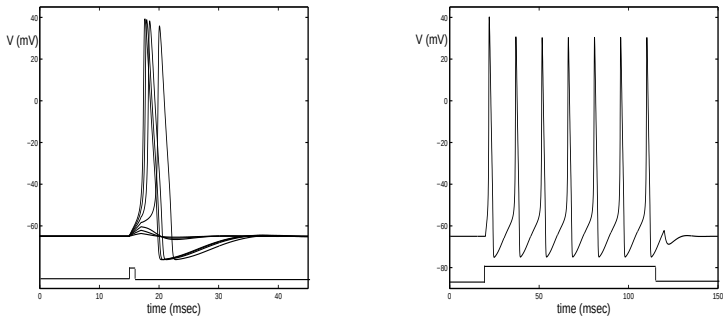

Figure 2.13. *Responses of the HH model to applied currents. Left: transient responses showing "all-or-none" behavior; Right: Sustained periodic response.*

Figure 2.14 shows of an action potential along with plots of the Na^+ and K^+ conductances, g_{Na} and g_K. Here, we start with the cell at rest and then depolarize the cell by 10 mV at $t = 0$. The cell then generates a single action potential. In Section 2.8, we described the events underlying the action potential in terms of

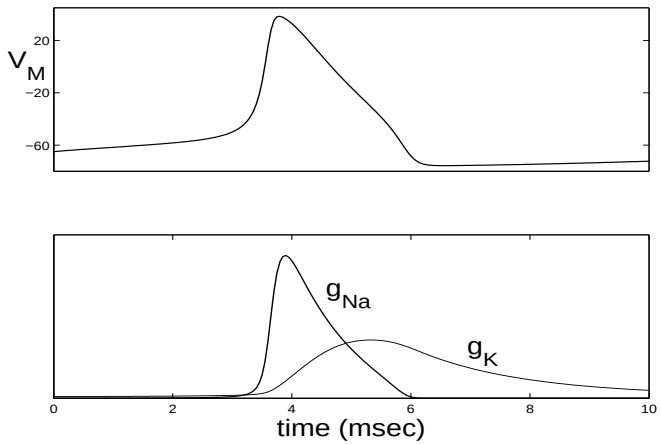

Figure 2.14. *Solution of the Hodgkin-Huxley equations showing an action potential. Also shown are the sodium and potassium conductances.*

the inward and outward flow of sodium and potassium ions. Here we give a more "mathematical" explanation in terms of the behavior of the dependent variables in the differential equations.

When we depolarize the cell, we change the values of the activation curves: $n_\infty(V)$ and $m_\infty(V)$ increase, while $h_\infty(V)$ decreases. Since n, m and h tend towards their activation curves, it follows that n and m initially increase, while h decreases. That is, potassium channels open, while sodium channels both activate and inactivate. However, τ_m is much smaller than both τ_h and τ_n. It follows that the Na^+ channels activate much faster than they inactivate or K^+ channels open. Therefore, the Na^+ conductance, $g_{Na} = \bar{g}_{Na} m^3 h$, increases faster than $g_K = \bar{g} n^4$.

The increase in the Na^+ conductance leads to a large increase in the Na^+ current, $I_{Na} = g_{Na}(V - E_{Na})$. As long as the cell is near rest, the driving force $V - E_{Na}$ is large (recall that $E_{Na} \approx +55mV$). Hence, the sodium current will dominate the equation for the membrane potential and V will increase towards the Na^+ Nernst potential. As V increases, $m_\infty(V)$ increases further, leading to further increase in Na^+ activation.

As V increases towards E_{Na}, sodium channels inactivate. This is because $h \to h_\infty(V) \approx 0$. Moreover, the sodium driving force $V - E_{Na}$ decreases. For both reasons, the Na^+ current turns off. Meanwhile, the potassium channel activates because $n \to n_\infty(V) \approx 1$. Moreover, the K^+ driving force $V - E_K$ becomes very large. It follows that eventually, the potassium current dominates and the membrane potential must fall back towards the K^+ Nernst potential. This corresponds to the down-stroke of the action potential.

After the action potential, the cell is hyperpolarized with $m_\infty \approx 0, n_\infty \approx 0$ and $h_\infty \approx 1$. After some time, m, n and h approach their steady state values and

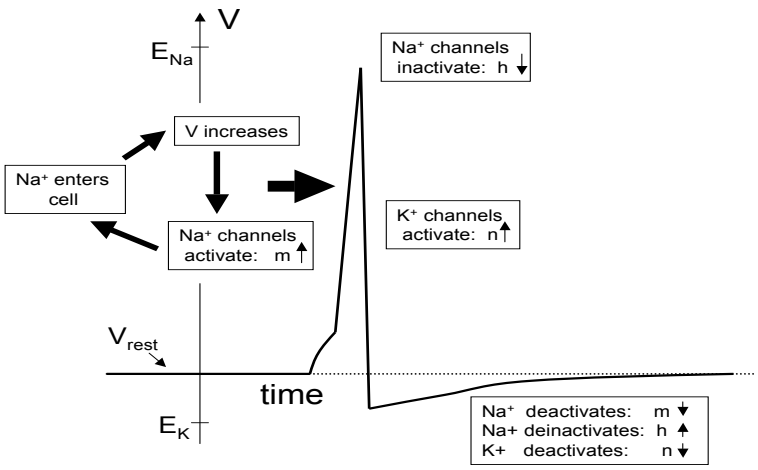

Figure 2.15. *Mechanisms underlying the action potential.*

the cell returns to rest.

2.12 Bibliography

There are many standard neuroscience textbooks that present the biological aspects covered in this chapter in much more detail. These textbooks include Kandel, Schwartz and Jessell [28], Hille [22] and Martin [36]. The reader is also highly recommended to look at Hodgkin and Huxley's original papers [1]. A review of these papers, along with a short history leading up to them, is given in Rinzel [42]. Excellent textbooks, which emphasize modeling and quantitative approaches, are Johnston and Wu [**?**], Koch [30], Jack et. al.[25], Izhikevich izhikevichbook, and Dayan and Abbott [10]. Keener and Sneyd [29] and Fall et. al. [14] give detailed introductions to mathematical aspects of cellular biophysics.

2.13 Exercises

1. Consider a passive, spherical cell with radius .003cm^2, a resting membrane potential of $-65mV$, a membrane capacitance of 1μF/cm^2 and a membrane resistance of $R_m = 700\Omega$cm^2. Suppose that the cell is injected with an applied current of $5nA/\mu m^2$ for two seconds and then turned off. What is the membrane potential at $t = 1, t = 2$ and $t = 3$?

2. Suppose that a passive axon has a diameter of half a millimeter, a resting membrane resistance of $R_m = 700\Omega$cm^2, and a transmembrane resistance of $R_i = 30\Omega$cm. Compute the space constant. If the axon is 5 centimeters long and one end of the axon is held at 120 mV above rest, then what is the

potential at the other end?

3. (Johnston and Wu, page 12) The membrane capacitance of a typical cell is 1 μF/cm^2 and the concentration of ions inside and outside of the cell is about .5 M. Calculate the fraction of uncompensated ions on each side of the membrane required to produce 100 mV in a spherical cell with a radius of 25 μm.

4. Numerically solve the Hodgkin-Huxley equations. Start the system at rest and, at some later time, inject an applied current to generate an action potential. Plot the time courses of the sodium and potassium conductances.

5. Numerically perform space-clamp experiments. That is, start the Hodgkin-Huxley model at rest and, at some later time, change the membrane potential and keep it as some "clamped" level. Plot the sodium and potassium conductances for when the membrane potential is stepped to different values.

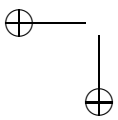

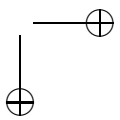

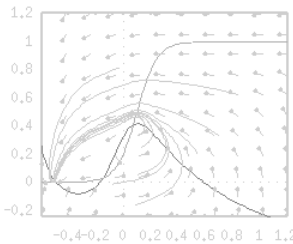

Chapter 3

Dendrites

In this chapter, we will derive mathematical theories for describing dendrites. Dendrites are very important for many reasons. Indeed, the majority of the total membrane area of many neurons is occupied by the dendritic tree. Dendrites enable neurons to connect to thousands of other cells, far more than would be possible with just a soma, as there is a huge membrane area to make connections. Dendrites may direct many subthreshold postsynaptic potentials (PSPs) towards the soma, which summates these inputs and determines if the neuron will fire an action potential. In addition to the tree-like structure of dendrites, many dendrites have additional fine structures at the ends of the branches called **spines**. During development, animals that are raised in rich sensory environments have more extensive dendritic tress and more spines.

3.1 Multiple compartments

A very useful way to treat complicated dendritic structures is the compartimental approach. Here one divides the dendritic tree into small segments or compartments that are all linked together. Examples are shown in Figure ??. Each compartment is assumed to be isopotential and spatially uniform in its properties. Differences in voltage and nonuniformity in membrane properties, including diameter, occur between compartments rather than within them.

As a simple example, consider the two-compartment model shown in Figure ??. An equivalent circuit for this model is shown in Figure ??. Each compartment is viewed as an isopotential cylinder with radius a_i and length L_i. Let V_i be the membrane potential of the i^{th} compartment and let c_i and r_{Mi} be the corresponding specific membrane capacitance and specific membrane resistivity, respectively. We assume that each compartment has an electrode current and the total electrode current is given by $I^i_{electrode}$. Finally, we assume that the intracellular, or longitudinal, resistivity is given by r_L.

Now the capacitive and ionic currents for each compartment must be balanced

by the longitudinal and electrode currents. That is,

$$i^i_{cap} + i^i_{ion} = i^i_{long} + i^i_{electrode} \tag{3.1}$$

where i^i_{cap} and i^i_{ion} are the capacitve and ionic currents per unit area of membrane for compartment i. As before,

$$i^i_{cap} = c_i \frac{dV_i}{dt} \quad \text{and} \quad i^i_{ion} = \frac{V_i}{r_{Mi}} \tag{3.2}$$

if we assume that the resting potential is 0. In order to compute i^i_{long}, we need to determine total axial resistance. Note that the total resistance between the centers of the two comparments is simply the sum of the two resistances of the half-cylinders that separate the compartment centers. That is the total resistance is given by:

$$R_{long} = \frac{r_L L_1}{2\pi a_1^2} + \frac{r_L L_2}{2\pi a_2^2} \tag{3.3}$$

Using Ohm's law, we can write the expressions for the current from comparments i to compartment j as

$$i^1_{long} = g_{1,2}(V_2 - V_1) \quad \text{and} \quad i^2_{long} = g_{2,1}(V_1 - V_2). \tag{3.4}$$

The coupling terms $g_{1,2}$ and $g_{2,1}$ are obtained by inverting (3.3) and dividing by the surface area of the compartment of interest. That is,

$$g_{1,2} = \frac{a_1 a_2^2}{r_L L_1 (a_2^2 L_1 + a_1^2 L_2}$$

and

$$g_{2,1} = \frac{a_2 a_1^2}{r_L L_1 (a_2^2 L_1 + a_1^2 L_2}.$$

Finally, to compute $i^i_{electrode}$, we divide the total electrode currents by the surface areas of the compartments. That is,

$$i^i_{electrode} = \frac{I^i_{electrode}}{A_i}$$

where $A_i = 2\pi a_i L_i$ is the surface area of compartment i.

Putting this all together, we find that the equations for two connected cylinders are:

$$\begin{aligned} c_1 \frac{dV_1}{dt} + \frac{V_1}{r_{m1}} &= g_{1,2}(V_2 - V_1) + \frac{I^1_{electrode}}{A_1} \\ c_2 \frac{dV_2}{dt} + \frac{V_2}{r_{m2}} &= g_{2,1}(V_1 - V_2) + \frac{I^2_{electrode}}{A_2} \end{aligned} \tag{3.5}$$

If instead of using conductances, $g_{i,j}$, we use $r_1 = 1/g_{1,2}$ and $r_2 = 1/g_{2,1}$ then we can express this system as:

$$\begin{aligned} c_1 \frac{dV_1}{dt} + \frac{V_1}{r_{m1}} &= \frac{V_2 - V_1}{r_1} + i_1 \\ c_2 \frac{dV_2}{dt} + \frac{V_2}{r_{m2}} &= \frac{V_1 - V_2}{r_2} + i_2 \end{aligned} \tag{3.6}$$

where $i_i = I^i_{electrode}/A_i$.

We can now explore the effects of two compartments on the input resistance of the "cell." Suppose that we inject current into cell 1 only. Moreover, each cylinder is identical with the same length and radius. Then $r_1 = r_2 \equiv r$. What is the input resistance due to the coupling? To solve this, we must compute the steady state potential due to the coupling. Without loss in generality, define $r_M = r_{M1} = r_{M2}$. A simple bit of algebra shows that

$$V_1/i_1 = \frac{r_M(r + r_M)}{r + 2r_M}$$

and thus the ratio of the coupled to the uncoupled input resistance is:

$$\frac{R_{input,coupled}}{R_{input,uncoupled}} = 1 - \frac{r_M}{r + 2r_m};$$

that is, the input resistance decreases. To get the same increment in potential the current required for the coupled system is more than the uncoupled system because some current is drained away by the second compartment.

In a similar way, we can derive a compartmental model for a general tree-like structure. A general algorithm for computing the correct equations is:

- For each cylinder, j, with radius and length a_j and L_j in microns, compute surface area, $A_j = 2\pi a_j L_j$ and the axial resistance factor: $Q_j = \frac{L_j}{\pi a_j^2}$.
- The membrane capacitance is $C_j = c_j A_j \times 10^{-8}$ and the membrane resistance is $R_j = (r_{mj}/A_j) \times 10^8$.
- The coupling resistance between compartment j and k is $R_{jk} = \frac{r_L}{2}(Q_j + Q_k) \times 10^4$.
- The equations are then

$$C_j \frac{dV_j}{dt} = -\frac{V_j}{R_j} + \sum_{k \text{ connected } j} \frac{V_k - V_j}{R_{jk}} + I_j.$$

The factors of $10^{\pm 8}$ and 10^4 are the conversion from microns to centimeters. For example, consider a two compartment model with (i) compartment 1 having a length of 200μ and radius of 30μ and (ii) compartment 2 having a length of 20μ and radius of 20μ. Then, $R_1 = 2.65 \times 10^7\Omega$, $C_1 = 3.77 \times 10^{-10}F$,$R_2 = 3.98 \times 10^8\Omega$, $C_2 = 2.52 \times 10^{-11}F$, and $R_{long} = 4.34 \times 10^4\Omega$, thus

$$10\frac{dV_1}{dt} = -V_1 + 611(V_2 - V_1), \quad 10\frac{dV_2}{dt} = -V_2 + 9181(V_2 - V_1)$$

where the time is in milliseconds and the coupling coefficients are dimensionless. Note how the ratio of the coupling strengths is the same as the reciprocal of the area ratios. The bigger compartment has a much greater effect on the smaller compartment than vice versa.

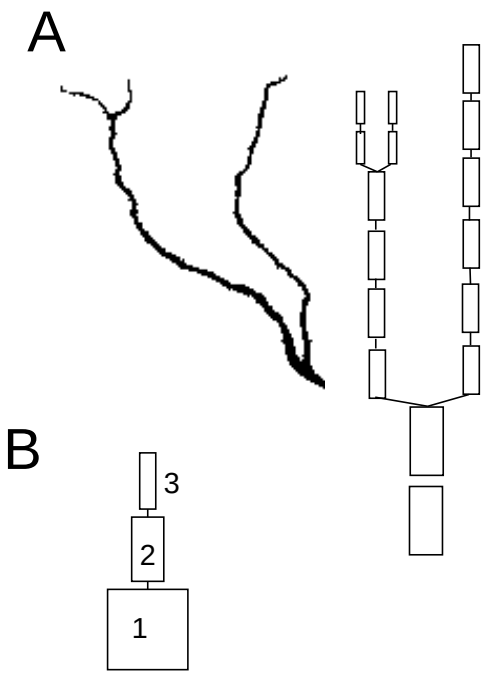

Figure 3.1. *A. Branched dendrite converted to a series of cylinders for modeling. B. Simple 3 compartment model.*

We also would like to remark that the standard units used in most compartmental models are $\mu F/cm^2$, mS/cm^2, and $\mu A/cm^2$ for the capacitance, conductance, and applied current. Experimentalists don't generally know the current density but only the total current injected. Typical currents injected into a cell are of the order of less than a nanoampere.

To generate arbitrary compartmental models, one needs only to compute the length, diameter, and the connectivity of the cylinders that make up the dendritic tree. The software NEURON enables an experimentalist to input a digitized picture of a neuron and the program will automatically produce a compartmental model of the neuron by linking together many cylinders.

3.1.1 Homework

1. Derive the differential equations for the three compartment model shown in figure 3.1 B, where you can take $R_{m,s} = 10000\Omega - cm^2$, $C_{m,s} = 1\mu F/cm^2$, and $R_{long,s} = 100\Omega - cm$. The compartments have dimensions, $(\ell_j, \rho_j) = (50, 25), (100, 15), (80, 10)$ respectively. Compute the input resistance for a current applied to compartments 1 and 3 (the "soma" and the "distal dendrite.")

2. Consider 3 identical compartments coupled in a chain by the same coupling resistance:

$$C\frac{dV_1}{dt} = -\frac{V_1}{R} + (V_2 - V_1)/R_{couple} + I$$
$$C\frac{dV_2}{dt} = -\frac{V_2}{R} + (V_3 - 2V_2 + V_1)/R_{couple}$$
$$C\frac{dV_3}{dt} = -\frac{V_3}{R} + (V_2 - V_3)/R_{couple}.$$

Compute the input resistance. What do you think happens with more and more compartments?

3. Consider an semi-infinite array of compartments with only the first one receiving injected current. Can you prove that

$$V_1/I_1 = \frac{R}{1 + \frac{R}{R_{couple}}(1-\mu)}$$

where

$$\mu = 1 + z - \sqrt{z^2 + 2z}, \quad z = \frac{R}{2R_{couple}}.$$

(Here is a hint. Show that the steady state voltages satisfy:

$$V_{j+1} - 2(1+z)V_j + V_{j-1} = 0$$

except for $j = 1$. The general solution to this difference equation is just $V_j = A\mu_1^j + B\mu_2^j$ where $\mu_{1,2}$ are roots to $\mu^2 - 2(1+z)\mu + 1 = 0$. One of these roots, say, μ_2, is greater than 1 so that as $j \to \infty$ you better choose $B = 0$. Choose A so that the correct equation for V_1 holds:

$$0 = -\frac{V_1}{R} + \frac{V_2 - V_1}{R_{couple}} + I.$$

)

4. Consider a general N-compartment model for a passive neuron with current injected into some or all of the compartments. This will obey the following differential equations:

$$C_j\frac{dV_j}{dt} = I_j + \sum_k g_{jk}(V_k - V_j) - g_{L,j}(V_j - V_{leak})$$

Suppose that $g_{jk} \geq 0$, $C_j > 0$, $g_{L,j} > 0$. Prove that there is a unique equilibrium point to this and that it is asymptotically stable. (Hint: This is a diagonally dominant system.)

5. Consider the infinite linear array of cells:

$$\tau \frac{dV_1}{dt} = V_0 - V_1 + \beta(V_2 - V_1)$$
$$\tau \frac{dV_j}{dt} = -V_j + \beta(V_{j+1} - 2V_j + V_{j-1})$$

Find the steady state solution to this. (Hint: The second group of equations has the form $V_{j+1} = V_j(2 + 1/\beta) - V_{j-1}$ which is a finite difference equation. The general solution to such equations is $V_j = C_1 r_1^j + C_2 r_2^j$.)

6. Consider a single compartment model with a sinusoidal current:

$$C\frac{dV}{dt} = -g_L(V - V_{leak}) + I_0 \sin \omega t.$$

Find the steady state solution to this equation.

7. Consider the single compartment model:

$$C\frac{dV}{dt} = I - g_L(V - V_{leak}) - g(t)(V - V_{syn})$$

where $g(t) = 0$ except when $t \in [t_1, t_2]$ where it is $\bar{g}$. Solve this equation assuming the cell starts from rest. For what values of V_{syn} does $V(t)$ increase above rest?

3.2 The cable equation.

Mathematically, dendrites and axons are regarded as continuous media rather than a series of compartments. Previously, we derived the cable equation for a simple cable in which the radius along the cable was assumed to be constant. Here we derive the cable equation for more general geometries. This is done by considering the limit as the number of compartments in an approximation of it tends to infinity.

Suppose the cable is defined on the interval $(0, \ell)$ with a circular cross-section and diameter $d(x)$. We break the cable into n pieces and define $x_j = jh$ where $h = \ell/n$. Each piece has a surface area $A_j = \pi d_j h$ where $d_j = d(x_j)$, and crossectional area, $\pi d_j^2/4$. Let c_M and r_M denote the specific membrane capacitance and resistance, and let r_L be the longitudinal resistance. Then, neglecting the end points, the voltage satisfies:

$$c_M A_j \frac{dV_j}{dt} = -\frac{V_j}{r_M/A_j} + \frac{V_{j+1} - V_j}{4r_L h/(\pi d_{j+1}^2)} + \frac{V_{j-1} - V_j}{4r_L h/(\pi d_j^2)}$$

Note that we use the larger diameter for the transmembrane resistance; in simulations, the average of the two would be preferred. Dividing by πh the coupling term simplifies to:

$$\frac{1}{h}\left(\frac{d_{j+1}^2(V_{j+1} - V_j)}{4r_L h} - \frac{d_j^2(V_j - V_{j-1})}{4r_L h}\right).$$

As $h \to 0$, this goes to the diffusion operator:

$$\frac{1}{4r_L}\frac{\partial}{\partial x}\left(d^2(x)\frac{\partial V}{\partial x}\right).$$

Thus, the cable equation has the form:

$$c_m\frac{\partial V}{\partial t} = -\frac{V}{r_M} + \frac{1}{4r_L}\frac{\partial}{\partial x}\left(d^2(x)\frac{\partial V}{\partial x}\right). \tag{3.7}$$

We remark that the term

$$\frac{d_j^2(V_{j-1} - V_j)}{4r_L h}$$

has dimensions of current and in the limit as $h \to 0$ is called the *longitudinal current*:

$$I_L = -\frac{\pi d^2(x)}{4r_L}\frac{\partial V}{\partial x}. \tag{3.8}$$

If one is interested only in the passive cable and $d(x) = d$ is constant, then it is convenient to multiply both sides by r_M and divide by d obtaining the linear cable equation:

$$\tau\frac{\partial V}{\partial t} = -V + \lambda^2\frac{\partial^2 V}{\partial x^2} \tag{3.9}$$

where

$$\lambda = \sqrt{\frac{dr_M}{4r_L}} \tag{3.10}$$

is the space constant. Since λ depends on the diameter of the cable, this parameter depends on the geometry of the cable. The quantity, $\tau = r_M c_M$ is the time constant and is independent of geometry. For example, if $c_M = 1\mu F/cm^2$, $r_M = 20000\Omega cm^2$, $r_L = 100\Omega cm$ and the diameter of the cable is 2 microns, then $\tau = 20$ msec and $\lambda = 1$ mm.

3.3 Linear cables with constant diameter.

3.3.1 The infinite cable

We first consider the infinite cable, so that $-\infty < x < \infty$, with some applied current:

$$\tau\frac{\partial V}{\partial t} + V(x,t) - \lambda^2\frac{\partial^2 V}{\partial x^2} = r_M I(x,t). \tag{3.11}$$

The current, $I(x,t)$ has units of $\mu A/cm^2$. Additionally, we also must provide an initial voltage distribution, $V(x,0) = V_0(x)$. We will solve this using Fourier transforms and then write the solution in terms of something called a *Green's function.* Let

$$\hat{V}(k,t) = \int_{-\infty}^{\infty} e^{-ikx}V(x,t)\,dx$$

$$\hat{V}_0(k) = \int_{-\infty}^{\infty} e^{-ikx} V_0(x)\ dx$$
$$\hat{I}(k,t) = \int_{-\infty}^{\infty} e^{-ikx} I(x,t)\ dx$$

denote the Fourier transforms of V, V_0, and I. Then $\hat{V}$ satisfies the differential equation

$$\frac{d\hat{V}}{dt} + (1+\lambda^2 k^2)\hat{V}/\tau = r_M \hat{I}/\tau$$
$$\hat{V}(0) = \hat{V}_0$$

where we have dropped the k dependence for simplicity. This is a linear first order ODE so we can write the solution:

$$\hat{V}(k,t) = e^{-(1+\lambda^2 k^2)t/\tau}\hat{V}_0(k) + (r_M/\tau)\int_0^t e^{-(1+\lambda^2 k^2)(t-s)}\hat{I}(k,s)\ ds.$$

Recalling that the inverse Fourier transform is

$$V(x,t) = \frac{1}{2\pi}\int_{-\infty}^{\infty} e^{ikx}\hat{V}(k,t)\ dk$$

we find that $V(x,t)$ is given by

$$V(x,t) = \int_{-\infty}^{\infty} G(x-y,t)V_0(y)\ dy + \frac{r_M}{\tau}\int_0^t \int_{-\infty}^{\infty} G(x-y,t-s)I(y,s)\ dy\ ds$$

where

$$G(x,t) = \frac{1}{\sqrt{4\pi\lambda^2 t/\tau}} e^{-t/\tau} e^{-x^2/(\lambda^2 t/\tau)}. \tag{3.12}$$

Note that $G(x,t)$ has dimensions of λ^{-1}.

Suppose that $V_0(x) = 0$ (that is, the membrane is at rest) and at $t = 0$, the membrane is perturbed by a delta function in space and time. That is, $I(x,t) = I_0\delta(x)\delta(t)$. Then

$$V(x,t) = \frac{r_M I_0}{\tau\lambda\sqrt{4\pi t/\tau}} \exp\left(-\frac{\tau x^2}{4\lambda^2 t}\right)\exp\left(-\frac{t}{\tau}\right). \tag{3.13}$$

In the exercises below, you are asked to analyze this. One interesting point is that at each spatial location x, the function $V(x,t)$ reaches its maximum at a value $t^*(x)$. You can obtain this expression using calculus and show that for x large, $t^*(x) \approx \tau x/2\lambda$, that is, the voltage is a rapidly decaying "wave".

For another example, consider an infinite cable with a step of constant applied current at a single point: $I(x,t) = I_0\delta(x)$. Plugging this into (3.12), we find that

$$V(x,t) = \frac{r_M I_0 \lambda}{4}\left[e^{-(x/\lambda)}\mathrm{erfc}\left(\frac{x\sqrt{\tau}}{2\lambda\sqrt{t}} - \sqrt{t/\tau}\right) - e^{(x/\lambda)}\mathrm{erfc}\left(\frac{x\sqrt{\tau}}{2\lambda\sqrt{t}} + \sqrt{t/\tau}\right)\right]$$

where

$$\operatorname{erfc}(x) = \frac{2}{\sqrt{\pi}} \int_x^\infty e^{-y^2} dy. \tag{3.14}$$

Note that $\operatorname{erfc}(0) = 1$, $\operatorname{erfc}(\infty) = 0$ and $\operatorname{erfc}(-\infty) = 2$. If we let $t \to \infty$ in (3.14) then $V(x,t)$ approaches the steady state solution

$$V_{ss}(x) = \frac{r_M I_0}{2\lambda} e^{-|x|/\lambda}.$$

Often a cable is described in terms of its *electrotonic length* which is $L = \ell/\lambda$, where ℓ is the physical length and λ is the space constant.

3.4 Finite and semi-infinite cables.

For the infinite cable, the only physically reasonable boundary condition is that $V(x) \to 0$ as $|x| \to \infty$. However, for the finite and semi-infinite cables there are several interesting boundary conditions that are often used:

- *sealed end* where no current can pass and so the longitudinal current $I_L = 0$. It then follows from (3.8) that $\frac{\partial V}{\partial x}(0) = 0$.
- *current injected at one end* where a current of magnitude $I(t)$ is injected at, say, the end $x = 0$. In this case, $\frac{\partial V}{\partial x}(0) = \frac{4r_L}{\pi d^2} I(t)$.
- *voltage clamp* in which the voltage is clamped to some fixed level, so that $V(0) = V_c$, a constant.
- *short circuit* or *open end* where the voltage is clamped to 0.
- *lumped soma* where we regard the soma as a single compartment attached to the nerve cable. Suppose that the soma has total resistance R_s and capacitance C_s. Then the boundary condition at $x = 0$ is

$$\frac{V(0,t)}{R_s} + C_s V_t(0,t) - \frac{\pi d^2}{4r_L} V_x(0,t) = 0$$

Note that the general steady-state equation, $0 = -V + \lambda^2 V_{xx}$ has solutions of the equivalent forms:

$$\begin{aligned} V(x) &= A_1 e^{-x/\lambda} + A_2 e^{x/\lambda} \\ V(x) &= B_1 \cosh((l-x)/\lambda) + B_2 \sinh((l-x)/\lambda) \\ V(x) &= C_1 \cosh(x/\lambda) + C_2 \sinh(x/\lambda) \end{aligned}$$

The constants are determined from the boundary conditions. First consider the semi-infinite cable. This has a solution of the form $V(x) = A \exp(-x/\lambda)$. Suppose

that we inject current, I_0 into the end of the cable. Recall that the longitudinal current is $I_0 = -(\pi d^2/4r_L)dV/dx$. Thus, we find that

$$A = \frac{4\lambda I_0 r_L}{\pi d^2}.$$

Recall that the *input resistance*, R_{inp} of a cable as the ratio of the steady state potential divided by the current injected. Thus, for the semi-infinite cable,

$$R_{inp} = V(0)/I(0) = \frac{4\lambda r_L}{\pi d^2} = \frac{2\sqrt{r_M r_L}}{\pi d^{3/2}}$$

and the input conductance is given by

$$G_{inp} = 1/R_{inp} = \frac{\pi d^{3/2}}{2\sqrt{r_M r_L}}.$$

For finite cables, it is convenient to use dimensionless space, $X = x/\lambda$ and the electrotonic length, $L = \ell/\lambda$. Assume that the voltage at $X = 0$ is V_0. Then the general solution to the steady-state equation is:

$$V(X) = V_0 \frac{\cosh(L - X) + B_L \sinh(L - X)}{\cosh L + B_L \sinh L}$$

where B_L is an arbitrary constant. This general solution is equivalent to asserting that the boundary condition at $X = 0$ is V_0 and that at $X = L$

$$B_L V(L) + \frac{dV}{dX}(L) = 0.$$

The free parameter, B_L, is the ratio of the terminal conductance for the cable, G_L, to that of the semi-infinite cable, G_{inp}. That is, $B_L = G_L/G_{inp}$.

For example, if we want the sealed end condition at $X = L$ we take $B_L = 0$ so that

$$V(X) = V_0 \frac{\cosh(L - X)}{\cosh L}.$$

If we want the open end conditions, we take $B_L = \infty$ so that

$$V(X) = V_0 \frac{\sinh(L - X)}{\sinh L}.$$

If we choose $B_L = 1$ then

$$V(X) = V_0 e^{-X}$$

which is precisely the solution to the semi-infinite cable.

From these equations for the membrane potential, we can compute the input resistance and input conductance of a finite-length cable. For example, consider the sealed end condition at $X = L$. Suppose that a current, I_0, is injected into the other end at $X = 0$. Then the input resistance is given by

$$R_{inp} = V(0)/I_0 = V_0/I_0.$$

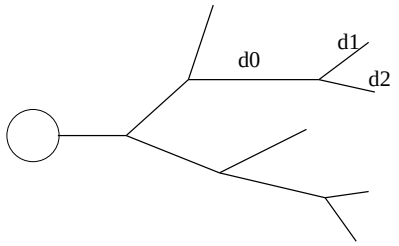

Figure 3.2. *A simple dendritic tree.*

Now,

$$I_0 = -\frac{1}{\lambda r_M}\partial V_m \partial X = \frac{V_0}{\lambda r_M}\frac{sinh(L-X)}{cosh(L)}$$

It follows that

$$I_0 = \frac{V_0}{\lambda r_M} tanh(L) \quad \text{at} \quad X = 0$$

Hence,

$$R_{inp} = \lambda r_M \frac{1}{tanh(l)} \quad \text{and} \quad G_{inp} = \frac{\lambda r_M}{tanh(L)}$$

3.5 Branching and equivalent cylinders.

The infinite cable and the finite cable are simple idealizations of the multi-branched structure of true neurites. Here, we briefly look at branch points and describe the Rall model for dendrites. Figure 3.2 hows a simple branched dendritic structure. Consider the cable with diameter d_0, length ℓ_0 and space constant λ_0 which branches at $x = x_1$ into two semi-infinite cables with diameters d_1 and d_2 and space constants λ_1 and λ_2. The cable equation for such a structure can be solved on the individual segments coupled with continuity of the voltages and the conservation of current. Under certain constraints on the geometry, we can attain a stronger result than continuity of the voltage and its derivative that is important physically and allows us to significantly simplify the problem. With these constraints on the geometry, we will show that having the branch point at x_1 is exactly equivalent to extending branch d_0 to infinity.

Conservation of current implies that the current leaving the branch d_0 equals the sum of the currents entering branches d_1 and d_2. That is,

$$\frac{\pi d_0^2}{4r_L} V_0'(x_1) = \frac{\pi d_1^2}{4r_L} V_1'(x_1) + \frac{\pi d_2^2}{4r_L} V_2'(x_1). \tag{3.15}$$

Here we assume that the material properties of the cables are the same; only their geometry differs. Now, if we let $V_0 \equiv V_0(x_1) = V_1(x_1) = V_2(x_1)$, then

$$V_1(x) = V_0 e^{\lambda_1 x} \quad \text{and} \quad V_2(x) = V_0 e^{-\lambda_2 x}$$

for $x > x_1$. Moreover, if $V_{eq}(x)$ is the membrane potential of the cable obtained by extending branch d_0 to infinity, then

$$V_{eq}(x) = V_0 e^{\lambda_0 x}.$$

Plugging these into (3.15), and recalling that $\lambda_j \propto \sqrt{d_j}$, we find that we can collapse the three cables 0, 1, and 2 into a single semi-infinite cable with diameter d_0 if

$$d_0^{\frac{3}{2}} = d_1^{\frac{3}{2}} + d_2^{\frac{3}{2}} \tag{3.16}$$

Will Rall was the first to recognize that if (3.16) is satisfied and the material properties of the cables are the same, then the three cables 0, 1 and 2 can be collapsed into an *equivalent cylinder.* For a complex structure, starting at the ends, we can recursively simplify the model to a single semi-infinite cylinder. In the previous example, we considered only two branches at the branch point; however, we could have had any number of branches at each branch point as long as

$$d_P^{\frac{3}{2}} = \sum d_D^{\frac{3}{2}}$$

where d_P is the parent dendrite and d_D are the daughter dendrites. If this condition holds at every branch point and the material properties of the cables are the same, then the entire dendritic tree can be reduced to an equivalent semi-infinite cable.

We have so far assumed that the branches attached to the final branch point extend to infinity; that is, they correspond to semi-infinite cables. A similar analysis holds if we assume that all of the branches have finite lengths. Here we must assume that all dendrites end at the same electrotonic length. Recall that the electronic length of a cable of length ℓ and space constant λ is ℓ/λ. Suppose, for example, that the cables 1 and 2 shown in Figure ?? have lengths ℓ_1 and ℓ_2. If we assume that $\ell_1/\lambda_1 = \ell_2/\lambda_2$, then we can collapse the three cables 0, 1 and 2 into a single cable of diameter d_0 and electrotonic length equal to $\ell_0/\lambda_0 + \ell_1/\lambda_1 = \ell_0/\lambda_0 + \ell_2/\lambda_2$.

Example

In the figure 3.3, we depict a dendritic tree consisting of several branches with their lengths and diameters in microns. (a) Can they be reduced to an equivalent cylinder (b) What is the electrotonic length (c) What is the input conductance. Assume sealed ends for all terminal dendrites and assume that $r_M = 2000\Omega\text{cm}^2$ and that $r_L = 60\Omega\text{cm}$.

Answer.

$$d_a^{3/2} + d_b^{3/2} + d_c^{3/2} = 1 + 1 + 1 = 3 = 2.08^{3/2} = d_d^{3/2}$$

$$d_d^{3/2} + d_e^{3/2} = 3 + 3 = 6 = 3.3^{3/2} = d_f^{3/2}$$

so the 3/2 rule is obeyed. Clearly a,b,c are all the same electrotonic length. The space constants are:

$$\lambda_a = \lambda_b = \lambda_c = \sqrt{d_a r_M / 4 r_L} = 289\mu$$

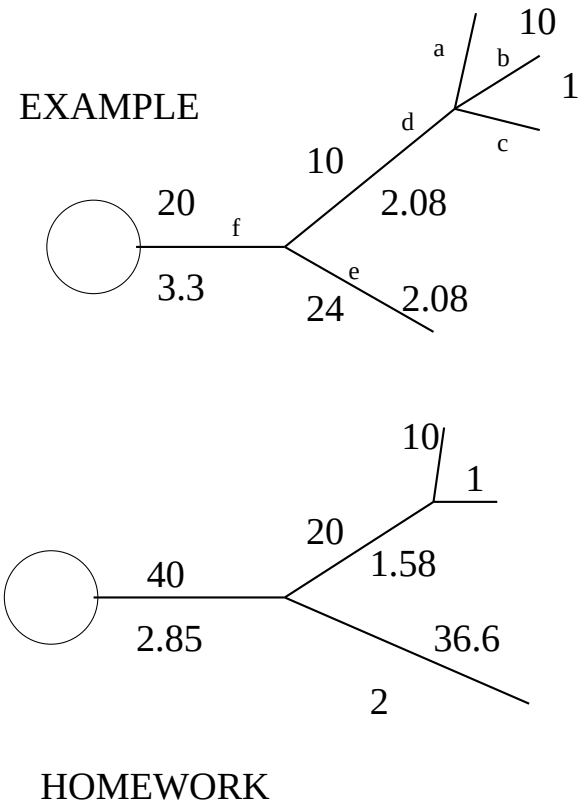

Figure 3.3. *Example of the Rall reduction to an equivalent cylinder.*

$$\lambda_d = \lambda_e = \sqrt{d_e r_M / 4 r_L} = 416\mu$$

$$\lambda_f = \sqrt{d_f r_M / 4 r_L} = 524\mu$$

Thus, the total electrotonic length of abc with d is

$$L_{abcd} = \frac{\ell_a}{\lambda_a} + \frac{\ell_d}{\lambda_d} = \frac{10}{289} + \frac{10}{416} = .0586$$

$$L_e = \frac{\ell_e}{\lambda_e} = \frac{24}{416} = .0576$$

which are close enough to be considered equal (2% difference). Thus, we can combine the whole thing into an equivalent cylinder. The total electrotonic length is then:

$$L = L_f + L_e = L_f + L_{abcd} = \frac{\ell_f}{\lambda_f} + L_e = 0.096 \approx 0.1$$

Finally, the input conductance is

$$G_{in} = G_\infty \tanh(L) = \frac{\pi d^{3/2}}{2\sqrt{R_M R_A}} \tanh(L)$$

which is

$$G_{in} = \frac{\tanh(0.1)(3.14159)(3.3 \times 10^{-4})^{3/2}}{2\sqrt{2000 \times 60}} = 2.7 \times 10^{-9}\text{S}$$

3.6 An isolated junction

The equivalent cylinder is a very useful method for reducing the analysis of complex dendritic trees to a simpler model. However, there are limitations. For example, one must assume that the so-called 3/2 law (see (3.16)) is satisfied. Another difficulty is related to the problem of determining the response of the dendritic tree to an injected current. Consider, for example, the simple dendritic tree shown in Figure 3.2. If the injection site is along the principle initial cylinder, then the equivalent cylinder will determine how the membrane potential responses at this and the daughter dendrites. However, if the injection site is along the daughter dendrites, then, in order to use the equivalent circuit, one must assume that the current is spread out evenly along all of the daughter dendrites that emerge from the same junction point. One cannot use the equivalent circuit if only one of the daughter dendrites receives input and the others receive none.

In this section, we consider a single isolated junction of three semi-infinite cables with a point source of current injection. We do not assume that the 3/2 law holds. We note that a considerably more general analysis for dendritic trees with complex geometries is given in [Rinzel/Rall].

We consider the branched cable shown in Figure ??. The three cables are denoted as C_0, C_1 and C_2. Assume that the diameters and specific membrane resistance of the cables are d_i and r_{Mi}, $i = 0, 1, 2$, respectively. Let r_L be the longitudinal resistivity. We assume that the junction point is at $x = 0$. Moreover, x will denote the distance along each cable to the junction point. Finally, we assume that there is an electrode current at an isolated point along C_0; the distance from this point to the junction point is denoted as y. Note that C_0 may be either the parent dendrite or one of the daughter dendrites.

We derive the steady-state solution to this problem. Except at the junction and the injection points, each membrane potential $V_i(x)$ satisfies the steady-state cable equation:

$$\lambda_i \frac{\partial^2 V_i}{\partial x^2} - V_i = 0$$

where

$$\lambda_i = \sqrt{\frac{d_i r_{Mi}}{4 r_L}}$$

is the space constant of corresponding cable. We now need to determine the boundary conditions that must be satisfied. At the junction point, the three membrane

potentials must be equal; moreover, the flow of current must be conserved. Hence,

$$V_0(0) = V_1(0) = V_2(0) \quad \text{and} \quad \sum d_i^2 \frac{dV_i}{dx}(0) = 0.$$

At the electrode site, the injection current is conserved and spreads towards (decreasing x) or away from (increasing x) the junction point. Recall that the longitudinal current is given by (3.8). It follows that the boundary condition at the junction point is:

$$\frac{dV_0}{dx}(y^-) - \frac{dV_0}{dx}(y^+) = \frac{4r_L}{\pi d_0^2} I_0$$

where I_0 is the total electrode current and the two terms on the left hand side represent the left-handed and right-handed derivatives of V_0 at y, respectively.

We leave it as an exercise to demonstrate that the solution of this problem is given by:

$$\begin{aligned} V_0(x) &= \frac{I_0 R_{\lambda_0}}{2}[\exp(-|y-x|/\lambda_0) + (2p_0 - 1)exp(-(y+x)/\lambda_0)] \\ V_1(x) &= p_1 I_0 R_{\lambda_1} exp(-x/\lambda_1 - y/\lambda_0) \\ V_2(x) &= p_2 I_0 R_{\lambda_2} exp(-x/\lambda_2 - y/\lambda_0) \end{aligned} \tag{3.17}$$

where, for $i = 0, 1, 2$,

$$p_i = \frac{d_i^{3/2}}{d_1^{3/2} + d_2^{3/2} + d_3^{3/2}} \quad \text{and} \quad R_{\lambda_i} = \frac{4r_L \lambda_i}{\pi d_i^2}.$$

An example is shown in Figure ??. If the injection site is along the thicker dendrite, then this has little effect on the attenuation of the potential along the thin branches. However, if the injection since is along on of the thinner dendrites, then the big dendrite has a much greater effect on the attenuation between the two thinner branches.

3.7 Exercises

1. (a) Plot profiles of $V(x,t)$ for the response of an infinite cable (3.13) at different spatial locations as a function of time. (b) Compute the time at which $V(x,t)$ reaches its maximum and show that for x large it is asymptotically linear in x. (c) Compute the maximum value of the voltage for each spatial position.

2. Compute the steady-state response of the cable to a sustained periodic input. That is $I(x,t) = I_0 \sin(\omega t)\delta(x)$. (Hint: Everything will be easier if write the current as proportional to $\exp(i\omega t)$ and use the linearity of the cable to assume a solution of the form $z(x)\exp(i\omega t)$.. Then use the steady state infinite cable result.) Compute the phase-shift as a function of the distance from the source. Plot the amplitude at $x = 0$ as a function of the frequency. Determine how quickly the amplitude falls off with distance as a function of frequency.

3. Solve the cable equation $\tau v_t = -v + v_{xx} + I(x,t)$ on the finite interval $0 < x < L$ subject to the boundary conditions $v(0) = 0$ and $v_x(L) = 0$. (Hint: You could compute a Green's function for this, or you could expand it in an eigenfunction expansion by solving $v'' = \beta v$ with $v(0) = 0$ and $v'(L) = 0$.).

4. Consider a cable with electrotonic length L and a sealed end at $x = L$. Suppose $V(0) = V_0$. Show that the input conductance at $X = 0$ is

$$G_L = G\infty \tanh(L).$$

5. Prove that the homogeneous solution to equation

$$\frac{1}{d(x)}\frac{d}{dx}\left(\frac{d^2(x)dV}{dx}\right) = V(x) \tag{3.18}$$

with boundary conditions $dV/dx(0) = 0$ and $V(L) = 0$ has no nonzero solutions. (Hint: Without loss of generality, you can assume $V(0) > 0$. Show that $V(x)$ must be concave up in the interval $(0, L)$.)

6. Numerically compute the solution to (3.18) with $d(x) = 1 - cx/L$ where $c < 1$, $V(0) = 1$ and $V'(L) = 0$. Compare the solutions for $c = 0$ to those with $c = .95$ when $L = 10$. Try $c = -0.5$ (corresponding to a fattening cable)

7. Do the equivalent cylinder reduction to the bottom dendrite in figure 3.3.

8. Advanced exercise. Consider a cable with three currents, as shown in figure equivcyl. Suppose that the concentrations of the ions are those given for the squid axon in table 2.3 and that the permeabilities are $P_K = 1, P_{Cl} = 0.1$ and $P_{Na} = .03$. Suppose the temperature is 20 C. Let $I(V)$ denote the total current as defined by (2.3). Simulate the response to the following cable:

$$C_m\frac{\partial V}{\partial t} = -I(V) + K\frac{\partial^2 V}{\partial x^2}$$

to a current step at $x = 0$. You can make $C_m = 1, K = 1$ without loss of generality since these just set the time and space scales. Compare this to the passive linear conductance cable model. Convince yourself that there is very little difference. In particular, you might want to solve the steady state boundary value problem for, say, $V(0) = V_0$ and $V_x(L) = 0$. You cannot do this analytically, but numerical solutions should be fairly simple.

3.8 Dendrites with active processes

We have, so far, primarily considered passive dendrites in which all of the conductances and currents are constant. However, it is now recognized that neurons may have active voltage-gated conductances along the dendritic trees and these active conductances may have a profound influence on the neuron's firing properties and how the neuron response to synaptic inputs. We note that active channels are typically unevenly distributed along the dendrites so, for example, there may be a higher

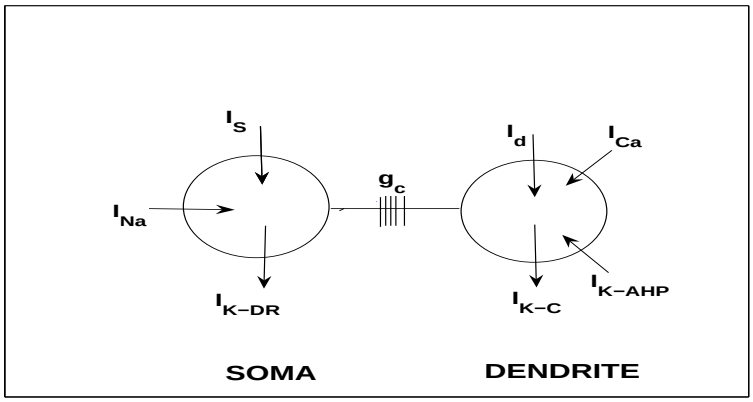

Figure 3.4. *Schematic of 2-compartment model showing applied currents and outward and inward currents to soma and dendrite compartments.*

distribution of, say, sodium channels in the proximal region near the soma than in the distal region far from the soma. A useful way to model neurons with active dendrites is to use the multicompartment approach. Here we present an example of this due to Rinzel and Pinsky.

Pinsky and Rinzel developed a two-compartment model for CA3 hippocampal pyramidal neurons in a guinea pig. This work was motivated by an earlier, considerably more complex model of Traub which consisted of 19 compartments. The reduced Pinsky-Rinzel model contained elements of the full model which were thought to be essential and was capable of reproducing many of the important stimulus-response properties of the Traub model. By considering a minimal reduced model, Pinsky and Rinzel were able to explain how interactions between the somatic and dendritic compartments generate bursting with unusual wave-forms which do not seem to arise in single-compartment models. The reduced model is also considerably easier to implement computationally.

A schemata of the two-compartment model is shown in Figure 3.4. Motivated by Traub's model, the fast spiking currents are restricted to the soma while most of the calcium and calcium modulated currents lie in the dendritic-like compartment. The soma-like compartment has two voltage-dependent currents, an inward sodium current and an outward delayed-rectifier potassium current. The dendritic compartment has three voltage dependent currents. There is a fast calcium current and two types of potassium currents: a Ca-activated potassium current and a potassium afterhyperpolarization. Electrotonic coupling between the compartments is modeled using two parameters, g_c and p, where g_c represents the strength of coupling and p represents the percentage of total area in the some-like compartment. Finally, the model includes terms for applied current to the soma and dendrite.

The model can generate bursting activity for appropriate values of the parameters. Figure 3.5 shows the wave-form of the spiking activity during a burst. This type of activity does not typically arise in single-compartment models; it results from interactions between the two compartments. Here we step through how this burst is generated; a more complete and detailed description is given in [?].

The burst shown in Figure 3.5 results from electrotonic interactions between soma and dendrite with significant coupling current that flows back and forth, alternately providing depolarizing or hyperpolarizing current to each compartment. The burst sequence is initiated by a somatic sodium spike. This is because I_{Na} is activated at lower voltages that I_{Ca}. The leading sodium action potential depolarizes the dendrite through the spread of electrotonic current. The soma then repolarizes, but only partially. This causes the dendritic membrane potential to fall below the threshold for calcium spike generation, thereby delaying the full dendritic spike. During this repolarization phase, current flows into the soma from the dendrite which then initiates a second somatic spike. The second somatic spike stops the drain of coupling current from the dendrite, enabling the dendrite to undergo a full I_{Ca}-mediated voltage spike with accompanying rapid increase in Ca. The dendritic spike then provides depolarization which drives soma activity. We note that the calcium dendritic spikes are considerably broader than the somatic spikes. The broad dendritic spike leads to strong stimulation of the soma which leads to damped, high frequency spiking. The dendritic calcium spike, and hence the burst, is terminated by the calcium-dependent potassium current. This builds up on a slow time-scale during the dendritic spiking activity. Hence, the burst duration is primarily determined by the amount of time required for Ca to build up. We note that the length of the silent phase is determined by slow variables q and Ca mediating the outward potassium currents. Both of these currents must decrease before a somatic action potential can be initiated.

3.9 Bibliography

Much of the pioneering work on the modeling of dendrites was done by Wilfred Rall. Reviews of this material can be found in Rall [39] and Koch and Segev [31]. The book [45] was written in honor of Wilfred Rall and contains many of his original papers, along with commentaries by leading researchers in this field. Other textbooks include Jack et. al. [25], Tuckwell [52], Johnston and Wu [26] and Koch [30].

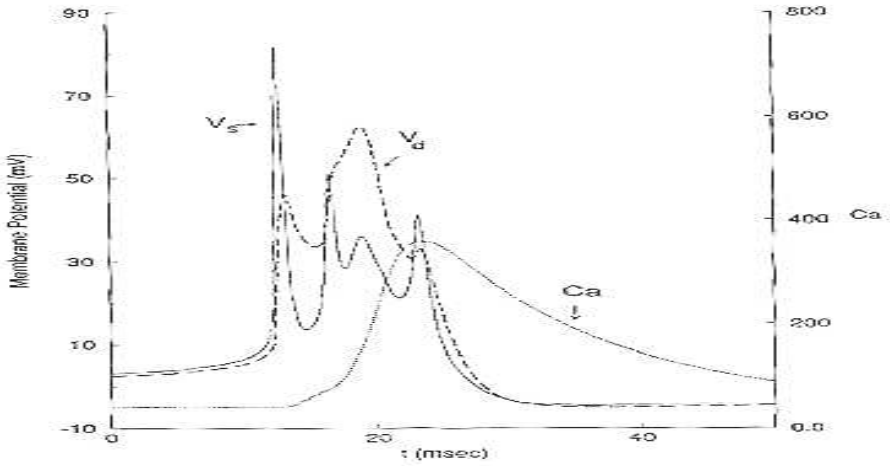

Figure 3.5. *Voltage and calcium traces of a bursting solution in the 2-compartment model.*

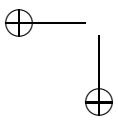

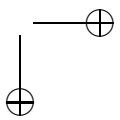

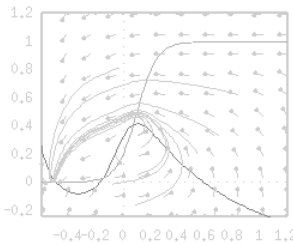

Chapter 4

Dynamics

4.1 Introduction to dynamical systems

Dynamical systems theory provides a powerful tool for analyzing nonlinear systems of differential equations, including those that arise in neuroscience. This theory allows us to interpret solutions geometrically as curves in a phase space. By studying the geometric structure of phase space, we are often able to classify the types of solutions that the model may exhibit and determine how solutions depend on the model's parameters. For example, we can often predict if a model neuron will generate an action potential, determine for which values of the parameters the model will produce oscillations and compute how the frequency of oscillations depends on parameters.

In this chapter, we introduce many of the basic concepts of dynamical systems theory using a reduced 2-variable model: the Morris-Lecar equations. Although this model is considerably simpler than the Hodgkin-Huxley equations, it still exhibits many important features of neuronal activity. For example, the Morris-Lecar model generates action potentials, there is a threshold for firing and the model displays sustained oscillations at elevated levels of an applied current. By considering a reduced model, we can more easily explain the geometric mechanisms underlying each of these phenomena. Moreover, we can introduce important mathematical concepts such as phase space analysis, bifurcation theory, oscillations and stability theory. Each of these concepts plays a fundamental role in the analysis of more complex systems discussed throughout the book.

4.2 The Morris-Lecar model

One of the simplest models for the production of action potentials is a model proposed by Kathleen Morris and Harold Lecar. The model has three channels: a potassium channel, a leak, and a calcium channel. In the simplest version of the model, the calcium current depends instantaneously on the voltage. Thus, the

Morris-Lecar equations (ML) have the form:

$$\begin{aligned} C_m \frac{dV}{dt} &= I_{app} - g_l(V - E_L) - g_k n(V - E_K) \\ &\quad -g_{Ca} m_\infty(V)(V - E_{Ca}) \;\equiv\; I_{app} - I_{ion}(V, n) \\ \frac{dn}{dt} &= \phi(n_\infty(V) - n)/\tau_n(V) \end{aligned} \tag{4.1}$$

where

$$\begin{aligned} m_\infty(V) &= \frac{1}{2}[1 + \tanh((V - V_1)/V_2)] \\ \tau_n(V) &= 1/\cosh((V - V_3)/(2V_4)) \\ n_\infty(V) &= \frac{1}{2}[1 + \tanh((V - V_3)/V_4)]. \end{aligned}$$

Here, $V_{1,2,3,4}$ are parameters chosen to fit voltage clamp data.

The solutions shown in Figure 4.1 demonstrate that the Morris-Lecar model exhibits many of the properties displayed by neurons. Here the parameters are listed in Table 4.2 under the Hopf case. Figure 4.1A demonstrates that the model is *excitable* if $I_{app} = 60$. That is, there is a stable constant solution corresponding to the resting state of the model neuron. A small perturbation decays to the resting state, while a larger perturbation, above some threshold, generates an action potential. The solution $(V_1(t), n_1(t)) \equiv (V_R, n_R)$ is constant; V_R is the resting state of the model neuron. The solution $(V_2(t), n_2(t))$ corresponds to a subthreshold response. Here, $V_2(0)$ is slightly larger than V_R and $(V_2(t), n_2(t))$ decays back to rest. Finally, $(V_3(t), n_3(t))$ corresponds to an action potential. Here, we start with $V_3(0)$ above some threshold. There is then a large increase of $V_3(t)$ followed by $V_3(t)$ falling below V_R and then a return to rest.

Figure 4.1B shows a periodic solution of (ML). The parameter values are exactly the same as before; however, we have increased the parameter I_{app}, corresponding to the applied current. If we increase I_{app} further, then the frequency of oscillations increase; if I_{app} is too large, then the solution approaches a constant value.

In the following, we will show how dynamical systems methods can be used to mathematically analyze these solutions. The analysis is extremely useful in understanding when this type of model, for a given set of parameters, displays a particular type of behavior. The behavior may change as parameters are varied; an important goal of bifurcation theory, which we describe below, is to determine when and what types of transitions take place.

4.3 The phase plane

It will be convenient to write (4.1) as

$$\begin{aligned} \frac{dV}{dt} &= f(V, n) \\ \frac{dn}{dt} &= g(V, n). \end{aligned} \tag{4.2}$$

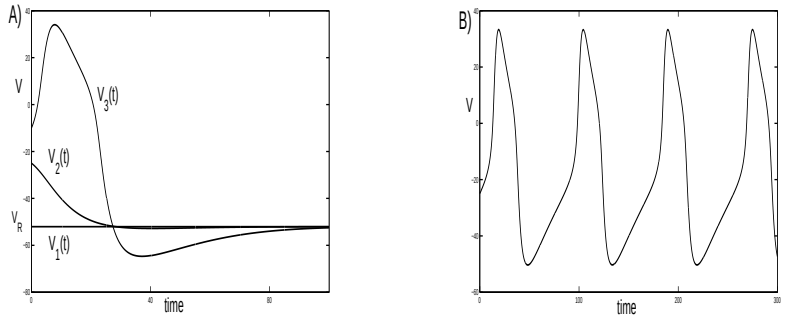

Figure 4.1. *Solutions of the Morris-Lecar equations. Parameters are listed in Table 4.2, the Hopf case. A) A small perturbation from rest decays to the resting state, while a larger perturbation generates an action potential. Here,* $I_{app} = 60$. *B) A periodic solution of (ML). Here,* $I_{app} = 100$.

Table 4.1. *Morris-Lecar parameters; the current,* I_{app}*, is a parameter.*

Parameter	**Hopf**	**SNLC**	**Homoclinic**
ϕ	0.04	.067	0.23
g_{Ca}	4.4	4	4
V_3	2	12	12
V_4	30	17.4	17.4
E_{Ca}	120	120	120
E_K	-84	-84	-84
E_L	-60	-60	-60
g_K	8	8	8
g_L	2	2	2
V_1	-1.2	-1.2	-1.2
V_2	18	18	18
C_m	20	20	20

The phase space for this system is simply the (V, n)-plane; this is usually referred to as the *phase plane*. If $(V(t), n(t))$ is a solution of (4.1), then at each time t_0, $(V(t_0), n(t_0))$ defines a point in the phase plane. The point changes with time, so the entire solution $(V(t), n(t))$ traces out a curve (or trajectory or orbit), in the phase plane.

Of course, not every arbitrarily drawn curve in the phase plane corresponds to a solution of the differential equations. What is special about solution curves is that the velocity vector at each point along the curve is given by the right hand side of (4.1). That is, the velocity vector of the solution curve $(V(t), n(t))$ at a point (V_0, n_0) is given by $(V'(t), n'(t)) = (f(V_0, n_0), g(V_0, n_)$. This geometric property – that the vector $(f(V, n), g(V, n))$ always points in the direction that the solution is

flowing – completely characterizes the solution curves.

Two important types of trajectories are *fixed points* (sometimes called *equilibria* or *rest points*) and *closed orbits*. At a fixed point, $f(V_R, n_R) = g(V_R, n_R) = 0$; this corresponds to a constant solution. Closed orbits correspond to periodic solutions. That is, if $(v(t), n(t))$ represents a closed orbit, then there exists $T > 0$ such that $(V(t), n(t)) = (V(t+T), n(t+T))$ for all t.

A useful way to understand how trajectories behave in the phase plane is to consider the *nullclines*. The V-nullcline is the curve defined by $V' = f(V, n) = 0$ and the n-nullcline is where $n' = g(V, n) = 0$. Note that along the V-nullcline, the vector field $(f(V, n), g(V, n))$ points either up or down and along the n-nullcline, vectors point either to the left or to the right. Fixed points are where the two nullclines intersect. The nullclines divide the phase plane into separate regions; in each of these regions, the vector field points in the direction of one of the four quadrants: (I) $f > 0,\ g > 0$; (II) $f < 0,\ g > 0$; (III) $f < 0,\ g < 0$; or (IV) $f > 0,\ g < 0$.

Stability of fixed points

One can determine the stability of a fixed point by considering the linearization of the vector field at the fixed point. The linearization of (4.2) at a fixed point (V_R, n_R) is the matrix

$$M = \begin{bmatrix} \frac{\partial f}{\partial V}(V_R, n_R) & \frac{\partial f}{\partial n}(V_R, n_R) \\ \frac{\partial g}{\partial V}(V_R, n_R) & \frac{\partial g}{\partial n}(V_R, n_R) \end{bmatrix}.$$

The fixed point is stable if both of the eigenvalues of this matrix have negative real part; the fixed point is unstable if at least one of the eigenvalues has positive real part. For (ML), the linearization is given by

$$M = \begin{bmatrix} -\frac{\partial I_{ion}(V_R, n_R)}{\partial V}/C_m & -g_K(V_R - E_K)/C_m \\ \phi n'_\infty(V_R)/\tau_n(V_R) & -\phi/\tau_n(V_R) \end{bmatrix} \equiv \begin{bmatrix} a & b \\ c & d \end{bmatrix}.$$

Moreover,

$$\begin{aligned} a &\equiv -\frac{\partial I_{ion}(V_R, n_R)}{\partial V}/C_m \\ &= (-g_L - g_K n_R - g_{Ca} m_\infty(V_R) + (E_{Ca} - V_R) g_{Ca} m'_\infty(V_R))/C_m. \end{aligned}$$

We now find conditions on the nonlinear functions in (4.1) for when the fixed point is stable.

Suppose that the equilibrium voltage lies between E_K and E_{Ca}, a reasonable assumption. Then $b < 0$, $c > 0$, and $d < 0$ in the linearization. Only a can be either negative or positive and the only term contributing to the positivity of a is the slope of the calcium activation function, $m_\infty(V)$. If $a < 0$, then the fixed point is asymptotically stable since the trace of M is negative and the determinant is positive. (Recall that the trace is the sum of the eigenvalues and the determinant is the product of eigenvalues.) Note that the slope of the V-nullcline near the fixed point is given by $-a/b$. Since $b < 0$, it follows that if this slope is negative then

the fixed point is stable; that is, if the fixed point lies along the left branch of the V-nullcline, then it is stable.

Now suppose that the fixed point lies along the middle branch of the V-nullcline, so that $a > 0$. Note that the slope of the n-nullcline, $-c/d$, is always positive. If the slope of the V-nullcline is greater than the slope of the n-nullcline, (i.e., $-a/b > -c/d$) then $ad - bc < 0$. In this case, the determinant is negative and the fixed point is an unstable saddle point. In contrast, if the slope of the n-nullcline is greater than that of the V-nullcline, then the fixed point is a node or a spiral. We leave it as an exercise to show that the fixed point is a spiral if the parameter ϕ is sufficiently small. In this case, the stability of the fixed point is determined by the trace of M: the fixed point is stable if $a + d < 0$ and it is unstable if $a + d > 0$. In summary, if the fixed point lies along the middle branch of the V-nullcline, then it is unstable if either the slope of the V-nullcline at the fixed point is sufficiently large, or ϕ is sufficiently small. Note that ϕ governs the speed of the potassium dynamics.

Excitable systems

Recall that for the parameters given in Table 4.2, the Hopf case, the system is *excitable.* As Figure 4.1A demonstrates, a small perturbation in voltage from the resting state decays back to rest, while a sufficiently large perturbation in voltage continues to increase and generates an action potential.

Phase plane analysis is very useful in understanding what separates the firing of an action potential from the subthreshold return to rest in this model. The projection of the solutions shown in Figure 4.1A onto the phase plane are shown in Figure 4.2A. This figure also shows the V- and the n-nullclines. Note that the V-nullcline separates points along trajectories in which $V' < 0$ and $V' > 0$. In particular, V increases below the V-nullcline and V decreases above the V-nullcline. We further note that the V-nullcline is 'cubic-shaped'. This suggests that a perturbation from rest that lies to the 'left' of the middle-branch of the V-nullcline will return quickly to rest, while a perturbation that lies to the 'right' of the V-nullcline will initially display an increase in membrane potential, corresponding to an action potential, before returning to rest. Therefore, the middle-branch of the V-nullcline in some sense separates the firing of an action potential from the subthreshold return to rest.

This analysis can be made more precise if we assume that the parameter ϕ is small. Looking at Table 4.2, it can be seen that ϕ is relatively smaller in the Hopf case than in the other two cases. For small ϕ, n will not change much so let's hold it at rest. Figure 4.3 shows the phase plane with a horizontal line drawn through the fixed point. If n does not change much, then the dynamics are governed by the behavior on the phase-line $n = n_R$. Since the V-nullcline intersects this line at 3 points, there are three equilibria to the system when n is held constant. The resting state (and true equilibrium of the full system) V_R is stable. There are two additional equilibria (which are not equilibria of the full model, just the model when n is held at its resting value): V_θ, which is unstable and V_e, which is stable. On this line, if the voltage is perturbed past V_θ then it will jump to the right fixed

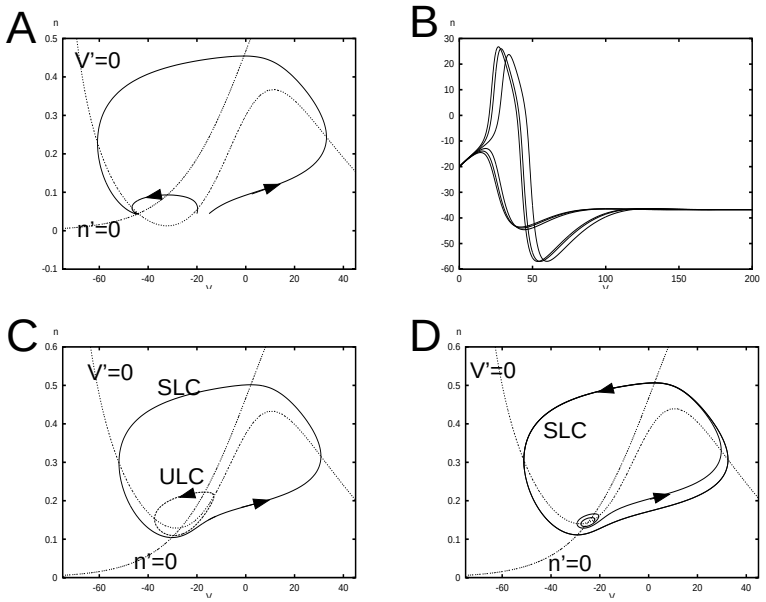

Figure 4.2. *Phaseplanes and time series for the ML model in the Hopf regime. (A) $I = 60$; an excitable system with threshold at about 20 mV. Nullclines are included as well, (B) Starting at $n = n_{rest}$ and varying V from -20 to -20.1 mV; (C) $I = 90$ showing bistability between a stable limit cycle (SLC) and a fixed point, separated by the unstable limit cycle (ULC); (D) $I = 95$, the fixed point is stable and only a limit cycle remains.*

point, V_e. Otherwise, it will decay to rest, V_R. This shows that for small ϕ, the "threshold" voltage for generating an action potential is roughly the intersection of the horizontal line through the rest state and the middle branch of the V-nullcline. Since experimentalists can only move the voltage through current injection, we can use this to estimate the magnitude of a current pulse needed to cross threshold. (See exercise 2 below.)

We note that the peak of the action potential occurs at some latency after the initial perturbation, but this latency can never get very large. The action potential itself is graded and takes on a continuum of peak values, as shown in Figure 4.2B. If ϕ is not "small" and it is increased, then the spike amplitudes are even more graded than those shown in Figure 4.2B. Recall that ϕ is related to the temperature of the preparation. Thus, increasing the temperature of a neuron should lead to a much less sharp threshold distinction and graded action potentials. Indeed, Cole et al demonstrated this in the squid.

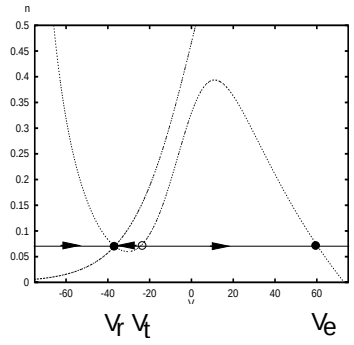

Figure 4.3. *Threshold construction for the ML model.*

Oscillations

We expect the phase plane to change if a parameter in the equations changes. Figure 4.2D shows the phase plane corresponding to the periodic solution shown in Figure 4.1B. Here, $I_{app} = 100$. Note that the periodic solution corresponds to a closed curve, or *limit cycle*. In general, whenever we wish to find periodic solutions of some model, we look for closed orbits in phase space. In Figure 4.2D, there is a unique fixed point; this is where the nullclines intersect. This fixed point is unstable, however.

If we change I_{app} to 90, then the model is *bistable* and the phase plane is shown in Figure 4.2C. Note that there exist both a stable fixed point and a stable limit cycle. Small perturbations from rest will decay back to the stable fixed point, while large perturbations will approach the stable periodic solution. Note that there also exists an unstable periodic solution. This orbit separates those initial conditions that approach the stable fixed point from those that approach the stable limit cycle.

It is often difficult to show that a given model exhibits stable oscillations, especially in higher dimensional systems such as the Hodgkin-Huxley model. Limit cycles are global objects, unlike fixed points that are local. In order to demonstrate that a given point is on a periodic solution, one must follow the trajectory passing through that point and wait to see if the trajectory returns to where it started. This is clearly not a useful strategy for finding periodic solutions. A powerful method for locating oscillatory behavior is bifurcation theory, which we describe in the following section.

4.4 Bifurcation analysis

Bifurcation theory is concerned with how solutions change as parameters in a model are varied. For example, in the previous section we showed that the Morris-Lecar equations may exhibit different types of solutions for different values of the applied current I_{app}. If $I_{app} = 60$, then there is a stable fixed point and no oscillations, while if $I_{app} = 100$, then the fixed point is unstable and there does exist a stable

limit cycle. Using bifurcation theory, we can classify the types of transitions that take place as we change parameters. In particular, we can predict for which value of I_{app} the fixed point loses its stability and oscillations emerge. There are, in fact, several different types of bifurcations; that is, there are different mechanisms by which stable oscillations emerge. The most important types of bifurcations can be realized by the Morris-Lecar model. These are described below.

The Hopf bifurcation

In Figure 4.4, we choose the parameters as in Table 1, the Hopf regime, and show the *bifurcation diagram* for (ML) as the current I_{app} is varied. For each value of I_{app}, there is a unique fixed point, $(V_R(I_{app}), n_R(I_{app}))$. In Figure 4.4A, we plot V_R vs. I_{app}. The fixed point is stable for $I_{app} < 94 \equiv I_1$ and $I_{app} > 212 \equiv I_2$; otherwise, it is unstable. A *Hopf bifurcation* takes place at $I_{app} = I_1$ and $I_{app} = I_2$. By this we mean the following: Recall that a fixed point is stable if all of the eigenvalues of the linearization have negative real part; the fixed point is unstable if at least one of the eigenvalues has positive real part. The fixed point loses stability, as a parameter is varied, when at least one eigenvalue crosses the imaginary axis. If the eigenvalues are all real numbers, then they can cross the imaginary axis only at the origin in the complex plane. However, if an eigenvalue is complex, then it (and its complex conjugate) will cross the imaginary axis at some point that is not at the origin. This latter case corresponds to the Hopf bifurcation and it is precisely what happens for the example we are considering. In this example, $(I_1, V_R(I_1), n_R(I_1))$ and $(I_2, V_R(I_2), n_R(I_2))$ are called *bifurcation points*. Sometimes, I_1 and I_2 are also referred to as bifurcation points. The *Hopf Bifurcation Theorem* states that (if certain technical assumptions are satisfied) there must exist values of the parameter I_{app} near I_1 and I_2 such that there exist periodic solutions that lie near the fixed points $(V_R(I_{app}), n_R(I_{app}))$. A more precise statement of the Hopf bifurcation theory can be found in numerous texts on dynamical systems.

The curves in Figure 4.4A represent fixed points and periodic solutions of the Morris-Lecar model. This diagram was generated using the numerical software XPPAUT. The curve above the fixed point curve represents the maximum voltages on the periodic orbits and the curve below the fixed point curve represents the minimum voltages. The solid curves represent stable solutions and the dashed curves represent unstable solutions. The bifurcation diagram shows many interesting and important features. Note that the periodic solutions near the two bifurcations points are unstable. These unstable, small amplitude periodic solutions lie on the same side of the bifurcation points as the stable fixed points. These are both examples of *subcritical Hopf bifurcations*. At a *supercritical Hopf bifurcation*, the small amplitude periodic solutions near the Hopf bifurcation point are stable and lie on the opposite side as the branch of stable fixed points.

If $88.3 < I_{app} < I_1$ and $I_2 < I_{app} < 217$, then (ML) is bistable. For these values of I_{app}, there exists both a stable fixed point and a stable periodic solution. The phase plane for $I_{app} = 95$ is shown in Figure 4.2C. Note that small perturbations of initial conditions from the resting state will decay back to rest; however, large perturbation from rest will generate solutions that approach the stable limit cycles.

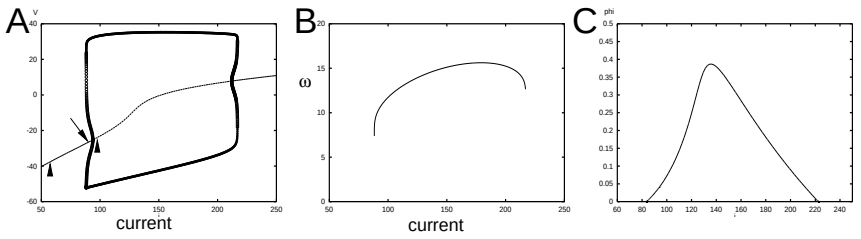

Figure 4.4. *Bifurcation diagram for the ML model in the Hopf regime. (A) Voltage as a function of current. The curves above and below the fixed point curve correspond to the maximum and minimum voltages along periodic orbits. Solid curves represent stable solutions and dashed curves represent unstable solutions. Arrows shown at* $I_{app} = 60, 90$ and 100 *correspond to the solutions shown in Figure 4.1, Figure 4.2A and Figure 4.2B, respectively. (B) Frequency (Hz) versus current. (C) Two-parameter bifurcation showing the curve of Hopf bifurcations as* ϕ *and* I_{app} *vary.*

Figure 4.4B shows the frequency of the periodic solutions versus current. Note that the frequency lies in a narrow range between 7-16 Hz. In particular, the frequency does not approach zero as I_{app} approaches the bifurcation points. This is a general property of periodic solutions that arise via the Hopf bifurcation. In the next section, we shall consider another mechanism for the generation of stable limit cycles. In that mechanism, the frequency does approach zero.

Finally, we can ask what happens if we change the speed of the potassium kinetics. Figure 4.4C shows a two-parameter diagram with ϕ along the vertical axis and I_{app} along the horizontal axis. This shows the locus of Hopf bifurcations in these two parameters. For fixed values of ϕ below about 0.4, there are two currents at which the Hopf bifurcation occurs. Inside the curve, the rest state is stable. One can numerically show that the Hopf bifurcation is subcritical outside the interval, $124.47 < I_{app} < 165.68$; inside this interval, the bifurcation is supercritical. The reader can choose, for example, $\phi = .35$ and show that both Hopf bifurcations are supercritical; the only oscillations are stable and have small amplitude.

Saddle-node on a limit cycle

The Hopf bifurcation is the best known mechanism through which one can go from a stable fixed point to an oscillation. Importantly, the fixed point persists through the bifurcation. Furthermore, the limit cycles which bifurcate are *small amplitude* and local, in the sense that it lies close to the branch of fixed points (although, as we saw in the ML model, the bifurcation is subcritical at low currents and thus bifurcating periodic orbits are unstable). Another mechanism through which an oscillation can emerges from a fixed point is called a *saddle-node on a limit cycle* or SNLC. It is also called a *saddle-node infinite cycle* or SNIC. This is an example of a global bifurcation.

The behavior of the ML model with these parameters is quite different as is seen by looking at Figure 4.5. First, unlike Figure 4.2B, the action potentials appear to occur with arbitrary delay after the end of the stimulus. Secondly, the shape of the action potentials is much less variable. The reason for this can be understood by looking at the phase plane in Figure 4.5B. Unlike the Hopf case, here there are three fixed points, only one of which (labeled N) is stable. The middle fixed point is a saddle point (labeled S). Thus, the linearized system at this fixed point has one positive and one negative eigenvalue. Associated with these eigenvalues are the stable and unstable manifolds. These manifolds consist of trajectories that approach the saddle point in either forward or backward time, respectively. The two branches of the unstable manifold, Σ^+, form a loop with the stable node N and the saddle point S. This loop in the plane plane constrains the spike shape; since trajectories cannot cross, any trajectory starting outside the loop must remain outside of it. Thus, the spike height cannot fall below a certain level. More importantly, the stable manifold, Σ^-, forms a hard threshold that is precisely determined. This contrasts with the pseudothreshold we saw in the Hopf case. Any perturbation which drives the potential to the right of Σ^- results in a spike and any to the left leads to a return to rest without a spike.

Figure 4.5 also explains the delay to firing. Suppose that a stimulus drives the voltage to a point exactly on the unstable manifold Σ^-. Then, the trajectory will go to the saddle point where it will remain. The closer a perturbation gets to Σ^- (but to the right of it), the longer the delay to spike. Indeed, the spike with the longest delay in Figure 4.5A stays at a nearly constant voltage close to the value at the saddle-point before finally firing.

Like the Hopf case, as current is increased, the model fires repetitively. A typical limit cycle is shown in Figure 4.5D. Figure 4.6A shows the bifurcation diagram as the current is increased. The steady-state voltage shows a region where there are three equilibria for I_{app} between about -15 and +40. Only the lower fixed point is stable. As I_{app} increases, the saddle-point and the stable node merge together at a saddle-node bifurcation, labeled SN_2. When $I_{app} = I_{SN_2}$, the invariant loop formed from Σ^+ becomes a homoclinic orbit; that is, it is a single trajectory that approaches a single fixed point in both forward and backward time. This type of homoclinic orbit is sometimes called a *saddle-node homoclinic orbit* or a SNIC. As I_{app} increases past $I_{app} = I_{SN_2}$, the saddle-point and node disappear; the invariant loop formed from Σ^+ becomes a stable limit cycle. The branch of limit cycles persists until it meets with a branch of unstable periodic solutions emerging from a subcritical Hopf bifurcation.

Figure 4.6B shows the frequency of the oscillations as a function of the current. Unlike Figure 4.4B, the frequency for this model can be arbitrarily low and there is a much greater dynamic range. Note that the nullclines in Figure 4.5C can be very close to touching each other and thus create a narrow channel where the flow is extremely slow. This suggests why the frequency of firing can be arbitrarily low. Moreover, as $I_{app} \to I_{SN_2}$, the limit cycles approach a homoclinic orbit. We expect that the frequency should approach zero as $I_{app} \to I_{SN_2}$. In an exercise below, the reader shows that the frequency scales as the square root of $I_{app} - I_{SN_2}$ and develops the theta model.

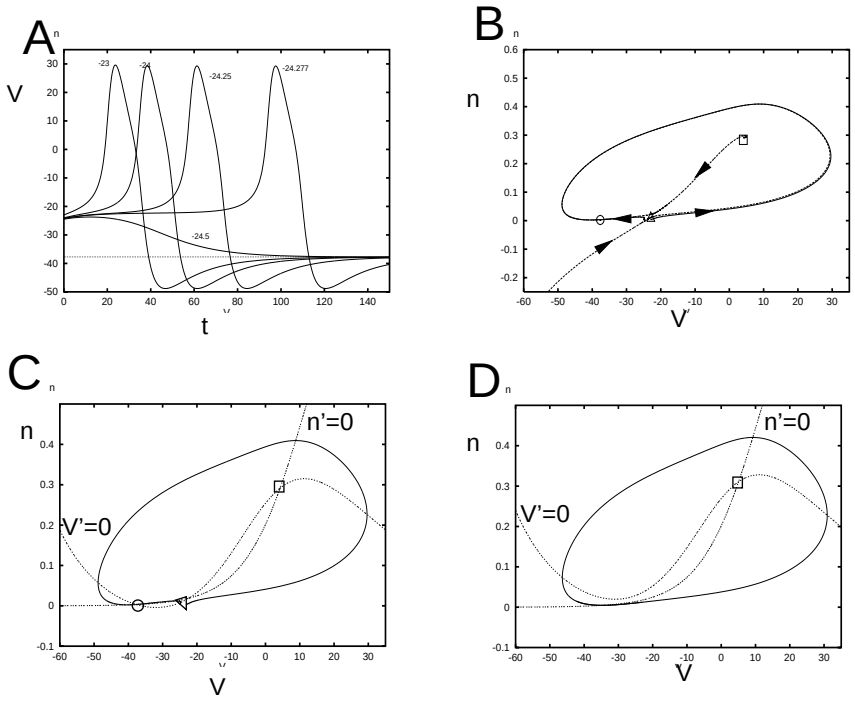

Figure 4.5. *Dynamics of the ML model with saddle-node dynamics. A) The delay to spike can be arbitrary but the spike height is invariant. B) and C) Phase-plane explaining A). The fixed points $N, S,$ and U are, respectively a stable node (the rest state), a saddle-point, and an unstable node. $\Sigma^{\pm}$ are the stable $(-)$ and unstable $(+)$ manifolds of S. D) There exists a stable limit cycle for sufficient current; the nullclines are also shown.*

Saddle-homoclinic bifurcation

By changing the rate of the potassium channel, ϕ, we can alter the dynamics of the model so that the SNIC is replaced by another type of global bifurcation; this is called a *saddle-homoclinic bifurcation*. In both types of bifurcations, the frequency of oscillations approach zero as the current approaches the bifurcation value. However, there are important differences.

Since ϕ only changes the rate of n, it has no effect on the number and values of the fixed points, only their stability. Figure 4.7 shows the bifurcation diagram for the model when ϕ is increased from 0.067 to 0.23. As before, the fixed points are lost at a saddle-node bifurcation. The Hopf bifurcation on the upper branch occurs at a much lower value of current than in Figure 4.6 but the branch of periodic orbits is still subcritical. The main difference is that the stable branch of periodic orbits does not terminate on the saddle node as in Figure 4.6. Rather it terminates on an orbit that is homoclinic to one of the saddle points along the middle branch of

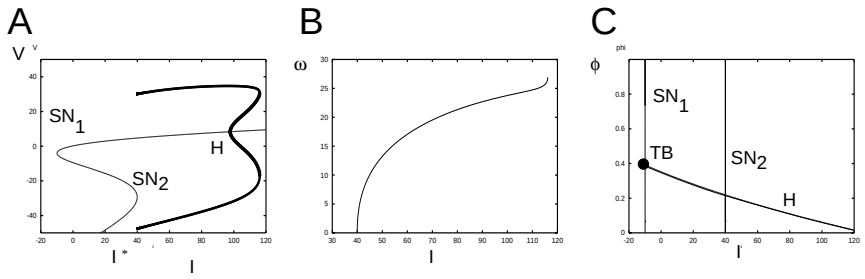

Figure 4.6. *Bifurcation for the ML model with saddle-node dynamics. A) Voltage vs current showing saddle-nodes, $SN_{1,2}$ and Hopf H bifurcations. B) Frequency as a function of current. C) Two-parameter bifurcation diagram showing the curves of Hopf and saddle-node bifurcations as the rate, ϕ, of the potassium channel varies. The Hopf curve meets the left-most saddle-node curve at a double zero eigenvalue characterizing a Takens-Bogdanov bifurcation (TB).*

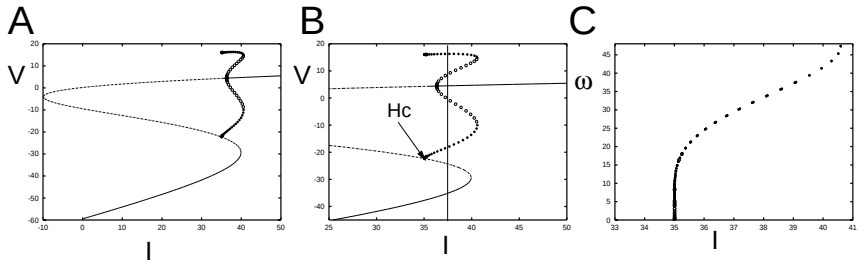

Figure 4.7. *Bifurcation for the ML model with increased ϕ. A) Voltage vs current. B) Zoom in of A) showing the homoclinic orbit (Hc). The vertical line at $I_{app} = 37$ shows tristability. (C) Frequency versus current; note the much steeper approach to I^* than in Figure 4.6.*

fixed points. Like the SNIC, this homoclinic orbit has an infinite period. However, the periods of the limit cycles approach infinity quite differently than before. In exercise ??? you are asked to show that the period scales as

$$T \sim \ln \frac{1}{I_{app} - I_{Hc}}$$

where I_{Hc} is the current at which there is a saddle-homoclinic orbit. The frequency T^{-1} approaches zero much more rapidly than the SNIC case.

Figure 4.8 shows the phase plane for the membrane model near the critical current, I_{Hc}. There are three fixed points. The lower left fixed point is always stable, the middle point is a saddle, and the upper right point is an unstable spiral. For $I_{app} < I_{Hc}$ (panel A), the right branch of the unstable manifold of the saddle wraps around and returns to the stable fixed point. The upper branch of the

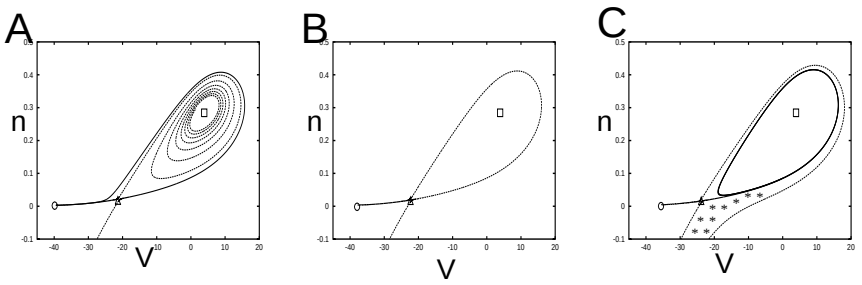

Figure 4.8. *Phaseplane for the ML system near the homoclinic bifurcation showing A) $I_{app} < I_{Hc}$, B) $I_{app} \approx I_{Hc}$ and C) $I_{app} > I_{Hc}$.*
. Perturbations from rest that lie in the starred region shown in C) will approach the stable limit cycles.

stable manifold wraps around the spiral (in negative time). Note that the unstable manifold passes on the outside of the stable manifold. In Figure 4.8B, the stable and unstable manifolds meet and form the homoclinic orbit at $I_{app} = I_{Hc}$. For $I_{app} > I_{Hc}$, the unstable manifold passes *inside* the stable manifold and wraps around a stable limit cycle. Thus, this model has a regime of bistability where there is a stable fixed point and a stable periodic orbit. Unlike the bistability in the Hopf case, the stable limit cycle does not surround the stable fixed point. In the Hopf case, an unstable periodic orbit acted to separate the stable fixed point from the stable limit cycle. In the present set of parameters, the stable manifold of the middle fixed point separates the two stable states. In order to get onto the limit cycle, it is necessary to perturb the potential into the starred region in Figure 4.8C. Consider a brief current pulse which perturbs the voltage. If this pulse is weak, the system returns to rest. If it is very strong and passes the starred region, then the model will generate a single spike and return to rest. However, for intermediate stimuli (like the baby bear's porridge – just right), the system will settle onto the stable limit cycle.

Finally, we look closely at the bifurcation diagram, Figure 4.7B. Near $I_{app} = 38$, there are two stable fixed points as well as a stable limit cycle. Thus, the model is actually "tristable". The reader is urged to explore this aspect of the model more carefully in exercise *

Class I and class II

The ML model illustrates several important features of neuronal firing. Three different mechanisms for switching from rest to repetitive firing were illustrated. In particular, the most common mechanisms are through the Hopf and SNIC bifurcations. In the 1940's Hodgkin classified three types of axons according to their properties. He called these Class I-II; with Class III being somewhere in between the first two classes which we describe:

Class I. Axons have sharp thresholds, can have long latency to firing, and can fire at arbitrarily low frequencies;

Class II. Axons have variable thresholds, short latency, and a positive minimal frequency.

From this description, we can see that these two classes fall neatly into the dynamics of the SNIC and the Hopf bifurcations, respectively. Rinzel and Ermentrout (1989) were the first to note this connection. Now there are many papers which classify membrane properties as Class I or Class II and mean SNIC and Hopf respectively.

Tateno et al (2004) have characterized regular spiking (RS) neurons (excitatory) and fast spike (FS) neurons (inhibitory) in rat somatosensory cortex using this classification. (Note that many authors call the dynamics Type I,II instead of Class I,II.) Figure 4.9 show some properties of cortical neurons. RS neurons appear to be Class I; the minimal frequency is close to zero. Note that RS neurons do not seem to have subthreshold oscillations (not shown). In contrast, FS neurons appear to be Class II; they have a minimum frequency of around 15 Hz. They also exhibit subthreshold oscillations. Near the critical current, they seem to switch back and forth between rest and firing. This suggests the possibility of a narrow range of bistability consistent with the subcritical Hopf bifurcation.

T. Tateno, A. Harsch, and H. P. C. Robinson Threshold Firing Frequency-Current Relationships of Neurons in Rat Somatosensory Cortex: Type 1 and Type 2 Dynamics J Neurophysiol, Oct 2004; 92: 2283 - 2294.

4.5 Bifurcation analysis of the Hodgkin-Huxley equations

We now consider the spaced-clamped Hodgkin-Huxley model (2.43). In the previous chapter, we discussed the response to a brief current pulse. Figure 2.13 shows the effects of a brief current pulse at amplitudes ranging from 1-5 $\mu A/cm^2$. There appears to be a very sharp transition between an action potential and a minimal response. A constant current can induce the membrane to oscillate repeatedly as seen in the right panel of Figure 2.13.

We can get a more global picture of the dynamics of the equations by looking at a bifurcation diagram. Figure 4.10A shows the behavior of the voltage as a function of the applied current, I_{app}. Lines represent fixed points and circles represent periodic orbits. The frequency of the oscillations is shown in Figure 4.10C. The range is from about 40 Hz to about 150 Hz.

Note that there is a unique equilibrium point for all I_{app}. At $I_{app} \approx 10$, the rest state loses stability at a Hopf bifurcation. At a large value of $I_{app} \approx 154$ there is another Hopf bifurcation. From the figure, it seems clear that the bifurcation is subcritical at the low current and supercritical at the high current. At the lower Hopf bifurcation, there is a subcritical branch of unstable periodic orbits. Hence, the transition from resting behavior to oscillations is Class II.

Figure 4.10B shows a blowup of the region near this Hopf bifurcation. Evidently, there are values of I_{app} near 7.88 where there are *four* different limit cycles.

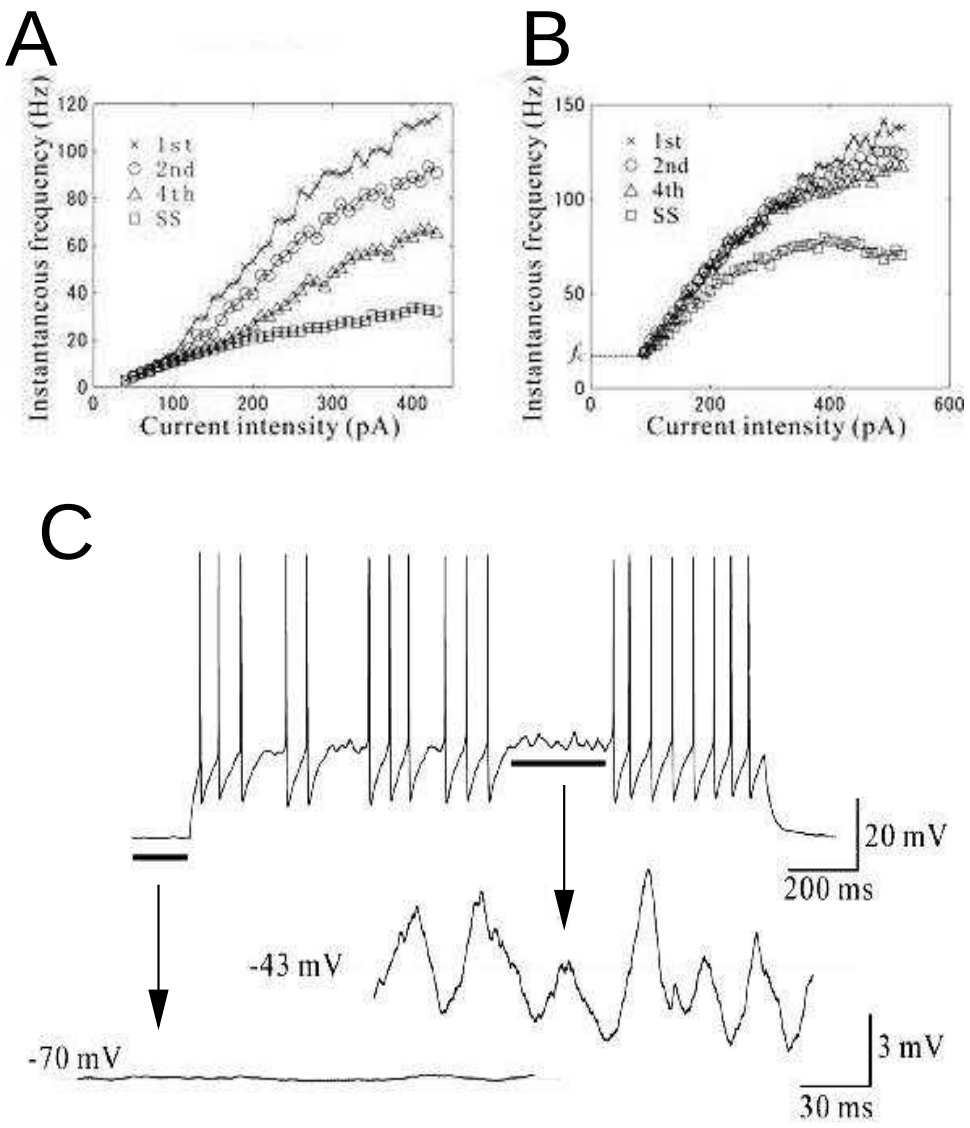

Figure 4.9. *From Tateno etal; Properties of RS and FS neurons in cortex. A. Firing rate versus current for RS neurons. (Note that these cells have spike-frequency adaptation so that the inter-spike interval (ISI) is not constant. Thus, this shows the ISI after several spikes as well as the steady-state.) (B) Same as A for FS neurons. (C) Mixture of spikes and subthreshold oscillations near the critical current for FS.*

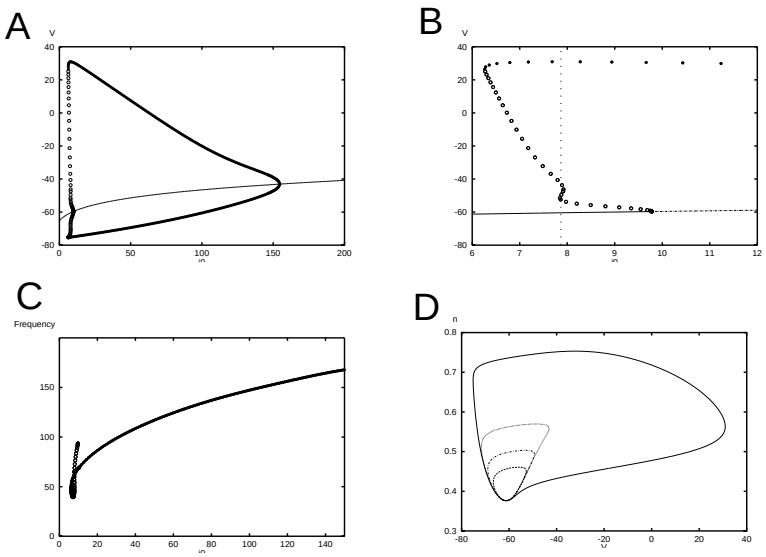

Figure 4.10. *Bifurcation diagram for the HH model. A) V versus I_{app}, the applied current; B) Expanded view of A); C) Frequency as a function of current; D) $(V, n)-$phase plane projection showing 4 different limit cycles.*

Figure 4.10D shows the projection of these limit cycles in the $(V, n)-$plane. Guckenheimer and Oliva (2002) provide convincing numerical evidence for chaotic behavior near this lower current value. The chaos that they compute is *unstable* so that it will not be observed in simulations. For large values of current, the rest-state stabilizes again through a supercritical Hopf bifurcation.

The apparent fact that there is a unique equilibrium point for all I_{app} has never been rigorously proved for the HH equations. At equilibrium, each of the gating variables m, n and h can be written as a function of V so that we find:

$$\begin{aligned} I_{app} = \bar{g}_L(V - E_L) + \bar{g}_{Na} m_\infty^3(V) h_\infty(V)(V - E_{Na}) \\ + \bar{g}_K n_\infty^4(V)(V - E_K) \;\equiv\; F(V). \end{aligned} \tag{4.3}$$

The statement that there is a unique equilibrium is a statement that $F(V)$ is monotone for all V. Since this monotonicity depends very much on the details of the steady-state gate functions, it is not likely that any general theory of the monotonicity of F exists. We leave it as an exercise to show that if $|V|$ is large enough, then there is a unique value of I_{app} for which there exists an equilibrium.

If we assume that the function $F(V)$ is monotone, then it is possible to rigorously prove the existence of the two Hopf bifurcation points. Troy (1979) proved under fairly general assumptions that there are two values of the current I_{app} at which the rest state loses stability at a pair of imaginary eigenvalues. Thus, from the Hopf bifurcation theorem, he was able to conclude that there is a branch of periodic solutions emerging from the fixed points. A rigorous proof of the direction

of the bifurcation remains an open question.

Troy's proof relies on an analysis of the linearized equations and application of Hurwitz' criteria to the characteristic polynomial. We can sketch out some of the details. Troy's assumption that the function $F(V)$ is monotone implies that for each I_{app}, there is a unique V that satisfies (4.3). Furthermore, this implies that there are never any zero eigenvalues of the linear system (see exercise ***). The linearization about the fixed point leads to a matrix with a very special form. It is zero except along the diagonal, across the first row, and down the first column:

$$M = \begin{pmatrix} -F_V & -F_m & -F_h & -F_n \\ m'_\infty/\tau_m & -1/\tau_m & 0 & 0 \\ h'_\infty/\tau_h & 0 & -1/\tau_h & 0 \\ n'_\infty/\tau_n & 0 & 0 & -1/\tau_n \end{pmatrix}.$$

The characteristic polynomial for such matrices (which are called *mammillary* because they resemble a mammal with many suckling babies; here the voltage is the mother and the gates are the babies) is easy to compute and the result is a fourth-order polynomial of the form:

$$P_M(\lambda) = \lambda^4 + a_3\lambda^3 + a_2\lambda^2 + a_1\lambda + a_0.$$

The coefficients are messy, but straightforward to compute. The Hopf bifurcation occurs when there are imaginary roots. The Routh-Hurwitz criterion provides the simplest test for this condition. (see Digression). For a 4th order polynomial, there will be a Hopf bifurcation if $a_0 > 0$, $a_3 > 0$, $a_3a_2 - a_1 > 0$, and $R \equiv a_3a_2a_1 - a_1^2 - a_3^2a_0$ vanishes. Thus, Troy uses assumptions on the shapes of the gating functions to prove that there is a Hopf bifurcation by showing that the quantity R changes sign.

Digression. The Routh Hurwitz Criterion. Consider the polynomial:

$$P(\lambda) = \lambda^n + a_{n-1}\lambda^{n-1} + \ldots a_1\lambda + a_0. \tag{4.4}$$

The Routh-Hurwitz determinants provide a simple way to tell of the real parts of the roots of P are negative. We define $a_n = 1$ and $a_j = 0$ for $j > n$ or for $j < 0$. We will form a series of matrices containing the coefficients a_j:

$$H_1 = a_{n-1}$$
$$H_2 = \begin{bmatrix} a_{n-1} & 1 \\ a_{n-3} & a_{n-2} \end{bmatrix}$$
$$H_3 = \begin{bmatrix} a_{n-1} & 1 & 0 \\ a_{n-3} & a_{n-2} & a_{n-1} \\ a_{n-5} & a_{n-4} & a_{n-2} \end{bmatrix}$$

and so on up to H_n. Each matrix is square and the first column contains every other coefficient, $a_{n-1}, a_{n-3}, \ldots$. The roots of $P(\lambda)$ have negative real parts if an only if $\det H_j > 0$ for $j = 1, \ldots, n$. For example:

$n = 1$. $a_0 > 0$

$n = 2$. $a_0 > 0$ and $a_1 > 0$;

$n = 3$. $a_0 > 0$, $a_2 > 0$, $a_1 a_2 - a_0 > 0$.

$n = 4$. $a_0 > 0$,$a_3 > 0$, $a_3 a_2 - a_1 > 0$, $a_3 a_2 a_1 - a_1^2 - a_3^2 a_0 > 0$.

We note the following:

- det $H_n = a_0 \det H_{n-1}$ so that this means $a_0 > 0$ is necessary. If $a_0 = 0$ then there is a zero eigenvalue.
- If det $H_{n-1} = 0$, $a_0 > 0$ and det $H_j > 0$ for $j < n - 1$, then there are imaginary roots.

These two criteria allow us to determine where possible saddle-node (eigenvalue 0) and Hopf (imaginary eigenvalues) bifurcations occur.

End digression.

4.6 Reduction of the HH model to a 2-variable model

We have seen that two-dimensional models, such as the Morris-Lecar equations, exhibit many important features of the more complicated Hodgkin-Huxley equations. The Morris-Lecar equations generate action potentials, there is a threshold for firing and, depending on parameters, there are several mechanisms for the generation of oscillatory behavior. In this section, we shall describe two ways in which dynamical systems methods have been used to formally reduce the four-dimensional Hodgkin-Huxley model to a two-dimensional system of equations. Reduction methods will be very useful in later sections when we consider networks of neurons.

Rinzel (Federation Proceedings ??) developed a simple method based on two observations. The first is that $\tau_m(V)$, the voltage-dependent time constant for the gating variable m, is much smaller than both τ_h and τ_n. Because τ_m is small, $m(t)$ is very close to $m_\infty(V(t))$. If we replace m by $m_\infty(V)$ in the voltage-equation, then this reduces the HH-model by one equation. The second observation, first observed by Krinskii and Kokoz (1973), is that $(n(t), h(t)$ lies nearly along a line $n = b - rh$ where b and r are constants. Figure 4.11 shows these curves at three different currents. The slope and the intercept depend somewhat on the current, but Rinzel ignored this. Hence, we replace n by $b - rh$ in the voltage-equation and obtain the reduction to a two-dimensional model. We leave the analysis of this model as an exercise.

A common method for comparing parameters which have different units is to render the model in terms of dimensionless variables. Kepler et al (1992) describe a method for comparing the time scales of all the gating variable. Each voltage-dependent gate $x(t)$ satisfies an equation of the form

$$x' = (x_\infty(V) - x)/\tau_x(V).$$

The functions $x_\infty(V)$ are monotonic, so that they are invertible. Thus, Kepler et al introduce a new variable V_x for each gate, where $x(t) = x_\infty(V_x(t))$. They obtain an

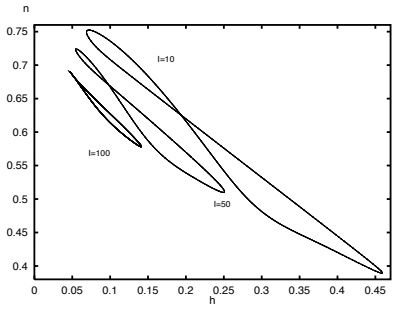

Figure 4.11. *Projection of limit cycles in HH equations in the* $(n, h)-$*plane.*

equivalent dynamical system, but now every variable has the dimensions of voltage. The equivalent potentials satisfy:

$$\frac{dV_x}{dt} = \frac{x_\infty(V) - x_\infty(V_x)}{\tau_x(V)x'_\infty(V_h)}$$

where $x'_\infty(V)$ is the derivative of x_∞ with respect to V. Now, we must simulate the equations in these new variables and this allows us to compare the amplitudes and the time courses of the responses of all the variables. Figure 4.12A shows a plot of the equivalent potentials for the four variable HH equations. From the figure, it looks as if V_m and V have roughly the same temporal dynamics while V_h and V_n have similar time courses. Thus, we create a reduced model by setting $V_m = V$ and $V_n = V_h$. There are two possible reduced models: use the dynamics of V_h and set $n = n_\infty(V_h)$ or use the dynamics of V_n and set $h = h_\infty(V_n)$. We leave the latter case to the reader and consider the (V, V_h)-system.

The two-dimensional (V, V_h)-system has the following form:

$$C\frac{dV}{dt} = I_{app} - g_{Na}m^3_\infty(V)h_\infty(V_h)(V - E_{Na}) - g_K n^4_\infty(V_h)(V - E_K) - g_L(V - E_L)$$
$$\frac{dV_h}{dt} = \frac{h_\infty(V) - h_\infty(V_h)}{\bar{\tau}_h(V, V_h)}$$

where $\bar{\tau}_h$ is the effective time constant, $\tau_h(V)h'_\infty(V_h)$. Figure 4.12B shows the bifurcation diagram for the reduced system. It cannot have any more fixed points than the full system since both have identical equilibria. There is a subcritical Hopf bifurcation at roughly $I_{app} = 6.8$ which is slightly lower than that for the original HH equations. What is strikingly different is that the reduced model continues to oscillate at an extremely large applied current. The second Hopf bifurcation does not occur until $I_{app} = 267$, much higher than the original 4-variable system. The phase-plane is shown for $I_{app} = 0$ in Figure 4.12C. A convenient aspect of the equivalent potential method is that the V_h-nullcline is just $V = V_h$. The $V-$nullcline

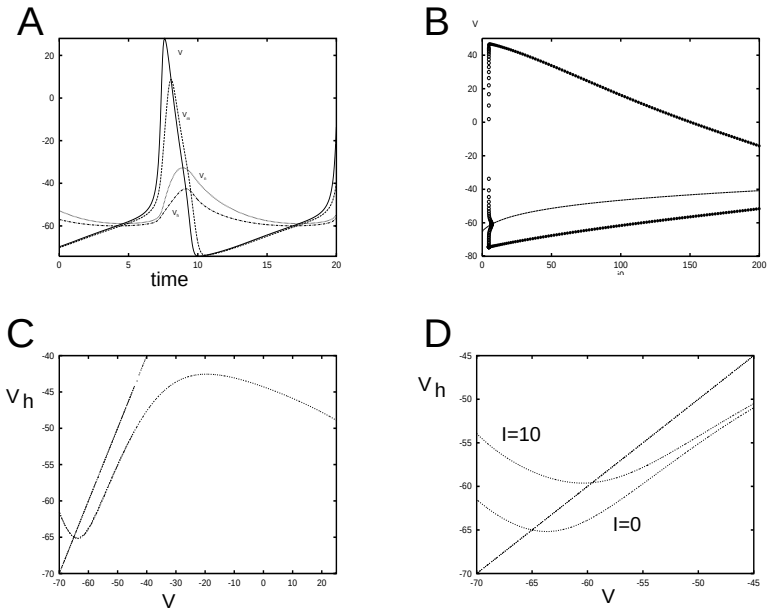

Figure 4.12. *Equivalent potentials for the Hodgkin-Huxley model. (A) the voltages of the 4 variables; (B) Bifurcation diagram for $(V, V_h)-$system; (C) Phase plane at rest; (D) Phase-plane showing how the fixed point moves to the middle branch as I_{app} increases.*

has a cubic form which is typical in many neural models and absolutely necessary in order to get oscillations.

4.7 Fitzhugh-Nagumo equations

The simplified (V, n) version of the Hodgkin-Huxley equations and the Morris-Lecar equations both share a common feature in so far as their nullclines are concerned. The $V-$nullcline has a cubic shape, while the recovery nullcline is a monotonically increasing function of the the voltage. In 1961 Dick Fitzhugh (Biophysical Journal 1) developed a simplified model which captures the essence of the cubic nature of the V-nullcline and has many of the properties of the more complicated models that we have already discussed. Because of its pivotal importance in the literature (particularly, the mathematical literature), we discuss it briefly at this point. We leave as an exercise, the numerical and qualitative analysis of these equations. The equations have the form:

$$\frac{dV}{dt} = V(V-a)(1-V) - w + I \tag{4.5}$$

$$\frac{dw}{dt} = \epsilon(V - \gamma w) \tag{4.6}$$

where $0 < a < 1$, $\epsilon > 0$ and $\gamma \geq 0$. The actual model is based on a modification of the van der Pol equation:

$$C\frac{dV}{dt} + F(V) + J = 0$$
$$L\frac{dJ}{dt} = V.$$

The van der Pol equation arises from an electrical circuit with a linear capacitor, linear inductor, and nonlinear resistor in parallel. C is the capacitance, L the inductance, $F(V)$ is a nonlinear current depending on the voltage, V, across the capacitor and J the current through the inductor. By adding a driving current and the additional $-\gamma w$, Fitzhugh created a model for the action potential. At about the same time, Nagumo and colleagues developed a similar model.

The FHN equation has been used to model many physiological systems from nerve to heart to muscle and is a favorite model for the study of excitability. In most applications, ϵ is small so that the recovery variable is much slower than the voltage. When $I = 0$ and γ is small enough there is a unique fixed point at the origin. As I increases, this fixed point becomes unstable through a Hopf bifurcation and a limit cycle emerges. We will provide an extensive exercise below for examining the behavior of this popular and much studied model.

4.8 Bibliography

An excellent reference for an introduction to dynamical systems is Strogatz [48]. More advanced textbooks include Guckenheier and Holmes [20], Perko [38] and Kuznetsov [**?**]. FitzHugh [17] was perhaps the first to use phase plane analysis to study the Hodgkin-Huxley and reduced models. Much of the analysis in this chapter builds on the paper by Rinzel and Ermentrout [43] who carefully described geometric methods, including phase planes and bifurcation theory, applied to reduced neuronal models. They also recognized the relationship between Class I and Class II excitability and the geometric properties of different types of bifurcations. Izhikevich [24] covers most of the material described in this chapter, but in more detail.

4.8.1 Exercises

There are a number of exercises about simplified neural models which are popular in the literature. Rather than discuss these in the text, we have chosen to leave them as an extended set of exercises. In later chapters, we will refer to these models and their properties. Thus, it would be a good idea to do those related to the leaky integrate and fire and quadratic integrate and fire models.

1. Show that the gating functions used by Morris and Lecar are derived from the Boltzman model.

2. Near rest, potential of the ML system can be approximated by its linearization:

$$C\frac{dV}{dt} = I(t) - aC(V - V_r)$$

where a is as computed above. Suppose that I is a square pulse of current with duration T and magnitude I_0. Estimate the value of I_0 needed to evoke an action potential assuming that one will occur if V crosses V_t (see figure 4.3.) Sketch the critical value I_0 as a function of T. This is called the *Strength-Duration Curve.* The minimum strength needed to elicit a response is called the *rheobase* and the stimulus duration needed to elicit an action potential when the stimulus is twice the strength of the rheobase is called the *Chronaxie.* Now you can drop terms with old time physiologists! Compute the rheobase and chronaxie using this estimate. Numerically determine them as well.

3. Simulate the ML model with the homoclinic parameters and $I = 36$ corresponding the phase-plane in figure 4.8C.(a) Starting at rest, give a 5 msec current pulse sufficient to produce a single spike. Weaken the current pulse to perturb the model to the stable limit cycle. (b) Set $I = 38$. This corresponds to the vertical line in figure 4.7B where there is tristability. Starting at rest, is it possible to inject a single pulse of current to get the system to go from the lower rest state to the upper rest state? If not, figure out a stimulation sequence that will let you go from rest to the upper state.

4. (Exploring the FHN model I.) The fixed points of this model satisfy $w = V/\gamma$ and $I = V/\gamma - V(V - a)(1 - V) \equiv h(V)$. The latter is a cubic. It can have at most three roots. Differentiating $h(V)$ and setting this to zero allows us to find local maxima and minima. (a) Find these as a function of a, γ. Show that $\gamma > 3/(1 - a + a^2) \equiv \gamma^*(a)$ in order for such extrema to exist. Next, set V to these roots and use this to find values of I where there are saddle-node bifurcations. This summarizes the steady state behavior of the model. (b) Consider the case when $\gamma < \gamma^*(a)$ so that there is only a single root. Since there is one root, there can be no bifurcation at a zero eigenvalue as I varies. Thus, the only way to lose stability is a Hopf bifurcation. Show that the trace of the linearization is

$$T = -3V^2 + (2 + a)V - a - \epsilon.$$

Show that there are two values of V such that the trace vanishes as long as $3\epsilon < a^2 - a + 1$. These correspond to two distinct values of current ($I = h(V)$) at which there is a Hopf bifurcation.

5. (Exploring the FHN model II.) (a) Choose $\epsilon = .02$ and $\gamma = 1$, and $a = 0.1$. For $I = 0$ show that the system is excitable – that is show that there is an action potential if the voltage is taken sufficiently past threshold. (b) Compute the bifurcation diagram and look at the frequency-current plot. Notice that the bifurcation is nearly vertical. Compute several limit cycles along the nearly vertical branch. Notice how they hug the middle branch of the nullcline. This

is an example of a phenomena called a *canard* and is common in systems with a small parameter (eg ϵ.)

6. (The integrate and fire model.) A classic approximation for the firing of a cell is the leaky integrate and fire model (Lapique,???). This model has the form:

$$\tau \frac{dV}{dt} = -(V - V_r) + R_m I \tag{4.7}$$

where R_m is the membrane resistance, τ the time constant, and V_r, the resting potential. In addition to this linear equation, there is a nonlinear reset condition. If $V(t^-) = V_{spike}$ then an action potential occurs and $V(t)$ is reset to V_{reset}. In many cases, an additional condition is imposed in which V is prevented from firing for a period, T_{ref}, the "refractory" period. Assume that $V_r < V_{spike}$ and $V_{reset} < V_{spike}$. Find the critical value of I, I_{min} under which the LIF fires repetitively. Compute the $F - I$ curve; the firing rate as a function of the applied current for $I > I_{min}$. Show that for large values of I, the firing rate is linear with respect to I when $T_{ref} = 0$.

7. (Spike-response model.) Consider the leaky integrate and fire model with a time-dependent current, $I(t)$:

$$\tau \frac{dV}{dt} = I(t) - V(t) - A \sum_j \delta(t - t_j)$$

where $A = \tau(V_{spike} - V_{reset})$. We have formally included the reset into the equations by adding the delta function term. The values, t_j are the times for which $V(t)$ crosses V_{spike} from below; that is, the spike-times. Integrate this equation to convert it to the following form:

$$V(t) = V(0)e^{-t/\tau} + \sum_j \eta(t - t_j) + \int_0^t k(t - s)I(s)\ ds$$

where

$$\eta(t) = \text{Heaviside}(t)(V_{reset} - V_{spike})e^{-t/\tau}$$

and

$$k(t) = \frac{1}{\tau} e^{-t/\tau}.$$

Gerstner and collaborators consider classes of models like this where η takes a more general form. These models are called *spike response models.* For example, $\eta(t)$ could include an additional spike frequency adaptation term, eg:

$$\eta(t) = \text{Heaviside}(t)[k_1 e^{-t/\tau} + k_2 e^{-t/\tau_a}].$$

Unfortunately, once these extra terms are added, it becomes difficult to compute even the steady state firing rate. Later on in the book, we will use this formulation to compute the velocity of waves in networks of coupled integrate-and-fire models.

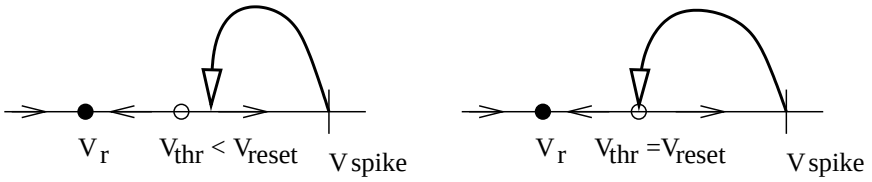

8. In the ML model with class I dynamics (the saddle-node), the potential near the bifurcation satisfies the following differential equation:

$$\frac{dV}{dt} = a(I - I_{SN}) + b(V - V_{SN})^2 \tag{4.8}$$

where a, b are positive numbers that can be determined from the actual dynamics (see Kuznetsov,2002). (What are the physical dimensions of a, b?) This is called the **quadratic integrate and fire** model or QIF. (a) By integrating this equation, show that V can go to infinity in finite time. When $V(t)$ goes to infinity, we say that a spike has been generated. (b) Suppose that $I < I_{SN}$ and find the fixed points for this, V_{rest} and V_{thr} corresponding to the stable and unstable fixed points respectively. Suppose $V(0) > V_{thr}$. Compute the time to spike as a function of $V(0) - V_{thr}$. (c) Show that if $I > I_{SN}$, then $V(t)$ goes to infinity no matter what the initial condition. In particular, compute the time it takes to reach infinity if $V(0) = -\infty$. (d) Let

$$V(t) = V_{SN} + \frac{c}{b}\tan(\theta/2).$$

where c^{-1} has dimensions of time. Show that $\theta(t)$ satisfies:

$$\frac{d\theta}{dt} = c(1 - \cos\theta) + \frac{ab}{c}(1 + \cos\theta)[I - I_{SN}]. \tag{4.9}$$

This is called the **theta model.** Kopell and Ermentrout (1986) showed that this was the normal form for a system near a saddle-node limit cycle bifurcation. Sketch the phase-line for this of $I < I_{SN}$, $I = I_{SN}$ and $I > I_{SN}$. Compute the $F - I$ curve when $c = 1$.

9. A variant of the QIF model truncates the spike and the reset. Latham first suggested the model:

$$\tau\frac{dV}{dt} = a(V - V_r)(V - V_{thr}) + R_m I \tag{4.10}$$

with the condition that if $V(t) = V_{spike} > V_{thr}$ then $V(t)$ is reset to V_{reset}. When $I = 0$, V_r is the resting state and V_{thr} is the threshold. If $V(0) > V_{thr}$, then the model will spike. (a) Compute the FI curve for this model . Note that it is somewhat different from the QIF in equation (4.8) due to the finite reset.

(b) Suppose that $V_{reset} > V_{thr}$. Then this model is bistable for $I = 0$ or I sufficiently small and has a fixed point near V_r and a periodic solution. As $V_{reset} \to V_{thr}^+$, the period goes to infinity and this model has the equivalent of a homoclinic orbit. (See the figure above.) Compute the period as a function of $V_{reset} - V_{thr}$. (c) Now suppose that $V_r < V_{reset} < V_{thr}$. As I increases, either the stable rest state will reach V_{reset} from below or the unstable fixed point will reach V_{reset} from above and form a homoclinic. Find conditions for the latter scenario and sketch the bifurcation diagram as I varies. Compare this to the diagram for the Morris-Lecar model in parameter set 3. From this exercise, it should be clear that the QIF model has much richer dynamics that the LIF precisely because it has a true spiking threshold which is different from the value of the actual spike.

10. Karbowski and Kopell introduce a linear model:

$$\tau \frac{dV}{dt} = R_m I + a|V| \tag{4.11}$$

where $a > 0$ is parameter. (a) Show that this is qualitatively like equation (4.10). How does the firing rate scale near $I = 0$? (b) One can define a class of scalar neural models by considering

$$\tau \frac{dV}{dt} = R_m I + f(V).$$

Suppose that $f(V) = |V|^p$ where $p > 1$. The model spikes when $V(t)$ reaches infinity in which case the neuron is reset to negative infinity. What is the firing rate of such a neuron for I large? That is how does it scale with p. For example, we know that when $p = 2$, the firing rate scales like the square root of I.

11. A class of models related to the theta model are called *ring* models (Winfree, 1980; Ermentrout and Rinzel 1984). These are models for excitable activity which lie on the unit circle:

$$\frac{dx}{dt} = f(x) + I$$

where $f(x + 2\pi) = f(x)$ is a bounded periodic function. For certain ranges of I, the system has two fixed points a saddle and a node. The saddle point acts as a threshold. Since $f(x)$ is bounded, for I large enough, there are periodic solutions to the equation and thus there is repetitive firing. Suppose that $f(x)$ is $C^2[0, 2\pi)$ and periodic. Write an expression for the period of the oscillations when there is repetitive firing. Discuss the mechanism from going from a stable rest state to repetitive firing. Can there ever be bistability?

12. Fourcaud et al have introduced the exponential integrate and fire model:

$$C \frac{dV}{dt} = -g_L(V - V_L) + a \exp(bV) + I.$$

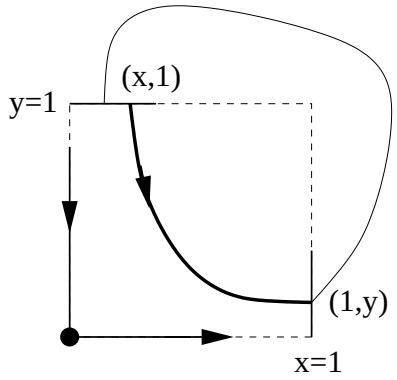

Set $g_L = 0$ and assume a, b, C are positive. Find an expression for the firing rate as a function of I.

13. (Period near a homoclinic.) This is actually an exercise in dynamical systems, but is instructive in that it does show the period of the homoclinic orbit. Assume the origin is a saddle point and the y-axis is the stable manifold with a decay rate of $-\mu$ and the $x-$axis is the unstable manifold with a decay rate of ν. Assume that $\mu > \nu$. Consider a point $(1, y)$ on the little interval at $x = 1$. This gets mapped into the little interval at $y = 1$, via $(1, y) \to (ay + b, 1)$. The parameter a is positive and won't really matter. The parameter b is the distance from the homoclinic orbit. Note that if $b = 0$, then $(1, 0) \to (0, 1)$ is the homoclinic orbit. Starting at $(x_0, 1)$, we follow the linear dynamics

$$x' = \nu x \quad y' = -\mu y.$$

This maps the $y = 1$ interval onto the $x = 1$ interval. Thus, we get a map from $(1, y_{old}) \to (1, y_{new})$. (a) Show that the map of the y values is:

$$y_{new} = (a y_{old} + b)^r$$

where $r = \mu/\nu > 1$. For b sufficiently small, show that $y = b^r + o(b^r)$ is a fixed point. Show that the fixed point is stable. (b) Since the map from $x = 1$ to $y = 1$ is instant, the period is the time it takes to go from $y = 1$ to $x = 1$. Show that at the fixed point

$$T \sim -\frac{1}{\nu} \log b.$$

(Note: this relies on the fact that $r > 1$. If $r < 1$, then the fixed point will be unstable and so the periodic orbit will also be unstable.)

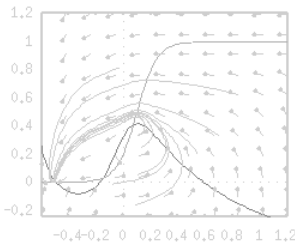

Chapter 5

On the variety of channels.

In the last several chapters, we have discussed several types of active (voltage-gated) channels for specific neuron models. The Hodgkin-Huxley model for the squid axon consisted of three different ion channels: a passive leak, a transient sodium channel, and the delayed rectifier potassium channel. Similarly, the Morris-Lecar model has a delayed rectifier and a simple calcium channel (with no dynamics). Hodgkin and Huxley were smart and supremely lucky that they used the squid axon as a model to analyze the action potential, as it turns out that most neurons have dozens of different ion channels. In this chapter, we briefly describe a number of them, provide some instances of their formulas and describe how they influence a cell's firing properties. The reader who is interested in finding other channels and other models for these channels should consult **http://senselab.med.yale.edu/modeldb/default.asp** which is a database for neural models.

5.1 Channels, channels, channels.

We briefly describe various ion channels in this section. Most of the voltage-gated channels follow the usual formulation that the delayed rectifier, the calcium model, and the transient sodium current we have already discussed. However, there are several important channels which are gated by the internal calcium concentration so that we will describe some simple models for intracellular calcium handling.

All of the channels that we describe below follow the classic HH formulation. The total current due to the channel is

$$I_{channel} = m^p h^q I_{drive}(V)$$

where m and h are dynamic variables lying between 0 and 1, p and q are non-negative integers, and V is the membrane potential. Thus, the channel current is maximal when m and h are both 1. By convention, h will generally inactivate (get smaller) with higher potentials of the cell and m will activate. Not all channels have both activation and inactivation. For example, the Hodgkin-Huxley potassium channel,

and both the Morris-Lecar calcium and potassium channels have no inactivation. The Hodgkin-Huxley sodium channel has both activation and inactivation.

The drive current generally takes two possible forms corresponding to the linear model or the constant field model respectively:

$$I_{lin} = g_{max}(V - V_{rev}) \tag{5.1}$$

and

$$I_{cfe} = P_{max}\frac{z^2F^2}{RT}V\left(\frac{[C]_{in} - [C]_{out}e^{\frac{-zVF}{RT}}}{1 - e^{\frac{-zVF}{RT}}}\right). \tag{5.2}$$

The constant g_{max} has units of siemens per square centimeter and the constant P_{max} has units of centimeters per second so that the driving current has dimensions of amperes per square centimeter.

The gates, m and h generally satisfy equations of the form:

$$\frac{dx}{dt} = a_x(1 - x) - b_x x$$

or

$$\frac{dx}{dt} = (x_\infty - x)/\tau_x$$

where the quantities a_x, b_x, x_∞ and τ_x depend on voltage or some other quantities. The functional forms of these equations often take one of the following three forms:

$$F_e(V, A, B, C) = Ae^{(V-B)/C}$$
$$F_l(V, A, B, C) = A\frac{(V - B)}{1 - e^{(V-B)/C}}$$
$$F_h(V, A, B, C) = A/(1 + e^{-(V-B)/C}).$$

Generally speaking, most of the voltage gated ion channels can be fit with functions of the form

$$x_\infty(V) = \frac{1}{1 + e^{(V-V_T)/k}} \tag{5.3}$$

and

$$\tau_x(V) = \tau_{min} + \tau_{amp}/\cosh\frac{V - V_{max}}{\sigma}. \tag{5.4}$$

5.1.1 Sodium channels

Roughly speaking, there are two types of sodium currents: the transient or fast sodium current and the persistent or slow sodium current. We have already described the former when we discussed the Hodgkin-Huxley model. The fast sodium current is found in the soma and axon hillocks of many neurons. The persistent sodium current (which activates rapidly; the "slow" in its name refers to inactivation) has been implicated as underlying both sub- and suprathreshold firing in many neurons by adding a small depolarizing current which keeps them active.

As an example of the utility of the persistent sodium we will introduce a simple model of the Pre-Botzinger complex, a group of neurons responsible for generating

the respiratory pacemaker oscillations in the brainstem. (That is, these are the cells that make us breathe.) Here the persistent sodium and its inactivation play a crucial role in generating the pacemaker potential for the oscillation. The model has the form:

$$\begin{aligned} C_m\frac{dV}{dt} &= -g_L(V-E_L) - g_K n^4(V-E_K) - g_{Na}m_\infty(V)^3(1-n)(V-E_{Na}) \\ &\quad - g_{Nap}w_\infty(V)h(V-E_{Na}) \\ \frac{dn}{dt} &= (n_\infty(V)-n)/\tau_n(V) \\ \frac{dh}{dt} &= (h_\infty(V)-h)/\tau_h(V) \end{aligned}$$

In the appendix, we provide all the exact values for the parameters and the functions. Note that for the fast sodium, the inactivation has been replaced by $1-n$ as in the Rinzel reduction of the HH equations. The variable h now corresponds to inactivation of the persistent sodium channel. The key feature in this model is that the inactivation of the persistent sodium has a time constant of ten seconds. Figure 5.1A shows a simulation of this model for 40 seconds. The voltage oscillates at a period of about 6 seconds which is commensurate with the 10 second time constant for inactivation of the persistent sodium channel. In a later chapter (on bursting), we will explore the role of the persistent sodium channel in producing the bursts. Here, we restrict our discussion to the pacemaker duties of the persistent sodium channel.

Butera etal showed that one of the key parameters in inducing the bursting is the leak potential E_L. If $E_L = -65$ mV, then the system stable resting behavior. By shifting this parameter from -65 mV to -60 mV, they obtained the pattern shown in Figure 5.1A. If we block the transient sodium by setting $g_{Na} = 0$, then we can see look at the bifurcation diagram of the "spikeless" model as a function of E_L. Figure 5.1B shows the voltage as a function of the leak current. There are two Hopf bifurcations: a subcritical bifurcation at about -60 mV and a supercritical bifurcation at about -54 mV. Thus, for a range of leak potentials there is a slow pacemaker potential. We can further understand this by noting that the variable h is much slower than (V, n). If we set $n = n_\infty(V)$, then this leads to a two-dimensional system in (V, h), the phaseplane of which we show in Figure 5.1C. At $E_L = -62$mV, there is a single stable fixed point. As E_L increases, the $V-$nullcline moves down and intersects the h nullcline in the middle branch. Since h is very slow, this leads to a relaxation oscillation shown in the phaseplane and in Figure 5.1D. The period of the pacemaker potential is about twice that of the full model (in Figure 5.1A). This is because the spikes produced by the full model cause more inactivation of the persistent sodium.

5.1.2 Calcium channels

Calcium channels are quite similar to sodium channels both in their form, function, and dynamics. However, because the concentration of calcium in the cell is very low (e.g. on the order of 10^{-8} M), the small amount of calcium coming into the cell

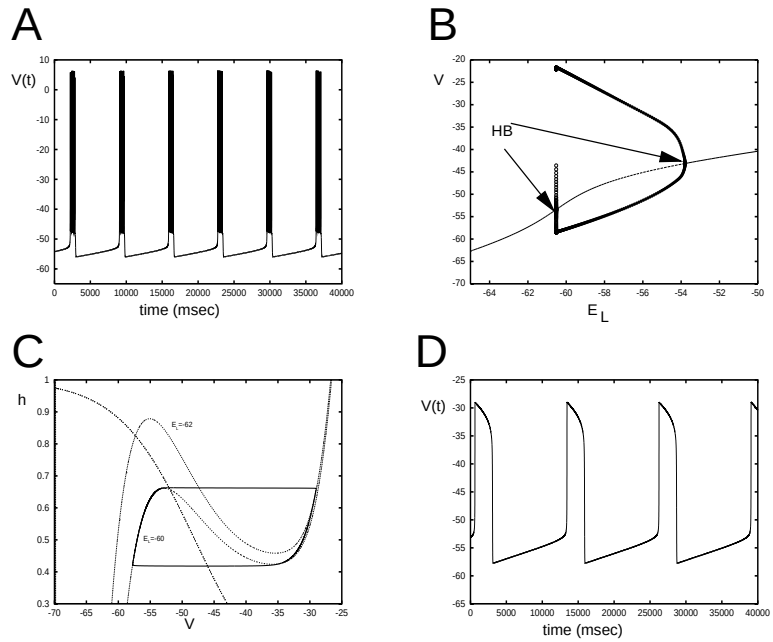

Figure 5.1. *Persistent sodium provides the pacemaker current for the model Pre-Botzinger cell. (A) Potential with $E_L = -60$ mV for the full bursting model. (B) Bifurcation diagram with fast sodium blocked showing onset of pacemaker oscillations at the Hopf bifurcation. (C) Phaseplane with $n = n_\infty(V)$ showing relaxation oscillation. (D) Potential of the simple relaxation model.*

from the channel opening can drastically alter the driving potential. Thus, many modelers (but no theoreticians!) use the constant field equation (5.2) rather than the simple ohmic drive (5.1). Using the CFE model requires an extra equation for the intracellular calcium concentration, but this is often ignored. The CFE just adds a nonlinearity to the current with little effect on the dynamics.

We can divide calcium channels into roughly two classes (although experimentalists describe many more): (i) $T-$type calcium currents $I_{Ca,T}$ which are low-threshold but inactivate and (ii) $L-$type calcium currents $I_{Ca,L}$ which have a high threshold and do not inactivate. $I_{Ca,T}$ is fast and both the activation and inactivation are voltage-dependent. This current is responsible for bursting in many neurons, particularly in the thalamus where it plays the dominant role in producing oscillatory activity during sleep. $I_{Ca,L}$ is responsible for spikes in some cells (such as the Morris Lecar model). It does in fact inactivate, but the inactivation is calcium- rather than voltage-dependent.

The $T-$current has some interesting properties such as the ability to produce rebound bursts and subthreshold oscillations. Let's see some of these features. We will look at a simple model in which the spiking currents (sodium and potassium)

are blocked so that all that is left is the T current and the leak:

$$\begin{aligned} C\frac{dV}{dt} &= I_0 - g_L(V - E_L) - I_T \\ \frac{dh}{dt} &= (h_\infty(V) - h)/\tau_h(V) \\ I_T &= m_\infty(V)^2 h I_{cfe}(V, [Ca]_o, [Ca]_i) \\ m_\infty(V) &= 1/(1 + \exp(-(V + 59)/6.2)) \\ h_\infty(V) &= 1/(1 + \exp((V + 83)/4)) \\ \tau_h(V) &= 22.7 + 0.27/(\exp((V + 48)/4) + \exp(-(V + 407)/50)). \end{aligned} \tag{5.5}$$

In order to simplify the analysis of this model, we have set the activation variable m to its steady state $m_\infty(V)$. Full parameters for the model are in the appendix. What sets the behavior for this model is the resting potential. Various neural modulators (chemicals which alter the behavior of neurons in a quasi-constant manner) set the resting potential from either relatively depolarized at, say, -60 mV to relatively hyperpolarized at -80 mV. The inactivation h has a half-activation at -83 mV in the present model so that if the resting potential is -60 mV, then $h \approx 0$. This means that no amount of depolarizing current can activate the current. In the sensory literature, when the thalamic neurons are depolarized like this, the network is said to be in "relay" mode. Inputs to the thalamus are transmitted as if the cell was just a nonlinear spiker like we have already encountered. However, if the network is hyperpolarized, then inactivation of the T-current, h, will be much larger and a subsequent stimulus will lead to an explosive discharge of the neuron.

Suppose that the leak is set so that the resting potential is around 60 mV. Figure 5.2A shows the response of the model to brief depolarizing and hyperpolarizing pulses. At -60 mV, the T-current is completely inactivated so that the response to depolarizing pulses is the same as if the current was not there. In this simplified model, the result is a passive rise in voltage followed by a passive decay. However, if the same membrane is provided with a brief and strong hyperpolarizing stimulus, it responds with a calcium action potential when released from the stimulus. This is called *rebound* and is a classic property of cells with a T-type calcium current. Figure 5.2B provides a geometric explanation for rebound. At rest, the membrane sits at the lower right fixed point. At this point $h \approx 0$. A hyperpolarizing input moves the V nullcline upward; if the hyperpolarization is maintained, the trajectory will move towards the new fixed point (upper left circle.) If, instead, the hyperpolarization is transient, then when the stimulus is removed, the V-nullcline moves to its original position. Since h is slow compared to V, the potential will rapidly move horizontally to reach the right-branch of the $V-$nullcline leading to the calcium spike.

In contrast, consider the the system when the leak is -80 mv. Then the rest state is about -78 mV and the T-current inactivation, h, is no longer negligible. Figure 5.2C shows that a small depolarizing input is now sufficient to elicit an action potential. Similarly, a small hyperpolarizing input will also result in the firing of an action potential. Figure 5.2D provides an explanation for why depolarization will work in this case. Depolarizing lowers the $V-$nullcline allowing the trajectory to

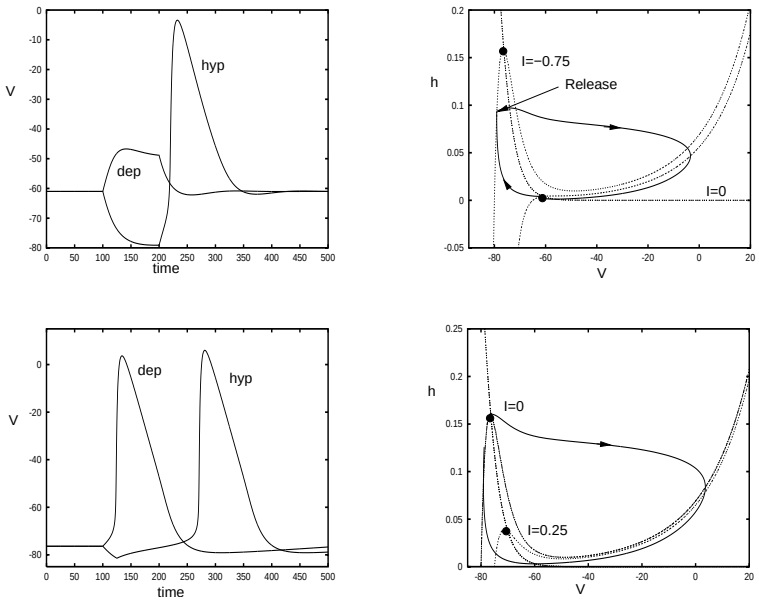

Figure 5.2. *Properties of the T-type calcium current.*

jump to the right branch of the nullcline and produce a spike.

The T-current also provides a mechanism for subthreshold calcium oscillations which can be pacemakers for bursting like the persistent sodium current. In exercise *, you are asked to find these oscillations and give a geometric explanation for them.

5.1.3 Voltage-gated potassium channels.

There is no doubt that the greatest variety of channels is found in those which involve potassium. We have already seen the workhorse for spiking, the delayed rectifier, in the Hodgkin-Huxley model, the Butera model of the Pre-Botzinger complex, and the Morris-Lecar model. The delayed rectifier is rather fast and has only an activation gate. Potassium channels provide the main repolarizing force for nerve cells. If they are fast, then the cell are allowed to rapidly repolarize so that very fast spike rates are possible. If they are slow, they cause the spike rate to slow down with sustained depolarization, an important form of adaptation. In addition to the voltage-gated potassium channels which we describe here, there are also calcium-gated potassium channels which perform similar roles.

A-current

The Hodgkin-Huxley model was based on a quantitative analysis of the squid axon. In 1971, Connor and Stevens introduced an alternative model for action potentials

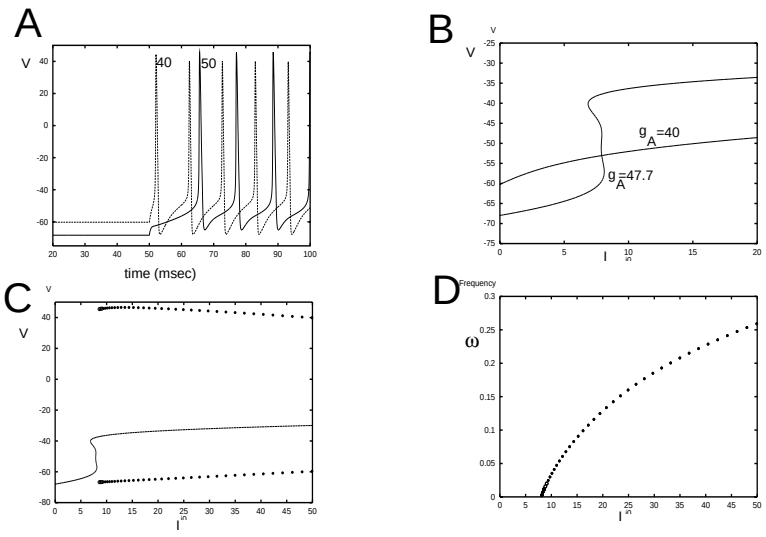

Figure 5.3. *Connor-Stevens model. (A) Delay to spiking depends on the A-current. Dashed curve shows* $g_K = 27.7, g_A = 40$ *and solid curve shows* $g_K = 17.7, g_A = 50$. *(B) Steady-state I-V curve with two different amounts of A-current. (C) Full bifurcation diagram for the CS model with default parameters. (D) Frequency-current curve for the CS model showing class I behavior.*

in the axons of crab legs. The transient sodium and delayed rectifier were similar to those in the HH model although they were faster. In addition, Connor and Stevens introduced a transient potassium current, the *A-current.* Like the transient sodium current, this current has both an activation and an inactivation gate:

$$I_A = g_A a^3 b (V - E_A).$$

The reversal potential E_A is close to that of the delayed rectifier. The activation variable a increases with voltage while the inactivation variable b decreases; $b_\infty(V)$ has a half-activation at about -78 mV. (The full Connor-Stevens model (CS) is given in the appendix.) One consequence of having this current is that it induces a delay to spiking when the cell is relatively hyperpolarized. Intuitively, the reason for this is that when the cell is somewhat hyperpolarized, b will be large. Depolarization engages a and thus there will be a large potassium current. However, when the membrane is depolarized, $b_\infty(V)$ will be small so that b will decrease leading to a gradual loss of the A-current. The neuron will spike only when this current is sufficiently small. Thus, the A-current causes a delay to spiking. Figure 5.3A shows an example of the delay to spiking due to the A current.

One of the most interesting dynamic consequences of the A-current in the Conner Stevens model is that it converts the transition to repetitive firing from class II (like the Hodgkin-Huxley model) to class I. Recall that for a class II neuron, the transition from resting behavior to oscillations if via a Hopf bifurcation;

moreover, the steady-state voltage-current (I-V) relationship is monotonic. For a class I neuron, the transition to oscillations is via a SNIC bifurcation and the I-V relationship is non-monotonic.

The A-current provides a means to make the I-V relationship non-monotonic since the steady state current,

$$I_{A,ss} = g_A a_\infty(V)^3 b_\infty(V)(V - E_A),$$

is nearly zero. Thus, if the majority of the potassium current is A-type rather than the delayed rectifier current, then the steady-state I-V curve will be dominated by the sodium current.

In order to explore this idea in more detail, we consider the CS model keeping the maximal total potassium conductance constant: $g_A + g_K = g_{total} = 67.7$. The choice of 67.7 for the total is so that the CS model is our default, $g_K = 20$ and $g_A = 47.7$. Figure 5.3B shows the steady state I-V curve for the standard CS parameters and also for when the A-current is reduced to 40 while the delayed rectifier is increased to 27.7. It is clear that the I-V curve is monotonic with the reduced A-current so that class I (SNIC) dynamics is impossible. Figure 5.3C shows the bifurcation diagram for the standard CS model as current is injected. A branch of periodic orbits emerges at high applied currents at a supercritical Hopf bifurcation (not shown). This branch terminates via a SNIC on the steady-state IV curve. The frequency is shown in Figure 5.3D and as predicted by the general theory has a square-root shape and vanishes at the critical current. We point out that the steady-state I-V curve in the standard parameter regime is not a simple "cubic" as the in the Morris-Lecar model. Rather, there are currents where there appear five fixed points. Rush and Rinzel (1995) were the first to notice this. The phenomena occurs over a very narrow range of values of g_A. In exercise * below, you are asked to explore the behavior of the system with slightly different values of g_A.

5.1.4 M-current.

There are several slow potassium currents which are responsible for a phenomenon known as spike frequency adaptation (SFA). That is, this slow low-threshold outward current gradually reduces the firing rate of a neuron which has been depolarized sufficiently to cause repetitive firing. The M-current and related slow potassium currents are able to stop neurons from firing if they are strong enough and thus can provide an effective brake to run-away excitation in networks.

Figure 5.4 shows an example of SFA in a simple cortical neuron model due to Destexhe and Pare (1999). The left-hand figure shows the voltage as a function of time when the current is instantaneously increased to 6 $\mu A/cm^2$. The initial interspike interval (ISI) is short but over time this lengthens. Figure 5.4B shows the instantaneous frequency (reciprocal of the ISI) as a function of spike number. The frequency drops from 130 Hz to 65 Hz over about a second of time.

The M-current does far more than just slow down the spike rate. Because it is active at rest (the threshold is -30 mV), the M-current can have profound effects on the steady state behavior. Figure 5.5A shows the bifurcation diagram of steady

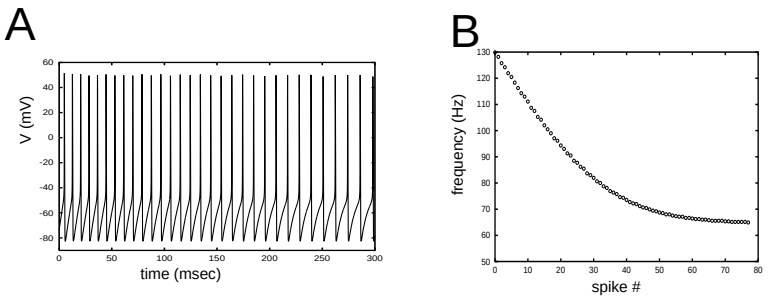

Figure 5.4. *Spike frequency adaptation from the M-type potassium current. The model is from Destexhe and Pare (1999) and represents a cortical pyramidal neuron. Applied current is 6 $\mu A/cm^2$ and $g_M = 2mS/cm^2$. (A) Voltage and (B) instantaneous frequency versus spike number.*

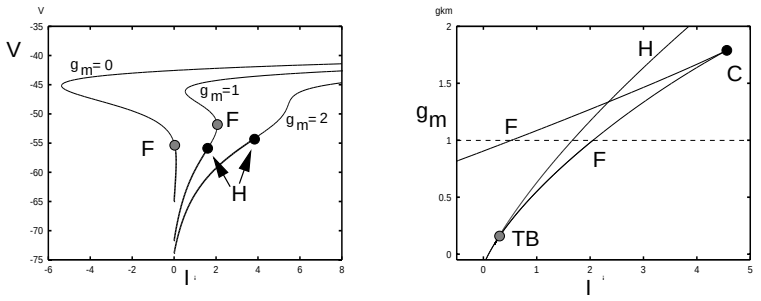

Figure 5.5. *Effects of M-current on equilibria. (A) Steady state as a function of current at three values of g_m. With no M-current, the neuron is class I and oscillations are borne via a SNIC along the fold curve F. With large enough M-current ($g_m = 2$), oscillations are borne via a Hopf (H) bifurcation and the fold points no longer exist since there is a unique equilibrium point. For intermediate values, the folds still exist, but the Hopf bifurcation occurs on the lower branch of fixed points. (B) Two-parameter diagram. The two fold curves (F) meet at a cusp point (C) at near $I = 4.8$ and $g_m = 1.8$. There is a curve of Hopf points (H) which terminates at a Takens-Bogdanov (TB) point when the Hopf curve meets a fold curve. Dashed line corresponds to $g_m = 1$; as I increases, there is first a Hopf point and then the fold. At $g_m = 0$, no Hopf is encountered and when $g_m = 2$, there are no folds.*

states as the conductance of the M-current (g_m) is increased. With no M-current, the model has a SNIC bifurcation to a limit cycle so that it is a class I membrane. For larger values of g_m (Destexhe and Pare used $2 < g_m < 5$) the rest state loses stability at a Hopf bifurcation so that the membrane is class II. The transition from class I to class II occurs for $g_m = 1$ where the fold points (saddle-nodes) remain but

the lower branch of fixed points loses stability at a Hopf bifurcation. Figure 5.5 B shows a two-parameter bifurcation diagram of this system where the applied current and g_m vary. As g_m increases, the two fold-points merge at a cusp point (labeled C) and for g_m larger, there is only a single fixed point. Additionally, there is a curve of Hopf points which terminates on the right-most fold point at a Takens-Bogdanov (TB) point. In some sense, the TB point marks the transition from class I to class II excitability. The global picture is complex. For example, when $g_m = 0$, there is a single branch of periodic solutions terminating at the fold point via a SNIC. However, when $g_m = 1$, a branch of periodic solutions must bifurcate from the Hopf. This branch must somehow either merge with the SNIC branch or disappear. The interested reader could attempt to put together a plausible global picture as a project.

5.1.5 The inward rectifier.

The inward rectifier is hyperpolarization activated. That is, if the neuron is hyperpolarized enough, the current is activated, further hyperpolarizing the model. This implies the possibility for bistability in the hyperpolarizing direction. The current has the form:

$$I_{Kir} = g_{Kir} h(V)(V - E_K)$$

where

$$h(V) = 1/(1 + \exp((V - V_{th})/k)).$$

Typical values for the parameters are $V_{th} = -85$ mV and $k = 5$ mV. With a leak current the steady state current satisfies:

$$I = g_L(V - E_L) + g_{Kir} h(V)(V - E_K).$$

Differentiating this equation, we obtain

$$\frac{dI}{dV} = g_l + g_{Kir} h(V) + g_{Kir} h'(V)(V - E_K).$$

The first two terms are positive. However, if $V > E_K$, then since $h'(V) < 0$, it is possible that this last term can be large and negative enough so that the $I - V$ curve is cubic-like. Necessary conditions are that $E_K < V_{th}$ and k must be small enough. Once there is bistability, it is possible to generate oscillations. Izhikevich points out that if you add a delayed rectifier potassium current, then it is possible to generate oscillations *with two potassium currents*! Given the fact that this current can induce bistability, this is not surprising. In exercise **, you can give this a try. Another way to induce oscillations in this model is to assume that there is extracellular potassium accumulation. This will result in the reversal potential for potassium becoming more positive, inactivating the channel. Thus, there will be negative feedback to a bistable system and possibly oscillations. See exercise *.

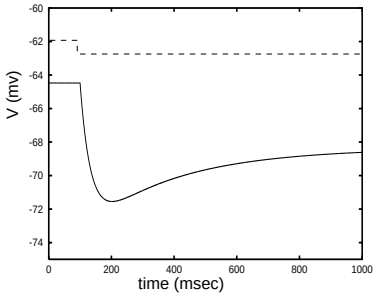

Figure 5.6. *The sag (I_h) current causes a slow repolarization of the potential to hyperpolarizing steps. (Parameters are those from McCormick et al.)*

5.1.6 Sag

We end our discussion of voltage-gated channels with a description of the so-called sag current, I_h. This is a slow inward current with a reversal potential of between -43 and 0 mV, but which requires hyperpolarization to become active; that is, the activation curve is monotone decreasing. The ions involved are a mixture of sodium an potassium so that the reversal potential lies between them. The sag current is implicated as a pacemaker in many different systems (Luthi et al, Maccaferri and McBain, Kocsis and Li). There are several models for this current; some have a single component and others have multiple components. The simplest model is due to McCormick and Huguenard:

$$I_h = g_h y(V + 43) \tag{5.6}$$

where

$$\begin{aligned} \frac{dy}{dt} &= (y_\infty(V) - y)/\tau_y(V) \\ y_\infty(V) &= 1/(1 + \exp((V - V_{th})/k)) \\ \tau_y(V) &= \tau_0 \text{sech}((V - V_m)/b). \end{aligned}$$

The time constant, τ_0 varies from 50 msec to over 1000. (Note that the function $\tau_y(V)$ used by McCormick et al is more complicated than the present version, but they are almost identical in shape.) Figure 5.6 shows how the sag gets its name. Hyperpolarizing the membrane causes the potential to drop and thus activates the sag current which then repolarizes the membrane. In exercise *, you combine this current with the I_{Kir} current from the previous section to obtain a slow pacemaker oscillation.

5.1.7 Currents and ionic concentrations.

So far, we have assumed that the ionic concentrations both inside and outside the cell are held constant. This is usually a good assumption except for the ion calcium.

Because the internal free calcium levels are very low in a cell (10^{-4} millimolar), the entrance of calcium through voltage-gated channels can substantially contribute to the intracellular calcium. Indeed, calcium is a very important signaling molecule and it often sets up complex reaction cascades within the cell. These reactions have both long and short-term effects on the cell. Thus, it is useful to understand how to model the flow of calcium due to voltage-gated channels. In certain pathological cases, the buildup of extracellular potassium can also have profound effects on neurons. Since normal extracellular media has quite low potassium, if many neurons are firing simultaneously, they are releasing large amounts of potassium into the medium. The surrounding nonneural cells (glia) buffer the potassium concentration, but this process can be slow.

Consider a current due to some ionic species I_X. Suppose that this is a positive ion. The current is typically measured in units of $\mu A/cm^2$. Recall that an ampere is a coulomb of charge per second. We need to convert this current to a concentration flux which has dimensions of millimolar. Recall that one molar is one mole per liter or one mole per 1000 cubic centimeters. Faraday's constant, 96,485 Coulomb/mole, is just what we need. Suppose the valance of the ion is z. Then $I_X/(zF)$ gives us the transmembrane flux in units of $\mu M/cm/s$. To convert this into a concentration flux, we suppose that the ions collect in a thin layer of depth d (in microns) near the surface of the cell. Thus, the change in concentration is $I_X/(zdF)$. Finally, we want out units of concentration to be in millimoles per liter per millisecond. Noting that a liter is a thousand cubic centimeters, we find that the total in(out)flux of an ion is

$$f_X = 10 I_X/(zFd) \tag{5.7}$$

where $F = 96,485$, d is depth in microns, and I_X is current in microamperes per square centimeter.

Having defined the flux of of ions moving through the cell, we need to write equations for the total concentration of ion, X:

$$\frac{dX}{dt} = \pm f_X - \delta(X)$$

where $\delta(X)$ is the decay of ion X through uptake or buffering. Which sign should we take? If we are interested in the intracellular concentration, then we take the negative sign and if we are interested in extracellular concentrations, we take the positive sign. The simplest form is

$$\delta_P(X) = (X - X_0)/\tau$$

which means that in absence of the ionic current, X tends to X_0. Another common form is

$$\delta_M(X) = \frac{K_1 X}{K_h + X}$$

which is a passive buffering model due to the reaction

$$X + B \rightleftharpoons XB \longrightarrow B + Y$$

where Y is the inactivated form of X. We finally note that the flux term f_X can have a factor multiplying it to account for buffering as well (see Keizer book). Thus, for intracellular accumulation, we can write:

$$\frac{dX}{dt} = -\gamma I_X - \delta(X) \tag{5.8}$$

where the parameter γ takes into account the buffering and depth of the membrane pool.

The main ion of interest is calcium. Wang (1998) uses $\gamma = .002$ in $\mu\text{M}(\text{msec}\mu\text{A})^{-1}\text{cm}^2$ in order to produce a 200 nM influx of calcium per spike. This amount is based on careful measurements by Helmchen et al (1996) in cortical pyramidal neurons. Wang also uses a simple decay for calcium, $\delta(X) = X/\tau$, where for the dendrite, $\tau = 80$msec.

5.1.8 Calcium-dependent channels.

The main reason to track calcium is that there are several important channels whose behavior depends on the amount of intracellular calcium. The two most important such channels are $I_{K,Ca}$, the calcium-dependent potassium current, and I_{can}, the calcium-dependent inward current. The former current appears in many neurons and is responsible for slow after-hyperpolarizations and spike-frequency adaptation. It is often referred to as the AHP current. The CAN current can last for many seconds and causes sustained depolarization. It has been implicated in graded persistent firing (Egorov et al 2002) and in the maintenance of discharges by olfactory bulb granule cells (Hall and Delaney, 2002). In order to model these currents, we need to keep track of the calcium. Thus, (i) there must be a source of calcium and (ii) we need to track it via equation (5.8).

Calcium dependent potassium - the AHP

A typical model for $I_{K,Ca}$ is due to Destexhe:

$$I_{K,Ca} = g_{K,Ca} m^2 (V - E_K) \tag{5.9}$$

$$\frac{dm}{dt} = (m_\infty(c) - m)/\tau_m(c) \tag{5.10}$$

$$m_\infty(c) = \frac{c^2}{K^2 + c^2} \tag{5.11}$$

$$\tau_m(c) = \max(\tau_{min}, \tau_0/(1 + (c/K)^2). \tag{5.12}$$

Typically K is 0.025 mM, $\tau_{min} = 0.1$ msec, and τ_0 varies. In Destexhe (1994) τ_0 is around 40 msec, but values as high as 400 msec can be found in the literature. A simple way to incorporate this model into one which has a calcium channel is to assume that it depends instantly on the calcium concentration:

$$m = m_\infty(c)$$

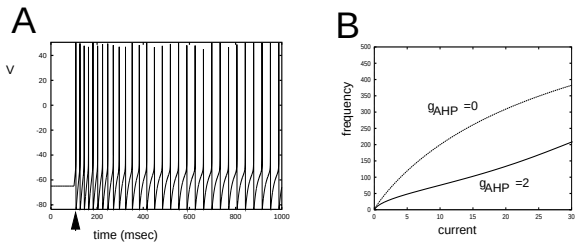

Figure 5.7. *Calcium-dependent potassium channel. (A) Spike frequency adaptation showing decrease in frequency over time. (B) Steady-state firing rate with and without adaptation.*

so that to incorporate this current into a spiking model one need only add an instantaneous calcium channel (if one is not present), the calcium dynamics, and the instantaneous AHP current. As with all the models, the equations for this are found in the appendix. Figure 5.7A shows the behavior of the firing rate over time when this current is added to the Morris-Lecar model. The onset of spiking is unaffected by the presence of this current because it turns on only when the cell is spiking (and calcium enters the cell). Thus, unlike the M-current, the AHP current cannot alter the stability of the rest state.

One very interesting effect of the AHP is shown in Figure 5.7B. It is not surprising that the current lowers the frequency-current curve. However, it also tends to make the curve more linear. This point was first described by Wang (1998) in a model similar to that depicted above. We now attempt to explain the origin of this linearization effect. We will first formulate this problem rather abstractly and then consider a full biophysical model.

Suppose that the unadapted neuron is able to fire at arbitrarily low rates and that the derivative of the firing rate function tends to infinity as the threshold for firing is approached. Let z be the degree of adaptation in the model and we suppose that $z = \alpha f$ where f is the firing rate. The adaptation acts negatively on the total current injected into the neuron, thus

$$f(I) = F(I - gz)$$

where $F(I)$ is the unadapted firing rate function and g is some constant. Since $z = \alpha f$ this leads us to

$$f(I) = \alpha F(I - g\alpha f). \tag{5.13}$$

Differentiating this with respect to I and rearranging, we obtain:

$$\frac{df}{dI} = \frac{F'(I - \alpha g f)}{1/\alpha + \alpha g F'(I - \alpha g f)}.$$

For large F', we see that

$$\frac{df}{dI} \approx \frac{1}{\alpha g}$$

showing that it is approximately linear. If we suppose that $F(I) = A\sqrt{I}$ so that the the neuron has a class I firing rate curve , we can exactly solve for f:

$$f(I) = -\kappa + \sqrt{\kappa^2 + A^2 I} \tag{5.14}$$

where $\kappa = A^2\alpha g/2$. **** Remark: this doesn't look very linear so it's not clear what the point is ***

What does this simple calculation have to do with the full biophysical model? We can exploit the slow dynamics of adaptation in order to justify equation (5.13). For simplicity, we assume that conductance of the adaptation is linear rather than the nonlinear model we have used as an illustration. Consider:

$$C\frac{dV}{dt} = I - I_{fast} - gz(V - E_K) \tag{5.15}$$

$$\frac{dz}{dt} = \epsilon[q(V)(1 - z) - z]. \tag{5.16}$$

here I_{fast} represent all the 'fast" currents which are responsible for spiking. There are three keys to the analysis (i) ϵ is very small; (ii) the fast system has class I dynamics; (iii) the width of the spikes does not change very much as a function of the firing rate. Figure 5.7B shows that the present model is class I. The interested reader can verify that the spike width is nearly independent of the frequency. Finally, we have chosen the calcium time constant to be 300 msec which is at least an order of magnitude slower than any of the other dynamics. (We remark that the calculations that follow will be used often to justify simplified firing rate dynamics of biophysical models.)

Slow-fast analysis.

Since ϵ is small, we can treat z as a constant as far as the dynamics of the fast variables is concerned. Thus, we can examine (5.15) using I and z as parameters. Since $gz(V - E_K)$ is essentially a constant hyperpolarizing current (when z is fixed), we expect that if we inject enough current into the cell, it will fire. We also expect that the onset of firing will be a SNIC at some critical current, $I_{SN}(z)$, depending on z. A numerical analysis of the model illustrated in Figure 5.7 shows that

$$I_{SN}(z) \approx I_0 + gI_1 z.$$

Recall that the firing rate of class I neurons is (at least near the bifurcation) a square-root function of the distance from the saddle node:

$$f(I, z) = A\sqrt{I - I_{SN}(z)} \approx A\sqrt{I - I_0 - gI_1 z}. \tag{5.17}$$

Thus, if $I < I_{SN}$, then the neuron does not fire and if $I > I_{SN}$ the neuron fires at a rate dependent on the distance from the saddle-node. Note that the function f need not be exactly a square root. However, we do assume that it depends only of the distance from the saddle-node and that the saddle-node value is a linear function of the degree of adaptation. Now we turn to the slow equation (5.16).

We assume the function $q(V)$ is such that if the neuron does not fire an action potential, then $q(V) = 0$. Thus, at rest, $q = 0$ and $z = 0$. Since the adaptation in this section is *high-threshold*, the subthreshold membrane behavior will have no effect on the degree of adaptation. Now, suppose the neuron is firing with period T. Then equation (5.16) is a scalar periodically driven equation:

$$\frac{dz}{dt} = \epsilon[q(V(t))(1 - z) - z].$$

Since ϵ is small, we can use the method of averaging (see chapter *) and replace z by its average Z:

$$\frac{dZ}{dt} = \epsilon < q > (1 - Z) - Z$$

where

$$< q >= \frac{1}{T}\int_0^T q(V(t))\ dt.$$

Now, we invoke the hypothesis that the spike width is independent of the frequency. Since $q(V)$ is zero except during a spike and the spike width is independent of the frequency, the above integral simplifies to

$$< q >= \frac{c}{T}.$$

Here c is the integral of $q(V(t))$, a frequency-independent constant. But $1/T$ is just the frequency and this is given by equation (5.17). Thus, we obtain a closed equation for the degree of adaptation:

$$\frac{dZ}{dt} = \epsilon[cA\sqrt{I - I_0 - I_1 Z}(1 - Z) - Z]. \tag{5.18}$$

The steady-states for this equation will yield the steady-state F-I curve. However, one has to solve a cubic equation to get the steady-states, so that it is not analytically tractable. (However, see exercise *).

CAN current.

The CAN current can be modeled very much like the AHP but instead of hyperpolarization, the current provides depolarization. We model the CAN current simply as

$$I_{CAN} = g_{CAN} m_{Can}^p (V - E_{CAN}).$$

The gate m_{CAN} obeys dynamics much like the AHP:

$$\frac{dm_{CAN}}{dt} = (q(c)(1 - m_{Can}) - m_{CAN})/\tau_{CAN}$$

where $q(c)$ is some monotone function of the calcium. Typically, $q(c) = \alpha(c/c_0)^2$. The CAN current has been implicated in sustained firing of many neurons, notably those in the entorhinal cortex (Egorov, et al). A simple illustration of sustained

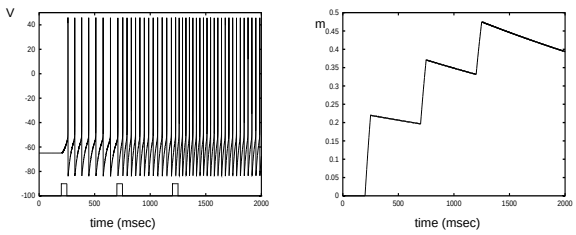

Figure 5.8. *The CAN current can explain long-lasting persistent activity. (A) The voltage of a spiking model with three calcium stimuli. (B) The gate for the CAN current.*

firing due to the CAN current is shown in Figure 5.8. We use the Destexhe-Pare spiking model for the generation of action potentials and add a small amount of the CAN current

$$I_{Can} = g_{can} m_c (V + 20)$$

where

$$\frac{dm_c}{dt} = 0.005[Ca]^2(1 - m_c) - m_c/3000.$$

Since the spiking model does not have any calcium channels, we suppose that the synaptic stimulation of the model produces a square pulse of calcium of width 50 msec and magnitude 1 mM. (See the section on synaptic channels below). The results of three pulses at $t = 200, 700, 1200$ shows the long-lasting graded persistent activity. (This model is quite naive and cannot maintain the firing rate since the CAN current decays. One way to rectify this is to have calcium channels in the model for spiking which will then provide positive feedback. Problems related to this are explored below in one of the exercises/projects.)

5.1.9 Exercises

1. Based on what you have seen in the ML system, one might guess that there is the possibility of getting oscillations in the Butera model when the fast sodium is blocked and the inactivation of the persistent sodium is held constant (that is $dh/dt = 0$). Thus, the model could be reduced to a planar system in V, n:

$$C_m \frac{dV}{dt} = -g_L(V - E_L) - g_K n^4 (V - E_K) - g_{NaP} w_\infty(V) h (V - E_{Na})$$

$$\frac{dn}{dt} = (n_\infty(V) - n)/\tau_n(V).$$

Compute the bifurcation diagram of this using h as a parameter at a variety of different values of E_L. Conclude that there can be no oscillations for this. How would you change the shape of $n_\infty(V)$ in order to generate oscillations in this model?

2. Compute the bifurcation diagram of the $T-$current model using E_L as a parameter starting it at -60 mV and decreasing it to -85 mV. Simulate the model when there are calcium oscillations.

3. Add sodium and potassium currents to the T-current model using the equations in the Appendix for `cat-spike.ode`. Show that when the resting potential is depolarized ($E_L = -65$), the application of sufficient depolarizing current leads to a train of action potentials. Show the analogues of figure 5.2A,C for the spiking model.

4. The $T-$type calcium current was shown to be capable of oscillations and rebound depending on the leak current. Explore the $L-$type calcium current which has calcium-dependent inactivation. The model equations for this are given in the appendix. The activation is set to its steady state so that the resulting model is planar. Explore the bifurcation to periodic solutions as a function of the applied current. Compute the bifurcation diagram as I_0 the applied current is increased.

5. The Connor-Stevens model has its parameters balanced at a nearly critical value in that there are many complicated bifurcations which can occur nearby. This has not been systematically explored although Rush and Rinzel make some mention of the unusual behavior. Use the CS model in the appendix in which the A- and delayed rectifier currents are balanced so that their total maximal conductance is fixed. (That is, let $g_K = 67.7 - g_A$ in the CS model.) The standard values are $g_A = 47.7$ and $g_K = 20$. (i) Change the model so that $g_A = 48.7$ and $g_K = 19$. Compute the bifurcation diagram and show that there are at most three fixed points. (ii) Change $g_A = 47.4$ and $g_K = 20.3$. Compute the bifurcation diagram as a function of the current. Show that there is a small range of currents where there are two stable fixed points. Now, use the parameters g_A and I_0 to create a two-parameter diagram of fold points and Hopf points. You should find something that looks like the figure below. There are three cusp points corresponding to the coalescence of fold points. There is also a curve of Hopf points which terminates on one to the folds at a Takens-Bogdanov point. Thus, the standard parameters for the CS model are quite weird!

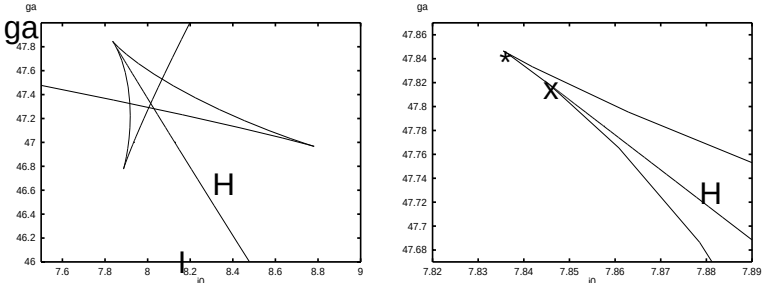

6. Compute the FI curve for the Destexhe-Pare model with $g_m = 0$ and with $g_m = 5$ and compare the two.

7. Create a figure like 5.4B for the DP model ($I = 6$, $g_m = 2.$) and try to fit the data to a function of the form:

$$F = F_{ss} + (F_{inst} - F_{ss})\lambda^{n-1}$$

where F_{ss} is the steady state firing rate, F_{inst} is the instantaneous rate, λ is a parameter and n is the ISI number. The parameters F_{ss}, F_{inst} characterize the degree of adaptation and the parameter λ characterizes the time scale of adaptation.

8. Make a neural oscillator using the inward-rectifier and a delayed rectifier model of the form

$$I_K = g_K n^4 (V - E_K)$$

where

$$\frac{dn}{dt} = (1/(1 + exp(-(V - a)/b)) - n)/\tau.$$

You should try to pick a, b, τ so that the model oscillates. Don't worry if the choices of a are pretty low. Use $g_{Kir} = 0.5$, $E_K = -90$, $E_L == 60$, $g_L = 0.05$, and V_{th}, k as in the text.

9. **Inward rectifier and potassium accumulation.** Let

$$I_K = g_K m_\infty(V)(V - E_K)$$

where

$$m_\infty(V) = 1/[1 + \exp((V + 71)/0.8)]$$

and

$$E_K = 85 \log_{10} K_{out}.$$

Consider the model with external potassium accumulation with passive uptake:

$$C\frac{dV}{dt} = I - g_L(V - E_L) - I_K$$
$$\tau\frac{dK_{out}}{dt} = \alpha I_K + K_0 - K_{out}$$

where $K_0 = 0.1$, $\alpha = 0.2$, $g_L = 0.1$, $g_K = 0.1$ Sketch the phaseplane for various hyperpolarizing currents. Show that if you choose I in some small range and τ sufficiently large, that you will obtain oscillations in the potential. (Hint: Show that the V-nullcline can be cubic and that it can intersect the K_{out} nullcline in the middle branch. Then increase τ until this fixed point is unstable.

10. Consider a combination of the sag current and the inward rectifier. Parameters should be taken from the model in the appendix. Draw the phaseplane and integrate the equations. Change the sag model from the McCormick to the Migliore parameters. Does the model still generate subthreshold oscillations? Compute the bifurcation diagram for the model using I as a parameter. How is the oscillation borne and how does it die?

11. Suppose that Z is small in equation (5.18) so that the equation is well approximated by
$$\frac{dZ}{dt} = \epsilon[cA\sqrt{I - I_0 - gI_1 Z} - Z].$$
Find the steady-states of Z and obtain the FI curve from this.

12. Repeat the calculations for the slow adaptation model by explicitly computing the averaged quantities for the theta model:
$$\frac{d\theta}{dt} = 1 - \cos\theta + (1 + \cos\theta)[I - gz]$$
$$\frac{dz}{dt} = \epsilon[\delta(\theta - \pi) - z]$$
The right-hand side of z says that each time θ crosses π, z is incremented by an amount ϵ. Numerically compute the FI curve for this model with different values of g (say 0,1,5). Since the firing rate of the unadapted theta model is known exactly (see exercise **), you should try to fit the numerically computed FI curves to equation (5.14).

13. A related model to the previous exercise adds spike-adaptation to the quadratic integrate and fire model. The simplest form of this model is:
$$V' = I + V^2 - u \tag{5.19}$$
$$u' = a(bV - u)$$
along with reset conditions such that when $V = V_{spike}$, V is reset to c and u is incremented by d. By rescaling V, you can set $V_{spike} = 1$ with no loss in generality. (Do this as an exercise.) The variable u plays several roles in this model. If $a = 0$, then it can have no effect on the local behavior of the rest point. However, if $a \neq 0$ the adaptation can change the stability of rest.

    (a) Suppose there is a rest state, $(\bar{V}, \bar{u})$. Linearize about the rest state and find the parameters (a, b, I) where there is a saddle-node bifurcation, a Hopf bifurcation, and where the two bifurcations merge at a Takens-Bogdanov point. This is not surprising as the next part of this exercise will show.

    (b) The Takens-Bogdanov bifurcation occurs when there is a double zero eigenvalue which has geometric multiplicity 1. The Takens normal form for this bifurcation takes the form:
$$\frac{dw}{dt} = z + \beta w + w^2, \qquad \frac{dz}{dt} = \alpha + w^2.$$
Let $r = w - z$ and write equations for the new (r, w) system. Next let
$$x = w + \frac{\beta + 1}{2}$$
$$z = \frac{r}{\beta + 1} + \frac{\alpha + (\beta + 1)^2/2}{\beta + 1}.$$

yielding:

$$\frac{dx}{dt} = -(\beta+1)z + x^2 + k, \qquad \frac{dy}{dt} = x - y$$

where

$$k = \alpha + (\beta+1)^2/4.$$

Thus, the local dynamics of the QIFA model is the same as that of the normal form. Note that we can get rid of the parameter a by rescaling time and V, z in (5.19). You should attempt this.

(c) The FI curve of this model cannot be analytically derived even when $a = 0$. Nor can we use AUTO or other bifurcation tools to obtain the FI curve since the reset condition makes the equations discontinuous. However, we can pose this as a boundary value problem which *is* smooth and so can be computed with AUTO. We suppose that there is a repetitively firing solution with period P. This means that $V(0) = c$ and $V(P) = 1$. Thus, the boundary conditions for V are specified. We also require that $u(0) = u(P) + d$ since u is incremented whenever V crosses 1. Since the period is unknown, we rescale time, $t = Ps$ and thus have the following equations:

$$\begin{aligned} V' &= P(V^2 + I - u) \\ u' &= Pa(bV - u) \\ V(0) &= c \\ V(1) &= 1 \\ u(0) &= u(1) + d. \end{aligned}$$

There are *three* boundary conditions, but only two differential equations. However, there is a free parameter P which can allow us to solve the equations. For example, take $(a, b, c, d) = (0.1, 1, -0.25, 0.5)$ and $I = 1$ and you will find a repetitive spiking solution with $u(0) = 1.211$ and period $P = 5.6488$. Try this, and then use AUTO or some other method to compute the FI curve. The analysis of the rest state that you did above should tell you the lowest possible current for repetitive firing.

14. (Izhikevich model) Eugene Izhikevich has adapted the quadratic integrate-and-fire model with linear adaptation (5.19) to look more like a biophysical model. The model has 4 free parameters as well as the current. The equations are

$$\begin{aligned} \frac{dV}{dt} &= 0.04V^2 + 5V + 140 + I - u \\ \frac{du}{dt} &= a(bV - u) \end{aligned} \tag{5.20}$$

along with the reset conditions if $V = 30$ then $V = c$ and $u = u + d$. Find a change of variables which converts (5.20) to (5.19). Izhikevich suggests the following sets of parameters (a, b, c, d, I) for various types of neurons. Try

these and classify the behavior: (.02,.2,-65,6,14); (.02,.2,-50,2,15); (.01,.2,-65,8,30); (.2,.26,-65,0) and let I vary on this example. In each of these, start with $I = 0$ and then increase I to the suggested value. Can you derive a method for numerically following a bursting solution as a function of some parameter? (It is likely you will have to fix the number of spikes in a burst.)

15. Sakaguchi has recently devised a simple model for a one-variable bursting neuron. The equation is as follows:

$$C\frac{dV}{dt} = \alpha(V_0 - V + DH(V - V_T)) \tag{5.21}$$

where $H(X)$ is the step function. There are two reset conditions. If V crosses V_T from below, then V is boosted to V_1. If V crosses V_{T2} from above, V is reset to V_2. Sakaguchi takes $\alpha = .035$, $C = 2$, $V_0 = 30$, $D = 5$, $V_T = -35$, $V_1 = 50$, $V_2 = -50$, and $V_{T2} = 40$. Compute the period of the Sakaguchi burster for these parameters. What are the conditions on the various resets and thresholds for this model to have sustained periodic behavior?

5.1.10 Projects

In this section, we lay out some projects that could be used in a classroom setting.

1. Artificial respiration. The Hering-Breuer reflex is a phenomena through which it has been shown that mechanical deformation of the lungs can entrain the respiratory pattern generator. Use the full Butera model as your simple pacemaker. This pacemaker provides the motor out put for the inspiratory phase of breathing. The ventilator provides both inflation and deflation. Inflation is known to inhibit the motoneuron pools for inspiration, so assume that the ventilator provides periodic inhibitory input. Explore the range of frequencies and patterns of entrainment and the conditions under which there is 1:1 locking.

2. Calcium feedback and bistability. Consider a spiking model

$$C\frac{dV}{dt} = -I_L - I_{Na} - I_{Kdr} - I_{Ca} - I_{Can} + I(t)$$

where you can take the Destexhe-Pare model of the leak, sodium, and potassium current. Choose a very small instantaneous high-threshold calcium current as was done in the calcium-dependent potassium current. Add calcium dynamics and a CAN current. Try to adjust parameters so that a sufficient stimulus generates sustained firing. If you give a very strong stimulus, you should be able to get more calcium into the system and thus increase the CAN current. This may lead you to believe that you can get graded persistent firing. But, simulations should convince you that the best you can get is bistability. Can you design a model (even an abstract one) which has many fixed points and thus admits a variety of steady state firing rates? (Hint: See recent papers by Loewenstein and Sompolinsky (2003) and Teramae and Fukai (2004) who find a solution to this problem.)

3. Bifurcation analysis of the aEIF. Brette and Gerstner (2005) propose the following simple two-variable integrate-and-fire model:

$$C\frac{dV}{dt} = I - g_L(V - E_L) + g_L\Delta_T e^{(V-V_T)/\Delta_T} - w$$
$$\tau_W\frac{dw}{dt} = a(V - E_L) - w$$

with the provision that when $V(t) = 20$, it is reset to V_r and w is increased by an amount b. A lengthy project would be to study the local behavior of this model using combined analytical and computational methods. For example, find the saddle-node and Hopf bifurcations. The above authors fit this model to a detailed biophysical model with parameters $C = 281$ pF, $g_L = 20$ nS, $E_L = -70.6$ mV, $V_T = -50.4$ mV, $\Delta_T = 2$ mV, $\tau_w = 144$ msec, $a = 4$ nS, $b = .0805$ nA. Note the units, w is a current and V is a voltage. The time constant of the cell at rest is roughly, 9 msec.

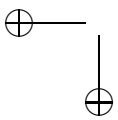

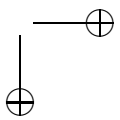

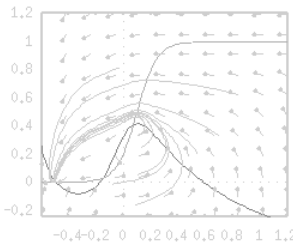

Chapter 6

Bursting Oscillations

6.1 Introduction to Bursting

Many neurons exhibit much more complicated firing patterns than simple repetitive firing. A common mode of firing in many neurons and other excitable cells is bursting oscillations. This is characterized by a silent phase of near steady state resting behavior alternating with an active phase of rapid, spike-like oscillations. Examples of bursting behavior are shown in Figure ??. Note that bursting arises in neuronal structures throughout the central nervous system. Bursting activity in certain thalamic cells, for example, are implicated in the generation of sleep rhythms, while patients with Parkinsonian tremor exhibit increased bursting activity in neurons within the basal ganglia. Cells involved in the generation of respiratory rhythms within the Pre-Botzinger complex also display bursting oscillations.

**** Figure of Bursting Cells as in Wang-Rinzel *****

At least two biophysical mechanisms are required to produce bursting: a mechanism responsible for the generation of spiking and a separate mechanism underlying the slow modulation, responsible for the switch between the silent and active phases. The spikes are action potentials and typically arise from interactions between an inward sodium current and an outward potassium current. In order to generate the slow modulation, there must be another process that slowly builds up (or possibly decays) during the spiking phase and then decays (builds-up) during the silent phase. This process typically involves an ionic current which either activates or inactivates at a rate slower than the other currents.

A classic example of an ionic current underlying the slow modulation is the calcium-dependent potassium current I_{KCa}. Calcium enters the cell during the active spiking phase and this leads to activation of the I_{KCa} current. Once this outward current is sufficiently large, the cell can no longer sustain spiking activity and the active phase terminates. During the silent phase, calcium leaves the cell and calcium-dependent potassium channels close. Spiking resumes once I_{KCa} is sufficiently small. This is just one of many mechanisms that may underlie the slow

modulation. In this example, an outward current slowly activates, because of the build-up of calcium, and this eventually terminates the spiking phase. Another possibility is that an inward current slowly inactivates, thereby weakening spiking activity. An example of such a current is the persistent sodium current I_{NaP} and this mechanism underlies bursting in models for cells in the Pre-Botzinger complex.

The examples shown in Figure ?? demonstrate that the firing properties of bursting cells may be quite different. There has been considerable effort to classify mechanisms underlying bursting oscillations. Mathematical classifications have been in terms of geometric properties of the corresponding phase space dynamics. Note that bursting cannot happen in a two-variable model such as the Morris-Lecar equations. This is because each spike corresponds to a loop in phase space and trajectories cannot cross each other in a two-dimensional phase plane. Hence, a minimal model for bursting must include at least three dependent variables.

Models for bursting typically involve multiple time scales and can often be written as

$$\begin{aligned} \frac{dx}{dt} &= f(x,y) \quad (FS) \\ \frac{dy}{dt} &= \epsilon g(x,y) \quad (SS) \end{aligned} \tag{6.1}$$

where $\epsilon > 0$ is a small singular parameter. Here, $x \in R^n$ are fast variables responsible for spike-generation, while $y \in R^m$ are slow variables responsible for the slow modulation of silent and active phases. Note that if $\epsilon = 0$, then y is constant. We denote to the first equation in (6.1), with y constant, as the fast subsystem (FS). During the silent phase, a bursting trajectory passes near a manifold of fixed points of (FS), while during the active phase of repetitive spikes the trajectory passes near a manifold of periodic solutions of (FS). The slow processes modulate the fast dynamics between these two phases. Different classes of bursting oscillations are distinguished by the mechanisms by which the bursting trajectory switches between the silent and active phases. This is closely related to the global bifurcation structure of the fast subsystem with the slow variables treated as parameters.

Models for bursting may exhibit other types of oscillatory activity, as well as more exotic behavior including chaotic dynamics. Geometric dynamical systems methods are extremely useful in determining what sorts of solutions may arise and how the solutions depend on parameters. The models contain multiple time scales and this often leads to very interesting issues related to the theory of singular perturbations. Transitions from one type of behavior to another usually involve global bifurcations. Homoclinic orbits, for example, often play an important role in the generation of bursting activity: the active phase of rapid oscillations may either begin or end (or both) as the bursting trajectory crosses near a homoclinic point in phase space. At these points, standard singular perturbation methods may break down, so more delicate analysis is required.

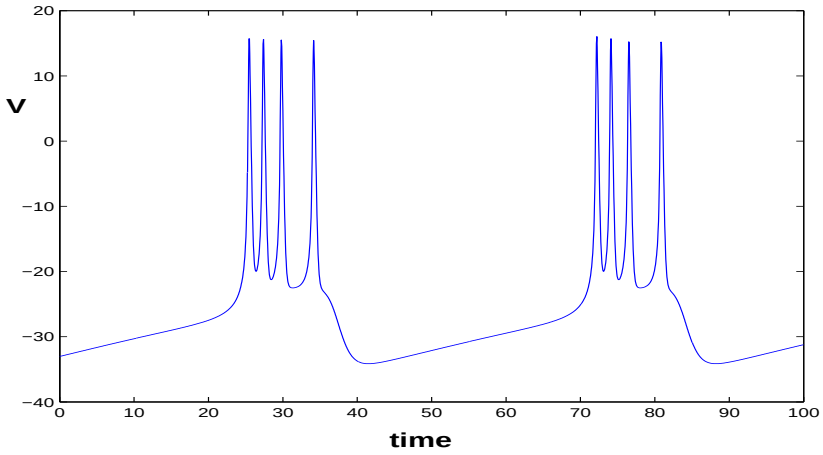

Figure 6.1. *Square-wave bursting. Note that the active phase of repetitive firing is at membrane potentials more polarized than during the silent phase. Moreover, the frequency of spiking slows down at the end of the active phase.*

6.2 Square-wave Bursters

Perhaps the best studied form of bursting is so-called *square-wave bursting*. This class of bursting was first considered in models for electrical activity in pancreatic-beta cells; these play an important role in the release of insulin. Another example of square-wave bursters is respiratory generating neurons within the Pre-Botzinger complex.

An example of a square-wave burster is shown in Figure 6.1. Note that the active phase of repetitive firing occurs at membrane potentials considerably more polarized than during the silent phase. Another feature of square-wave bursting is that the frequency of spiking slows down during the active phase. These firing properties reflect geometric properties of the trajectory in phase space corresponding to the bursting solution. In fact, it is these geometric properties which uniquely characterize square-wave bursters and what distinguishes them from other classes of bursters.

We have already noted that bursting cannot arise in two-variable models. There is simply not enough room in a two-dimensional phase plane to generate the repetitive spiking. However, it is rather simple to generate bursting activity if we periodically drive a two-variable model. Consider, for example, the Morris-Lecar equations (4.1) with parameters given in Table 4.2 for the homoclinic regime. The bifurcation diagram, with bifurcation parameter I_{app}, is shown in Figure 6.2. The set of fixed points forms an S-shaped curve. There is a branch of periodic orbits which originates at a subcritical Hopf bifurcation along the upper branch of fixed points and terminates at an orbit homoclinic to the middle branch of fixed points.

(The fact that the Hopf bifurcation is subcritical is not important here.) Moreover, there is an I_{app}-interval between $I_{app} = I_{HOM}$ and $I_{app} = I_{SN}$ for which the model is bistable: there are stable rest states along the lower branch of fixed points and stable, more depolarized, limit cycles. When $I_{app} = I_{HOM}$, there is a homoclinic orbit and when $I_{app} = I_{SN}$ there is a saddle-node bifurcation. Now suppose that I_{app} slowly varies back and forth across this interval. Because of the bistability, it is easy to see how a hysteresis loop is formed in which the membrane potential alternates between resting and spiking activity. Note that the frequency of firing slows down near the termination of the active phase. This is because the active phase ends as the solution crosses the homoclinic orbit.

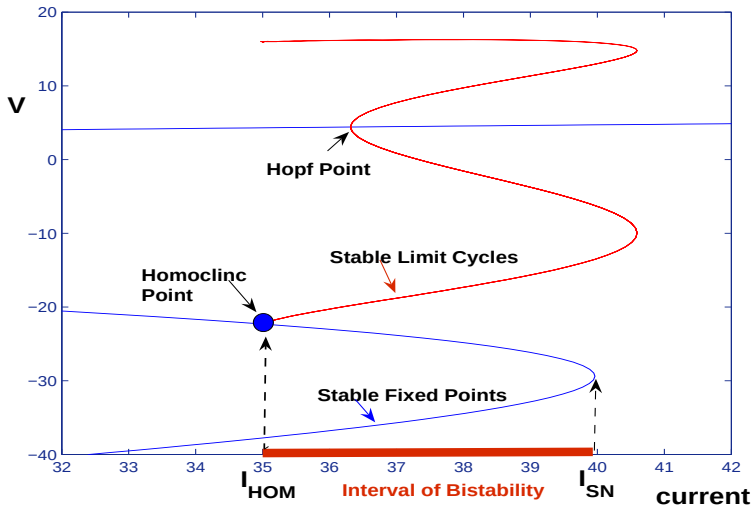

Figure 6.2. *A bifurcation diagram of the Morris-Lecar equations, homoclinic case. The set of fixed points form an S-shaped curve (not all of which is shown). A branch of limit cycles originates at a Hopf point and terminates at a homoclinic orbit. There is an interval of applied currents for which the system displays bistability.*

This example provides a simple mechanism, and geometric interpretation, for square-wave bursting. However, this mechanism is unsatisfactory since we imposed an external, periodic applied current. What we really wish to understand is autonomous bursting; that is, bursting that arises due to interactions among intrinsic properties of the cell. One way to achieve autonomous square-wave bursting is to again consider the Morris-Lecar model except now we redefine I to be a dynamic dependent variable that decreases during the active phase of repetitive firing and increases during the silent phase. This example demonstrates the basic principle that slow negative feedback together with hysteresis in the fast dynamics underlie square-wave bursting.

Many different ionic current mechanisms could produce the slow negative feed-

back. Here, we construct an autonomous model for square-wave bursting by starting with the Morris-Lecar model (4.1) and adding a calcium-dependent potassium current. The complete model can be written as:

$$\begin{aligned} C_m \frac{dV}{dt} &= -g_L(V - E_L) - g_K n(V - E_K) \\ &\quad -g_{Ca} m_\infty(V)(V - E_{Ca}) - I_{KCa} + I_{app} \\ \frac{dn}{dt} &= \phi(n_\infty(V) - n)/\tau_n(V) \\ \frac{d[Ca]}{dt} &= \epsilon(\mu I_{Ca} - k_{Ca}[Ca]) \end{aligned} \tag{6.2}$$

where the calcium-dependent potassium current I_{KCa} is given by

$$I_{KCa} = g_{KCa} z (V - V_K). \tag{6.3}$$

Here, g_{KCa} is the maximal conductance for this current and z is the gating variable with a Hill-like dependence on $[Ca]$, the near-membrane calcium concentration. Hence,

$$z = \frac{[Ca]^p}{[Ca]^p + 1}.$$

For simplicity, we set the Hill exponent $p = 1$. The third equation in (6.2) represents the balance equation for [Ca]. The parameter μ is for converting current into a concentration flux and involves the ratio of the cell's surface area to the calcium compartment's volume. The parameter k_{Ca} represents the calcium removal rate and ϵ is the ratio of free to total calcium in the cell. Since calcium is highly buffered, ϵ is small so that the calcium dynamics is slow. We shall refer to the first two equations in (6.2) as the fast-subsystem (FS) and the third equation as the *slow equation*.

Note that I_{KCa} is an outward current. If its conductance $g_{KCa}z$ is large, then the cell is hyperpolarized and the cell exhibits steady-state resting behavior. If, on the other hand, this conductance is small, then the cell can fire action potentials. Figure 6.3 shows the bifurcation diagram of (6.2), in which z is the bifurcation parameter. Note that the curve of fixed points is now Z-shaped, not S-shaped. There is a branch of limit-cycles that begins at a subcritical Hopf point and terminates at an orbit homoclinic to the middle-branch of fixed points. Finally, there is an interval of z-values for which the fast-subsystem exhibits both a stable fixed point and a stable limit cycle.

Now the full system exhibits square-wave bursting, as shown in Figure 6.1. Parameter values are given in Table 6.2. When the membrane is firing, intracellular calcium slowly accumulates, turning on the outward I_{KCa} current. When this current is sufficiently activated, the membrane can no longer maintain repetitive firing thus terminating the active phase. During the silent phase, intracellular calcium concentration decreases thereby closing KCa channels. Once enough outward channels are closed, the cell may resume firing.

The projection of the bursting solution onto the bifurcation diagram of the fast subsystem is shown in Figure 6.3B. During the silent phase, the solution trajectory

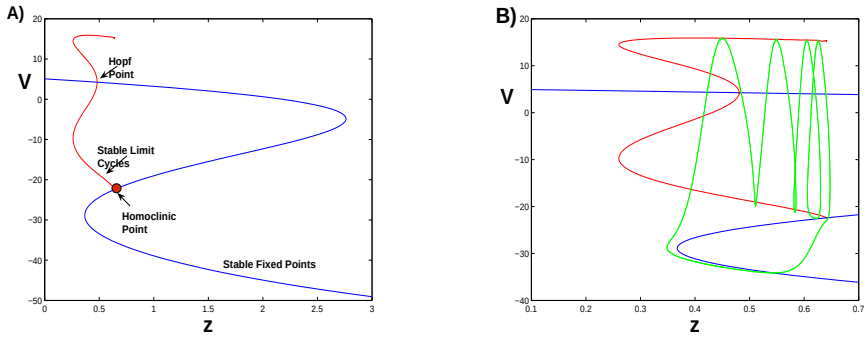

Figure 6.3. *(A) Bifurcation diagram of the fast-subsystem for square-wave bursters. (B) The projection of the bursting trajectory onto the bifurcation diagram.*

lies close to the lower branch of fixed points of the fast subsystem. The silent phase ends when the trajectory reaches the saddle-node of fixed points at which point the trajectory jumps close to the branch of stable limit cycles of the fast subsystem. While the membrane is spiking, the solution remains close to this branch until it crosses the homoclinic orbit of the fast-subsystem. The trajectory is then forced to jump down to the lower branch of fixed points and this completes one cycle of the bursting trajectory.

This example illustrates some of the basic features of square-wave bursting. We now consider a more general class of fast/slow systems and describe in more detail what geometric properties are needed to generate square-wave bursting. In general, square-wave bursting can arise in a system of the form (6.1) in which there are at least two fast variables and one slow variable. In order to obtain square-wave bursting, we must make assumptions on both the bifurcation structure of the fast subsystem and the slow dynamics. In order to describe these assumptions, we consider a three-variable model of the form:

$$\begin{aligned} v' &= f(v, w, y) \\ w' &= g(v, w, y) \\ y' &= \epsilon h(v, w, y, \lambda). \end{aligned} \tag{6.4}$$

In the third equation, λ represents a fixed parameter. Later, we discuss complex bifurcations that arise when λ is varied. What distinguishes square-wave bursting is the bifurcation diagram of the fast subsystem: the set of fixed points of the fast subsystem forms a Z- (or possibly S-) shaped curve and there is a branch of stable limit cycles that terminate at a homoclinic orbit. The fixed points along the lower branch are stable with respect to the fast subsystem, while those fixed points along the middle branch are saddles with one stable and one unstable direction. The branch of limit cycles terminates at an orbit homoclinic to one of these saddles. In what follows, we denote the curve of fixed points of the fast subsystem as C_{FP} and the branch of stable limit cycles as P.

Table 6.1. *Bursting parameters.*

Parameter	Square-wave	Elliptic	Parabilic
ϕ	4.6	.8	1.33
g_{Ca}	4.4	4.4	4
V_3	2	2	12
V_4	30	30	17.4
E_{Ca}	120	120	120
E_K	-84	-84	-84
E_L	-60	-60	-60
g_K	8	8	8
g_L	2	2	2
V_1	-1.2	-1.2	-1.2
V_2	18	18	18
C_m	1	1	1
I_{app}	45	65	65
ϵ	.1	.04	.01
k_{Ca}	1	1	1
μ	.02	.0167	.025
k	1	1	1
g_{KCa}	.25	1	1
$\tau_s,\ g_{CaS}$			.05, 1

Assumptions are also needed for the slow dynamics. The slow variable y must decrease during the silent phase and increase during the active phase. (Here we are assuming that the set of fixed points of the fast subsystem is Z-shaped, not S-shaped.) Note that the y-nullsurface $\{h = 0\}$ is two-dimensional. We assume that this surface intersects C_{FP} at a single point that lies along the middle branch of C_{FP} below the homoclinic point. Moreover, $h > 0$ above $\{h = 0\}$ and $h < 0$ below $\{h = 0\}$. This allows for y to slowly increase (decrease) while the bursting solution is in the active (silent) phase. Note that the point where the y-nullsurface intersects C_{FP} is a fixed point of the full system (6.4) with $\epsilon > 0$.

It is important that the slow nullsurface $\{h = 0\}$ intersects C_{FP} below the homoclinic point; in particular the nullsurface must lie between the lower branch of C_{FP} and the branch of stable limit cycles P. If this condition is not satisfied, then the system may exhibit other types of solutions. For example, suppose that $\{h = 0\}$ intersects the lower branch of C_{FP}. This point of intersection will be a stable fixed point of (6.4), corresponding to a resting state of the neuron. If, on the other hand, $\{h = 0\}$ intersects C_{FP} along its middle branch above the homoclinic point, then the (6.4) may exhibit a stable limit cycle which lies near P. This type of solution is often referred to as either *continuous* or *tonic spiking*.

Rigorous results concerning the existence and stability of bursting oscillations and continuous spiking are presented in [??]. In order to describe these results, we suppose that there exists λ_0 such that if $\lambda < \lambda_0$ then $\{h = 0\}$ intersects C_{FP} along its middle branch below the homoclinic point while if $\lambda > \lambda_0$ then $\{h = 0\}$

intersects C_{FP} along its middle branch above the homoclinic point. The results in [?] state that if ϵ is sufficiently small, then (6.1) exhibits bursting oscillations for $\lambda < \lambda_0$ and continuous spiking for $\lambda > \lambda_0$, just as expected. However, it is important to realize that how small ϵ needs to be depends on how close λ is to λ_0. In particular, $\epsilon \to 0$ as $\lambda \to \lambda_0$. This is illustrated in Figure 6.4. Note that there is a wedge-shaped region emanating from $(\lambda, \epsilon) = (\lambda_0, 0)$ where we cannot conclude that there exists bursting or spiking. Numerical studies and rigorous analysis have shown that as λ varies across this wedge-shaped region, between the bursting and continuous spiking regimes, the bifurcation structure of solutions must be very complicated. In particular, there will be solutions in which the number of spikes per burst varies considerably. Further discussion of chaotic dynamics in models for bursting oscillations will be given later.

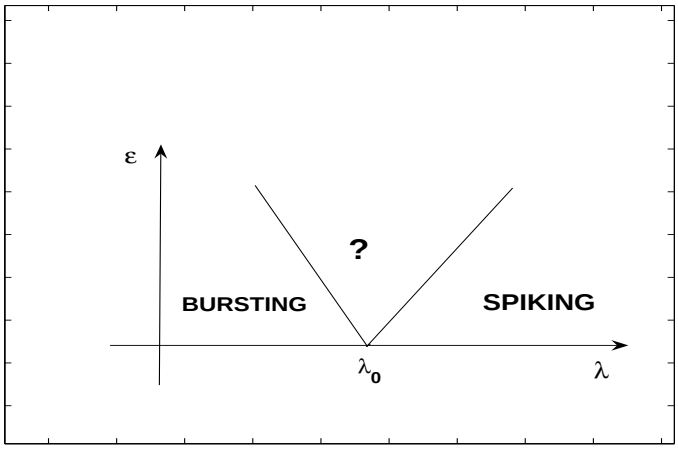

Figure 6.4. *Dependence of bursting oscillations and continuous spiking with respect to* ϵ and λ. *Bursting exists if* $\lambda < \lambda_0$ *and spiking exists if* $\lambda > \lambda_0$. *However, how small* ϵ *must be depends on how close* λ *is to* λ_0. *There is an wedge-shaped region in which chaotic dynamics exist.*

6.3 Elliptic Bursting

Square-wave is only one type of bursting. Examples of two other types are shown in Figure 6.5; these are commonly known as *elliptic* and *parabolic* bursters. Elliptic bursters exhibit small amplitude oscillations during the silent phase and the amplitude of spikes gradually wax and wane. An important feature of parabolic bursters is that the frequency of spikes first increases and then decreases during the active phase. Both elliptic and parabolic bursters arise in models for neuronal activity and other excitable systems. Elliptic bursters arise in models for thalamic

neurons, rodent trigeminal neurons, certain neurons within the basal ganglia and 40-Hz oscillations. Parabolic bursting is found in models for Aplysia R-15 neurons.

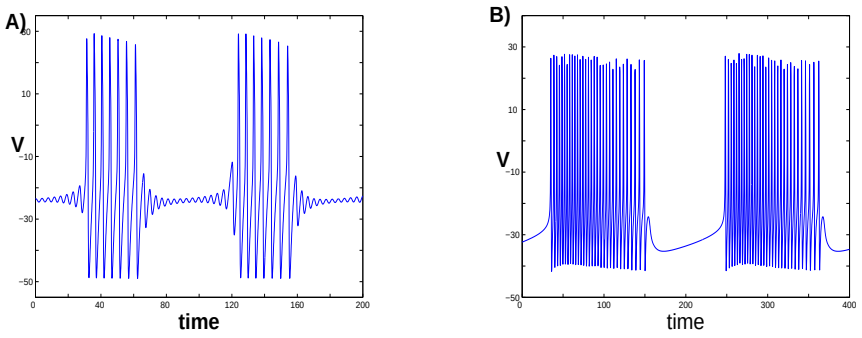

Figure 6.5. *(A) Elliptic burster. Note the subthreshold oscillations. (B) Parabolic bursting. The frequency of spiking first increases and then decreases during the active phase.*

Elliptic bursting can arise in a system of the form (6.1) in which there are two fast variables and one slow variable. Parabolic bursting, on the other hand, requires at least two slow variables. What characterizes each class of bursting are properties of the bifurcation diagram of the fast subsystem in which the slow variables are considered as bifurcation parameters.

The elliptic burster shown in Figure 6.5 is a solution of (6.2) and (6.3) with parameter values given in Table 6.2 . As before, we denote the first two equations in (6.2) as the fast subsystem (FS) and the third equation for calcium as the slow equation. The bifurcation diagram of (FS) is shown in Figure 6.6; the bifurcation parameter is the slow variable $[Ca]$. Note that (FS) exhibits bistability: there is a range of values of $[Ca]$ for which there exist both a stable fixed point and a stable limit cycle. Bistability is also an important feature of square-wave bursting. An important difference, however, between square-wave and elliptic bursting is that for elliptic bursting the curve C_{FP} of fixed points of (FS) need not be Z-shaped; there may be only one fixed point of (FS) for each value of $[Ca]$. The branch of periodic solutions P now originates at a subcritical Hopf bifurcation along C_{FP}. Suppose that the Hopf point is at $[Ca] = [Ca]_{HB}$. Then the fixed points of (FS) are stable for $[Ca] > [Ca]_{HB}$ and unstable for $[Ca] < [Ca]_{HB}$. Since the Hopf bifurcation is subcritical, the branch of periodic orbits which bifurcates from the Hopf point are unstable. This branch "turns around" at some $[Ca] = [Ca]_{SN} > [Ca]_{HB}$ giving rise to a stable branch of limit cycles for $[Ca] < [Ca]_{SN}$. There are two limit cycles for $[Ca]_{HB} < [Ca] < [Ca]_{SN}$, one of which is stable and the other unstable. The two limit cycles come together at $[Ca] = [Ca]_{SN}$ where there is a fold or saddle-node bifurcation of limit cycles. This is where that active phase of the bursting trajectory terminates.

To obtain bursting, we must make some assumptions on the slow variable

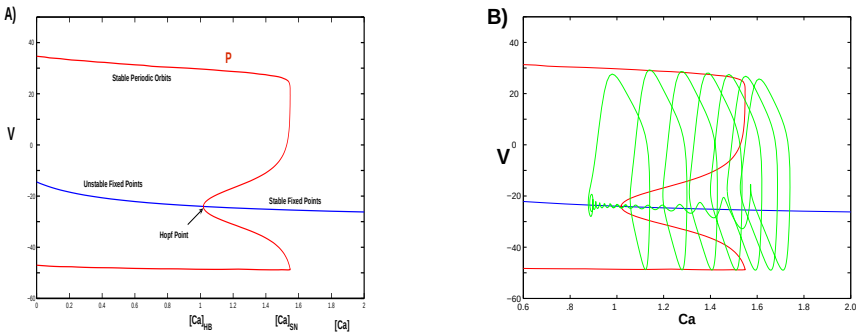

Figure 6.6. *Bifurcation diagram associated with elliptic bursting. The projection of the elliptic bursting trajectory onto the bifurcation diagram is shown in (B).*

dynamics so that $[Ca]$ decreases during the silent phase and (on average) increases during the active phase. In what follows, we define $h(V, n, [Ca])$ so that the right hand side of the third equation in (6.2) can be written as

$$\frac{d[Ca]}{dt} = \epsilon h(V, n, [Ca]).$$

We hypothesize that $h(V, n, [Ca]) < 0$ near C_{FP}. During the silent phase, the bursting solution evolves near the stable portion of C_{FP}, with $[Ca]$ decreasing, until it passes the Hopf point, beyond which the fixed points along C_{FP} are no longer stable. Note, however, that the trajectory does not jump up to the active phase immediately after crossing the Hopf point. The slow variable $[Ca]$ may traverse a distance that is $O(1)$ with respect to ϵ past the Hopf point before jumping up. This type of delayed behavior or slow-passage past a Hopf point has been studied extensively in the singular perturbation literature.

We next consider the active phase. We cannot expect that $h(V, n, [Ca]) > 0$ near all of P, as was the case for square-wave bursting. This follows from geometric considerations. For square-wave bursting, the two-dimensional surface $\{h = 0\}$ separates the curve C_{FP} and the cylindrical-shaped surface P. For elliptic bursting, C_{FP} lies "inside" of P, so $\{h = 0\}$ cannot separate them. Since $h < 0$ near C_{FP}, it follows that we must expect that $h < 0$ near at least some part of P; that is $[Ca]$ must decrease during some portion of the active phase. The best we can hope for is that there is a net increase of $[Ca]$ as the bursting trajectory passes near P.

In order to make this more precise, we consider the average increase or decrease of $[Ca]$ along the bursting trajectory. For each $[Ca] \leq [Ca]_{SN}$, let $(v_{[Ca]}(t), w_{[Ca]}(t))$ denote the periodic solution along the outer branch of P and let $T([Ca])$ be the corresponding period. Then

$$\bar{h}([Ca]) = \frac{1}{T([Ca])} \int_0^{T([Ca])} h(v_{[Ca]}(t), w_{[Ca]}(t), [Ca])dt$$

represents the average of h along this fixed limit cycle. We assume that $\bar{h}([Ca]) > 0$ for each $[Ca] < [Ca]_{SN}$. This assumption implies that in the limit $\epsilon \to 0$, the net change in $[Ca]$ during the active phase is positive. Thus during the active phase, $[Ca]$ slowly increases, on average, until the bursting solution passes the fold along P. The fast dynamics then forces the trajectory back towards C_{FP} and a new silent phase begins.

Both square-wave and elliptic bursting depend on bistability and hysteresis. An important difference is how the active phase is initiated and terminates. For square-wave bursting, the silent phase ends at a saddle-node of fixed points and the active phase ends at a homoclinic orbit of the fast subsystem. For elliptic bursting, the silent phase ends when there is a slow passage through a Hopf bifurcation and the active phase ends at a saddle-node of limit cycles. These contrasting mechanisms reflect differences in firing properties. For square-wave bursting, the frequency of spiking slows down at the end of each active phase; for elliptic bursting there are subthreshold oscillations during the silent phases.

6.4 Parabolic Bursting

Both square-wave and elliptic bursting can be achieved in a system with only one slow variable. Moreover, both depend on bistability of the fast dynamics. Parabolic bursting, on the other hand, requires at least two slow variables and does not arise from a hysteresis phenomenon. The parabolic burster shown in Figure 6.5B satisfies the equations:

$$\begin{aligned} C_m \frac{dV}{dt} &= -I_L - I_K - I_{Ca} - I_{KCa} - I_{CaS} + I_{app} \\ \frac{dn}{dt} &= \phi(n_\infty(V) - n)/\tau_n(V) \\ \frac{d[Ca]}{dt} &= \epsilon(\mu I_{Ca} - [Ca]) \\ \frac{ds}{dt} &= \epsilon(s_\infty(v) - s)/\tau_s \end{aligned} \tag{6.5}$$

where I_L, I_K, I_{Ca} and I_{KCa} are leak, potassium, calcium and calcium-dependent potassium channels, respectively, as described in (6.2) and (6.3). Here, we have added a new calcium current

$$I_{CaS} = g_{CaS} s(V - E_{Ca}) \tag{6.6}$$

which depends on the gating variable s. Here, $s_\infty(V) = .5(1 + tanh((v - 12)/24))$. Parameter values are given in Table 6.2. Note that in this model there are two fast variables, V and n, and two slow variables, $[Ca]$ and s.

A geometric model for parabolic bursting is the following. Consider a system of the form (6.1) where $x \in R^n, n \geq 2$, and $y = (y_1, y_2) \in R^2$. There are now two slow variables, namely y_1 and y_2. We first describe the bifurcation structure of the fast subsystem with both slow variables considered as parameters. We then discuss properties which the slow dynamics must satisfy.

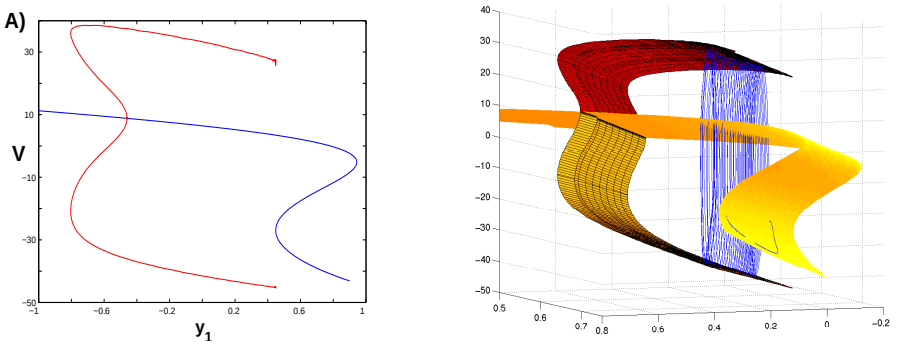

Figure 6.7. *Bifurcation diagram of the fast-subsystem for parabolic bursting. (A) One of the slow variables is fixed. Note that the branch of periodic orbits end at a SNIC. (B) With both slow variables as bifurcation parameters, the sets of fixed points and limit cycles form surfaces. Also shown is the projection of the bursting trajectory onto the bifurcation diagram.*

The bifurcation diagram of the fast subsystem is illustrated in Figure 6.7 where we plot one component of the fast variable, corresponding to the membrane potential. In Figure 6.7A, we fix one of the slow variables to be constant and compute the bifurcation diagram with the other slow variable as constant. Note that there is a Z-shaped curve of fixed points and a branch of periodic orbits that originate at a subcritical Hopf point and that terminate at a SNIC. If we allow both slow variables to vary, as shown in Figure 6.7B, then the set of fixed points and branch of limit cycles become surfaces, while there is a curve of Hopf points, as well as SNIC's. The fixed points along the lower branch are assumed to be stable fixed points of (FS). In Figure 6.7B, we also show the maximum and minimum values of the fast variable along each of these periodic solutions along with the projection of the parabolic bursting solution shown in Figure 6.5. In Figure 6.8, we show regions in the slow phase plane where the fast dynamics exhibit spiking and stable resting behavior along with the projection of the bursting solution. Note that these regions do not overlap; that is, the fast dynamics do *not* exhibit bistability. The spiking and resting regions are divided by a curve at which the fast dynamics exhibit a SNIC; this curve also corresponds to the fold of the fixed-point surface.

The existence of a parabolic bursting solution also requires hypotheses on the slow dynamics. There must be a mechanism by which the slow variables drift back and forth between the spiking and resting regions. In what follows, we exploit the singular nature of the fast/slow system to obtain reduced equations for just the slow variables y_1 and y_2. This is done in two steps, one for the silent phase and one for the active phase. The method we describe here is quite general and can be applied to any bursting model of the form (6.1).

First consider the silent phase. We change to the slow time-scale $\tau = \epsilon t$ in

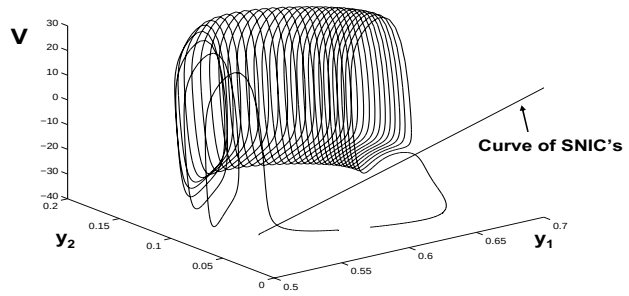

Figure 6.8. *Projection of the parabolic bursting solution onto (V, y_1, y_2)-space. There is a curve in the slow (y_1, y_2)-plane corresponding to SNIC's. This curve separates the regions where the fast subsystem exhibits spiking and resting behavior.*

(6.1) and then set $\epsilon = 0$ to obtain:

$$\begin{aligned} 0 &= f(x, y) \\ \frac{dy}{d\tau} &= g(x, y). \end{aligned}$$

The first equation in (10.9) simply states that during the silent phase, the (singular) solution lies close to the lower branch of the fixed-point surface. If we write this branch as $x = \Phi(y)$, then the second equation in (10.9) becomes:

$$\frac{dy}{d\tau} = g(\Phi(y), y). \tag{6.7}$$

This is then the reduced system for the evolution of the slow variables during the silent phase.

To obtain the reduced equations for the evolution of the slow variables in the active phase we use the method of averaging. Suppose that $y = (y_1, y_2)$ lies in the region where there exists a stable limit cycle of (FS). Let $x_y(t)$ be the corresponding periodic solution of (FS) with period $T(y)$ and consider the averaged quantity

$$\bar{g}(y) \;=\; \frac{1}{T(y)} \int_0^{T(y)} g(x_y(t), y) dt.$$

The evolution of the slow variables during the active phase is then given by the averaged equations

$$\frac{dy}{d\tau} = \bar{g}(y). \tag{6.8}$$

Parabolic bursting corresponds to the existence of a closed curve in the slow (y_1, y_2) phase plane which passes through both the region of stable fixed points and the region of stable limit cycles. While passing through the silent and active regions, the curve must satisfy (10.35) and (6.8), respectively.

The active phase of the bursting solution both begins and ends along a curve of homoclinic bifurcations. Since the limit cycles have frequencies which approach infinity at the homoclinic bifurcations, the inter spike interval is longer at both the beginning and the end of each burst. This accounts for the parabolic nature of the period of fast oscillations.

6.5 Classification of Bursters

We have now described three types of bursters. Other types are possible and do, in fact, arise in important applications. There has been considerable effort to classify the types of bursters, beginning with Rinzel who was the first to analyze bursting models using fast/slow geometric methods. He described square-wave, parabolic and elliptic bursting and this classification scheme was extended by Bertram et.al. Izhikevich has given a complete topological classification of bursters arising from co-dimension-1 bifurcations; he identified 120 different topological types. All of these classification schemes are based on the bifurcation structure of the fast-subsystem in which the slow variables are considered to be bifurcation parameters. Different types of bursters correspond to different ways in which there can be transitions between resting behavior and repetitive spiking. Since resting behavior and repetitive spike correspond to branches of stable equilibria and periodic limit cycles of the fast subsystem, it follows that different classes of bursters represent different bifurcations of these branches. For example, square-wave bursting corresponds to a saddle-node, or fold, bifurcation of the branch of stable fixed points and a saddle-homoclinic bifurcation of the branch of stable limit cycles of the fast-subsystem. It follows that in order to classify bursters, we need to understand all possible co-dimension-1 bifurcations of equilibria and limit cycles.

It turns out that there are just four types of bifurcations of equilibria and four types of bifurcations of limit cycles. Hence, there are 16 types of bursting in which the resting state is a stable equilibrium point and its spiking state is a stable limit cycle. The four bifurcations of equilibria are: saddle-node (fold), saddle-node on an invariant circle (SNIC), supercritical Hopf, and subcritical Hopf. The four types of of bifurcations of limit cycles are: saddle-node on invariant circle (SNIC), saddle homoclinic orbit, supercritical Hopf and subcritical Hopf. In Izhikevich's classification scheme, each type of bursting is named according to: *bifurcation of equilibria / bifurcation of limit cycle.* Hence, the square-wave burster is denoted as *fold/homoclinic*, while an elliptic burster is referred to as *subHopf/fold cycle*.

An example of a bursting-type not discussed earlier is shown in Figure 6.9. Here the branch of stable fixed points of the fast subsystem ends at a saddle-node bifurcation (fold) and the branch of stable limit cycles of the fast subsystem end at a fold limit cycle bifurcation. Note that the branch of limit cycles that bifurcate from the homoclinic orbit are unstable with respect to the fast subsystem. This branch

"turns around" at the fold limit cycle bifurcation to form the branch of stable limit cycles. Bertram et. al. referred to this as *Type IV* bursting; it corresponds to a fold/fold cycle in Izhikevich's classification scheme. This type of bursting was first discovered in the Chay-Cook model for bursting in Pancreatic β-cells. It also arises in a model for a leech heart interneuron and in a model for synaptically Pre-Botzinger cells, where it was referred to as *top hat* bursting.

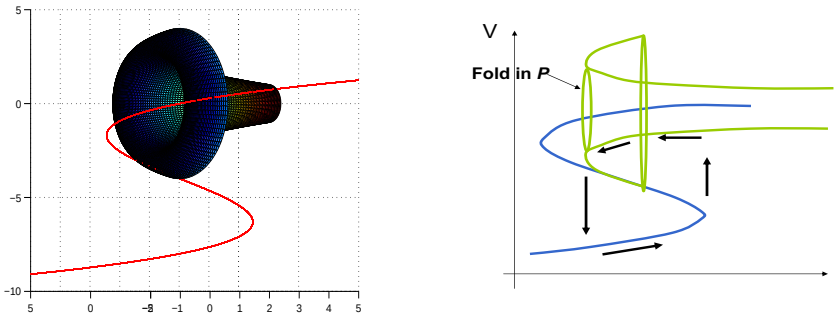

Figure 6.9. *Top hat bursting.*

6.6 Chaotic Dynamics

6.6.1 Chaos in Square-wave Bursting Models

Even three-variable minimal bursting models can exhibit complex dynamics as parameters are varied. There are at least two ways in which square-wave bursters, for example, may generate chaotic behavior. As the singular perturbation parameter ϵ decreases, the number of spikes per bursts increases. The process of adding a spike may be quite complicated. It was shown in [ ] that chaotic dynamics may arise during this transition. For example, Figure 6.10A) and C) show solutions of (6.2) in which there are 3 and 2 spikes per burst. The parameters are given in Table 6.2 with $\epsilon = .0072$ and $\epsilon = .0073$, respectively. For the solution shown in Figure 6.2), $\epsilon = .00721998$. Note that there are bursts which possess 2, 3 and 4 spikes. The pattern of spikes per burst does not appear to repeat in a periodic manner. We note that this mechanism for chaotic dynamics only arises for a very small range of parameter values. It was shown in [?] that the size of this range is of the order $e^{-k/\epsilon}$ for some $k > 0$. This is indeed very small, so the chaos is probably not of much biological interest.

A second mechanism for chaos arises during the transition from bursting to continuous spiking. Figure 6.11 shows four solutions of (6.2); the parameters are chosen as in Table 6.2 except for k_{Ca}. In Figures 6.11) A)-D), we set $k_{Ca} = 1, 1.225, 1.228$ and 1.3, respectively. Note that as we increase k_{Ca}, the systems appears to transition from exhibiting periodic bursting, chaotic bursting,

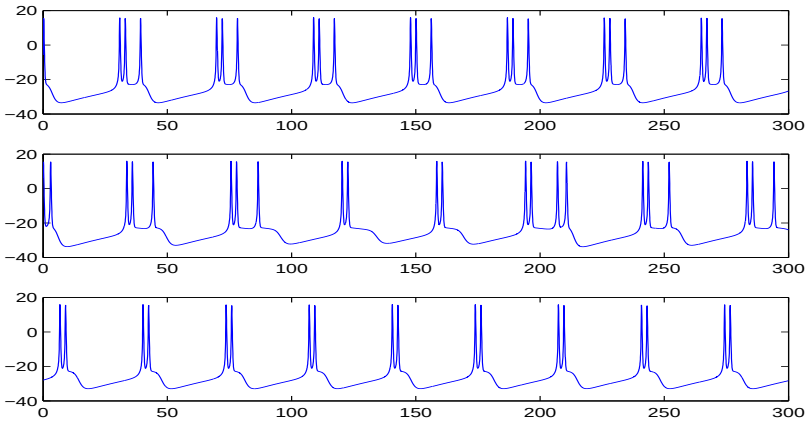

Figure 6.10. *Chaotic dynamics may arise during the transition of adding spikes. As we increase ϵ, the number of spikes per burst will increase. As B) demonstrates, during this transition, there may exist solutions in which the number of spikes per burst is not constant.*

chaotic spiking and finally periodic spiking. For the chaotic bursting shown in Figure (6.11))B), some bursts are much longer than others; the occurrence of long or short bursts appear to be random.

A standard way to analyze oscillatory behavior, including chaos, is in terms of a Poincare return map. We start with a given periodic bursting orbit and then consider a two-dimensional cross-section $\mathcal{S}$ that is transverse to the flow; i.e., trajectories cross $\mathcal{S}$ at a non-zero angle. Then the Poincare map is defined from some subset of $\mathcal{S}$ back to $\mathcal{S}$ as follows: For each $p_0 \in C_{FP}$ let $\gamma(t, p_0)$ be the solution starting at p_0. If p_0 is sufficiently close to the original periodic orbit, then this trajectory must eventually cross $\mathcal{S}$ at some time $T_0 > 0$. The Poincare map is defined as $\pi(p_0) \equiv \gamma(T_0, p_0)$. This is where the solution starting at p_0 "returns" to the cross-section.

Consider the example illustrated in Figure 6.11C). Here, the solution exhibits repetitive firing that is not regular. We compute a Poincare map by recording the value of n and $[Ca]$ each time that V decreases through 0. For this model, the recorded values of n are all about .35; however, the value of calcium varies between 18.7 and 20.8. The solution is approximately represented by the time series of values of calcium, $[Ca]_1, [Ca]_2, ...$ We can generate a one-variable map whose solutions approximate this time series as follows. With initial conditions $n = 0$ and $n = .35$, we specify a value for calcium, and then integrate the full differential equations until V crosses 0 again, obtaining the next value of calcium. This is then the Poincare map, which we denote as $y = F([Ca])$, and is shown in Figure 6.12. From the figure, it is evident that there is an intersection of the

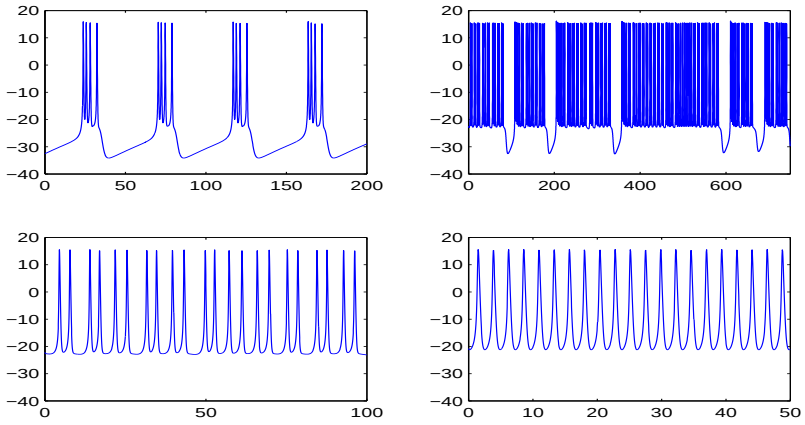

Figure 6.11. *A chaotic burst arising during the transition between bursting and continuous spiking. As we increase the parameter k_{Ca}, the model may exhibit A) regular bursting; B) chaotic bursting; C) chaotic spiking; and D) continuous spiking.*

line $y = [Ca]$ and $y = F([Ca])$. This means that there is a single concentration of calcium $[Ca]^*$, to which the trajectory returns after one cycle. This corresponds to a periodic solution to the mode equations. If $|F'([Ca]^*)| > 1$, as is the case here, then the periodic solution is unstable. This type of map is characteristic of dynamics that have chaotic behavior. Further analysis of the map is presented in the exercises.

6.6.2 Symbolic Dynamics

In the preceding section, we saw that the complex dynamics that arise during the transition from bursting to continuous spiking in square-wave bursting models can be described in terms of a one-dimensional map. This description must be an approximation of the full dynamics since the model has three dependent variables and the Poincare section, along with the return map, must be two-dimensional. Terman analyzed this two-dimensional map and rigorously demonstrated that chaotic dynamics must arise during the transition from bursting to continuous spiking; moreover, the dynamics can be described in terms of symbolic dynamics. Here, we will present the main result in [?].

In order to state this result, we need to recall some basic properties of two-dimensional maps and how they relate to symbolic dynamics. The most famous two-dimensional map that exhibits complex dynamics is the Smale-horseshoe map, which we will now quickly describe. A more detailed discussion of this map can be found in [?].

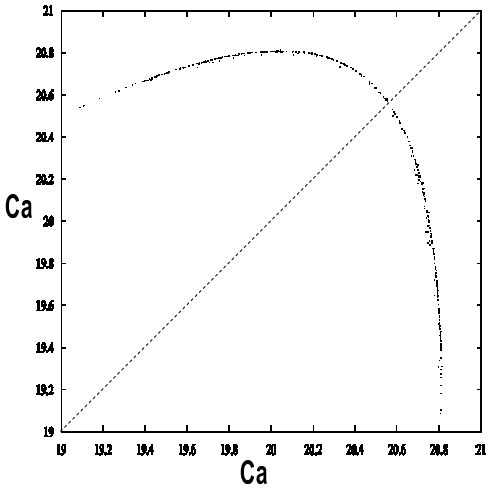

Figure 6.12. *Poincare map.*

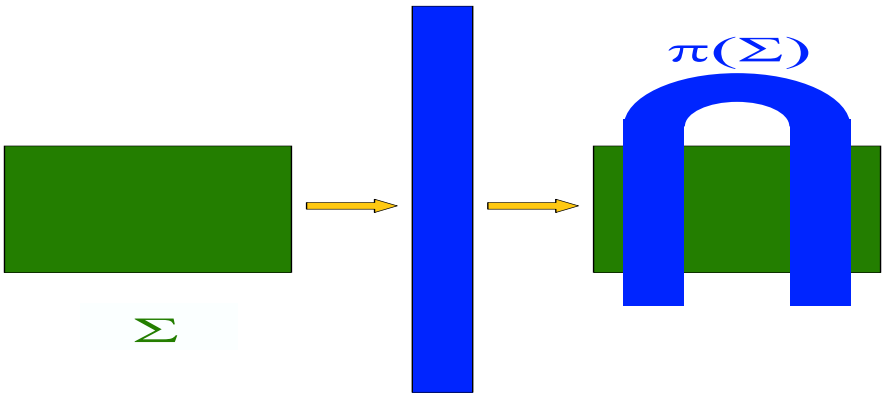

Figure 6.13. *The Smale Horseshoe. The square $\mathcal{S}$ is stretched in the vertical direction, contracted in the horizontal direction and then folded. The intersection of $\pi(\mathcal{S})$ with $\mathcal{S}$ forms two vertical strips.*

Let $\mathcal{S}$ be the unit square in $\mathcal{R}^2$. Then the Smale-horseshoe map is a map, which we denote as π, from $\mathcal{S}$ to $\mathcal{R}^2$. The construction of this map consists of two steps, as shown in Figure 6.13. First we contract $\mathcal{S}$ by an amount μ in the horizontal direction and expand $\mathcal{S}$ in the vertical direction by an amount λ. Here, $0 < \mu < 1$ and $\lambda > 1$. The second step is to fold the resulting rectangle so that

$\pi(\mathcal{S}) \cap \mathcal{S}$ consists of two vertical rectangles as shown in the Figure.

While the Smale-horseshoe map is easy to define, it is not at all clear if it has any interesting properties. Note, for example, that not every point in $\mathcal{S}$ is mapped back into $\mathcal{S}$. It is not obvious if there is any point x_0 whose entire orbit $\{\pi^k(x_0) : k = 0, \pm 1, \pm 2, ...\}$ lies entirely in $\mathcal{S}$. In what follows, we let

$$\Lambda = \{x_0 : \ \pi^k(x_0) \in \mathcal{S} \ \text{ for all } k\}.$$

We can also ask if there are any fixed points or periodic orbits of π; that is, does there exist $x_0 \in \mathcal{S}$ and an integer k such that $\pi^k(x_0) = x_0$? If there do exist periodic orbits, then how many are there? Or, does there exist an orbit in $\mathcal{S}$ that is not periodic; that is, does there exist $x_0 \in \mathcal{S}$ such that $\pi^k(x_0) \in \mathcal{S}$ for every integer k but $\pi^k(x_0) \neq x_0$ unless $k = 0$? As it turns out, this map does indeed have infinitely many periodic orbits and uncountably many aperiodic orbits. There is a very eloquent way to prove this result and this involves symbolic dynamics.

Let Σ be the set of all bi-infinite sequences of two symbols; that is,

$$\Sigma = \{a_i : -\infty < i < +\infty\}, \quad \text{where} \ \ a_i = 0 \text{ or } 1.$$

Consider the shift map $\sigma : \Sigma \to \Sigma$ defined as follows: Suppose that $\mathbf{a} = \{a_i\}$ and $\sigma(\mathbf{a}) = \mathbf{b}$ where $\mathbf{b} = \{b_i\}$. Then $b_i = a_{i-1}$. That is, σ shifts the indices of $\mathbf{a}$. Now σ defines a dynamical system on Σ and it easy to see that this dynamical system contains infinitely many periodic orbits. For example, if

$$\mathbf{a} = \{.... \ 0 \ 1 \ 0 \ 1 \ 0 \ 1 \ .....\}$$

then the orbit $\{\sigma^k(\ a)\}$ has period two. It is also easy to see that there are uncountable many aperiodic orbits. This is left as an exercise.

A remarkable fact is that Σ and Λ are topologically equivalent. There is a one-to-one correspondence between points in Σ and points in Λ; moreover, there is a one-to-one correspondence between orbits generated by σ and orbits generated by π. It follows that π has a countably infinite number of periodic orbits and uncountably many aperiodic orbits.

To state the result concerning chaotic dynamics in square-wave bursting models, we will need to consider another two-dimensional map. This is shown in Figure 6.14. We start with two squares, denoted as $\mathcal{S}_1$ and $\mathcal{S}_2$. Each square is expanded, contracted, folded and mapped into $\mathcal{R}^2$ as shown in the Figure. Note that $\pi(\mathcal{S}_1)$ intersects both $\mathcal{S}_1$ and $\mathcal{S}_2$ in a single vertical strip; $\pi(\mathcal{S}_2)$ intersects $\mathcal{S}_1$ in a vertical strip but does not intersect $\mathcal{S}_2$. This map also generates symbolic dynamics; however, the symbolic dynamics is somewhat different than that generated by the Smale-horseshoe map. A description of the symbolic dynamics is given in [ ]. Finally, we will need to consider generalizations of this map. These are shown in Figure 6.4. For each integer $K > 1$, there are K-squares; each rectangle is contracted, expanded, folded and then mapped into $\mathcal{R}^2$ as shown. We denote the map corresponding to K-rectangles as π_K. These maps generate increasingly more complicated symbolic dynamics.

We can now describe the main result in [?]. Consider the (λ, ϵ) parameter plane shown in Figure 6.4. Recall that there is a wedge shaped region, arising

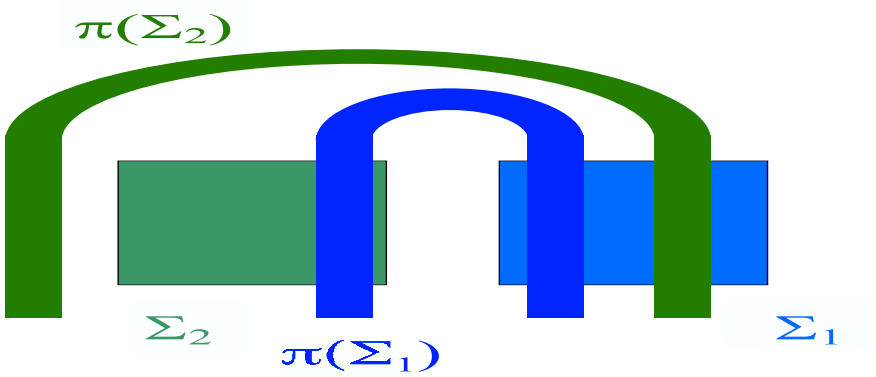

Figure 6.14. *A generalized Smale horseshoe-type map that generates symbolic dynamics. The two squares* $\mathcal{S}_1$ and $\mathcal{S}_2$ *are stretched, contracted and then folded onto each other as shown.*

from $(\lambda, \epsilon) = (\lambda_0, 0)$, in which we could not conclude whether the system exhibits bursting or continuous spiking. The results in [?] state that there are infinitely many wedge-shaped regions that emanate from $(\lambda_0, 0)$ as shown in Figure 6.15. There is a return map $\pi(\lambda, \epsilon)$ such that in each odd sector S_{2j-1}, the map gives rise to dynamics topologically equivalent to that shown in Figure 6.15 with j-rectangles. Hence, as we fix $\epsilon > 0$ sufficiently small and we increase λ from the bursting to the spiking regions, then the system must undergo a series of increasingly more complicated global bifurcations. We note that each sector may only be defined for ϵ sufficiently small. Hence, each line segment $\epsilon = \epsilon_0$ may only intersect finitely many sectors. However, the number of sectors which the line segment $\epsilon = \epsilon_0$ intersects becomes unbounded as $\epsilon_0 \to 0$.

6.6.3 Bistability and the Blue-Sky Catastrophe

Shilnikov et.al. described a mechanism in which a model can exhibit coexistence of both stable continuous spiking and stable bursting oscillations. The system also generates chaotic dynamics, through a mechanism known as the *blue-sky* catastrophe. The mechanism underlying bistability between spiking and bursting is shown in Figure 6.16. Note that the fast-subsystem has the bifurcation structure of the fold/fold or top hat burster. This bifurcation structure is actually not that crucial for what follows; a square-wave burster would work just as well. Here we consider the top hat burster, since this is what was used in the original papers.

For bistability, what is important is that there are two periodic orbits of the full system that lie close to the branch of limit cycles of the fast-subsystem. See

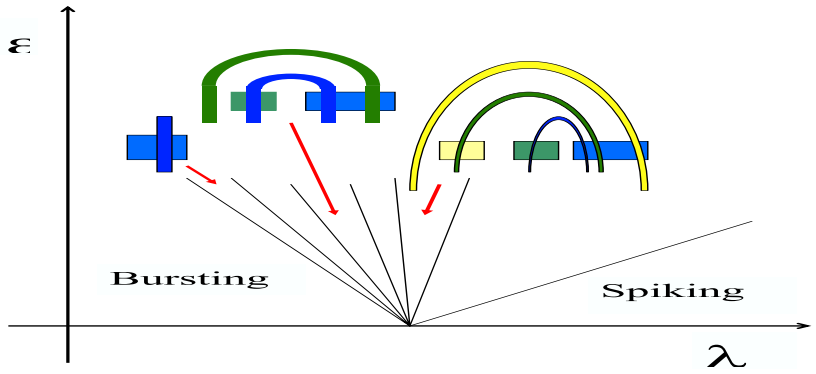

Figure 6.15. *The transition from bursting to spiking in the square-wave bursting model. If one fixed $\epsilon > 0$ and increases λ, then there is a series of increasingly more complex global bifurcations in which the system exhibits symbolic dynamics.*

Figure 6.16A. One of these periodic orbits is stable, while the other is unstable. The unstable periodic orbit is a saddle with a two-dimensional stable manifold. Trajectories which lie on one side of this manifold will approach the stable periodic orbit and exhibit continuous spiking, while trajectories that lie on the other side will display bursting. In order to explain the geometry in more detail, we need to say more about the fast-subsystem and how it perturbs if the singular perturbation parameter is positive.

Consider a fast/slow system of the form (6.1) in which there are two fast variables and one slow variable; that is, $x \in \mathcal{R}^2$ and $y \in \mathcal{R}^1$. Suppose that the set of fixed points of (FS) forms a Z-shaped curve whose left knee is at $y = y_{LK}$. Moreover, there is a branch of stable limit cycles of (FS), which we denote as $\mathcal{P}$. Recall that, for $\epsilon > 0$ small, the dynamics near $\mathcal{P}$ is determined by the averaged equations. That is, let $x(y;t)$ denote the limit cycle of (FS) for some y and suppose that this periodic orbit has period T_y. Then the evolution of the slow variable near $\mathcal{P}$ for $\epsilon > 0$ is determined by the averaged equation:

$$\frac{dy}{d\tau} = \hat{g}(y) \equiv \frac{1}{T_y}\int_0^{T(y)} g(x(y;t),y)dt. \tag{6.9}$$

Here, $\tau = \epsilon t$ is the slow time variable. A fixed point of this equation corresponds to a periodic solution of the full system. If $\hat{g}(y_0) = 0$, then there is a periodic solution $\gamma_\epsilon(t) = (x_\epsilon(t), y_\epsilon(t))$ of the full system (6.1) such that $|y_\epsilon(t) - y_0| = O(\epsilon)$ for all t and ϵ sufficiently small. This periodic solution is stable, with respect to the full system, if $\hat{g}'(y_0) < 0$ and unstable if $\hat{g}'(y_0) > 0$. In general, a solution $(x(t), y(t))$

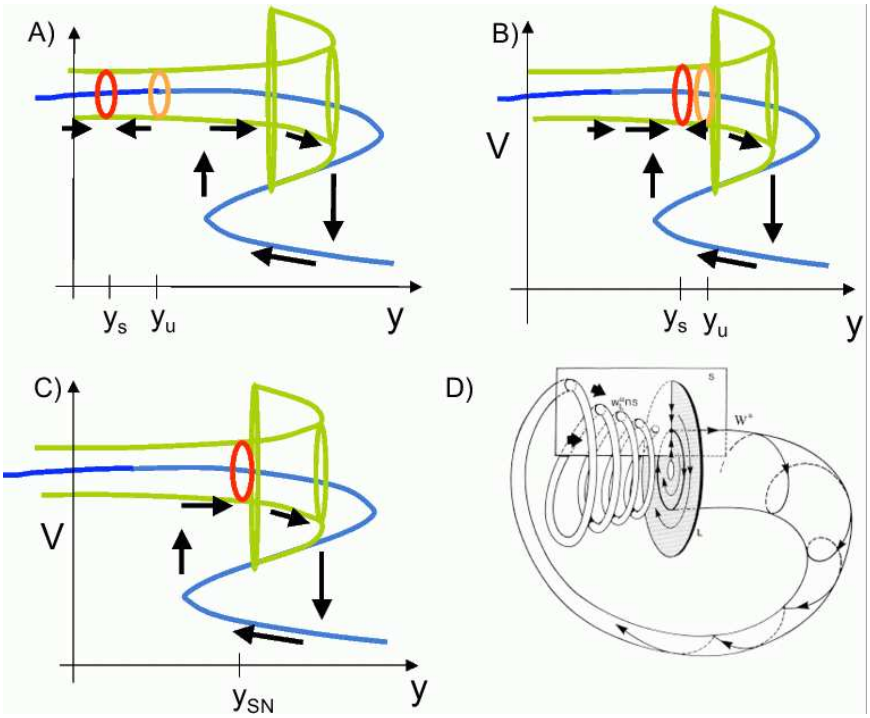

Figure 6.16. *A) Bistability of bursting and spiking. There are stable and unstable limit cycles of the full system that lie close to $\mathcal{P}$, the branch of periodic solutions of the fast-subsystem. The stable manifold of the unstable limit cycle separates those orbits that approaching the bursting solution from those that exhibit continuous spiking. B) The periodic orbits lie to the right of the left knee. Bursting no longer exhibits; however, there are orbits heteroclinic between the two limit cycles. C) and D) A blue-sky catastrophe occurs if the two limit cycles form a saddle-node bifurcation.*

with $|y(0) - y_0|$ small, will first evolve according to the fast dynamics to near $\mathcal{P}$ and then evolve according to the slow averaged equation either towards or away from $\gamma_\epsilon(t)$.

Suppose that $\hat{g}'(y_0) > 0$ so that $\gamma_\epsilon(t)$ is unstable. Then the stable manifold of γ_ϵ separates those solutions which drift to the left from those that drift to the right. To understand this stable manifold further, consider the case $\epsilon = 0$. The local stable manifold of $\gamma_0(t) = (x(y_0; t), y_0)$ is the set of points in the plane $\{y = y_0\}$ that lie close to $\mathcal{P}$. (By *local* we mean near the periodic orbit.) It follows that for $\epsilon > 0$, the two-dimensional local stable manifold of $\gamma_\epsilon(t)$ lies very close, i.e. $O(\epsilon)$, to the plane $\{y = y_0\}$.

It is now easy to see how the model can display both stable spiking and stable bursting. Suppose that the averaged equations has both a stable and a unstable

fixed point at $y_s > y_u$, respectively. Fix $\epsilon > 0$ and denote the corresponding periodic solutions of the full system as $\gamma_s(t)$ and $\gamma_u(t)$. We further assume that $y_u < y_{LK}$ so that the right knee lies to the "right" of the unstable periodic orbit. The two-dimensional stable manifold of $\gamma_u(t)$ divides phase-space into two regions. Trajectories in the region $y < y_u$ will approach $\mathcal{P}$ and then drift towards γ_s, while trajectories in the region $y > y_u$ will drift away from γ_u towards the fold in $\mathcal{P}$. Once these trajectories cross $\mathcal{P}$ they will be forced down towards the branch of stable fixed points of (FS). Since $y_{LK} > y_u$, a stable bursting oscillations will result.

Chaotic dynamics can arise in this model as follows. Suppose that as some parameter changes, the positions of y_u and y_s change. In particular, suppose that both move to the right so that at some parameter value, $y_s > y_{LK}$. This is shown in Figure 6.16B. In this case, if a trajectory begin near $\mathcal{P}$ in the region where $y > y_u$, then this solution will drift away from γ_u towards the fold in $\mathcal{P}$, fall down to the silent phase and eventually jump back up. Since $y_u > y_{LK}$, the trajectory will approach γ_s as $t \to \infty$. We note that this solution will approach γ_u as $t \to -\infty$. This corresponds to an orbit that is heteroclinic between the two periodic orbits.

We now suppose that as a parameter changes the stable and unstable periodic orbits come together at a saddle-node of periodic bifurcation. This is shown in Figure 6.16C. In this case, there will be orbits that are homoclinic to the saddle-node periodic orbit. A more detailed diagram of this is shown in Figure 6.16D. Once the periodic orbit near $\mathcal{P}$, disappears, the system exhibits bursting oscillations. However, it has been demonstrated that the bursting is chaotic. The dynamics illustrated in Figure 6.16 has been called the 'blue-sky catastrophe' and the behavior described in this section has been observed in neuronal models. Details can be found in [silnikov].

6.7 Bibliography

Rinzel [40, 41] was the first to classify bursting oscillations using fast/slow analysis and to consider their geometric properties in phase space. He described square-wave, parabolic and elliptic bursting, and this classification scheme was extended by others, including Bertram [5]. A complete classification of bursting oscillations. has been given by Izhikevich [23]; a detailed description of his classification scheme is presented in his book [24], where there is also a discussion of possible roles of bursting oscillations in neuronal computations.

Several authors have studied the transitions between resting behavior, bursting and continuous spiking. References include Ermentrout and Kopell [12], Terman [35, 49, 50], Destexhe and Gaspard [**?**], Shilnikov and Cymbalyuk [46]and Medvedev [**?**].

A recently published book edited by Coombes and Bressloff [9] contains many review articles pertaining to various aspects of bursting oscillations.

6.8 Exercises

1) For the square-wave, elliptic, and parabolic bursting models:

a) compute the bifurcation diagrams of the fast-subsystem

b) draw the phase planes of the fast-subsystem for various values of the slow variable

c) in Matlab, draw the projection of the bursting solution onto the bifurcation diagram

d) change parameters to see how the transitions are made

2) Poincare map. Consider the square-wave bursting model and choose parameters so that it exhibits nice continuous spiking. Compute the Poincare map. Now change parameters so that it goes into bursting. Identify parameters where periodic doubling bifurcations of the Poincare map take place. Find parameter values where the map is chaotic.

3) Bistability of the fast subsystem. Start with a square-wave burster and solve it until the solution is in the silent phase. Now introduce a short perturbation to "kick" it into the spiking regime. How long is the subsequent burst of spiking activity? How does the length of spiking activity depend on the phase at which the perturbation was introduced? Next, introduce the perturbation while the bursting solution is spiking so that the perturbation kicks the solution into the silent phase. How does the length of the subsequent silent phase depend on the phase at which the perturbation was introduced? Do the same thing for elliptic bursters.

3) Smale horseshoe.

a) Prove that the Smale horseshoe map exhibits a countable number of periodic orbits and uncountably many aperiodic orbits.

b) How many periodic orbits are there with period N.

c) Prove that there is a dense orbit.

4) Wang's 2-compartment model for 40hz oscillations.

5) Rinzel-rush model for triangular bursting.

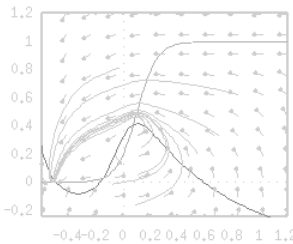

Chapter 7

Propagating Action potentials.

Neurons need to communicate over long distances. This is accomplished by electrical signals, or action potentials, that propagate along the axon. We have seen that linear cables cannot transmit information very far; neural signals are able to reach long distances because there exist voltage-gated channels in the cell membrane. The combination of ions diffusing along the axon, together with the nonlinear flow of ions across the membrane, allows for the existence of an action potential that propagates along the axon with a constant shape and velocity.

One of the great successes of the Hodgkin-Huxley model is that it exhibits the propagating action potential; moreover, it accurately predicts the speed of the action potential. We remark that the Hodgkin-Huxley equations is a system of a nonlinear partial differential equation coupled with three ordinary differential equations. It is not at all clear how Hodgkin and Huxley were able to numerically solve these equations in order to compute the speed of the propagating action potential.

Mathematically, the Hodgkin-Huxley model is an example of a system reaction diffusion equations. The propagating action potential corresponds to a traveling wave solution; that is, it is a solution that 'moves' with constant shape and velocity. Motivated to a large part by the Hodgkin-Huxley model, there was a flowering of papers in the mid seventies and eighties in which mathematicians developed sophisticated techniques in order to rigorously analyze the existence, uniqueness and stability properties of traveling wave solutions to reaction diffusion equations.

In this chapter, we will begin by describing a geometric way to think about the propagating action potential. As we shall see, the traveling wave corresponds to a homoclinic orbit of a system of ordinary differential equations. Hodgkin and Huxley numerically computed the speed of the wave by considering this system of ODE's and we shall briefly describe how Hodgkin and Huxley did this. We will then describe mathematical methods for analyzing the existence and stability properties of traveling waves. Here we will consider reduced models such as the Morris-Lecar equations. We will also consider periodic wave trains and models for myelinated axons and discrete diffusion.

7.1 Traveling waves and homoclinic orbits

The propagating action potential corresponds to a traveling wave solution of the Hodgkin-Huxley model. By this we mean the following: We rewrite the Hodgkin-Huxley model from Chapter 2 as

$$\begin{aligned} C_m \frac{\partial V}{\partial t} &= \frac{4d}{R_i}\frac{\partial^2 V}{\partial x^2} - I_{ion} + I \\ \frac{\partial \Gamma}{\partial t} &= \alpha_\Gamma(V)(1-\Gamma) - \beta_\Gamma(V)\Gamma \end{aligned} \tag{7.1}$$

where $\Gamma = m, h$, or n. Figure 7.1 shows a simulation of the action potential down a 10 centimeter axon with a diameter of a millimeter. The time between the two action potentials at 6 and 7 centimeters is about 8 milliseconds so that the velocity of this action potential is 1.25 meters per second. The spatial profile looks just like the temporal profile in backwards time and scaled by the velocity. The propagating action potential thus corresponds to a solution of (7.1) that 'travels' with constant shape and velocity; that is, it is a *traveling wave solution*. If we denote the shape of the wave as $\hat{V}(x)$ and the speed of the wave as c, then the traveling wave solution satisfies $V(x-ct,t) = \hat{V}(x)$.

Suppose we change coordinates and replace x by $\xi = x - ct$. For convenience, we will also write V instead of $\hat{V}$. Then the new equations are

$$\begin{aligned} C_m \frac{\partial V}{\partial t} &= C_m c\frac{\partial V}{\partial \xi} + \frac{4d}{R_i}\frac{\partial^2 V}{\partial \xi^2} + I - I_{ion} \\ \frac{\partial \Gamma}{\partial t} &= c\frac{\partial \Gamma}{\partial \xi} + \alpha_\Gamma(V)(1-\Gamma) - \beta_\Gamma(V)\Gamma \end{aligned} \tag{7.2}$$

where, again, $\Gamma = m, h$ or n. A traveling wave is thus a time-independent solution in ξ and satisfies a system of ordinary differential equations. We will consider an infinite domain. Then the traveling wave solution must also satisfy $V(\xi = \pm\infty) = V_{rest}$.

It will be more convenient to write (7.2) as a first-order system; that is, we set $\frac{dV}{d\xi} = U$. Then (7.2) is equivalent to the following system of five ordinary differential equations:

$$\begin{aligned} \frac{dV}{d\xi} &= U \\ \frac{dU}{d\xi} &= \frac{R_i}{4d}(I_{ion} - I - cC_m U) \\ \frac{d\Gamma}{d\xi} &= -(\alpha_\Gamma(V)(1-\Gamma) - \beta_\Gamma(V)\Gamma)/c \end{aligned}$$

The solution must also satisfy the boundary conditions

$$(V, U, m, h, n)(\pm\infty) = (V_{rest}, 0, 0, 0, 0).$$

If follows that the propagating action potential corresponds to a homoclinic orbit of (7.3). Figure 7.1C shows a projection of this orbit in the coordinates $(V, n, c\frac{dV}{d\xi})$.

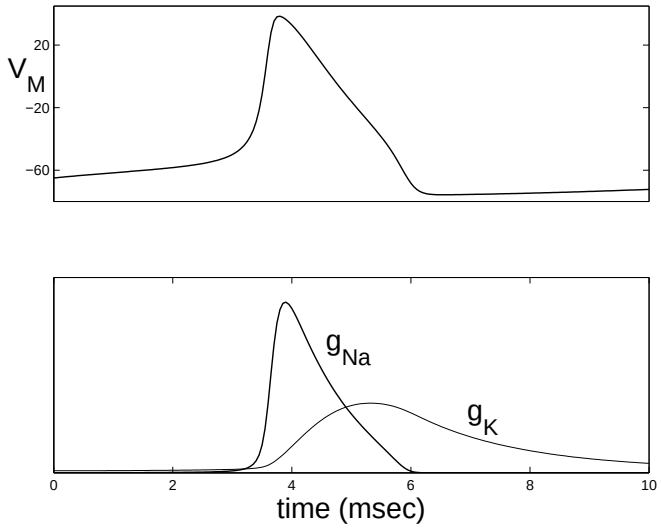

Figure 7.1. *Action potential propagation for the HH equations. Discretization of the nonlinear PDE for a 10 cm axon into 150 segments.*$R_i = 100\Omega cm$ *and* $d = 0.1cm$. *(A) Voltage at* $x = 6$ *cm and* $x = 7$ *cm, showing velocity if about 1.25 meters/second (B) Spatial profile at* $t = 20$ *msec; (C) Three-dimensional trajectory of the wave at grid point 50; axes are voltage, potassium gate and the voltage derivative.*

This system is parameterized by c and one only expect homoclinic orbits to exist for discrete values of c. This is because homoclinic orbits are generically codimension 1 bifurcations. The mathematical question is to prove that there *is* such a c for which there is a homoclinic orbit. Once the homoclinic has been found, we have to determine whether it is a stable stationary solution to equation (7.2). We generally expect that for parameters near the homoclinic orbit, there are periodic orbits with arbitrarily long periods in the space-like variable ξ. Furthermore, in some cases, we can find very complex dynamics for equations (7.3).

Hodgkin and Huxley did not attempt to numerically solve the full partial differential equation (**??**) as they did not have the necessary computing equipment. (Although, we can now do it in less than a few seconds on a laptop!). Rather, they used a shooting procedure to estimate the speed of the wave. What they did was to first fix a value of c and find a solution that decays to rest as $\xi \to -\infty$. Denote this solution as $\hat{U}(\xi, c)$. They then needed to find a value of c for which $\lim_{\xi\to+\infty} U(\xi, c_0) = 0$. For most values of c, the solution $\hat{U}(\xi, c)$ satisfies either $\lim_{\xi\to+\infty} U(\xi, c) = +\infty$ or $\lim_{\xi\to+\infty} U(\xi, c) = -\infty$. If one finds two values of c, say c_1 and c_2, such that $\lim_{\xi\to+\infty} U(\xi, c_1) = -\infty$ and $\lim_{\xi\to+\infty} U(\xi, c_2) = +\infty$, then there must be a value c_0 between c_1 and c_2 for which $\lim_{\xi\to+\infty} U(\xi, c_0) = 0$; that

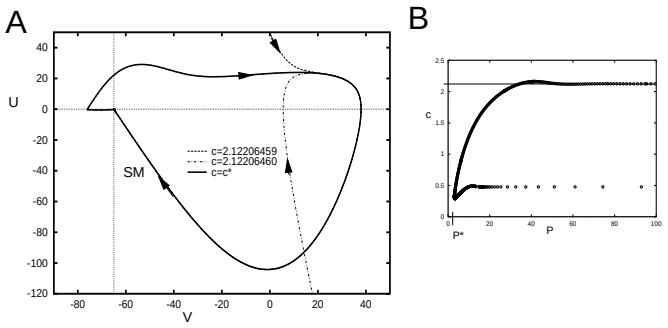

Figure 7.2. *Numerical shooting for the HH ODE. (A) Shooting from the one-dimensional stable manifold (SM) by integrating backward in time. For c too low, the stable manifold gos off the top and for c too high, out the bottom. (B) Numerically computed dispersion relation. This shows the speed c as a function of the spatial period, P. For each period $P > P^*$ there are two velocities; one fast and one slow.*

is, $\hat{U}(\xi, c_0)$ is a homoclinic orbit and c_0 is the speed of the traveling wave. Using an iteration scheme, Hodgkin and Huxley used this idea to estimate the speed of the wave. Figure 7.2A shows an example of numerical shooting in order to find the homoclinic orbit.

7.2 Scalar bistable equations.

There have been numerous papers in which mathematical methods were developed to rigorously analyze the existence and stability of traveling waves. Most of these studies considered simplified neuronal models such as the FitzHugh-Nagumo or the Morris-Lecar equations. These papers also often assume that the recovery dynamics ((h, n) in the Hodgkin-Huxley equations) is slow. One then lets the rates of these equations go to zero and this leads to a singular perturbation problem. The basic idea is to then piece together a traveling wave or periodic orbit. This basic idea has also been used to analyze the stability of the wave.

We will discuss some of these methods in detail. However, before considering to a two-dimensional example, we first review the general theory of bistable scalar reaction-diffusion equations. This theory will be important in the construction of traveling waves in higher dimensional systems. Moreover, by considering a simpler example, we can more easily introduce some of the geometric constructions that will be needed later.

Consider the following equation defined on the real line:

$$\frac{\partial u}{\partial t} = f(u) + \frac{\partial^2 u}{\partial x^2}, \quad -\infty < x < \infty. \tag{7.3}$$

We assume, for now, that $f(u) = u(1-u)(u-\alpha)$ where $0 < \alpha < 1/2$. Then, 0 and 1

are stable equilibria to the equation $du/dt = f(u)$ and α is an unstable equilibrium. We would like to find traveling wave solutions to (7.3) which join the two stable states. That is, we want a solution of the form $u(x,t) = U(\xi),\ \xi = x - ct$, that satisfies

$$lim_{\xi\to-\infty}U(\xi) = 1 \quad \text{and} \quad lim_{\xi\to+\infty}U(\xi) = 0.$$

Here, c is the velocity of the wave. Note that $U(\xi)$ satisfies the ordinary differential equation

$$c\frac{dU}{d\xi} = f(U) + \frac{d^2U}{d\xi^2}. \tag{7.4}$$

We rewrite this as the first order system

$$\begin{aligned}\frac{dU}{d\xi} &= Y\\ \frac{dY}{d\xi} &= cY - f(U).\end{aligned} \tag{7.5}$$

We want to show that there exists a unique value of c for which there is a solution that satisfies the boundary conditions

$$lim_{\xi\to-\infty}(U(\xi), Y(\xi)) = (1,0) \quad \text{and} \quad lim_{\xi\to+\infty}(U(\xi), Y(\xi)) = (0,0).$$

Hence, we need to show that there is a (unique) value of the wave-speed c for which (7.5) exhibits a heteroclinic orbit. One proves the existence of a heteroclinic orbit using a standard shooting argument. Here we will only outline the geometric construction and leave details to the reader as exercises.

Note that for every value of c, the fixed points at $(0,0)$ and $(1,0)$ are saddles. Both the stable and unstable manifold of each of these fixed points has dimension one. A heteroclinic orbit corresponds to a trajectory that lies in both the unstable manifold of $(1,0)$ and the stable manifold of $(0,0)$. The phase planes of (7.5) for $c = 0$ and c very large are shown in Figures 7.3. Note that when $c = 0$, the unstable manifold of $(1,0)$ lies "below" the stable manifold of $(0,0)$ (in the region $0 < U < 1$), while if c is very large, then opposite is true. Since these manifolds depend in a continuous way on the parameter c, one can show that there must exist at least one value of c for which the manifolds "cross". This then corresponds to the heteroclinic orbit, or traveling wave solution of (?). In the exercises, you are asked to fill in the details and prove that the wave speed is uniquely determined.

We note that this construction does not depend on the precise form of $f(u)$. More generally, we may assume that f is any smooth 'cubic=shaped' function such that $f(0) = f(1) = 0$, $f'(0) < 0$ and $f'(1) < 0$. (In fact, we don't even need that f is 'cubic-shaped'; it may have an arbitrary number of zeros.) Then the shooting argument outlined above can be used to demonstrate the existence of the traveling wave solution.

A key point of interest for us is how c depends on f. Multiply (7.4) by $dU/d\xi$ and integrate over the real line:

$$c\int_{-\infty}^{\infty}\left(dU(\xi)/d\xi\right)^2 d\xi = \int_{-\infty}^{\infty}\left(dU(\xi)/d\xi\right) f(U(\xi))d\xi + \int_{-\infty}^{\infty}\left(dU(\xi)/d\xi\right)\left(d^2U/d\xi^2\right)d\xi.$$

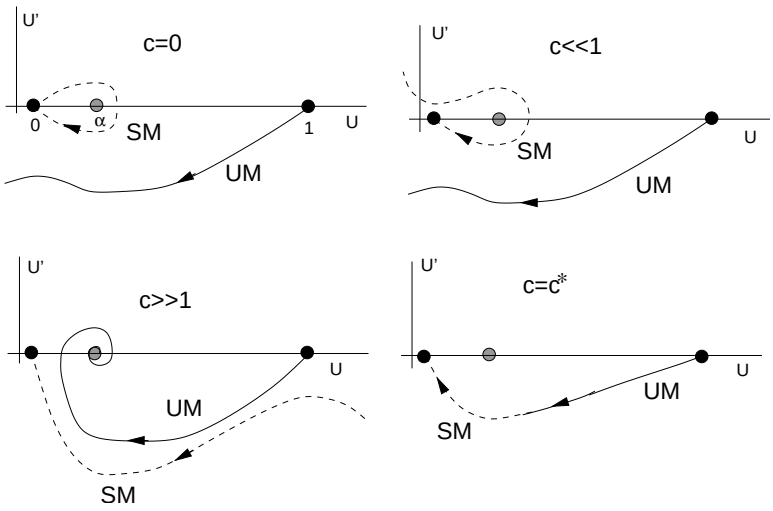

Figure 7.3. *Existence of fronts in equation (7.4). For $c = 0$, the system is integrable. For c small, the unstable manifold of the right fixed point (UM) falls below the stable manifold of the left-fixed point (SM). For large c, the positions of the manifolds are reversed. For a single intermediate value of $c = c^*$, the manifolds intersect for a homoclinic.*

Since $U(\xi)$ is monotone, we let $u = U(\xi)$ be a new variable. Then $du = (dU/d\xi)d\xi$ so that the first integral on the right-hand side is now $\int_0^1 f(u)du$. The second integral vanishes since

$$(dU/d\xi)(d^2U/d\xi^2)d\xi = \frac{1}{2}d\left(\frac{dU}{d\xi}\right)^2$$

which integrates to zero because $dU/d\xi(\pm\infty) = 0$. Thus we have

$$c\int_{-\infty}^{\infty}(U'(\xi))^2 d\xi = \int_0^1 f(u)du. \tag{7.6}$$

Since the integral in (7.6) is positive, this shows that the sign of the velocity, c, is the same as the area of f between the two-stable equilibria. What does it mean intuitively? Suppose that the middle root α is close to 0. Then the region where $f(u)$ is negative, $(0, \alpha)$, is small compared to where f is positive. Thus the integral will be positive and the wave will move to the right converting the medium from the 0-state to the 1-state. On the other hand, if α is close to 1, then the area will be negative, the velocity will be negative, the wave will move to the left and the 1-state will be converted to the 0-state. Finally, if the positive and negative areas balance exactly, the velocity of the wave will be zero. The case of more than two-stable equilibria can be similarly handled and under fairly general circumstances; there can be multiple wave fronts with multiple speeds joining these fixed points.

7.2.1 Numerical shooting.

How do we obtain the velocity c numerically? let us write the traveling wave equations as a system:

$$U' = Y, \quad Y' = -cY - f(U).$$

Consider the fixed point at $(1, 0)$. The linearization is:

$$A \equiv \begin{pmatrix} 0 & 1 \\ -f'(1) & -c \end{pmatrix}.$$

Since $f'(1) < 0$, the determinent of A is negative, so the fixed point is a saddle and the eigenvalues are

$$\lambda^{\pm} = \frac{-c \pm \sqrt{c^2 - 4f'(1)}}{2}.$$

The unstable manifold is tangent to the eigenvector corresponding to λ^+ which is simply $[1, \lambda^+]^T$. Thus, we take initial conditions, $(U, Y) = (1 - a, -a\lambda^+)$ where a is a small positive number. We then integrate the equations until the trajectory crosses either the $U-$axis or the $Y-$axis. If the $U-$axis is hit, then c is too big while if the $Y-$axis is hit, c is too small. In exercise *, we have you try your hand at shooting for the problem $f(u) = u(u - \alpha)(1 - u)$.

7.3 Singular construction of waves.

We now describe the construction of a traveling pulse for the equation:

$$\frac{\partial v}{\partial t} = f(v, w) + \frac{\partial^2 v}{\partial x^2}$$
$$\frac{\partial w}{\partial t} = \epsilon g(v, w)$$

where ϵ is a small positive number. We will consider a general class of nonlinear functions f and g. We assume that the v-nullcline, $\{f(v, w) = 0\}$, is a cubic-shaped curve; moreover, $f > 0$ (< 0) below (above) this nullcline. We further assume that the w-nullcline, $\{g(v, w) = 0\}$, is a monotone increasing function that intersects the v-nullcline at precisely one point which we denote as (v_r, w_r). Moreover, this point lies along the left branch of the cubic-shaped v-nullcline. Finally, assume that $g > 0$ (< 0) below (above) the w-nullcline. Note that (v_r, w_r) corresponds to a stable (resting) state of the kinetic equations

$$\frac{dv}{dt} = f(v, w)$$
$$\frac{dw}{dt} = \epsilon g(v, w).$$

We remark that these assumptions are satisfied for many two-variable models for neurons including the FitzHugh-Nagumo equations and the Morris-Lecar equations.

A traveling wave solution is a solution of the form $(v(x,t), w(x,t)) = (V(\xi), W(\xi))$ where $\xi = x + ct$. As before, c is the (yet to be determined) wave speed; (V, W) now corresponds to the profile of the wave. We note that we have now chosen $\xi = x + ct$ instead of $\xi = x - ct$ as was done in the preceeding section. The wave is now 'moving' to the left.

The traveling wave equations are:

$$\begin{aligned} \frac{dV}{d\xi} &= U \\ \frac{dU}{d\xi} &= cU - f(V,W) \\ \frac{dW}{d\xi} &= \frac{\epsilon}{c} g(V,W) \end{aligned} \tag{7.7}$$

along with the boundary conditions

$$\lim_{\xi \to \pm\infty} (V, U, W)(\xi) = (v_r, 0, w_r). \tag{7.8}$$

Hence, we seek values of c for which there exists an orbit homoclinic to the fixed point $(v_r, 0, w_r)$. There may, in fact, be at least two waves. This was demonstrated for the FitzHugh-Nagumo model by Hastings, Carpenter and Conley. It has been demonstrated that the wave with the larger speed is the stable one and this is what we will concentrate on. In a later section, we will consider the stability of this wave.

We demonstrate the existence of a homoclinic orbit using methods from the geometric theory of singular perturbations. The idea is to formally set $\epsilon = 0$ and construct a singular homoclinic trajectory. Once we construct the singular trajectory, we worry about proving that this trajectory perturbs to an actual homoclinic orbit for $\epsilon > 0$. The singular trajectory will consist of four pieces; these correspond to the jump-up from the silent to the active phase, the active phase, the jump-down to the silent phase, and the return to rest in the silent phase. See Figure 7.4. We note that the jumps up and down take place on a fast time scale ξ, while the active phase and the return to rest take place on a slower time scale $\eta = \epsilon\xi$. It will be important to exploit this separation of time-scales in the construction of the singular orbit.

It will be convenient to introduce some notation. Recall that the nullcline $f(V, W) = 0$ is cubic-shaped. For fixed W, let $(V_L(W), W)$ and $(V_R(W), W)$ be the points that lie on the left and right branch of the cubic, respectively. (Here we are assuming that W lies below the local maximum of the cubic.) Note that $V_L(w_r) = v_r$, since (v_r, w_r) is a fixed point of the kinetic equation (7.7).

We first consider the jump-up to the active phase. Let $\epsilon = 0$ in (7.7); this leads to the reduced system

$$\begin{aligned} V' &= U \\ U' &= cU - f(V,W) \\ W' &= 0. \end{aligned} \tag{7.9}$$

Note that W must be constant. For the jump up, we take $W \equiv w_r$ and (7.9) becomes just the traveling equation for the scalar equation. From the discussion

in the previous section, we know that there exists a unique value of c, which we denote as c^*, for which there exists a unique heteroclinic orbit of (7.9) that connects $(v_r, 0, w_r)$ along the left branch of the cubic nullcline to $(V_R(w_r), 0, w_r)$ along the right branch. This heteroclinic orbit corresponds to the jump-up piece of the full singular orbit and c^* corresponds to the $(\epsilon = 0)$ velocity of the traveling pulse. For the remainder of the analysis we assume that $c = c^*$.

We next consider the active phase. Here we introduce in (7.7) the slow variable $\eta = \epsilon\xi$ and then set $\epsilon = 0$ to obtain the reduced system

$$\begin{aligned} 0 &= U \\ 0 &= cU - f(V, W) \\ \frac{dW}{d\eta} &= \frac{1}{c} g(V, W). \end{aligned} \tag{7.10}$$

The first two equations state that this piece of the singular orbit lies on the cubic nullcline $f(V, W) = 0$ and the third equation gives the rate at which the orbit evolves along the cubic. For the active phase, the singular orbit lies on the right branch of the cubic beginning at the point $(V_R(w_r), 0, w_r)$. See Figure ??

Now consider the jump down. Once again we use the fast time scale and consider the reduced system (7.9) with $c = c^*$. Now W is constant, say W_{jd}, along this piece; however, it is not clear how we should choose this constant. Analysis similar to that given in the preceding section demonstrates for each such W that lies below the local maximum of the cubic, there exists a wave-speed $c(W)$ for which there exists a solution of (**??**) that approaches $(V_R(W), 0, W)$ along the right branch as $\xi \to -\infty$ and approaches $(V_L(W), 0, W)$ along the left branch as $\xi \to +\infty$. Now the pulse must maintain a constant width, so the speed of the jump up and the jump down must be the same. That is, we must choose the position of the jump down so that $c(W_{jd}) = c^*$. This condition determines W_{jd} uniquely. We remark that this condition may not be satisfied. In this case, the jump-down is at the local maximum of the v-nullcline. Such systems admit traveling waves for a continuum of velocities. (See exercise *). For some models, it is possible to compute W_{jd} explicitly. In the exercises, the reader is asked to do this for the FitzHugh-Nagumo equations in which $f(v, w) = v(1 - v)(v - \alpha) - w$.

Finally, we consider the return to rest. Here, we use the slow time scale η and consider the reduced system (**??**). This piece of the singular orbit lies along the left branch of the cubic, as shown in Figure 7.4, and approaches the rest state as $\xi \to \infty$.

Note that during the active phase, the traveling wave lies along the right branch of the cubic V-nullcline; moreover, the slow-variable W satisfies (7.10). From this we can compute the width, Ξ, of the action-potential. Using the slow variable η, we find that

$$\Xi = c^* \int_{w_r}^{W_{jd}} \frac{dw}{g(V_R(w), w)}.$$

For the membrane models that we have considered, $g(v, w) = \epsilon(w_\infty(v) - w)/\tau(v)$. If $w_\infty(v)$ is very sharp, then, $w_\infty(v_R(w))$ will be close to 1. Assuming that $\tau(v)$

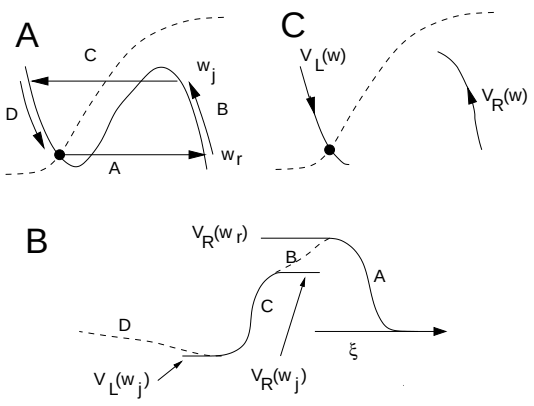

Figure 7.4. *Singular construction of the traveling wave. (A) Projection of the wave onto the $(V, w)-$phase plane. Initiation of the action potential is a front from the rest state to the right-branch with w held constant. Then along the right-branch of the nullcline w increases until w_j where a wave back goes to the left branch. w then decays to rest along the left branch. (B) Pieces of the wave and the relevant voltages. Solid lines are front dynamics governed by (**??**) and dashed are branch dynamics governed by (**??**). (C) Details of the left and right branches.*

does not vary much, we can approximate $g(V_R(w), w)$ by $(1 - w)/\tau_R$ where τ_R is a constant. Then, it is easy to show that the width of the action potential is

$$\Xi = \tau_R c^* \ln \frac{1 - w_r}{1 - W_{jd}}.$$

7.3.1 Wave trains.

How do we compute the periodic wave trains for this model? Basically, the method is relatively easy. Instead of jumping from w_r, we jump at a slightly higher value of w, say, w_P. Thus, we first compute a jump from $V_L(w_P)$ to $V_R(w_P)$. This will have a smaller velocity than the solitary pulse (why?); call it c_P. As before, we need to find a jump-back point, w_Q, such that the velocity of the wave from $V_R(w_Q)$ to $V_L(w_Q)$ matches c_P. Then we compute the dynamics on the left branch until w reaches w_P and the process repeats. The up-jump and down-jump are relatively fast compared to the evolution time of w along the two branches. Thus the actual period of these wave trains is approximately:

$$\Xi_P \approx \frac{c_P}{\epsilon} \left[\int_{w_P}^{w_Q} \frac{dw}{g(V_R(w), w)} + \int_{w_Q}^{w_P} \frac{dw}{g(V_L(w), w)} \right].$$

7.4 Dispersion relations

In general, if a dynamical system has a homoclinic orbit for at a special parameter value, then for parameters nearby, we expect to find periodic orbits. What do such orbits correspond to in equation (7.2)? Consider the following "experiment:" We initiate an action potential at one end of a semi-infinite cable. Then, after a period of time T, we initiate another one, and so on. This will asymptotically produce a traveling wave train. Denote the temporal period by T, the spatial separation between the successive action potentials by P and assume that the wave train travels at a velocity c. Note that c, P and T are not independent of each other: $P = cT$, since the spatial period is dictated by the velocity and the temporal period. The velocity c will not be the same as the velocity of the homoclinic orbit (solitary action potential) because sucessive action potentials travel on a cable which may be refractory from the prior activity. As we will see below, this can lead to either lower values of c or, surprisingly, higher values of c. Thus, we expect that c will be a function of T or P. This notion is well known from nonlinear wave theory. The spatial and temporal frequencies ($1/P$ and $1/T$) are related through the so-called *dispersion relation.* Traditionally, in mathematical neuroscience, the relationship is given by $c = c(P)$, the spatial period between waves. A way to think about this is to suppose that we make the axon into a ring. A periodic wave train with spatial period P is a solitary wave propagating around the ring with circumference P.

The dispersion relationship is very important since it tells us how the axon respond to multiple stimuli. As with the homoclinic orbit, it is possible to numerically compute the dispersion relationship by looking for a periodic orbit and varying c, the speed. Figure 7.2B shows the dispersion relationship for the HH equations. There are several important points to note. There is a minimum period, P^*, below which waves do not seem to exist. This means that there is a limit to how closely spaced action potentials can be on the axon; not surprising, given the refractoriness (recovery from the hyperpolarization). For each $P > P^*$, there are two possible speeds, one is fast and the other slow. What is perhaps most interesting is that the velocity exhibits damped oscillations around the solitary wave speed c_∞. This means that for some spatial periods, the waves move *faster* than the solitary wave. The reason for this is complex, but we can provide a bit of intuition. Consider the recovery to rest after the wave is passed. This is dominated by the behavior of the linearization of (7.3) at rest. We note that this linearization has a single negative eigenvalue and all the remaining eigenvalues have positive real parts. Two of these eigenvalues are complex, $\alpha \pm i\beta$, so that we expect that there will be some damped oscillations on return to rest. (Note that we shoot backward in ξ, the traveling coordinate, so the oscillations are damped rather than growing.) This means that the membrane potential shows damped oscillations near rest, e.g.

$$V(\xi) \approx V_{rest} + Ae^{\alpha\xi} \cos \beta\xi$$

for ξ large and negative. This implies that for some values of ξ, $V(\xi)$ is larger than V_{rest} so that it takes less current to produce an action-potential. Thus, waves which are spaced close to the characteristic length $2\pi/\beta$ would have the added "boost" and would travel faster.

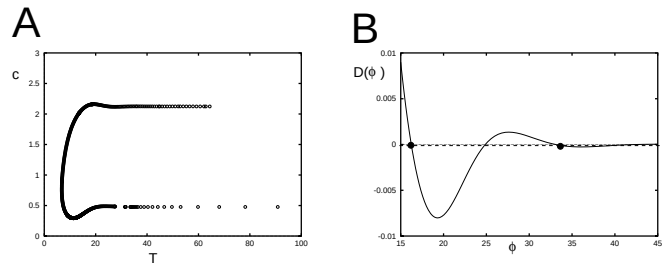

Figure 7.5. *Velocity versus temporal period $T = P/c$ for the HH equations. (A) Full dispersion relation; (B) The function $D(\phi) = 1/c(\phi) - 1/c_\infty$.*

7.4.1 Dispersion kinematics.

Rinzel and Maginu (1984) came up with a clever method for studying multiple waves along axons without using the full neuron model. The idea is to use the dispersion relation to compute the instantaneous velocity of an action potential which is a certain distance (in space or time) from an initial impulse. Suppose that an initial pulse is initiated at $x = 0$ and at time t_1. Then the time at which this first impulse reaches a point x is $T_1(x) = t_0 + x/c_\infty$ where c_∞ is the spead of the solitary pulse. Suppose we introduce a new spike at $x = 0$ at time t_2. The instaneous velocity of this new spike at $x = 0$ will depend on the time since the last spike occured at $x = 0$; that is, $t_2 - t_1$. Rinzel and Maginu suggest that the instantaneous velocity should be approximated by $c(t_2 - t_1)$ where $c(T)$ is the velocity of a wave with *temporal period* T. (If one has the dispersion curve as a function of the spatial period, P, divide this by $c(P)$ to get the temporal period.) Figure 7.5 replots the data from Figure 7.2B to show the temporal dispersion relationship for the HH equations. Given this Rinzel-Maginu approximation, the time that a second action potential reaches a point x will evolve as:

$$\frac{dT_2}{dx} = \frac{1}{c(T_2(x) - T_1(x))}. \tag{7.11}$$

The time interval, $\phi \equiv T_2(x) - T_1(x)$, between two action potentials initiated at $x = 0$ will evolve (in space, x) as

$$\frac{d\phi}{dx} = \frac{1}{c(\phi)} - \frac{1}{c_\infty} \equiv D(\phi). \tag{7.12}$$

If $D(\phi)$ has a zero(s), $\bar{\phi}$, then the time-difference between the two action potentials will lock at these zeros. Figure 7.5B shows a plot of $D(\phi)$ and two zeros of this function. Viewed as an evolution equation, we see that if $D'(\phi) < 0$, then the timing difference is stable. Intuitively, this says the following: Suppose that ϕ is slightly larger than $\bar{\phi}$ so that $D(\phi) < 0$. This means that $c(\phi) > c_\infty$ so that the trailing action potential will speed up and the temporal difference, ϕ, decreases. The case of multiple action potentials is easily analyzed by assuming that the only action

potential which matters is the one preceding. The timing of the $(j+1)^{st}$ action potential will depend only on the time since the j^{th},

$$\frac{dT_{j+1}}{dx} = \frac{1}{c(T_{j+1} - T_j)}.$$

7.5 Morris-Lecar revisited and Shilnikov dynamics

Here we will briefly describe additional properties of traveling wave solutions for the Morris-Lecar equations. In particular, we point out that these properties depend on whether the model cells exhibit class I or class II dynamics.

7.5.1 Class II dynamics

The Morris-lecar model is two-dimensional, so that the analysis of propagating action potentials leads to a three-dimensional dynamical system of the form:

$$\begin{aligned} \frac{dV}{dt} &= U \\ \frac{dU}{dt} &= -U/c - f(V,W) \\ \frac{dW}{dt} &= -g(V,W)/c. \end{aligned} \tag{7.13}$$

We start as in Chapter *, with the ML model with class II dynamics. There is a unique fixed point, $(v_r, 0, w_r)$, and as shown in exercise *, it has a one-dimensional stable manifold and a two-dimensional unstable manifold. Figure 7.6 shows the dispersion relation for the the ML model in this regime. As expected, it looks very similar to Figure 7.2B as both types of cells are class II. At $I = 80$, the linearization of (7.13) at the fixed point has eigenvalues, $-\nu$ and $\mu \pm i\omega$ with $\nu > \mu > 0$. Thus, we can apply a very powerful theorem from dynamical systems due to Shilnikov. This theorem implies that if (7.13) has a homoclinic orbit for $c = c^*$, and if the linearization of the fixed point has a real eigenvalue, r, and a pair of complex conjugate eigenvalues, $\alpha \pm i\beta$, with r and α of opposite signs and $0 < |\alpha| < |r|$, then there must exist infinitely many periodic orbits for values of c near c^*. Furthermore, the system contains so-called Smale horseshoe dynamics. This implies very complex behavior. Indeed, we can expect very complicated sequences of action potentials to persist on the axon. An interesting project would be to use the kinematics of the dispesrion relationship to find some of these complex orbits.

We note that Shilnikov-type dynamics may also exist for the FitzHugh-Nagumo model:

$$\begin{aligned} \frac{\partial v}{\partial t} &= \frac{\partial^2 v}{\partial x^2} + f(v) - w + I \\ \frac{\partial w}{\partial t} &= b(v - kw) \end{aligned}$$

where $f(v) = v(1-v)(v-a)$, $0 < a < 1$, $b > 0$ and $k \geq 0$. Here we assume that $I = k = 0$. Hastings and Carpenter proved the existence of traveling wave

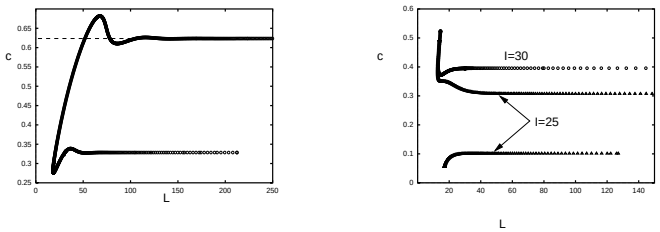

Figure 7.6. *Dispersion relation for the ML model. (A) Class II dynamics showing characteristic damped oscillatory form with fast and slow wave branches connected ($I = 80$.) (B) Class I dynamics showing disconnected fast and slow waves (slow waves for $I = 30$ are on the $c = 0$ axis.)*

solutionss (or homoclinic orbits) for this model when the recovery variable b is sufficiently small. These results will be described in some detail later. However, it is easy to show that when the recovery is very slow, then all the eigenvalues of the linearized system are real. Thus, one cannot obtain Shilnikov-type dynamics in this case. However, Hastings (1982) proved that the homoclinic orbit exists when the recovery is fast enough such that the linearized system does have complex eigenvalues. In a related paper, Feroe (1982) shows the existence of the Shilnikov structure for the piecewise-linear McKean model, $f(v, w) = I - v + H(v - a) - w$ where H is the step function. Finally, Evans Fenichel and Feroe (1982) proved a theorem similar to the Silnikov theorem and applied it to the question of double-impulse solutions. They show that if the return to the fixed point is damped oscillatory, then there are double pulse solutions and that if the return is monotonic, then there are none. (See exercise *)

7.5.2 Class I dynamics.

Surprisingly, no one has looked at the propagation of action potentials in Class I membranes, except in a scalar case. Figure 7.6B shows the dispersion relationship for the ML equations with class I dynamics at two different currents. At $I = 30$, there is only a fast branch of waves. At $I = 25$, there is a new slow branch of waves. The explanation of this is somewhat complicated and not suitable for a textbook. However, Ermentrout (2005) has provided an analysis of waves in the class I system. Rather than go through the details, we consider the scalar model for an excitable medium.

Class I excitability is characterized by dynamics which lies on a circle. Figure 7.7A shows the phase-space for simple scalar dynamics which is equivalent to the θ-model:

$$\frac{dV}{dt} = f(V)$$

where V lives on the circle of radius 1 and $f(V)$ is $2\pi-$periodic. We assume that $f(V)$ has two roots in $[0, 2\pi)$ and denote the unique root r where $f(r) = 0$ and

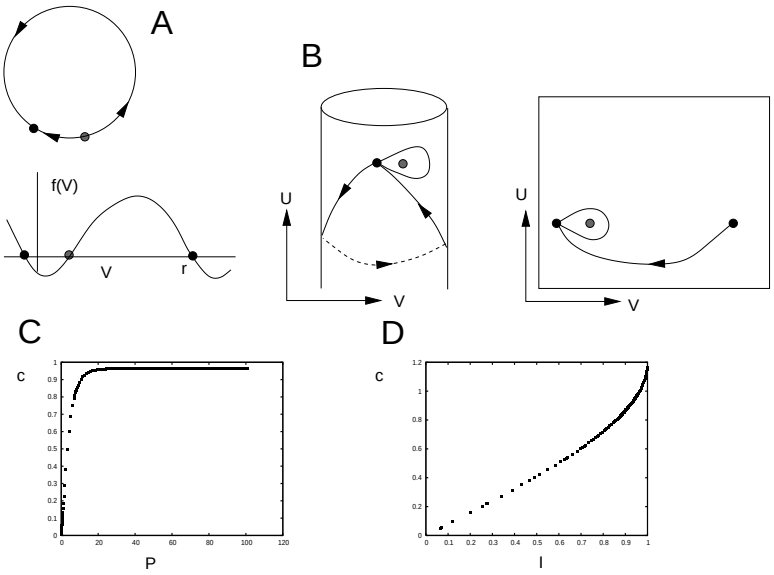

Figure 7.7. *Ermentrout-Rinzel excitable model. (A) Dynamics lies on a circle; the nonlinearit is periodic with period 2π and two fixed points. (B) Phase-space of the travelling wave equations is a cylinder. For $c = c_\infty > 0$ there is a "big" homoclinic which wraps around the cylinder; for $c = 0$, there is also a small homoclinic. These are depicted on the unfolded cyclinder; the "big" homoclinic is now a heteroclinic joining $(2\pi + r, 0)$ to $(r, 0)$ where $f(r) = 0$ and $f'(r) < 0$. (C) Dispersion relation for $f(V) = I - cos(V)$ when $I = 0.95$. (D) Velocity of a large period (100) wave as I varies.*

$f'(r) < 0$. Ermentrout and Rinzel (1982) considered

$$\frac{\partial V}{\partial t} = \frac{\partial^2 V}{\partial x^2} + f(V)$$

where $V(x,t) \in S^1$, the unit circle. In exercise *, we have the reader prove the existence of a fast wave and the associated dispersion curve. In travelling coordinates, we obtain

$$-cV' = V'' + f(V),$$

the dynamics of which lie on a cylinder. There are two types of homoclinic solutions: a "big" homoclinic and a "small" homoclinic. Figure 7.7B shows these solutions as well as their projections onto the unfolded cylinder. The small homoclinic occurs when $c = 0$, for then the dynamics is

$$V'' = -f(V)$$

which is an integrable equation. That is, all solutions lie on a curve defined by

$$E = (V')^2/2 + F(V)$$

where $F'(V) = f(V)$. There is a family of periodic orbits (inside the small homoclinic) whose period varies between p_{min} and ∞. This branch of solutions for $c = 0$ corresponds to the "slow" branch of solutions we have seen in other models. The "big" homoclinic is actually a heteroclinic orbit joining r and $r - 2\pi$. But in the cylindrical phase space, these two are the same point, so that, projected on the cylinder, the solution is a homoclinic. The theory of bistable reaction-diffusion equations provides the existence of a unique value of c for the heteroclinic.

7.6 Stability of the wave.

Perhaps the most influential work done concerning the stability of traveling wave solutions of nerve impulse equations was that done by John Evans. In a series of four papers, he developed a general mathematical framework in which to study a general class of models that include the Hodgkin-Huxley equations. In his fourth paper, Evans constructed a complex analytic function, now called the Evan's function, with the property that eigenvalues of the equations linearized about the traveling wave correspond to zeros of the Evan's function. Using other properties developed by Evans, this implies that the stability of the traveling wave is determined by computing the roots of the Evans' function. Here we will briefly describe issues surrounding stability of waves and define the Evans' function. Actually defining the Evans' function is not that hard; what is difficult is to compute the Evans' function and say something concrete about the eigenvalues. Jones applied the Evan's function to the FitzHugh-Nagumo equations and completed the rigorous proof of the stability of the traveling wave solution. Another stability proof was given by Maginu.

Here we consider the FitzHugh-Nagumo equations and we denote the traveling wave solution as $(V(\xi), W(\xi))$, $\xi = x + ct$. For stability, we need to consider the initial value problem

$$\begin{aligned} v_t &= v_{xx} + f(v) - w \\ w_t &= b(v - kw) \\ (v(x,0), w(x,0)) &= (v_0(x), w_0(x)). \end{aligned} \tag{7.14}$$

It is not completely obvious how one should define asymptotic stability of the traveling wave. Intuitively, we would like to say that the wave is asymptotically stable if we start with initial data that is "close" to the wave, then the corresponding solution will asymptotically approach the wave as $t \to \infty$. One issue is how do we define "close"; that is, what norm or function space should we use? This turns out not to be a problem and any reasonable norm, such as the sup-norm, works. A more serious issue is that the traveling wave is, in fact, not unique; every translate of a traveling wave is also a traveling wave. That is, if $(V(\xi), W(\xi))$ is a traveling wave solution, then so is $(V(\xi+\xi_0), W(\xi+\xi_0))$ for any constant ξ_0. Now if take our initial data to be $(V(\xi+\xi_0), W(\xi+\xi_0))$ with ξ_0 very small, then the initial data lies very close to the original traveling wave; however, the solution with this initial data does not approach the original traveling wave as $t \to \infty$. In general, the best that we can hope for is that a perturbation of a traveling wave solution will approach

some translate of the original traveling wave solution. With this in mind, we define asymptotic stability as follows. By $||\cdot||$ we mean the usual sup or L^∞ norm.

Definition: The traveling wave $(V(\xi), W(\xi))$ is asymptotically stable if for each $\delta_0 > 0$ there exists $\delta_1 > 0$ and ξ_0 such that if $||(V(x), W(x)) - (v_0(x), w_0(x))|| < \delta_1$ then $||(V(x+ct), W(x+ct)) - (v(x,t), w(x,t))|| < \delta_0$ for all $t > 0$. Moreover, $\lim_{t\to\infty}||(V(x+ct+\xi_0), W(x+ct+\xi_0)) - (v(x,t), w(x,t))|| = 0$.

7.6.1 Linearization

A common approach to proving the stability of the wave is to use the method of linearization. In fact, this is one of the few mathematical methods available to treat the initial value problem for the system of partial differential equations (7.14). The first step in applying this method is to reduce the issue of stability to an eigenvalue problem. This is done as follows. We first change to the moving coordinate frame $\xi = x + ct$. In this new variable, (7.14) becomes

$$\begin{aligned} v_t &= v_{\xi\xi} - cv_\xi + f(v) - w \\ w_t &= \epsilon(v - kw) - cw_\xi \\ (v(\xi,0), w(\xi,0)) &= (v_0(\xi), w_0(\xi)). \end{aligned} \tag{7.15}$$

Note that the traveling wave is a steady solution of this system. We then look for solutions of (7.15) that are perturbations of the traveling wave. In particular, we look for solutions of the form:

$$(v(\xi,t), w(\xi,t)) = (V(\xi) + p(\xi)e^{\lambda t}, W(\xi) + r(\xi)e^{\lambda t}).$$

This solution either grows or decays (in time) with rate λ. If we plug a solution of this form into (7.15), "linearize" around the traveling wave, drop higher order terms, use the fact that the traveling wave is a steady solution and let $q = p'$, then we find that $(p(\xi), q(\xi), r(\xi))$ must solve the eigenvalue problem

$$\begin{aligned} p' &= q \\ q' &= cq + (\lambda - f'(V(\xi))p + r \\ r' &= \frac{b}{c}(p - kr) - \frac{\lambda}{c}h. \end{aligned} \tag{7.16}$$

Note that we are interested in solutions of (7.16) that satisfy the boundary conditions

$$\lim_{\xi\to\pm\infty}(q,p,r)(\xi) = (0,0,0). \tag{7.17}$$

Now λ is an eigenvalue if there exists a bounded, nonzero solution of (7.16) that satisfies the boundary conditions (7.17). We note that $\lambda = 0$ must be an eigenvalue because every translation of the wave is also a wave; in particular, $(p,q,r) = (V', V'', W')$ is the corresponding eigenvector. Evans proved that if all the remaining eigenvalues are in the left half complex plane (and 0 is a simple eigenvalue), then the traveling wave is asymptotically stable.

7.6.2 The Evan's Function

Here we will show how to define the Evan's functions for a broad class of reaction-diffusion systems. Unfortunately, this class does not include the nerve impulse equations, for reasons we point out below. Our discussion will at least give a taste for how such a function is defined and why it has the properties that it does. It is not too difficult to extend this definition to nerve impulse equations; however, this becomes somewhat technical so we simply refer the interested reader to [ ].

We consider a general class of reaction-diffusion equations of the form:

$$U_t = DU_{xx} + F(U). \tag{7.18}$$

Here, $U(x,t) \in R^n$ and $F : R^n \to R^n$ is sufficiently smooth. We assume that D is a $n-$dimensional diagonal matrix with nonzero, positive entries along the diagonal. Note that this rules out the nerve impulse equations since these do not have diffusion in the recovery variables. We assume that $U = A$ and $U = B$ are fixed points (that is, $F(A) = F(B) = 0$) and there is a traveling wave solution $V(\xi)$ of (7.18), with speed c, which connects A with B. Note that we do not rule out $A = B$.

As before, we change to a moving coordinate frame, $\xi = x + ct$, and consider perturbations of the wave of the form $p(\xi)e^{\lambda t}$. This leads to an eigenvalue problem of the form:

$$\begin{aligned} p' &= q \\ q' &= D^{-1}\{cq + (\lambda - F'(V))p. \end{aligned} \tag{7.19}$$

Then λ is an eigenvalue if there is a nontrivial solution (eigenfunction) $(p(\xi), q(\xi))$ of (?) that satisfies

$$\lim_{\xi\to\pm\infty}(p,q)(\xi) = (0,0). \tag{7.20}$$

Note that an eigenfunction is a pair of (complex) functions that satisfy (?) and decays at $\pm\infty$. In order to define the Evan's function, we consider the two sets of solutions that decay at either $+\infty$ or decay at $-\infty$. That is, let

$$\begin{aligned} \mathcal{E}^+(\lambda) &= \{\text{solutions of (?) such that } \lim_{\xi\to+\infty}(p(\xi), q(\xi)) = (0,0)\} \\ \mathcal{E}^-(\lambda) &= \{\text{solutions of (?) such that } \lim_{\xi\to-\infty}(p(\xi), q(\xi)) = (0,0)\}. \end{aligned}$$

It is obvious that λ is an eigenvalue if the intersection of $\mathcal{E}^+(\lambda)$ and $\mathcal{E}^-(\lambda)$ is nontrivial. It is important to realize that $\mathcal{E}^+(\lambda)$ and $\mathcal{E}^-(\lambda)$ are linear subspaces. This is because (7.19) is linear. A standard result from the theory of linear ODE's implies that the dimension of each of these linear subspaces is n. We choose a basis for each of these linear subspaces. That is, suppose that

$$\mathcal{E}^+(\lambda) \;=\; \text{span}\{Q_1^+(\xi), ..., Q_n^+(\xi)\}$$

and

$$\mathcal{E}^-(\lambda) \;=\; \text{span}\{Q_1^-(\xi), ..., Q_n^-(\xi)\}.$$

Note that each Q_j^+ and Q_j^- is an $2n$-dimensional vector. We next form the $2n$ x $2n$-dimensional matrix in which the first n columns are $Q_1^+, ..., Q_n^+$ and the next n columns are $Q_1^-, ..., Q_n^-$. We denote this matrix by $\mathcal{M}(\xi)$.

We are now ready to define the Evan's function. Let

$$\mathcal{D}(\lambda) = \det\mathcal{M}(\xi_0) \tag{7.21}$$

where ξ_0 is some arbitrary point (say 0).

Now the Evan's function is certainly well defined. Evan's proved that this function has many important properties. Perhaps the most important property is that λ is an eigenvalue if and only if $\mathcal{D}(\lambda) = 0$. This is actually trivial to prove. The proof is simply:

$\mathcal{D}(\lambda) = 0$
if and only if $\det\mathcal{M}(\lambda) = 0$
if and only if The rows of $\mathcal{M}(\lambda)$ are linearly dependent
if and only if There exist constants $c_1, c_2, ..., c_{2n}$ such that

$$c_1Q_1^+ + c_2Q_2^+ + ... + c_nQ_N^+ + c_{n+1}Q_1^- + c_{n+2}Q_2^- + ... + c_{2n}Q_n^- \;=\; 0$$

if and only if

$$c_1Q_1^+ + c_2Q_2^+ + ... + c_nQ_N^+ = -(c_{n+1}Q_1^- + c_{n+2}Q_2^- + ... + c_{2n}Q_n^-)$$

if and only if $\mathcal{E}^+(\lambda)$ and $\mathcal{E}^-(\lambda)$ have nonzero intersection
if and only if λ is an eigenvalue.

Another important property of the Evan's function is that it is analytic. Moreover, if λ is a zero of $\mathcal{D}$, then the order of this zero is equal to the algebraic multiplicity of λ as an eigenvalue. These two properties are considerably more difficult to prove.

While it is straightforward to define the Evan's function, it is quite challenging to actually compute this function in any given example. For stability, one needs to prove that there are no roots of $\mathcal{D}$ in the right-half plane, there are no roots on the imaginary axis except at the origin (because of translation) and zero is a simple eigenvalue. Methods that have been developed for computing $\mathcal{D}$ go well beyond the scope of this book.

7.7 Myelinated axons and discrete diffusion.

Many vertebrate axons are covered a fatty substance called myelin which serves to both insulate the axons and decrease the membrane capacitance. Myelin consists of the membranes of glial cells which wrap around the axons to make a thick layer. At regularly spaced intervals, the *nodes of Ranvier*, the axon is exposed to the extracellular medium and there is a high density of sodium channels. The decreased resistivity implies that little current leaks out along the myelinated portions of the axon, so that we can expect the velocity of propagation to be greatly enhanced. (See below.)

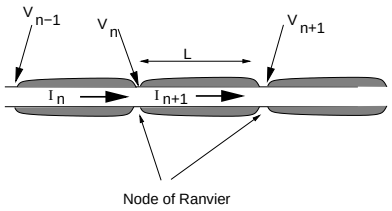

Figure 7.8. *Myelinated axon. Currents in myelinated region are confined to the axial direction. Potentials at the nodes are governed by active currents.*

Let a_1 denote the diameter of the axon and a_2 denote the diameter of the myelinated axon. Dayan and Abbot (2001) show that the total capacitance due to the myelination is

$$\frac{1}{c_m} = \frac{\ln(a_2/a_1)}{2C_m \pi d_m L}$$

where L is the length of the myelinated region, C_m is the usual material constant for capacitance, and d_m is the thickness of a cell layer. Because of the large transmembrane resistance and small capacitance, the potential in the myelinated membrane satisfies the diffusion equation:

$$\frac{c_m}{L}\frac{\partial V}{\partial t} = \frac{4\pi a_1^2}{R_L}\frac{\partial^2 V}{\partial x^2} \tag{7.22}$$

where R_L is the transmembrane resistivity. Dividing by c_m/L, this is the diffusion equation with $D = 4a_1^2 \ln(a_2/a_1)/(2C_m R_L d_m)$. The larger the diffusion coefficient the faster the propagation. Suppose we fix the outer diameter, a_2. Then, we can ask what inner diameter maximizes the diffusion coefficient. It is easy to show that this occurs when $a_1 = a_2 \exp(-1/2) \approx 0.6a_2$. At the optimal diameter, $D = Ka_2^2$ so the velocity of propagation (which scales as $\sqrt{D}$) scales linearly with diameter. The velocity of propagation for unmyelinated axons scales as the square root of the diameter.

Figure 7.8 shows a cartoon of a myelinated axons with nodes of Ranvier spaced a distance of L apart. We assume that the nodes are sufficiently small so that they are isopotential. Let V_n denote the potential at a node. The transmembrane conductance and the capacitance of myelinated regions are roughly 100-fold smaller than the unmyelinated portions of the axon (the nodes of Ranvier.) Thus, there is a sense in which we can regard the myelinated axon as a collection of discrete active nodes separated by a purely resistive medium. Take the limit as $c_m \to 0$ in equation (7.22). Then $V_{xx} = 0$ between nodes $n-1$ and n. The voltage at $x = 0$ and $x = L$ must match the voltage at the nodes. Thus, the potential is linear between nodes: $V(x) = V_{n-1} + (V_n - V_{n-1})x/L$. The current flowing into node n is proportional to the gradient of the voltage in the myelinated segments. Thus, at a node n, the voltage satisfies:

$$AC_m \frac{dV_n}{dt} = -AI_{ionic}(V_n, \ldots) + I_n - I_{n+1} \tag{7.23}$$

where A is the area of membrane exposed at the node, and the longitudinal current (recall equation (3.8))

$$I_n = -\frac{4a_1^2}{R_l}\frac{\partial V}{\partial x} = 4\pi a_1^2 \frac{(V_n - V_{n-1})}{R_l L}.$$

The area A is $\pi\mu a_1$ where μ is the length of the node. Dividing through by the area, we obtain:

$$C_m \frac{dV_n}{dt} = -I_{ionic}(V_n, \ldots) + D(V_{n+1} - 2V_n + V_{n-1}) \tag{7.24}$$

where $D = 4a_1/(R_l L\mu)$. Thus the continuous axon equation, in the presence of myelin, becomes a discrete system of differential equations. Surprisingly, this is much more difficult to analyze, even in the simple bistable case. A traveling wave, if it exists, satisfies $V_{n+1}(t) = V_n(t-\tau)$; that is, translating by one space unit results in a time shift of τ. The speed of the wave is thus L/τ since L is the distance between nodes. With the traveling wave ansatz, we must solve the differential-delay equations:

$$\begin{aligned} C_m \frac{dV}{dt} &= D[V(t+\tau) - 2V(t) + V(t-\tau)] - I_{ionic}(V, w, \ldots) \\ \frac{dw}{dt} &= g(V, w) \end{aligned}$$

where w represents the gating variables, calcium, etc. In the scalar bistable case, we set $f(V) = -I_{ionic}(V)$ and assume that $f(V)$ has three roots, $V_{rest}, V_{thr}, V_{ex}$, the rest state, threshold, and excited state. We seek solutions to the delay equation where $V(-\infty) = V_{ex}$ and $V(+\infty) = V_{ex}$. There have been a few results on this problem (Zinner, 1992; Carpio et al 2001.)

Keener and Sneyd offer the following approximate analysis. Approximate $V(t+\tau) - 2V(t) + V(t-\tau)$ by $\tau^2 V''$ so that we have to solve

$$C_m V' = f(V) + \frac{\tau^2}{L\mu}\frac{4a_1}{R_l}V''$$

with τ an unknown parameter. In order to compare this to the continuous cable, we contast the term multiplying V'' with that in equation (**??**). We introduce the new space-like variable, $\xi = \sqrt{L\mu}/\tau$. Then, the traveling wave equation is:

$$C_m \frac{\sqrt{L\mu}}{\tau} V_\xi = f(V) + \frac{4a_1}{R_l} V_{\xi\xi}.$$

Let c be the traveling wave speed of the unmyelinated axon. Then, we can immediately identify $c = \sqrt{L\mu}/\tau$, so that

$$c_{myelin} = L/\tau \approx \sqrt{\frac{L}{\mu}}c.$$

Since μ is often a micron and L is around a hundred microns, the increase in velocity of myelinated axons can be almost ten times that of unmyelinated. In practice, the factor is closer to 6, but we have made a rather crude approximation here.

7.8 Bibliography

There have been a great deal of papers devoted to a rigorous treatment of propagating waves in reaction diffusion models, including nerve impulse equations. Two of the most influential papers concerning scalar reaction diffusion equations were those by Aronson and Weinberger [4] and Fife and McLeod [16].

As we have described in this chapter, the propagating action potential corresponds to a homoclinic orbit in phase space. Conley [8] developed a very powerful topological method (known as the Conley index) for rigoursly proving the existence of heteroclinic and homoclinic orbits, as well as other invariant sets such as periodic orbits. This approach was used by Carpenter [2] to prove the existence of homoclinic orbits for the Hodgkin-Huxley model. Hastings also considered this problem, using a topological shooting arguments [21]. Analyis of homoclinic orbits often involves fast/slow analysis and methods from the geometric singular perturbation theory. A seminal paper on geometric singular perturbation theory was that of Fenichel [15].

The most influential papers concerning the stability of the traveling wave solution were those by Evans [13], who developed what is now known as the Evan's function. In these papers, Evan's developed the mathematical machinary needed to begin to analyze the stability of the waves; however, he did not consider whether the traveling wave solution of a specific nerve inpulse equation is stable. This step was carried out for the FitzHugh-Nagumo model by Jones [27]. The Evan's function has also been used to study integro-differential equations that arise as neuronal models; see, for example, Zhang [55], Coombes [3].

7.9 Projects

1. Consider the Morris-Lecar model with no potassium:

$$C_m \frac{dV}{dt} = I - g_L(V - E_L) - g_{Ca} m_\infty(V)(V - E_{Ca})$$

with parameters as in chapter *. This is bistable when there is enough injected current. Compute the velocity of wave-fronts for this as a function of the current, I. Now, in the original ML model, m is a dynamic variable, but we have set it to its steady state. Study the velcoity of wave fronts for the ML model:

$$\begin{aligned} C_m \frac{dV}{dt} &= I - g_L(V - E_L) - g_{Ca} m(V - E_{Ca}) \\ \epsilon \frac{dm}{dt} &= m_\infty(V) - m \end{aligned}$$

as ϵ increases.

2. *Aglantha digitale*, a lovely jellyfish (see the figure), has an interesting axon (Mackie and Meech, 1985). When the animal is moving through the water, slow moving spikes are generated in the axon, but when trying to escape, the animal produces fast action potentials. The slow waves occur at a lower

Aglantha digitale

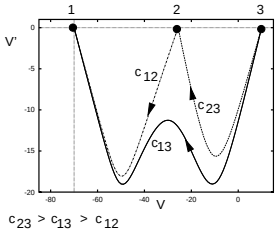

Figure 7.9. *The jellyfish,* A. digitale *and the phaseplane for a tristable system*

threshold stimulus, have low amplitude, and are produced by a calcium spike. The fast waves are generated by a high threshold sodium current. One way to think about this behavior theoretically is to study the initiation of the spike by looking at a model with no recovery. That is, imagine a tristable system in which there are five fixed points, three of which are stable and two unstable. The slow wave is a front from rest to the middle fixed point. The fast wave is a front from the rest to the highest fixed point. Consider a simple model like (**??**) with

$$I_{ion}(V) = g_L(V - E_L) + g_{Ca}m_1(V)(V - E_{Ca}) + g_{Na}m_2(V)(V - E_{Na}).$$

Find parameters using $E_L = -70$, $E_{Na} = 55$, $E_{Ca} = 150$, and $m_j(V) = 1/(1 + \exp(-(V - V_{tj})b_j))$ so that I_{ion} has five zeros.Arrange these zeros so that there are the requisite fronts. Figure 7.9 shows our attempt at this. The figure shows three different fronts at three different speeds.

7.10 Exercises

1. Simulate the reduced HH cable model using $m = m_\infty(V)$ and $h = 0.8 - n$. Deduce that the velocity of an action potential is about 2-3 times faster than that of a full model. Why do you think this is?

2. Use shooting to estimate the velocity of an action potential for the Rinzel reduction. Try to find the slow velocity wave and then use continuation software (such as AUTO) to draw the dispersion relation.

3. What is the velocity of an action potential using the HH dynamics for an axon of diameter d in centimeters and axial resistance R_i is ohm-centimeters? (Use the numerically computed value above in your formula; that is when $d = 0.1$ and $R_i = 100$, you should get 1.25 m/sec.)

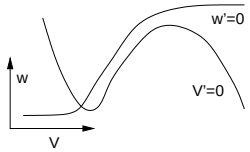

4. Consider a two-dimensional model such as the ML class II or reduced HH equations. At rest with no current, assume the nullclines are as shown above. Show that if the velocity, c is large enough, then there is exactly one negative real root and two roots with positive real parts to the linearization of the traveling wave equation. Thus, there is a one-dimensional stable manifold and a two-dimensional unstable manifold.

5. Analyze equation (**??**) for $k > 0$ and show that the rest state can become unstable as I increases. (Hint: Show that the Hopf bifurcation occurs when $f'(\bar{V}) = k$ and solve this for two values of $\bar{V}$ and plug these into the expression for equilibria to get two values of I, thus showing there are two possible HB points. Find a relationship between a and k guaranteeing that these points exist.)

6. Suppose that the stable dispersion relation satisfies:

$$c(P) = c_\infty(1 - \alpha e^{-\beta(P-P_{min})})$$

where $\alpha = (c_\infty - c_{min})/c_\infty$. Analyze the kinematics of this type of dispersion curve. What happens to a pair of spikes on an axon? ($c_\infty > c_{min} > 0$ and $\beta > 0$. More generally, suppose that $c = F(P)$ and F is monotone increasing. Show that if $F(P) > PF'(P)$, then $D(\phi)$ has no roots. Thus, show that if the dispersion relation is monotonic, there are no double pusle solutions. (See Evans et al 1982).

Suppose that the dispersion curve $c = F(P)$ has infinitely many local extrema with the peaks and valleys centered aroind c_∞. Does that imply that $c = G(T)$ has infinitely many extrema and thus, that there are infinitely many roots to $D(\phi) = 0$?

7. For many class II axons, the dispersion relation $c(P)$ is oscillatory. For simplicity, suppose that

$$\frac{1}{c(P)} = \frac{1}{c_\infty} + \eta e^{-aP}\cos bP$$

where a, b are positive constants and $\eta > 0$ is smaller than c_∞^{-1}. Find an equation for the interspike interval of a pair of pulses on the cable. What is the minimal interval? Pick some values of a, b, η and look at the kinematics of pulse triplets, etc.

8. (a) Find the velocity to 3 decimal places for the traveling front to the equation $V_t = f(V) + V_{xx}$ where $f(V) = V(1-V)(V-\alpha)$ and $\alpha = 0.1$. (b) Consider the same equation where $f(V) = I - \cos V$ and $0 < I < 1$. There are two fixed points of interest, $V_0 = -\arccos(I)$ and $V_1 = 2\pi - \arccos(I)$. For $I = 0.95$, find the velocity of the front joining V_1 to V_0. (c) Find the velocity exactly for the model with $f(V) = H(V - \alpha)$ where $\alpha < 1/2$ and $H(V)$ is the step function.

9. Consider the simple ring model for excitability:

$$V_t = I - \cos V + V_{xx}.$$

In the previous exercise, you computed the front from $V_1 = 2\pi - \arccos(I)$ to $V_0 = -\arccos(I)$. Let $c_\infty(I)$ be the velocity of the front. Since the state space for this system is a cylinder (recall figure 7.7), we can also look for "periodic" solutions. Take it as a fact that if $c < c_\infty$, then the unstable manifold of V_1 hits the V'-axis before it hits the V axis. Show that, on the cylinder, the unstable manifold approaches a periodic solution, that is $V(\xi + P) = V(\xi) - 2\pi$. (See Ermentrout & Rinzel, 1984).

10. Here is a cool trick. Consider

$$f(u) = Au(u-a)(1-u)$$

where $a \in (0,1)$. The front satisfies:

$$-cu' = f(u) + u''$$

with $u(-\infty) = 1$ and $u(+\infty) = 0$. Consider the equation

$$u' = -bu(1-u)$$

Find a value of b and c so that the solution to the second equation is a solution to the first. Thus, find an exact expression for the velocity. Solve the second equation by quadrature to get a closed form expression for ther wave front! Compare the value of the velocity to that computed numerically in exercise *(a).

11. Consider the equation:

$$-cV' = V'' + V^2(1-V)$$

$V = 0$ is a double root. Show that there are infinitely many values of c for which there is a front joining 0 and 1.

12. (Propagation failure.) (A).Consider the equation

$$\frac{dv_n}{dt} = f(v_n) + D(v_{n+1} - 2v_n | v_{n-1}).$$

Suppose that f has roots $0, 1, a$ with $0 < a < 1$ and $0, 1$ stable fixed points to $v' = f(v)$. Let $U_n(t), V_n(t)$ be two solutions to this equation with initial data such that $V_n(0) > U_n(0)$ for all n. Prove that $V_n(t) \geq U_n(t)$ for all $t > 0$. (B) Part A implies that if there is a stationary front (that is, a zero velocity front) with $V_n \to 1$ as $n \to \infty$ and $V_n \to 0$ as $n \to -\infty$, then there will be no traveling front, since this static front blocks the propagation. It is clear that if $D = 0$, such a stationary front exists, just take $V_n = 0$ for $n < 0$, $V_0 = a$, and $V_n = 1$ for $n > 0$. This is a hyperbolic fixed point, so that for small D, it

will persist. Thus, we expect that the dtationary front exists for D sufficiently small. Keener (1987) showed that there is a $D^* > 0$ such that if $D \leq D^*$, there is a stationary front. Suppose that $f(v) = -v + H(v - a)$ where H is the step function. Find D^* for this model. (Hint: consult Keener & Sneyd, p 280.) Ans: $D^* = a(1-a)/(2a-1)^2$.

13. Show that the G for the HH equations satisfies the cubic hypothesis for the Carpenter theorem.

14. Use the computer to check assumption (6) in the hasting HH theorem.

15. Consider the equation $v_t = v_{xx} + f(v) - w$ where $f(v)$ is as above and w is constant. Note that there is a range of w for which there are three fixed points; we denote these as $v_L(w) < v_M(w) < v_R(w)$. For which values of w does there exist a TWS such that $\lim_{\xi\to-\infty} V(\xi) = v_L(w)$ and $\lim_{\xi\to\infty} V(\xi) = v_R(w)$? How does the wave speed depend on w? For which value of w is the wave speed equal to zero? For which values of w does there exist a TWS such that $\lim_{\xi\to-\infty} v(\xi) = v_R(w)$ and $\lim_{\xi\to\infty} v(\xi) = v_L(w)$? For which value of w does the speed of this wave equal to $c*$.

16. Prove that the traveling wave solution of the bistable equation (7.3) exists for a unique value of the wave-speed. In what sense is the traveling wave unique?

17. Suppose that $f(v) = v(1-v)$ in (7.3). Prove that there exist a value c^* such that there is a traveling wave solution for wave-speeds $c > c^*$.

18. Consider the FitzHugh-Nagumo equations (?) with $k > 0$ and $I = 0$. Note that if k is sufficiently large, then there are three fixed points. One of these is at the origin $\mathcal{O}$ and we denote the fixed point on the right branch of the cubic as q_0. As above, we can construct singular heteroclinic orbits that connect either $\mathcal{O}$ to q_0 or q_0 to $\mathcal{O}$ (for some value of the wave speed). For which values of k does there exist a singular heteroclinic orbit? For which values of k does there exist a singular homoclinic orbit to the origin?

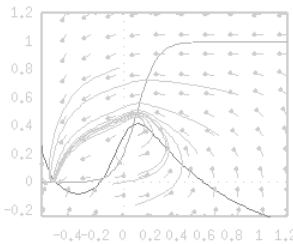

Chapter 8

Synaptic channels.

So far, we have restricted our modeling and analysis efforts to single neurons. In order to begin to develop networks and the theoretical background for networks, we need to introduce an additional class of membrane channels. We have already looked at voltage-gated and ion-gated channels. However, there are many other channels on the surface of nerve cells which respond to various substances. Among the most important of these, at least theoretically, are synaptic channels.

The events leading to the opening of synaptic channels involve several steps. The action potential travels down the axon and terminates at many presynaptic sites invading regions called synaptic terminals. These terminals contain calcium channels which when depolarized, cause (a) release of calcium; (b) calcium activates a calcium binding protein which promotes transmitter release by binding to vesicles containing the transmitter; (c) these "docked" vesicles release their transmitter into the synaptic cleft; (d) the transmitter diffuses through the cleft where it binds to various receptors on the postsynaptic neuron (often on protuberances on the dendrites called spines); (e) these receptors open channels which either depolarize or hyperpolarize the neuron depending on the nature of the transmitter.

Transmitter release can get quite complex for there are sometimes presynaptic receptors near the site of transmission which can be modulated by various chemicals. Furthermore, the release of transmitter is probabilistic and occurs in discrete amounts called *quanta.* Presynaptic stimulation can lead to more vesicles becoming docked to the membrane so that on the next presynaptic spike, more transmitter is released than on the first spike. This increase is called *potentiation.* Additionally, after several presynaptic spikes, the transmitter release per spike can decrease through various means (such as depletion) and take some time to recover. Decrease of transmitter over successive firings of action potentials is called synaptic *depression.*

The consequences of synaptic dynamics and short-term plasticity (e.g. depression and facilitation) have not been thoroughly explored in terms of dynamical systems theory. Here, we will develop several models for both the release and for the plasticity of synaptic release. In a later chapter, when we look at networks, we

will show some interesting behavior which occurs because of synaptic depression.

8.1 Synaptic dynamics.

In this section, we deal with the five most common classes of synaptic dynamics. The main transmitters associated with cortical neurons are glutamate and γ-aminobutyric acid (GABA). A good rule of thumb is that glutamate excites the postsynaptic cell while GABA inhibits it. However, the reversal potential of some GABA receptors is mainly dependent on chloride concentration so that it can be close to rest and even above rest. Thus, (particularly, early in development) some GABA synapses can be excitatory. Like other currents, we model the synaptic currents as the product of a conductance with a voltage difference:

$$I_{syn} = g(t)(V_{post} - V_{rev}).$$

Unlike our previously studied channels, the conductance $g(t)$ depends on the presynaptic neuron.

There are several ways to model the conductance $g(t)$. A popular method among computational neuroscientists is to assume that $g(t)$ is the sum of fixed functions which depend only on the times that the presynaptic cell has spiked:

$$g(t) = \bar{g} \sum_k \alpha(t - t_k) \equiv \bar{g} z(t) \tag{8.1}$$

where $\bar{g}$ is a constant conductance and $\alpha(t)$ is a prescribed function of time, vanishing for $t < 0$ and positive for $t > 0$. The times t_k are when the presynaptic cell has spiked. The most general form for the function $\alpha(t)$ is:

$$\alpha(t) = \frac{a_d a_r}{a_r - a_d}(e^{-a_d t} - e^{-a_r t}). \tag{8.2}$$

The parameter a_r characterizes the rise rate of the synaptic conductance and a_d the decay. Many modelers assume that $a_d = a_r$ in which case, the function has the form

$$\alpha(t) = a_d^2 t e^{-a_d t}.$$

Letting $a_r \to \infty$ reduces the model to a single exponential. The maximum of $\alpha(t)$ occurs at $t^* = \ln(a_r/a_d)/(a_r - a_d)$. The constants multiplying these functions are chosen so that the area under $\alpha(t)$ is 1. Other normalizations are possible; for example, choosing the value of $\alpha(t^*) = 1$ for some $t^* > 0$.

If one uses alpha functions in simulations, then equation (8.1) implies that it is necessary to keep track of all the incoming spikes at times t_k. Since $z(t)$ in (8.1) is the solution to a second order linear differential equation:

$$z'' + (a_r + a_d)z' + a_r a_d z = 0, \tag{8.3}$$

we need only solve this equation in time with the proviso that each time t_k that a presynaptic spike arises, $z'(t)$ is incremented by an amount $a_d a_r$. Formally, we can write

$$z'' + (a_r + a_d)z' + a_r a_d z = a_r a_d \sum_k \delta(t - t_k).$$

If the spike train is random (say Poisson) with a time varying rate, $\nu(t)$, then we can formally average this equation to obtain

$$z'' + (a_r + a_d)z' + a_r a_d z = a_r a_d \nu(t). \tag{8.4}$$

The solution to this linear equation provides a formula for the average net synaptic input for a time varying random stimulus.

Choosing a fixed function $\alpha(t)$ for the synaptic response has some advantages which will become apparent when we study networks. However, from a physical point of view, the use of alpha functions is unsatisfying. First, as noted above, we need to track the time of a spike which could be ambiguous. Furthermore, this approach does not connect well with our notion of voltage and ligand-gated channels. We introduce a simple model for synapses which is identical to the formalism that we previously described. Let $[T]$ denote the concentration of transmitter released into the synaptic cleft by a presynaptic spike. Note that $[T]$ will be time dependent since synaptic transmitter is rapidly taken up and/or degraded. Then the conductance $g(t) = \bar{g}s(t)$ where $s(t)$ denotes the fraction of open channels. $s(t)$ satisfies:

$$\frac{ds}{dt} = a_r[T](1-s) - a_d s. \tag{8.5}$$

Suppose that at $t = t_0, [T]$ jumps to T_{max} and at $t = t_1$, $[T]$ falls back to zero. Then

$$s(t - t_0) = s_\infty + (s(t_0) - s_\infty)e^{-(t-t_0)/\tau_s}, \quad \text{for } t_0 < t < t_1,$$

where

$$s_\infty = \frac{a_r T_{max}}{a_r T_{max} + a_d} \quad \text{and} \quad \tau_s = \frac{1}{a_r T_{max} + a_d}.$$

After the pulse of transmitter is gone, $s(t)$ decays as

$$s(t) = s(t_1)e^{-a_d(t-t_1)}.$$

While it may appear that, like the alpha function, there is a rise rate and a decay rate, the formula for τ_s shows that the rates are not independent. If $a_r T_{max}$ is large, the synapse will saturate near 1 so that it is not possible to make this rise rate arbitrary. However, by varying the residence time of the transmitter, $t_1 - t_0$, it is possibe to mimic the alpha function quite closely. We now must connect the transmitter release $[T]$ with the presynaptic neuron. We assume a model of the form:

$$[T](V_{pre}) = \frac{T_{max}}{1 + \exp(-(V_{pre} - V_T)/K_p)}. \tag{8.6}$$

Destexhe at al (1994) suggest that T_{max} =1 mM, V_T = 2 mV, and K_p = 5 mV. [Destexhe A, Mainen ZF, Sejnowski TJ (1994) Synthesis of models for excitable membranes, synaptic transmission and neuromodulation using a common kinetic formalism. J Comput Neurosci 1:195-230

Saftenku EE (2005) Modeling of slow glutamate diffusion and AMPA receptor activation in the cerebellar glomerulus. J Theor Biol 234:363-82]

We now have a complete model of the conductance changes of a simple synapse connected to the presynaptic voltage. We turn next to the four main classes of synaptic transmission used in models of cortical neurons. Figure 8.1 shows the conductance changes due to each of our four model synapses.

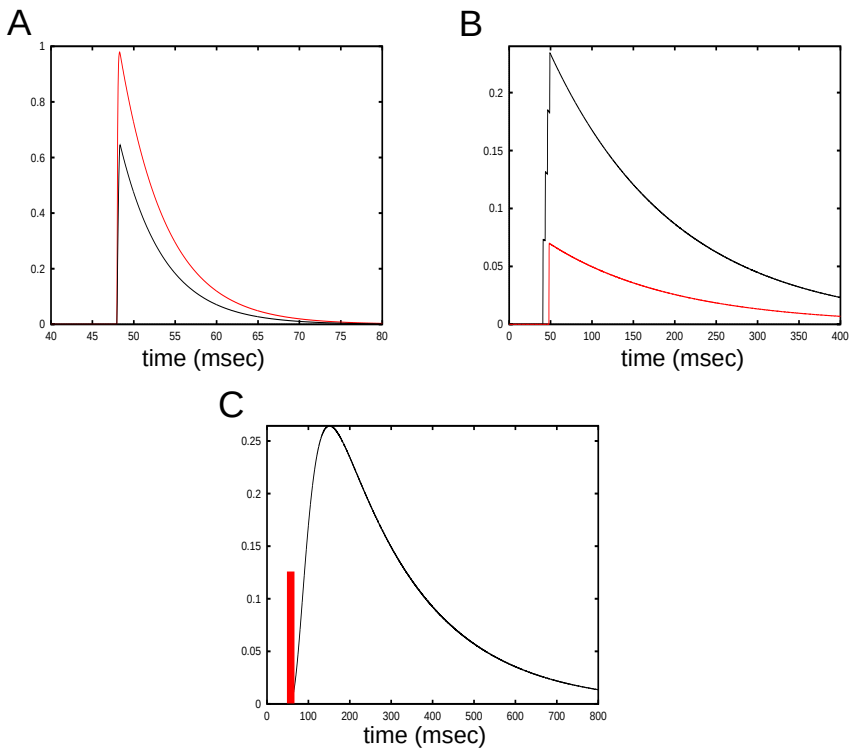

Figure 8.1. *Model synaptic conductances. (A) AMPA (black) and GABA-B conductance due to a single presynaptic spike. (B) NMDA conductance to a single (red) and a burst of four (black) spikes. (C) GABA-B conductance to a burst of 8 spikes. Single spike response is negligible.*

8.1.1 Glutamate

The neurotransmitter glutamate activates two different kinds of receptors: AMPA/kainate which are very fast and NMDA which is implicated in memory and long-term potentiation of synapses. Both of these receptors lead to excitation of the membrane.

AMPA/Kainate.

The current from a fast AMPA synapse is

$$I_{AMPA} = \bar{g}_{AMPA} s (V - V_{AMPA}) \tag{8.7}$$

where $V_{AMPA} = 0\ mV$. For the synapse shown in Figure 8.1A, s satisfies equations (8.5) and (8.6) with $a_r = 1.1\ mM^{-1} ms^{-1}$, and $a_d = 0.19\ ms^{-1}$.

The AMPA synapses can be very fast. For example, in some auditory nuclei, they have submillisecond rise and decay times. In typical cortical cells, the rise time is 0.4 to 0.8 milliseconds. Using the above model with a transmitter concentration

of 1 mM, the rise time would be 1=/(1.1 + 0.19) = 0.8 msec. Decay is about 5 milliseconds. As a final note, AMPA receptors onto inhibitory interneurons are about twice as fast in rise and fall times as those onto excitatory neurons.

Real AMPA synapses show quite strong depression. That is, the peak amplitude of the AMPA current decreases with each subsequent spike. We will address this short term plasticity in the next section. Figure 8.1A shows the conductance change for a single presynaptic spike.

8.1.2 NMDA

The NMDA receptor is also sensitive to glutamate but has effects that last considerably longer than those of AMPA. However, under normal physiological conditions, the NMDA receptor is blocked by magnesium ions. The magnesium block can be removed if the postsynaptic neuron is depolarized. Thus, if the postsynaptic cell is already active, then the NMDA receptor opens and the effect of the current will be long lasting. Because of the property that both the pre- and postsynaptic cells must be active in order for the NMDA current to flow, the presence of these receptors is believed to be necessary for many types of long term changes in the synapses. Indeed, one of the ions carried by NMDA current is calcium which is a main player in long term changes in neurons. The NMDA current is modeled as:

$$I_{NMDA} = \bar{g}_{NMDA} s B(V)(V - V_{NMDA}) \tag{8.8}$$

where s obeys equations (8.5,8.6) and $B(V)$ represents the magnesium block (Jahr and Stevens, J. Neuroscience 10, 1830-183):

$$B(V) = \frac{1}{1 + e^{-0.062V}[Mg^{++}]/3.57}.$$

It is convenient to rewrite this is

$$B(V) = \frac{1}{1 + e^{-(V-V_T)/16.13}}$$

where V_T is the half activation and is given by

$$V_T = 16.13 \ln \frac{[Mg^{++}]}{3.57}.$$

At the physiological concentration of 2 mM, $V_T \approx -10$ mV so that the post-synaptic cell has to be quite depolarized. Even at the relatively low concentrartion of 1 mM, $V_T \approx -20$ mV. The synaptic parameters for s are well fit by the choices $a_r = 0.072\ mM^{-1}ms^{-1}$, $a_d = 0.0066$, and $V_{NMDA} = 0$ mV. Figure 8.1B shows the conductance change for a model NMDA synapse when there is a single spike and when there are four spikes. The rise time is fast enough so that each spike can be seen in the model trace.

8.1.3 GABA

GABA is the principle inhibitory neurotransmitter in the cortex. There are two main receptors for GABA: GABA_A and GABA_B.

GABA$_A$

GABA$_A$ is responsible for fast inhibition and, like AMPA and NMDA, requires a single presynaptic spike to be evoked. The current is

$$I_{\mathrm{GABA}_A} = \bar{g}_{\mathrm{GABA}_A} s(V - V_{\mathrm{GABA}_A}) \tag{8.9}$$

where s obeys (8.5) and (8.6) with $a_r = 5\ mM^{-1}ms^{-1}$, $a_d = 0.18\ ms^{-1}$ and V_{GABA_A} varying between -81 and -60 mV. This GABA current is carried by chloride (among other ions) and thus there is a wide range of values depending on the physiological conditions and the developmental stage of the neurons. (Early in develoment GABA is mainly depolarizing with a reversal potential well above rest.) In most models in the literature, $V_{\mathrm{GABA}_A} = -75$ mV. Figure 8.1A shows the conductance change for our model GABA$_A$ synapse.

GABA$_B$

The three synapses described so far (AMPA/Kainate, NMDA and GABA$_A$) share the common feature that the ion channel and the receptor are the same protein. Thus, the effects of transmitter on these synaptic recptors is *direct.* However, there are other synaptic events which are *indirect* in that the activation of the receptor sets off a cascade of intracellular events which eventually alter the conductivity of an ion channel. The GABA$_B$ receptor is an example of this indirect effect: transmitter binds to a receptor protein which activates an intracellular complex called a G-protein which in turn activates a potassium channel to hyperpolarize the membrane. Such indirect effects can have several consequences. The responses can be: (i) nonlinear; (ii) slow to activate; and (iii) long-lasting. There are several models for the activation of GABA$_B$ synapses; we will consider only the simplest one. There is a receptor r which is activated exactly as described by equations (8.5) and (8.6). This receptor activates the ionic channel, s, and results in the GABA$_B$ current. The current is a nonlinear saturating function of s. Thus, the model for GABA$_B$ is

$$\begin{aligned} I_{GABA_B} &= \bar{g}_{GABA_B} \frac{s^n}{K_d + s^n}(V - E_K) \qquad (8.10)\\ \frac{dr}{dt} &= a_r T(1-r) - b_r r \\ \frac{ds}{dt} &= K_3 r - K_4 s. \end{aligned}$$

For the synapse shown in Figure 8.1C, $a_r = 0.09\ mM^{-1}ms^{-1}$, $a_d = 0.0012\ ms^{-1}$, $n = 4$, $K_d = 100$, $K_3 = 0.18\ ms^{-1}$, and $K_4 = 0.034\ ms^{-1}$. We use the same function (8.6) for the transmitter release, T, as we have in the other synaptic models. The nonlinearity in equation (8.10) means that s must become large enough for the synapse to take effect. GABA$_B$ is more effective when several action potentials occur in a row. Note also that the reversal potential is that of potassium; in a cortical cell this can be around -90 to -105 mV. GABA$_B$ is unambiguously hyperpolarizing. Figure 8.1C shows the effective synaptic conductance, $s_{eff} = s^4/(s^4 + K_d)$ for a burst of eight spikes. The conductance for a single spike is very close to zero.

8.1.4 Gap or electrical junctions.

Many cells can directly communicate with each other via tight junctons between their membranes. These act as resistors connecting compartments in two different cells and are called either electrical or gap junctions. The difference between gap junctions and chemical synapses is that the former always keep the cells in communication while the latter occur only when there is a presynaptic action potential. (Although, there are some neurons which release transmitter in a graded fashion, these are rare and atypical. The granule cells in the olfactory bulb of mammals are the best known example.) We model the current for this type of synapse as:

$$I_{gap} = \bar{g}_{gap}(V_{post} - V_{pre}) \tag{8.11}$$

where g_{gap} is the conductance.

8.2 Short term plasticity.

Our conceptual model for synapses treats them as though there is no history dependence. That is, the magnitude of the post synaptic current (PSC) is independent of how many times that it has been invoked in recent history. However, the experimental work of many groups over the years shows that many synapses exhibit *short term plasiticity.* Here, the emphasis is on the words *short-term* as opposed to long-term changes that are associated with learning and memory. Short term plasticity occurs over times scales of the order of milliseconds to minutes and takes the form of short term depression (the magnitude of successive PSCs decreases), facilitation (the magnitude of successive PSCs increases) or possibly both. We point out that the $GABA_B$ model in section * shows facilitation in that several closely timed action potentials lead to a much larger current. Markram et al (1998), Castro-Alamancos (2002) and Beierlein et al (2003) are among those who have quantified synaptic plasticity in mammalian brains. Abbott was among the first to recognize the computational consequences of short term plasticity. Here, we briefly describe some models and some consequences of this plasticity. Later on, we will see that the effects on networks or neurons can be much more interesting.

Figure 8.2A shows examples of synaptic depression (SD) and facilitation (SF) in cortical neurons. We now describe phenomenological and mechanistic models for short term plasticity. The phenomenological model is due to Dayan and Abbott but is closely related to many other models. We suppose for that we want to characterize the magnitude, $M(t)$, of synaptic release per presynaptic spike. We write this magnitude as the product of two factors, the depression $d(t)$ and the facilitation $f(t)$, so that:

$$M(t) = d(t)f(t).$$

We could also call $M(t)$ the probability of release if one is interested in treating the process stochastically. Both $f(t), d(t)$ lies between 0 and 1 and each has a resting value of f_0, d_0 respectively, to which it returns with a time constant, τ_f, τ_d, respectively. Thus, in absense of any inputs,

$$\tau_f \frac{df}{dt} = f_0 - f \quad \text{and} \quad \tau_d \frac{dd}{dt} = d_0 - d.$$

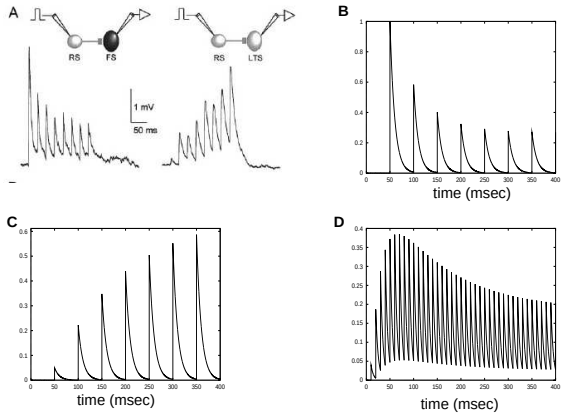

Figure 8.2. *(A) Short-term synaptic plasticity in cortical neurons (From Beierlein et al 2003). Connections between cortical excitatory cells (RS) and cortical fast spike units (inhibitory) show synaptic depression to 20 Hz stimuli while RS to low threshold spike (LTS) inhibitory cells show facilitation. (B-D) simulations of equations (8.12) and (8.13) to periodic stimuli.Parameters for B are* $\tau_d = 300$, $a_d = 0.5$, $d_0 = 1$, $\tau = 10$ *and there is no facilitation. Parameters for C are* $\tau_f = 500$, $a_f = 0.2$, $f_0 = 0$, $\tau = 10$ *with no depression. Frequency is 20 Hz. D has both depression and facilitation with* $f_0 = 0, d_0 = 1$, $\tau_f = 50, \tau_d = 400$, $a_f = 0.2, a_d = 0.05$ *and* $\tau = 5$. *The frequency is 100 Hz.*

Each time there is a spike, $f(t)$ is incremented by an amount $a_f(1-f)$ and $d(t)$ is decremented by an amount $a_d d$. In both cases, the change is multiplied by a factor which keeps the variables bounded between 0 and 1. We assume that both a_f and a_d are less than one. Formally, we can write the facilitation equation as:

$$\frac{df}{dt} = \frac{f_0 - f}{\tau_f} + \left(\sum_j \delta(t - t_j) \right) a_f (1 - f) \tag{8.12}$$

where t_j are the times of the incoming spikes. Similarly, for the depression equation, we have:

$$\frac{dd}{dt} = \frac{d_0 - d}{\tau_d} - \left(\sum_j \delta(t - t_j) \right) a_d d. \tag{8.13}$$

We leave the analysis of these equations when stimuli are periodic as an exercise. Figures 8.2B-D show the results of a simulation of these equations when there is a periodic input. Each time a stimulus comes in, the synaptic variable $s(t)$ is incremented by $M(t)$ and both $d(t), f(t)$ are updated. Between stimuli, $s(t)$ decays exponentially with a time constant of τ.

Suppose that the inputs to the synapse are Poisson with rate r. (See Chapter

* for a definition of Poisson). Averaging equation (8.12), we obtain:

$$\frac{df}{dt} = (f_0 - f)/\tau_f + a_f r(1 - f).$$

The steady state value of f is:

$$f_{ss} = \frac{f_0 + a_f \tau_f r}{1 + a_f \tau_f r}.$$

A similar calculation for d yields:

$$d_{ss} = \frac{d_0}{1 + a_d \tau_d r}.$$

The effective average rate is

$$r_{eff} = r f_{ss} d_{ss} = r d_0 \frac{f_0 + a_f \tau_f r}{(1 + a_f \tau_f r)(1 + a_d \tau_d r)}.$$

If there is depression, then this function saturates as the true rate goes to infinity.

Abbott points out that SD has a useful computational property in that it emphasizes changes in input rates. That is, starting at a low rate and jumping to a high rate results in a huge jump of r_{eff}. Suppose that $d_0 = 1$ and the input jumps from r_{lo} to r_{hi}. At the moment before the jump

$$r^-_{eff} = \frac{r_{lo}}{1 + a_d \tau_d r_{lo}}.$$

Right after the jump,

$$r^+_{eff} = \frac{r_{hi}}{1 + a_d \tau_d r_{lo}}$$

since the depression has not had a chance to take effect. That is, the denominator is still that for the low rate. Over time, the effective rate will decrease to the steady state:

$$r_{eff} = \frac{r_{hi}}{1 + a_d \tau_d r_{hi}}.$$

By the same argument, if the rate is suddenly lowered again, the effective rate will be very small since the denominator is large from the high prior rate. Thus, SD behaves much like a differentiator of the input rate and allows for very strong temporal contrast. We note that Bertram (2001) calls our depression model a *vesicle depletion mechanism* as one can regard the variable d as the amount of transmitter available for release.

8.2.1 Other models.

The above models for plasticity require that one track the time of spikes. In this sense, they are analogous to using alpha functions for synapses rather than the mechanistic models. Bose and Nadim (2005) use a channel-like model for synaptic

depression. They combine an activation model like (8.5) with a depression model of the form:

$$\frac{dd}{dt} = \frac{d_\infty(V) - d}{\tau_1 + \tau_2 d_\infty(V)}$$

where

$$d_\infty(V) = \frac{1}{1 + e^{k(V - V_{thr})}}$$

and $k > 0$ and V_{thr} are parameters. The threshold is set close to $V = 0$ and k is somewhat large so that when V is near rest, $d_\infty(V)$ is close to 1 and $d(t)$ will relax to 1 with a time constant roughly like $\tau_1 + \tau_2$. When the neuron spikes, d_∞ is nearly zero and $d(t)$ will decay to 0 with a time constant of τ_1. Thus, $1/\tau_1$ is like a_d and τ_2 is like τ_d in the heuristic model. Given the equation for $d(t)$ and a model such as (8.5) for $s(t)$, the total synaptic conductance is $\bar{g}s(t)d(t)$. Similar models can be built for potentiation of synapses, but $k < 0$ so that at rest the potentiation variable goes to a low value which is increased with each spike. A more direct mapping that has been used in the past is:

$$\frac{dd}{dt} = (d_0 - d)/\tau_d - a_d(V)d$$

where

$$a_d(V) = \frac{a}{1 + e^{-k(V - V_{th})}}.$$

When the neuron spikes $a_d(V)$, is large; otherwise it is negative.

We close this section with a three state model for depression which is based on a simple physical model:

$$\begin{aligned} A &\longrightarrow S \\ S &\longrightarrow U \\ U &\longrightarrow A. \end{aligned}$$

A is the available transmitter, S is the conducting state which produces the synaptic conductance, and U is the transmitter which is unavailable for release. Since $A + S + U$ is conserved, we can eliminate A and obtain the following pair of differential equations:

$$\frac{ds}{dt} = \alpha(V)(1 - s - u) - \beta s \quad \text{and} \quad \frac{du}{dt} = \beta s - \beta_2 u.$$

By varying β_2, we can incorporate various degrees of synaptic depression. This simple model does not have the degree of freedom that other models have; there is only one free parameter β_2 since β determines the decay rate of the synapse and $\alpha(V)$ is voltage dependent.

8.3 Exercises.

1. Simulate and recreate all of Figure 8.1 using the parameters in the text.

2. If inputs come into a synapse periodically, determine the steady state values of $d(t)$ and $f(t)$ at the moment after a stimulus arrives.

3. What rate r maximizes the probability of release for a synapse which has both facilitation ($f_0 = 0$) and depression ($d_0 = 1$)?

4. Simulate
$$\frac{dd}{dt} = \frac{1-d}{\tau_d} - a_d r(t) d$$
with $a_d = .4$, $\tau_d = 500$ msec, and $r(t)$ changes as follows: for the first 200 msec, it is 25 Hz. It jumps to 100 Hz for the next 300 msec. Then it falls to 10 Hz and at $t = 1000$ msec it junps to 40 Hz. Plot the effective firing rate $d(t)r(t)$.

5. Castro-Alamancos (2002) describes a synapse with the following peoperties. The ratio of the first spike to the second spike is 0.6 when the time between spikes is 50 msec. If the time between spikes is 25 msec, the ratio is 0.4. Given that $d_0 = 1$, find parameters a_d, τ_d which match this assuming there is no potentiation.

6. Given an alpha function (8.2), compute the steady state value of $s(t)$ assuming that the presynaptic spikes, $t_k = kP$ are periodic with period P.

7. Suppose that $\nu(t)$ in (8.4) is sinusoidal, $\nu(t) = \sin \omega t$. Find $z(t)$. Find the magnitude of the response.

8. Gulledge and Stuart (Neuron 2003 37:299-309) demonstrate an interesting example of GABA enhancing the post-synaptic response to an excitatory synapse. They record from pyramidal neurons in rat somatosensory cortex and produce both dendritic and somatic GABA stimulation. (pas_in.ode)

Beierlein M, Gibson JR, Connors BW. Two dynamically distinct inhibitory networks in layer 4 of the neocortex. J Neurophysiol. 2003 Nov;90(5):2987-3000. Epub 2003 Jun 18.

Castro-Alamancos MA. Properties of primary sensory (lemniscal) synapses in the ventrobasal thalamus and the relay of high-frequency sensory inputs.J Neurophysiol. 2002 Feb;87(2):946-53.

Markram H, Wang Y, Tsodyks M. Differential signaling via the same axon of neocorticalpyramidal neurons. Proc Natl Acad Sci U S A. 1998 Apr 28;95(9):5323-8.

Abbott LF, Regehr WG. Synaptic computation.Nature. 2004 Oct 14;431(7010):796-803.

Abbott LF, Varela JA, Sen K, Nelson SB. Synaptic depression and cortical gain control. Science. 1997 Jan 10;275(5297):220-4.

Varela JA, Sen K, Gibson J, Fost J, Abbott LF, Nelson SB. A quantitative description of short-term plasticity at excitatory synapses in layer 2/3 of rat primary visual cortex. J Neurosci. 1997 Oct 15;17(20):7926-40. Bertram R. Differential filtering of two presynaptic depression mechanisms. Neural Comput. 2001 Jan;13(1):69-85.

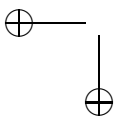

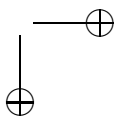

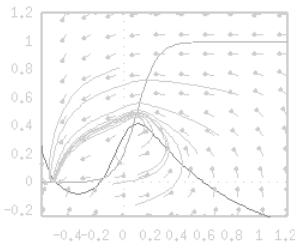

Chapter 9

Neural oscillators: Weak coupling

This chapter begins the second part of the book. By now, we hope that the reader has a thorough knowledge of single cell dynamics and is ready to move onto networks. There are two main approaches to the analysis and modeling of networks of neurons. In one approach, the details of the action potentials (spikes) matter a great deal. In the second approach, we do not care about the timing of individual neurons; rather, we are concerned only with the firing rates of populations. This division is reflected in the sometimes acrimonious battles between those who believe that actual spike times matter and those who believe that the rates are all that the brain cares about. On these issues, we have our own opinions, but for the sake of the reader, we will remain agnostic and try to present both sorts of models.

If spikes matter, then it is important to understand how the spikes of one neuron affect the timing of the spikes of another neuron to which it is synaptically (or otherwise) connected. *General* theories on the influence of inputs on the dynamics of single neurons do not exist. Here we have emphasized the word "general" as there has been some work on the influence of transients on firing patterns of cells. In order to say something rigorously, we consider, in this chapter, a very specific situation in which the individual neurons intrinsically oscillate. This is not an unreasonable assumption at least in the short time scale. a neuron receiving a slowly varying current may throw off a few fairly regularly spaced spikes; thus, at least for those few moments, it can be regarded as an oscillator. Hence, we are interested in how networks of neural oscillators behave when the are are allowed to interact. Such oscillatory (or transiently oscillatory) networks arise in many areas of neuroscience. There is absolutely no doubt that these networks play a critical role in motor patterns for repetitive activity such as locomotion, feeding, breathing, and mating. Such *central pattern generators* (CPGs) consist of networks of neurons which produce robust rhythmic output. Kopell (1988) was among the first to recognize the connection between the mathematical theory of coupled oscillators and CPGs. This alone should be sufficient motivation for studyng the properties of coupled neural oscillators. However, a more controversial role for neural oscillations and synchrony has emerged over the last twenty years. A major question in cog-

nitive psychology concerns how different sensory modalities are brought together to produce a unified percept. The problem of how such different aspects of, say, an object, are brought together is called the *binding problem.* von der Malsberg and Schneider (1986) were among the first to suggest that neural oscillations could "solve" this problem. That is, different areas of the brain would synchronize when there was a common percept. Wolf Singer's group found tantalizing evidence for this theory in electrical recordings of the cat visual cortex. So called gamma oscillations (30-80 Hz) were found to have a high degree of synchrony under certain situations presumably related to perceptual grouping. Thus, an industry was born and there are now hundreds of papers which concern the role of gamma oscillations and synchrony in perception. We list some of the in the references below. Our point here is not to ask whether these synchronous oscillations do in fact play a role, but rather, use this possibility to motivate the study of spike synchronization between neurons.

9.1 Neural oscillators, phase, and isochrons

A single neuron often fires repetitively when it is injected with a constant current. Indeed, we studied the onset of these oscillations in many different neural models in previous chapters. Thus, it is not unreasonable to regard a stimulated neuron as a limit cycle at least in the short-term (over a period of several spikes.) Thus it behooves us to consider some general properties of limit cycles. Unlike a stable fixed point, a stable limit cycle oscillator has a degeneracy associated with it; namely, the fact that any solution $X(t)$ can be arbitrarily translated in time and still be a solution. In the first two exercises, we explore the notion of linear stability for limit cycles. In particular, one can never get the same kind of asymptotic stability as with fixed points. Instead, one gets orbital asymptotic stability.

Consider the differential equation in R^n:

$$\frac{dX}{dt} = F(X) \tag{9.1}$$

and suppose that Γ is a $T-$periodic limit cycle. Recall that the limit cycle is said to be orbitally asymptotically stable if nearby initial conditions approach Γ as $t \to \infty$. We can parametrize Γ by time modulo the period T (see Figure 9.1A) and thus define a phase, $\theta \in [0, T)$ along the limit cycle. Let $\Theta(x)$ denote the phase of the oscillator for a point x on Γ. When the cycle is asymptotically stable, it is possible to define a phase for points y in a neighborhood of the cycle. Let $X(t; y)$ be the solution to (9.1) with initial condition y. Suppose that y is a point in the neighborhood of the limit cycle and x is a point on the limit cycle such that $||X(t; x) - X(t; y)|| \to 0$ as $t \to \infty$. Then we define $\Theta(y) = \Theta(x)$. That is, as $t \to \infty$, the solutions are indistinguishable. The set of points y which have the same asymptotic phase are called the isochrons of the limit cycle (see Figure 9.1B.) We denote the isochron through a point $x \in \Gamma$ as $N(x)$. Isochrons are local sections; that is, for a point $y \in N(x)$, $X(y, T) \equiv y' \in N(x)$. The map $y \to y'$ is a Poincare map for the limit cycle which takes time *exactly* T to return. The existence of isochrons allows us to define the phase of any point in the neighborhood of the limit cycle which as above

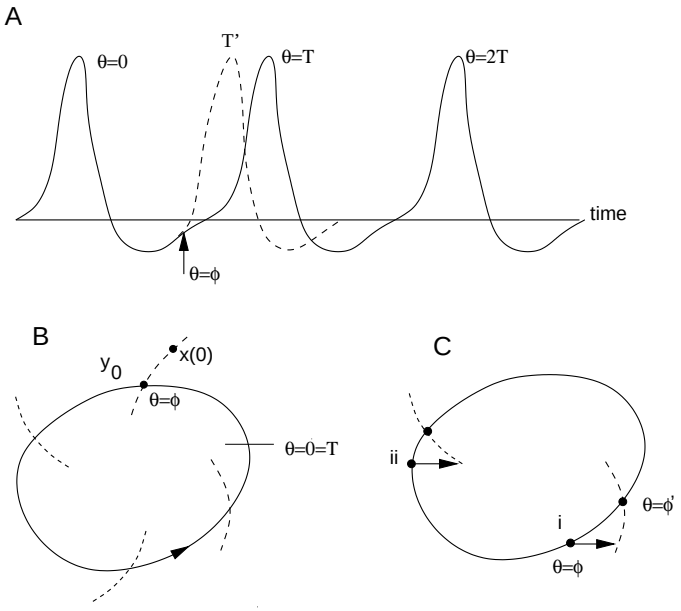

Figure 9.1. *Phase for a limit cycle. (A) Time trace showing definition of the phase zero as the peak of the potential. (B) Limit cycle in the phase plane showing contours with the same asymptotic phase. These are called isochrons. Initial condition $x(0)$ is mapped to y_0 on the limit cycle with phase ϕ. (C) Geometry of phase-resetting. At point (i) a perturbation along the $x-$axis at phase ϕ tends to a new asymptotic phase ϕ' which is closer to spiking with respect to the original phase. The same perturbation at (ii) delays the next spike time.*

we call $\Theta(x)$. In most of this chapter, we define the zero phase to be the peak of the voltage, so that any point on the limit cycle has a uniquely defined phase lying between 0 and T.

In practice, the isochrons can only be computed numerically. However, for some simple models, an exact formula can be found (cf Exercise *). Izhikevich (2006) provides MatLab code for computing isochrons for planar models limit cycles. Figure 9.2 shows the color-coded isochrons for the Morris-Lecar model. The function $\Theta(x)$ is not at all isotropic and shows very slow changes near the spike and very rapid changes near the "ghost" of the saddle-node bifurcation. For example, the time difference between the isochrons labeled a and b is about 2.5 msec while the time difference between those labeled c and d is about 40 msec. This says that small changes in the variables near the points c and d will have a much greater effect on the phase of the oscillator than similar magnitude perturbations near a and b. We will see the implications of this next.

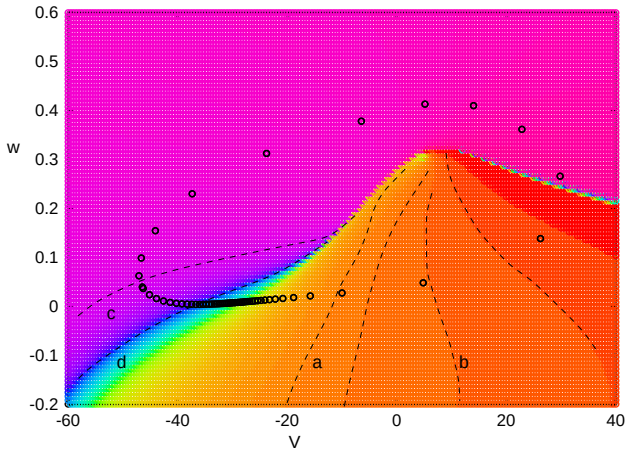

Figure 9.2. *Morris-Lecar oscillator (Class I parameters, $I = 42$) showing the asymptotic phase function $\Theta(x)$ and some representative isochrons. Black dots show values on the limit cycle in increments of 2.5 msec. Period of the limit cycle is 145 msec.*

9.1.1 Phase resetting and adjoints.

Suppose that we are merrily rolling along the limit cycle and a brief stimulus is given. For example, in Figure 9.1C, we have applied a horizontal perturbation to the vector field at phase ϕ. This perturbation puts us on the isochron for ϕ' so that the phase of the oscillator is reset to a different value which depends on its initial phase. For each phase ϕ at which the stimulus is applied, we get a new phase ϕ'. The map from old phase ϕ to new phase, ϕ' is called the *phase transition curve* (PTC), $\phi' = P(\phi)$. Winfree (1980) and others have noted that the PTC has two different topological forms that are called type 0 (strong) and type 1 (weak) resetting. In weak resetting, the map $P(\phi)$ is an invertible map of the interval $[0, T)$ to itself. With strong resetting, the map is not invertible. For example, suppose the stimulus is so strong that the phase is always reset to 0 (that is, the neuron spikes immediately). For the classic integrate-and-fire model, any finite increase of the voltage always results in type 0 resetting (see exercise *) while for the QIF model with infinite reset, all perturbations show type 1 resetting. For the normal form at a Hopf bifurcation, resetting can be both type 1 and type 0 depending on the size of the perturbation.

In this chapter, we will be concerned almost exclusively with type 1 resetting, where the function $P(\phi)$ is invertible. In the next chapter, where there is strong coupling applied to relaxation oscillators, we will analyze the opposite extreme in which essentially all resetting is type 0.

Experimentalists are often interested not in the phase transition curve, but rather in the actual *change* in phase due to the perturbation. This function, knows

as the *phase resetting curve* is defined as the difference between the new phase and the old phase:

$$\Delta(\phi) \equiv \phi' - \phi = P(\phi) - \phi.$$

Figure 9.3 shows some examples of experimentally computed PRCs from cortical and related neurons. In each case, if the stimulus is given at the moment of spiking, the PRC is zero. This says that a stimulus given at the moment of the action potential is ignored.

Figure 9.1A shows the time trace of, say, the voltage of a neuron, with and without the brief perturbation given at time (phase) ϕ. Suppose that the time of the spike given the perturbation is at T'. We now relate T' with the PRC. Note that the phase of a limit cycle satisfies:

$$\frac{d\theta}{dt} = 1 \mod T.$$

Suppose that at time ϕ the stimulus is applied and this causes a shift to a new phase ϕ'. Assume for the moment that the new phase is less than T, the period of the limit cycle. (This is not an unreasonable assumption for neurons since it says that the perturbation will never cause an immediate spike; rather there is some delay.) The time until the next spike is just $\tau = T - \phi'$ so that the time of the next spike, $T' = \phi + \tau = \phi + T - \phi' = T - \Delta(\phi)$. Thus, we have:

$$\Delta(\phi) = T - T'. \tag{9.2}$$

Typically, if one is trying to measure a PRC either experimentally or from a numerical simulation, the time of the phase zero defining event is measured as a function of the time of the stimulus. This is just T'. If $T' < T$, then the stimulus advances the phase (speeds up the cycle) and vice versa. Figure 9.3A,B show that excitatory stimuli can lengthen the time to spike if they occur very shortly after the spike, but otherwise shorten the time to spike. Figure 9.3C essentially shows only lengthening. Inhibitory stimuli (Figure 9.3A,B (ii)) always appear to lengthen the time to the next spike – they phase delay the oscillator.

Many people normalize the phase to lie between 0 and 1 or 0 and 2π so that we have to rescale ϕ and Δ, e.g. multiply by $1/T$ or $2\pi/T$. The rescaling is useful if we want to compare the PRCs for oscillators at different frequencies since they then have the same domain and range. Unless otherwise noted, we will not rescale the phase and the PRC.

We now relate the PRC to the phase function $\Theta(x)$ defined by the isochrons of an attracting limit cycle. Let $x = X_0(\phi)$ be the point on the limit cycle, $X_0(t)$, with phase (time) $\phi \in [0, T)$. Note that $\Theta(x) = \phi$ by definition. Consider an arbitrary perturbation, $y \in R^n$, of the vector field. The new phase is

$$\phi' = \Theta(x + y) = \phi + \nabla_X \Theta(x) \cdot y + O(|y|^2).$$

Thus for small perturbations

$$\Delta(\phi; y) = \nabla_X \Theta(x) \cdot y.$$

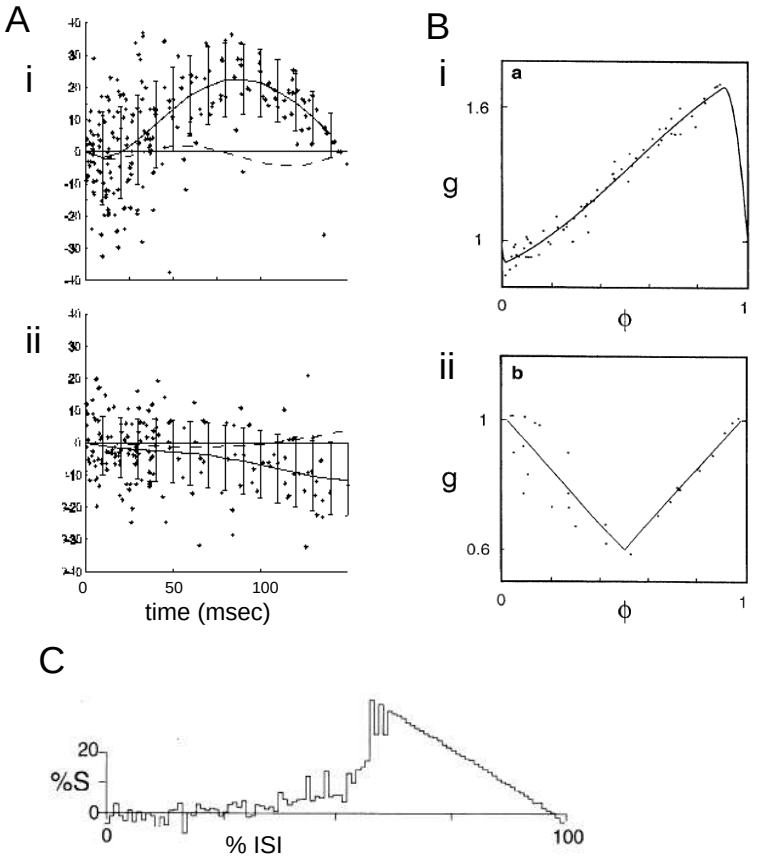

Figure 9.3. *Some experimentally measured PRCs from neurons. (A) Entorhinal cortex cells (Netoff et al 2005) for excitatory (i) and inhibitory (ii) synaptic perturbations; (B) rat barrel cortex pyramidal cells (Stoop et al 2000) with inhibitory (i) and excitatory (ii) perturbations; (C) cat motor cortex neurons. Note that in B, what is plotted is* $T'(\phi)/T = g(\phi) = 1 + \Delta(\phi)/T$

(We have included y in the PRC to emphasize that this corresponds to a very general perturbation.) If we suppose that the first component of the differential equation is the voltage of the neuron and take $y = (a, 0, \ldots, 0)$ where a is the scalar size of the perturbation of the potential, then we see that the PRC is approximately the first component of the gradient of the phase function $\Theta(x)$ evaluated at $X_0(\phi)$. Indeed, for neuroscientists, the PRC comes from some experimental perturbation which typically involves only at most a few of the variables which make up the dynamical systems governing the oscillation. The vector function

$$Z(\phi) \equiv \nabla_X \Theta(X_0(\phi)) \tag{9.3}$$

provides a complete description of how infinitesimal perturbations of the limit cycle change its phase. Kuramoto (1980) introduced the function $Z(\phi)$ and Winfree (1967) was a long-time proponent of the utility of the PRC. In the correct limit, we see that they are related. The PRC is exactly related to $\Theta(X_0(\phi)+y)-\phi$, but in practice the function $\Theta(x)$ for arbitrary x is very difficult to calculate. However, the gradient evaluated at the limit cycle, the function $Z(\phi)$, is very simple to compute as we will now see.

9.1.2 The adjoint

.

As we have noted, the phase function $\Theta(x)$ is not easy to compute. The function $Z(\phi)$ could be computed by applying small stimuli to the limit cycle along each of the $n-$components of the limit cycle and then linearly interpolating the results to zero amplitude. The reader with time on her hands is urged to try this! However, it turns out that the function $Z(\phi)$ is the solution to a linear differential equation which is closely related to the linearization of (9.1) about the limit cycle.

Suppose that $X_0(t)$ is a $T-$periodic limit cycle solution to (9.1). Let

$$A(t) = D_X F(X)|_{X_0(t)}$$

be the $n \times n$ matrix resulting from linearizing (9.1) around the limit cycle. Then solutions to the linearized equation satisfy:

$$\frac{dy(t)}{dt} - A(t)y(t) \equiv (Ly)(t) = 0. \tag{9.4}$$

Let

$$(u(t), v(t)) = \int_0^T u(t) \cdot v(t)\ dt \tag{9.5}$$

be the standard inner product on $T-$periodic functions in R^n. Recall that if L is a linear operator, then the adjoint linear operator, L^*, satisfies $(u, Lv) = (L^*u, v)$ for all u, v. As shown in exercise *, the adjoint L^* is

$$(L^*y)(t) = -\frac{dy(t)}{dt} - A(t)^T y(t). \tag{9.6}$$

We now use Brown etal's (2003) simple proof that $Z(t)$ satisfies the adjoint equation.

Recall that the asymptotic phase to an infinitesimal perturbation $y(t)$ is given by $Z(t) \cdot y(t)$. By definition, this phase is independent of time. Note that $y(t)$ satisfies $Ly = 0$ since y is arbitrarily close to the limit cycle. Thus

$$\begin{aligned} 0 &= \frac{d}{dt} Z(t) \cdot y(t) \\ &= \frac{dZ(t)}{dt} \cdot y(t) + Z(t) \cdot \frac{dy}{dt} \\ &= \frac{dZ(t)}{dt} \cdot y(t) + Z(t) \cdot A(t)y(t) \end{aligned}$$

$$= \frac{dZ(t)}{dt} \cdot y(t) + A(t)^T Z(t) \cdot y(t)$$
$$= [\frac{dZ(t)}{dt} + A(t)^T Z(t)] \cdot y(t).$$

Note that the operator inside the [ ] is $-L^*$. Since $y(t)$ is arbitrary, we must have that

$$L^* Z(t) = 0.$$

If $X_0(t)$ is a stable limit cycle, then the operator $L(t)$ has a nullspace spanned by scalar multiples of $dX_0(t)/dt$ (see exercise *) which is a periodic function. The adjoint has a one-dimensional nullspace (in the space of $T-$periodic functions in R^n) as well, so that $Z(t)$ must be proportional to this eigenfunction. It remains to determine the appropriate normalization. But this follows immediately from the observation that $\Theta(X_0(\phi)) = \phi$. Differentiate this with respect to ϕ and see that

$$Z(\phi) \cdot \frac{dX_0(\phi)}{d\phi} = 1.$$

This uniquely defines $Z(t)$ as the solution of the $L^*Z = 0$ and $Z \cdot dX_0/dt = 1$.

Numerically solving $L^*y = 0$ is done by integrating the equation:

$$\frac{dy}{dt} = -A(t)^T y$$

backward in time. Since the limit cycle is aymptotically stable, backward integration damps out all components except the periodic one which is the solution of the adjoint equation. Suitable multiplication by a scalar provides the necessary normalization.

Examples.

Ring models. Consider the differential equation:

$$x' = f(x)$$

where $f(x) > 0$ and $x \in S^1$. Thus, $f(x+1) = f(x)$. This equation has a $T-$periodic solution $x_0(t)$ with period

$$T = \int_0^1 \frac{dx}{f(x)}.$$

The adjoint is just $z(t) = 1/f(x_0(t))$ since $z(t)dx_0/dt = 1$. For example, consider the function $f(x) = 1 + a\cos 2\pi x$ where $|a| < 1$. This has a period $T = 1/\sqrt{1-a^2}$ and a bit of algebra shows that the adjoint is just

$$x^*(t) = \frac{1 - a\cos 2\pi t/T}{1 - a^2}. \tag{9.7}$$

In particular, note that $x^*(t)$ is always positive. One can only phase advance the oscillator when the stimulus is positive. On the other hand, plotting $-x^*(t)$ as

would be the response to an inhibitory stimulus looks a great deal like the PRC in Figure 9.3Bii. In general for any ring model, the PRC/adjoint is always non-negative, a fact that should be obvious. Exercise * asks the inverse problem – given a positive PRC, find a ring model.

$\lambda - \omega$ systems. Kopell and Howard (197?) introduced a class of nonlinear oscillators (which is closely related to the normal form for the Hopf and Bautin bifurcations):

$$u' = \lambda(r)u - \omega(r)v, \quad v' = \lambda(r)v + \omega(r)u \tag{9.8}$$

where $r^2 = u^2 + v^2$. Suppose that $\lambda(0) = 0$, $\omega(1) = 1$ and $\lambda'(1) < 0$. Then there is a stable limit cycle solution $(u, v) = (\cos t, \sin t)$. Kopell and Ermentrout (1984) were the first to compute the adjoint for this system; we leave it as an exercise to prove that

$$(u^*(t), v^*(t)) = (a\cos t - \sin t, a\sin t + \cos t) \tag{9.9}$$

where $a = -\omega'(1)/\lambda'(1)$. Note that the normal form of the Hopf bifurcation, $\lambda(r) = 1 - r^2$ and $\omega(r) = 1 + q(r^2 - 1)$, so $a = q$.

QIF model. The quadratic integrate-and-fire model with infinite reset:

$$V' = V^2 + I$$

is a singular example of a scalar "ring" model. The solution to this is

$$V(t) = -\sqrt{I}\cot\sqrt{I}t.$$

The adjoint is thus, $V^*(t) = 1/V'(t)$:

$$V^*(t) = \sin^2(\sqrt{a}t)/a = (1 - cos(2\sqrt{a}t))/a.$$

An alternate way to find $V^*(t)$ is to compute the PTC for a finite perturbation, b (exercise *), differentiate with respect to b and evaluate at $b = 0$.

We note that for a finite reset and finite spike, the model is essentially a ring model. In exercise *, you will compute the adjoint for this case.

Singularly perturbed systems. In exercise *, you find a general formula for the adjoint of any stable planar limit cycle. The result is not particularly transparent. However, for a relaxation oscillator, the singular limit makes the calculation more useful. Izhikevich was the first to do this and we follow his presentation here. Figure 9.4 shows the singular trajectory ($\mu = 0$) for the system:

$$\begin{aligned} \mu x' &= f(x, y) \\ y' &= g(x, y). \end{aligned}$$

Let $\Gamma(t)$ be the singular trajectory. The $x-$component of $\Gamma(t)$ has jumps at $t = t_j$ corresponding to the jumps in the phase-plane from a_j to b_j. The linearized equation is

$$\begin{aligned} 0 &= f_x(\Gamma(t))x + f_y(\Gamma(t))y \\ y' &= g_x(\Gamma(t))x + g_y(\Gamma(t))y. \end{aligned}$$

The linearized system has a solution $\Gamma'(t) = (f(\Gamma(t)), g(\Gamma(t)))$ which, because of the jumps at t_j in $\Gamma(t)$, will consist of a smooth part and a singular part (with Dirac delta functions at t_j.). The adjoint equation is

$$0 = -f_x(\Gamma(t))u - g_x(\Gamma(t))v \tag{9.10}$$
$$v' = -f_y(\Gamma(t))u - g_y(\Gamma(t))v. \tag{9.11}$$

The normalization is

$$ux' + vy' = uf(\Gamma(t)) + vg(\Gamma(t)) = 1.$$

Consider, first, the smooth parts of the trajectory, $t \neq t_j$. Along the singular trajectory, $f(\Gamma(t) = 0$ so that the normalization yields:

$$v = 1/g(\Gamma(t)). \tag{9.12}$$

Since $f_x(\Gamma(t))$ is nonzero away from the jump points the equality (9.10) implies that

$$u = -\frac{g_x(\Gamma(t))}{g(\Gamma(t))f_x(\Gamma(t))}. \tag{9.13}$$

At $t = t_j$, $v(t)$ jumps from $1/g(a_j)$ to $1/g(b_j)$. From (9.11):

$$u(t) = -\frac{1}{f_y(\Gamma(t))}\left(v'(t) + g_y(\Gamma(t))\right).$$

Since v jumps, u must have a Dirac delta function singularity. Integrating across this we have to have

$$u(t_j^+) - u(t_j^-) = -\frac{1}{f_y(a_j)}\left(\frac{1}{g(b_j)} - \frac{1}{g(a_j)}\right) \equiv c_j.$$

Thus, at $t = t_j$ we have

$$(u, v) = \left(c_j\delta(t - t_j), 1/g(a_j)\right). \tag{9.14}$$

Equations (9.12), (9.13), and (9.14) provide the complete adjoint solution

9.1.3 Bifurcations and adjoints.

In general, except for the few examples described above, it is not possible to find the adjoint explicitly for a limit cycle. Certainly, the minimal condition is that an explicit solution for the limit cycle be provided and there are very few examples of that. However, several of the examples are suggestive that they may be more general than they first appear. For example, in class I excitability, the behavior near the bifurcation is the same as that of the QIF/theta model. Thus, we expect that near the onset of rhythmicity, the adjoint of *any* class I oscillator should look like $1 - \cos t$. How well does this actually work in practice? We can numerically compute the adjoint for any oscillator and compare the shape to that predicted near the bifurcation.

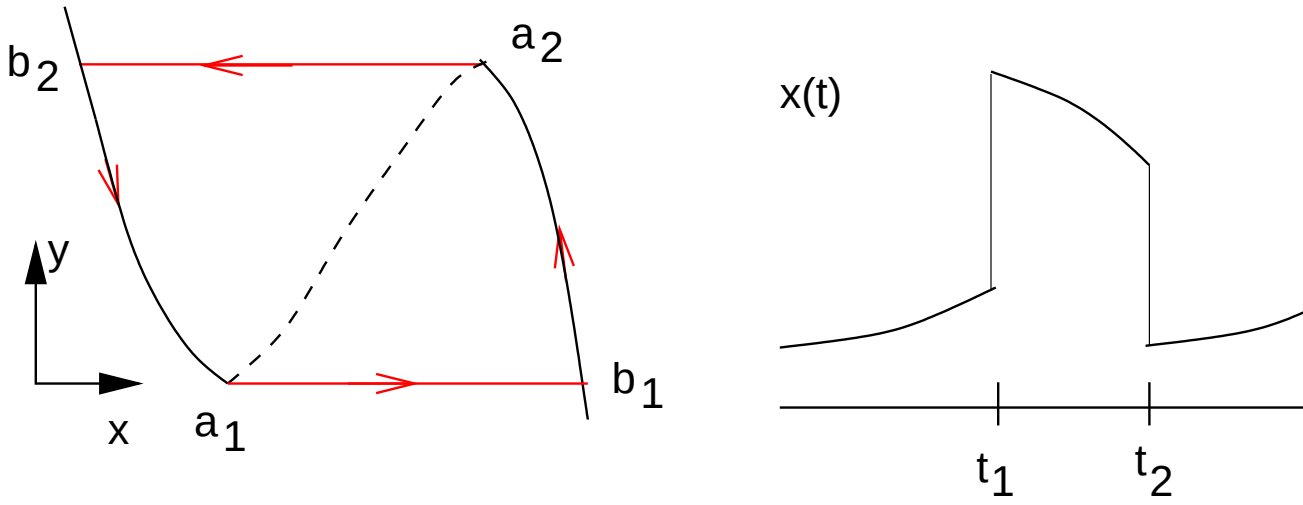

Figure 9.4. *Singular trajectory and the fast variable as a function of time.*

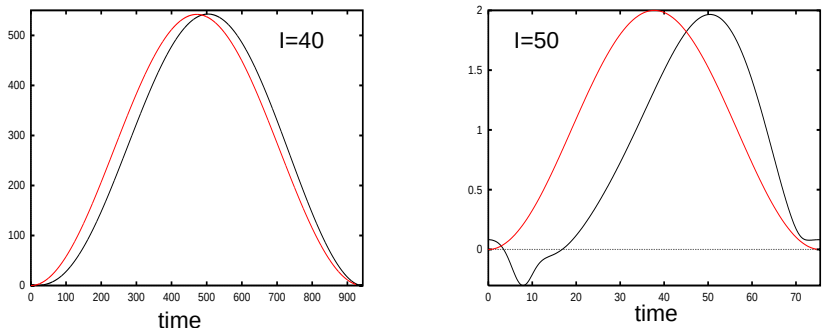

Figure 9.5. *The numerically computed adjoint for the ML model near the saddle-node bifurcation and its comparison to the asymptotic solution. Left panel,* $I = 40$ *and* $T = 943$*; right panel,* $I = 50$ *and* $T = 75.5$.

Class I excitability.

From equation (9.7) we expect that near a saddle-node on a circle bifurcation, the adjoint should be proportional to $1 - \cos\theta$. As an example, we will look at the Morris-lecar model about which we have already exhausted a great deal of ink.

Figure 9.5 shows the numerically computed adjoint (black) and the approximation (red) for two different currents. When $I = 40$, the model is very close to the bifurcation as can be seen from the length of the period, which is nearly 1000 msec. The adjoint is quite close to the theoretical value from equation (9.7). When $I = 50$, the period drops more than ten-fold and the approximation is not as good, but remains qualitatively similar.

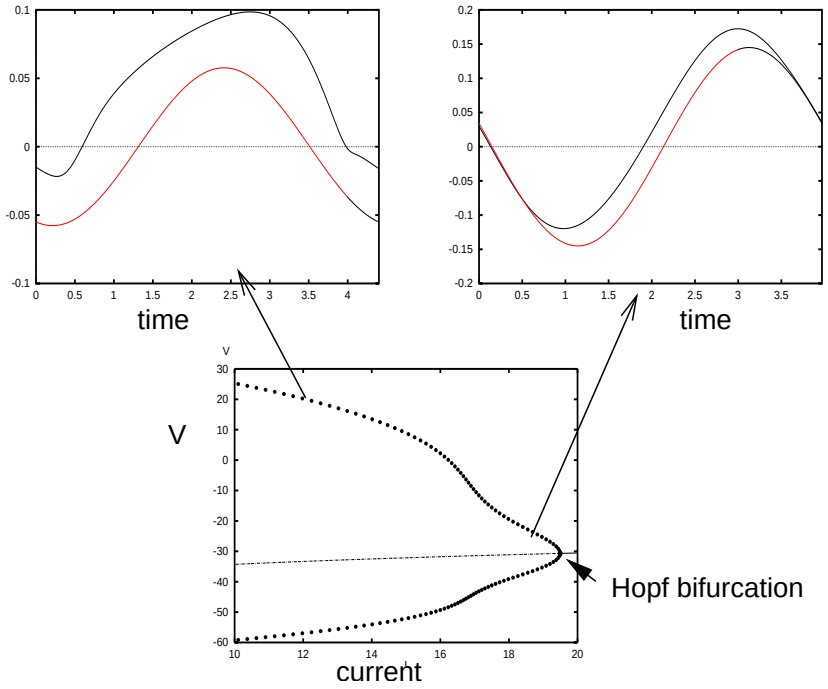

Figure 9.6. *The numerically computed adjoint for the Golomb-Amitai model near the supercritical Hopf bifurcation. Bottom figure shows the bifurcation diagram as a function of the current. Top two curves show the adjoint (black) and the approximation (red) $a\sin\theta + b\cos\theta$. Choices of a, b come from the Fourier expansion of the numerically computed adjoints.*

Hopf bifurcation.

Very few neural models actually undergo *supercritical* Hopf bifurcation at least at the onset of the rhythmic behavior. Thus, it is difficult to make comparisons. However, for illustrative purposes, we use a model from Golomb and Amitai which has a supercritical Hopf bifurcation at high applied currents. The normal form for the supercritical Hopf bifurcation is of the form (9.8) and, for this model, each component of the adjoint is a pure sinusoid:

$$u^*(\theta) = \alpha\sin\theta + \beta\cos\theta.$$

We thus compute the adjoint numerically and see how well it is approximated by pure sinusoids. Figure 9.6 shows the results for currents close to the Hopf bifurcation and further away. The key take-home lesson here is that models near a Hopf bifurcation have regimes of phase advance and phase delay in contrast to class I models which are dominated by phase advance dynamics.

Limit point.

In most Class II neural models, the Hopf bifurcation is subcritical but the unstable branch folds back to become stable. Thus, there is a saddle-node bifurcation of limit cycles. What can we expect the adjoint to look like in this case? A hint of the behavior can be found in returning to the lambda-omega system (9.8) since we can easily obtain this type of bifurcation by choosing:

$$\lambda(r) = p + r^2 - r^4$$

where p is a bifurcation parameter. For $p < 0$ and small, there are two roots to $\lambda(r) = 0$, $r_1 < r < 2$, corresponding to a stable and unstable limit cycle. They coalesce when $r_1 = r_2$ which occurs when $\lambda'(r) = 0$. From equation (9.9), we see that the magnitude of the adjoint is dominated by the terms multiplied by $\omega'(r)/\lambda'(r)$ since $\lambda'(r)$ goes to zero as the limit point is approached. Thus, we expect that the magnitude of the adjoint will tend to infinity as the limit point is approached. This may seem somewhat counter-intuitive since we know that $u^*(t) \cdot u'(t) = 1$. Thus, all of the growth of the adjoint is in a direction orthogonal to the limit cycle. Exercise * gives an explicit formula for the adjoint to any planar system. The computation depends on solving a scalar equation of the form:

$$dc/dt = (f_u + g_v)c + p(t).$$

For a planar limit cycle the attraction is determined by

$$\nu = \int_0^T f_u + g_v \; dt.$$

As a limit point or saddle-node of limit cycles is approached, the eigenvalues, ν tends to zero so that the quantity $c(t)$ will grow like $1/\nu$. This $c(t)$ multiplies a vector which is orthogonal to the limit cycle, so we expect to see that adjoint grow rapidly as the bifurcation is approached. Figure 9.7 confirms this fact for the ML model. As we approach the bifurcation, the adjoint rapidly increases. Intuitively, this makes sense: if the attraction to the limit cycle is weak, then the motion around the limit cycle will be very fast compared to the motion into the limit cycle so the isochrons will have a very pronounced twist.

Takens-Bogdanov.

In chapter **channel** we showed that the M-type potassium channel (an outward current which acts at voltages near rest) can convert the transition to oscillations from Class I (saddle-node on a circle) to Class II (Hopf bifurcation). The mechanism for this transition is organized around the Takens-Bogdanov bifurcation (see figure 5.5B). Our results so far suggest that this should have a big effect on the shape of the PRC. Figure 9.8A shows the effects of adding an M current to the Destexhe-Pare model described in chapter **channel**. The PRC (where we have added sufficient current so that the cell fires at about 40 Hz) switches from strict positivity to a substantial negative region.

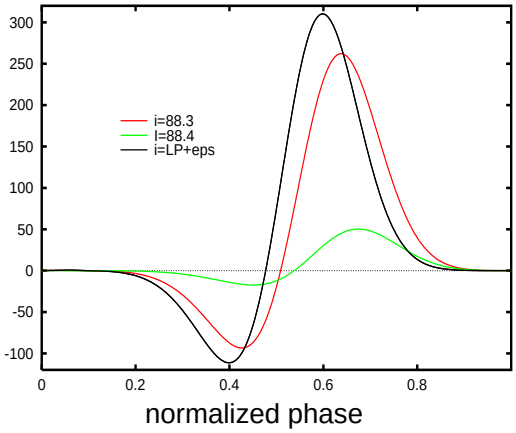

Figure 9.7. *The adjoint for the ML model near the turning point bifurcation. Black curve is closest to the limit point and the adjoint has been scaled by a factor of 10 to fit on the same figure. Phase is normalized from 0 to 1 for easier comparison since the periods are different.*

How can we understand this switch? In exercise * in chapter **channel**, you show that the quadratic integrate and fire model with adaptation (5.19) is locally equivalent to the normal form for the Takens-Bogdanov. We compute a PRC for this model by injecting a brief current (the discontinuous resetting makes the adjoint difficult to compute accurately) at different times in the spike cycle. Recall the equations:

$$V' = I + V^2 - u, \quad u' = a(bV - u)$$

with reset of V to c when there is a spike and at the same time the variable u is incremented by an amount d. The adaptation is manifested in two ways: the parameter b governs subthreshold effects and the parameter d governs effects due to spikes. Since only the parameter b (which acts at rest) can switch the cell from class I to class II, we expect that this parameter will produce a negative component in the PRC. This is illustrated in figure 9.8B. With no adaptation ($b = d = 0$), the PRC is close to the canonical form, $1 - \cos t$. When $b = 1$, the rest state loses stability at a Hopf bifurcation and the excitability class is II. The PRC shows a pronounced negative component. However, if $b = 0$ and d is nonzero, then the PRC stays positive but is flattened in the early part of the cycle. In exercise * below, you explore this effect more systematically in a biophysical model.

Other currents.

Other currents affect the PRC in subtle ways. A good project would be to explore these currents in a systematic fashion. Exercises ** explore the roles of adaptation and the sag current. The reader should look at some of the other oscillators from

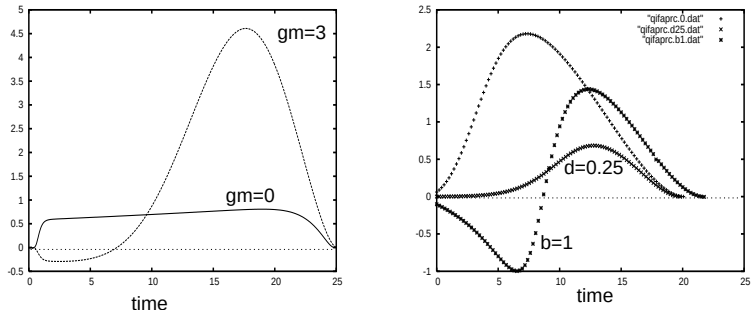

Figure 9.8. *The effects of outward currents on the PRC. (A) Adding an M-type potassium current to the Destexhe-Pare model adds a negative component to the adjoint. (B) PRCs for the quadratic integrate and fire model with adaptation computed by injecting a pulse with amplitude 1 for 0.2 time steps.*

chapter **channel** and examine the adjoints of these models.

9.1.4 Spike-time response curves.

With the advent of the *dynamic clamp*, it is possible to add and subtract channels and synapses in real neurons in a slice. Thus, several experimental groups now use the dynamic clamp to look at the behavior between two or more cells when they are coupled with artificial (that is computer) synapses. The first step in understanding the behavior of these coupled neurons is to understand how a single neuron responds to a synaptic current. If this current is an infinitesimal perturbation of the membrane potential, then we know that the response is precisely the adjoint. More generally, we can compute a phase resetting curve to any stereotypical input. Indeed, we already used this idea to compute the PRC for the QIF model by applying a small rectangular pulse of current at different times.

Let's consider this generally. Let X be the vector of variables satisfying

$$\frac{dX}{dt} = F(X)$$

and let $G(t, t_0)$ be the vector of inputs parametrized by the onset time t_0. Our system is thus

$$\frac{dX}{dt} = F(X) + G(t, t_0).$$

We assume that $X' = F(X)$ has a stable limit cycle. We multiply by the phase gradient function (9.3) and find that the phase of the oscillations satisfies:

$$\frac{d\theta}{dt} = 1 + Z(t) \cdot G(t, t_0).$$

This is an exact equation for the phase. We start with $\theta = 0$ and ask when $\theta(T') = T$, the period the unperturbed limit cycle. T' is a function of t_0 and is the time of

the spike. When $G(t,t_0)=0$, $T'(t_0)\equiv T$. We integrate this function and find:

$$\theta(T')=T'+\int_0^{T'} Z(t)\cdot G(t,t_0)\ dt=T.$$

Solving this for T' tells us when the next spike occurs. The PRC for a stimulus $G(t,t_0)$ is just $\mathrm{PRC}(t_0)=T-T'(t_0)$ which tells us how much the stimulus advances or delays the next spike. Suppose that $G(t,t_0)$ is small, say $G(t,t_0)=\epsilon g(t,t_0)$. Then we can expand $T'(t_0)$ as

$$T'(t_0)=T+\epsilon\tau(t_0)+\ldots.$$

This leads to

$$0=\tau(t_0)+\int_0^T Z(t)\cdot g(t,t_0)\ dt$$

so that to lowest order

$$\mathrm{PRC}(t_0)=\int_0^T Z(t)\cdot G(t,t_0)\ dt. \tag{9.15}$$

This is the time advance/delay due to the input G. Often one expresses it in terms of the fraction of a cycle in which case we divide by T. Note that if $G(t)$ is a Dirac delta function along one of the components of X, then the PRC is exactly the same as the adjoint as it is just a component of Z.

When $X(t)$ is a membrane equation and $G(t,t_0)$ is a synaptic current generated by an alpha function type of synapse:

$$G(t,t_0)=\alpha(t-t_0)(V_{syn}-V(t)),$$

then the function (9.15) is called the spike time response curve or STRC. It tells us how the spike time of a neuron is changed by a stereotypical input as a function of when that input arrives. In the reduction to maps and phase equations which follows later in this chapter, we do not distinguish between the STRC and the usual PRC.

9.2 Who cares about adjoints?

At long last, we come to the core of this chapter. We have spent several pages extolling the virtues of PRCs, STRCs, and adjoints. There are at least two ways in which these response functions are useful. First, we can use them directly to create systems of pulse coupled equations which we can reduce to maps. Secondly, we can use the weak coupling assumption and averaging to reduce arbitrarily coupled networks of neurons to systems of equations on a torus. The most obvious application of a PRC is to study the effects of periodic drive on an oscillator; the subject of the next section.

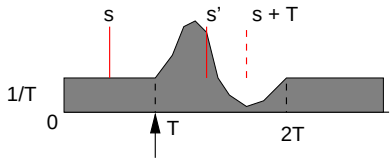

Figure 9.9. *Post stimulus time histogram for a neuron.*

9.2.1 Relationship of the adjoint and the response to inputs.

The adjoint and its cousin the PRC are relevant beyond purely oscillating neurons and they provide information about how a neuron responds to inputs *even when it is not a regular oscillator.* Clearly, if the neuron is at a stable rest state, then a weak input will, by definition, have no effect on it and only strong inputs will produce a spike. In this case, there is dependence of the response on time of the inputs since the cell is at rest. However, if the neuron is subject to sufficient depolarization that it is firing (irregularly, perhaps) then even "weak" inputs can alter the time of a spike. The amount by which the spike time is altered depends on when the neuron last spiked and thus we can expect that there is some relationship to the PRC. Gutkin et al (2005) numerically showed that the shifting of spikes in a nonstationary system (that is, a non-constant stimulation, either slowly varying input currents or fast noisy inputs) is determined by the steady-state PRC of the neuron. That is, the PRC can tell us how an input shifts a spike even when the neuron is not a regular oscillator.

One of the most common measurements done by neurophysiologists is the post-stimulus time histogram (PSTH). The PSTH is the probability of a spike occurring at a given time t after the onset of a stimulus. It is measured by collecting the spike times of a neuron over many repetitions of the same stimulus. Implicit in the usefulness of the PSTH is that the dynamics are stationary. For example, the mean firing rate of the neuron before the stimulus is constant and the time between repetitions is long enough so that the effect of the stimulus wears off. A cartoon of the PSTH is shown in Figure 9.9. A brief stimulus is applied at $t = 0$ causing the probability of firing for the neuron to increase transiently before returning to the baseline uniform probability. Gutkin et al (2005) show that the PSTH can be related to the PRC, an argument that we now repeat. We assume that

i. The mean firing rate of the neuron is $1/T$ prior to the stimulus and the probability over trials of firing is uniform.

ii. The stimulus is sufficiently weak so that *no new spikes are added.* That is, the probability of firing is shifted, but there are no new spikes.

iii. The neuron rapidly returns to its baseline mean firing rate after one cycle.

Assumptions (ii) and (iii) imply that the area between $t = T$ and $t = 2T$ is 1 since no new spikes are added and all the rearranging of spikes is finished within one average period. Consider the spike at time s in the figure. In the absence of the

stimulus, the expected time of the next spike is $s + T$ since the mean firing rate is $1/T$. But, because of the stimulus, the expected spike time is shifted to s'. The mean period of the neuron is T so that with respect to the spike at time s, the stimulus comes $T - s$ milliseconds after the neuron last fired. From the definition of the PRC, the expected time of s' is:

$$s' = s + T - \Delta(T - s) \equiv F(s).$$

Note that $F(0) = T$ and $F(T) = 2T$. Furthermore, $F'(s) = 1 + \Delta'(T - s) > 0$ since the stimulus is assumed to be weak. Thus, $F(s)$ is an invertible map from the interval $[0, T]$ to $[T, 2T]$. The PSTH is the probability that a spike occurs in a given window of time after the stimulus. Thus, the probability that $s' < t$ for some $t \in [T, 2T]$ is just:

$$\Pr\{s' < t\} = \int_T^t \text{PSTH}(t')\ dt'.$$

However,

$$\begin{aligned} \Pr\{s' < t\} &= \Pr\{F(s) < t\} \\ &= \Pr\{s < F^{-1}(t)\} \\ &= \frac{1}{T} F^{-1}(t). \end{aligned}$$

The last equality comes from the fact that the distribution of spikes before the stimulus arrives is uniform. We thus have the relationship between the PSTH and the PRC:

$$F^{-1}(t) = T \int_T^t \text{PSTH}(t')\ dt'. \tag{9.16}$$

9.2.2 Forced oscillators.

PRCs are directly computable from experimental data, thus they provide a way of creating a model of a specific biological oscillator without needing a mechanistic basis. Let us first explore how one can use the PRC to develop a map for the dynamics of a single oscillator which is periodically forced by an external pulsatile stimulus. This type of analysis has a long history and the reader should consult the comprehensive book by Glass and Mackey for references and applications to cardiac and other oscillators. Stoop and colleagues as well as several older references have also used PRCs to compute the behavior of forced systems.

Suppose that an oscillator $X(t)$ has a PRC, $\Delta(t)$ which describes the advance or delay as a function of the time of the stimulus, $0 \leq t < T$, where T is the period of the oscillator. Suppose that a stimulus is applied every T_f time steps and let ϕ_n denote the phase of the oscillator at the instant before the stimulus arrives. Right after the stimulus, the phase is given by $P(\phi_n) \equiv \phi_n + \Delta(\phi_n)$. Recall that $\phi \in [0, T)$. Between stimuli, the oscillator advances by an amount T_f in phase. Thus, at the moment of the next stimulus, we have

$$\phi_{n+1} = \phi_n + \Delta(\phi_n) + T_f = P(\phi_n) + T_f \equiv M(\phi_n) \tag{9.17}$$

where $P(\phi)$ is the phase transition map. This is a map on the circle and there is a huge literature on such maps. Since PRC theory is valid mainly when stimuli are weak, the size of Δ is assumed to be small. Therefore, $P(\phi)$ is monotonic and its derivative is

$$P'(\phi) = 1 + \Delta'(\phi)$$

Invertible maps on the circle are completely characterized by their *rotation number* which is defined as the average number of cycles covered per stimulus. We can make this more precise as follows. Instead of considering ϕ_n to be defined modulo T, we let it evolve on the real line. The rotation number is defined as

$$\rho \equiv \lim_{n\to\infty} \frac{1}{T}\frac{\phi_n}{n}. \tag{9.18}$$

This quantity has a nice intuitive appeal. For example, if $\rho = 1$ then, on average, the oscillator completes one cycle per stimulus and we say that there is $1:1$ locking. On the other hand, if $\rho = 2/3$, then the oscillator completes two cycles for each three of the stimulus and we call this $2:3$ locking. The rotation number is described by a beautiful theorem which we state without proof. This version of the theorem appears in Hale and Kocak (1991).

Theorem. (Denjoy) The rotation number is well-defined; that is, the limit exists and is independent of the initial condition. Furthermore, if $M(\phi)$ is twice continuously differentiable then

(i) ρ is rational if and only if $M(\phi)$ has a periodic orbit of some period: $\phi_{n+N} = \phi_n \bmod T$.

(ii) ρ is irrational if and only if every orbit $\{\phi_n\}$ is dense in the circle.

(iii) ρ is a continuous function of any parameters in the function M.

We turn to the analysis of the map (9.17). We first find conditions for $1:1$ locking, $2:1$ locking, and $1:2$ locking and determine the stability. We then look at the rotation number of two relevant simple maps as a function of T_f the period of forcing.

For 1:1 locking, we must have $\phi_{n+1} = \phi_n + T$; that is, the oscillator must complete one cycle per stimulus. This means that

$$\phi + T = \phi + \Delta(\phi) + T_f$$

so that we must solve:

$$\Delta(\phi) = T - T_f \tag{9.19}$$

for ϕ. In class I neurons, the PRC is typically non-negative everywhere so that in order to entrain this type of neural oscillator, the period of the forcing stimulus must be smaller than the natural period. In the other hand, for class II firing, the PRC can be both positive and negative so that the period of the forcing stimulus can be both shorter and longer than the natural period. Since $\Delta(\phi)$ is a periodic function,

we expect that there will be at least two roots to (9.19) except at bifurcation points (see below). To determine the stability, we linearize and obtain:

$$y_{n+1} = (1 + \Delta'(\phi))y_n \equiv cy_n.$$

We know that $c > 0$ since the PTC is monotone. If $\Delta'(\phi) > 0$, then $c > 1$ and the fixed point is unstable while if $\Delta'(\phi) < 0$, then $0 < c < 1$ and the fixed point is stable. The only bifurcation that can occur corresponds to $c = 1$ or $\Delta'(\phi) = 0$ which means ϕ is a double root and occurs at a local maximum or minimum of $\Delta(\phi)$.

2:1 locking occurs when $\phi_{n+1} = \phi_n + 2T$; that is, the oscillator fires twice for every cycle of the stimulus. In this case, we have to solve

$$\Delta(\phi) = 2T - T_f.$$

Note that if $\Delta(\phi)$ is centered around zero, then we can solve this equation when T is close to $T_f/2$. Stability follows in the same way as the 1:1 case. In general, phase-locking of the form $m : 1$ is very simple to analyze and is done in a manner similar to the 1:1 case.

1:2 locking means that the oscillator fires only once for every two stimuli so that

$$\phi_{n+2} = \phi_n + T.$$

We note that $\phi_{n+2} = M(\phi_{n+1}) = M(M(\phi_n))$ where $M(\phi)$ is as in (9.17) so that we must solve:

$$T = 2T_f + \Delta(\phi) + \Delta[\phi + \Delta(\phi) + T_f]. \tag{9.20}$$

Obviously, this is more difficult to solve than the $m : 1$ case. However, we note that if Δ is small, then this can be solved only when $2T_f \approx T$. That is, the stimulus must be roughly twice as fast as the intrinsic period of the oscillator, another intuitively appealing observation. Stability proceeds in a similar manner and we require that $c = M'(M(\phi))M'(\phi)$ be less than one for stability. This gives a condition on $\Delta(\phi)$ and its derivatives:

$$c = [1 + \Delta'(\phi)][1 + \Delta'(\phi + \Delta(\phi) + T_f)] < 1.$$

In general, for $m : r$ locking, in which the stimulus fores r times and the oscillator fires m times, we have to solve

$$\phi + mT = M^r(\phi)$$

where M^r is r iterates of $M(\phi)$. We note that

$$M^r(\phi) = \phi + rT_f + \ldots$$

where the remaining terms depend on Δ. Thus, for small PRCs, we want $T_f/T \approx m/r$.

The analysis above hints that whenever T_f/T is near a rational number, m/r, then there can be phaselocking and thus a rational rotation number. If the PRC

is nontrivial (that is, it is not constant), then we should be able to solve for ϕ and thus find $m : r$ locked solutions for some open set of forcing periods, T_f. This means that if T_f is a parameter, then $\rho(T_f)$ should be constant over the open regions where there is locking. Figure 9.10 shows the rotation number for (9.17) for two different PRCs: $\Delta_1(\phi) = 0.8(1 - \cos\phi)$ and $\Delta_2(\phi) = c\phi^6(2\pi - \phi)$ where c is chosen so that the maximal magnitude of the slope is the same as Δ_1. The shape of this PRC is meant to mimic that of Figure 9.3C. Since the magnitude of Δ_2 is much smaller than that of Δ_1, the width of the plateaus is much shorter. In both cases, the rotation number increases with T_f and is punctuated with regions where it is constant. This diagram is called "the Devil's staircase." We note an interesting pattern in the steps. The largest steps are 2:1, 1:1, 0:1. The next largest are 3:2 and 1:2. Between any flat regions $a : b$ and $c : d$, the largest regime is always the one obeying the Farey addition rule, $(a + c) : (b + d)$. Allen (1983) was the first to notice this pattern in the context of neural firing.

If the slope of the PRC becomes more negative than -1, the invertibility of $M(\phi)$ is violated and it is possible to get very complex behavior in these simple maps, such as chaos. In neural models, a slope of -1 means that the neuron fires at the instant of the stimulus. Thus it is impossible to get slopes more negative than -1.

9.2.3 Coupled oscillators.

We now turn our attention to the case of two mutually coupled cells where we use the computed PRC to create a dynamical system. The cells are both oscillators and to start, we assume that they are identical with the same period, T_0. Each time one cell spikes, the cycle of the other cell is perturbed according to the PRC. This is the only time there is interaction between the cells. There are at least two ways to derive the dynamics. One is to derive equations for the spike times of the cells. The second is to derive equations for the phase of one cell when the other cell fires. The latter is considerably more convenient and can be formally generalized in a more straightforward manner. So that we can close this section on a good note, we start with the firing time idea.

Firing time maps.

Consider the spike times shown in Figure 9.11. Our goal is to derive a map for t'_j given t_j. If there was no spike t_2 then $t'_1 = t_1 + T_0$, since the cell is oscillatory with period T_0. The spike from cell 2 occurs at a time $t_2 - t_1$ after cell 1 spikes so that the time of the next cell 1 spike is shifted according to the PRC. Recalling the definition (9.2), we obtain

$$t'_1 = t_1 + T_0 - \Delta(t_2 - t_1).$$

Now, we turn our attention to t'_2, the time of the next spike from cell 2. As with cell 1, without coupling, $t'_2 = t_2 + T_0$, but the intervening spike at t'_1 produces a phase-shift in the cell 2 spike. Thus, we obtain:

$$t'_2 = t_2 + T_0 - \Delta(t'_1 - t_2).$$

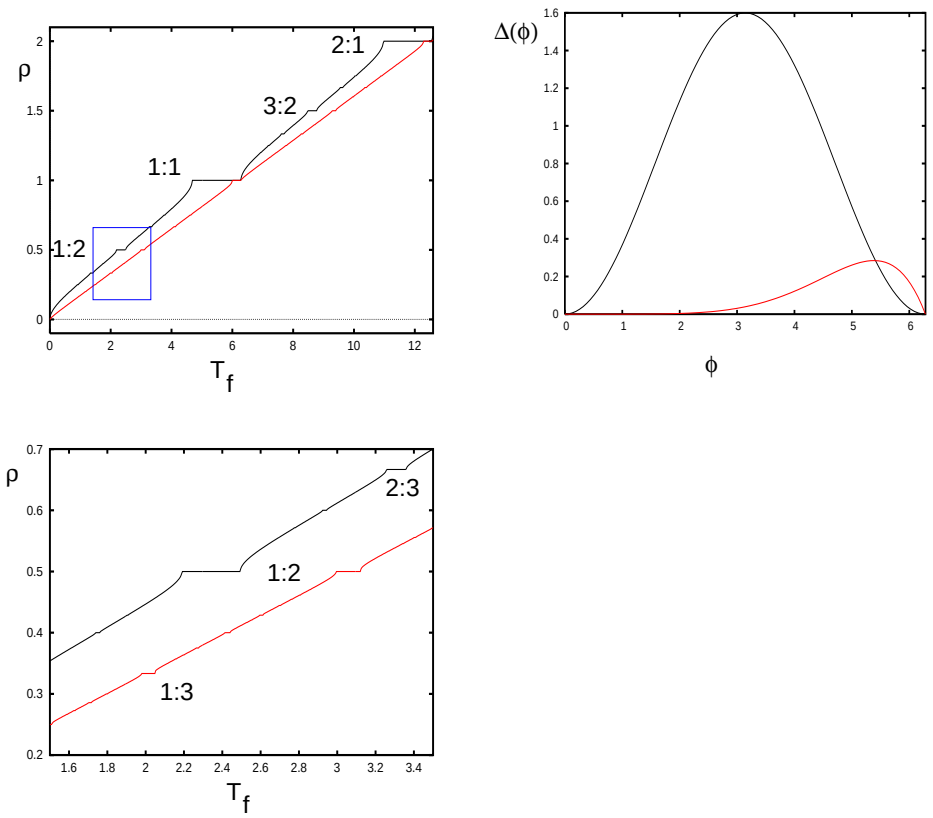

Figure 9.10. *The rotation number for the map* $M(\phi) = \phi + \Delta(\phi) + T_f$ *for* $\Delta(\phi) = 0.8(1 - \cos\phi)$ *(black) and* $\Delta(\phi) = 0.000013\phi^6(2\pi - \phi)$ *(red) as* T_f *varies. Expanded region is shown on below. Some rational rotation numbers are shown. The right panel shows the relative sizes of the two PRCs. The slope of the red PRC at* $\phi = 2\pi$ *is the same as that of the black at* $\phi = 3\pi/2$.

Note that t_2' depends on the difference between t_1' and t_2, *not* the difference between t_1 and t_2 since t_1' is the spike occurring between t_2 and t_2'. These equations are valid provided that no cell spikes twice before the other cell spikes. Thus, the spike alternation must be maintained for all finite time. We can reduce this equation to a one-dimensional map for the time difference between the cell 2 spike and the cell 1 spike. Let $\tau = t_2 - t_1$ and let $\tau' = t_2' - t_1'$. Now,

$$t_1' - t_2 = t_1 - t_2 + T_0 - \Delta(t_2 - t_1) = T_0 - \phi - \Delta(\tau) \equiv D(\tau),$$

so the t_2' equation is:

$$t_2' = T_0 + t_2 - \Delta[T_0 - \tau - \Delta(\tau)].$$

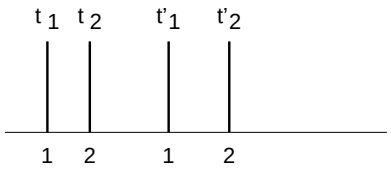

Figure 9.11. *Spike times of 2 coupled oscillators*

We subtract the t_1' equation from the t_2' equation to obtain

$$\tau_{n+1} = \tau_n - \Delta[T_0 - \tau_n - \Delta(\tau_n)] + \Delta(\tau_n) = D[D(\tau_n)]. \tag{9.21}$$

The new time difference between cell 1 and cell 2 is just the composition of two identical maps, $D(\tau) = T_0 - \tau - \Delta(\tau)$. The map $D(\tau)$ tells us how much longer we have to wait for a spike when a stimulus arrives τ after the previous spike. This map is the "time" equivalent of the phase transition curve. Recall that a fixed point of a scalar map $x \to M(x)$ satisfies $x = M(x)$ and it is stable provided that $|M'(x)| < 1$. We seek a fixed point for (9.21); thus,

$$0 = \Delta(\tau) - \Delta(T_0 - \tau - \Delta(\tau)).$$

For most of the PRCs which we have encountered (see Figures 9.3 or 9.5, e.g.) $\Delta(0) = \Delta(T_0) = 0$. That is, the oscillator is not affected by stimuli at the moment it spikes. In this case, $D(0) = 0$ so that synchrony $\tau = 0$ is a fixed point. Synchrony is a stable fixed point if:

$$|1 + \Delta'(0) + \Delta'(T_0)(1 + \Delta'(0))| = |[1 + \Delta'(0)][1 + \Delta'(T_0)]| < 1.$$

We have not assumed that $\Delta'(T_0) = \Delta'(0)$ since for experimental PRCs (see Figure 9.3C, e.g) this may not be the case. We can also remove the absolute value since throughout this section we have assumed that the phase transition map $\tau + \Delta(\tau)$ is monotone. Thus synchrony is stable when:

$$[1 + \Delta'(0)][1 + \Delta'(T_0)] < 1. \tag{9.22}$$

For "nice" PRCs such as the adjoint (in which the PRC is continuously *differentiable*), this condition is reduces to $\Delta'(0) < 0$. There may be other fixed points as well. Indeed, since $D^2(\tau)$ is a monotonic map of the circle to itself, there must be at least one other fixed point corresponding to the so-called antiphase solutions in which $\tau \approx T_0/2$. We can see this if, for example, $\Delta(\tau) = a \sin \tau$ (or any odd periodic function for that matter). In this case, it is clear that $\tau = \pi$ is also a fixed point; as with the synchronous case, it is stable if $\Delta'(\pi) < 0$.

In the derivations, we have assumed that the oscillators are identical. We leave it as an exercise for the reader to show that, in this case, the map becomes:

$$\tau_{n+1} = T_2 - T_1 + \tau_n + \Delta_1(\tau_n) - \Delta_2[T_1 - \tau_n - \Delta_1(\tau_n)] \tag{9.23}$$

where T_j is the natural period of oscillator j and Δ_j is the PRC.

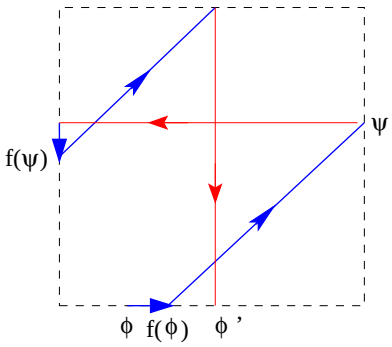

Figure 9.12. *Coupling of two phase equations.*

Phase equations.

The firing time methods that we derived above are useful for pairs of oscillators, but it is difficult to generalize them to many oscillators. Instead, we will turn to the phase-description of oscillators. The phase of an oscillator is complimentary to its firing time in that, for our purposes, the phase is the amount of time since the oscillator last fired. Many researchers define phase so that it is normalized and represents, not an absolute time, but rather the percent or fraction of a cycle covered. As we pointed out earlier in this chapter, normalization of phase makes it easier to compare cells with different frequencies. Since the remainder of this chapter deals with phase equations, we will normalize the PRC. In order to prevent confusion with the un-normalized PRC, we define the normalized PRC as:

$$d(\phi) = \frac{1}{T_0}\Delta(T_0\phi). \tag{9.24}$$

$d(\phi)$ is unitless and is $1-$periodic. The derivative of d has the same magnitude as that of Δ.

We now derive equations for a pair of cells coupled by their normalized PRCs:

$$\theta_1' = \omega_1 + \delta_1(\theta_2)d_1(\theta_1) \tag{9.25}$$
$$\theta_2' = \omega_2 + \delta(\theta_1)d_2(\theta_2). \tag{9.26}$$

$\delta_1(\phi)$ is the "periodized" Dirac delta function – a unit impulse at every integer. We interpret this equation to mean that each time θ_2 crosses an integer (completes a cycle), θ_1 is incremented by its normalized PRC, $d_1(\theta)$. This equation is a flow on the torus and if the PRCs are not too big and the frequencies are close, then, we expect that there will be a cycle of θ_1 for each cycle of θ_2. Thus we can define a Poincare map; we take the Poincare section to be $\theta_2 = 0$. That is, we let ϕ denote the *phase* of oscillator 1 at the moment that oscillator 2 fires but before oscillator 1 is reset. Figure 9.12 shows the setup. Between spikes, each oscillator runs according to its frequency until it hits 1, is reset, and jolts the other oscillator. Let $d_{1,2}(\phi)$ be the response of oscillator 1 (respectively 2) to a spike from oscillator 2 (respectively

1). Let $f_j(\phi) = d_j(\phi) + \phi$ be the phase transition curve. This is the new phase *after* a stimulus as a function of the current phase. ψ is the phase of oscillator 2 when oscillator 1 reaches 1:

$$\psi = \frac{\omega_2}{\omega_1}[1 - f_1(\phi)].$$

To see this, note that the solution to (9.25) is $\theta_1 = \omega_1 t + f_1(\phi)$ so that θ_1 fires at $t_1 = (1 - f_1(\phi))/\omega_1$. In that time, θ_2 has advanced by $\omega_2 t_1$. Oscillator 2 is reset to $f_2(\psi)$ and fires again at $t_2 = (1 - f_2(\psi))/\omega_2$. At this point, θ_1 has advanced, to $\phi' = \omega_1 t_2$. Thus we find that

$$\phi' = \frac{\omega_1}{\omega_2}[1 - f_2(\psi)]$$

where ψ is as above. We can think of the map $\phi \to \phi'$ as the composition of two maps:

$$\begin{aligned} \phi' &= G_2(G_1(\phi)) \\ G_1(\phi) &= \frac{\omega_2}{\omega_1}[1 - \phi - d_1(\phi)] \\ G_2(\phi) &= \frac{\omega_1}{\omega_2}[1 - \phi - d_2(\phi)]. \end{aligned} \tag{9.27}$$

We must be *very careful* in applying this map and using it since it requires that the spikes of the two oscillators *alternate*. If one oscillator is sufficiently fast compared to the other, then the fast oscillator may spike twice before the slow oscillator can spike. This violates the premise of alternation which we used to derive the map. Thus, we will assume that the ratio ω_2/ω_1 is sufficiently close to 1 to guarantee that this happens. In fact, the main role of the map is to examine the existence and stability of fixed points which we now do. We note that the map (9.27) is quite similar to the time map (9.23) in that it is the composition of the effects of one oscillator on the other. Let us first suppose that $\rho \equiv \omega_1/\omega_2 = 1$. As in the rest of this chapter, we assume that $d_j(0) = d_j(1) = 0$. Then, $G_j(0) = 1$ and $G_j(1) = 0$, so that $\phi = 0$ is a fixed point to the composed map (9.27). A fixed point $\bar{\phi}$ is linearly stable if

$$\lambda = G_2'(G_1(\bar{\phi}))G_1'(\bar{\phi})$$

is less than 1 in magnitude. That is

$$[1 + d_1'(0)][1 + d_2'(1)] < 1. \tag{9.28}$$

This is exactly the same condition as we saw for stability of the synchronous state for the time map (9.22) since $d(\phi) = \Delta(T\phi)/T$. Other locking patterns besides 1:1 are possible. In the exercises, the reader is asked to derive equations for 2:1 locking in which oscillator 1 fires twice for each firing of oscillator 1.

Mirollo and Strogatz.

It is possible to analyze larger systems of pulse-coupled oscillators, but due to the singular nature of the coupling, only special types of solutions can be easily analyzed.

In particular, "all-to-all" identical pulse coupling was first analyzed by Mirollo and Strogatz (1990). These authors studied strong coupling between oscillators – that is the phase-transition curve is not invertible. Specifically, they assume that in absence of coupling each oscillator obeys dynamics governed by $x_j(t) = f(t)$ where $f(t)$ is a prescribed function satisfying $f(0) = 0$, $f(1) = 1$, $f'(t) > 0$ and $f''(t) < 0$. When $x_j(t) = 1$, it is reset to 0. For example, if $f(t)$ is a solution to the integrate and fire model, then with rescaling of time, $f(t)$ will satisfy the assumptions. Note that the QIF models do not satisfy the concavity assumption so the MS theorem does not hold. Oscillators communicate to each other by advancing those which have not fired by an amount $\epsilon > 0$. Each oscillator is coupled identically to all the others with the following rules:

1. At time t^-, if m oscillators fire (cross 1), then all other oscillators which are below 1 are incremented by $m\epsilon$;

2. If this increment is sufficient to cause an oscillator to fire (cross 1), then it is set to 1 but does not contribute a pulse to the others;

3. All oscillators at 1 are immediately reset to 0.

Because the oscillators are *identical*, rule 2 implies that once an oscillator joins a group which has fired (by crossing 1 due to the inputs) it is *absorbed* into the group for all times and will remain synchronous with them. Intuitively, it is clear how this type of strong coupling will lead to synchronization of the entire group by the process of absorption. Indeed, as more and more oscillators become absorbed, their effect on the remaining oscillators becomes very large and will rapidly bring them into the fold.

Mirollo and Strogatz prove that, with the above assumptions on $f(t)$ and on the coupling, the set of initial conditions for which the oscillators are not completely absorbed has measure zero. We sketch the proof for $N = 2$ as it is the basis for the general proof and it also exposes some problems with basic assumptions of the model. As with the rest of this section, we reduce the analysis of the behavior of a pair of oscillators to a simple map.

Since $f(t)$ is monotonic and $f(0) = 0, f(1) = 1$, $f(t)$ has an inverse, $t = g(x)$ which provides the phase (or time) in the cycle given the value $x \in [0, 1)$. Let ϕ be the phase of oscillator B right after A fires; that is, after B has received a kick from A. If B is pushed past 1, we are done since now B and A are synchronous; we therefore assume that $\phi < 1$. B will fire at time $1 - \phi$ and at this point A is at $x_A = f(1 - \phi)$. A receives a kick of size ϵ and if this now exceeds 1, we are done since the two are synchronous. Thus, suppose that $f(1-\phi)+\epsilon < 1$. The phase of A is now $g(f(1 - \phi) + \epsilon) \equiv h(\phi)$. We are exactly where we started before except that the roles of A and B are reversed. Since the oscillators are identical, the complete map is just two iterates of $h(\phi)$. Thus our map is:

$$\phi \to h(h(\phi)) \equiv R(\phi).$$

Note that the domain of $R(\phi)$ is not the whole interval $[0, 1]$ because for any finite ϵ, if ϕ is sufficiently close to 0, then $f(1 - \phi) + \epsilon$ will cross 1. Let δ be such

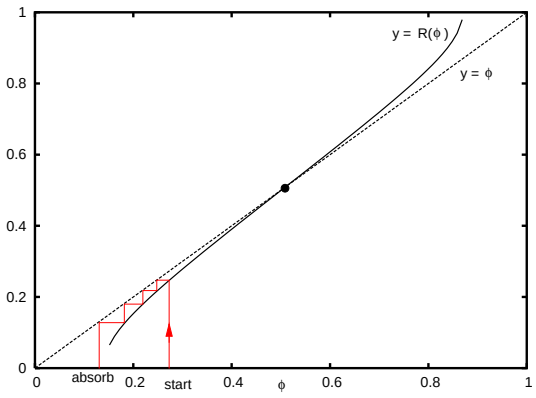

Figure 9.13. *Mirollo-Strogatz map with* $f(t) = t(2-t)$ *and* $\epsilon = 0.02$

that $f(1-\delta)+\epsilon = 1$. The function $h(\phi)$ is defined for $\phi \in (\delta, 1)$. f and g are monotonically increasing so $h' < 0$; that is, h is monotonically decreasing. Since $R(\phi) = h(h(\phi))$, we must have $h(\phi) > \delta$ as well. That is, $\phi < h^{-1}(\delta)$ because h is a decreasing function. Thus the domain of R is the interval $(\delta, h^{-1}(\delta))$. We need to prove that this is nonempty. That is $\delta < h^{-1}(\delta)$ or, equivalently, $h(\delta) > \delta$. But, clearly, $h(\delta) = 1 > \delta$.

We can define the map on the whole of [0,1) as follows. For $\phi > h^{-1}(\delta)$, we set $R(\phi) = 1$ and for $\phi < \delta$ we set $R(\phi) = 0$. These conditions correspond to absorption, that is, once you hit 0 or 1, you stay there for all time. Since the phase-space is the circle, the point 1 is identified with 0.

Before continuing with the analysis, it is useful to consider a specific example, say, $f(t) = t(2-t)$. Then $g(x) = 1 - \sqrt{1-x}$. Figure 9.13 shows $R(\phi)$ for this example when $\epsilon = 0.02$. Note that the map is only defined for a subinterval of $[0, 1]$. There is a single fixed point at $\phi = 1/2$ and it is evidently a repellor (since the slope at the fixed point is greater than 1). The red curve shows successive iterates of the map until there is absorption and $\phi = 0$. Any initial condition except the fixed point will be absorbed into either 0 or 1 after a finite number of cycles.

Thus, we can prove that almost all initial data are eventually absorbed if we can prove two things about $R(\phi)$: (i) there is a single fixed point and (ii) it is unstable. Since $R(\phi) = h(h(\phi))$, we can prove (ii) if we can show that $|h'(\phi)| > 1$ for all ϕ where it is defined. Since f and g are inverses, $f'(y) = 1/g'(f(y))$ so:

$$h'(\phi) = -g'(f(1-\phi)+\epsilon)f'(1-\phi) = -\frac{g'(f(1-\phi)+\epsilon)}{g'(f(1-\phi))}.$$

Let $u = f(1-\phi)$. Then

$$h' = -g'(u+\epsilon)/g'(u).$$

By hypothesis, $f'' < 0$ so that $g'' > 0$; thus, $g'(u)$ is monotone increasing. This means that $g'(u+\epsilon) > g'(u)$ for $\epsilon > 0$. Thus the above ratio is less than -1 and we have proven that any fixed points (if the exist) are unstable.

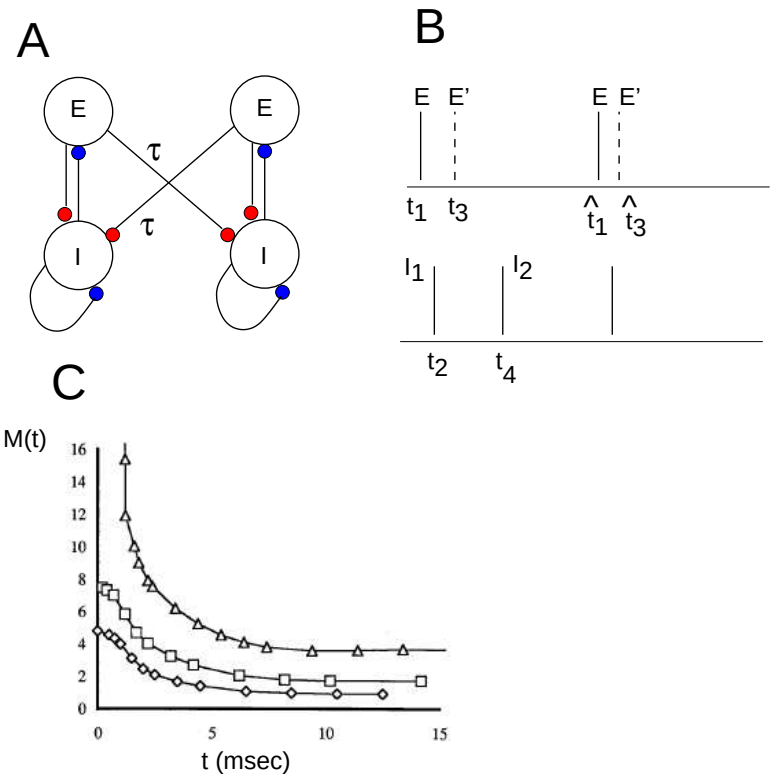

Figure 9.14. *Hippocampal oscillatory circuit. Two "columns" coupled via E to I synapses with a delay.*

All that is left to do is to prove that there is a unique fixed point. If there is a fixed point to $\phi = h(\phi)$, then this is also a fixed point for $\phi = R(\phi)$ since $R(\phi) = h(h(\phi))$. Let $F(\phi) = \phi - h(\phi)$. Note that $F(\delta) = \delta - h(\delta) = \delta - 1 < 0$. On the other hand, $F(h^{-1}(\delta)) = h^{-1}(\delta) - \delta > 0$ so that there is root between $(\delta, h^{-1}(\delta))$. Since $F'(\phi) = 1 - h'(\phi) > 2$, this root is unique.

Mirollo and Strogatz prove the all:all case for N oscillators in a similar manner. The original motivation for their work was a conjecture by Charles Peskin for the leaky integrate and fire model. For the LIF, the profile of $x(t)$ is $1 - \exp(-t)$ so this satisfies the concavity assumption which is critical. On the other hand, the QIF and other models like it rise to the spiking threshold in a manner which can be concave up. What happens in this case is for the reader to explore.

9.2.4 Other map models.

Ermentrout and Kopell (1998) studied the circuit shown in Figure 9.14 in order to understand results from the Whittington lab (1996, nature). Specifically, gamma (40 Hz) rhythms were induced in brain slices which contained both halves of the

hippocampus. Long fibers connected the two halves and there was consequently a delay in the coupling between the two networks. The experiments showed that for each spike forced by the excitatory cells, the local inhibitory cells fired "doublets" or pairs of spikes. But the doublets only occurred when the two halves were synchronized. The figure shows a simple abstraction of the circuit (A) and the spiking pattern of one side near synchrony (B). The single excitatory-inhibitory pair is driven by the E cell. That is, without the synaptic excitation, the I cell would not fire. The feedback inhibition from the I cell slows the E cell down to about a 40 Hz rhythm. Thus, the first spike, I_1, is a consequence of the excitation from the local circuit and the second spike, I_2, comes from the distant excitation.

Let us devise a simple map for this model and then use this to analyze the existence and stability of the synchronous state. In order to do this, we will make some simplifying assumptions:

a. The E cell spikes a *fixed* time after the last I spike that it receives.

b. All I spikes produce the *same* amount of inhibition on their target E cells.

c. The second I spike (I_2) occurs at a time which depends on the time difference between its two excitatory inputs.

d. The first I spike (I_1) occurs a *fixed* time after the local E spike received.

e. The delay τ between columns is not long compared to the period of the uncoupled system.

Assumption (a) implies that the E cells have no memory of when they last spiked and what keeps them from spiking is the inhibition. They can only spike when the inhibition has worn off sufficiently. Assumption (b) says that the inhibition from the same cell does not facilitate or add up. Each time the I cell spikes, the total inhibition to the E cell is reset to the maximum where it then decays. Assumption (c) is crucial. It says that the I cell has some memory of when it last fired since a second E input does not necessarily make it spike immediately. Assumption (d) says that the effect referred to in (c) wears off quickly. Assumption (e) is a necessary one to make the map well-defined.

We now put these assumptions into mathematical terms to derive a simple map for the timing difference between the E cells. In the figure, we have labeled several different times. Assumptions (a) and (b) say that the time between $\hat{t}_1$ and t_4 is a fixed number we will call T_{ie}. Assumption (d) says that the time between t_1 and t_2 is fixed at T_{ei}. Thus, the key to the derivation of the map is to determine t_4. In absence of coupling, the period of the single circuit is $T_{ie} + T_{ei}$ by assumptions (a) and (d). If the distant E cell spikes at time t_2, then the local I cell receives the input at a time $t_3 + \tau$ where τ is the delay. Assumption (c) says that t_4 is a function of the time difference, $t_3 + \tau - t_2$. Call this function $M(t)$; $t_4 = M(t_3 + \tau - t_1) + t_3 + \tau$. That is, the second I spike occurs with a delay M after its second excitatory input. We are now done, since we can write:

$$\begin{aligned} \hat{t}_1 &= T_{ie} + t_4 \\ &= T_{ie} + M(t_3 + \tau - t_1) + t_3 + \tau \end{aligned}$$

We can write exactly the same type of equation for $\hat{t}_3$:

$$\hat{t}_3 = T'_{ie} + M(t_1 + \tau - t_3) + t_1 + \tau.$$

We have put a prime on T_{ie} above to account for possible heterogeneities between the two circuits. For example, if the drive to the right-hand circuit is larger than that of the left-hand circuit, we would expect the right circuit to recover from inhibition quicker and hence, T'_{ie} would be less than T_{ie}. Let $\zeta = t_3 - t_1$ and $\hat{\zeta} = \hat{t}_3 - \hat{t}_1$ and $\mu = T'_{ie} - T_{ie}$. Then, subtracting these two equations leads to

$$\hat{\zeta} = \mu - \zeta + M(-\zeta + \tau) - M(\zeta + \tau) \equiv F(\zeta). \tag{9.29}$$

Note that because of the delay, the distant I input always occurs after the local I input even if $t_3 < t_1$. This means that, unlike our timing maps above, we do not require that the E spikes keep the same order. Indeed, with effective inhibition coupling the cells and with the delay, we never have to worry about a distant input making the local E cell fire immediately.

Let us turn our attention to the map $M(t)$. This can be numerically computed as follows. Create the single circuit so that the E and I cells fire exactly one spike per period. At a time t after the E cell spikes, stimulate the I cell with an excitatory synaptic input and then examine when the I cell spikes. This sounds, at first, like a PRC since the I cell fires periodically and receives a stimulus. However, the basic premise of PRC theory is that the stimulus is weak enough to *move* the spike but not strong enough to *add* new spikes. In the present setting, the input from the distant E cell is strong enough to cause the I cell to produce an extra spike. Thus, this is a large-amplitude theory, rather than an infinitesimal one. What accounts for the shape of this map? A biophysical interpretation is that if the input comes in right after the I cell has spiked, then the cell will not be able to fire again at all. As the second input is delayed, the I cell just manages to cross threshold. Since the I cell is class I (cf chapter CHANNEL), the delay to spiking can be arbitrarily large. This accounts for the vertical asymptote. Finally, for long times after spiking, the I cell has forgotten the previous spike so that it fires at a finite delay after the input. In exercise *, we put some mathematical meat on these meager heuristic bones.

Turning back to equation (9.29), we know that $M(t)$ is a strictly decreasing function which has a rather steep slope for small t. Phaselocking between the two columns occurs if there is a fixed point to the map in (9.29). Let $\bar{\zeta}$ be such a fixed point. It is linearly stable if $|F'(\bar{\zeta}| < 1$ which means that

$$0 < \frac{1}{2}[M'(-\bar{\zeta} + \tau) + M'(\bar{\zeta} + \tau)] < -1.$$

The left hand inequality is always true since M' is a decreasing function. However, if M is very steep, then this condition can be violated. Since the slope decreases with large delay τ, increasing τ can stabilize a given fixed point. If the two columns are identical, $\mu = 0$, and $\zeta = 0$ is the synchronous fixed point. The stability condition reduces to $M'(\tau) < -1$. Thus, the delay must be large enough to prevent the destabilization. However, the delay should also not be too long (see exercise **).

9.2.5 Weak coupling.

We will now analyze a pair of nonlinear oscillators which are coupled in an arbitrary fashion, but the coupling is "weak." Kuramoto (1984) popularized the methods and ideas of weak coupling using a very intuitive geometric concept which employs the gradient of the phase map $\nabla_X \Theta(x)$ – an object which we have seen is the solution to the adjoint.

Geometric idea.

Suppose that $X' = F(X)$ has an asymptotically stable limit cycle, $U(t)$. Consider two identical oscillators which are coupled:

$$\frac{dX_j}{dt} = F(X_j(t)) + \epsilon G_j(X_j(t), X_k(t)) \tag{9.30}$$

where $j = 1, 2$ and $k = 3 - j$. Kuramoto (1984) suggests a simple approach to this. We make the change of coordinates along the limit cycle, $\theta_j = \Theta(X_j)$ where Θ is the asymptotic phase function as in Figure 9.1. Then

$$\begin{aligned}\frac{d\theta_j}{dt} &= \nabla\Theta(X_j) \cdot \frac{dX_j}{dt} \\ &= \nabla\Theta(X_j) \cdot F(X_j(t)) + \epsilon \nabla\Theta(X_j) \cdot G_j(X_j, X_k) \\ &= 1 + \epsilon \nabla\Theta(X_j) \cdot G_j(X_j, X_k). \end{aligned} \tag{9.31}$$

This equation is exact but quite useless since we do not know what $X_j(t)$ is so that we cannot evaluate the right-hand side. However, if ϵ is small, then $X_j(t)$ is close to $U(\theta_j)$. Thus, equation (9.31) becomes an equation which only involves the phases, $\theta_{1,2}$:

$$\frac{d\theta_j}{dt} = 1 + \epsilon \nabla\Theta[U(\theta_j)] \cdot G[U(\theta_j), U(\theta_k)]. \tag{9.32}$$

Equation (9.32) is intuitively appealing since it shows that the evolution of the phase is determined by a product of the coupling with the response function. Winfree (1967) deduced this equation on first principles. For neurons, the coupling is often only through input currents to the membrane potential of the cell leading to a simpler pair of equations:

$$\begin{aligned}\frac{d\theta_1}{dt} &= 1 + \epsilon P_2(\theta_2) d_1(\theta_1) \\ \frac{d\theta_2}{dt} &= 1 + \epsilon P_1(\theta_1) d_2(\theta_2)\end{aligned}$$

where $d_j(\theta)$ is the PRC for the oscillator and $P_j(\theta)$ is the synaptic input of the presynaptic oscillator. Note the similarity between this simple equation and equations (9.25,9.26). One can regard (9.32) as a smooth equivalent of the pulsatile coupling we considered above.

We exploit the fact that ϵ is small once more to further reduce equation (9.32). Let us introduce the variables, $\phi_j = \theta_j - t$. Then (9.32) becomes:

$$\frac{d\phi_j}{dt} = \epsilon \nabla\Theta[U(t + \phi_j)] \cdot G[U(t + \phi_j), U(t + \phi_k)]. \tag{9.33}$$

All functions involved are smooth and U is itself $T-$periodic. Thus, we have a system of the form

$$y' = \epsilon M(y,t)$$

and we can apply the method of averaging which says that $y(t)$ is close to $\bar{y}$ where

$$\bar{y}' = \epsilon \frac{1}{T}\int_0^T M(\bar{y},t)\ dt.$$

Recall that $\nabla_X \Theta(X)$ is exactly the solution to the adjoint equation, $Z(t)$. Applying averaging to (9.33), results in the following equations

$$\begin{aligned} \frac{d\phi_1}{dt} &= \epsilon H_1(\phi_2 - \phi_1) \\ \frac{d\phi_2}{dt} &= \epsilon H_2(\phi_1 - \phi_2) \end{aligned} \tag{9.34}$$

where

$$H_j(\phi) = \frac{1}{T}\int_0^T Z(t)\cdot G_j[U(t), U(t+\phi)]\ dt. \tag{9.35}$$

The beauty of equation (9.34) is that the interactions between the two oscillators only show up in the phase-differences between them: $\phi_2 - \phi_1 = \theta_2 - \theta_1$. Indeed, let $\psi = \phi_2 - \phi_1$ denote the phase difference between the two oscillators. Then subtracting the two equations in (9.34) results in the following *scalar* equation for the phase-difference:

$$\frac{d\psi}{dt} = \epsilon[H_2(-\psi) - H_1(\psi)]. \tag{9.36}$$

Stable (unstable) fixed points of (9.36) correspond to stable (unstable) periodic solutions to the full equations (9.30). For example, if $\psi = 0$ is a stable fixed point of (9.36), then the two oscillators will synchronize.

Equation (9.34) generalizes to N coupled neural oscillators leading to the following system of differential equations:

$$\frac{d\phi_j}{dt} = \epsilon H_j(\phi_1 - \phi_j, \phi_2 - \phi_j, \ldots, \phi_N - \phi_j), \quad j = 1, \ldots, N. \tag{9.37}$$

While (9.37) represents a considerable simplification of a general system of N coupled oscillators, it is by no means a trivial system to analyze and there are many open problems concerning the behavior of this dynamical system on the $N-$torus. An entire book could easily be devoted to the subject! We define a **phase-locked** state of (9.37) to be a solution of the form:

$$\phi_j(t) = \Omega t + \xi_j$$

where Ω is called the *ensemble* frequency, $\xi_1 = 0$, and ξ_j are constants called the relative phases. We pin ξ_1 to zero since you can add an arbitrary constant to all of the phases $\phi_j(t)$ corresponding to the arbitrary translation in time of any autonomous limit cycle oscillator. Thus, the existence os a phase-locked solution

to (9.37) reduces to solving a set of N algebraic equations in the N unknowns, $\Omega, \xi_2, \ldots, \xi_N$:

$$\Omega = \epsilon H_j(-\xi_j, \xi_2 - \xi_j, \ldots, \xi_N - \xi_j), \quad , j = 1, \ldots, N. \tag{9.38}$$

If we can find such states, then there is a convenient theorem which provides sufficient (*but not necessary*) conditions for stability.

Theorem. (Ermentrout,1992). Let $S = \{\Omega, 0, \xi_2, \ldots, \xi_N\}$ be a phase-locked solution to (9.37). Let a_{jk} denote the partial derivative of $H_j(\eta_1, \ldots, \eta_N)$ with respect to η_k evaluated at S. Suppose that $a_{jk} \geq 0$ and that the matrix $A = (a_{jk})$ is irreducible. Then S is asymptotically stable.

We provide an intuitive definition for irreducibility. Draw N points on a paper. Draw a directed line from point j to point k if $a_{jk} > 0$. The matrix A is irreducible if and only if it is possible to start at any point n and go to any other point m following the directed lines.

Applications of weak coupling.

Before proceeding to specific neural examples, we examine (9.36) more closely. Recall that H_j is the average of the interaction with the PRC. Let's break G_j into two parts:

$$G_j(X, Y) = B_j(X) + gC_j(X, Y)$$

where g is the strength of the coupling between the two cells and B_j represents intrinsic differences between the two neurons. For membrane models, the main coupling is through the membrane potential so that $B_j(X)$ may be something as simple as a small bias current and $C_j(X, Y)$ is the synaptic current. In this case, equation (9.38) becomes the equation typically studied:

$$\Omega = \epsilon \left(\omega_j + \sum_k H_{jk}(\xi_k - \xi_j) \right) \tag{9.39}$$

with $\xi_1 = 0$.

We consider two cases for the synaptic current: chemical synapses and electrical synapses:

$$C_{syn}(X, Y) = -s_Y(V_X - V_{syn})\vec{e}_V$$
$$C_{gap}(X, Y) = (V_Y - V_X)\vec{e}_V$$

where $\vec{e}_V$ is the vector of all 0's except for a 1 in the voltage component. $s_Y(t)$ is the synaptic response of the presynaptic cell. If we define $V^*(t)$ to be the voltage component of the adjoint solution, $V(t)$ the potential, and assume that except for the heterogenity, both cells are identical, then we see that

$$H_j(\phi) = \omega_j + h(\phi)$$

where

$$h(\phi) = h_{syn}(\phi) \equiv \frac{1}{T}\int_0^T V^*(t)s(t+\phi)[V_{syn} - V(t)]\ dt \tag{9.40}$$

$$h(\phi) = h_{gap}(\phi) \equiv \frac{1}{T}\int_0^T V^*(t)[V(t+\phi) - V(t)]\ dt \tag{9.41}$$

We remark that these equations have a nice intuitive interpretation. The adjoint is (at least for weak perturbations) a scaled version of the PRC of a neuron. When the PRC is computed, it is done so by perturbing with a brief *current.* However, chemical synapses between cells are best modeled as *conductances.* Thus, the effect of a presynaptic conductance change on the postsynaptic cell is the product, $Q(t) \equiv V^*(t)(V_{syn} - V(t))$. The presynaptic cell alters the phase of the postsynaptic cell by averaging the effective response, $Q(t)$, with the time course of the synapse. The function $Q(t)$ will not differ substantially from the adjoint, $V^*(t)$, for excitatory conductances since $V_{syn} - V(t)$ is positive except for a a short period when the neuron spikes. (Recall that $V_{syn} = 0$mV for excitatory synapses.) However, there can be a rather large difference between $Q(t)$ and $V^*(t)$ for inhibitory synapses since the reversal potential can sometimes be very close to the resting state of the neuron. In project ** below, you can explore how the reversal potential of the inhibition affects the synchronization properties of pairs of cells. Since the reversal potential of inhibition varies a great deal during the development of the nervous system, this could have important implications in setting up local cortical circuits.

9.2.6 Synaptic coupling near bifurcations.

Equation (9.40) provides a formula for the interaction function between a presynaptic and postsynaptic neural oscillator. Equation (9.36) provides the equations for the phase-difference between two coupled neurons. Suppose that both neurons are identical. Then the phase difference, ψ satisfies

$$\psi' = -2H_{odd}(\psi) \tag{9.42}$$

where $2H_{odd}(\psi) = H(\psi) - H(-\psi)$. Any continuous odd periodic function vanishes at $\psi = 0$ and $\psi = T/2$ where T is the period of the function. Thus a pair of mutually coupled neural oscillators will always have a synchronous and an *anti-phase* pattern of behavior. If $\bar{\psi}$ is a zero of $H_{odd}(\psi)$, then from equation (9.42), it will be stable if and only if $H'_{odd}(\bar{\psi}) > 0$. (Note the $-$ sign in the equation!) For a pair of mutually coupled identical oscillators, the key function is the odd part of the interaction function. Zeros of this function are phase-locked states. In general computing H and its odd part must be done numerically since the explicit form for the adjoint is not generally available. However, near bifurcations, we have formula for the adjoint and thus we can study some of the effects of frequency and synaptic parameters on the ability of a pair of neurons to synchronize.

Suppose that we choose

$$s(t) = \frac{e^{-\beta[t]_+} - e^{-\alpha[t]_+}}{\alpha - \beta}$$

as out synaptic conductance. Here $[t]_+$ is the positive part of t; the alpha-function synaptic conductances vanish for $t < 0$.

$$H(\phi) = \frac{1}{T}\int_0^T V^*(t) \sum_{j=-\infty}^{\infty} s(t + jT + \phi)\ dt.$$

The sum arises since the synaptic function $s(t)$ is not itself periodic so that we have to "periodize" it by adding the synaptic response for every spike at intervals of the period. We leave it as an exercise to the reader to show that

$$H(\phi) = \frac{1}{T}\int_0^\infty V^*(t-\phi)s(t)\ dt.$$

Since the interval of integration is non-negative, we can drop the $[\ ]_+$ and just evaluate the integrals. Finally, we can rescale the period of the oscillations allowing us to express $V^*(t)$ and $H(\phi)$ in simple sines and cosines. Thus, a long period oscillation is like an oscillation of period 2π, but with very fast synapses: $\alpha \to \alpha/\omega$ and $\beta \to \beta/\omega$ where $T = 2\pi/\omega$.

Near bifurcations we have explicit formula for the adjoint so that we can analyze $H(\phi)$ explicitly by evaluating the integrals. Suppose that the neural oscillator is class I so that the adjoint is $V^*(t) = 1 - \cos t$. If the synaptic current is $Is(t)$ with $I > 0$ for excitatory synapses and $I < 0$ for inhibitory, then

$$H_{odd}(\phi) = -I \sin\phi \frac{\alpha+\beta}{(\alpha^2+1)(\beta^2+1)}.$$

We recover the well-known result (van Vreeswijk et al 1994; Ermentrout 1996 - Type I) that excitatory coupling ($I > 0$) results in stable anti-phase and inhibitory coupling ($I < 0$) results in stable synchrony.

The behavior near a Hopf bifurcation depends on the parameters in the normal form. The adjoint can be written as $V^*(t) = -\sin(t) + q\cos(t)$ where q is a parameter from the normal form. Evaluation of the integral yields:

$$H_{odd}(\phi) = I \sin\phi \frac{q(\alpha+\beta)+\alpha\beta-1}{(\alpha^2+1)(\beta^2+1)}.$$

Unlike systems near a saddle-node, the stability of, say, synchrony, depends on the timing of the synapses and the parameter q. Even when $q = 0$, it is possible to switch from stable synchrony to stable anti-phase as the frequency of the oscillator (the timing of the synapses) changes.

In neither case does there exist bistability between synchrony and anti-phase, nor are any other phase-locked patterns possible. The reason for this is that the adjoint has only pure sines and cosines without any higher modes. Looking at, say, Figure 9.3Ai or C, it is clear that these two simple models for the adjoint (PRC) are not particularly good approximations. We can combine the two types and add two more terms to obtain a pretty good approximation for neural PRCs:

$$V^*(t) = a(1-\cos(t)) + c(1-\cos(2t)) + b\sin(t) + d\sin(2t). \tag{9.43}$$

With this model, we find

$$H_{odd}(\phi) = \left(\frac{-a(\alpha+\beta) - b(\alpha\beta - 1)}{(\alpha^2+1)(\beta^2+1)}\right)\sin\phi + \left(\frac{-2c(\alpha+\beta) - d(\alpha\beta - 4)}{(\alpha^2+4)(\beta^2+4)}\right). \tag{9.44}$$

We remark that since we have normalized the period to be 2π, the parameters α, β should be scaled as $\alpha = \alpha_0 T$ and similarly for β where α_0 is the true synaptic time scale and T is the period of the oscillator. Note that for T large, the terms b, d dominate.

9.2.7 Small central pattern generators.

A central pattern generator (CPG) is a network of neurons which is able to produce a patterned oscillator output to motor neurons. For example, in chapter *, we looked at a model for the respiratory oscillation driven by the so-called preBotzinger complex. Much research has been done on simple locomotor CPGs which govern the different gaits for walking, running, etc. Most mammalian CPGs are poorly understood and their actual location in the brain is not known. However, the story for certain fish and invertebrates is much clearer. There are numerous review articles on CPGs and their modeling (see Grillner et al for a recent review with many references to other reviews or Yuste et al for a call to treat cortical circuits in the way that motor patterns have been treated.) We will consider three examples: finger tapping, hand clapping, and quadrupedal locomotion.

In a clever series of experiments Kelso and collaborators (see his book for a complete discussion and analysis) studied the transition from one pattern to another as the frequency increased. In the experiment (and you can do this yourselves) the subject is asked to tap his fingers in an alternating rhythm. The subject is asked to speed up the rhythm and try to maintain the pattern. However, at high enough frequencies, the subject tends to switch into synchronous tapping. The subject is able to tap fingers synchronously at all frequencies, thus there appears to be bistability between the two types of coupling.

Imagine that each finger is controlled by an oscillatory circuit and that the two sides are synaptically coupled. Then we can ask whether this kind of model can explain the bistability and the switch as the frequency increases. Figure 9.15 shows a numerical computation for the Wang-Buszaki model with inhibitory and excitatory synapses as the frequency changes. At low frequencies with inhibitory coupling (about 9 Hz) both the synchronous and the anti-phase state are stable since the odd part of H has a positive slope. However at higher frequencies (30 Hz) only the synchronous state is stable. Thus, there is a transition from bistability to monostability at high frequencies. In contrast, with excitatory coupling (right figure), the synchronous state is unstable for both high and low frequencies. This simple model of mutually coupled inhibitory circuits shows that we can induce a switch from the anti-phase state to synchrony as the frequency increases. van Vreeswijk et al (1994) demonstrated this phenomena for weakly coupled integrate

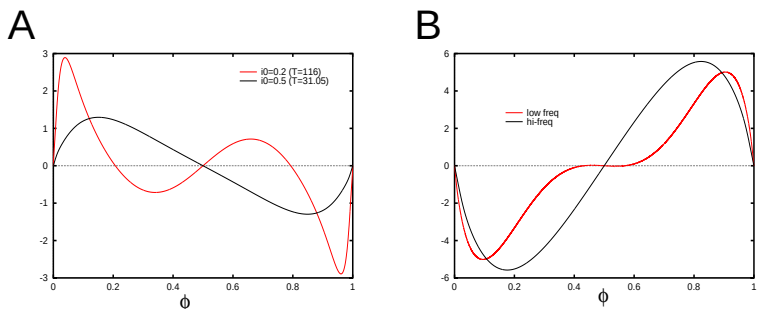

Figure 9.15. *Weakly coupled WB model for inhibitory (left) and excitatory (right) coupling*

name	left rear (LR)	right rear (RR)	left front (LF)	right front (RF)
pronk	$x_1(t)$	$x_1(t)$	$x_1(t)$	$x_1(t)$
rack/pace	$x_1(t)$	$x_1(t+\frac{1}{2})$	$x_1(t)$	$x_1(t+\frac{1}{2})$
bound	$x_1(t)$	$x_1(t)$	$x_1(t+\frac{1}{2})$	$x_1(t+\frac{1}{2})$
trot	$x_1(t)$	$x_1(t+\frac{1}{2})$	$x_1(t+\frac{1}{2})$	$x_1(t)$
jump	$x_1(t)$	$x_1(t\pm\frac{1}{4})$	$x_1(t\pm\frac{1}{4})$	$x_1(t)$
walk	$x_1(t)$	$x_1(t\pm\frac{1}{2})$	$x_1(t\pm\frac{1}{4})$	$x_1(t\pm\frac{3}{4})$

Table 9.1. *Common simple quadruped gaits*

and fire neurons and also showed that a similar effect occurs in the Hodgkin Huxley model. We can use the simple adjoint approximation (9.43) to analytically obtain this result. We leave this as an exercise to the reader.

Quadruped gaits. An interesting and well-studied problem is the existence and stability of patterns of movement in four-legged animals (quadrupeds). There are many subtly different gaits; here we present only the so-called primary gaits. Table 9.1 shows the relative phases of the six primary gaits. $x_1(t)$ is the dynamics of a single limb, so that all the other limbs can be specified in terms of their relative phase with the left rear limb. Golubitsky and his collaborators have derived minimal circuits which can explain the gaits using symmetry arguments. Their methods are elegant and from them they conclude that the minimal number of oscillators required is eight corresponding to two oscillators per limb. Their reasoning goes something like this. Suppose there are only four oscillators and suppose an animal has both a stable walk and a stable trot. Then by symmetry, it must also have a stable pace. Since no animal both paces and walks, there must be additional structure to break the symmetry. We can see this for ourselves by considering the following network of 4 coupled oscillators:

$$\begin{aligned}\theta_1' &= H_a(\theta_2-\theta_1)+H_b(\theta_3-\theta_1)+H_c(\theta_4-\theta_1)\\ \theta_2' &= H_a(\theta_1-\theta_2)+H_b(\theta_4-\theta_2)+H_c(\theta_3-\theta_2)\\ \theta_3' &= H_a(\theta_4-\theta_3)+H_b(\theta_1-\theta_3)+H_c(\theta_2-\theta_3)\end{aligned} \tag{9.45}$$

$$\theta_4' = H_a(\theta_3 - \theta_4) + H_b(\theta_2 - \theta_4) + H_c(\theta_1 - \theta_4).$$

Here $\theta_1 - \theta_4$ are the left front, right-front, right-rear, and left-rear limb oscillators, respectively. Connections labeled H_a are left-right coupling, those labeled H_b couple "diagonal" limbs, and H_c couple the same side. Phase-locked solutions have the form

$$\theta_j = \omega t + \phi_j$$

where $\phi_1 = 0$, Ω is the ensemble frequency, and $\phi_{2,3,4}$ are the phases of the other limbs relative to the left front limb, θ_1. We are interested in several types of solutions. The walk corresponds to $W = (0, \pi, 3\pi/2, \pi/2)$, the trot, $T = (0, \pi, 0, \pi)$, the pace $P = (0, \pi, \pi, 0)$ and the bound, $B = (0, 0, \pi, \pi)$. The "pronk" is a fully synchronous state. If you walk your dog slowly, you will notice that she moves using the walk while as you speed up, she will switch to a trot, the gait used in the show ring. (Hopefully, your dog will have nice long legs to make this evident; my dog, a corgi, makes the observation somewhat difficult.) We leave as an exercise, the analysis of this network. If the functions $H_{a,b,c}$ are general and periodic, then there will be a walk state if and only if $H_b = H_c$. From this, you can deduce that there is also a trot and a pace state and that they must have the same stability properties. This result (easily deduced in the present case) actually follows from the symmetry arguments of Golubitsky and others.

Schoner G, Jiang WY, Kelso JA. A synergetic theory of quadrupedal gaits and gait transitions. J Theor Biol. 1990 Feb 9;142(3):359-91.

Kelso, J.A.S. (1995). Dynamic Patterns: The Self-Organization of Brain and Behavior. Cambridge: MIT Press

Grillner S, Markram H, De Schutter E, Silberberg G, LeBeau FE. Microcircuits in action–from CPGs to neocortex. Trends Neurosci. 2005 Oct;28(10):525-33.

Yuste R, MacLean JN, Smith J, Lansner A. The cortex as a central pattern generator. Nat Rev Neurosci. 2005 Jun;6(6):477-83.

Excitatory/inhibitory coupling.

We have already seen that near a saddle-node bifurcation, weak excitatory coupling tends to push pairs of oscillators into anti-phase. However, most cortical networks consist of networks with both excitation and inhibition. Can the inhibition affect the response of coupled networks? Naturally, this depends on the nature of the individual neurons, but, at least near bifurcations, we can explore these questions using simple models like the theta model. Consider a single "column" consisting of an E and an I cell:

$$\theta_e' = 1 - \cos\theta_e + (1 + \cos\theta_e)(0.25 - 2s_i) \tag{9.46}$$
$$\theta_i' = 1 - \cos\theta_i + (1 + \cos\theta_i)(-0.2 + 2s_e) \tag{9.47}$$
$$s_e' = 4[1 + \exp(-20(1 + \cos\theta_e))](1 - s_e) - s_e/3 \tag{9.48}$$
$$s_i' = 4[1 + \exp(-20(1 + \cos\theta_i))](1 - s_i) - s_i/8. \tag{9.49}$$

When simulated, this produces a nearly 40 Hz rhythm. (In absence of inhibition, the network fires at 200 Hz.) Figure 9.16 shows the results of a weak coupling

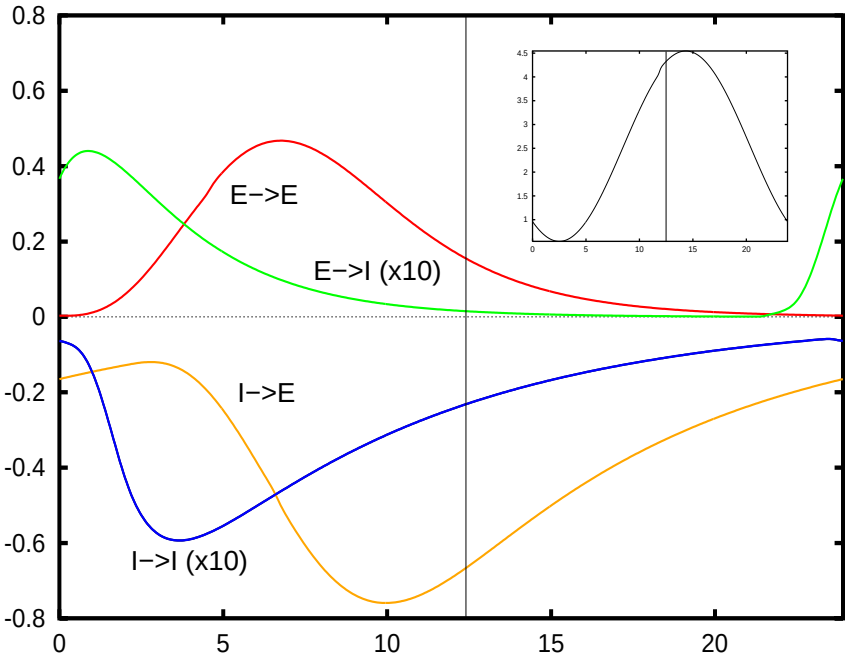

Figure 9.16. *Interaction functions for an excitatory-inhibitory pair. Inset shows pure excitatory network.*

analysis of the above network. There are several important points. The inset shows the interaction function for a purely excitatory network adjusted so that frequency is about 40 Hz. $H(\phi)$ has a positive slope at the anti-phase solution and a negative slope at $\phi = 0$ so that synchrony is unstable but the anti-phase state is stable. This, of course, was anticipated from our results above. However, in an EI network, the period (at least for strong recurrent inhibition) is largely determined from the decay of the inhibition. In this case, E-E coupling no longer stabilizes the anti-phase state. Instead, there is a near synchronous state which is stabilized. Coupling in which the I cell is the recipient is an order of magnitude less efficacious than coupling to the E cell. This is because the E cell is really the driver of the rhythm with the I cell firing only because of the strong transient E cell input. Note that I→E coupling is quite strongly synchronizing but also produces a stable anti-phase solution. We leave it as an exercise to the reader to simulate a pair of these simple models and show that the weak coupling results predict what happens for the full model.

It should not be surprising to the reader that the effect of, say, excitatory coupling between a pair of cells in isolation is quite different from the same pair in the presence of recurrent inhibition. In this case, we can regard the inhibition as a delayed negative feedback – much like an additional outward current. Since

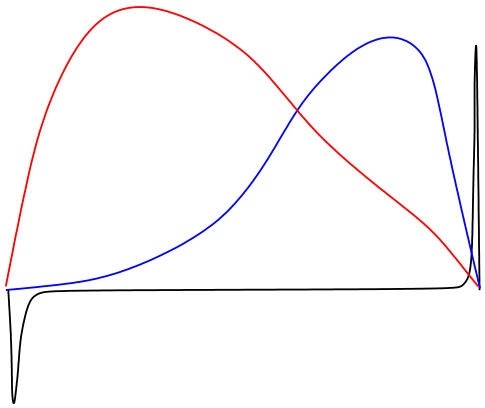

Figure 9.17. *$V'(t)$ and two different adjoints.*

the phase-resetting curve of an oscillator is sensitive to the presence of different currents, so should the effects of coupling pairs of oscillators.

Pfeuty et al explore how synchrony between neurons coupled with gap junctions depends strongly of the shape of the PRC. We can see this geometrically by recalling that the interaction function for a pair of cells coupled with gap junctions has the form:

$$H_{gap}(\phi) = \frac{1}{T}\int_0^T V^*(t)[V(t+\phi) - V(t)]\ dt.$$

Here, $V(t)$ is the somatic potential and $V^*(t)$ is the adjoint. Synchrony is stable if $H'_{gap}(0) > 0$ which we write as:

$$H'_{gap}(0) = \frac{1}{T}\int_0^T V^*(t)V'(t)\ dt.$$

Figure 9.17 provides a geometric interpretation for how the shape of the PRC can alter synchrony for gap junctions. If the area of the product of $V'(t)$ (the black curve) and the adjoint (red or blue curves) is positive (negative) then synchrony will be stable (unstable). Since the bulk of the PRC is towards the left for the blue curve, the total area is positive and synchrony will be stable while for a PRC like that in the red curve, synchrony will be unstable. Ermentrout and Kopell (Handbook) were the first to make this argument. Pfeuty et al show how the addition of a persistent sodium current or removing some potassium current can shift the PRC from the rightward leaning to the leftward leaning case and thus demonstrate how intrinsic membrane properties alter the stability of the synchronous state.

Dendritic structure. All of the results for weak neural coupling have considered only point neurons. The same methods here can be applied to models with active dendrites by discretizing them to a finite number of compartments and then computing the adjoint. However, if the dendrites are nothing more that passive cables, then we can treat the dendrite as a cable with a sealed end at the apical tip

and a periodic current at the somatic end due to the oscillating soma. Suppose that there is a synapse at a point x on the dendrite (where $x = 0$ is the soma). Then the synaptic current felt at the soma from a synaptic current $I(t)$ at x is:

$$I_{soma}(t) \int_0^\infty G(x;s)I(t-s)\ ds$$

where $G(x;t)$ is the Green's function associated with the dendrite. That is, the dendrite acts as a linear filter. Thus, if $H(\phi)$ is the interaction function for a synapse occurring at the soma, then the interaction function for a synapse a distance x from the soma on a passive dendrite is simply

$$H(x;\phi) = \int_0^\infty G(x;s)H(\phi - s)\ ds. \tag{9.50}$$

Crook et al showed how stability of synchrony between two oscillators changes as the position of the synapse is changed. For example, if we take $H(\phi) = \sin\phi$ and $G(x;t) = \exp(-t)\exp(-x^2/t)/\sqrt{\pi t}$ (which is the Greens function for an infinite dendrite) then at $x \approx 1.25$, the slope of $H(x;\phi)$ at $\phi = 0$ changes sign. Thus, distal synapses (further away than about 1 space constant) will have opposite synchronization properties to proximal synapses.

9.2.8 Linear arrays of cells.

There are a number of neural systems which can be regarded as a one-dimensional array of oscillators at least at a crude level. The locomotor pattern generator of the lamprey (a eel-like fish vampire) is among the best characterized examples of such a model. The leech swim generator is also organized in a linear array. However, some sensory systems are similarly organized, notably, the procerebral lobe ("olfactory brain") of the slug. In both the lamprey and the slug brain, the network of oscillators produces oscillatory waves which propagate down the network. Interestingly, similar waves have been observed in cortical brain slices in which the magnesium is reduced. In all of these systems, the local uncoupled network appears to oscillate so that the idea of a locally coupled network of intrinsic oscillators is a good first approximation. Some jellyfish have swim generators which are organized into a ring so that one-dimensional arrays of oscillators with periodic boundary conditions could also be biologically relevant.

For simplicity, we discuss only nearest neighbor coupling. The more general types of coupling can also be analyzed but not as transparently. Consider a linear array of N oscillators, possibly with heterogeneity in the frequencies:

$$\theta_j' = \omega_j + H_{j+1,j}(\theta_{j+1} - \theta_j) + H_{j-1,j}(\theta_{j-1} - \theta_j). \tag{9.51}$$

These equations are valid for $j = 2, \ldots, N-1$ and at the ends, we can impose a number of different boundary conditions. For example, if we identify θ_0 with θ_N and θ_{N+1} with θ_1, then we have a periodic array. On the other hand, identifying $\theta_0 = \theta_1$ and $\theta_{N+1} = \theta_N$ gives reflecting conditions. Finally, the "cut" conditions assume

that the interactions with $j = 0$ and $j = N + 1$ do not exist. Both the reflecting and periodic boundary conditions lead to a homogenization of the network while the cut condition can produce waves even in absence of any heterogeneities.

Homogeneous networks. Consider the case in which $H_{j,k} = H$ for all j and such that there is no heterogeneity: $\omega_j = \omega$. For the reflecting and the periodic boundary conditions, there is a synchronous state, $\theta_j = \Omega t$ where $\Omega = \omega + 2H(0)$ which is stable if and only if $H'(0) > 0$. (Note the "if" follows from Theorem **, but the only if requires explicit calculation of the eigenvalues. Since the linearized matrix is just tri-diagonal, this is a relatively simple calculation. See exercise **). For periodic boundary conditions, there is also a wave solution of the form: $\theta_j = \Omega t + 2\pi j/N$ where $\Omega = \omega + H(2\pi/N) + H(-2\pi/N)$. In the exercises, you are invited to examine this solution in more detail.

Cut ends. The "cut" end case is rather interesting, even when there is no frequency gradient. The oscillators at $j = 1$ and $j = N$ receive less input than the rest of the oscillators. Thus, unless, $H(0) = 0$ there will be no synchronous solution. That being the case, what happens? Suppose that $H(\phi)$ is positive near the origin. Then since the end oscillators receive less inputs than the middle ones, we expect that they will oscillate faster so that we expect a phase gradient symmetric about the center of the chain so that the phase increases from oscillator 1 until it reached the middle and then the phase decreases back to zero at oscillator N. If the chain is anisotropic, then we expect to see a traveling wave. To understand why this is, consider the following model:

$$\begin{aligned} \theta_1' &= \omega_1 + H_a(\theta_2 - \theta_1) \\ \theta_j' &= \omega_j + H_a(\theta_{j+1} - \theta_j) + H_d(\theta_{j-1} - \theta_j) \\ \theta_1' &= \omega_N + H_d(\theta_{N-1} - \theta_N). \end{aligned} \tag{9.52}$$

Now, set $\omega_j = \omega$ and suppose that $H_a(\phi) \equiv 0$ so that there is only coupling from the lower numbered oscillator. Then, clearly $\theta_1 = \omega t$ and in order for there to be a phase-locked solution, oscillator 2 must be of the form $\theta_2 = \omega t + \xi_d$. This means that $H_d(-\xi_d) = 0$. Continuing down the chain in this manner, we see that $\theta_{j+1} - \theta_j = \xi_d$. If H_d has a nondegenerate zero (that is, one such that $H'(x) \neq 0$), then, since it is continuous and periodic, it must have at least two and one of these has a positive slope. This stable zero sets the wavelength of the traveling wave, so that $\theta_j = \omega t + \xi(j - 1)$. If $\xi > 0$ then the wave travels to the left and if $\xi < 0$ it travels to the right. (If oscillator 2 has a positive phase difference with respect to oscillator 1, then it fires earlier so that the wave travels to the left.) So, for unidirectional coupling, if there is a nondegenerate zero to $H_{a,f}(x) = 0$, then this sets the phase difference between successive oscillators in the chain. If the chain is anisotropic but bidirectional, then the two types of coupling will "fight it out." For large N, it can be shown that the oscillators will form a wave (except near one end) of the form $\theta_j = \Omega t + \xi(j - 1)$ where ξ is either ξ_a or ξ_d and $H_a(\xi_a) = 0$ and $H_d(-\xi_d) = 0$. A proof of this result appears in Kopell and Ermentrout (1986). If the chain is completely isotropic, $H_a(\phi) = H_d(\phi)$ and H has a zero with a positive slope, then for large N, the chain will organize into a pattern that consists of a pair

symmetric waves moving toward or away from the center of the chain. Let ξ be such that $H(-\xi) = 0$ and $H'(-\xi) > 0$. Then, the phase-locked solution will look roughly like:

$$\theta_j = \Omega t - |(N+1)/2 - j|\xi, \quad , j = 1, \ldots, N, \tag{9.53}$$

where $\Omega = \omega + H(\xi)$. Figure 9.19A shows the phase-locked solutions to a chain of 50 nearest-neighbor coupled oscillators along with the above approximation. Since $H(\phi) = \sin\phi + 0.5\cos\phi$, $\xi = \tan^{-1}(0.5)$. Except near the center, this approximation matches extremely well.

By manipulating the two end frequencies, ω_1 and ω_N while keeping the middle frequencies the same, we can produce waves of the form $\theta_j = \Omega t + \xi(j-1)$. Choose ξ so that $H_a'(\xi) > 0$ and $H_d'(-\xi) > 0$. Then choose

$$\omega_1 = \omega + H_d(-\xi) \quad \text{and} \quad \omega_N = H_a(\xi).$$

One must be cautious in using a linear array of oscillators for a cortical slice because of the importance of boundary effect and the fact that they can have global effects on the behavior of the network. For this reason, it is best to use some type of homogeneous condition so as to avoid waves which are driven solely from the boundaries. Weak coupling theory, nevertheless, works quite well and one may be tempted to suggest that the organized oscillations seen in pharmacologically treated cortical slice preparations may be a consequence of nothing more than coupled heterogeneous oscillators. Figure 9.18 shows an example of application of weak coupling to a linear array of cells. 50 Wang-Buszaki neurons were coupled with nearest neighbor inhibition and a a small degree of heterogeneity was introduced in the form of constant randomly chosen applied currents. The figure shows approximately one period of the cycle after a steady state is reached. While the currents were random, the network organizes itself into a rather simple pattern which consists of a right-ward moving wave which collides with a leftward moving wave. Using a single neuron model, we have computed the interaction function $H(\phi)$ and used this to derive the phase model (9.52). The heterogeneous currents become heterogeneous frequencies for the phase model. (In the full model, we have a frequency current relationship for an individual cell, $\omega = F(I)$. Since I is close to I_0, we obtain, $\omega \approx F(I_0) + c(I - I_0)$ so that the frequency in the phase model is just a scalar multiple of the heterogeneity of the currents.) The phase model produces a pattern very close to that of the full model. Such colliding waves are seen in experiments as the small inset in the figure shows.

Richard A. Satterlie Neuronal control of swimming in jellyfish: a comparative story1 Can. J. Zool. 80: 16541669 (2002) (notably figure 6)

Bao W, Wu JY. Propagating wave and irregular dynamics: spatiotemporal patterns of cholinergic theta oscillations in neocortex in vitro.

Ermentrout-B; Flores-J; Gelperin-A, Minimal model of oscillations and waves in the Limax olfactory lobe with tests of the model's predictive power. J-Neurophysiol. 1998 May; 79(5): 2677-89

Wu JY, Guan L, and Tsau Y. Propagating activation during oscillations and evoked responses in neocortical slices. J Neurosci 19: 5000-5015,1999

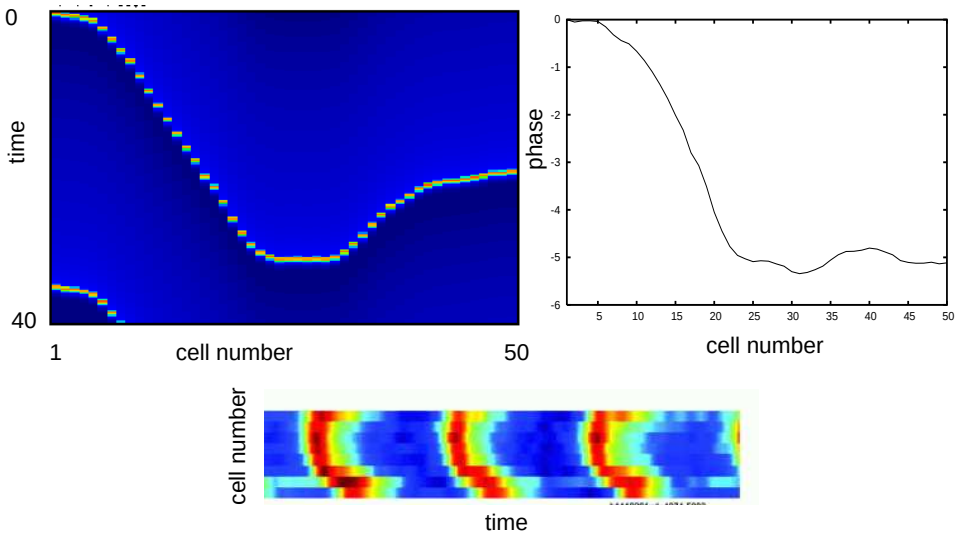

Figure 9.18. *50 Wang-Buszaki neurons coupled to nearest neighbors with inhibitory synapses (Reversal potential -80 mV, decay 6 msec). Each oscillator is driven by a constant current of* 0.5 *plus a small random value(between* -0.0035 *and* 0.0035*) to produce heterogeneity. Coupling strength is 0.02. Right-hand side is the phase-locked solution to the corresponding phase model. Below shows the space-time plot from Bao & Wu for a carbachol-treated slice.*

A.H. Cohen, G.B. Ermentrout, T. Kiemel, N. Kopell, K.A. Sigvardt, T.L. Williams, 1992, Modeling of intersegmental coordination in the lamprey central pattern generator for locomotion, TINS 15:434-438.

S. Grillner, T. Deliagina, O. Ekeberg, A. El Manira, R.H. Hill, A. Lansner, G.N.Orlovsky, P. Wallen, 1995, Neural networks that coordinate locomotion and body orientation in lampreys, TINS 18:270-279.

P.D. Brodfuehrer, E.A. Debski, B.A. O'Gara, and W.O. Friesen, 1995, Neuronal control of leech swimming, J. Neurobiology, 27:403-418.

M. Steriade, D. McCormick, and T.J. Sejnowski, 1993, Thalamocortical oscillations in the sleeping and aroused brain, Science 262:679-685.

9.2.9 Two-dimensional arrays.

There are fewer studies (both experimentally and theoretically) of two-dimensional arrays of neural oscillators. Ren and Ermentrout proved that phase-locked solutions of two-dimensional arrays coupled to the four neighbors (left, right, above, below) decomposed into the product of one-dimensional chains. This behavior is only "interesting" if the boundary effects dominate so the one-dimensional chains themselves produce interesting patterns. For example, consider an isotropic two-dimensional array of oscillators with "cut" boundary conditions. Let $H(\phi)$ have a

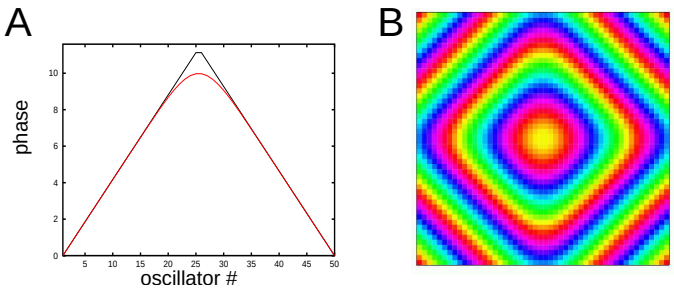

Figure 9.19. *Steady state phases for a chain of 50 oscillators,* $H(\phi) = \sin\phi + 0.5\cos\phi$ *with cut ends. Black line is equation (9.53). Right panel shows an array of* 50×50 *oscillators with the same* H.

zero with $H'(\phi)$ positive at the zero. Then the Ren theorem says that

$$\theta_{j,k} \approx \Omega t - \xi(|j-(N+1)/2| + |k-(N+1)/2|).$$

Figure 9.19B shows an example. The pattern of phases is like a square target pattern. This pattern completely disappears when the boundary condition is homogeneous; it is driven by the boundary. Intuitively, as with the chain, neurons along the edges get less input than those in the center and if $H(0) > 0$, this means that they will lag the oscillators in the middle producing waves which begin at the center of the array. If $H(0) < 0$, then they will lead the center oscillators and waves start at the edges and propagate to the center.

Patterns such as shown in Figure 9.19 are derived from the inhomogeneities at the boundaries which act like pacemakers along the edges of the medium. There are, however, patterns which arise from the intrinsic two-dimensional nature of the coupling. Spiral waves are well-known in the reaction-diffusion literature and are distinct from the target waves shown in the above figure in that they do not require any heterogeneity in the medium. Figure 9.20 shows examples of rotating waves from a variety of neural systems. The first example (of which these authors know) of rotating electrical activity in the CNS was on rabbit cortex treated with penicillin (which makes the network "epileptic"). Petsche et al reconstructed the spatio-temporal activity from a 4×4 array of electrodes placed on the surface of the occipital lobe (back of the brain). Fuchs and others reconstructed activity from the human electroencephalogram during resting (alpha) activity. Prectl et al used voltage-sensitive dyes to extract spatio-temporal activity from turtle cortex when certain stimuli were presented. Most recently, Huang et al created tangential slices of cortex and using voltage-sensitive dyes were able to record over thirty rotations of a spiral wave on the slice.

The classic model for spiral wave in the reaction-diffusion literature consists of an excitable medium with local coupling. However, there is no need for the medium to be excitable and intrinsically oscillator media can exhibit rotating waves and

spiral waves as seen in Figure 9.20D,E. A simple discrete model has the form:

$$\theta'_{i,j} = \omega + \sum_{k,l} H(\theta_{k,l} - \theta_{i,j})$$

where the sum is over the 4 neighbors. The figure shows the phase distribution for $H(\phi)$ a pure sine and also with a cosine component. The existence and stability of the first pattern has been established through a theorem due to Paullet (1994). For any $2N \times 2N$ array with nearest neighbor coupling such that $H(\phi)$ is odd and $H'(\phi) > 0$ for $-\pi/2 < \phi < \pi/2$, then Paullet and Ermentrout prove that there exists a rotating wave and it is asymptotically stable. The pattern of phases for the wave is such that in the upper left corner the phase is 0, the upper right, $\phi/2$, the lower right, π and the lower left $3\pi/2$. The diagonals from these 4 corners have the same phase as their respective corners and all meet in the central 2×2 array of oscillators. We leave the 4×4 case as an exercise to the reader. If $H(\phi)$ is not odd, then the behavior can be quite complex. For a small amount of even periodic coupling, the pattern evolves into a spiral wave (see Figure 9.20E) but as the even component increases, the "core" of the spiral breaks away and complicated (even chaotic) behavior ensues. (See Sakaguchi et al and Ermentrout 1995). The existence of stable phase patterns for this case has yet to be proven.

Sakaguchi, H, Shinimoto, S, and Y.Kuramoto, 1988, Mutual entrainment oscillator lattices with nonvariational coupling, Prog Theor Physics 79:1069-1079.

Paullet, J.E., and Ermentrout, G.B. (1994). Stable rotating waves in two-dimensional discrete active media. SIAM J. Appl. Math. 54, 17201744.

Prechtl, J.C., Cohen, L.B., Mitra, P.P., Pesaran, B., and Kleinfeld, D. (1997). Visual stimuli induce waves of electrical activity in turtle cortex. Proc. Natl. Acad. Sci. USA 94, 76217626.

Prechtl, J.C., Bullock, T.H., and Kleinfeld, D. (2000). Direct evidence for local oscillatory current sources and intracortical phase gradi- ents in turtle visual cortex. Proc. Natl. Acad. Sci. USA 97, 877882.

Ermentrout-B, A heuristic description of spiral wave instability in discrete media, Physica D, 82:154-164, 1995

Huang X, Troy WC, Yang Q, Ma H, Laing CR, Schiff SJ, Wu JY. Spiral waves in disinhibited mammalian neocortex. J Neurosci. 2004 Nov 3;24(44):9897-902. Petsche H, Prohaska O, Rappelsberger P, Vollmer R, Kaiser A. Cortical seizure patterns in multidimensional view: the information content of equipotential maps. Epilepsia. 1974 Dec;15(4):439-63.

Petsche H, Rappelsberger P, Trappl R. Properties of cortical seizure potential fields. Electroencephalogr Clin Neurophysiol. 1970 Dec;29(6):567-78

Fuchs A., Friedrich R., Haken H., Lehmann D.: 'Spatio-Temporal Analysis of Multichannel alpha-EEG Map Series', in: Computational Systems – Natural and Artificial, H. Haken, ed., Springer, Berlin (1987)

Friedrich R., Fuchs A., Haken H.: 'Spatio-Temporal EEG Patterns', in: Rhythms in Physiological Systems, H. Haken, H.P. Koepchen, eds., Springer, Berlin (1991)

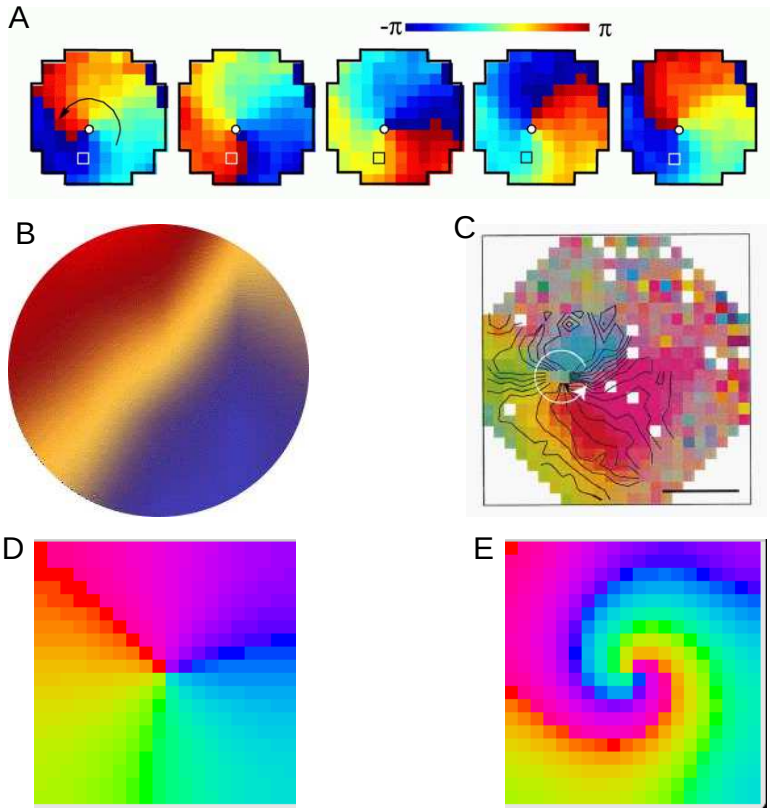

Figure 9.20. *Rotating and spiral wave patterns seen in neural tissue. (A) From Huang et al in a tangential dis-inhibited cortical slice; (B) From Fuchs et al reconstructed from EEG electrodes in a human during alpha activity; (C) from Ermentrout and Kleinfeld optical activity in the turtle visual area; (D) steady state phases in a* 20×20 *array of nearest neighbor phase oscillators* ($H(\phi)=\sin\phi$)*; (E)as in (D) but* $H(\phi)=\sin\phi+0.5(\cos\phi-1)$.

9.2.10 All-to-all coupling.

(Note that this section may be a bit technical and could easily be skipped.) In this section, we consider the so-called Kuramoto model and in so doing introduce a powerful method for analyzing large networks of neurons. We will start with a very general system of phase models with additive noise and heterogeneities in their frequency:

$$\theta_j' = \omega_j + \frac{K}{N}\sum_k H(\theta_k-\theta_j) + \sigma dW_j. \tag{9.54}$$

Here dW_j is the usual white noise process. K is the strength of the coupling which we will regard as a parameter. We can assume without loss of generality that the average value of $H(\phi)$ is zero for if it is nonzero, we can write $H(\phi)=H_1(\phi)+\bar{H}$ and

then replace ω_j by $\omega_j + K\bar{H}$. The frequencies, ω_j are taken from some distribution (see below). Since we can always replace θ_j by $\theta_j + Ct$, where C is a constant, we can assume that the mean frequency is zero.

Rather that looking at the individual neurons, θ_j, the idea of the *population density* method is to consider the distribution of phases, θ that any randomly chosen neuron might take. Kuramoto studied a particular case when the noise is zero and $H(\phi) = \sin\phi$. His method was formal and we refer the reader to the excellent review article by Strogatz (2000) to see how Kuramoto proceeded. Strogatz and Mirollo devised a method based on the phase density which was more rigorous and can be readily generalized such as to equation (9.54). (Strogatz describes his burst of insight for using the population density method in his popular book, *Sync.* It reminded one of the authors of the present volume of Kekule's insight into the structure of benzene, both occurring in a near dreamlike state.) Neu (1978) was the first to introduce the notion of density to coupled oscillators, but he did not take it to the extent that Strogatz and those who followed him did.

We will not attempt to rigorously derive the equations; rather we write down an equation for the population density which should allow the reader to apply to her own results and models. We assume that $N \to \infty$ and let $\rho(\theta, \omega, t)$ denote the density of oscillators with uncoupled frequency ω and phase θ at time t. Note that the oscillators cannot change their uncoupled frequency. Let $g(\omega)$ denote the density function for the distribution of frequencies. We will define g on the real line with

$$\int_{-\infty}^{\infty} g(\omega)\ d\omega = 1.$$

The density, ρ, satisfies the continuity equation:

$$\frac{\partial \rho}{\partial t} = -\frac{\partial}{\partial \theta} J(\theta, \omega, t)\rho.$$

This equation simply says that the phase of a given oscillator evolves in time and that total "mass" of the oscillators, $\int_0^{2\pi} \rho(\theta, \omega, t)d\theta$, is conserved. The flux is given by $d\theta/dt$ so that

$$J(\theta, \omega, t) = \omega - \frac{\sigma^2}{2}\frac{\partial \rho}{\partial \theta} + KQ(\theta, t).$$

The first term is pretty obvious, the second is the diffusive flux from the noisy inputs, dW_j which as usual are independent. The last term is:

$$Q(\theta, t) = \lim_{N\to\infty} \sum_{k=1}^{N} H(\theta_k - \theta).$$

The reader will recognize this as the average of H over the phases of the other oscillators so that we can write:

$$Q(\theta, t) = \int_{-\infty}^{\infty} g(\omega) \int_0^{2\pi} H(\phi - \theta)\rho(\phi, \omega, t)\ d\phi\ d\omega. \tag{9.55}$$

Thus, we have the following continuity equation:

$$\frac{\partial \rho}{\partial t} = \frac{\sigma^2}{2}\frac{\partial^2 \rho}{\partial \theta^2} - \frac{\partial}{\partial \theta}\left(\left(\omega + KQ(\theta, t)\right)\rho\right). \tag{9.56}$$

Unlike the Fokker-Planck equations which we studied in earlier chapters, equation (9.56) is nonlinear since Q is a functional of the density ρ. Because of the nonlinearity, it is difficult to write down any closed form solutions. However, one solution is the fully *asynchronous state* in which the distribution of phases is uniform. Substitute $\rho = 1/2\pi$ into equation (9.55) to see that $Q = \bar{H}$, the average value of $H(\theta)$ over $[0, 2\pi)$.. We can always absorb the average value of H into the frequency and thus we suppose $\bar{H} = 0$. Plugging this into equation (9.56), we see that the uniform density is in fact a solution. The key to Strogatz' analysis (and, in fact, all other analysis) is that we can linearize (9.56) about this stationary solution and study stability as a function of the coupling strength, K. Let $\rho = 1/2\pi + z$. Then to lowest order

$$\begin{aligned}\frac{\partial z}{\partial t} &= \frac{\sigma^2}{2}\frac{\partial^2 z}{\partial \theta^2} - \omega\frac{\partial z}{\partial \theta} \\ &\quad + \frac{K}{2\pi}\int_{-\infty}^{\infty} g(\omega)\int_0^{2\pi} H'(\phi - \theta)z(\phi, \omega, t)\; d\omega\; d\phi.\end{aligned}$$

Note that the dependence on θ appears through the convolution of z with the derivative of $H(\theta)$. This linear equation is homogeneous with respect to t and to θ and they must be $2\pi-$periodic int θ so we can look for solutions of the form:

$$z(\theta, \omega, t) = e^{in\theta}e^{\lambda t}f(\omega).$$

$f(\omega)$ is an unknown function which we must compute. Since $H(\theta)$ is periodic and square integrable (well, we never actually asserted this, but for reasonable models, it is), we can expand it in a trigonometric series:

$$H(\theta) = \sum_{n=-\infty}^{\infty} a_n e^{in\theta}$$

and since H is real, $a_{-n} = \bar{a_n}$. Finally, since $\bar{H} = 0$, we also assume $a_0 = 0$. If H is differentiable, then

$$H'(\theta) = i\sum_{n=-\infty}^{\infty} n a_n e^{in\theta}.$$

With these preliminaries, we plug the solution z into the linearized equation and obtain:

$$\lambda f(\omega) = (-in\omega - \frac{\sigma^2 n^2}{2})f(\omega) - in\bar{a_n}K\int_{-\infty}^{\infty} g(\omega)f(\omega)\; d\omega. \tag{9.57}$$

The last part of the equation follows from the fact that

$$\frac{1}{2\pi}\int_0^{2\pi} e^{im(\phi-\theta)}e^{in\phi}\; d\phi$$

vanishes unless $n = m$ in which case it is $e^{in\theta}$. We shall not worry about the essential spectrum for this problem (Crawford and others ??? have proven that it lies in the left half plane) and instead will focus on the discrete spectrum. Let

$$A = \int_{-\infty}^{\infty} g(\omega) f(\omega)\ d\omega.$$

Then from equation (9.57), we can solve for $f(\omega)$:

$$f(\omega) = \frac{-ina_{-n}KA}{\lambda + in\omega + \sigma^2 n^2/2}.$$

Recalling how A is defined, we find the equation for A must satisfy:

$$A = -inAKa_{-n} \int_{-\infty}^{\infty} g(\omega) \frac{1}{\lambda + in\omega + \sigma^2 n^2/2}\ d\omega.$$

Dividing through by A (since $A = 0$ is the zero solution) we obtain:

$$1 = -inKa_{-n} \int_{-\infty}^{\infty} g(\omega) \frac{1}{\lambda + in\omega + \sigma^2 n^2/2}\ d\omega. \tag{9.58}$$

We will study two cases: (i) no noise and (ii) no heterogeneity. In the first case, we must have:

$$1 = -inKa_{-n} \int_{-\infty}^{\infty} \frac{\lambda - in\omega}{\lambda^2 + n^2\omega^2} g(\omega)\ d\omega. \tag{9.59}$$

This is an equation for λ which depending on the function $g(\omega)$ may or may not be possible to evaluate in closed form. Suppose that $g(\omega)$ is symmetrically distributed around 0. Then equation (9.59) becomes:

$$1 = -2inKa_{-n} \int_{0}^{\infty} \frac{\lambda}{\lambda^2 + n^2\omega^2} g(\omega)\ d\omega.$$

Finally, we make one last simplification. Suppose that $H(\phi)$ is an odd function,

$$H(\phi) = \sum_n b_n \sin n\phi$$

so that $a_n = -ib_n/2$ and the eigenvalue equation is then:

$$1 = nKb_n \int_{0}^{\infty} \frac{\lambda}{\lambda^2 + n^2\omega^2} g(\omega)\ d\omega.$$

Stability of the asynchronous solution occurs as K changes if λ crosses the imaginary axis. Clearly,$\lambda = i\beta$ is impossible, so that the only way to lose stability is through a real eigenvalue. (We remark that if H has even components or if the frequency distribution is asymmetric, then the zero eigenvalue will not generally occur and instead stability will be lost through imaginary eigenvalues.) We will let λ tend to

zero and use this to compute the critical value of the parameter, K. Let $\omega = \lambda\gamma$ be a change of integration variables. Then

$$\int_0^\infty \frac{\lambda}{\lambda^2 + n^2\omega^2} g(\omega)\, d\omega = \int_0^\infty \frac{g(\lambda\gamma)}{1 + n^2\gamma^2}.$$

As $\lambda \to 0$, this integral is just

$$g(0)\frac{\pi}{2n}.$$

This, we find that for each n,

$$K_c(n) = \frac{2}{\pi g(0) b_n}.$$

In particular, for Kuramoto's case of a pure sinusoidal coupling, $b_1 = 1$ and all other $b_m = 0$, $K_c = 2/\pi g(0)$. If all the $b_j < 0$, then the asynchronous state is always stable. However, as long as $g(0) > 0$, if there is a single positive b_n, then for strong enough coupling the asynchronous state will destabilize. Since the mode $\exp(in)$ becomes unstable with stronger coupling, standard bifurcation methods (see later chapters when we explore spatial models), predict that the new solutions which bifurcate from the asynchronous state will have the form:

$$\rho(\omega, \theta) = \frac{1}{2\pi} + cf(\theta)\cos n\theta.$$

where c is some small parameter.

We will leave case (ii) of noise with no heterogeneity as an exercise to the reader. But we provide a start here. Referring to equation (9.57), we can set $f(\omega) = 1$ a constant since there is no frequency dependence. The integral with respect to ω becomes 1 and we have:

$$\lambda = (-in\omega - \frac{\sigma^2 n^2}{2}) - in\bar{a_n}K. \tag{9.60}$$

If stability is lost for $n > 1$, then the solution which emerges will generally have n peaks and is called a clustered state. Noise-free two-clustered states are left as an exercise to the reader.

9.3 Pulse-coupled networks: solitary waves

The method of phase reduction provides a very general way to reduce systems of coupled oscillatory neurons to simple phase models. However, it presumes that the individual cells are intrinsically oscillatory. In the next chapter, we address the behavior of networks with strong coupling, some of which are not intrinsically oscillating. Recall that when a single nerve cell is stimulated, an action potential propagates down the axon mediated by the diffusion of the potential along the unmyelinated axon. Similar propagation of electrical activity can be found in *networks* of neurons in which a spatially localized region is stimulated and results in the outward spread of activity over distances of several millimeters. Figure 9.21 shows

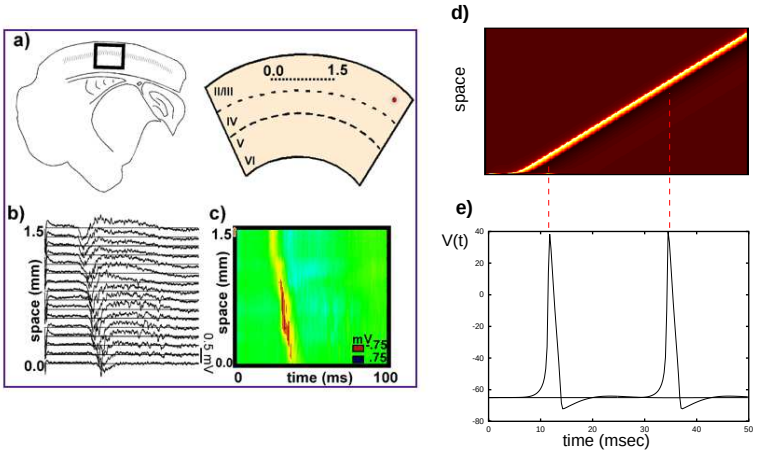

Figure 9.21. *Propagating wave of activity in a brain slice preparation in which the inhibition has been blocked (Pinto et al 2006) (a) shows where the slice comes from (b) the exracellular potential recorded from a 16 electrode array (c) plot of (b) in pseudocolor (d) simulation of an array of 200 HH neurons with excitatory synaptic coupling and exponentially decaying spatial connectivity, (e) the membrane potential from cells at position 25 and 125 in the array*

an example of an experimental demonstration of synaptically generated waves in a network of cortical cells with the inhibition blocked. A slice is removed from the brain of a rat and bathed in a medium which blocks the effects of synaptic inhibition. A stimulating electrode produces a brief local shock which causes neurons to fire and this activity is transmitted via excitatory synapses to neighboring cells exciting them and so on. The result is a wave which propagates at a ?? mm/sec. This is slower than axonal propagation since the wave depends on the activation of synapses rather than direct diffusive coupling. The figure also shows a simulation of the Hodgkin-Huxley model coupled in a network of 200 neurons with excitatory synapses.

We consider the following general system:

$$C\frac{\partial V}{\partial t} = -I_{ion}(V,z,\ldots) - \left(g_{syn}\int_{-\infty}^{\infty} W(x-y)s(y,t)\,dy\right)(V(x,t)-V_{syn}) \quad (9.61)$$

$$\frac{\partial z}{\partial t} = Z(V,z,\ldots)$$

$$s(x,t) = \sum_m \alpha(t-t^m(x))$$

where the sum is taken over all spikes produced by the neuron at spatial location x, and $\alpha(t)$ is a predefined function which vanishes for $t<0$ and represents the time course of the synaptic conductance. z represents the possibly many gating variables (such as the activation of potassium and inactivation of sodium). $W(x)$ describes the distance-dependent strength of interactions between neurons. We assume that

W is symmetric, non-negative, and integrates to 1 over the whole line. For the model in the figure, $\alpha(t) = \exp(-t/5)$ and $W(x) = \exp(-|x|)/2$. We define the time of a spike to be that time at which the potential crosses so predefined threshold, V_T. In figure 9.21d each neuron spikes exactly one time during the course of the wave. We can exploit this to construct and analyze the propagation of waves. Suppose that (as in the simulation, but not in the experiment), each neuron fires exactly once at time $T(x)$. Then that cell contributes $\alpha(t-T(x))$ to the other cells and the total conductance produced by the wave is:

$$G(x,t) = g_{syn} \int_{-\infty}^{\infty} W(x-y)\alpha(t-T(y))\ dy.$$

A constant speed traveling wave satisfies, $T(x) = x/\nu$ where ν is the velocity of the wave. The simulations in the figure suggest that we look for traveling wave solutions to the integro-differential equation. That is, we seek solutions of the form, $V(x,t) = v(x-\nu t), z(x,t) = u(x-ct)$ where v, u are functions of the single variable, $\xi = x - ct$. We note that in these coordinates, the conductance, $G(x,t)$ can be written as

$$G(x,t) = g(\xi,\nu) = g_{syn} \int_{-\infty}^{0} W(\xi-\eta)\alpha(-\eta/\nu)\ d\eta.$$

The traveling waves start at rest and end at rest. Thus equation (9.61) becomes the non-autonomous ODE:

$$\begin{aligned} -\nu C\frac{dv}{d\xi} &= -I_{ion}(v,u) - g(\xi,\nu)(v-V_{syn}) \\ -\nu\frac{du}{d\xi} &= Z(u,z). \end{aligned} \tag{9.62}$$

We must solve this for $v(\xi), u(\xi)$ satisfying:

$$\begin{gathered} (u(\pm\infty), z(\pm\infty) = (V_{rest}, z_{rest}) \\ u(0) = V_T. \end{gathered}$$

Here (V_{rest}, z_{rest}) is the resting state for the each neuron. Since traveling waves are translation invariant, the second condition set the origin of the wave $\xi = 0$ to be the point at which the neuron crosses threshold. We note that $g(\xi) \to 0$ as $\xi \to \pm\infty$ since $W(x)$ is integrable, $\alpha(t)$ decays as $t \to \infty$ and vanishes for $t < 0$. If the velocity, ν is positive, then the boundary condition at $-\infty$ is simple to achieve since the rest state is asymptotically stable and g decays to zero. On the other hand, it is natural to ask how we can attain the decay of (v,u) to rest as $\xi \to \infty$ since the rest state is unstable as a solution to (9.62) for $\nu > 0$ and for $\xi \to \infty$. There is no proof for the existence of a wave speed, ν such that $(v(\xi), u(\xi))$ go to the rest state as $\xi \to \infty$. However, for simple models like the integrate-and-fire, the solution can be explicitly computed.

9.3.1 Integrate-and-fire model.

The analogue of (9.61) for an integrate and fire model is

$$\tau \frac{\partial V}{\partial t} = V_{rest} - V + a(V_{syn} - V)S(x,t)$$

where $a = g_{syn}R_m$ and

$$S(x,t) = \int_{-\infty}^{\infty} W(x-y) \sum_k \alpha(t - t_k(y))\ dy. \tag{9.63}$$

Here, $\alpha(t)$ is the proscribed synaptic gating variable (e.g., it could be a simple exponential, or difference of exponentials) and $t_k(x)$ represents the firing times of a neuron at spatial point x. This says that the effect of other neurons on a neuron at spatial point x depends on the distance (the function $W(x)$) and the times that those neurons fire, $T_k(y)$. We note that in this formalism, there could be delays to the synapse and it is clear that we could also introduce delays that depend on the distance. This makes the model more complex but it remains solvable. We have absorbed any applied current to the model into the constant V_{rest} which we assume is less than the threshold for firing. (Otherwise, the neuron would spontaneously fire and we are interested on evoked waves, so we don't want spontaneous activity.) We shift the potential by V_{rest}, $\hat{V} = V - V_rest$ so that the driving force for the synaptic coupling is

$$V_{syn} - V_{rest} - \hat{V}.$$

The equation is still difficult to analyze since the potential, $\hat{V}$ is multiplied by the synaptic activity, $S(x,t)$ making it difficult to integrate the equation. Thus, we make one more simplification. We replace the voltage-dependent drive by a constant drive, $V_{syn} - V_{rest}$. Noting that a is dimensionless, we absorb it into the drive, $V_{drive} = (V_{syn} - V_{rest})g_{syn}R_m$ and now turn our attention to the simpler problem:

$$\tau \frac{\partial V}{\partial t} = -V + V_{drive}S(x,t) \tag{9.64}$$

with $S(x,t)$ as defined in (9.63). We have dropped the hats on the voltage for notational simplicity. As in the conductance-based model, we suppose that there is only one spike per neuron so that the index k can be dropped from the sum in (9.63). By assuming that there is only one spike per wave, we don't have to worry about what happens after the wave passes through. This makes our work much simpler. Equation (9.64) can be integrated with the integrating factor $\exp(-t/\tau)$ leading to the following equation:

$$V(x,t) = Ce^{-t/\tau} + V_{drive} \int_{-\infty}^{\infty} W(x-y)A(t - T(y))\ dy \tag{9.65}$$

where

$$A(t) = \frac{1}{\tau} \int_0^t \alpha(t-s)e^{-s/\tau}\ ds.$$

(The proof of this statement is left as an exercise.) We take $C = 0$ since we are interested in what happens when the neurons all start from rest. The function $A(t)$ vanishes for $t < 0$ since the function $\alpha(t)$ vanishes for $t < 0$. $A(t)$ is the response to a passive membrane with time constant τ to a synaptic current of the form $\alpha(t)$. An obvious generalization of equation (9.65) could include passive dendrites between the synapse and the spike-generating zone of the neuron. In this case, $A(t)$ is the convolution of $\alpha(t)$ with the spatio-temporal Green's function for the dendrite evaluated at the spatial location of the synapse (see chapter ???). (Coombes, Bressloff, and others have considered many of these cases; there are differences as expected, but the basic theory remains identical.) Since each neuron fires exactly once, this means that the membrane potential of a neuron at $t = T(x)$ must be equal to it's firing threshold, V_T (which has been shifted by V_{rest}) thus, we must have

$$V(x, T(x)) = V_T.$$

Evaluating (9.65) at $t = T(x)$, we have the following functional differential equation:

$$V_T = V_{drive} \int_{-\infty}^{\infty} W(x-y) A(T(x) - T(y))\ dy. \tag{9.66}$$

We note that if the neuron fires multiple times, we have to take into account the resetting properties of the integrate and fire model and also that there will be a family of firing times, $T_k(x)$. This problem has been investigated by Osan, et al.

A traveling wave with velocity, ν satisfies, $T(x) = x/\nu$. Keeping in mind that $A(t)$ is nonzero only if $t > 0$, expression (9.66) reduces to

$$\begin{aligned} \frac{V_T}{V_{drive}} &= \int_{-\infty}^{x} W(x-y) A((x-y)/\nu)\ dy \\ &= \int_{0}^{\infty} W(y) A(y/\nu)\ dy \\ &\equiv Q(\nu). \end{aligned}$$

This is just an algebraic equation for ν as a function of V_T/V_{drive}. For example, if $W(x) = \exp(-|x|\sigma)/(2\sigma)$ and $\alpha(t) = \exp(-\beta t)$, then

$$Q(\nu) = \frac{1}{2} \frac{\sigma\nu}{\nu^2\tau + \sigma\nu(1+\tau\beta) + \beta\sigma^2}.$$

Notice that $Q(0) = 0$ and as $\nu \to \infty$, $Q(\nu) \to 0$. Note also that $Q(\nu)$ has a single maximum. Thus if V_T/V_{drive} is too big, we cannot solve

$$V_T/V_{drive} = Q(\nu)$$

but that if it is small enough, then there are always two roots, ν. In exercise ???, you are asked to draw this function and solve for ν. For most functions $W(x)$, one cannot evaluate the integral, Q; however, it is possible to prove some properties (see exercise ***). Figure 9.22A shows a typical plot of $Q(\nu)$ and the calculation of roots to $Q(\nu) = V_T/V_{drive}$. As long as this latter quantity is small enough,

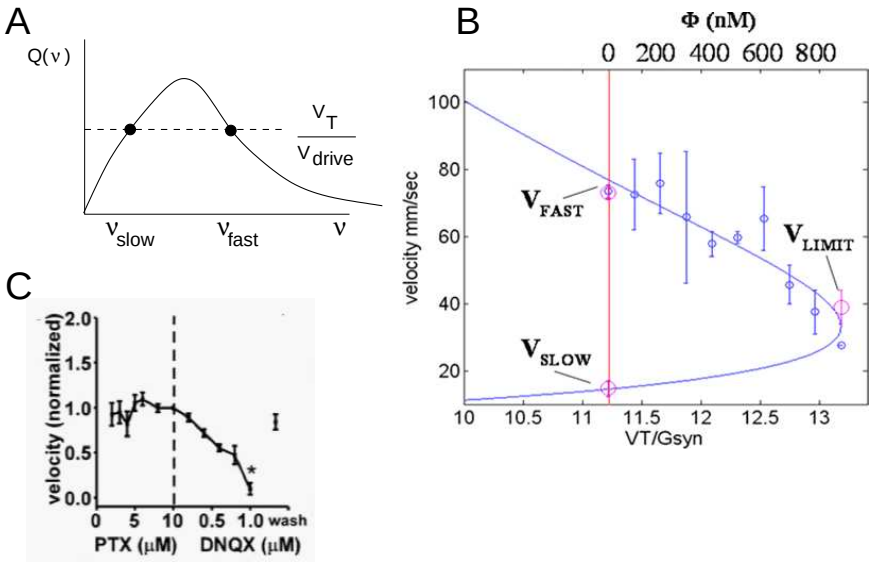

Figure 9.22. *(A) Calculation of the wave speed for single-spike traveling waves as a function of the threshold and drive (B) Experimental velocity in a one-dimensional cultured network as a function of the amount of excitatory synaptic blocker, DNQX; (C) Same for a disinhibited slice.*

there are two possible wave velocities, one slow and one fast. Intuition tells us that if we increase the drive, the wave should travel faster; increasing the drive corresponds to lowering the dashed line. The fast wave increases in speed and the slow decreases. Thus, we would like to conclude that the fast wave is the one that is observed experimentally and numerically. Indeed, that is the case as would appear from figures 9.22B,C which show experimentally determined wave velocities in two different preparations as the strength of the recurrent excitatory connections is pharmacologically decreased. In 9.22B, neurons are grown in a one-dimensional cultured array (Feinerman, et al) and the velocity of evoked waves is measured while different concentrations of the excitatory synaptic blocker, CNQX are applied. The authors of this paper have attempted to fit their data to a curve similar to that in figure 9.22A. The slow velocity is estimated by applying a minimal stimulation which results in a slow initial propagation that switches to the fast wave after a small transient. Pinto et al (Figure 9.22C) observe a similar qualitative dependence of the velocity on the strength of connections in a disinhibited cortical slice preparation.

9.3.2 Stability.

The stability problem for the traveling waves is difficult. However, we can explore a simple version of stability called spatial stability. We suppose that $T(x) = x/\nu + b\exp(\lambda x)$ where b is a small deviation. Plugging this into equation (9.66) we see

that

$$0 = b\int_{-\infty}^{\infty} W(x-y)A'((x-y)/\nu)[e^{\lambda x} - e^{\lambda y}]\ dy.$$

Factoring out $e^{\lambda x}$ and using the fact that $A(t)$ and therefore $A'(t)$ vanishes for $t < 0$, we must have

$$0 = \int_{0}^{\infty} W(y)A'(y/\nu)[1 - e^{-\lambda y}]\ dy \equiv E(\lambda).$$

This is the "Evans" function and zeros correspond to eigenvalues. Any eigenvalues with positive real parts will lead to an exponential growth of $T(x)$ away from the traveling wave as x increases. In exercise ***, you show that if $W(x)$ is a monotone decreasing function of x on the positive real line and if $A(t) \geq 0$, then the slow wave (cf figure 9.22) is unstable. The stability of the fast wave is proven in Bressloff (2000). Bressloff also considers periodic traveling waves and their stability as well as some extensions to two-dimensional spatial domains.

Bressloff P C 2000 Traveling waves and pulses in a one-dimensional network of excitable integrate-and-fire neurons J. Math. Biol. 40 16998

9.4 Adjoints and weak coupling using XPP

XPPAut contains an algorithm for finding the adjoint of any stable limit cycle by integrating the adjoint equation backward. It also allows you to compute the interaction function from the weak coupling reduction. subsectionComputing a limit cycle and the adjoint. To use XPP to compute the adjoint, a necessary first step to computing the interaction function H, we first have to compute exactly one full cycle of the oscillation. We will use the Traub model with no adaptation and with both gap junctional and synaptic coupling. The file in the appendix should do the trick. We will look at:

$$v_1' = \ldots + g_{syn}s_2(V_{syn} - v_1)$$
$$v_2' = \ldots + g_{syn}s_1(V_{syn} - v_2)$$

when $g_{syn} \ll 1$. Since the method of averaging depends on the two oscillators being identical except possibly for the coupling, all you need to do is integrate the isolated oscillator. Use the Traub file with $g_m = g_{ahp} = 0$ and $I = 1$. Integrate the equations for about 30 msec and click on **Initialconds Last** a few times to make sure you have gotten rid of all transients. Now you are pretty much on the limit cycle. To compute the adjoint, you need one full period. In many neural systems, coupling between oscillators occurs only through the voltage and thus, the integral average involves only one component of the adjoint, the voltage component. For whatever reason, the numerical algorithm for computing the adjoint for a given component converges best if you start the oscillation at the *peak* of that component. Thus, since we will only couple through the potential in this example, we should start the oscillation at the peak of the voltage. Here is a good **trick** for finding that maximum. In the **Data Browser** click on **Home** which makes sure that the first entry of the data is at the top of the window. Click on **Find** and in the dialog box,

choose the variable v and for a value, choose 1000and then **Ok**. XPP will find the closest value of v to 1000 which is obviously the maximum value of v. Now click on **Get** in the Data window which grabs this as initial conditions. In the main window, click on **Initialconds Go** to get a new solution. Plot the voltage versus time. Use the mouse to find the time of the next peak (With the mouse in the graphics window, click the button and move the mouse around. At the bottom of the windows, read off the values). The next peak is at 23. In the Data window scroll down to this time and find exactly where v reaches its next maximum. Note that it is, as we suspected, at $t = 23$. In the main window , click on the **nUmerics** menu and then **Total** to set the total integration time. Choose 23. Escape to the main menu and click on **Initialconds Go**. Now we have one full cycle of the oscillation! The rest is easy.

Computing the adjoint.

Click on **nUmerics Averaging New adjoint** and after a brief moment, XPP will beep. (Sometimes, when computing the adjoint, you will encounter the `Out of Bounds` message. In this case, just increase the bounds and it recompute the adjoint.) Click on **Escape** and plot v versus time. This time, the adjoint of the voltage is in the Data window under the voltage component.

9.4.1 Averaging

Now we can compute the average. Recall that the integral depends on the adjoint, the original limit cycles and a phase-shifted version of the limit cycle:

$$X^*(t) \cdot G(X_0(t+\phi), X_0(t)).$$

In XPP, you will be asked for each component of the function G. For unshifted parts, use the original variable names, e.g., `x,y,z` and for the shifted parts, use primed versions, `x',y',z'`. The coupling vector in our example is

$$(s(t+\phi)(V_{syn} - V(t), 0, \ldots, 0).$$

We will take $V_{syn} = 0$ for excitatory coupling. Thus, for our model, the components for the coupling are `(s'*(0 - v), 0, ..., 0)`. This says that we take the phase-shifted version of the variable `s`, called `s'` by XPP and multiply it by the drive. With these preliminaries, it is a snap to compute the average. Click on **nUmerics Averaging Make H**. Then type in the first component of the coupling, `s'*(0-v)` and the `0` for the rest of the components. Then let it rip. In a few moments, the calculation will be done. If your system has more than two columns in addition to time, `t` (as this example does) then the first column contains the average function $H(\phi)$, the second column contains the odd part of the interaction function, and the third column contains the even part. Plot the function H by escaping back to the main menu and plotting v versus time – remember v is the first column in the browser after the `t` column. This is a periodic function.

Summarizing,

1. Compute exactly one period of the oscillation – you may want to phase-shift it to the peak of the dominant coupling component.
2. Compute the adjoint from the **nUmeric Averaging** menu.
3. Compute the interaction function using the original variable names for the unshifted terms and primed names for the shifted terms.

9.5 Projects.

- Use the Izhikevich model or a similar "integrate-and-fire" model to compute a PSTH for a weak perturbation and then use this to reconstruct the PRC.
- Synchrony without coupling. Two oscillators which are driven with common weak noise can synchronize even if they are not coupled (Teramae and Tanaka, 2004). To see this, start with any two oscillators (for example, the Izhikevich model) and drive them with a common white noise process, started from slightly different initial conditions. Over time, they will converge to a synchronous solution. In this project, you use the results of chapter Noise to analyze the resulting equations. To simplify the analysis, we restrict our attention to simple ring model oscillators which are continuous and differentiable:

$$dx_1 = a(x_1)dt + \sigma dW$$
$$dx_2 = a(x_2)dt + \sigma dW$$

Assume that $a(x) > 0$, $a(x+2\pi) = a(x)$ and $P = \int_0^{2\pi} \frac{dx}{a(x)} < \infty$. Then we can regard each x as an oscillator

Step 1. Make a change of variables $x = U(\theta)$ where $U' = a(U)$. Since $a(U) > 0$, this is an invertible transformation. Let $f(x)$ be the inverse, so that $\theta = f(x)$. Recall Ito's formula when you make the change of variables.

Step 2. Recall that for the scalar oscillator, the adjoint, $Z(\theta)$ is given by $Z(\theta) = 1/a(U(\theta))$. Use regular calculus to show that with the change of variables in step 1, the equations are:

$$d\theta_1 = [1 + \frac{\sigma^2}{2} Z'(\theta_1)Z(\theta_1)]dt + \sigma Z(\theta_1)dW$$
$$d\theta_2 = [1 + \frac{\sigma^2}{2} Z'(\theta_2)Z(\theta_2)]dt + \sigma Z(\theta_2)dW.$$

Step 3. One solution to this SDE is $\theta_1 = \theta_2 = \theta$. Let $\phi = \theta_2 - \theta_1$. Then ϕ satisfies:

$$d\phi = \frac{\sigma^2}{2}[Z'(\theta)Z(\theta)]'\phi dt + \sigma Z'(\theta)\phi dW.$$

Again, using Itos, formula, let $y = \log(\phi)$ and show that y satisfies:

$$\frac{dy}{=} \frac{\sigma^2}{2}\{[Z'(\theta)Z(\theta)]' - Z'(\theta)^2\}dt + \sigma Z'(\theta)dW.$$

Step 4. The long time behavior of $y(t)$ determines the stability of the synchronous state. That is, if

$$\lambda \equiv \lim_{T\to\infty} \frac{1}{T}(y(T) - y(0))$$

is negative, then $\phi(t)$ will decay to zero. λ is the time average of $y(t)$ and we can replace this with the ensemble average:

$$\lambda = \frac{\sigma^2}{2} \int_0^{2\pi} P_{st}(\theta)\{[Z'(\theta)Z(\theta)]' - Z'(\theta)^2\}d\theta.$$

Here $P_{st}(\theta)$ is the stationary distribution of θ which satisfies the SDE:

$$d\theta = [1 + \frac{\sigma^2}{2}Z'(\theta)Z(\theta)]dt + \sigma Z(\theta)dW.$$

If the noise is small, then θ is nearly uniform and you can approximate $P_{st}(\theta) = 1/(2\pi)$. Show that with approximation:

$$\lambda = -\frac{\sigma^2}{2}\frac{1}{2\pi}\int_0^{2\pi} Z'(\theta)^2 \; d\theta.$$

Conclude synchrony is stable.

Supplement the analysis with some numerical simulations. Additionally, add independent noise to each oscillator, say, 10% of the common noise. Solve this numerically and look at the stationary distribution of the phase-differences.

- Development and synchrony. During the development of the nervous system, there are two important features of neural communication. First, there are many electrical or gap junctions between cells. Second, the reversal potential of GABA-ergic synapses is such that they actually act to depolarize rather than hyperpolarize. In this project, you should perform the weak coupling analysis for a pair (or more) of coupled neurons as the reversal potential of the inhibition changes from, say -40 mV down to -75 mV. You should also apply the weak coupling analysis to a gap junctionally coupled neuron. A good choice for the membrane model is the Wang-Buszaki model (found in the list of models in the appendix and also available on the web). Drive the WB model so that it fires at about 40 Hz and use a fast GABA synapse such as defined in the synapse chapter. Vary the reversal potential of the synapse and compute the interaction function $H(\phi)$. Use this to predict whether a pair of synaptically coupled neurons will synchronuze or fire in anti-phase. With this "prediction", couple two WB membrane modesl with weak inhibition and see if the theoretical results agree. Look at larger networks either using a phase model or the full blown network.

- Kuramoto and coupling. Suppose that instead of heterogenity in the frequencies of the Kuramoto model, there is instead heterogenity in the coupling. In

general, there is little one can do to analyze this case, but there is one type of coupling which lends itself to rigorous analysis. Suppose that $H(0) > 0$ and consider:

$$\theta_j = \omega + \frac{1}{N}\sum_k C_j C_k H(\theta_k - \theta_j).$$

The coupling coefficients C_j are taken from some distribution with mean μ and variance σ. Develop a population density theory for this and analyze the stability (and existence) of the asynchronous state. (You could probably do this with C_j, C_k different.)

- Integrate and fire neurons and phase-locking. Consider a system of integrate and fire neurons which we write simply as:

$$\frac{dV_j}{dt} + V_j = I_j + \sum_{k,l} C_{jk}\alpha(t - t_k^l) - B\sum_l \delta(t - t_j^l)$$

where C_{jk} are the coupling currents and t_k^l are the firing times. The delta function appearing on the right-hand side represents the reset when the neuron fires. B is the distance between threshold and reset. Let $E(t) = \exp(-\max(t, 0))$ and let $A(t)$ denote the integral

$$A(t) = \int_0^t e^{-t+s}\alpha(s)\ ds.$$

Show that we can rewrite this equation as:

$$V_j(t) = V_j(0)e^{-t} + I_j(1 - e^{-t}) - B\sum_l E(t - t_j^l) + \sum_{k,l} C_{jk}A(t - t_k^l).$$

Now suppose that the integrate-and-fire neurons all fire with a period T (unknown) so that they are phase locked. That is, $t_j^l = lT + \zeta_j$. Let V_{th} denote the threshold for firing; that is $V_j(t_j^l) = V_{th}$. Let

$$A_T(t) = \sum_l A(t + lT) \quad \text{and} \quad E_T(t) = \sum_l E(t + lT).$$

Show that a phase-locked solution for the integrate-and-fire model must satisfy:

$$V_{th} = I_j - \frac{B}{1 - e^{-T}} + \sum_k C_{jk}A_T(\zeta_k - \zeta_j).$$

This equation is very similar to equation ** which provides a set of algebraic conditions for locking in weakly-coupled oscillators. The only difference here is that the coupling function A_T depends on the ensemble period. Bressloff and his collaborators have shown that many of the results proven for weakly coupled oscillators also hold for synaptically coupled integrate and fire models. As a project, you should evaluate some of these functions and look at, say, a pair of neurons or an array of neurons in a circle and compute the conditions for phaselocking. In the case of neurons in a circular array, you could also find the algebraic conditions for a traveling wave.

- Solve the identical frequency, noisy, Kuramoto density model numerically as follows. Assume that $\rho(\theta, t)$ can be written as a finite number of terms:

$$\rho(\theta, t) = \sum_{n=-N}^{N} p_n(t) e^{in\theta}.$$

Write

$$H(\phi) = \sum_m h_m e^{im\theta}.$$

Show that

$$\int_0^{2\pi} H(\phi - \theta)\rho(\phi, t)\ d\phi = 2\pi \sum_n h_{-n} p_n(t) e^{in\theta}.$$

From this, you should be able to write a series of ordinary differential equations for $p_n(t)$ satisfying:

$$p_n'(t) = -\sigma^2 n^2/2 p_n - 2\pi i n \sum_k h_{-k} p_k p_{n-k}.$$

Write these in real coordinates to get $2N + 1$ differential equations. If, for example, $H(\phi) = K \sin\phi$, then h_k vanishes except when $k = \pm 1$ so this is a very simple set of equations. In the case for which H is the pure sine model, show that the equations reduce to:

$$p_n' = -\sigma^2 n^2/2 p_n + K\pi n[p_1 p_{n-1} - p_{-1} p_{n+1}].$$

Finally, since H is odd, we can assume that the density is symmetric so that $p_{-j} = p_j$ and thus, this becomes a set of N ODEs:

$$p_n' = -\sigma^2 n^2/2 p_n + K\pi n p_1[p_{n-1} - p_{n+1}], \quad , n = 1, \ldots, N.$$

The end conditions are $p_0 = 1/(2\pi)$ and $p_{N+1} = 0$. The condition at $n = 0$ comes from the fact that

$$\int_0^{2\pi} \rho(\theta, t)\ d\theta = 1.$$

The condition at $n = N + 1$ is just our truncation. Use whatever methods you have at your disposal (analytic, numerical) to study the stability of the state $p_j = 0$, $j = 1, \ldots, N$ and compute the bifurcation diagram for K as a parameter. (Note that this numerical approximation of the PDE is considerably better than simply applying the method of lines to the density model.) If you are ambitious, you can try $H(\phi)$ as a sum of several sines and analyze the emergence of clustered states.

- (Noisy synchrony.) A model that has been used for a pair of coupled neurons in the presence of noise is:

$$d\theta_1 = (\omega_1 + H(\theta_2 - \theta_1))dt + \sigma dW_1$$
$$d\theta_2 = (\omega_2 + H(\theta_1 - \theta_2))dt + \sigma dW_2$$

where dW_j is white noise. Subtract these two equations and let $\phi = \theta_2 - \theta_1$ to obtain:

$$d\phi = (\delta - 2G(\phi))dt + \sigma\sqrt{2}dW$$

where $\delta = \omega_2 - \omega_1$ and $G(\phi)$ is the odd part of $H(\phi)$. The $\sqrt{2}$ factor arises because the sum of two wiener processes with unit variance and zero mean is also a wiener process with variance 2. Write a Fokker-Planck equation for this Langevin equation. For the case $\delta = 0$ write the steady state probability density for ϕ. (The more general case is doable but not so compactly.) Pfeuty et al have shown that this density function is related to the spike-time cross correlation of the two neural oscillators.

9.6 Exercises

1. Suppose that $X_0(t)$ is a $T-$periodic solution to the differential equation:

$$\frac{dX}{dt} = F(X)$$

where $F(X)$ is C^1. Show that $X_0(t + t_0)$ is also a solution foe any number t_0. Let $A(t) = D_X F(X_0(t))$ be a the matric formed by linearizing the above ODE around the limit cycle. Show that

$$\frac{dY}{dt} = A(t)Y(t)$$

has a nontrivial periodic solution, $Y(t) = dX_0(t)/dt$. Consider the adjoint equation:

$$\frac{dX^*}{dt} = -A(t)^T X^*(t).$$

Show that if $X^*(t)$ is a periodic solution to the adjoint, then

$$X^*(t) \cdot \frac{dX_0}{dt} = 1$$

for all t.

2. Floquet theory is the periodic analogue of stability theory for fixed points. Floquet's theorem states the following: Consider the homogeneous linear periodic system:

$$\frac{dx}{dt} = A(t)x, \qquad A(t+T) = A(t), \quad T > 0. \tag{9.67}$$

Then every fundamental solution, $X(t)$ to (9.67)has the form

$$X(t) = P(t)e^{Bt}$$

where $P(t)$ is a $T-$periodic matrix and B is a matrix. The matrix $C = e^{BT}$ is called the monodromy matrix and the eigenvalues of C are called the Floquet

multipliers. If the Floquet multipliers are all inside the unit circle then the origin is an asymptotically stable solution to (9.67).

If $A(t)$ is as in the previous exercise, show that there is always at least one Floquet multiplier with value 1.

A classic result from linear differential equations is

$$\det X(t) = e^{\int_0^t \mathrm{Tr}\ A(s)\ ds} \det X(0).$$

Use this to show that a planar limit cycle:

$$u' = f(u,v) \quad v' = g(u,v)$$

is asymptotically stable if

$$\int_0^T f_u(t) + g_v(t)\ dt < 0.$$

Note that f_u means the partial derivative of $f(u,v)$ with respect to u evaluated along the limit cycle.

3. Show by direct calculation that the adjoint L^* of the operator L in equation (9.4) under the inner product (9.5) is:

$$L^* y = -\frac{dy(t)}{dt} - A(t)^T y(t).$$

4. Let $\Phi(t)$ ba a fundamental solution to the differential equation:

$$\frac{dX}{dt} = A(t)X(t).$$

Show that $\Psi(t) = \left(\Phi(t)^{-1}\right)^T$ satisfies the adjoint equation:

$$\frac{dY}{dt} = -A^T(t)Y(t).$$

Suppose that $A(t)$ is as in exercise 1 so that there is a unique (up to scalar factor) periodic solution to (9.67). Let the first column of $\Phi(t)$ be this periodic solution. Show that the first column of $\Psi(t)$ is also periodic.

5. Consider the normal form for a Hopf bifurcation in polar coordinates:

$$r' = r(1-r^2) \qquad \theta' = 1 + q(r^2 - 1).$$

Suppose that $(r(0), \theta(0)) = (r_0, \theta_0)$ and $r(0) > 0$. Find the asymptotic phase and use this to sketch the isochrons. (Hint: let $R = r^2$ and rewrite the equations in terms of R.) When $q = 0$, this oscillator is sometmes called the radial isochron clock. Why?

6. Consider the LIF model:
$$\tau \frac{dV}{dt} = I - V$$
with $I > 1$ such that when $V = 1$, it is reset to 0. Define phase zero as the moment of reset to 0. Suppose that at time (phase) $t < T$ the voltage is incremented by an amount a. If $V + a > 1$ the voltage is immediately reset to 0. Compute the PTC for this model and show that for any $a > 0$, the PTC is type 0.

7. Consider the model oscillator
$$r' = r(1 - r) \quad \theta' = 1.$$
The period of this is 2π. In rectangular coordinates, $(u, v) = r(\cos\theta, \sin\theta)$, we define the zero phase to be the peak of $u(t)$. Thus, $\theta = 0$ is the zero phase. Suppose at time (phase) t $u(t)$ is instantly incremented by an amount a. Compute the PTC for this model as a function of a. For what values of a is this type 1 resetting? Can you offer a geometric interpretation of this?

8. Consider the QIF on the whole line:
$$\frac{dV}{dt} = V^2 + I$$
where $I > 0$ and such that when $V = +\infty$ it is reset to $-\infty$. Define phase zero to be the time of reset. You have already shown that the period of this oscillator is $T = \pi/\sqrt{I}$. Suppose that at time (phase) $t \in [0, T)$, the voltage is instantly incremented by an amount a. Compute the PTC for this and show that no matter how big a is, it is always type 1 resetting.

9. Davis Cope derives a formula for the adjoint equation for arbitrary nonlinear planar systems, $u' = f(u, v)$, $v' = g(u, v)$. He shows that
$$\begin{pmatrix} u^*(t) \\ v^*(t) \end{pmatrix} = \begin{pmatrix} \frac{u'(t)}{u'(t)^2+v'(t)^2} \\ \frac{v'(t)}{u'(t)^2+v'(t)^2} \end{pmatrix} + c(t) \begin{pmatrix} -v'(t) \\ u'(t) \end{pmatrix} \tag{9.68}$$
where $c(t)$ is periodic and satisfies:
$$\frac{dc}{dt} = -(f_u + g_v)c + \frac{2u'(t)v'(t)[f_u - g_v] + (v'(t)^2 - u'(t)^2)[f_v + g_u]}{(u'(t)^2 + v'(t)^2)^2}. \tag{9.69}$$
Here f_u is the derivative of $f(u, v)$ with respect to u evaluated along the limit cycle. f_v, g_u, g_v are similarly defined. Prove this formula satisfies the adjoint equation:
$$u_t^* = -f_u u^* - g_u v^*, \quad v_t^* = -f_v u^* - g_v v^*$$
along with the condition that $u^*u' + v^*v' = 1$. Also, prove that if the limit cycle is asymptotically stable, then the equation for $c(t)$ has a periodic solution.

10. We saw how a ring model has a strictly positive PRC. So, suppose that you are given a model with a continuous positive PRC, $\Delta(t)$. Given the positive PRC, does there exist a function $f(x) > 0$ such that the ring model

$$x' = f(x)$$

has the given PRC? (Note that the ring length is unspecified and it depends on the choice of PRC.) For the most part, you cannot arrive at a closed form solution for $f(x)$. However, for some problems, it is possible. Try, $\Delta(t) = a + t(1-t)$. Try $\Delta(t) = \exp(t)$.

11. Compute the adjoint for

    (a) the LIF model:

$$\tau \frac{dV}{dt} = V_0 - V$$

    with the condition that if $V(t) = V_{spike} < V_0$, the voltage is reset to V_{reset}.

    (b) the QIF model with finite reset:

$$\frac{dV}{dt} = aV^2 + I$$

    with $I > 0$ and such that if $V = V_{spike}$ then V is reset to V_{reset}.

12. Ermentrout et al considered the QIF with infinite reset and with a delayed inhibition. Consider

$$\frac{dV}{dt} = V^2 + I$$

such that at time $\tau < T$ after firing, the voltage is decremented by an amount $b > 0$. If T is the period of the oscillation without the inhibition, compute the period as a function of τ and b. For τ, b fixed, compute the PRC for this model for a stimulus which arrives at time t after the spike and increments V by $a > 0$. How does the shape of this PRC compare to the uninhibited PRC.

13. In this exercise, you consider the Traub model for hippocampal pyramidal cells (see the appendix for the equations) in which a small high-threshold calcium current is added (to produce calcium only when the cell spikes) and two types of adaptation are included. There is a M-type voltage dependent calcium current acting at rest and a calcium-dependent potassium current acting only when there is a spike. The conductances for these are respectively g_m and g_{ahp}. You should first compute the bifurcation diagram for this model when both are set to zero as the current varies. Now change the adaptation to $0.5, 1.0, 1.5$ and compute the bifurcation diagram. Note that the onset of spiking is still via a saddle-node. Do a similar analysis with g_m and see that the onset of spiking is via a Hopf bifurcation. Pick $g_{ahp} = 0, g_m = 0$ and add sufficient current to get a 40 Hz oscillation. Compute the adjoint. Add $g_{ahp} = 0.5$ and enough current so that the frequency stays at 40 Hz. Compute

the adjoint and compare to the adaptation-free adjoint. Finally, set $g_{ahp} = 0$ and $g_m = 0.5$ and add sufficient current to keep the frequency at 40 Hz. Compute the adjoint. Thus show that the type of adaptation has a drastic effect on the adjoint.

14. In the previous exercise, you show how some outward currents can affect the PRC. Take the above Traub model without the calcium and adaptation currents. Add to this the sag current (which is an inward current - this is in the appendix in the sag+inward rectifier model) using the McCormick parameters and pick $g_h = 4$. Apply current so that the frequency is 40 Hz. Compute the adjoint. You should see that there is a negative region in it. Check the nature of the bifurcation to a limit cycle. Is it now a Hopf? Conclude that like the $M-$type potassium current (previous exercise), the sag converts a saddle-node limit cycle to a Hopf.

15. Derive the analogue of equation (9.21) when the oscillators have slightly different periods, say, T_0 and $T_0 + c$ Suppose $\Delta(\phi) = a \sin \phi$ with $-1 < a < 0$. Study the existence of fixed points as c varies with a held fixed. Use a computer to solve for the fixed points and determine the maginitude of c such that there exists a stable fixed point.

16. Suppose the PRC is $\Delta(\phi) = b(1 - \cos \phi)$. What is the behavior of the map (9.21)? Can you prove that the synchronous state is asymptotically stable? (Hint: What is the behavior of the map $x \to x + cx^2$?)

17. (i) Consider the map (9.27) and use $d(\phi) = a \sin 2\pi\phi$. For what values of a is synchrony a stable fixed point when $\rho = \omega_1/\omega_2 = 1$. Fix $a = -.1$ and vary ρ. Plot the map and figure out for what values of ρ there is a saddle-node and locking is lost. You should be able to do this analytically, since a saddle-node occurs when (9.28) is exactly equal to 1. (ii) Suppose that $d_j(\phi) = a_j \sin 2\pi\phi$. Even though the two PRCs are different, show that synchrony is still a solution and find conditions for which it is stable.

18. Derive a map for 2:1 locking of two oscillators satisfying (9.25), (9.26) with $\omega_1 \approx 2\omega_2$. That is suppose the firing pattern is 1 1 2 and so on. Let ϕ denote the phase of 2 when 1 fires the first time. Assume that ϕ is close enough to 0.5 so that oscillator 1 fires *again* before oscillator 2 fires. Use this sequence to devise a map for ϕ. Find a condition like (9.28) for determining stability. Suppose that the normalized PRC is an odd periodic function so that $d(0) = d(1/2) = 0$. Show that if the frequency ratio is exactly 2:1, then $\phi = 1/2$ is the fixed point.

19. In order to better understand the shape of the map $M(t)$ in section x.2.3, we will examine the behavior near threshold. Recall that the I cell is a class I neuron so that at threshold, it undergoes a saddle-node bifurcation. Thus, we approximate its dynamics as

$$V' = qV^2. \qquad (*)$$

Suppose that after it fires, the I cell is set to $V = -V_0 < 0$. The larger is V_0 the more refractory the cell is. Now, t^* milliseconds later the second E spike arrives to the I cell and suppose that all it does is increment $V(t)$ by an amount A. If $V(t^*) + A > 0$, then the I cell will fire (reach infinity) in finite time. Compute this firing time, t_f and show that it can be written as

$$t_f(t^*) = c + \frac{a}{t^* + b}$$

where c, a, b are parameters. In particular, the parameter b can be positive or negative. This simple function provides a good fit to the map $M(t)$ and each parameter has a nice physical interpretation in terms of the size of the input A and the degree of refractoriness, V_0. (Hint: Solve (*) starting at $t = 0$ with the given inital data up to t^*. Then increment $V(t)$ by A and solve (*) up to the point that $V(t)$ becomes infinite. This is $t_f(t^*)$.)

20. What is the nature of the bifurcation which occurs in the map (9.29) when $M'(\tau) = -1$? (If you need to recall what sorts of bifurcations occur in maps, see the appendix for a review of dynamical systems.) Since we know that for sufficient delay, the synchronous state can be stable, explain why a very long delay (thus, where $M'(t)$ is small) might also be bad. (Hint: If $M'(t) = -\epsilon$ where ϵ is a small positive parameter, then the map reduces to:

$$z_{n+1} = \mu - z_n + 2\epsilon z_n$$

What is the fixed point for this and how long does it take to settle into it?)

21. (Mirollo and Strogatz) (a) Analyze the map for two coupled Mirollo-Strogatz oscillators when $\epsilon < 0$. (b) Analyze the map for $f''(t) > 0$ for $\epsilon < 0$ and $\epsilon > 0$.

22. (Mirollo and Strogatz II.) Plot $h(\phi)$ and $R(\phi)$ when

    a.

    $$f(t) = \frac{1 - e^{-ct}}{1 - e^{-c}}$$

    for different values of c and ϵ. This, of course, is the profile for the LIF. Explicitly compute the interval of existence for $R(\phi)$.

    b. Repeat (a) for the firing map:

    $$f(t) = \frac{\tan[a(x - 1/2)] + \tan(a/2)}{2\tan(a/2)}$$

    where $0 < a < \pi$. This is the map which occurs for a quadratic integrate-and-fire model with finite reset. It is both concave and convex!

23. Using the following model for the PRC:

$$V^*(t) = 1 - cos(t) - sin(t) + sin(2t)/2$$

and $s(t) = I_0 t e^{-\beta t}$ as the synaptic current,compute $H_{odd}(\phi)$. (Hint, use formula (9.44) and set $\alpha = \beta$.) Compute the derivative of H_{odd} at $\phi = 0$ and $\phi = \pi$ and plot the result for excitatory ($I_0 = 1$) and inhibitory ($I_0 = -1$) coupling as a function of β. Recalling that β large means low frequency, conclude that this simple model with inhibition could explain the results of the finger tapping experiment.

24. Find conditions for when the pronk is stable. Prove that the walk exists as a solution to equation (9.45) if and only if $H_b(x) = H_c(x)$. Show that under these assumptions the pace, trot, and bound all exist as phase-locked solutions. Find conditions such that the walk is asymptotically stable. Prove that if the trot is asymptotically stable, then so is the pace. Prove that it is possible for the bound to be stable, but the trot and pace could be unstable. Find conditions such that the walk is stable and the trot/pace is unstable and vice versa. (Hint: you will have a 4×4 matrix, but it will have a great deal of symmetry so you should be able to explicitly write down the eigenvalues since the eigenvectors will be chosen from the 4^{th} roots of unity.)

25. Make a model consisting of two sets of the excitatory-inhibitory pair (9.46) and couple them with all four types of coupling (one at a time), E-¿E, E-¿I, etc and start with a variety of initial conditions. Describe all the stable states and compare this to the predictions you would get from figure 9.16.

26. Consider the anisotropic chain for $j = 1, \ldots, N$:

$$\theta_j' = \omega + H_a(\theta_{j+1} - \theta_j) + H_b(\theta_{j-1} - \theta_j).$$

Suppose that the end conditions are either periodic $\theta_0 = \theta_N$ and $\theta_{N+1} = \theta_N$ or reflecting, $\theta_0 = \theta_1$ and $\theta_{N+1} = \theta_N$. Prove that the synchronous solution is asymptotically stable if and only if $H_a'(0) > 0$ and $H_d'(0) > 0$.

27. Consider the same chain as in the previous problem with periodic boundary conditions. Show that there is a wave-like solution of the form, $\theta_j = \Omega t + 2\pi j/N$, determine Ω and also the stability of this solution. (This leads to a tridiagonal matrix, whose eigenvalues are pretty easy to compute.) If synchrony (previous problem) is stable, then you should be able to prove that this traveling wave is also stable if N is sufficiently large.

28. Show that a 4×4 network of nearest neighbor phase oscillators has the following phase-locked pattern and compute the unknown quantity $0 < \xi < \pi/2$. Prove that this solution is also asymptotically stable using theorem ???.

$$\begin{array}{cccc} 0 & \xi & \pi/2 - \xi & \pi/2 \\ -\xi & 0 & \pi/2 & \pi/2 + \xi \\ 3\pi/2 + \xi & 3\pi/2 & \pi & \pi - \xi \\ 3\pi/2 & 3\pi/2 - \xi & \pi + \xi & \pi \end{array}$$

29. Show that the only terms contributing to instability of the asynchronous state for the all-all coupled oscillator model with noise and no heterogeneity are the

odd parts of $H(\phi)$. Equation (9.60) should provide the crucial clues. Compute the critical values of K for each n.

30. (Two-cluster states.) Suppose that there are N all-all oscillators with identical frequencies and no noise:

$$\theta_j' = \omega + \frac{1}{N}\sum_{k=1}^{N} H(\theta_k - \theta_j).$$

Let us look for a solution such that the first m oscillators are synchronized and the remaining $N-m$ oscillators have a phase difference ϕ with respect to the first group. As long as $m < N$ and $\phi \neq 0$, this is called a two-cluster state. Let $p = m/N$. Show that a two cluster state exists if and only if

$$\Omega = \omega + pH(0) + (1-p)H(\phi)$$
$$\Omega = \omega + pH(-\phi) + (1-p)H(0).$$

Here Ω is the unknown ensemble frequency. You can parametrize this using p as:

$$p = \frac{H(\phi) - H(0)}{H(\phi) + H(-\phi) - 2H(0)}.$$

Show that there is always a solution to this for $\phi = \pi$ and $p = 1/2$. This is a balanced cluster state with half of the oscillators in antiphase with the others. If H is an odd function, show that p can be anything and $\phi = \pi$ (since $H(\pi) = H(0) = 0$). Stability of the general clustered state is a more difficult problem, but with some decent linear algebra skills, you should be able to do it. The stability matrix has a nice simple block form.

31. Derive equation (9.65) from (9.64)

32. Derive the equation in the text for $Q(\nu)$ when $W(x) = \exp(-|x|/\sigma)/(2\sigma)$ and $\alpha(t) = \beta\exp(-\beta t)$ Plot the wave speed as a function of the ratio, V_T/V_{drive}.

33. Suppose that $W(x) \geq 0$ and $A(t) \geq 0$, $A(0) = 0$ and both functions are integrable over $[0, \infty)$. Consider the expression:

$$Q(\eta) = \int_0^\infty W(y)A(y/\nu)\, dy.$$

Prove that $Q(0) = 0$ and $Q(\infty) = 0$. What happens if you relax the assumption that $A(0) = 0$? If $W(y) > 0$ and $A(t) > 0$ except at $t = 0$ where it vanishes, prove $Q(\nu) > 0$ for $0 < \nu < \infty$.

34. Suppose that $\alpha(t) = \beta\exp(-\beta(t - \tau_d))$ where τ_d is a delay (fixed and space-independent). Analyze the existence and stability of the one spike waves in this case. (See Golomb & Ermentrout, 2000).

35. Suppose that there is a delay due to the conduction velocity so that it depends on distance. Justify the expression below for $S(x,t)$ below and analyze the existence of traveling waves in this case when there is an exponential weight $W(x) = \exp(-|x|/\sigma)/(2\sigma)$ and $\alpha(t) = \exp(-\beta t)$.

$$S(x,t) = \int_{-\infty}^{\infty} W(x-y)\alpha(t - T(y) - |x-y|/c)\, dy$$

where $c > 0$ is the conduction velocity.

36. (Instability of the slow wave.) In this exercise, you prove that the slow wave is unstable by showing that there is a real positive root to the Evans function:

$$E(\lambda) = \int_0^{\infty} W(y)A'(y/\nu)[1 - e^{-\lambda y}]\, dy.$$

Consulting figure 9.22, it is clear that for the slow wave, $Q'(\nu_{slow}) > 0$. We suppose that $W(x)$ is monotone decreasing for $x > 0$, differentiable, and that $A(t) > 0$ for $t > 0$.

(a) Clearly $E(0) = 0$. As $\lambda \to \infty$,

$$E(\lambda) \to \int_0^{\infty} W(y)A'(y/\nu)\, dy \equiv E_{\infty}.$$

By integrating E_{∞} by parts, conclude that $E_{\infty} > 0$.

(b) Differentiate $Q(\nu)$ with respect to ν and differentiate $E(\lambda)$ with respect to λ. Show that the sign of $E'(0)$ is the opposite of $Q'(\nu)$.

(c) Use the previous two parts of this exercise to show that at $\nu = \nu_{slow}$, $E(\lambda) < 0$ for small positive λ and $E(\lambda) > 0$ for large λ. Thus conclude that there is a real positive value of λ such that $E(\lambda) = 0$ and that the slow wave is unstable.

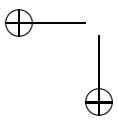

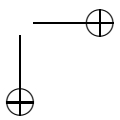

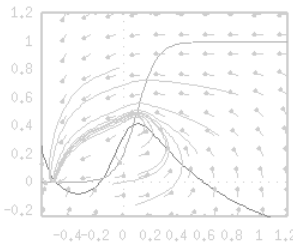

Chapter 10

Networks

10.1 Introduction

In this chapter, we discuss a very different approach to studying networks of neurons than that presented in the previous chapter. In the previous chapter, we assumed that each cell is an intrinsic oscillator, the coupling is weak and details of the spikes are not important. By assuming weak coupling, we were able to exploit powerful analytic techniques such as the phase response curve and the method of averaging. In this chapter, we do not assume, in general, weak coupling or the cells are intrinsic oscillators. The main mathematical tool used in this chapter is geometric singular perturbation theory. Here, we assume that the model has multiple time-scales so we can dissect the full system of equations into fast and slow subsystems. As we shall see, this will allow us to reduce the complexity of the full model to a lower-dimensional system of equations; these will be equations for the slow variables. We have, in fact, introduced this approach in earlier chapters when we discussed bursting oscillations and certain aspects of the Morris-Lecar model.

Complex population firing patterns, similar to those described in this and subsequent chapters, are believed to play a critical role in many brain functions. For example, oscillatory behavior has been observed in many systems; it has been implicated in sensory processing, the generation of sleep rhythms, Parkinsonian tremor and motor activity. The spatiotemporal structure of spiking activity can be very complicated. For example, neurons may fire action potentials in a synchronous or partially synchronous manner, or the spiking of different neurons may be uncorrelated. The activity may propagate through the population in a wave-lake manner or may remain localized.

We note that population rhythms arise through interactions between three network components. These are: (1) the intrinsic properties of cells within the network; (2) the synaptic properties of connections between neurons; and (3) the topology of network connectivity. Each of these may depend on numerous parameters and the first two usually involve multiple time-scales. We have described intrinsic properties of cells in the preceding chapters. A cell's dynamics depends

primarily on its channel gating variables. These may activate or inactivate on disparate time-scales and a single cell may exhibit a variety of firing patterns including continuous spiking, bursting oscillations or even chaotic dynamics. As described in Chapter ??, there are several classes of synapses. Synapses may be chemical or electrical and chemical synapses may be excitatory or inhibitory. Different types of excitatory or inhibitory synapses have distinct properties that determine how one cell influences another. Finally, we note that there are many possible classes of network architectures. The connectivity may be sparse or dense; that is, each cell may communicate with a small number or a large number of other cells. The connectivity may be random or it may be highly structured. We also note that a given neuronal system may include many different types of cells with different types of synaptic connections.

A goal of this chapter is to consider reduced two-variable neuron models and classify the types of activity patterns that emerge. We also wish to understand how the activity depends on the types of cells and synapses in the network, as well as the network architecture. One traditional view is that excitatory synapses always tend to promote synchronous activity in which different cells fire spikes at the same time. Inhibitory synapses, on the other hand, are thought to promote out-of-phase behavior. This traditional view is, in fact, often true. However, simple examples demonstrate that it may not always be the case. The network behavior may depend not only on whether the synapses are excitatory or inhibitory, but on the rates at which the synapses turn on or turn off. The dynamics also depends on how synaptic properties interact with intrinsic properties of cells within the network.

10.2 Mathematical Models for Neuronal Networks

Recall that a network consists of three components. These are: (1) the individual cells within the network; (2) the synaptic connections between cells; and (3) the network architecture. We now describe how each of these components is modeled for the analysis presented in this chapter. We also describe different categories of cells, synapses and network architectures.

Individual Cells

Throughout this chapter, we consider a general two-variable neuron model of the form

$$\begin{aligned} \frac{dv}{dt} &= f(v,w) \\ \frac{dw}{dt} &= \epsilon g(v,w). \end{aligned} \tag{10.1}$$

We have seen several examples of models that can be written in this form. This includes the Morris-Lecar equations. We write the equations in a rather general form to emphasize that the analysis does not depend on the specific forms of the equations.

In (10.1), v is the membrane potential of the cell, w is a channel gating variable and ϵ is a small positive parameter. Hence, w represents a channel state variable that

either activates or inactivates on a time-scale slower than the other processes. The main mathematical technique used throughout this chapter is geometric singular perturbation theory.

We need to make some assumptions on the nonlinear functions f and g. We assume that the v-nullcline $\{f = 0\}$ defines a cubic-shaped curve and the w-nullcline $\{g = 0\}$ is a monotone increasing curve. Moreover, $f > 0$ ($f < 0$) below (above) the v-nullcline and $g > 0$ (< 0) below (above) the w nullcline. Note that these assumptions are satisfied by the Morris-Lecar model for a robust range of parameter values.

We would like to understand how firing properties of individual cells influence network behavior. For this reason, it would be useful to somehow classify the firing properties of cells. One simple way to do this is that the cells may be *oscillatory* or *excitable*; that is, a cell may or may not fire intrinsically without any synaptic input. Recall that this depends on whether (10.1) has a fixed point that lies along the middle or left branches of the cubic shaped v-nullcline.

If (10.1) is oscillatory, then there are several possible ways to classify the dynamics. One is in terms of the frequency of oscillations. Another is in terms of the duty-cycle. This is defined to be the ratio of the time the cell spends in the active phase over the time it spends in the silent phase. We sometimes interpret oscillations with a long duty cycle as corresponding to bursting activity and oscillations with a short duty cycle as corresponding to a spiking neuron.

In the following sections, we will demonstrate that the frequency or duty cycle of a cell may have a significant influence on network behavior. In particular, it may be crucially important in determining whether neurons synchronize or not.

Synaptic Connections

We model the synaptic current as described in Chapter ??. Most of the discussion will be concerned with chemical synapses. In this case, the synaptic current can be written as:

$$I_{syn} = g_{syn} s(V_{post} - v_{syn}) \tag{10.2}$$

where g_{syn} is a constant maximal conductance, V_{post} is the membrane potential of the post-synaptic cell and v_{syn} is the synaptic reversal potential. The dependent variable s represents the fraction of open channels and, as in (??), depends on the presynaptic membrane potential. We will usually assume that s satisfies a first order equation of the form:

$$\frac{ds}{dt} = \alpha(1 - s)H_\infty(V_{pre} - V_T) - \beta s. \tag{10.3}$$

Here, α and β represent the rates at which the synapse turns on and turns off, respectively. Recall that different types of synapses may turn on or turn off at very different rates. For example, GABA_B synapses are slow to activate and slow to turn off, compared with GABA_A and AMPA synapses. We assume that H_∞ is a smooth approximation of the Heaviside step function (or actually is the Heaviside step function) and V_T is some threshold.

The model of a pair of mutually coupled neurons is then:

$$\begin{aligned}\frac{dv_i}{dt} &= f(v_i, w_i) - g_{syn} s_j (v_i - v_{syn}) \\ \frac{dw_i}{dt} &= \epsilon g(v_i, w_i) \\ \frac{ds_i}{dt} &= \alpha(1 - s_i) H_\infty (v_i - V_T) - \beta s_i\end{aligned} \tag{10.4}$$

Here i and j are 1 or 2 with $i \neq j$. We are assuming that the cells are identical so that the nonlinear functions f and g do not depend on the particular cell. Later, we consider networks with heterogeneities.

Note that the coupling between the cells is through the synaptic variables s_j. In particular, suppose that cell 1 is the pre-synaptic cell. When cell 1 fires a spike, its membrane potential v_1 crosses the threshold V_T. The synaptic variable s_1 then activates at a rate that depends on both α and β and this then changes the membrane potential of the cell 2, the post-synaptic cell. When cell 1 is silent, so that $v_1 < V_T$, then s_1 decays at the rate β.

We wish to classify different types of synapses in order to study how synaptic interactions influence network behavior. A traditional way to classify synapses is whether they are *excitatory* or *inhibitory*. This depends primarily on the synaptic reversal potential v_{syn}. For example, the reversal potential of the AMPA receptor is $V_{AMPA} = 0\ mV$. This is greater than the post-synaptic cell's resting potential, so the AMPA synapse is excitatory. The principal inhibitory synapses involve the neurotransmitter GABA. Recall that the reversal potential of GABA_A varies between -81 and $-60mV$; this is usually less than the cell's resting potential. However, there are examples of cells in which the GABA_A reversal potential is very near or even above rest and GABA_A synapses may be excitatory.

We can further classify synapses depending on the rates at which they activate or deactivate. For example, GABA_A synapses are often refereed to as fast-inhibitory synapses, while GABA_B synapses are referred to as slow-inhibitory synapses. As discussed above, the rates at which the synapses turns on or off depend on the parameters α and β.

We will also classify synapses as being *direct* or *indirect*. The synapses we have considered so far are direct synapses since they are activated as soon as a membrane crosses the threshold. To more fully represent the range of synapse dynamics observed biologically, it will sometimes be necessary to consider more complicated connections. These will be referred to as indirect synapses, and they are modeled by introducing a new independent variable x_i for each cell in the network. To model indirect synapses, we replace the third equation in (10.4) with following the equations for each (x_i, s_i):

$$\begin{aligned}\frac{dx_i}{dt} &= \epsilon\alpha_x(1 - x_i) H_\infty (v_i - V_T) - \epsilon\beta_x x_i \\ \frac{ds_i}{dt} &= \alpha(1 - s_i) H(x_i - \theta_x) - \beta s_i.\end{aligned} \tag{10.5}$$

The constants α_x and β_x are assumed to be independent of ϵ. The variable x

corresponds to a secondary process that is activated when transmitters bind to the postsynaptic cell. The effect of the indirect synapses is to introduce a delay from the time one cell jumps up until the time the other cell feels the synaptic input. For example, if the first cell jumps up, a secondary process is turned on when v_1 crosses the threshold V_T. The synapse s_1 does not turn on until x_1 crosses some threshold θ_x; this takes a finite amount of (slow) time since x_1 evolves on the slow time scales, like the w_i.

Network Architecture

There are many possibilities for network architecture. For example, the architecture may be *global* or *local*, *dense* or *sparse*, *random* or *structured*. In general, we model an arbitrary network as:

$$\begin{aligned}
\frac{dv_i}{dt} &= f_i(v_i, w_i) - g^i_{syn}(\sum W_{ij} s_j)(v_i - v^i_{syn}) \\
\frac{dw_i}{dt} &= \epsilon g_i(v_i, w_i) \\
\frac{ds_i}{dt} &= \alpha_i(1 - s_i)H_\infty(v_i) - \beta_i s_i
\end{aligned} \tag{10.6}$$

Here we are assuming that the cells are heterogeneous so that the nonlinear functions f and g may depend on the cell i. Moreover, the reversal potential v_{syn}, as well as the rates at which the synapses turn on and turn off, depends on the cell, so some of the cells may be excitatory while some of the cells may be inhibitory. The sum in (10.6) is over all presynaptic cells and the constants W_{ij} represent synaptic weights. They can viewed as the probability that there is a connection from cell j to cell i.

It is sometimes convenient to consider the limiting equations as the number of cells in the network becomes unbounded. We assume that the cells lie in some domain $\mathcal{D}$ and $v(x,t)$ represents the membrane potential of the cell at position $x \in \mathcal{D}$ at time t. We now assume that the cells are homogeneous; it is straightforward to generalize this to heterogeneous networks. Then, after an appropriate rescaling, (10.6) becomes

$$\begin{aligned}
\frac{\partial v}{\partial t} &= f(v(x,t), w(x,t)) - g_{syn}(v(x,t) - v_{syn}) \int_{y \in \mathcal{D}} W(x,y) s(y,t) dx \\
\frac{\partial w}{\partial t} &= \epsilon g(v(x,t), w(x,t)) \\
\frac{\partial s}{\partial t} &= \alpha(1 - s(x,t))H_\infty(v(x,t) - V_T) - \beta s(x,t).
\end{aligned} \tag{10.7}$$

10.3 Examples of Firing Patterns

We now describe some of the firing patterns that can arise in a network of the form (10.6). In the following examples, each cell is modeled by the Morris-Lecar equations. We begin by considering a network with just two mutually coupled cells.

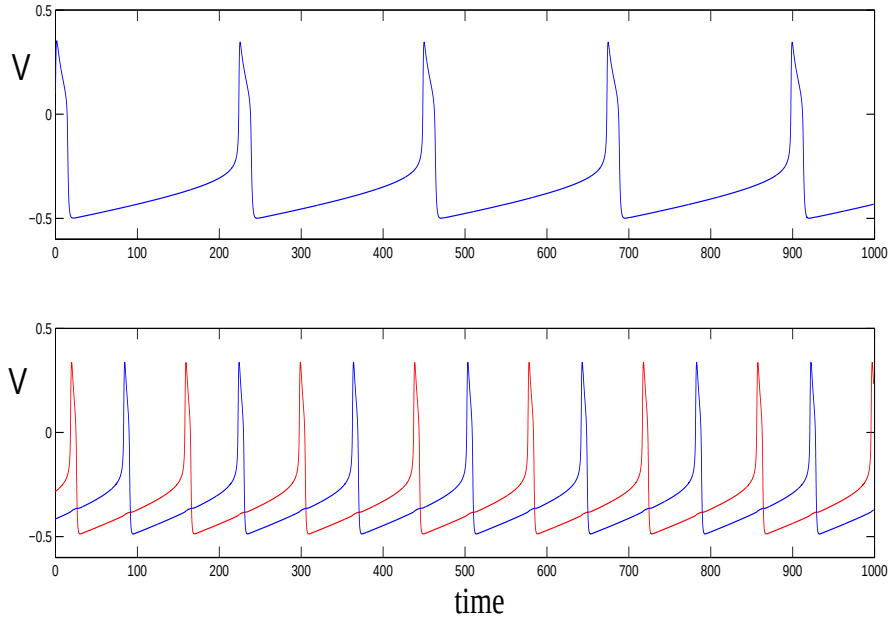

Figure 10.1. *Solutions of a network of two mutually coupled Morris-Lecar neurons with excitatory coupling. A) Synchronous solution. The membrane potentials are equal so only one is shown. B) Anti-phase behavior. The solutions shown in A) and B) are for the same parameter values but different initial conditions. Hence, the system is bistable.*

The model can then be written as:

$$\begin{aligned}
\frac{dV_i}{dt} &= I - I_{ion}(V_i, w_i) - g_{syn} s_j (V_i - v_{syn}) \\
\frac{dw_i}{dt} &= (w_\infty(V_i) - w_i)/\tau_w(V_i) \\
\frac{ds_i}{dt} &= \alpha(1 - s_i) H_\infty(V_i - V_T) - \beta s_i
\end{aligned} \tag{10.8}$$

where i and j are 1 or 2 and $i \neq j$.

Figure 10.1 shows two solutions of (10.8) in which $v_{syn} = .5$. In this case the synapses are excitatory. A stable synchronous solution is shown in Figure 10.1A. Here, $(v_1(t), w_1(t)) = (v_2(t), w_2(t))$ for all t. Figure 10.1B shows a solution with anti-phase behavior. This solution is stable; moreover, the synchronous solution is also stable. Hence, for this choice of parameters, the system is bistable.

Figure 10.2 shows solutions of (10.8) in which $v_{syn} = -.5$ so that the synapses are inhibitory. The other parameters are ??=??. We note that for these parameter

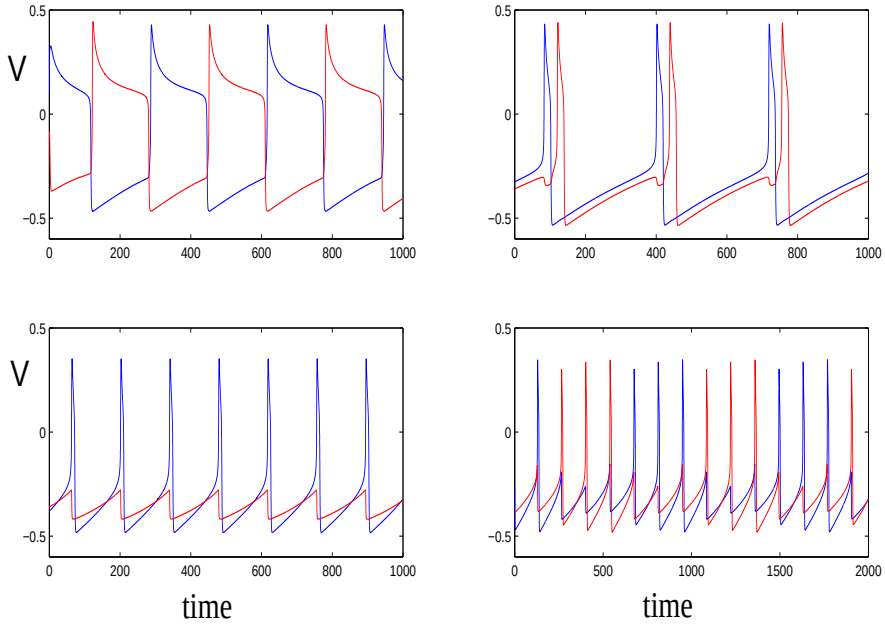

Figure 10.2. *Solutions of a network of two mutually coupled Morris-Lecar neurons with inhibitory coupling. A) Each cell fires due to post-inhibitory rebound. B) An almost-synchronous solution. C) A suppressed solution. D) The cells take turns firing three spikes while the other cell is silent.*

values, a single cell, without any input, is excitable; that is, it does not generate oscillations. Therefore a network of two cells, which by themselves are silent, can generate oscillatory behavior with inhibitory synaptic coupling. In Figure 10.2A, the cells take turns firing. The mechanism underlying this rhythm is *post-inhibitory rebound* (PIR). As one cell spikes, it sends inhibition to the other cell, thereby hyperpolaring the silent cell's membrane potential. When the active cell stops firing, it releases the silent cell from inhibition so that the silent cell rebounds and generates an action potential. Mechanisms underlying PIR will be described later.

Figure 10.2B shows a solution in which one of the cells fire shortly after the other; there is then a delay until the first cell fires again. This is sometimes referred to as an *almost synchronous solution*. We note, in fact, that an inhibitory network can generate a stable synchronous solution. In Figure 10.2C, one of the cells fires periodically and the other cell never generates an action potential. This is sometimes referred to as a *suppressed solution*. Finally, Figure 10.2D illustrates a more exotic solution in which one cell generates three spikes while the other cell is silent and then the roles of the cells are reversed. All of the solutions shown in Figure 10.2 are stable.

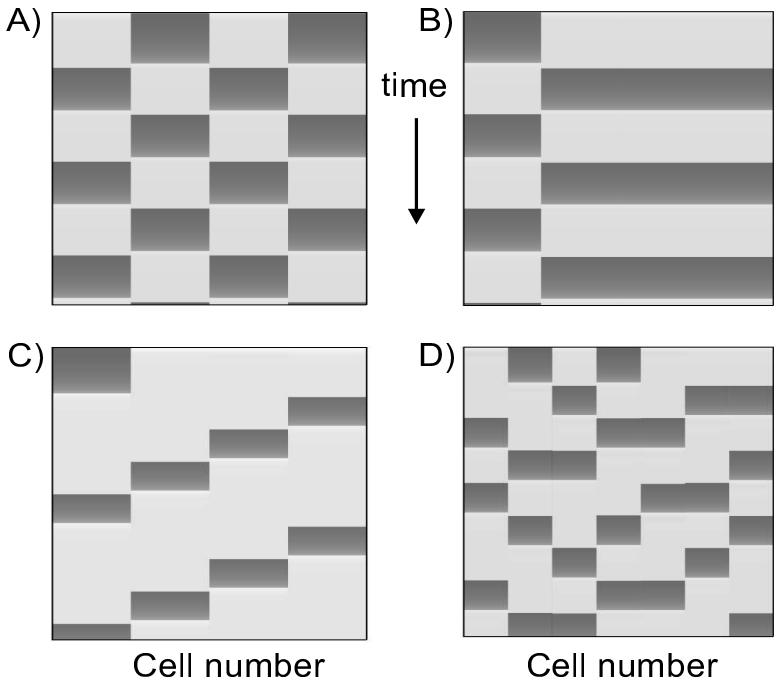

Figure 10.3. *Firing patterns in inhibitory network. A) and B) show examples of clustering. Wave-like is shown in C) and dynamic clustering in D).*

We next describe firing patterns in larger networks with inhibitory connections. An example of *clustering* is shown in Figure 10.3 A and B. Here, the network of four breaks up into different groups or clusters; cells within each cluster are synchronized but different clusters fire out-of-phase. We note that these two solutions correspond to the same network with the same parameter values. The only difference between the solutions is the initial conditions. Figure 10.3 C shows a solution in which the four cells take turns firing in a wave-like manner. Waves may arise in both excitatory and inhibitory networks. Figure 10.3 D shows an example of *dynamic clustering*. Here there are seven cells in the network ad different groups of cells take turns firing. However, membership of the groups change so that two different cells may fire together during the one episode but not fire together during later episodes.

10.4 Singular Construction of the Action Potential

The main mathematical tool that will be used throughout this chapter to analyze neuronal networks is geometric singular perturbation theory. Here one exploits the fact that neuronal systems typically involve separate processes that evolve on much different time-scales. For example, the membrane potential may jump-up or

jump-down on a much faster time-scale than some ionic gating or synaptic variable. By exploiting this discrepancy in time-scales, one can often reduce a complicated neuronal system to a lower-dimensional system of equations, one that is easier to analyze and implement numerically. We have, in fact, already seen examples of this method when we considered traveling wave solutions and bursting oscillations. Recall, for example, that for parabolic bursting, we reduced the full four-dimensional system to equations for just the two slow variables. Similar methods will be used to study networks of coupled cells.

In this section, we consider a single neuron modeled by (10.1). By considering a single neuron, we are able to illustrate important features of the geometric singular perturbation method with a rather simple example. We note that (10.1) is an example of a relaxation oscillator. The Morris-Lecar equations will be used for all of the numerics. The analysis, however, is quite general and does not depend on details of the equations. In what follows, we refer to the v-nullcline as '*the cubic*' and the minimum and maximum of the cubic as the *left-* and *right knee*, respectively.

Assume that the cubic intersects the w-nullcline at a single point that lies along its middle branch. This fixed point is unstable and there exists a stable periodic orbit. The periodic solution is shown in Figure 10.4A and its projection onto the phase-plane is shown in Figure 10.4B. Using geometric singular perturbation methods, we will give a rather explicit description of this periodic solution, in the limit $\epsilon \to 0$.

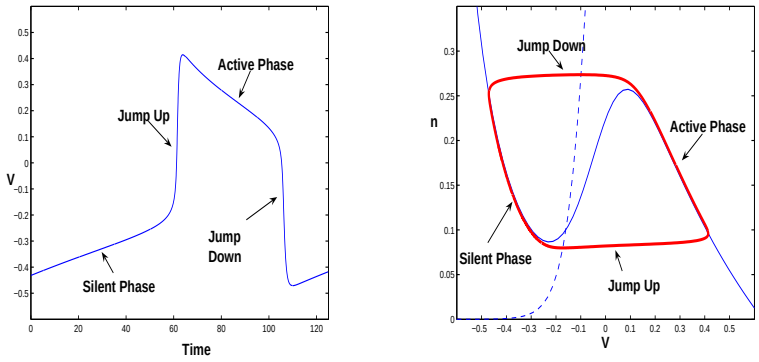

Figure 10.4. *Periodic solution of the Morris-Lecar equations corresponding to an action potential. The projection of this solution onto the* (v, w)*-phase plane is shown in B).*

We dissect the periodic orbit into four pieces; these are referred to as: (i) *the silent phase*, (ii) *the jump up*, (iii) *the active phase* and (iv) *the jump-down*. Note that during the silent and active phases, the solution lies close to the left and right branches of the cubic, while the jump-up and jump-down occur when the trajectory reaches the left and right knees. In order to obtain a more detailed description of each piece, we consider two time-scales: a fast time-scale corresponding to the original variable t and a slow time-scale defined as $\tau = \epsilon t$. The fast time-scale is

used to describe the evolution of the solution during the jumps up and down, while the slow time-scale is used to describe evolution during the silent and active phases.

First consider the slow time-scale. If we let $\tau = \epsilon t$ and then set $\epsilon = 0$, then (10.1) becomes:

$$\begin{aligned} 0 &= f(v,w) \\ \frac{dw}{d\tau} &= g(v,w). \end{aligned} \tag{10.9}$$

The first equation in (10.9) states that singular periodic orbit lies along the left and right branches of the cubic during the silent and active phases, respectively. The second equation determines the time evolution along these branches. This evolution can be written as a scalar equation for the single (slow) variable w. Suppose that the left and right branches can be written as $v = \Phi_L(w)$ for $w > w_L$ and $v = \Phi_R(w)$ for $w < w_R$, respectively. Here, w_L and w_R represent the positions of the left and right knees. Then (10.9) can be written as

$$\frac{dw}{d\tau} = w(\Phi_\alpha(w), w) \;\equiv\; \Lambda_\alpha(w) \tag{10.10}$$

where $\alpha = L$ or R.

Now consider the jumps up and down. These take place on the fast time-scale. Let $\epsilon = 0$ in (10.1) to obtain the reduced system:

$$\begin{aligned} \frac{dv}{dt} &= f(v,w) \\ \frac{dw}{dt} &= 0. \end{aligned} \tag{10.11}$$

The second equation in (10.11) implies that w is constant during the jumps. During the jump-up, $w = w_L$ and v is a solution of (10.11) that approaches the left knee as $t \to -\infty$ and approaches the right branch of the cubic as $t \to +\infty$. During the jump-down, $w = w_R$ and v is a solution of (10.11) that approaches the right knee as $t \to -\infty$ and approaches the left branch of the cubic as $t \to +\infty$.

An important feature of geometric singular perturbation theory is that it gives a systematic way to reduce complicated models to lower dimensional systems of equations. In the example illustrated here, the full model (10.1) is two-dimensional, while each piece of the singular periodic solution corresponds to a solution of a single differential equation: the jumps up and down satisfy the fast equation (10.11), while the silent and active phases correspond to solutions of the slow equation (10.9). We have therefore reduced the original two-dimensional model to four first-order equations. This may not seem like such a big deal, since two-dimensional systems can be easily analyzed using phase-plane methods; however, for larger cell models or networks of cells, such a reduction may be crucially important when analyzing the dynamics.

We conclude this section by considering how the geometric singular perturbation approach can be used to analyze the response of a neuron to a time-varying injected current. This analysis will be very useful when we consider networks of

cells. It will illustrate, with a simple example, how a neuron may respond to excitatory or inhibitory input.

Consider the system

$$\begin{aligned} \frac{dv}{dt} &= f(v,w) + I(t) \\ \frac{dw}{dt} &= \epsilon g(v,w). \end{aligned} \tag{10.12}$$

We assume that when $I(t) = 0$, the system is excitable; that is, the v- and w-nullclines intersect at a stable fixed point along the left branch of the cubic. We further assume that there exist I_0 and $T_{on} < T_{off}$ such that

$$I(t) = \begin{cases} I_0 & \text{if } T_{on} < t < T_{off} \\ 0 & \text{otherwise} \end{cases} \tag{10.13}$$

We consider two cases: either $I_0 > 0$, in which case the injected current is said to be *depolarizing*, or $I_0 < 0$ and the injected current is *hyperpolarizing*. Figure 10.5 illustrates the neuron's response when (top) $I_0 = .1$ and (bottom) $I_0 = -.1$. In the depolarizing case, the neuron fires an action potential immediately after the injected current is turned on. The cell then returns to rest. In the hyperpolarizing case, the neuron's membrane potential approaches a more negative steady state until the current is turned off, at which time the neuron fires a single action potential. This last response is an example of *post-inhibitory rebound*.

The geometric approach is very useful in understanding these responses. As before, we construct singular solutions in which ϵ is formally set equal to zero. The singular solutions lies along the left or right branches of some cubic-shaped nullcline during the silent and active phases, as shown in Figure 10.6. The cubics depend on the value of $I(t)$. We denote the cubic corresponding to $I = 0$ as C and the cubic corresponding to I_0 as C_0. Note that if $I_0 > 0$, then C_0 lies 'above' C, while if $I_0 < 0$, then C_0 lies 'below' C.

Consider the depolarizing case $I_0 > 0$. This is illustrated in Figure 10.6 (left). For $t < T_{on}$, $I(t) = 0$ and the solution lies at the fixed point p_0 along the left branch of C. When $t = T_{on}$, $I(t)$ changes to $I_0 > 0$ and the cubic switches from C to C_0. If the left knee of C_0 lies above p_0, then the cell jumps up to the right branch of C_0; this corresponds to the firing of an action potential. If the w-nullcline intersects C_0 along its left branch, then the cell approaches the stable fixed point along the left branch of C_0 until the input is turned off. It is possible that the w-nullcline intersects C_0 along its middle branch. In this case, the cell continues to oscillate, firing action potentials, until the input is turned off at $t = T_{off}$. The number of action potentials depends on the size of $T_{off} - T_{on}$. If the w-nullcline intersects C_0 along its right branch, then the cell will approach this fixed point until the input is turned off at $t = T_{off}$ and then return to rest.

Next consider the hyperpolarizing case $I_0 < 0$, shown in Figure 10.6 (right). In this case, C_0 lies below C and the w-nullcline intersects C_0 at a point denoted by p_1. At $t = T_{on}$, the solution jumps to the left branch of C_0 and then evolves along

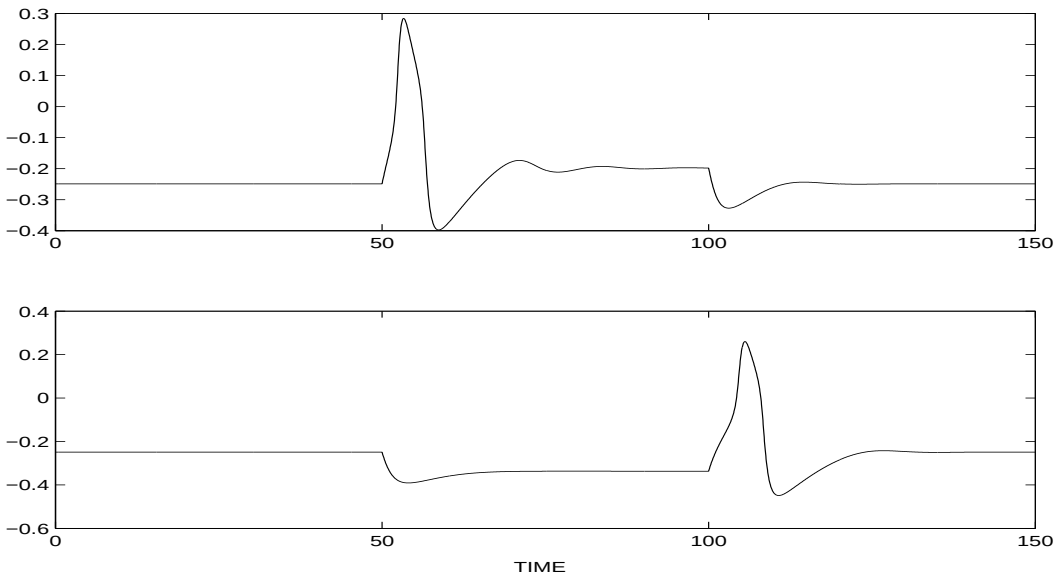

Figure 10.5. *Response of a model neuron to applied current. Current is applied at time $t = 50$ and turned off at $t = 100$. In the top figure, the current is depolarizing ($I_0 = .1$), while in the bottom figure the current is hyperpolarizing ($I_0 = -.1$) and the neuron exhibits post-inhibitory rebound.*

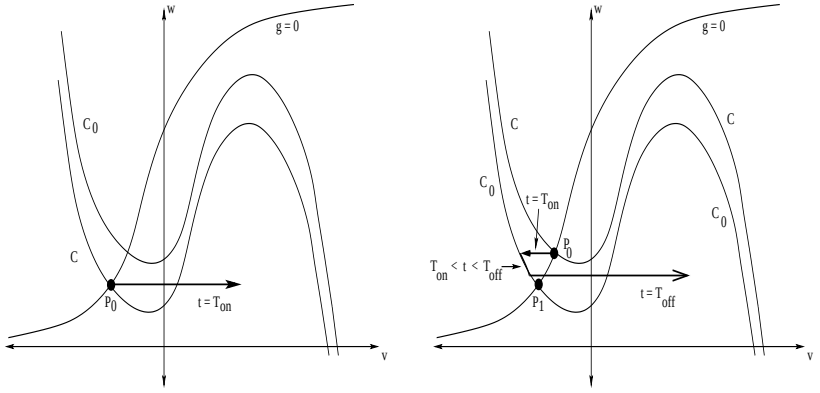

Figure 10.6. *Phase space representation of the response of a model neuron to applied current. Current is applied at time $t = T_{on}$ and turned off at $t = T_{off}$. (Left) Depolarizing current. The cell jumps up as soon as the current is turned on. (Right) Hyperplorizing current. The cell jumps to the left branch of C_0 when the current is turned on and jumps up to the active phase due to post-inhibitory rebound when the current is turned off.*

this branch approaching p_1 for $T_{on} < t < T_{off}$. When $t = T_{off}$, $I(t)$ switches back to 0 and the cell now seeks the left or right branch of C. If, at this time, the cell lies below the left knee of C, then the cell jumps up to the active phase giving rise to post-inhibitory rebound.

Note that in order to generate post-inhibitory rebound, the hyperpolarizing input must be sufficiently large and last sufficiently long. I_0 must be sufficiently negative so that p_1 lies below the left knee of C. Moreover, $T_{off} - T_{on}$ must be sufficiently large; the cell needs enough time to evolve along the left branch of C_0 so that it lies below the left knee of C when the input is turned off.

10.5 Excitatory Synapses

Throughout this section, we consider excitatory synapses. We find conditions for when excitatory networks exhibit stable synchronous oscillations. Later we will find conditions for when excitatory connections lead to stable out-of-phase behavior. As we shall see, the network behavior depends crucially on whether the individual cells have thick or thin spikes; that is, whether they have long or short duty cycles.

We use geometric singular perturbation methods to analyze solutions. As before, we formally set $\epsilon = 0$ and construct singular solutions. The singular trajectory corresponding to each cell lies along either the left or right branch of the cubic shaped v-nullcline during the silent or active phase. The jumps up and down between the silent and active phases occur when a singular trajectory reaches the left or right knee of some cubic. There are now a family of cubic-shaped nullclines, depending on the total synaptic input.

It will be convenient to introduce some notation that will be used throughout the remainder of the chapter. Let $\Phi(v, w, s) \equiv f(v, w) - g_{syn}s(v - v_{syn})$. Then the right hand side of the first equation in (10.4) is $\Phi(v_i, w_i, s_j)$. If g_{syn} is not too large, then each $C_s \equiv \{\Phi(v, w, s) = 0\}$ defines a cubic-shaped curve. We express the left branch of $\mathcal{C}_s$ as $\{v = \Phi_L(w, s)\}$ and the right branch of $\mathcal{C}_s$ as $\{v = \Phi_R(w, s)\}$.

We assume that $H_\infty(v) = H(v - V_T)$ where H is the Heaviside step function. That is, $H_\infty(v) = 0$ if $v < V_T$ and $H_\infty(v) = 1$ if $v > V_T$. It follows that if the presynaptic membrane potential V_{pre} satisfies $V_{pre} > V_T$, then we can rewrite (10.3) as

$$\frac{ds}{dt} = (\alpha + \beta)(\frac{\alpha}{\alpha + \beta} - s) \tag{10.14}$$

In this case,

$$s \ \rightarrow \ \frac{\alpha}{\alpha + \beta} \equiv s_A$$

at the rate $\alpha + \beta$. While a cell receives synaptic input, it lies along the cubic $\mathcal{C}_{s_A}$. We will often write $\mathcal{C}_A$ instead of $\mathcal{C}_{s_A}$. We denote the positions of the left and right knees of $\mathcal{C}_0$ as $w = w_L$ and $w = w_R$, respectively, and the positions of the left and right knees of $\mathcal{C}_A$ as $w = w_L^A$ and $w = w_R^A$, respectively.

10.5.1 Synchrony in a Network of Two Mutually Coupled Neurons

In this section, we describe when excitatory networks exhibit stable, synchronous solutions. We begin by considering a simple network of two mutually coupled cells. We assume throughout this section that each cell, without any coupling, is oscillatory.

It is straightforward to show that there exists of the synchronous solution. This is because along a synchronous solution, $(v_1, w_1, s_1) = (v_2, w_2, s_2) \equiv (v, w, s)$ satisfy the reduced system

$$\begin{aligned}
\frac{dv}{dt} &= f(v,w) - g_{syn} s (v - v_{syn}) \\
\frac{dw}{dt} &= \epsilon g(v,w) \\
\frac{ds}{dt} &= \alpha(1-s) H_\infty(v) - \beta s.
\end{aligned}$$

The singular trajectory consists of four pieces and is shown in Figure 10.7 (left). During the silent phase $s = 0$ and (v, w) lies along the left branch of $\mathcal{C}_0$. During the active phase, $s = s_A$ and (v, w) lies along the right branch of the cubic $\mathcal{C}_A$. The jumps between these two phases occur at the left and right knees of the corresponding cubics. A similar construction holds if the synapses are inhibitory.

We next consider the stability of the synchronous solution to small perturbations. We begin with both cells close to each other in the silent phase with cell 1 at the left knee of $\mathcal{C}_0$ ready to jump up. We follow the cells around in phase space until one of the cells returns to the left knee of $\mathcal{C}_0$. We wish to show that the cells are closer to each other after this cycle than they were initially.

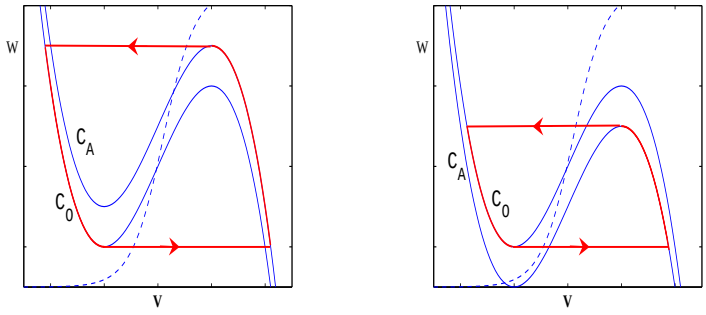

Figure 10.7. *Synchronous singular trajectories corresponding to A) excitatory synapses and B) inhibitory synapses.*

The singular solution consists of four pieces. The first piece begins when cell 1 jumps up. When $v_1(t)$ crosses V_T, $s_1(t) \to s_A$. This raises the cubic corresponding

to cell 2 from $\mathcal{C}_0$ to $\mathcal{C}_A$. If $w_2(0) - w_1(0)$ is sufficiently small, corresponding to a sufficiently small perturbation, then cell 2 lies below the left knee of $\mathcal{C}_A$. The fast equations then force cell 2 to also jump up to the active phase, as shown in Figure 10.8. Note that this piece takes place on the fast time scale. Hence, on the slow time scale, both cells jump up together at precisely the same time.

During the second piece of the singular solution, both oscillators lie in the active phase along the right branch of $\mathcal{C}_A$. Note that the ordering in which the oscillators track along the left and right branches has been reversed. While in the silent phase, cell 1 was ahead of cell 2. In the active phase, cell 2 leads the way. The oscillators remain on the right branch of $\mathcal{C}_A$ until cell 2 reaches the right knee of $\mathcal{C}_A$.

The oscillators then jump down to the silent phase. Cell 2 is the first to jump down. When $v_2(t)$ crosses V_T, s_2 switches from s_A to 0 on the fast time scale. This lowers the cubic corresponding to cell 1 from $\mathcal{C}_A$ to $\mathcal{C}_0$. If, at this time, cell 1 lies above the right knee of $\mathcal{C}_A$, then cell 1 must jump down to the silent phase. This will certainly be the case if the cells are initially close enough to each other.

During the final piece of the singular solution, both oscillators move down the left branch of $\mathcal{C}_0$ until cell 1 reaches the left knee. This completes one full cycle.

To prove that the synchronous solution is stable, we must show that the cells are closer to each other after this cycle; that is, there is compression in the distance between the cells. There are actually several ways to demonstrate this compression; these correspond to different ways to define what is meant by the 'distance' between the cells. Here we consider a Euclidean metric. Sommers and Kopell gave an alternative stability proof using a time metric. They referred to the mechanism by which one cell fires, and thereby raises the cubic of the other cell such that it also fires, as *Fast Threshold Modulation*. We will use a time metric in later sections when we discuss other types of solutions of (10.8).

By the Euclidean distance between the cells, we mean the following. Suppose that both cells lie along the same branch of the same cubic and the coordinates of cell i are (v_i, w_i). Then the distance between the cells is defined as simply $|w_1 - w_2|$. We wish to demonstrate that this distance decreases along the solutions described above. Since the singular solution consists of four pieces, we need to consider four cases. Note, however, that during the jump up and the jump down, the Euclidean distance does not change. This is because the jumps are horizontal so the values of w_i do not change. If there is compression, therefore, it must take place as the cells evolve along the left and right branches of the cubics in the silent and active phases. We now show that this is indeed the case if we make some very mild assumptions on the nonlinearities f and g.

The first step in the analysis is to reduce the full model to equations for just the slow variables w_1 and w_2. We introduce the slow time scale $\tau = \epsilon t$ and then let $\epsilon = 0$ in (10.4). This leads to the equations

$$\begin{aligned} 0 &= f(v_i, w_i) - g_{syn} s_j (v_i \; v_{syn}) \\ \frac{dw_i}{d\tau} &= g(v_i, w_i) \\ 0 &= \alpha(1 - s_i) H_\infty(v_j) - \beta s_i. \end{aligned} \tag{10.15}$$

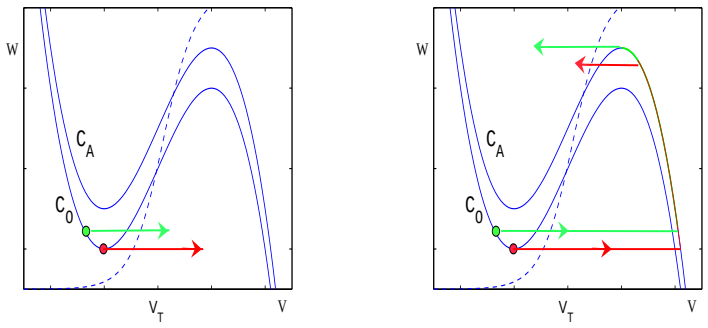

Figure 10.8. *Fast Threshold Modulation.*

The first equation in (10.15) states that each (v_i, w_i) lies on the cubic-shaped null-cline determined by s_j. Let

$$G_L(w,s) \;=\; g(\Phi_L(w,s),w) \quad \text{and} \quad G_R(w,s) \;=\; g(\Phi_R(w,s),w)$$

where Φ_L and Φ_R were defined earlier. Then the second equation in (10.15) can be written as

$$\frac{dw_i}{d\tau} = G_\rho(w_i, s_j) \tag{10.16}$$

where $\rho = L$ if cell i is silent and $\rho = R$ if cell i is active. Note that the third equation in (10.15) implies that either $s_i = 0$ or $s_i = s_A$ depending on whether the presynaptic cell is silent or active.

We now return to the stability analysis of the synchronous solution. We demonstrate that the Euclidean distance between the cells decreases as both cells evolve in either the silent or the active phases. Here we consider the silent phase; the analysis for the active phase is similar.

Suppose that when $\tau = 0$, both cells lie in the silent phase. Hence, each (v_i, w_i) lies on the left branch of C_0. We assume, for convenience, that $w_2(0) > w_1(0)$. We need to prove that $w_2(\tau) - w_1(\tau)$ decreases as long as the cells remain in the silent phase. Now each $w_i(\tau)$ satisfies (10.16) with $\rho = L$ and $s_j = 0$. Hence,

$$w_i(\tau) \;=\; w_i(0) \;+\; \int_0^\tau G_L(w_i(\xi),0)d\xi$$

and, using the Mean Value Theorem,

$$\begin{aligned} w_2(\tau) - w_1(\tau) &= w_2(0) - w_1(0) \\ &\quad + \int_0^\tau \; G_L(w_2(\xi),0) - G_L(w_1(\xi),0)\; d\xi \\ &= w_2(0) - w_1(0) \\ &\quad + \int_0^\tau \frac{\partial G_L}{\partial w}(w^*,0)(w_2(\xi) - w_1(\xi))d\xi \end{aligned} \tag{10.17}$$

for some w^*. Now $G_L(w,0) = g(\Phi_L(w,0),w)$. Hence,

$$\frac{\partial G_L}{\partial w} = g_v \frac{\partial \Phi_L}{\partial w}(w,0) + g_w.$$

Note that

$$\frac{\partial g}{\partial v} \geq 0 \quad \text{and} \quad \frac{\partial g}{\partial w} \leq 0 \tag{10.18}$$

near the synchronous solution. This follows from our assumption that $g > 0$ (< 0) below (above) the w-nullcline. We now make the additional assumption that there is a strict inequality in (10.18). We further note that $\frac{\Phi_L}{\partial w}(w,0) < 0$. This is because $v = \Phi_L(w,0)$ defines the left branch of the cubic C_0 which has negative slope. It follows that $\frac{\partial G_L}{\partial w} < 0$ and therefore,

$$w_2(\tau) - w_1(\tau) < w_2(0) - w_1(0).$$

This gives the desired compression. We note that if there exists $\gamma > 0$ such that $\frac{\partial G_L}{\partial w} < -\gamma$ along the left branch, then Gronwall's inequality can be used to show that $w_2(\tau) - w_1(\tau)$ decreases at an exponential rate.

We remark that this analysis generalizes to arbitrarily large networks of homogeneous cells with excitatory synaptic coupling. Suppose that initially all of the cells are in the silent phase and are sufficiently close to each other. When one cell, say cell 1, jumps up, then those cells that receive excitatory input from cell 1 will be induced to jump up as long as they lie below the left knees of the cubics corresponding the excitatory input. These cells will then induce other cells to jump up and so forth. In this way, all of the cells will fire at the same time (on the slow time-scale). There are, in fact, subtleties in the jumping-down process. A detailed analysis of synchronous behavior in larger networks with excitatory synapses can be found in [??].

10.6 Post-Inhibitory Rebound

10.6.1 Two Mutually Coupled Cells

We now consider two mutually coupled cells with inhibitory synapses. Figure 10.2 shows that this network can exhibit a wide variety of activity patterns. In this section, we consider the pattern shown in Figure 10.2A in which the cells take turns firing due to post-inhibitory rebound. In general, an oscillating network with two cells in antiphase is known as a "half-center" oscillator. This type of behavior is found in many applications including networks governing locomotion or other motor patterns.

The antiphase solution shown in Figure 10.2A exists and is stable only if certain conditions on the nonlinearities and parameters are satisfied. In particular, the coupling strength g_{syn} must be sufficiently strong and the duty cycle must be sufficiently long. Recall that by the duty cycle, we mean the ratio of the times a cell spends in the active and silent phases.

We assume throughout this section that the w-nullcline intersects the left branches of both $\mathcal{C}_0$ and $\mathcal{C}_A$. We denote these points as p_0 and p_A. In particular, individual cells, without any coupling, are excitable. We also note that the resting state $(v_1, w_1) = (v_2, w_2) = p_0$ is a stable solution of the coupled network. Hence, if the system exhibits stable oscillations, as shown in Figure 10.2, then the system is bistable.

There does exist a synchronous solution with $(v_1, w_1, s_1) = (v_2, w_2, s_2)$; however, this solution is unstable. The singular trajectory corresponding to the synchronous solution is shown in Figure 10.7 (right). During the silent phase, it lies along the left branch of $\mathcal{C}_0$ and during the active phase, it lies along the right branch of $\mathcal{C}_A$. A proof that the synchronous solution is unstable is given in [?].

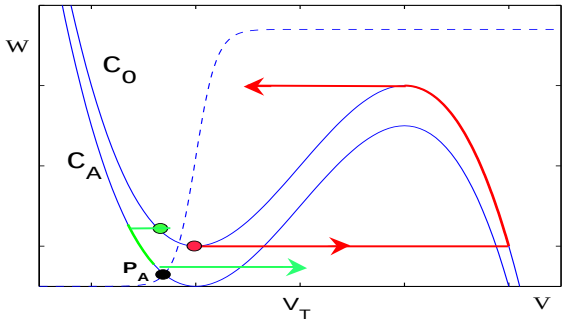

Figure 10.9. *Post-Inhibitory Rebound.*

We now step through the construction of the singular solution corresponding to the solution shown in Figure 10.2A. We begin with cell 1 at the right knee of $\mathcal{C}_0$ ready to jump down. We further assume that cell 2 is silent and lies along the left branch of $\mathcal{C}_A$ below the left knee of $\mathcal{C}_0$. When cell 1 jumps down, $s_1 \to 0$. Since (v_2, w_2) lies below the left knee of $\mathcal{C}_0$, cell 2 exhibits post-inhibitory rebound and approaches the right branch of $\mathcal{C}_0$.

Cell 2 then moves up the right branch of $\mathcal{C}_0$ and cell 1 moves down the left branch of $\mathcal{C}_A$ towards p_A. Eventually, cell 2 reaches the right knee of $\mathcal{C}_0$ and jumps down. If at this time, cell 1 lies below the left knee of $\mathcal{C}_0$, then it jumps up due to post-inhibitory rebound. The roles of cell 1 and cell 2 are now reversed. The cells continue to take turns firing when they are released from inhibition.

The preceding construction requires several assumptions. Firstly, the coupling strength g_{syn} needs to be sufficiently large. In particular, the fixed point p_A must lie below the left knee of $\mathcal{C}_0$. The duty cycle must also be sufficiently large. The active cell must spend enough time in the active phase so that the silent cell can evolve along the left branch of $\mathcal{C}_A$ to below the left knee of $\mathcal{C}_0$. We note that if either g_{syn} or the duty cycle is too small, then the only stable solution will be the resting state $(v_1, w_1) = (v_2, w_2) = p_0$. This last statement depends on our assumption that both cells are excitable.

Wang and Rinzel distinguish between "escape" and release" in producing out-

of-phase oscillations. In the preceding construction, we assumed that both cells are excitable for all levels of synaptic input. Then the silent cell can only jump up to the active phase once the active cell jumps down and releases the silent cell from inhibition. This is referred to as the release mechanism. To describe the escape mechanism, suppose that each cell is oscillatory for some fixed levels of synaptic input. Then the inactive cell may reach a left knee of its cubic and escape the silent phase. When the silent cell jumps up, it inhibits the active cell. This lowers the cubic of the active cell, so it may be forced to jump down before reaching a right knee.

Another mechanism for generating antiphase oscillations is to relax the restriction that the synaptic threshold lies between the active and silent branches. If the synaptic threshold lies along one of the branches, then the synaptic input given from one cell to the other changes as the cell traverses along its branch, not during its jump between branches. As shown in [?], this may have a large effect on the wave-form and frequency of the resulting oscillation.

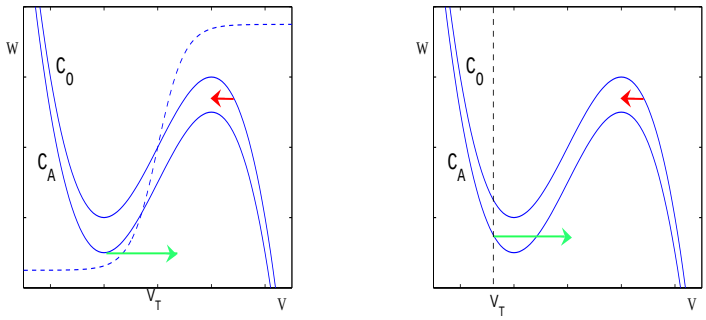

Figure 10.10. *A) Cellular and B) synaptic escape mechanisms.*

10.6.2 Clustering

We now consider larger networks with inhibitory synapses. By a *clustered solution* we mean one in which the population of cells breaks up into distinct groups or clusters. Cells within each cluster fire in synchrony; while cells in different clusters fire out-of-phase. The basic mechanism underlying clustering is simply post-inhibitory rebound. Examples of clustered solutions are shown in Figure 10.3. There are for a network with four cells and all-to-all coupling. The solution shown in Figure 10.3A consists of two clusters with two cells within each cluster. The existence of this solution is equivalent to the antiphase solution for a two-cell network described in the previous section. We note that there are subtleties associated with proving the stability of this two-clustered solution. One must demonstrate that cells within each cluster are stable with respect to perturbations along with proving that the different clusters remain separated. Discussion of these issues can be found in [ ].

Other types of clustered solutions are possible. For the solution shown in Figure 10.3B, there are two clusters; however, one of the clusters consists of three cells, while the other cluster has only one cell. The projection of this solution onto the (v, w)-phase plane is shown in Figure ??B. This is very similar to the clustered solution described above; however, note that now the clusters live on different nullclines in phase space. This is because the amount of inhibition that the cells receive depends on the number of cells within the active cluster.

Figure 10.3C shows a solution in which all the cells fire out-of-phase with each other. This can be viewed as a as a 4-cluster solution. When one of the cells jumps down, another is released from inhibition. The cells then take turns firing. Note that the existence of such a solution depends on the relative times the cells spend in the silent and active phase. The active phase cannot be too long or the network will exhibit a 2-clustered solution. In order to obtain the 4-clustered state, the time in the active phase must be roughly one-third the time the cell spends in the silent phase.

These considerations easily carry over to larger networks. There may exist a 2-clustered solution in which the entire networks breaks up into two groups and the two groups take turns jumping up when the other group releases them from inhibition. The existence of such a solution clearly requires certain assumptions on the length of the active phase and the strength of synaptic coupling. One can also easily obtain activity with more than two clusters under certain conditions. Which type of clustered solution the network exhibits depends on the duty cycle along with the strength of coupling. A more detailed analysis can be found in [??].

10.6.3 Dynamic Clustering

Dynamic clustering differs from clustering in that the membership of the active groups may change. That is, two different cells may fire together during the same episode, but fire separately during subsequent episodes. An example of such a solution is shown in Figure 10.3D. Note that cell 1 sometimes fires with cell 2, but sometimes it does not. In this section, we will explain a simple mechanism for the generation of dynamic clustering. The mechanism depends on both post-inhibitory rebound and network architecture. We will explain the mechanism with a rather simple example; however, this generalizes in a straightforward manner to larger networks. A complete analysis of this type of solution is given in [ ].

The example network consists of seven cells and the network architecture is shown in Figure 10.11. All connections are assumed to be inhibitory. Two different responses, for the same parameter values, are shown in the middle panel of the Figure. Each response consists of episodes in which some subset of the cells fire in near synchrony. These subsets change from one episode to the next; moreover, two different cells may belong to the same subset for one episode but belong to different subsets during other episodes. After a transient period the response becomes periodic. For example, consider the solution shown in A) of the middle panel. The cells which fire during the third episode are cells 2, 3 and 7. These are precisely the same cells which fire during the eighth episode. This subset of cells continues to fire together every fifth cycle. We say that this solution has a

periodic attractor consisting of 5 episodes (or simply, the period is 5). Note that the solution shown in the second panel has the same periodic attractor, although the initial response is different. These two panels demonstrate that two responses may have different initial transients but approach the same periodic attractor. There may be many periodic attractors, however, with different transients and different attractor:

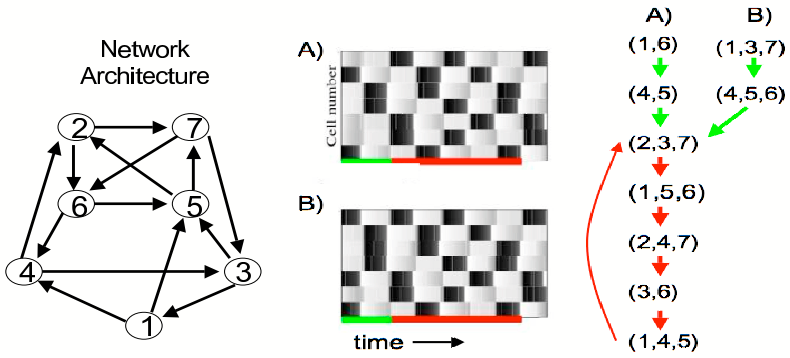

Figure 10.11. *An example of dynamic clustering and reduction to discrete dynamics.*

We next describe an algorithm which will allow us to determine how the network responds to initial conditions and analyze properties of the periodic attractors. If we know which subset of cells fire during one episode, then the algorithm determines which subset of cells fire during the next episode. In order to derive the algorithm, we need two assumptions. The first is that if a cell fires during an episode, then every cell that receives input from that cell and which does not fire during that episode must fire during the next episode. The second assumption is that no E-cell can fire in two subsequent episodes.

Consider the solution shown in the B) of middle panel in Figure 10.11. The cells which fire during the first episode are $1, 3$ and 7. Because of the two assumptions, these induce the cells $4, 5$ and 6 to fire during the second episode. Continuing in this way, we can determine which cells fire during each subsequent episode.

Note that if the number of cells as N (in this example $N = 7$), then those cells which fire during an episode represents a subset of $\mathcal{P}_N \equiv \{1, ..., N\}$. Let $\mathcal{S}_N$ denote the set of subsets of $\mathcal{P}$. The algorithm represents a map Φ from $\mathcal{S}_N$ to itself. For the example shown in the second panel of Figure 1B, we represent the cells which fire during the first and second episodes by indices $\{1, 3, 7\}$ and $\{4, 5, 6\}$, respectively. Hence, $\Phi(\{1, 3, 7\}) = \{4, 5, 6\}$. Iterating Φ, we obtain an orbit of subsets; these correspond to those cells that fire during successive episodes. The orbits corresponding to the three solutions illustrated in Figure ??B are shown in Figure ??. Note that each orbit consists of two components: there is an initial transient until the orbit returns to a subset that it has already visited. The orbit must then repeat itself. We remark that every orbit must eventually become periodic; this is because there are only a finite number of subsets of $\mathcal{P}_N$.

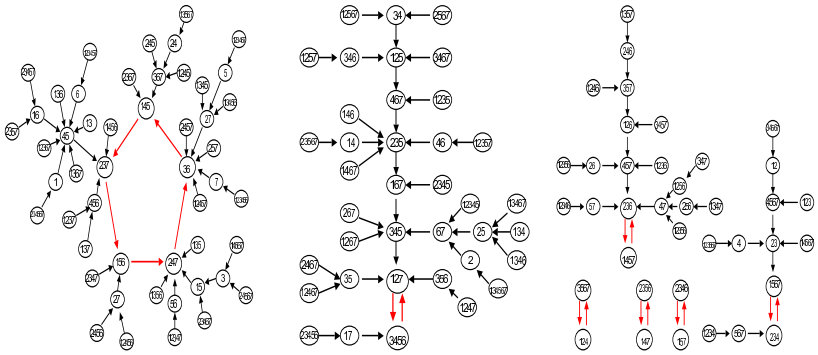

Figure 10.12. *Discrete graph of dynamics associated with the network shown in Figure 10.3.*

By considering every subset of $\mathcal{P}_N$, one obtains a directed graph. This graph has 2^N nodes. Hence, even for the seemingly simple example shown in Figure 1A, there are 128 nodes and the directed graph is quite complicated. The entire graph is shown in Figure 10.12. Examining this directed graph, we find that the model exhibits seven periodic attractors. The periods of the attractors are either 2 or 5. Attractors with period 5 generate dynamic clustering.

Further details and analysis of this algorithm can be found in [?], where precise conditions are given for when the differential equations model can be rigorously reduced to discrete dynamics.

10.7 Thin Spikes

We have, so far, found conditions for when excitatory coupling leads to synchrony and inhibitory coupling leads to antiphase oscillations. The existence and stability of these patterns depend on various assumptions. For example, in order generate antiphase behavior with inhibitory synapses, we required that the active phase, and therefore the duty cycle, is sufficiently long. Note that a cell with a long duty cycle can be viewed as a bursting oscillator; the active phase represents the envelope of spiking activity. In this section, we consider what happens if the duty cycle is short. We also assume that each cell, without coupling, is oscillatory. We may, therefore, think of the cell as exhibiting single, periodic spikes instead of bursts. We find conditions for when excitatory coupling leads to stable antiphase behavior. The analysis also demonstrates when the antiphase solution is unstable for inhibitory coupling.

We will demonstrate that stable antiphase solutions exist if the synapses are excitatory and both the coupling strength g_{syn} and the duty cycle are sufficiently small. The antiphase solution will exist but be unstable if the synapses are inhibitory.

10.7.1 Existence of Antiphase Oscillations

Throughout this section we consider two mutually coupled cells. In this subsection, we find conditions for when there exists an antiphase solution. The stability of this solution will be discussed in the next subsection.

Figure 10.1B shows an antiphase solution with excitatory synapses. The projection of this solution onto the (v, w) phase plane is shown in Figure 10.13A. We now step through the various pieces of this trajectory. We start with both cells are in the silent phase with cell 1 at the left knee of $\mathcal{C}_0$ ready to jump up. Suppose that $w_2(0) = w_*$. When cell 1 jumps up, $s_1 \to s_A$. If $w_* > w_L^A$, so that cell 2 lies above the left knee of $\mathcal{C}_A$, then cell 2 approaches the left branch of $\mathcal{C}_A$. Cell 1 then moves up the right branch of $\mathcal{C}_0$ and cell 2 moves down the left branch of $\mathcal{C}_A$. If the active phase is sufficiently brief, then cell 1 reaches the right branch of $\mathcal{C}_0$ and jumps down before cell 2 reaches the left knee of $\mathcal{C}_A$. Suppose that this happens when $\tau = T_A$. (Here we are considering the slow time-scale.) After cell 1 jumps down, both cells evolve along the left branch of $\mathcal{C}_0$ until cell 2 reaches the left knee of $\mathcal{C}_0$. Suppose that this happens when $\tau = T_0$. If $w_1(T_0) = w_*$, then the roles of cell 1 and cell 2 are reversed and this completes one-half of a complete antiphase cycle.

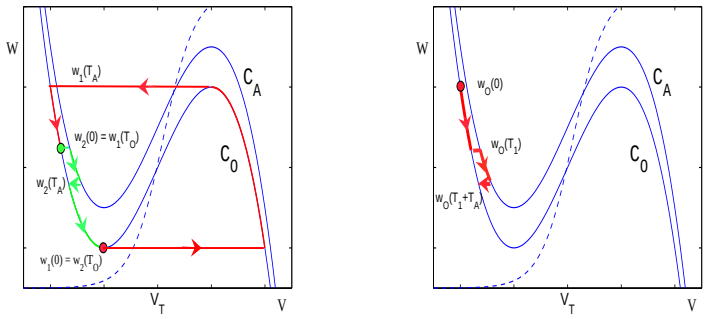

Figure 10.13. *Singular construction of antiphase solution. A) Cell 1 is shown in red and cell 2 in green. B) The auxiliary function $w_0(\tau)$ needed in the existence proof.*

We prove the existence and stability of an antiphase solution by constructing a one-dimensional map, which we denote as π. The definition of π is simply $\pi(w_*) = w_1(T_0)$ where w_* and T_0 are defined above. Clearly, a stable fixed point of π corresponds to a stable antiphase solution. Note that in order to define $\pi(w_*)$ we need that cell 1 jumps up to the active phase and then jumps back to the silent phase before cell 2 is able to jump up. This requires a number of assumptions. In particular, the duty cycle cannot be too long, g_{syn} cannot be too big and $(w_* - w_L)$ cannot be too small. We now derive precise conditions for when π is well defined and has a stable fixed point.

As was done in the preceding section, we reduce the analysis to equations for just the slow variables w_1 and w_2. Each of these variables satisfies (10.16) where

$\rho = L$ or R if cell i is silent or active, and $s_j = 0$ or s_A if the presynaptic cell is silent or active. In particular, if both cells are silent then each w_i satisfies

$$\frac{dw_i}{d\tau} = G_L(w_i, 0). \tag{10.19}$$

If cell i is silent and cell j is active, then

$$\frac{dw_i}{d\tau} = G_L(w_i, s_A) \tag{10.20}$$

and

$$\frac{dw_j}{d\tau} = G_R(w_j, 0). \tag{10.21}$$

Let T_A denote the duration of the active phase. More precisely, this is the time needed for a solution of (10.21) starting at w_L to reach w_R.

We will need to consider the distance between the cells and determine how the distance changes as trajectories evolve in phase space. Here we use a *time metric*. For now, we only consider the case when both cells are silent; that is, $(v_1(0), w_1(0))$ and $(v_2(0), w_2(0))$ lie along the left branch of $\mathcal{C}_0$. Suppose that $w_1(0) < w_2(0)$. Then the time metric $\rho_L(w_1(0), w_2(0))$ is defined to be the time it takes for the solution of (10.19) starting at $w_2(0)$ to reach $w_1(0)$. Note that this metric is time invariant in the following sense: Suppose that $w_i(\tau),\ i = 1, 2$, are solutions of (10.19). Then

$$\rho_L(w_1(\tau), w_2(\tau)) = \rho_L(w_1(0), w_2(0))$$

for all $\tau > 0$, as long as the cells remain on the left branch of $\mathcal{C}_0$. The proof of this statement is left as an exercise.

Note that π is not defined for all $w_* \in (w_L, w_R)$. We need that cell 1 jumps up and down before cell 2 jumps up. This will be true if T_A is sufficiently small and $w_* - w_L$ is sufficiently large. We assume, for the moment, that this is true. Once we characterize w_*, we will demonstrate that it is indeed in the domain of π.

We now find conditions for π to have a fixed point. Since

$$w_L < w_2(T_A) < w_* < w_R$$

it follows that

$$\rho_L(w_L, w_R) \ = \ \rho_L(w_L, w_2(T_A)) \ + \ \rho_L(w_2(T_A), w_*) \ + \ \rho_L(w_*, w_R).$$

Let $T_S = \rho_L(w_L, w_R)$ be the length of the silent phase. If w_* is a fixed point of π, then $w_2(T_0) = w_L,\ w_1(T_0) = w_*$ and $w_1(T_A) = w_R$. Hence,

$$\begin{aligned} T_S &= \rho_L(w_2(T_0), w_2(T_A)) + \rho_L(w_2(T_A), w_*) + \rho_L(w_1(T_0), w_1(T_A)) \\ &= (T_0 - T_A) + \rho_L(w_2(T_A), w_2(0)) + (T_0 - T_A) \\ &= 2(T_0 - T_A) + \rho_L(w_2(T_A), w_2(0)) \end{aligned} \tag{10.22}$$

We view (10.22) as an equation for $T_1 \equiv T_0 - T_A$. To do this, we first define an auxiliary function $w_0(\tau)$. Suppose that $w_0(0) = w_R$, $w_0(\tau)$ satisfies (10.19) for $0 < \tau < T_1$, and satisfies (10.20) for $T_1 < \tau < T_1 + T_A$. See Figure 10.13B. Note that if $w_1(\tau)$ and $w_2(\tau)$ correspond to an antiphase solution, then $w_0(\tau) = w_1(\tau + T_A)$ for $0 < \tau < T_1$ and $w_0(\tau) = w_2(\tau - T_1)$ for $T_1 < \tau < T_0$. Hence, we can rewrite (10.22) as

$$T_S = 2T_1 + \rho_L(w_0(T_1 + T_A), w_0(T_1)). \tag{10.23}$$

This is an equation for T_1. Once we solve for T_1, then $w_* = w_0(T_1)$ is the desired fixed point of π. Note that the last term in (10.23) $\to 0$ as $T_A \to 0$. Hence, in this limit, the solution of (10.22) is $T_1 = \frac{1}{2}T_S$. It follows that (10.23) has a solution, and there exists a fixed point of π, if the duration of the active phase is sufficiently small.

It remains to prove that the fixed point w_* lies in the domain of π. Recall that cell 1 must jump up and jump down before cell 2 jumps up. Choose $\omega_D > w_L^A$ so that the time it takes a solution of (10.20) starting at ω_D to reach w_L^A is T_A. Then cell 1 will jump up and jump down before cell 2 jumps up if if $w_* > \omega_D$. This will be the case if

$$\rho_L(w_L, w_*) > \rho_L(w_L, \omega_D). \tag{10.24}$$

We show that this is true if the coupling strength g_{syn} and the duration of the active phase T_A are sufficiently small. Note that the right hand side of (10.24) can be written as

$$\rho_L(w_L, \omega) = \rho_L(w_L, w_L^A) + \rho_L(w_L^A, \omega).$$

Since $w_L^A \to w_L$ as $g_{syn} \to 0$ and $\omega_D \to w_L^A$ as $T_A \to 0$, it follows that the right hand side of (10.24) is as small as we please if g_{syn} and T_A are small. On the other hand, the left hand side of (10.24) can be rewritten as

$$\begin{aligned} \rho_L(w_L, w_*) &= \rho_L(w_L, w_R) - \rho_L(w_*, w_R) \\ &= T_S - T_1 \\ &\to \frac{1}{2}T_S \end{aligned} \tag{10.25}$$

as $T_A \to 0$. Hence, (10.24) is satisfied if g_{syn} and T_A are sufficiently small. This completes the proof that π has a fixed point corresponding to an antiphase solution.

10.7.2 Stability of Antiphase Oscillations

We now consider the stability of the fixed point w_*. To prove the stability, we must show that $|\pi'(q_0)| < 1$. We demonstrate that this is the case if the synapses are excitatory and some rather natural assumptions on the nonlinearities f and g are satisfied. The analysis also demonstrates that the fixed point is unstable if the synapses are inhibitory.

We begin by describing another way to geometrically visualize the antiphase solution. Consider the projection of the solution onto the (w_1, w_2) slow phase plane as shown in Figure ??. Note that the solution lies within the rectangular region:

$$\mathcal{R} \;=\; \{(w_1, w_2) : w_L \le w_1 \le w_R,\; w_L \le w_2 \le w_R\}.$$

Denote the left, right, top and bottom sides of $\mathcal{R}$ as $\mathcal{R}_L, \mathcal{R}_R, \mathcal{R}_T$ and $\mathcal{R}_B$, respectively. These correspond to positions where one of the cells reaches a left or right knee of $\mathcal{C}_0$; that is, where cell 1 jumps up, cell 2 jumps up, cell 2 jumps down and cell 1 jumps down, respectively.

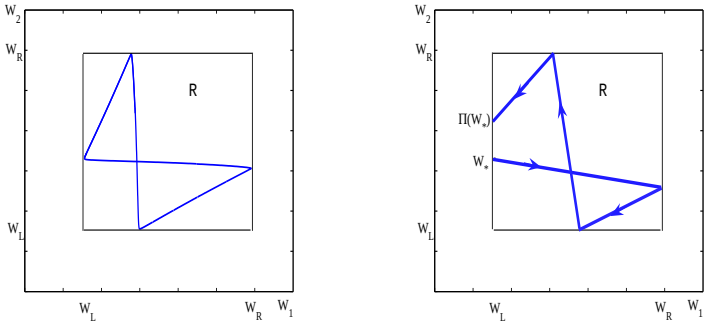

Figure 10.14. *A) Projection of the antiphase solution onto the slow* (w_1, w_2) *phase plane. B) The one-dimensional map.*

We now view π as a map defined on $\mathcal{R}_L$ and denote this new map as Π. That is, suppose we start at a point $(w_L, w_*) \in \mathcal{R}_L$. Then cell 1 is ready to jump up and cell 2 is silent. We follow the trajectory until it reaches $\mathcal{R}_L$ again. If the position of cell 2 at this time is w_0, we let $\Pi(w_*) = w_0$. Since here we are considering a full cycle, and in the definition of π we only considered one-half of a cycle, it follows that $\Pi(w_*) = \pi^2(w_*)$. It suffices to show that $|\Pi'(q_0)| < 1$. We will, in fact, demonstrate that $|\Pi'(w_*)| < 1$ for each w_* such that $\Pi(w_*)$ is well defined.

Since the antiphase solution consists of four pieces, we can decompose Π into four pieces. We write $\Pi(w_*) = (\Pi_4 \circ \Pi_3 \circ \Pi_2 \circ \Pi_1)(w_*)$ where each Π_k is a flow defined map from one side of $\mathcal{R}$ to another. Then

$$\Pi'(w_*) \;=\; \Pi_4'\Pi_3'\Pi_2'\Pi_1'(w_*) \tag{10.26}$$

Note that $|\Pi_2'| = |\Pi_4'| = 1$. This follows because the time metric ρ_L is time-invariant and each of these maps correspond to when both cells are silent and lie along the left branch of $\mathcal{C}_0$. We leave the details as an exercise. We must, therefore, prove that $|\Pi_1'| < 1$ and $|\Pi_3'| < 1$. Here we consider $|\Pi_1'|$ since the other inequality is similar. Note that Π_1 corresponds to when cell 1 is active and cell 2 is silent. Hence w_1 satisfies (10.21) and w_2 satisfies (10.20).

In order to calculate the derivative of Π_1, we write it as a difference quotient:

$$\Pi_1'(a) = \lim_{b\to a} \frac{\rho_L(\Pi_1(a), \Pi_1(b))}{\rho_L(a,b)} \tag{10.27}$$

Here, we are assuming that $a < b$. We now need a formula for ρ_L in terms of the nonlinearities f and g. Recall that $\rho_L(a,b)$ is the time for a solution of (10.19) starting at $w = b$ to reach $w = a$. Hence,

$$\rho_L(a,b) = \int_b^a \frac{1}{G_L(w,0)} dw. \tag{10.28}$$

This formula is not convenient to work with because w_2 does not satisfy (10.19); it satisfies (10.20) instead. For this reason, we define a new time-metric $\rho_A(a,b)$ to be the time it takes a solution of (10.20) starting at $w = b$ to reach $w = a$. Changing variables in (10.28), we find that if $w_2(\tau, b)$ is the solution of (10.20) with $w_2(0,b) = b$, then

$$\rho_L(a,b) = \int_0^{\rho_A(a,b)} \frac{G_L(w_2(\tau,b), s_A)}{G_L(w_2(\tau,b),0)} d\tau \tag{10.29}$$

Since this holds for all a and b such that $w_L^A < a < b < w_R$, we also have that

$$\rho_L(\Pi_1(a), \Pi_1(b)) = \int_0^{\rho_A(\Pi_1(a),\Pi_1(b))} \frac{G_L(w_2(\tau, \Pi_1(b)), s_A)}{G_L(w_2(\tau,\Pi_1(b)),0)} d\tau \tag{10.30}$$

We now insert these expressions into (10.27) and use L' Hopital's rule to conclude that

$$\Pi_1'(a) = \left(\frac{G_L(\Pi_1(a), s_A)}{G_L(\Pi_1(a),0)}\right)\left(\frac{G_L(a,0)}{G_L(a,s_A)}\right). \tag{10.31}$$

We show that if the synapses are excitatory, then $\frac{G_L(w,s_A)}{G_L(w,0)}$ is an increasing function of w; that is

$$\frac{\partial}{\partial w}\left(\frac{G_L(w,s_A)}{G_L(w,0)}\right) > 0. \tag{10.32}$$

Note that $\Pi_1(a) < a$. This is because $w_2(\tau)$ decreases while in the silent phase. This together with (10.31) implies that $|\Pi_1'(a)| < 1$ and the antiphase solution is stable. A similar analysis shows that if the synapses are inhibitory, then $\frac{G_L(w,s_A)}{G_L(w,0)}$ is a decreasing function of w; hence, the antiphase solution is unstable.

Let $\Delta(w,s) = G_L(w,s) - G_L(w,0)$. Then

$$\frac{\partial}{\partial w}\left(\frac{G_L(w,s_A)}{G_L(w,0)}\right) = \frac{G_L(w,0)\Delta_w(w,s_A) - G_{Lw}(w,0)\Delta(w,s_A)}{{G_L}_w^2(w,0)}.$$

We derive conditions on the nonlinear functions f and g so that

$$G_L < 0, \quad G_{Lw} < 0, \quad \Delta > 0 \text{ and } \Delta_w < 0.$$

To do this, we need to express each of these inequalities in terms of f and g and their derivatives.

Recall that $G_L(w,s) = g(\Phi_L(w,s),w)$ where $v = \Phi_L(w,s)$ represents the left branch of $\mathcal{C}_0$. In particular, $f(\Phi_L(w,s),w) - g_{syn}s(v - v_{syn}) = 0$. Suppose that $g(v,w)$ can be written in the usual form $g(v,w) = (h_\infty(v) - w)/\tau_w(v)$. To simplify the analysis, we assume that $\tau_w(v) = \tau_w$ is constant while the cell is in the silent phase. For convenience, we assume that $\tau_w = 1$.

Clearly, $G_L(w,0) < 0$; that is, w decreases in the silent phase. Moreover,

$$\frac{\partial G_L}{\partial w} = \frac{\partial g}{\partial v}\frac{\partial \Phi_L}{\partial w} + \frac{\partial g}{\partial w} \;=\; h'_\infty(v)\frac{\partial \Phi_L}{\partial w} - 1 \;<\; 0.$$

if $h'_\infty(v) > 0$ and the left branch of the cubic $\mathcal{C}_0$ has negative slope. It is not hard to give precise conditions on the nonlinear function f for when this last statement is true.

We next consider Δ and Δ_w. Note that

$$\Delta(w,s_A) = \int_0^{s_A} \frac{\partial G_L}{\partial s}(w,\gamma)d\gamma \;\text{ and }\; \Delta_w(w,s_A) = \int_0^{s_A} \frac{\partial^2 G_L}{\partial w \partial s}(w,\gamma)d\gamma.$$

Now

$$\frac{\partial G_L}{\partial s} = \frac{\partial g}{\partial v}\frac{\partial \Phi_L}{\partial s} = h'_\infty(v)\frac{\partial \Phi_L}{\partial s} \;>\; 0$$

if $h'_\infty(v) > 0$ and the cubics 'increase' as s increases; that is, if $s_1 > s_2$ then the cubic corresponding to s_1 lies above the cubic corresponding to s_2. Again, it is not hard to derive precise conditions on f so that this is the case. Finally, note that

$$\frac{\partial^2 G_L}{\partial w \partial s} \;=\; h''_\infty(v)\frac{\partial \Phi_L}{\partial w}\frac{\partial \Phi_L}{\partial s} + h'_\infty(v)\frac{\partial^2 \Phi_L}{\partial w \partial s}.$$

We assume that $h'_\infty(v) > 0$ and $h''_\infty(v) > 0$; this is true for most neuronal models including the Morris-Lecar equations. We have already seen that $\frac{\partial \Phi_L}{\partial w} < 0$ and $\frac{\partial \Phi_L}{\partial s} > 0$. Hence, it remains to find conditions on f so that $\frac{\partial^2 \Phi_L}{\partial w \partial s} < 0$. We leave this as an exercise.

10.8 Almost-Synchronous Solutions

In this section, we consider the *almost-synchronous solution* shown in Figure 10.2B. Note that one of the cells fires shortly after the other and there is then a delay until the cells fire again. Here we assume that the coupling is inhibitory and the cells, without any coupling, are oscillatory. We also assume that the duty cycle is small. In this case, we will demonstrate that the almost-synchronous solution exists and is stable. Note that results from the previous section demonstrate that both the synchronous and the antiphase solution exist but are unstable. Here, we consider a network consisting of two mutually coupled cells. The analysis carries over to larger networks.

10.8.1 Almost-Synchrony in a Network of Two-Mutually Coupled Cells

Figure 10.15 shows the projection of the almost-synchronous solution onto the (v, w) phase plane. We now step through this solution as it evolves in phase space. This description leads to a one-dimensional map, a fixed point of which corresponds to the almost-synchronous solution.

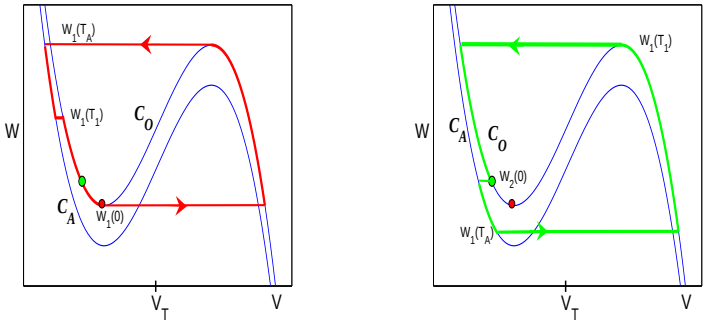

Figure 10.15. *Singular construction of the almost-synchronous solution. Cell 1 is shown in red and cell 2 in green.*

We start with both cells in the silent phase with cell 1 at the left knee ready to jump up. When cell 1 jumps up, cell 2 approaches the left branch of $\mathcal{C}_A$. Then cell 1 moves up the right branch of $\mathcal{C}_0$ and cell 2 moves down the left branch of $\mathcal{C}_A$. We assume that the active phase is sufficiently short so that cell 1 reaches the right knee of $\mathcal{C}_A$ and jumps down before cell 2 reaches the left knee of $\mathcal{C}_0$. Note that this assumption is not necessary if the w-nullcline intersects the left branch of $\mathcal{C}_A$ at some point p_A. We further assume that $w_2(0) - w_1(0)$ is sufficiently small so that when cell 1 jumps down, cell 2 lies below the left knee of $\mathcal{C}_0$. Then cell 2 exhibits post-inhibitory rebound. Suppose that cell 1 jumps down at time $\tau = T_A$.

Cell 2 then moves up the right branch of $\mathcal{C}_0$ and cell 1 moves down the left branch of $\mathcal{C}_A$. If the active phase is sufficiently small, then cell 2 jumps down before cell 1 can jump back up. Suppose that this happens at time $\tau = T_1$. We assume that $w_1(T_1) > w_L$ so that cell 1 does not rebound at this time. This will be the case if the active phase is short enough.

Finally, both cells move down the left branch of $\mathcal{C}_0$ until cell 1 reaches the left knee. Suppose that this happens at time T_2. If $w_2(T_2) = w_2(0)$, then we have constructed an almost-synchronous periodic solution. We define the one-dimensional map $\pi(w_2(0)) = w_2(T_2)$. We now derive conditions for when this map is well-defined and has a stable fixed point.

We first consider the domain of π. In order for π to be well-defined, three conditions need to be satisfied: (1) cell 2 cannot jump up before cell 1 jumps down; (2) cell 2 must rebound when cell 1 does jump down; and (3) cell 1 cannot rebound

when cell 2 jumps down. We consider the time-metrics ρ_L and ρ_A defined in the preceding section.

Note that condition (1) must be satisfied if the the w-nullcline intersects the left branch of $\mathcal{C}_A$. If this is not the case, then condition (1) will be satisfied if $w_2(0) > w_L$ and $T_A < \rho_A(w_L^A, w_L)$. We next choose $\omega > w_L$ so that $\rho_A(w_L, \omega) = T_A$. If $w_L < w_2(0) < \omega$, then $w_2(T_A) < w_L$ and condition (2) is satisfied. Finally, condition (3) is satisfied if we assume that $T_A < \rho_A(w_L, w_R)$.

We now show that π has a stable fixed point. A fixed point satisfies $\pi(w_2(T_2)) = w_2(0)$; that is, $\rho_L(w_L, w_2(0)) = \rho_L(w_L, w_2(T_2))$. Now cell 1 and cell 2 both lie on the left branch of $\mathcal{C}_0$ for $T_1 < \tau < T_2$. Since ρ_L is time-invariant, it follows that

$$\begin{aligned}\rho_L(w_L, w_2(T_2)) &= \rho_L(w_1(T_2), w_2(T_2)) = \rho_L(w_1(T_1), w_2(T_1)) \\ &= \rho_L(w_1(T_1), w_R).\end{aligned}$$

Hence, it suffices to show that

$$\rho_L(w_L, w_2(0)) = \rho_L(w_1(T_1), w_R). \tag{10.33}$$

To do this we consider two limiting cases: $w_2(0) = w_L$ and $w_2(0) = \omega$. In each of these limiting cases, we assume that cell 2 rebounds once cell 1 jumps down. If $w_2(0) = w_L$, then $\rho_L(w_L, w_2(0)) = 0$. Clearly, $\rho_L(w_1(T_1), w_R) > 0$. Hence,

$$\rho_L(w_L, w_2(0)) < \rho_L(w_1(T_1), w_R).$$

We will prove that if $w_2(0) = \omega$ then $\rho_L(w_L, w_2(0)) > \rho_L(w_1(T_1), w_R)$. It then follows that there must exist $w_2(0) \in (w_L, \omega)$ such that (10.33) is satisfied. Moreover, this fixed point is stable.

So assume that $w_2(0) = \omega$. Then $\rho_A(w_L, w_2(0)) = \rho_A(w_L, \omega) = T_A$ and cell 2 jumps up at $w_2(T_A) = w_L$. Moreover, cell 2 lies in the active phase for $T_A < \tau < T_1$ with $w_2(T_A) = w_L$ and $w_2(T_1) = w_R$. Recall that T_A is the time it takes for a solution of (10.21) to go from w_L to w_R. Hence, $T_1 - T_A = T_A$. Since $w_1(T_A) = w_R$, it follows that

$$\rho_A(w_1(T_1), w_R) \;=\; \rho_A(w_1(T_1), w_1(T_A)) \;=\; T_1 - T_A \;=\; T_A$$

Therefore,

$$\rho_A(w_L, w_2(0)) \;=\; \rho_A(w_1(T_1), w_R) \;=\; T_A.$$

Using (10.29), we find that if $w(\tau, b)$ is the solution of (10.21) with $w(0, b) = b$, then

$$\rho_L(w_L, \omega) = \int_0^{T_A} \frac{G_L(w(\tau, \omega), s_A)}{G_L(w(\tau, \omega), 0)} d\tau$$

and

$$\rho_L(w_1(T_1), w_R) = \int_0^{T_A} \frac{G_L(w(\tau, w_R), s_A)}{G_L(w(\tau, w_R), 0)} d\tau.$$

Finally, recall that $\frac{G_L(w, s_A)}{G_L(w, 0)}$ is a decreasing function of w. Moreover, $\omega < w_R$ and, therefore, $w(\tau, \omega) < w(\tau, w_R)$ for each $\tau \in (0, T_A)$. It follows that if $w_2(0) = \omega$, then $\rho_L(w_L, w_2(0)) > \rho_L(w_1(T_1), w_R))$. This then completes the proof.

10.9 Slow Inhibitory Synapses

Recall that different types of synapses may turn on or turn off at very different rates. For example, GABA_B synapses are slow to activate and slow to turn off compared with GABA_A synapses. The rates at which the synapses turn on or turn off may have a profound affect on the network behavior. For example, the solutions shown in Figures 10.2C and 10.2D were generated by choosing the rate at which the inhibitory synapse turns off to be small.

Note that α and β determine the rates at which the synapse turns on and turns off. We have, so far, considered *fast synapses*. By this we mean that α and β are O(1) with respect to ϵ. When a cell either jumps up or jumps down, the corresponding synaptic variable either approaches s_A or approaches 0 on the fast time-scale. In this section, we consider *slow synapses*; that is, either α or β (or both) are $O(\epsilon)$. We will use fast/slow geometric analysis to construct singular trajectories corresponding to synchronous and antiphase solutions, as well as the solutions shown in Figures 10.2C and 10.2D.

10.9.1 Fast/Slow Decomposition

The first step in the analysis is to decompose the full network (10.4) into fast and slow equations. Here we assume that $\alpha = O(1)$ with respect to ϵ and $\beta = \epsilon K$ where K does not depend on ϵ. Hence, the synapses activate on the fast time-scale and turn off on the slow time-scale.

We derive slow subsystems valid when the cells lie in either the silent or the active phase. There are several cases to consider and we only discuss two of these in detail. First suppose that both cells are silent. Then each $v_i < V_T$ and $H_\infty(v_i - V_T) = 0$. Hence, after letting $\tau = \epsilon t$ and setting $\epsilon = 0$, (10.4) becomes

$$\begin{aligned} 0 &= f(v_i, w_i) - s_j g_{syn}(v_i - v_{syn}) \\ \frac{dw_i}{d\tau} &= g(v_i, w_i) \\ \frac{ds_i}{d\tau} &= -K s_i. \end{aligned} \tag{10.34}$$

This system can be simplified as follows. We write the left branch of C_s as $v = \Phi_L(w, s)$ and let $G_L(w, s) = g(\Phi_L(w, s), s)$. Each (w_i, s_j) then satisfies the system

$$\begin{aligned} \frac{dw}{d\tau} &= G_L(w, s) \\ \frac{ds}{d\tau} &= -Ks. \end{aligned} \tag{10.35}$$

These equations determine the evolution of the slow equations while in the silent phase. The equations are well defined as long as each (v_i, w_i) lies along the left branch of the cubic determined by s_j. Note that the left knee of the cubic $\mathcal{C}_s$ depends on s; we denote the position of this left knee as $w_L(s)$. This defines a jump-up curve $w = w_L(s)$ as shown in Figure 10.16. The cells remain in the silent

phase and each (w_i, s_j) satisfies (10.35) as long as $w_i > w_L(s_j)$. If $w_i(\tau) = w_L(s_j)$, then cell i jumps up to the active phase.

Now suppose that cell i is active and cell j is silent. Then s_i activates on the fast time-scale, while s_j decays on the slow time scale; that is, s_i is a fast-variable, while s_j is a slow variable. The slow equations for cell j are (10.34), while the slow equations for cell i are

$$\begin{aligned} 0 &= f(v_i, w_i) - g_{syn} s_j (v_i - v_{syn}) \\ \dot{w}_i &= g(v_i, w_i) \\ 1 &\equiv s_i. \end{aligned} \tag{10.36}$$

We reduce these systems to equations for just the slow variables as before. Denote the right branch of C_s by $v = \Phi_R(w, s)$ and let $G_R(w, s) = g(\Phi_R(w, s), s)$. Then (w_j, s_j) satisfies the reduced equations

$$\begin{aligned} \dot{w}_j &= G_R(w_j, s_i) \\ \dot{s}_j &= -K s_j \end{aligned} \tag{10.37}$$

while w_i satisfies the scalar equation

$$\dot{w}_i = G_L(w_i, 1). \tag{10.38}$$

These equation are well defined as long as cell i lies on the right branch of the cubic determined by s_j and cell j is on the left branch of the cubic determined by s_i. Cell i jumps down if (v_i, w_i) reaches the right knee of the cubic $\mathcal{C}_{s_j}$. We denote the position of this knee as $w = w_R(s_j)$.

10.9.2 Antiphase and Suppressed Solution

In this section, we construct singular trajectories corresponding to antiphase and suppressed solutions of (10.4). We assume throughout that the synapses are inhibitory and decay on the slow time-scale. Throughout the analysis, we consider the projection of the solution onto the (w, s) slow phase plane. As we shall see, the existence of a particular type of solution depends on the relative size of the rate at which the synapse decays and the rate at which the cells evolve during the silent phase.

The projection of an antiphase solution onto the (w, s) phase plane is shown in Figure 10.16. We step through the evolution of this solution starting at the time when both cells lie in the silent phase and cell 1 has just jumped down from the active phase. This implies that the inhibition s_1 felt by cell 2 satisfies $s_1(0) = 1$. Both cells then evolve in the silent phase; each (w_i, s_j) satisfies (10.35). This continues until cell 2 reaches the jump-up curve $w = w_L(s)$. Suppose that this occurs at time $\tau = \tau_1$. At this time, the inhibition s_1 felt by cell 1 jumps up to the line $s \equiv 1$. Cell 2 then evolves in the active phase; we illustrate the projection of cell 2's trajectory during the active phase with a dotted curve in Figure ??. Note that $s_1(\tau)$ still satisfies the second equation in (10.37); hence, it keeps decreasing while cell 2 is active. During this time, cell 1 lies in the silent phase with $s_1 = 1$. This continues

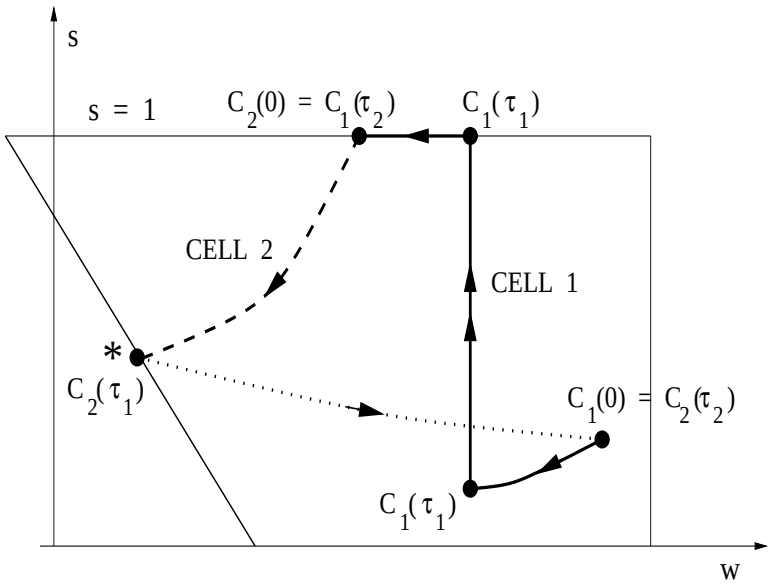

Figure 10.16. *Geometric construction of an antiphase solution for slow synapses.*

until cell 2 reaches the jump-down curve $w = w_R(s)$. We denote this time as τ_2. Cell 2 then jumps down and this completes one-half of a complete cycle. For this to be an antiphase solution, we must have that $w_1(\tau_2) = w_2(0)$ and $s_2(\tau_2) = s_1(0)$.

We next consider the so-called *suppressed solutions* shown in Figure 10.2C. In such rhythms, one cell remains quiet while the other oscillates. Here we assume that a single cell, without coupling, is oscillatory. Moreover, the cells are excitable for sufficiently high levels of inhibition. That is, the w-nullcline intersects $\mathcal{C}_0$ along it's middle branch but intersects the left branch of $\mathcal{C}_s$ for some $s \in (0, 1]$.

Suppressed solutions arise if the rate at which the synapse turns off is sufficiently slower than the rate at which the cells evolve in the silent phase. The reason for this is easy to understand: if the inhibition decays slowly enough, the leading cell can recover and fire again before the inhibition from its previous active phase wears off enough to allow the other cell to fire. This type of solution cannot exist if the cells are excitable rather than oscillatory, since there is no input from the quiet cell to drive the active one. On the other hand, suppressed solutions only arise if the cells are excitable for some fixed levels of inhibition; i.e. some $s \in (0, 1]$. If this is not the case, then the $w-$coordinate of the suppressed cell must keep decreasing until that cell eventually reaches the jump-up curve and fires.

If the synaptic inhibition decays at a rate comparable to the recovery of the cell, complex hybrid solutions can occur, in which one cell is suppressed for several cycles, while the other fires, and then fires while the other is suppressed. An example is shown in Figure 10.2D. In this example, each cell is excitable when uncoupled

but is oscillatory for intermediate higher levels of inhibition. small, A cell can fire a number of times while the other cell is suppressed. The inhibition of the firing cell must eventually wear off, such that that cell can no longer fire. This then allows the inhibition of the suppressed cell to wear off to the level from which it can fire. The roles of the two cells are then reversed.

10.9.3 Synchronous Oscillations With Slow Inhibitory Synapses

It may be surprising that networks with only inhibitory synapses can generate stable synchronous oscillations; however, this has indeed been demonstrated, both numerically and analytically, in several studies. Here we describe some rigorous results given in [tbk].

We first construct the singular synchronous solution. We begin with both cells at the right knee of the right branch of C_1. From this point, the cells jump down to the silent phase. While in the silent phase, the slow variables evolve according to (10.35). The cells can only leave the silent phase once they reach a left knee of one of the left branches. If the cells are able to reach such a point, then they will jump up to the active phase and return to the starting point. Hence, the existence of the synchronous solution depends on whether the cells can reach one of the jump-up points while in the silent phase.

If the cells are oscillatory, then the synchronous trajectory must reach one of the jump-up points. This is demonstrated in [tbk] where it is also shown that a synchronous solution can exist even though both cells, without any coupling, are excitable. This will be the case if the rate K of decay of inhibition is small enough and the cells are oscillatory for some fixed values of $s \in (0, 1)$; if the cells are excitable for all $s \in [0, 1]$, then the only stable solution is the quiescent resting state. Exit from the silent phase is not possible if K is too large, since then the inhibition decays quickly and the system behaves in the slow regime like the uncoupled excitable system with $s = 0$.

We next consider the stability of the synchronous solution. It turns out that the synchronous solution will always be unstable for the simple model of synaptic dynamics given in (10.3); that is, if the synapse turns on instantaneously with respect to the slow time-scale. However, if we introduce a slow delay in the response of the synapse, then it is possible for the synchronous solution to be stable. To model the delay, we introduce a new variable, denoted by x, in the model given in (10.3). That is, we replace (10.3) with the equations:

$$\begin{aligned} \frac{dx}{dt} &= \alpha_x(1-x)H(V_{pre} - V_T) - \beta_x x \\ \frac{ds}{dt} &= \alpha(1-s)H(x - \theta_x) - \beta s \end{aligned} \tag{10.39}$$

where H is the Heaviside step function. Note that the variable x represents the delay in synaptic response. When the presynaptic potential v_i crosses threshold V_T, it immediately activates x. Then the postsynaptic variable $s_j,\ j \neq i$ must wait until x crosses some threshold θ_x before it turns on. We refer to the original model (10.3) as a *direct synapse* and the new model (10.39)) as an *indirect synapse*. We

now demonstrate that the synchronous solution is unstable if the synapse is direct. We then give conditions for when the synchronous solution is stable if the synapse is indirect.

The reason why the synchronous solution is not stable when the synapses are direct is because with direct synapses, when one cell jumps, the other cell begins to feel inhibition as soon as the first cell's membrane potential crosses threshold. This instantly moves the second cell away from its threshold by an amount that stays bounded away from zero no matter how close to the first cell the second cell starts. Thus, infinitesimally small perturbations are magnified, at this stage of the dynamics, to finite size, and the synchronous solution cannot be stable.

We next consider indirect synapses and describe a Theorem proved in [tbk] which shows that the synchronous solution can be stable in some parameter ranges. This result implies that there are two combinations of parameters that govern the stability. Furthermore, only one of those two combinations controls stability in any one parameter regime.

For this result, it is necessary to make some further assumptions on the nonlinearities and parameters. It will be necessary to assume that

$$f_w \ < \ 0, \quad g_v \ > \ 0, \quad \text{and} \quad g_w \ < \ 0 \tag{10.40}$$

near the $v-$nullcline. For the Theorem stated below, we also assume that $f(v,w)$ is given by

$$f(v,w) = f_1(v) - g_c w(v - v_R)$$

where $g_c > 0$ and $v_R \leq v_{syn}$ represent a maximal conductance and reversal potential, respectively. Note that this holds for the Morris-Lecar equations. The analytical framework we develop, however, also applies to more general nonlinearities which satisfy (10.40). Some technical assumptions are also required on the nonlinear function $g(v,w)$. We need to assume that g_v is not too large near the right branches of the cubics C_s, for example.

We assume that the parameters α_x and β_x are sufficiently large, and $\frac{\alpha_x}{\alpha_x+\beta_x} > \theta_x$. This guarantees that each x_i can cross its threshold in order to turn on the inhibition. Precise conditions on how large α_x and β_x must be are given in [tbk].

We also need to introduce some notation. Let a_- be defined as the minimum of $-\partial g/\partial w$ over the synchronous solution in the silent phase. Note from (10.40) that $a_- > 0$. Let $(w^*, s^*) = (w_L(s^*), s^*)$ be the point where the synchronous solution meets the jump-up curve, and let $\lambda = w_L'(s^*)$ be the reciprocal slope of the jump-up curve at this point in (w,s)-space. Finally, let a_+ denote the value of $g(v,w)$ evaluated on the right hand branch of C_0 at the point where the synchronous solution jumps up. The main result in [tbk] is then the following.

Theorem: Assume that the nonlinear functions and parameters satisfy the assumptions stated above. If $\beta = \epsilon K$ with $K < a_-$ and $Ks^* < a_+/|\lambda|$, then the synchronous solution is asymptotically stable.

We note that the first condition in the Theorem is consistent with the numerical simulations of [wangrinz], who obtained synchronized solutions when the

synapses recovered at a rate slower than the rate at which the neurons recovered in their refractory period.

To interpret the second condition in the Theorem note that Ks^* is the rate of change of s at the point at which the synchronous solution jumps, while a_+ is the rate of change of w on the right hand branch right after the jump. Since $\lambda = dw_L/ds$, multiplication by $|\lambda|$ transforms changes in s to changes to w. One may think of $|\lambda|$ as giving a relationship between the time constants of inhibitory decay and recovery of the individual cells; a larger $|\lambda|$ (corresponding to a flatter jump-up curve) means that a fixed increment of decay of inhibition (Δs) has a larger effect on the amount of recovery that a cell must undergo before reaching it (inhibition-dependent) threshold for activation.

10.10 Propagating waves

We now consider propagating activity patterns. These may arise in both excitatory and inhibitory (as well as excitatory-inhibitory) networks and there have been numerous theoretical studies of mechanisms underlying both the existence and stability of this phenomenon. Wave-like activity has been observed experimentally in several brain regions.

Here we will consider conductance-based model of the region of the brain called the thalamus. At its simplest, the network consists of two layers of neurons, the thalamocortical cells (TC) and the reticular nucleus cells (RE). These nuclei have been shown to play a key role in the generation of sleep rhythms. Each neuron is modeled with single compartment, conductance based model that includes the usual potassium and sodium channels for spike generation, as well as a low threshold T-type calcium channel. This last channel allows the cells to produce rebound excitation. Details of the model can be found in [ ].

The phaseplane for an individual cell is shown in Figure 10.17A. Note that if a cell receives inhibitory input, then this raises the $V-$nullcline. If the cell receives inhibition for some period of time then the equilibrium moves toward the new fixed point. If the inhibition is rapidly removed, the $V-$nullcline falls back to the original position ($s = 0$) which leaves (V, h) above h_{max}. This causes the voltage to jump to the right branch of the nullcline (a rebound spike), before returning to rest. If the two layer network of these cells is wired up as in Figure 10.17B, then under some circumstance, the result is a wave of activity across the network. Such a wave is shown in Figure 10.17C. This is not a smooth wave; rather we call this a lurching wave. Here is what happens. A group of TC cells fires. This excites RE cells nearby causing them to fire. They inhibit the TC cells including those surrounding the original population of firing cells. The fresh population is inhibited and when the inhibition wears off, they fire as a group.

We now attempt to explain this and find a formula for the size of the groups that fire as well as the time it takes for them to fire. In order to do this, we will simplify a bit and consider a single layer of cells with inhibitory coupling. Thus, when a group of cells fires, it inhibits a neighboring group. After the inhibition wears off, the next group fires and so on. (In the next section, we will look at the transition

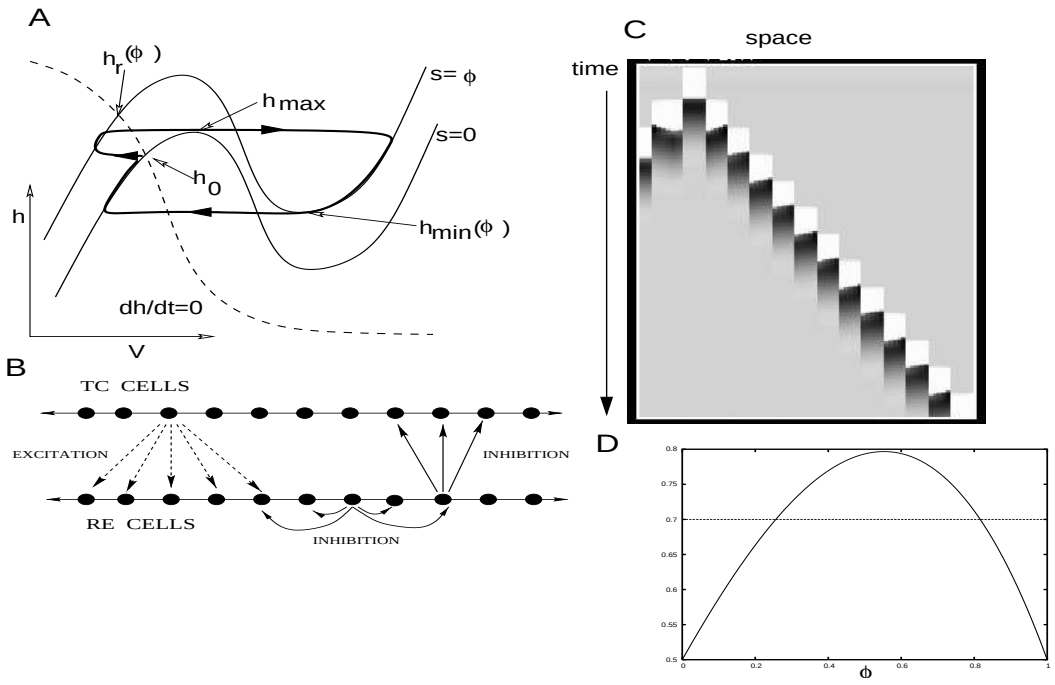

Figure 10.17. *Thalamic network model. (A) Phaseplane showing the h-nullcline (dashed) and V-nullcline at rest ($s = 0$). Several important values of h are shown. The approximate singular trajectory of a lurching wave is drawn in thick lines. (B) The architecture of the full model. (C) A simulation of a lurching wave. Grey scale depicts voltage; white=-40mV and black=-90mV. (D) The function $F(\phi)$ from equation (10.44 with $h_{max} = .7, h_{min}(\phi) = .2 + .5\phi, h_r(\phi) = .5 + \phi, \tau_R/\tau_L = .2$*

from smooth waves to lurchers through a different set of simplified models.) To analyze this model, we use singular perturbation. The present exposition will be a drastic approximation to a fuller analysis of the model which can be found in Terman et al. The equations of interest are

$$\epsilon \frac{\partial V}{\partial t} = f(V,h) - g \int_{-\infty}^{\infty} W(x-y)s(y,t)\, dy(V - V_{in}) \tag{10.41}$$

$$\frac{\partial h}{\partial t} = (h_\infty(V) - h)/\tau(V) \tag{10.42}$$

$$\epsilon \frac{\partial s}{\partial t} = \alpha H(V - V_T)(1 - s) - \beta s. \tag{10.43}$$

$f(V,h)$ is all the intrinsic currents of the cell. We suppose that the interaction kernel, $W(x)$ is a square and without generality, assume it is zero outside of $x = (-1/2, 1/2)$. We assume that $\tau(V)$ takes on two values, τ_R when V is on the right branch of the $V-$nullcline and τ_L when V on the left branch. The parameter ϵ is

small indicating that the dynamics is governed by the calcium recovery variable, h. (We should really start with ϵ multiplying the right-hand side of the h equation and then rescale time. In the interest of brevity, we have already done this.) By letting $\epsilon \to 0$, we analyze the singular trajectory and compute the properties of the wave. Figure 10.17A shows the singular trajectory of a group of cells. Suppose that ϕ is the size of the group of cells that is turned on. This inhibits a neighboring group, which are all at rest, h_0. As long as the first group remains on the right-branch of the $V-$nullcline, the second group crawls up the left branch of $V-$nullcline toward $h_r(\phi)$ the resting state. When the first group reaches the bottom of the inhibited ($s = \phi$) $V-$nullcline, the inhibition disappears. All cells that are above h_{max} will jump to the right branch, starting the cycle again. With this simple description of the wave, we can derive formulas for the time between jumps and the size of group that jumps. Suppose the group that jumps is on $x \in (-\phi, 0)$. This means that all the synaptic variables, $s(x,t)$, in the group are at their equilibrium values, $a \equiv \alpha/(\alpha+\beta)$. Thus

$$S_{tot}(x) \equiv \int_{-\infty}^{\infty} W(x-y)s(y,t)\ dy = a\int_{-\phi}^{0} W(x-y)\ dy.$$

We assume that ϕ is smaller than the synaptic footprint, so that $S_{tot}(x) = a\phi$ for $x \in (0,\phi)$. For the time in which this group of cells in on the right branch of the $V-$nullcline, All cells in $(-\phi,\phi)$ feel the same common inhibition parametrized by ϕ and the see the $V-$nullcline labeled $s = \phi$ in the figure. At the up-jump, all the cells roughly jump horizontally with $h = h_{max}$, the maximum of the $s = 0$ $V-$nullcline. They remain on the right branch until they reach $h_{min}(\phi)$ where they jump back. For V on the right branch, $h_\infty(V) = 0$, so the time it takes is

$$T = \tau_R \ln \frac{h_{max}}{h_{min}(\phi)}.$$

In the meantime, the group of cells at $x \in (0,\phi)$ is feeling the inhibition, so,starting from rest, they are heading toward the upper equilibrium point at $h_r(\phi)$. During this period h satisfies

$$\tau_L \frac{dh}{dt} = h_\infty(V_L(h)) - h, \quad h(0) = h_0,$$

where $V_L(h)$ is the value of the voltage on the $s = \phi$ $V-$nullcline. We approximate $h_\infty(V_L(h))$ as $h_r(\phi)$ so that we can solve for h in this time period:

$$h(x,t) = h_r(\phi) + (h_0 - h_r(\phi))e^{-t/\tau_L}.$$

When the inhibition wears off at $t = T$ only the cells above h_{max} will make the jump. Thus, for self-consistency, we must have

$$h(\phi, T) = h_{max}$$

or:

$$h_{max} = h_r(\phi) + (h_0 - h_r(\phi))\left(\frac{h_{min}(\phi)}{h_{max}}\right)^{\tau_R/\tau_L} \equiv F(\phi). \tag{10.44}$$

Thus, we reduce the problem to a single equation for ϕ. $F(0) = h_0 < h_{max}$ so that for small ϕ, $F(\phi) < h_{max}$. If the synaptic coupling g is large enough and τ_R/τ_L is also large, then $F(\phi)$ will be larger than h_{max} for ϕ in some range. Indeed, the function $F(\phi)$ is parabolic in shape (see figure 10.17, so there will either e two roots or no roots to this equation. Having found ϕ we can then plug it back to get T and thus get the speed of the lurching wave. In Terman, et al, a more correct and precise analysis is presented and compares very closely to the solutions obtained by numerically simulating the full model.

10.11 Bibliography

Half-centered oscillations, in which two mutually coupled cells can generate antiphase oscillations, was first described by Brown [7]. Another early paper that recognized the importance of postinhibitory rebound was that of Perkel and Mulloney [37].

The geometric singular perturbation approach decribed here began with papers by Kopell and Somers [33], who introduced the phrase "fast threshold modulations" and Terman and Wang [51]. Reviews of this and subsequent work can be found in Rubin and Terman [**?**] and Kopell and Ermentrout [32]..

Many papers have addressed the issue of when excitation or inhibition leads to synchrony or antiphase oscillations. Early papers are those of Van-Vreeswijk, Abbott and Ermentrout [53], Gerstner, van Hemmen and Cowen [18], and Wang and Rinzel [54]. Our approach follows most closely Wang and Rinzel's paper who recognized the importance of slow inhibitory dynamics in synchronizing the neuronal oscillations.

The issues described in this chapter are motivated by several neuronal systems, including thalamocortical sleep rhythms, olfaction and rhythmic behavior in the basal ganglia. References include [47, 11, 19, 44, 34, 6].

10.12 Exercises

1. Consider a system of the form (10.1). Assume that the system is oscillatory. Moreover, $g(v, w) = 0$ along the left branch of the cubic-shaped v-nullcline and $g(v, w) = 1$ along the right branch of this cubic. Finally, assume that the left and right knees of the cubic are at $w_L < w_R$, respectively. Compute the period of the singular periodic solution, with respect to the slow time-scale.

2. Construct a network of two mutually coupled cells with excitatory synapses that exhibits both a stable synchronous solution and a stable antiphase solution.

3. Construct a network of two mutually coupled cells with inhibitory synapses that exhibits antiphase (PIR) behavior and, by adjusting a single parameter, an almost synchronous solution. By adjusting another parameter, the network should exhibit a suppressed solution.

4. Construct a network of four mutually coupled cells that exhibits (for different values of parameters): a) synchronous behavior; b) a two-clustered solution in which there are two clusters with two cells in each cluster; c) a two-clustered solution in which there are three cells in one cluster and only one cell in the other cluster; c) a three-clustered solution in which there are two cells in one cluster and only one cell in the other two clusters; d) a four-clustered solution in which the cells take turns firing and the phase between the firings is constant; e) an almost-synchronous solution in which the cells take turns firing; the phase between the 'trailing cell' and the 'leading cell' is longer than the phase difference between other cells; e) a suppressed solution in which one cell fires periodically but the other cells are suppressed; f) a solution in which two of the cells fire in antiphase and the other two cells are suppressed.

5. Consider the synchronous solution with excitatory coupling. How does the frequency depend on the parameters I and $g_{syn}\epsilon$? Compute these curves using XPPAUT. Justify your answer using the singular constructions.

6. Give a detailed construction of the singular solutions corresponding to antiphase solutions arising from post-inhibitory rebound for the following cases: A) cellular escape; B) synaptic escape; and C) synaptic release.

7. Consider the antiphase solutions arising from post-inhibitory rebound. How does the frequency and duty cycle depend on the parameters I, g_{syn} and ϵ? You should consider separate cases: the cellular escape and release mechanisms and the synaptic escape and release mechanisms. Justify your answers using the singular constructions.

8. Use Gronwall's inequality to justify the last statement of Section 2.3.

9. In Section ??, we constructed the singular antiphase solution for excitatory synapses when the cells have a short duty cycle. Do the same thing for inhibitory synapses. Show that this solution is unstable.

10. Prove that as cells move along the same left or right branch of a cubic, the time metric between the cells is invariant.

11. Prove that $\Pi_2' = \Pi_4' = 1$ where Π_2 and Π_4 were defined in the Section ??.

12. Let $\Phi_L(w, s)$ be as in Section ??. Find conditions on $f(v, w)$ so that $\frac{\partial^2 \Phi_L}{\partial w \partial s} < 0$.

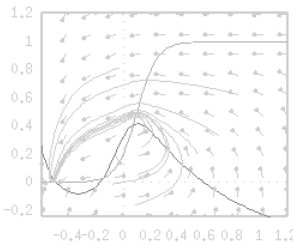

Chapter 11

Noise.

Neurons live in a noisy environment. That is, they are subjected to many sources of noise. For example, we treat ion channels deterministically, but in reality, opening and closing is a probablistic event. Similarly, there is spontaneous release of neurotransmitter which leads to random bombardment of small depolarizations and hyperpolarizations. *In vivo*, there is increasing evidence that cortical neurons live in a high conductance state due to the asynchronous firing of the cells which are presynaptic to them. Noise in neural and other excitable systems has been the subject of research since the early 60's. There are a number of good books and reviews about the subject. We single out the extensive review by Lindner et al (2004) and the book by Tuckwell.

Our goal in this chapter is to look at several aspects of the role of noise in neural models. Most of the analysis that we do will be on scalar models for the firing of action potentials, such as the integrate-and-fire. However, we also look at more general ionic models and stochastic channel dynamics. Since few textbooks in theoretical neuroscience address the issue of noise, we felt that a few words on the subject were warranted. There is no way to introduce a comprehensive theory of stochastic differential equations in the allotted space so we refer the reader to a number of good texts; notably Gardiner (1987) and the first five chapters of Kloeden and Platen(1995). The main point of the analysis in this chapter is to see the effects of noise on the subthreshold properties of neurons. This will allow us to develop heuristics for the firing rates of neurons in networks later on in the book.

Since the treatment of noise in this chapter is somewhat informal, we will not describe the beautiful mathematical constructions such as the Ito integral. Our main interest is the Langevin equation:

$$dX = A(X,t)dt + B(X,t)dW(t). \tag{11.1}$$

Here $X \in R^n$, $A : R^n \times R \to R^n$, B is an $n \times n$ matrix of functions, $B_{jk} : R^n \times R \to R$, and $W(t)$ is a vector of independent Wiener processes. (A Wiener process is formally defined below.) To get a feeling for this, it is helpful to solve this numerically:

$$X(n+1) = X(n) + hA(X(n), t_n) + B(X(n), t_n)\sqrt{h}\hat{N}(0,1) \tag{11.2}$$

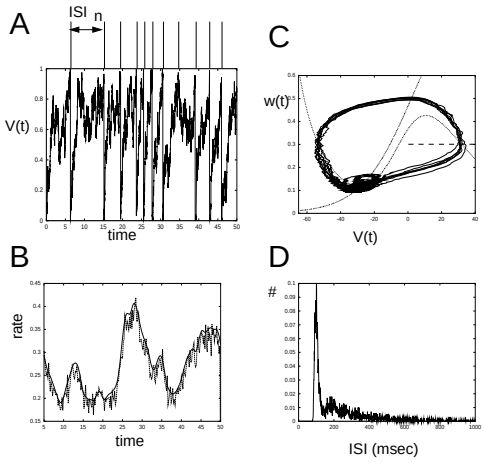

Figure 11.1. *Noisy neurons. (A) Integrate-and-fire model* $dV = (I - V)dt + \sigma dW(t)$ *with* $I = 0.75$ *and* $\sigma = 0.1$. *This numerical solution was computed using (11.2) with* $h = 0.01$. *Vertical lines represent times at which the model crosses* $V = 1$ *and is reset to 0. (B) Noise allows a subthreshold stimulus to be encoded. (C) Noisy ML model with class II parameters,* $I = 85$ *and unit variance noise in the voltage component. (D) Distribution of crossings of* $w = 0.3$.

where h is the discretization time step and $\hat{N}(0,1)$ is a vector of normally distributed independent random numbers with unit variance. (We will explain the strange $\sqrt{h}$ scaling below; you will just have to trust us on this for now.)

What does noise do to neurons? One of the main effects is that it allows them to fire in the presence of subthreshold inputs. That is, if a current is applied that will not cause the deterministic model to fire, the addition of zero mean noise can induce the neuron to fire. Figure 11.1A shows a simulation of the integrate and fire model with additive noise:

$$dV = (I - V)dt + \sigma dW_t$$

which is simulated with the simple scheme:

$$V_{n+1} = V_n + h(I - V_n) + \sigma\sqrt{h}\hat{N}(0,1).$$

In this figure, the threshold is $V = 1$ but $I = 0.75$ so that in the deterministic model ($\sigma = 0$), V will never fire. The addition of noise allows the model to fire occasionally. In fact, with sufficient noise, the neuron is able to sample stimulus and, over many trials, reconstruct it as in Figure 11.1B.

Figure 11.1C shows the effects of noise on the ML model with class II parameters. With $I = 85$, there is only a stable fixed point to the noiseless dynamics. Noise allows the neuron to spike with some regularity. How does one detect a spike in a stochastically driven model? Because the voltage itself is the driven variable,

then mathematically, the trajectory will not be differentiable so that theoretically it could cross a fixed value arbitrarily many times in a given time interval. This is not an issue with the integrate-and-fire model since as soon as it crosses threshold, the voltage is reset far away from threshold. In a simulation, we have access to all of the variables; in particular, the potassium gate. Figure 11.1C shows that crossing levels of w is a very reliable indicator of a spike. Thus, we collect all the times at which $w = 0.3$ is crossed from below. The interspike intervals (ISIs) are the times between spikes. Figure 11.1D shows a histogram of the distribution for these times. The distribution shows a sharp peak at about 100 msec and a broader, smaller peak at about 175 msec. In exercises 1-3 you are asked to look at these distributions more carefully.

The goal of this chapter is to provide some theoretical analysis of the results shown in figure 11.1. To set this up, we next provide a rather terse review of the theory of stochastic differential equations.

11.1 Stochastic differential equations.

Our main interest in this chapter is equation (11.1). Almost everything that can be done with this both practically and analytically concerns the scalar case where X is one-dimensional. The more general theory goes through as expected but the equations that we get are not easily solved either numerically or analytically. Thus, we start with the scalar equation. We can rewrite (11.1) as

$$x(t) = x(t_0) + \int_{t_0}^{t} a(x(s), s)\ ds + \int_{t_0}^{t} b(x(s), s) dW(s).$$

The first integral is the standard integral that you are probably familiar with, but the second integral is a stochastic integral. Let us briefly discuss some differences in the interpretation since this will come up when we introduce the Fokker-Planck equation.

11.1.1 The Wiener process.

We suppose that $W(t)$ is a *Wiener process.* This is just the limiting case of a random walk as the steps and the time between steps gets smaller such that $(\Delta x)^2/\Delta t$ tends to the finite limit of 1. That is, $W(t)$ is a simple diffusion process satisfying:

1. $W(0) = 0$
2. The probability distribution of $W(t)$ is Gaussian; that is, the density function satisfies
$$\frac{\partial p(x,t)}{\partial t} = \frac{\sigma^2}{2}\frac{\partial^2 p(x,t)}{\partial x^2}, \quad p(x,0) = \delta(x).$$
3. For any finite collection of times $t_1 < t_2 < \ldots < t_n$, the random variables $W(t_j) - W(t_{j-1})$ are independent.
4. $E[W(t)] = 0$ and $E[(W(t) - W(s))^2] = \sigma^2(t - s)$ for all $0 \le s \le t$.

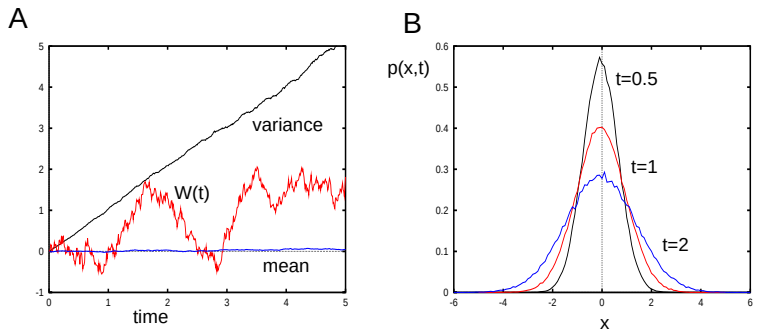

Figure 11.2. *Simulated Wiener process, $h = 0.01$. (A). Sample path and mean and variance of 1000 sample paths (B).Probability histogram for 100000 sample paths starting at $W(0) = 0$.*

5. $W(t)$ is a continuous process.

where $E[U]$ is the expected value of the random process U. As we pointed out in the introduction of this chapter, you can simulate a standard Wiener process by the iteration:

$$W(t+h) = W(t) + \sqrt{h}N(0,1) \tag{11.3}$$

where $N(0,1)$ is a normally distributed random variable with zero mean and unit variance. Figure 11.2 shows an example of such a simulation. Property (4) is illustrated in panel A; the mean is zero and the variance grows linearly in time. Panel B shows that the distribution is a Gaussian and a solution to the diffusion equation:

$$p(x,t) = \frac{1}{\sqrt{2\pi t}} e^{-x^2/(2t)}.$$

11.1.2 Stochastic integrals.

We now come to the main issue in stochastic calculus, the interpretation of an integral:

$$I = \int_{t_0}^{t} G(s)dW(s) \tag{11.4}$$

where $G(t)$ is a piecewise continuous function. As with usual integration, we divide the interval $[t_0, t]$ into finitely many points and write the partial sums

$$S_n = \sum_{j=1}^{n} G(\tau_j)[W(t_j) - W(t_{j-1})]$$

where we choose $t_{j-1} \le \tau_j \le t_j$. In Riemann integration, it doesn't matter where we take τ_j. However, for stochasic integration, the choice of τ_j matters (Gardiner, p

84.) For mathematical manipulation of the stochastic integrals, it turns out that one should take $\tau_j = t_{j-1}$. In this case, the resulting integral is called the *Ito* integral. The Ito calculus allows one to prove many rigorous results about stochastic integrals and also allows one to evaluate the integrals. An alternative choice of $\tau_j = (t_{j-1} + t_j)/2$ results in the *Stratonovich* integral and regular Stratonovich calculus. There is a relationship between the two integrals in the context of stochastic differential equations and there is a formula relating one to the other. The only reason we bring these technical issues up is that when we define the Fokker-Planck equations for (11.1), the choice of Ito versus Sratonovich matters. As far as neural modeling is concerned, some people prefer the Stratonovich calculus since it is the appropriate model is we assume that the "noise" has correlations and we take the limit as the correlation time goes to zero. *We cannot emphasise enough the point that if B is constant in (11.1), then the two are exactly the same.*

11.1.3 Change of variables: Ito's formula.

Later on (when we discuss the theta model), we will need to make a change of variables. In ordinary calculus, changing variables is a simple application of the chain rule. However, in the stochastic calculus, certain higher order terms are important. From equation (11.3), it follows that:

$$E[(W(t+h) - W(t))^2] = hE[N(0,1)^2] = h,$$

since $N(0,1)$ is a normal random variable with unit variance. Thus, we formally find

$$E[dW(t)^2] = dt.$$

Now suppose that x satisfies

$$dx = a(x,t)dt + b(x,t)dW(t).$$

Let $y = f(x)$ where f is twice differentiable. What differential equation does the new variable y satisfy (Gardiner,p 95) ?

$$\begin{aligned} dy &= f(x+dx) - f(x) \\ &= f'(x)dx + \frac{1}{2}f''(x)dx^2 + \dots \\ &= f'(x)[a(x,t)dt + b(x,t)dW(t)] + \frac{1}{2}f''(x)b^2(x,t)(dW(t))^2 + \dots \\ &= [f'(x)a(x,t) + \frac{1}{2}f''(x)b^2(x,t)]dt + f'(x)b(x,t)dW(t) + \dots . \end{aligned}$$

Unlike the standard chain rule, there is an additional term $f''(x)b^2(x,t)/2$ which appears in the determinsitic part of the equation for y. We call the equation:

$$df[x(t)] = \{f'[x(t)]a(x(t),t) + \frac{1}{2}f''[x(t)]b^2(x(t),t)\}dt + f'[x(t)]b(x(t),t)dW(t) \tag{11.5}$$

Ito's formula. There is an obvious multi-dimensional analogue of this equation.

11.1.4 Fokker-Planck Equation – General Considerations.

The Fokker-Planck equation (FPE) is the fundamental method that we have for studying stochastic differential equations. There is a cost to this in terms of practicality. The FPE is a diffusion equation on R^n so that instead of solving an $n-$dimensional stochastic differential equation (SDE), one has to solve a partial-differential equation. For the scalar case, the trade-off is not too bad and we can learn a lot from the analysis and simulation of the FPE. Beyond the scalar case, we have to say that it is probably more efficient to simulate the SDE.

Let us start with a general continuous scalar random process. Let $P(x,t)$ be the probability that a random variable, $X = x$ at time t. We will assume that the new state of the system depends only on the current state. (This is called the *Markov property* and such a process is called a Markov process.) Let $M(x',x,t)dt$ denote the rate at which the process whose state is $X = x'$ at time t jumps to x at time $t + dt$. Then

$$\frac{\partial P}{\partial t} = \int [M(x',x,t)P(x',t) - M(x,x',t)P(x,t)]\ dx'. \tag{11.6}$$

This is the *Master equation* and simply says that the rate of change of P is just the difference between the rate at which X goes from x' to x times the probability that one is in state x' and the rate at which the process leaves state x for some other state time the probability in state x. If X takes on discrete values then the integral is replaced by a sum. Let $Q(y,x,t) = M(x,x+y)$ be the rate of making a jump of size y from the point x. Equation (11.6) can be written as:

$$\frac{\partial P}{\partial t} = \int [Q(y,x-y,t)P(x-y,t) - Q(y,x,t)P(x,t)]\ dy.$$

The third order *Kramers-Moyal* expansion is an approximation in which we expand in y to second order:

$$\frac{\partial P}{\partial t} = \int\ dy[-y\frac{\partial Q(y,x,t)P(x,t)}{\partial x} + (y^2/2)\frac{\partial^2 Q(y,x,t)P(x,t)}{\partial x^2}. \tag{11.7}$$

Letting

$$\alpha_1(x,t) = \int\ dyyQ(y,x,t), \quad \alpha_2(x,t) = \int\ dyy^2Q(y,x,t)$$

we get an approximate PDE:

$$\frac{\partial P}{\partial t} = -\frac{\partial \alpha_1(x,t)P}{\partial x} + \frac{1}{2}\frac{\partial^2 \alpha_2(x,t)P}{\partial x^2}.$$

Note that α_1 is the mean jump size and α_2 is the variance. By assuming a diffusion process, all odd moments (y^3, y^5, etc) vanish and the higher even moments turn out to be expressible in terms of the second moment. Thus, for a diffusive process, the Kramer's-Moyal expansion is exact.

Let us return to the discretization of the scalar SDE:

$$x(t+h) = x(t) + ha(x,t) + \sqrt{h}b(x,t)N(0,1).$$

We can view this as a jump process in steps of h. The mean jump size is $ha(x,t)$ and the variance is $hb^2(x,t)$. Since the mean and variance in the Master equation are defined in terms of the rate per unit time, we divide by h and obtain the Fokker-Planck equation for the scalar Langevin equation (11.1)

$$\frac{\partial P}{\partial t} = -\frac{\partial a(x,t)P}{\partial x} + \frac{1}{2}\frac{\partial^2}{\partial x^2}\left(b(x,t)^2 P\right). \tag{11.8}$$

This equation can be more rigorously derived (see Gardiner), but, the present expansion provides the intuition behind it. The general n-dimensional FP equation for (11.1) is:

$$\frac{\partial P(X,t)}{\partial t} = -\sum_{i=1}^{n}\frac{\partial A_i(X,t)P(X,t)}{\partial x_i} + \frac{1}{2}\sum_{i,j=1}^{n}\frac{\partial^2}{\partial x_i \partial x_j}\left(B(X,t)B^T(X,t)P(X,t)\right). \tag{11.9}$$

In general, this PDE is intractable and numerical solutions must be computed. Since it is a PDE, it may be impractical to actually solve this and instead, the best to approach is to run the stochastic equation many times and take averages. Below, we introduce a method for obtaining equations for the moments; in particular, the mean and the variance in the small noise case.

Derivation from Ito's formula.

Here we derive the FPE using Ito's formula and taking averages. This derivation is adapted from Rudolph & Destexhe (NC 2003). We only derive the scalar model version. Consider the stochastic differential equation:

$$dx = f(x,t)dt + g(x,t)dW.$$

Let $y = h(x)$ be a transformation where h is arbitrary but twice differentiable. From Ito's formula,

$$dh(x) = h'(x)f(x,t)dt + h''(x)g^2(x,t)/2dt + h'(x)gdW.$$

Here primes mean differentiation with respect to x. Taking the expectation of this, we obtain:

$$\frac{d}{dt}E[h(x)] = E[h'(x)f(x,t)] + E[h''(x)g^2(x,t)/2].$$

Let $\rho(x,t)$ be the probability distribution for the variable x. Note that

$$E[U(x,t)] = \int U(x,t)\rho(x,t)dx.$$

The integral is over the domain of x, often the real line, but not always. Using the definition of the expectation, we find:

$$\frac{d}{dt}\int h(x)\rho(x,t)\ dx = \int [h'(x)f(x,t) + h''(x)g^2(x,t)/2]\rho(x,t)\ dx.$$

If we integrate the right hand side by parts, we obtain:

$$\frac{d}{dt}\int h(x)\rho(x,t)\ dx = \int [-(f(x,t\rho(x,t))' + (g^2(x,t)/2\rho(x,t))'']h(x)\ dx.$$

Since this must hold for any function $h(x)$, we must have:

$$\frac{\partial \rho}{\partial t} = \frac{\partial}{\partial x}\left(-f(x,t)\rho(x,t) + \frac{1}{2}\frac{\partial}{\partial x}[g^2(x,t)\rho(x,t)]\right).$$

This is the Fokker-Planck equation.

11.1.5 Scalar with constant noise

Here we are interested in the equation:

$$dx = f(x,t)dt + \sigma dW(t) \tag{11.10}$$

where $W(t)$ is the standard Wiener process. We are interested in the distribution of x as well as various rates such as how quickly x leaves a region. We can integrate (11.10) to obtain

$$x(t) = x(0) + \int_0^t f(x(s),s)\ dt + \sigma \int_0^t dW(t).$$

We start with the Fokker-Planck equation for this process. By assuming *additive* noise, we avoid issues about the interpretation of the stochastic integral. For a full discussion of this topic, see Gardiner (1995). From (11.8), the *forward* Fokker-Planck equation for (11.10) is:

$$\frac{\partial P(x,t)}{\partial t} = -\frac{\partial f(x,t)P(x,t)}{\partial x} + \frac{\sigma^2}{2}\frac{\partial^2 P(x,t)}{\partial x^2}. \tag{11.11}$$

This can also be written as a conservation law for probability:

$$\frac{\partial P(x,t)}{\partial t} + \frac{\partial J(x,t)}{\partial x} = 0,$$

where $J(x,t)$ is the probability current (in dimensions of dx/dt):

$$J(x,t) = f(x,t)P(x,t) - \frac{\sigma^2}{2}\frac{\partial P(x,t)}{\partial x}.$$

The current J consists of two parts: an active transport term $f(x,t)P(x,t)$ and a diffusive term $(\sigma^2/2)\partial P/\partial x$. The probability current is similar to the current that we saw earlier in our models of the cable equation. Unlike the axon equations, however, here we have *drift* or transport terms $f(x,t)$ which actively direct the probability flow according to the spatial location. Consider an interval $[a,b]$. The

change in probability in the interval must equal inward current minus the outward current. Thus, we have

$$\frac{\partial}{\partial t}\int_a^b P(x,t)\ dx = J(a,x) - J(b,x) = -\int_a^b \frac{\partial}{\partial x} J(x,t)\ dx.$$

Since the interval is arbitrary, we obtain the standard continuity equations:

$$\frac{\partial P(x,t)}{\partial t} = -\frac{\partial J(x,t)}{\partial x}.$$

We note that this simple continuity equation assumes infinitesimal jumps (in order to write this as a partial *differential* equation), but as we will encounter below, there may be large jumps so that the corresponding conservation equations must be amended.

In order to solve the Fokker-Planck PDE, we need boundary and initial conditions. If we choose positive initial data, then the maximum principle for the diffusion equation guarantees that $P(x,t) \geq 0$. Furthermore, if

$$\int_\Omega P(x,0)\ dx = 1$$

then

$$\int_\Omega P(x,t)\ dx = 1$$

from conservation of probability. (Here Ω is the domain of x.) There are numerous possible boundary conditions which are physically reasonable. If the domain is the real line, then obviously we want $P(x,t) \to 0$ as $|x| \to \infty$. In some examples the domain will be periodic so that $P(a,t) = P(b,t)$ and $J(a,t) = J(b,t)$.

We discuss two particularly important boundary conditions. If $P(x,t) = 0$ at a boundary point, a, we say that the boundary is *absorbing*. A particle reaching the boundary is absorbed. In this case, we lose conservation of probability. So, if this condition occurs, then it is necessary to add other terms to the continuity equations or have the flux out of that end point appear somewhere else to keep the total probability at 1. (In the scalar neuron models, described below, this condition occurs at the "spike" of the cell.) If $J(x,t) = 0$ at a boundary point, a, we say it is a *reflecting* boundary. A particle reaching the boundary cannot cross it (the current is zero) so that it bounces back.

Often one is only interested in stationary distributions ($f(x,t)$ is independent of t, for example). Then we obtain

$$\frac{\sigma^2}{2}P'' - (fP)' = 0,$$

where P' is the derivative with respect to x. This is an ODE and can be integrated once:

$$-\frac{\sigma^2}{2}P'(x) + f(x)P(x) = J. \tag{11.12}$$

J is just a constant of integration; the current described above. Suppose the domain is the real line. Then $P(\pm\infty) = P'(\pm\infty) = 0$ since P must be integrable. Thus, $J = 0$ and we can solve for the steady state:

$$P(x) = K \exp \frac{2F(x)}{\sigma^2} \tag{11.13}$$

where $F'(x) = f(x)$ and K is a normalization constant so that $\int P(x) = 1$. The function $-F(x)$ is called the potential for this process and local peaks in the probability correspond to minima of the potential. Consider, as an example, $f(x) = -x$. Then

$$P(x) = \frac{1}{\sigma\sqrt{\pi}} e^{-(x/\sigma)^2}.$$

If the domain is not infinite, then, J may be nonzero. However, if one of the boundaries is reflecting, then $J = 0$ which means that the other boundary must also be reflecting *unless there are additional terms in the continuity equation such as jumps.* Suppose the domain is (a, b). In general, with $J \neq 0$, we can still solve the steady state. Let

$$\Psi(x) = \exp\left((2/\sigma^2)\int_a^x f(y)dy\right).$$

Then we integrate (11.12) to obtain:

$$P(x) = \Psi(x)[P(a) - \frac{2J}{\sigma^2}\int_a^x dy/\Psi(y)].$$

Suppose, for example, the boundary conditions are periodic. Then we require $P(a) = P(b)$. Then, we obtain

$$J = P(a)\frac{[\Psi(b) - 1]\sigma^2}{2\Psi(b)\int_a^b dy/\Psi(y)}. \tag{11.14}$$

$P(a)$ is found by the normalization condition, $\int_a^b P(x) = 1$.

11.1.6 First passage times

Consider the equation (11.10). We now ask the following question: what is the distribution of exit times from the domain $[a, b]$ for the stochastic process? Suppose that $x(0) = x$. Let $p(x', t|x, 0)$ be the probability that the process defined by (11.10) is at x' at time t given it started at x at time 0. Define

$$G(x, t) \equiv \int_a^b dx' p(x', t|x, 0).$$

$G(x, t)$ is the probability that x is still in the interval $[a, b]$ at time t. Thus, if T is the time that x *leaves* the interval, then $G(x, t) = \text{Prob}(T \geq t)$. Why do we care

about this function? Below, when we discuss scalar models like the integrate-and-fire, we will be interested when the voltage crosses the threshold. These crossing times correspond to "spikes" and their distribution is the ISI distribution. Gardiner shows that $G(x,t)$ satisfies the *backward* FP equation:

$$\frac{\partial G(x,t)}{\partial t} = f(x,t)\frac{\partial G(x,t)}{\partial x} + \frac{\sigma^2}{2}\frac{\partial^2 G(x,t)}{\partial x^2}. \tag{11.15}$$

What are the initial and boundary conditions? Clearly $G(x,0) = 1$ if $a < x < b$. The boundary conditions depend on the nature of the problem. We will often take absorbing conditions at $x = b$.

For many problems, we are interested in the mean exit time, $T(x)$, defined as the expected time to leave the interval given a starting value at x. Suppose that f is independent of time. The definition of $G(x,t)$ implies that

$$G(x,t) = \int_t^\infty \rho(x,t')\ dt' \tag{11.16}$$

where $\rho(x,t)dt$ is the probability that x exits the domain in the interval $(t, t+dt)$. The mean first passage time is thus

$$< T > (x) = \int_0^\infty t\rho(x,t).$$

Integration by parts (exercise ??) shows that

$$< T > (x) = \int_0^\infty G(x,t)\ dt.$$

In the same exercise you show that equation (11.15) implies that $< T >$ satisfies the simple ODE:

$$-1 = f(x) < T >' + \frac{\sigma^2}{2} < T >'' . \tag{11.17}$$

Finally, a closed form solution is provided in the exercise, although, the integrals cannot generally be evaluated except numerically. In addition to the mean first passage time, one is often interested in higher moments such as the variance, $< T^2 >$. The n^{th} moment, T_n satisfies a simple second order equation like (11.17) depending only on the previous moments (exercise ?). Since the first passage time is realted to the firing rate of a noisy neuron, spike statistics can be found from the solution to the moment equations. For example the *coefficient of variation* (CV) is a measure of the irregularity of a process and is defined as the ratio of the standard deviation to the mean. The standard deviation of the firing rate is just

$$\sigma = \sqrt{E[(T - E[T])^2]} = \sqrt{E[T^2] - E[T]^2}$$

so that the CV is

$$\mathrm{CV}_T = \sqrt{E[(T/E[T])^2] - 1}.$$

Simple derivation of the first passage time.

Larry Abbott (personal communication) provides a very simple derivation of the first passage time. As above, we let $T(x)$ denote the mean first passage. On a given trial, x moves from x to $x + \Delta x$ in time Δt. Then on average, $< T(x + \Delta x) >= T(x) - \Delta t$. (Note that Δx is a random variable but $T(x), x, \Delta t$ are not.) From equation (11.10), we note that

$$\Delta x = f(x)\Delta t + \sigma\sqrt{\Delta t}\xi$$

where ξ is a normally distributed random variable with zero mean and unit variance. Thus, the mean of Δx is $f(x)\Delta t$. The mean of $(\Delta x)^2$ is

$$< \Delta x^2 >= \left\langle [f(x)\Delta t + \sigma\sqrt{\Delta t}\xi]^2 \right\rangle = [f(x)\Delta t]^2 + \sigma^2\Delta t = \sigma^2\Delta t + O((\Delta t)^2).$$

Now, expand $T(x + \Delta x)$, in small Δx, to get:

$$T(x + \Delta x) \approx T(x) + \Delta x T'(x) + \frac{1}{2}(\Delta x)^2 T''(x) + \ldots.$$

Taking the mean, using the above fact that $< (\Delta x)^2 >= \sigma^2\Delta t + O((\Delta t)^2)$, and dividing by Δt we get:

$$\frac{\sigma^2}{2}T''(x) + f(x)T'(x) = -1$$

as $\Delta t \to 0$.

Some comments on the utility of first passage times.

First passage time methods are an elegant tool for determining various questions like the firing rate of a neuron in the presence of noise. However, it is crucial that one be able to actually determine what the crossing threshold is for the model. In one-dimensional neurons, this is very clear – we set a point at which the cell is said to fire and that is that. (Technically, we apply an absorbing boundary condition at the spike, $P(V_{spike}, t) = 0$.) However, consider model that actually does produce spikes like the Morris-Lecar model, for example. The phase-space is no longer an interval on the line with a well-defined boundary. Rather, the domain is the whole plane. Given this, what do we mean when we say a neuron produces a spike? We could, for example, look for a peak in the membrane potential and call that a spike. This is what neuroscientists do when they attempt to detect spikes from the extra- or intracellular recordings of a neurons. However, with additive white noise stimuli, the voltage can cross a set threshold arbitrarily many times in any given interval so that a peak will not make any sense. There are two ways around this difficulty. One way is to use *colored* noise, that is, noise which has been low-pass filtered so that the right hand sides of the voltage equation are continuous. In this case, the peak of the voltage is well defined so that we can, at least, run reasonable stochastic simulations. Using colored noise presents a more realistic scenario for the environment of a neuron, but the analysis of this process is far more difficult as

we no longer obatin simple ODEs. Another way around the problem (which is not available to an experimentalist) is to consider crossing of one of the other variables in the ODE. For example, in the Morris-Lecar, we could say that a spike is emitted if $w(t)$ crosses some set value, $\bar{w}$. This was done in the Monte-Carlo simulation in figure 11.1C. Analytically (but, rather impractically), we could write down the full Fokker-Plank equations on a large enough domain and compute the flux through some region in the domain of the model and call this the firing rate. For example, if the model is planar, $dV = f(V,w)dt + \sigma dW$, $dw = g(V,w)dt$, then we solve the appropriate Fokker-Plank equation:

$$P_t = \frac{\sigma^2}{2} P_{VV} - [f(V,w)P]_V - [g(V,w)P]_w$$

on a large rectangle (large enough to ignore the boundaries, since the real problem is actually defined on the whole plane). Suppose that we obtain the stationary distribution, $P(V,w)$. We can say that a spike has fired if, e.g., w crosses some proscribed value, $\bar{w}$, while V lies in some specified interval. The total flux is the firing rate:

$$F = \int_{V_1}^{V_2} J_w(V,\bar{w})dV$$

where, $J_w(V,w) = g(V,w)P(V,w)$.

In sum, from a practical view point, most of the noise calculations that are done for neuron models make sense only for simple one-dimensional dynamics. Once we get to biophysical models, it is best to just simulate them as in figure 11.1C.

11.2 Firing rates of scalar neuron models.

We now turn to the applications to scalar neuron models of the methods we outlined above. Most scalar neuron models (such as the integrate-and-fire) have a reset condition when the voltages reaches a particular value, V_{spike}. Often, this particular value is the maximum value that the potential can take, thus, the probability of finding the neuron at this value vanishes – there is an absorbing boundary condition. However, the probability current out of that point (which represents the neuron's firing rate) is "re-injected" at the reset potential, V_{reset} so that the total probability is conserved. We begin with a generic scalar model with additive white noise:

$$dV = f(V,t)dt + \sigma dW(t) \tag{11.18}$$

with the stipulation that when $V(t)$ reaches V_{spike} from below, to is reset to V_{reset}. If $f(V,t) = -aV + I$, then we have the leaky integrate and fire model while if $f(V,t) = aV^2 + I$, we have the quadratic integrate and fire model. To obtain the mean firing rate, we can either solve the steady-state Fokker-Planck equation (11.11) or the mean first-passage time equation (11.17). We can also use the backward equation (11.15) to obtain interspike-interval histograms for these scalar models. In the rest of this section, we apply the above theory. Unfortunately, the resulting integrals are basically impossible to explicitly evaluate. On the other hand, the fact

that the steady-state Fokker-Planck equation and the first passage time equation are ordinary differential equations allows us to find smooth numerical solutions as parameters vary.

11.2.1 The Fokker-Planck equation.

The probability density for (11.18) subject to reset can be formally written as:

$$\frac{\partial P(V,t)}{\partial t} = -\frac{\partial}{\partial V} J(V,t) + \delta(V - V_{reset}) J(V_{spike}, t) \tag{11.19}$$

where

$$J(V,t) = f(V,t)P(V,t) - \frac{\sigma^2}{2}\frac{\partial P(V,t)}{\partial V}. \tag{11.20}$$

This equation is defined on the interval $-\infty < V < V_{spike}$. The boundary conditions are $P(-\infty, t) = 0$ and $P(V_{spike}) = 0$. The latter condition is *absorbing*. However, probability is conserved due to the delta-function term appearing in (11.19). Indeed, the reader can integrate this equation over the interval on which it is defined and see that

$$\frac{\partial}{\partial t}\int_{-\infty}^{V_{spike}} P(V,t)\ dV = 0.$$

Stationary solutions satisfy

$$0 = -\frac{d}{dV} J(V) + \delta(V - V_{reset}) J(V_{spike}).$$

We integrate this with respect to V to obtain:

$$J_0 = -J(V) + J(V_{spike}) H(V - V_{reset}),$$

where $H(V)$ is the Heaviside step function. Since $P(V)$ and its derivatives must vanish at $V = -\infty$, we conclude that $J_0 = 0$. Since $P(V_{spike} = 0)$ equation (11.20) implies that at steady-state:

$$J(V_{spike}) = -\frac{\sigma^2}{2}\frac{dP(V_{spike}}{dV} \equiv \nu.$$

The firing rate of the neuron is just $J(V_{spike}, t)$. Thus, we have the simple first-order linear differential equation:

$$J(V) \equiv f(V)P(V) - \frac{\sigma^2}{2}\frac{dP(V)}{dV} = \nu H(V - V_{reset}).$$

We let $P_{\pm}(V)$ denote the solutions to this equation for $V < V_{reset}$ and for $V > V_{reset}$. Then, with normalization we have:

$$f(V)P_-(V) - \frac{\sigma^2}{2}P'_-(V) = 0 \quad -\infty < V < V_{reset}$$
$$f(V)P_+(V) - \frac{\sigma^2}{2}P'_+(V) = \nu \quad V_{reset} < V < V_{spike}$$

$$\begin{aligned} P_-(-\infty) &= 0 \\ P_-(V_{reset}) &= P_+(V_{reset}) \\ P_+(V_{spike}) &= 0 \\ \int_{-\infty}^{V_{reset}} P_-(V)\, dV + \int_{V_{reset}}^{V_{spike}} P_+(V)\, dV &= 1. \end{aligned}$$

The solution to the stationary state depends on a single constant ν and this constant is determined by the normalization. Define $F(x)$ as $F'(x) = f(x)$. After a bit of simple manipulation, we find:

$$\begin{aligned} \nu^{-1} &= \frac{2}{\sigma^2} \int_{-\infty}^{V_{reset}} e^{\frac{2F(x)}{\sigma^2}}\, dx \int_{V_{reset}}^{V_{spike}} e^{\frac{-2F(y)}{\sigma^2}}\, dy \\ &+ \frac{2}{\sigma^2} \int_{V_{reset}}^{V_{spike}} e^{\frac{2F(x)}{\sigma^2}} \int_{x}^{V_{spike}} e^{\frac{-2F(y)}{\sigma^2}}\, dy\, dx \\ &= \frac{2}{\sigma^2} \int_{-\infty}^{V_{spike}} e^{\frac{2F(x)}{\sigma^2}} \int_{\max(x, V_{reset})}^{V_{spike}} e^{\frac{-2F(y)}{\sigma^2}}\, dy\, dx. \end{aligned} \tag{11.21}$$

This equation and three dollars will get you a small cup of coffee at Starbucks. We can simplify this equation for some particular cases although the evaluation of the resulting expressions is still nontrivial. We note that the flux is always positive *because of the absorbing boundary* at $V = V_{spike}$. The reason for this is that the flux is proportional to $-\partial_V P(V)$ at V_{spike}. Since P is positive and vanishes at V_{spike}, its derivative at V_{spike} must be negative.

Constant drift.

Suppose that $f(V) = I$; there is no dependence on the potential. Then we leave it as an exercise to the reader to show that the expression (11.21) is independent of σ and the firing rate is just

$$\nu = \frac{I}{V_{spike} - V_{reset}}.$$

Leaky integrate and fire.

For the leaky integrate and fire, $f(x) = I - x$, so that $F(x) = Ix - x^2/2$. Fourcaud and Brunel (2002) provide the most compact form for the firing rate of the leaky-integrate-and fire model:

$$\nu^{-1} = \sqrt{\pi} \int_{\frac{V_{reset}-I}{\sigma}}^{\frac{V_{spike}-I}{\sigma}} e^{s^2}(1 + \mathrm{erf}(s))\, ds, \tag{11.22}$$

where

$$\mathrm{erf}(x) = \frac{1}{\sqrt{\pi}} \int_{-x}^{x} e^{-s^2}\, ds.$$

In spite of the simple form, this is not a simple function to compute. Indeed, evaluating the integral numerically requires dealing with the very large $\exp(x^2)$ and

the very small $1 + \mathrm{erf}(x)$. In figure 11.3, we plot some representative firing curves for the LIF (and other models) by solving an appropriate boundary value problem. We can, however, do some asymptotic analysis is the cases of either large I or large σ. We leave all of this, including the derivation of (11.22) as exercises to the reader.

Quadratic integrate-and-fire.

In the quadratic integrate and fire model, $f(V) = V^2 + I$, $V_{spike} = +\infty$ and $V_{reset} = -\infty$. With some simple rescaling of the resulting integral, we arrive at a formula first derived by Lindner and Longtin:

$$\nu^{-1} = \left(\frac{18}{\sigma^2}\right)^{1/3} \int_{-\infty}^{\infty} dx\ e^{-ax-x^3} \int_{-\infty}^{x} dy e^{ay+y^3}, \tag{11.23}$$

where

$$a = \left(\frac{12}{\sigma^4}\right)^{1/3}.$$

Sigeti and Horsthemke (1989) evaluated this integral exactly for the case in which $I = 0$ (at the saddle-node) and obtain

$$\nu(I=0) = [\Gamma(1/3)]^{-2} \left(\frac{3\sigma}{2}\right)^{1/3} = 0.1595\ldots\sigma^{2/3}.$$

Not surprisingly, for $I > 0$ and small noise, $\nu \sim \sqrt{I}/\pi$, the deterministic firing rate. More interestingly, for $I < 0$ (the resting neuron), noise induced firing occurs and the rate is given by

$$\nu = \frac{\sqrt{|I|}}{\pi} \exp\left[-\frac{8|I|^{3/2}}{3\sigma^2}\right]$$

for $\sigma^2 \ll |I|^{3/2}$. (See Lindner and Longtin, 2004).

Ring models.

In the exercises of chapters ? and ?, we introduced ring models defined on the unit circle:

$$\frac{dV}{dt} = f(V) + I$$

where $f(V)$ is continuous and 2π-periodic. We can consider the noisy version of this:

$$dV = (f(V) + I)dt + \sigma dW(t). \tag{11.24}$$

The stationary distribution, $P(V)$ must also be periodic, so that it must satisfy

$$J = (f(V) + I)P(V) - \frac{\sigma^2}{2}\frac{dP}{dV}.$$

The constant J is the current and is also the firing rate of the neuron. Unlike the integrate-and-fire models, there is no reset condition so the current is equal at every

point. In particular, if I is large enough, then $f(V)+I$ is positive so that in absence of noise, we have

$$J^{-1} = \int_0^{2\pi} \frac{dV}{f(V)+I}.$$

More generally, we can apply equation (11.14) where

$$\Psi(x) = \exp\left((2/\sigma^2)\int_0^x (f(y)+I)dy\right).$$

We remark that, unlike integrate-and-fire type models, the current can be either positive or negative. (For I large and negative the oscillator runs couterclockwise.) Thus, one has to be careful with the interpretation of ring models as neural oscillators. One special case of a ring model was analyzed by Ritt:

$$d\theta = [1-\cos\theta + (1+\cos\theta)(I - \frac{\sigma}{2}\sin\theta)]dt + \sigma(1+\cos\theta)dW(t).$$

Here firing occurs when $\theta = \pi$. This model is equivalent to the QIF under the transformation $V \to \tan(\theta/2)$. Unlike the ring models with simple additive noise, (11.24), the noise is state-dependent and vanishes at $\theta = \pi$. Evaluation of the right-hand side at $\theta = \pi$ shows that the current is always positive. Without the singular noise, we cannot guarantee that the current will always be positive in general ring models.

11.2.2 First passage times.

The Fokker-Planck equation gives us more than just the firing rate – it also provides the distribution of the potentials. However, it is rare that one would need this information. (Although, in a very clever paper, Rudolphe et al show that by measuring the distribution of the noisy subthreshold potential in a neuron, it is possible to extract estimates of the mean and variance of excitatory and inhibitory conductances. See exercise ???.) Instead, the interspike interval distribution, the mean firing rate and the variance of the firing rate are much more useful. In section ** we developed equations for the mean time to reach a given point as well as the evolution of those times. We have

$$dV = f(V) + \sigma dW(t)$$

with $V(0) = V_{reset}$ and we want to determine the distribution of times at which $V(t) = V_{spike}$. The domain of interest is $-\infty < V < V_{spike}$. The average time between spikes is just the epected time it takes to go from V_{reset} to V_{spike} and the inter-spike interval histogram (ISI) is just the probability density function for the exit times given that the starting point is V_{reset}. From equation (11.16), the quantity $\rho(V_{reset}, t)$ is this probability density function and is just the derivative of the solution to the backward equation (11.15). Because there is no reset involved, it is often the case that the mean first passage time solution results in a simpler,

more compact, expression for the firing rate in contrast to equation (11.21). From equation (11.17), the mean first passage time equation is

$$\frac{\sigma^2}{2}T''(V) + f(V)T' = -1 \tag{11.25}$$

with appropriate boundary conditions. Recall that $T(V)$ is the expected time to exit some prescribed boundary given that at $t = 0$ the voltage is V. If we are working with an integrate-and-fire type model where there is a spike at V_{spike} and a reset to V_{reset}, then one of the boundary conditions is $T(V_{spike}) = 0$. Gardiner (p 139) shows that the other desired condition is that $T'(V) \to 0$ as $V \to -\infty$. However, this does not imply that the $T(V)$ itself remain bounded. Equation (11.25) is just a first order equation in $T'(V)$. We can use asymptotics to examine the large negative V behavior. If $f(V) = KV^p + \ldots$ where the remaining terms are lower order in V and $p > 0$, then clearly, we must have that

$$T'(V) = -\frac{1}{KV^p} + \ldots$$

as $V \to \infty$. If, as in the case of the leaky integrate-and-fire model, $p = 1$, then $T'(V)$ does go to zero as $V \to -\infty$ but, $T(V)$ diverges. The intuition behind the divergence of T is that with the LIF, solutions to the deterministic problem are exponentials which remain finite for all time – a solution with $V(0)$ arbitrarily large and negative reaches firing at a time proportional to $log(|V(0)|$ which can be arbitrarily large. In contrast, the quadratic integrate and fire model has $p = 2$ and thus $T(V)$ converges as $V \to \infty$ since the quadratic equation $V' = a + bV^2$ "blows up" in finite time.

With the condition $T(V_{spike} = 0$ and $T'(-\infty) = 0$, the solution to (11.25) is:

$$T(V) = \frac{2}{\sigma^2}\int_V^{V_{spike}} e^{\frac{-2F(x)}{\sigma^2}} \int_{-\infty}^{x} e^{\frac{2F(y)}{\sigma^2}} dy\ dx. \tag{11.26}$$

where $F(x) = \int f(x)dx$. (See exercise ???). Analogous expressions for periodic boundary conditions can be found for ring models *as long as the current* is nonzero. The current vanishes if and only if the average of $f(V)$ over the domain is zero. Equation (11.26) allows us (up to actually evaluating the integrals) to compute the FI curve in the presence of noise. By definition, $T(V_{reset})$ is the mean time to fire a spike so the firing rate is just $1/T(V_{reset})$. We can either numerically evaluate the double integral, numerically solve the boundary value problem (11.25), or numerically solve the Fokker-Planck equation (11.19). We find that the solution to the BVP seems to be the simplest choice.

Since we will use the noisy FI curves later in the book, we illustrate them in Figure 11.3 for two levels of noise. Both the solutions to the BVP and the Monte-Carlo simulations are shown. (For the Monte-Carlo simulations, we solve the equations for a time interval of 2000 and count the number of spikes.) The main differences between the smaller and large noise cases is that the FI curve is more linear with larger noise. This is a classic result: noise linearizes the response. In all cases, the deterministic model is smeared by the noise resulting in a smoother

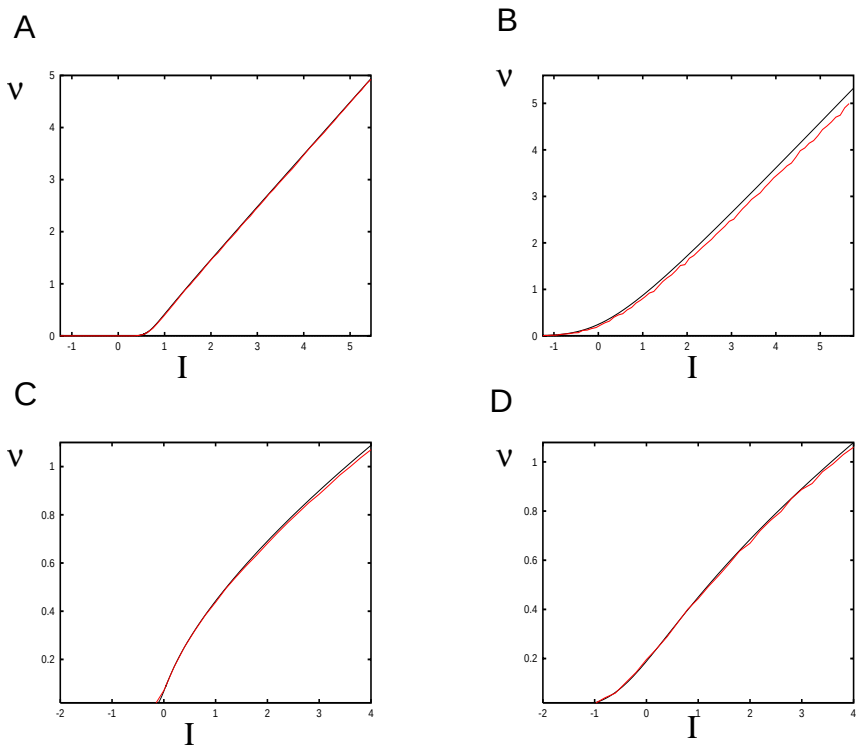

Figure 11.3. *F-I curves for the leaky (spike is at 1 and reset at 0) and quadratic (spike is at 10 and reset at -1) integrate and fire models. Solutions to the BVP are shown in black and Monte-Carlo simulations are shown in red. (A,B) LIF with* $\sigma = 0.25$ *(A) and* $\sigma = 1.0$ *(B). QIF with* $\sigma = 0.25$ *(C) and* $\sigma = 1$ *(D).*

sigmoidal curve. The firing rate curves will be useful for network models, thus, we will attempt to create easily computed approximations of them. Suppose that $F(I)$ is the deterministic FI curve when there is zero noise. We will approximate the noisy FI curve by the composition of $F(I)$ with a a function $M(I,p)$ which has the following properties. $M(I,p)$ is positive, monotone, and asymptotically approaches I for large I, independent of p. As $p \to 0^+$, $M(I,p) \to [I]_+$, the positive part of I. Several choices come to mind:

$$\begin{aligned} M_1(I,p) &= \frac{I}{1-\exp(-I/p)} \\ M_2(I,p) &= p\log(1+\exp(I/p)) \\ M_3(I,p) &= \frac{1}{2}\left[x(1+\mathrm{erf}(I/p)) + \frac{p}{\sqrt{\pi}}\exp(-(I/p)^2)\right]. \end{aligned} \tag{11.27}$$

The last function is the convolution of a gaussian with the positive part of I. Thus

we approximate the noisy FI curve by

$$\nu(I) = F(M_j(I,p))$$

where p is chosen to best fit the true FI curve. We find that the third choice provides a pretty good fit with the FI curves in figure 11.3. The parameter p is roughly linearly proportional to the noise, σ.

Other statistics.

There are other statistics besides the mean firing rate which may be useful. For example, one might desire to compute the variance, σ^2 and thus the standard deviation, σ. A much-used characteristic of the "noisiness" of a neuron is the coefficient of variation (CV), which is σ/T. Recall that the variance is just

$$\sigma^2 = \left\langle (T - < T >)^2 \right\rangle = < T^2 > - < T >^2 .$$

Exercise ** shows the second moment $T_2(V)$ obeys a simple second order ODE:

$$\frac{\sigma^2}{2} T_2''(V) + f(V) T_2' = -T(V)$$

where $T(V)$ is the already determined mean first passage time. The boundary conditions are the same as for $T(V)$.

Aside: Solving the BVP.

Ideally, we would like to numerically solve (11.25) on the interval $(-\infty, V_{spike})$, however,this obviously impossible. Thus we solve the problem on the interval $(-A, V_{spike})$ where we pick A large enough. We will use AUTO to do this since it is very efficient and works better than simple shooting. Our estimates above indicate that $T(V) = O(V^{-p})$ where $p = 1$ for the LIF and $p = 2$ for the QIF. Thus, we expect we will have to make A larger for the LIF in order to better approximate a reflecting boundary condition $T'(-A) = 0$. Since our asymptotics actually provide an estimate for $T'(-A)$ for large A, we use the boundary condition $T'(-A) = KA^{-p}$ for better accuracy.

11.2.3 Interspike intervals

Recall that the backward equation, (11.15) provides a solution to $G(V,t)$ which is the probability that no spike has fired up to time t given that the initial voltage is at V. Each time there is a spike, V is reset to V_{reset}. Thus, if T is the time to spike after resetting, $G(V_{reset}, t) = \text{Prob}\{T > t\}$. The interspike interval (ISI) histogram is the probability of a spike in a given interval of size Δt. This means that in limit as $\Delta t \to 0$, we have

$$G(V_{reset}, t) = \int_t^\infty \text{ISI}(s)\ ds.$$

So the ISI is found by solving the backward equation and computing the negative $t-$derivative of $G(V,t)$ at $V = V_{reset}$. To obtain the ISI distribution for an integrate and fire model, we must solve the backward equation (11.15):

$$\frac{\partial G(V,t)}{\partial t} = f(V)\frac{\partial G(V,t)}{\partial V} + \frac{\sigma^2}{2}\frac{\partial^2 G(V,t)}{\partial V^2}$$

along with the boundary and initial conditions $G(V,0) = 1$ for $V < V_{spike}$, $G(V_{spike},t) = 0$. Additionally, as with the mean first passage time, we require that $G_V(V,t) \to 0$ as $V \to -\infty$. In general, we cannot write down a useable closed form solution for the backward equation (except when $f(V) = I$, a constant – the so-called perfect integrator; Mandelbrot ??) so we must resort to numerical approximations. We solve a discretized version of the backward equation on an interval $(-A, V_{spike})$ where A is chosen large enough. Figure 11.4 shows some comparisons between the Monte Carlo simulations of equation (11.18) and the solutions to (11.15). We show both the LIF and the QIF models for subthreshold currents/high noise and suprathreshold currents/low noise.

11.2.4 Colored noise.

The sources for noise in neurons are manifold and include both channel noise (see below) as well as *synaptic noise* which comes about from the constant bombardment of other cells within the same milieu. Our model for white noise is simple and has the advantage of being tractable at least in so far as providing some simple scalar PDEs for the probability density and firing rates. While the formulae are not exactly useful, they are easy to numerically evaluate as are the PDEs which result. The white noise model is a somewhat crude approximation for synaptic noise especially if the time constants of the synapses are not real short. Thus, some researchers replace white noise by the following model:

$$\tau dz = -z dt + \sqrt{\tau} dW. \tag{11.28}$$

Here $\tau > 0$ approximates the decay properties of the synapses. This SDE is called an Ornstein-Uhlenbeck (OU) process and has an exact solution; the stationary distribution is Gaussian. Unlike the white noise case which is uncorrelated in time, OU noise has an autocorrelation function which decays exponentially like $\exp(-t/\tau)$. A natural question to ask is how this can affect the responses of neurons to stimuli, e.g. the FI curve. Lindner (2004) computes statistics for the interspike intervals of a perfect integrator ($dV/dt = I$) when there is colored noise. Brunel and Sergi (1998) and Brunel and Latham (2003) compute the FI curve for the noisy LIF and QIF models respectively with this kind of colored noise in the limits of small and large τ as well as a uniformly valid approximation over all ranges of τ. The calculations are heroic, but the bottom line is that the effect of colored noise has only a small effect on the steady-state firing rate. For example, if the applied current to the QIF is 0.5 and $\sigma = 0.5$, then the firing rate varies from 21.5 Hz to 23 Hz for all values of τ. We should point out that colored noise does have a rather important effect on the behavior of these models when periodic stimuli are added (see the next section as well as the last project in this section.)

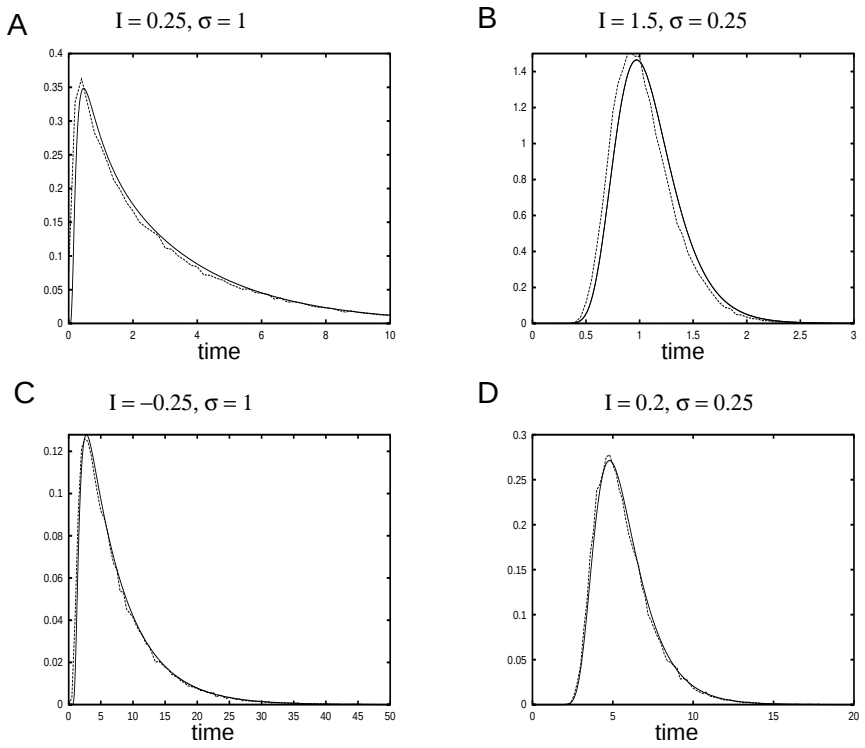

Figure 11.4. *Interspike interval distributions for noisy scalar models. Monte Carlo simulations are dashed and solid lines are solutions to (11.15). Monte Carlo simulations are 50000 ISIs from an Euler simulation of (11.18). the PDE is solved by the method of lines on a finite interval divided into 200 bins. (A,B) Leaky integrate and fire, $f(V) = I - V$. PDE is solved on the interval (-4,1) with $V = 1$ absorbing and $V = 0$ as the reset value. (C,D) Quadratic integrate and fire, $f(V) = I + V^2$. PDE is solved on the interval (-5,5) with $V = 5$ absorbing and $V = -1$ as the reset value. Currents and noise are indicated in the figure.*

11.2.5 Nonconstant inputs & filtering properties.

So far, we have considered situations in which the inputs to the noisy model are constant. However, real inputs to neurons change in time, so we would like to ask what can be said about the time-dependent firing rate. Figure 11.1B shows that one advantage of noise is that it allows subthreshold inputs to be recovered and a complex stimulus can be accurately encoded in the rates. Contrast this to a noise free model in which the neuron will not fire at all over a large range of inputs. The analysis of the output from a nonautonomous model is considerably more difficult than the stationary distribution. However, either Monte Carlo or numerical solutions to the FP equation provide a good way to study the dynamics

noisy neurons to stimuli. Figure 11.5 shows the response of the leaky integrgate and fire model (LIF) to aperiodic and periodic stimuli. Brunel et al (2001) and Lindner and Schimasky-Geier (2001) provide a formula for the response to weak periodic stimuli which involves various special functions and is well beyond the scope of this book. We point out two conclusions of their work: (i) with white noise the system behaves as a low pass filter whose magnitude decreases as $1/\sqrt{\omega}$ and the response lags the input by about 45° in phase; (ii) with colored noise (eg $dx = -x/\tau + dW$) the lag disappears.

In the example shown in figure 11.5A, the stimulus is encoded with almost no lag even though the noise is white. One approximation for slowly varying stimuli is to treat them statically and use the steady-state FI curve. We compute the FI curve for the level of noise in the model ($\sigma = 0.4$) and fit this to a smooth function, $F(I)$ as in (11.27) so that we can approximate the time-dependent firing rate as

$$\nu(t) = F(I(t))$$

where we use

$$F(I) = 0.16 \log(1 + \exp((I - .51)/0.16)).$$

The red and green curves in figure 11.5A show that the static approximation works quite well. Similarly, to periodic stimuli shown in figure 11.5B,C, the static response is also very close to the numerically computed response. However, at high frequencies as shown in 11.5D, there is a substantial diminution in the amplitude and there is a clear lag. Thus, we introduce a slightly more complicated model for the firing rate:

$$\tau \frac{d\nu}{dt} = -\nu + F(I(t)). \tag{11.29}$$

The results for $\tau = 0.2$ are shown in the black curves – this model provides a much better fit. In fig 11.5B,C, we also show the results from the dynamic model; they are nearly identical to the static model since the frequency is very low compared to τ. We chose τ in an ad hoc manner and expect that its choice would depend on the amount of noise as well as other aspects of the particular neural model.In one of the exercises/projects below, we illustrate that the situation is not so simple with a noisy conductance-based model. Nevertheless, equation (11.29) is the simplest dynamic model for the responses of neurons to time-varying stimuli and we will use equations like this to model populations of coupled neurons later in the book.

11.3 Weak noise and moment expansions

Rodriguez and Tuckwell (1998) heve developed a clever approximation for analyzing neural models (and any other models) in the presence of small noise. The idea of these methods is to assume that the probability distributions are Gaussian, centered at the mean values, $\bar{X}_j = E[X_j]$, with covariances $K_{ij} = E[(X_i - \bar{X}_i)(X_j - \bar{X}_j)]$. (Note, that $E[x]$ is the expectation of the process x. Then one does an expansion and derives equations for the means and covariances. We briefly outline the idea and then apply it to a simple polynomial neural model. Rodriguez and Tuckwell

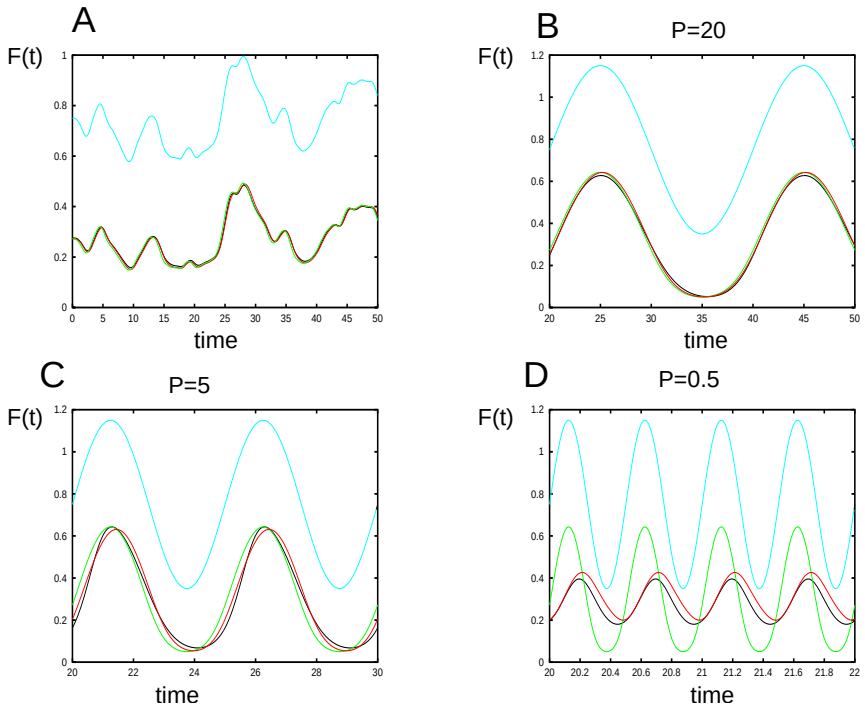

Figure 11.5. *Response of a noisy LIF model to non-constant stimuli. LIF model has* $I = 0.75$, $V_{spike} = 1$, $V_{reset} = 0$, $\sigma = 0.4$. *(A) A non-periodic stimulus. Blue curve shows the stimulus. Lower curves show the response of the FP equation (red) and the instantaneous firing rate (green) predicted by the steady-state FI curve. (B-D) Periodic stimuli at different periods (denoted by* P *in the figures). Blue curve shows the stimulus and red the solution to the FP equation. The instant response is shown in green and the solution to the simple dynamic model (see text) is shown in black (*$\tau = 0.2$.*)*

consider the case of general multiplicative noise. In order to simplify the description here, we restrict the method to additive noise. We start with

$$dX_j = f_j(X,t)dt + \sum_k g_{jk} dW_k(t). \tag{11.30}$$

The $W_j(t)$ are standard Wiener processes (zero mean, independent, delta correlated). Of the n^2 quantities, K_{ij}, n of them are variances, $V_i = K_{ii}$, and, the $n(n-1)/2$ remaining are the distinct covariances between the n variables. Taking the mean of equation (11.30), we immediately find

$$\frac{d\bar{X}_j}{dt} = E[f_j(X,t)]. \tag{11.31}$$

We note that $E[dW] = 0$ so this is an exact equation for the mean. Unfortunately, we need to approximate the right-hand side in order to get a closed system, of equations, since X is a random variable which we do not know except through (11.30). Similarly, the covariances satisfy

$$\frac{dK_{ij}}{dt} = E\left[(X_i - \bar{X}_i)f_j(X,t) + (X_j - \bar{X}_j)f_i(X,t) + \sum_k g_{ik}g_{jk}.\right] \tag{11.32}$$

This equation is obtained by differentiating the quantity

$$(X_i - \bar{X}_i)(X_j - \bar{X}_j)$$

with respect to t, taking expectations and using (11.31). We also use the fact that

$$E[(X_i - \bar{X}_i)E[f_j(X,t)]] = 0$$

since $E[f_j(X,t)]$ is deterministic and $(X_i - \bar{X}_i)$ has zero mean. Equations (11.31,11.32) are exact, but of course involve stochastic quantities whose values are not known. (Note that we can also obtain the moment equations by applying Ito's formula to the quantities $(X_i - \bar{X}_i)(X_j - \bar{X}_j)$ and then taking expectations of the resulting differential equation.)

If we make the assumption that the distributions are concentrated near the means and the third and higher moments are small relative to the second moment, we can approximate the right-hand sides of these equations. If $G(x_1, \ldots, x_n)$ is a function of n variables, then

$$E[G(X,t)] \approx G(m,t) + \frac{1}{2}\sum_{l=1}^{n}\sum_{p=1}^{n}\left\{\frac{\partial^2 G(m,t)}{\partial x_l \partial x_p}C_{lp},\right\} \tag{11.33}$$

where m is the approximation to $\bar{X}$,and C_{lp} is the approximation to K_{lp}. Applying (11.33) to (11.31), we get:

$$\frac{dm_j}{dt} = f_j(m,t) + \frac{1}{2}\sum_{l=1}^{n}\sum_{p=1}^{n}\frac{\partial^2 f_j(m,t)}{\partial x_l \partial x_p}C_{lp} \tag{11.34}$$

We now have an approximate equation for the means. Note that if we ignore the covariances, we correctly recover the noise free dynamics. The correction term in (11.34) makes intuitive sense since it depends on the sensitivity of the functions f_j on the variables. The approximation for $C_{lp}$is more difficult to obtain, but can be derived in steps. We replace $\bar{X}_j$ by its approximation, m_j, to obtain:

$$E[(X_i - m_i)f_j(X,t)] \approx \frac{1}{2}\sum_{l,p=1}^{n}\frac{\partial^2}{\partial x_l \partial x_p}[(x_i - m_i)f_j(m,t)]C_{lp}.$$

This partial derivative is just:

$$\delta_{il}\frac{\partial f_j}{\partial x_p} + \delta_{ip}\frac{\partial f_j}{\partial x_l}$$

where $\delta_{jk}$is 0 unless $j = k$,wherein it is 1. We obtain a similar approximation for $E[(X_j - m_j)f_i(X,t)$ which now leads to our approximation for the covariances:

$$\frac{dC_{ij}}{dt} = \sum_{l=1}^{n} \left(\frac{\partial f_i}{\partial x_l} C_{lj} + \frac{\partial f_j}{\partial x_l} C_{il} + g_{il} g_{lj}.equation \right) \tag{11.35}$$

It is instructive to apply this to a simple planar model with noise only in the first variable:

$$dV = f(V,U)dt + \sigma dW, \quad dU = g(V,U)dt,$$

such as the Morris-Lecar equations. Let v, u be the approximate means of the two equations and let w, y, z be, respectively, the variance of V, the variance of U, and the covariance between V, U. Then from (11.34,11.35) we get the following equations

$$\begin{aligned} v' &= f(v,u) + \frac{1}{2}(f_{vv}w + f_{uu}y + 2f_{vu}z) \\ u' &= g(v,u) + \frac{1}{2}(g_{vv}w + g_{uu}y + 2g_{vu}z) \\ w' &= \sigma^2 + 2f_v w + 2f_u z \\ y' &= 2g_v z + 2g_u y \\ z' &= (f_v + g_u)z + f_u y + g_v w. \end{aligned} \tag{11.36}$$

Here f_v means the derivative of f with respect to v,etc. With no noise, $\sigma = 0$,the solution, $(v(t), u(t), 0, 0, 0)$ is an invariant solution, so we can ask if it is a stable invariant solution. It turns out as you will show in an exercise below, that if $(\bar{u}, \bar{v})$ is a stable fixed point of

$$u' = f(u,v) \quad \text{and} \quad v' = g(u,v)$$

then $(\bar{u}, \bar{v}, 0, 0, 0)$ is also a stable fixed point of (11.36) when $\sigma = 0$. Thus, for small values of σ, the fixed point still exists, is stable, and the covariances are finite. However, if there are periodic orbits to the (u, v) system, then the covariances grow linearly in time for any positive σ. Thus, the moment equations do not admit any bounded periodic solutions if there is noise. They are only valid for a finite amount of time.

The use of the moment equations is limited mainly to fixed points. However, we can use them to see how stability and existence of fixed points changes as a function of the noise. Figure 11.6 shows an application of equation (11.36) to the Morris-Lecar model when the dynamics are Class I and II. Consider the noise-free case first. When there is a Hopf bifurcation for the noiseless system, the moment equations have a zero eigenvalue (exercise ??). Thus, in the computer analysis of the full moment equations, there appears to be a branch point. Solutions along the branch point can often correspond to negative values of w which is not physically possible. Thus, they should be ignored. The same "feature" occurs at the fold point for the class II example (figure 11.6B). When there is a small amount of noise, the loss of a stable fixed point occurs at lower values of the current as is intuitively expected. What is surprising is that the branch of solutions for the noiseless system

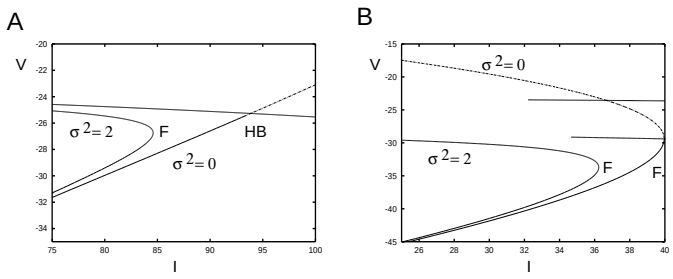

Figure 11.6. *Bifurcation diagram for Morris-Lecar moment expansion for (A) Class II and (B) class I excitability as the current varies at zero noise and with large noise ($\sigma^2 = 2$). In each case, the addition of noise shifts the loss of the stable fixed point to a lower value of I.*

disappears at a fold point in the noisy system (figure 11.6A). The fold for Class I is shifted to the left in the presence of noise. In exercise ???, you show that this will be generically the case.

As you will see in exercise *, these equations are of limited utility since they generically grow without bound when there are limit cycles to the deterministic equations. However, it has been noted that if higher order terms are kept in the moment equations (that is beyond the simple linear dependences), then it is possible to keep solutions bounded even away from stable fixed points. (See Tanabe and Pakdaman (2001) PRE 63:031911). The key point is that in the Gaussian approximation, all moments can be expressed in terms of the variances. For example $E[x^4] = 3E[x^2]$. For equations with polynomial right-hand sides, then *all* the expressions like $E[f(X)]$ can be expressed in terms of only the means and the variances with a finite number of terms. (For nonpolynomial systems, one can approximate f by a finite number of Taylor series terms.) Exercise * below takes the reader through a planar system and applies it to a variant of the Fitzhugh-Nagumo equations.

11.4 Poisson processes.

Many of the processes which occur at the molecular level in neuroscience are event-related and random. For example, the opening of a single channel is a single event and is random. The release of transmitter from an excited axon is also stochastic. The usual assumption that is made about these processes is that they are Poisson:

1. The number of events in non-overlapping intervals of time are independent for all intervals;

2. The probability of exactly one even occurring in an interval Δt is $P = r\Delta t$ where r is the rate of events and Δt is sufficiently small;

3. The probability of more than one event occurring in a sufficiently small interval

is zero.

11.4.1 Basic statistics

Consider the interarrival times, that is the times between events. Since the number of events in any non-overlapping interval is independent, the intervals between events are also independent. Let the events occur at time $t_1, t_2, \ldots$ and let $I_1 = t_1$, and $I_k = t_k - t_{k-1}$ for $k > 1$ be the interarrival times. That these are all dependent means that the process has no memory of what has already happened. (This has the following unfortunate consequence: if you have been waiting at the bus stop for a half an hour, then your expected waiting time for the next bus is exactly the same as the fellow who has just arrived at the bus stop!). Formally this means:

$$P(I > t + s | I > s) = P(I > t)$$

for all $s, t \geq 0$. Bayes theorem says:

$$P(x|y) = \frac{P(x, y)}{P(y)}.$$

But, because the Poisson process "forgets" everything that happens, the joint probability, $P(I > t + s, I > s) = P(I > t + s)$. Combining these two equations, we obtain:

$$\frac{P(I > t + s)}{P(I > s)} = P(I > t)$$

so that

$$P(I > t + s) = P(I > t)P(I > s).$$

Let $G(t) = P(I > t + s)$. Note that $G(0) = 1$. It is straightforward to show that the only solution to the functional equation $G(t + s) = G(t)G(s), G(0) = 1$ is

$$G(t) = e^{-rt}.$$

Let $F(t) = 1 - G(t) = P(I \leq t)$ be the cumulative probability. Then the density function is the derivative of the distribution funtion, $f(t) = re^{-rt}$. For this reason, we say that the intervals of a constant rate Poisson process are exponentially distributed. The mean inter-event interval is

$$E[I] = \int_0^\infty t f(t)\ dt = \frac{1}{r}.$$

The second moment is

$$E[I^2] = \frac{2}{r^2}$$

thus the variance ($\sigma^2 = E[(I - E[i])^2]$) is $1/r^2$. The *coefficient of variation* or CV is defined as $\sigma/E[I]$ and this a 1 for Poisson process. The inter-spike interval distributions for cortical neurons have a CV close to one (Softky and Koch, 1993).

Given we have the density function for the interval arrival times, we can now determine the density of the k^{th} arrival time. Let's approach this inductively. The

probability that the second event occurs at time t is the probability that the first event occurs at time $s < t$ and that the interspike interval is $t - s$. The first probability is $F(s) = 1 - \exp(-rs)$ and the second is $f(t - s)$. Thus

$$F_2(t) \equiv P(2^{nd}\text{event} < t) = \int_0^t (1 - e^{-rs}) r e^{-r(t-s)}\ ds.$$

The density of the second event ($k = 2$) distribution is the derivative of this and is just the convolution of the density function with itself:

$$f_2(t) = \int_0^t f(s) f(t - s)\ ds.$$

Evaluating this integral, we find

$$f_2(t) = (rt) r e^{-rt}.$$

Inductively, we find that the density of the k^{th} event is the so-called gamma distribution:

$$f_k(t) = (rt)^{k-1} r e^{-rt}/(k-1)!.$$

Finally, we can use this result to determine the distribution for the *number* of events in a given interval T. Let N_T denote the number of arrivals by time T. Then clearly $N_t \geq k$ when the k^{th} arrival time is less than or equal to T. That is

$$P(N_T \geq k) = \int_0^T f_k(s)\ ds.$$

This integral can be readily evaluated to yield:

$$P(N_T \geq k) = 1 - e^{-rT} \sum_{j=0}^{k} (rT)^j/j!.$$

Thus the density function for k spikes is

$$P(N_T = k) = \frac{(rT)^k}{k!} e^{-rT}.$$

This is called the Poisson distribution. The m^{th} moment for the Poisson distribution is found by evaluating the sum:

$$E[N^m] = \sum_{j=1}^{\infty} k^m \frac{(rT)^k}{k!} e^{-rT}. \tag{11.37}$$

This is not an easy task to do directly. Instead, it is easier to use a clever trick called the moment generating function. Consider the sum:

$$H(s) = e^{-rT} \sum_{k=0}^{\infty} \frac{(rT)^k}{k!} e^{sk}. \tag{11.38}$$

The m^{th} derivitive of $H(s)$ with respect to s evaluated at $s = 0$ is precisely equation (11.37). The sum is (11.38) can be rewritten as

$$H(s) = e^{-rT} \sum_{k=0}^{\infty} \frac{(rTe^s)^k}{k!} = e^{-rT} \exp rTe^s.$$

We thus find that $E[N] = rT$, $E[N^2] = rT + (rT)^2$ and the variance is rT. The ratio of the varaince in the number of events with the mean is called the *Fano factor* and for a Poisson process is exactly 1.

11.4.2 Channel simulations

. The easiest way to simulate an exponential waiting time with a constant rate r is to draw random numbers from the exponential distribution. That is, let $I_n = -\log(X_n)/r$ where X_n are uniformly distributed numbers in the interval (0,1). This is the key to the so-called Gillespie algorithm which is used to model chemical kinetics. For example the opening and closing of channels is a simple random process:

$$C \rightleftharpoons O$$

between the closed and open states. Let α, β be the respective rates for going from closed to open and vice versa. Let N denote the total number of channels and o the number of open channels. Since the channels are independnet, the rate of making a closed to open transition is $r_1 = \alpha(N - o)$ and the rate of making an open to closed transition is $r_2 = \beta o$. The rate of any event occurring is thus $r = r_1 + r_2$. So we can choose a time to the next event as

$$t_{new} = -log[X_1]/r$$

where X_1 is uniform in $(0, 1)$. Now we have to pick which event occurred. We choose another random number, X_2 uniformly distributed between 0 and r. If $X_2 < r_1$ then the first reaction (closed to open) occurs and otherwise the second reaction (open to closed) occurs. In the former case o is incremented and in the latter o is decremented. The total fraction of channels open is just o/N. Chow and White applied this idea to study the effects of a finite number of channels in the Hodgkin-Huxley equations. We proceed here with a simpler model, the Morris-Lecar since all of the channel equations are simple open/close events. Unlike the reduced Morris-Lecar model in which we let the calcium channel equal its equilibrium value $m_\infty(V)$, we must retain the temporal dynamics of the channel for a stochastic model. We have four possible events: (i) calcium channel opens, (ii) calcium channel closes, (iii) potassium channel opens, and (iv) potassium channel closes. The rates are dependent on the voltage which satisfies:

$$C_m \frac{dV}{dt} = I - g_l(V - E_l) - (g_K/N_w)W(V - E_K) - g_{Ca}(M/N_m)(V - E_{Ca})$$

where W, M are the total number of open potassium and calcium channels. We divide this by the number of each type of channel since maximal conductances

should be defined as conductance per channel. Thus the total maximal conductance possible will be indepenendt of the numbers of channels. This voltage equation is linear in V for any fixed W, M. Between events, both W, M will be constant, so that we can write down the solution to the voltage equation exactly. We can rewrite the V equation as :

$$\frac{dV}{dt} = (V_\infty - V)g$$

where V_∞ and g are functions of the parameters and W, M. Suppose the voltage was V_0 at the end of the last event. The next event comes at a time t_{new} later. Thus the voltage at the beginning of the next event is

$$V(t_{new}) = V_\infty + (V_0 - V_\infty)e^{-gt_{new}}.$$

We use this new voltage to update the transition rates and calculate the next event. The only numerical approximation we make is holding the rates constant between events. Chow and White (1996) address some of these numerical issues. Figure 11.7 shows a simulation of the Morris-Lecar model with 100 potassium and calcium channels and a subthreshold current. The noise due to the fluctuations in channels is enough to cause the neuron to fire sporadically.

Computation of the channel openings and closing as in the above algorithm can be laborious in more complex models or if the number of channels is large. (With a large number, N, of channels, events occur very frequently so that advancing even a small amount of time can take thousands of steps – indeed the time step is $O(1/N)$) Thus, there are a number of approximations which are often made. The most straightforward is to add noise to the deterministic channel models. That is, solve:

$$dx = [a(1-x) + bx]dt + \sigma_x dW(t). \tag{11.39}$$

The key question is the choice for σ_x. Greg Smith (chapt 11, Computational Cell Biology) suggests the following approximation:

$$\sigma_x^2 = \frac{a(1-x) + bx}{N} \tag{11.40}$$

where N is the number of channels. This has the right behavior for large N; from the law of large numbers, we expect the standard deviation to scale as $1/\sqrt{N}$. Fox and Lu (1994) make this approximation rigorous by (i) producing a Master equation for the channels, (ii) approximating this by a Fokker-Planck equationm and finally (iii) writing down the corresponsing Langevin equation. They make one more simplification of equation (11.40) by replacing x with $x_\infty = a/(a+b)$ and thus obtain

$$\sigma_x^2 = \frac{1}{N}\frac{ab}{a+b}$$

which is independent of x. Figures 11.7 C,D show the result of a simulation of the Morris-Lecar model using the approximation (11.40). One issue that must be dealt with in using these approximations is that the variable x can fall out of the valid range $(0, 1)$, thus it is necessary cap x when it leaves the interval. Finally,

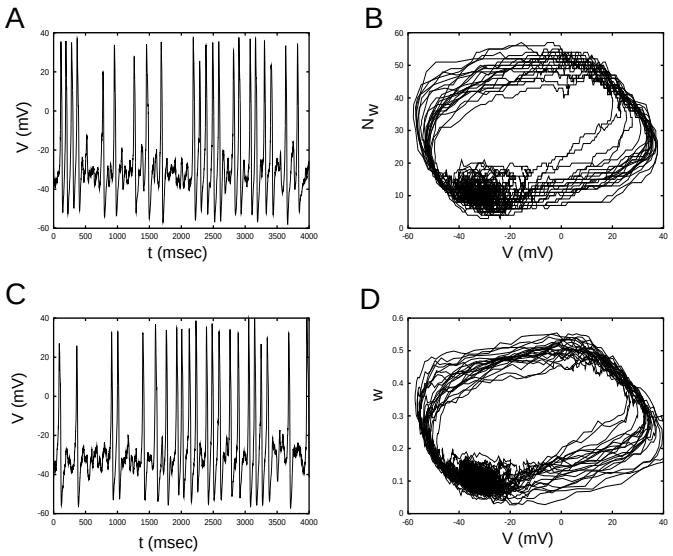

Figure 11.7. *Stochastic simulation of the Morris-Lecar model with 100 potassium and 100 calcium channels. $I = 80\mu A/cm^2$ injected is subthreshold for repetitive firing. (A) Time seris of the voltage (B) projection onto the (V, W) plane showing stochastic limit cycle. (C,D) Langevin approximations to the channel dynamics.*

we can ask whether the behavior of these noisy versions of the Morris-Lecar model differ substantially from the model with voltage noise only. A comparison of figures 11.7C,D with figure 11.1C would lead one to suspect that there is little difference between the figures. We would expect the difference in this physically derived model for stochasticity from the *ad hoc* additive-noise model to become important only when there are very few channels.

11.4.3 Stochastic spike models: beyond Poisson.

Rather than generating spikes with a nosiy deterministic model (such as described above) or with a fully deterministic model, sometimes it is desireable to create a completely stochastic model for the spike times. For example, one could simulate the spike times of a neuron with a purely Poisson process. However, biological neurons rarely have perfectly exponential interspike interval (ISI) histograms (see for example figure 11.1D). One reason for this is that once a neuron fires, the probability of a spike occurring again is very low due to refractoriness – there is history to the firing pattern. We now derive distributions for such history-dependent models. Let $f(t)$ denote the ISI density function (this is the ISI histogram when defined in discrete time intervals). The probability of a spike occurring before t is $F(t) = \int_0^t f(s)\ ds$. The probability that no spike has occurred up to time t is thus

$1 - F(t)$. Now, we introduce a notion of history-dependence. Let $h(t)\Delta t$ denote the probability that a spike occurs in the interval $[t, t + \Delta t]$ but *not* not at any time before. Let W be the random spike time. Then, formally:

$$h(t)\Delta t = P[t \leq W \leq t + \Delta t | W \geq t].$$

For a pure Poisson process, $h(t) = r$ the spike rate since the probability of the spike occurring is independent of the previous history. The probability of a spike between t and $t + \Delta t$ is just $f(t)\Delta t$ and the probability of no spike before t is $1 - F(t)$, thus we have:

$$h(t) = \frac{f(t)}{1 - F(t)} = -\frac{d}{dt} \log(1 - F(t))$$

where we use the fact that $F'(t) = f(t)$. Given $h(t)$ we can solve this differential equation for to find

$$F(t) = 1 - \exp\left(-\int_0^t h(s)\ ds\right). \tag{11.41}$$

The density fucnton $F'(t)$ is

$$f(t) = h(t) \exp\left(-\int_0^t h(s)\ ds\right). \tag{11.42}$$

As a first example, suppose that $h(t) = r$ so there is no history dependence. Then we recover the usual exponential function, $f(t) = re^{-rt}$. Suppose that when the neuron fires, the rate is set ot zero and recovers exponentially. Then $h(t) = r[1-\exp(-t/\tau)]$ and we get a density function shown in figure 11.8A. In this example, the baseline frequency is 40 Hz and $\tau = 50$ msec. Note the peak in the ISI histogram at about 50 msec. The mean ISI is 74 msec and the CV is about 0.66. Figure 11.8B plots the CV for this model at three different baseline frequencies over 6 orders of magnitude refractory period. Obviously, as $\tau \to 0$ the process approaches a pure Poisson process. Some more examples are provided as exercises.

Chapter 5 in the book by Gerstner and Kistler provides many examples of stochastic neural models. In particular, thy have a very readabl;e discussion of statistics of these generalized point processes such as the spike time autocorrelation function and the spectral power. The interested reader should consult this book as it is beyond the scope of the present text. Softky WR, Koch C. The highly irregular firing of cortical cells is inconsistent with temporal integration of random EPSPs. J Neurosci. 1993 Jan;13(1):334-50.

B. Lindner and L. Schimansky-Geier Transmission of noise coded versus additive signals through a neuronal ensemble, Phys. Rev. Lett., 86, 2934 (2001)

N Brunel and S Sergi (1998), Firing frequency of leaky integrate-and-fire neurons with synaptic currents dynamics, J. Theor. Biol., 195, 87-95

Firing rate of the noisy quadratic integrate-and-fire neuron. N. Brunel and P.E. Latham Neural Comput. 15:2281-2306 (2003) B. Lindner Interspike interval statistics for neurons driven by colored noise, Phys. Rev. E 69, 022901 (2004)

Brunel , N., & Hakim , V. (1999) . Fast global oscillations in networks of integrate - and- fire neurons with low firing rates . Neural Computation, 11, 1621

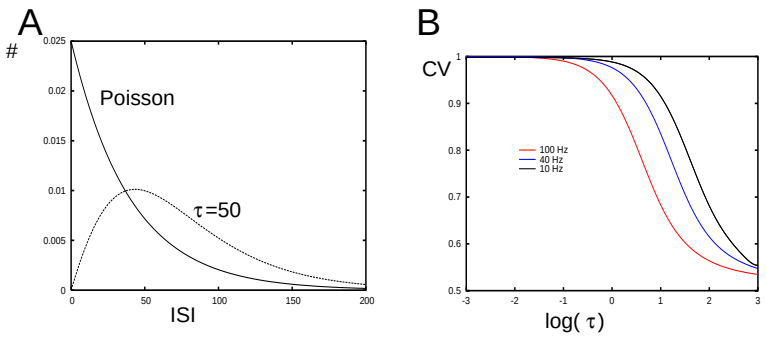

Figure 11.8. *Poisson process with a relative refractory period.* $r(t) = r_{max}(1 - \exp(-t/\tau))$. *(A) Density function for a pure Poisson process with a 40 Hz rate and one with a refractory period,* $\tau = 50$ *msec. (B) CV for different rates and refractory periods.*

1671. Chow, C. C. and J. A. White (1996). "Spontaneous action potentials due to channel fluctuations." Biophysical Journal 71: 3013-3021. Gillespie, D. T. (1977). "Exact stochastic simulation of coupled chemical reactions." J. Physical Chemistry 81(25): 2340-2361.

Ronald F. Fox and Yan-nan Lu , (1994) Emergent collective behavior in large numbers of globally coupled independently stochastic ion channels, PRE 49, 3421-3431

11.5 Projects

1. Develop computer code to solve the FP equation for the ML model. In particular, compute the noisy FI curve as follows.

   (a) Solve the steady state:

   $$0 = -\partial_v(f(v,w,I)P(v,w)) - \partial_w(g(v,w)P(v,w)) + (\sigma^2/2)\partial_{vv}P(v,w).$$

   The domain is the plane, but if you choose a large rectangle, $D \equiv (v_{min}, v_{max}) \times (w_{min}, w_{max})$, this should be sufficient. You should use reflecting boundaries, $J(\partial D) = 0$.

   (b) For each I, define the firing rate as

   $$f = -\int_{v_{min}}^{v_{max}} J(v, w_{th})\, dv,$$

   where we choose w_{th} as in the Monte Carlo simulations. The reason we don't choose a voltage threshold is that the noise is in the voltage variable and since we are using a Brownian motion, V can cross any specific point infinitely many times in any interval of time. Thus, we use

a section which is transverse to the flow in the recovery variable as this is a continuous process.

Compare the result to Monte Carlo simulations.

2. Consider the stochastic differential equation corresponding to the Izhikevich model (normal form for the Takens-Bogdonov bifurcation with finite reset):

$$dV = (I + V^2 - z)dt + \sigma dW, \quad dz = a(bV - z) \tag{11.43}$$

with the reset condition that if $V(t^-) = 1$ then $V(t^+) = c$ and $z(t^+) = z(t^-) + d$. Explain why the probability density satisfies:

$$\frac{\partial P}{\partial t} = -\frac{\partial}{\partial V}(fP) - \frac{\partial}{\partial z}(gP) + \frac{\sigma^2}{2}\frac{\partial^2 P}{\partial V^2} + J[\delta(V - c) + P(V, z - d) - P(V, z)]$$

where

$$J = -\int_{-\infty}^{\infty} dz \frac{\sigma^2}{2}\frac{\partial P(V, z)}{\partial V}|_{V=1}$$

and $f = I + V^2 - z$, $g = a(bV - z)$. This PDE is defined on the domain $(V, z) = (-\infty, 1) \times (-\infty, \infty)$. The stationary distribution will give you the firing rate, J. Try to develop an expansion for the stationary distribution for small a, d. This will be a fast-slow system. Tuckwell et al (2003) have developed expansions for the Fitzhugh-Nagumo equation that may be of use. Here is a suggested attack on the problem. For small a, d, z does not change very much, so we can hold z constant. If z is fixed, suppose that one can obtain the steady state firing rate, J as well as the density function, $P(V; z, I)$. Then z formally satisfies:

$$z' = d\nu + a(b < V > -z) \equiv G(z)$$

where ν is the firing rate of the cell and $< V >$ is the average potential. Note that both ν and $< V >$ depend on z. Find a fixed point, $G(z^*) = 0$ and substitute back into $P(V; z, I)$ to obtain the stationary density at steady state. One can continue this expansion to higher order to get the variance of z as well. We suspect that methods related to the moment expansions in this chapter could be of use for the z dynamics.

Another interesting phenomena to explore is the ISI distribution for this model. For example, choose $I = 0.05, \sigma + .015, a = 0.03, b = 1, c = 0.2, d = 0$ and perform a Monte Carlo simulation. You will see that there is a bimodal ISI. (See exercise ?? below for some comments on bimodal ISIs). Is it possible to get a bimodal ISI distribution in the limit as a gets small but b remains finite?

3. Set some parameters for the Morris-Lecar model with noise. A good choice is to add a modest amount of noise (say, $\sigma = 2$ and $I = 35$) in the Class I regime. First, numerically compute the FI curve for a range of applied currents. Now

add a small periodic term as in section ?? and compute the spike-time histogram (STH). (That is, present the periodic stimulus, say, 10000 times and count the number of spikes [crossings of $w = 0.3$] in each bin of say, 2 msec. From this, you get the number of spikes per millisecond which is the firing rate.) Compare the STH to a model for the firing rate as in section **:

$$u(t) = L[f(I(t))]$$

where L is some simple linear filter and f is the steady-state firing rate. Can you come up with a simplified firing rate model for the ML system based on these ideas? Repeat the Monte Carlo simulations above, but replace the white noise with the following noise:

$$\tau dz = -zdt + \sqrt{\tau} dW$$

for different values of τ. You should find that the lag between the stimulus and the firing rate disappears for τ roughly of the order of 10 msec.

11.6 Exercises

1. Compute the ISI distribution for the ML model with type II dynamics and $I = 95$ which is in the oscillatory regime. Use noise of amplitude 1, *i.e.* $V' = f(V, w) + \sigma\xi(t)$, $w' = g(V, w)$, where $\sigma = 1$. Show that the bimodality of the ISI is lost. Change I to 85 and set $\sigma = 2$ and then to 0.5. Compare the ISI histograms for these with that in figure 11.1D. Based on these computations can you offer an explanation for the bimodality of the distribution?

2. Compute the ISI distribution for the ML model with type I dynamics, unit noise and $I = 30$. Change the amount of noise. Is the distribution always unimodal?

3. Research problem? Consider the scalar neuron model:

   $$V' = f(V) + \sigma\xi(t)$$

   where ξ is the usual noise. Let $V = V_{reset}$ be the reset voltage and let V_{spike} be the voltage for a spike. Can the ISI distribution of this model ever be bimodal?

4. Suppose that $f(x)$ has zero mean on the interval (a, b). Show that $J = 0$ for the FP equation (11.12) with periodic boundary conditions.

5. Consider the simple model on the circle:

   $$dx = (I - cos(x))dt + \sigma dW.$$

   Write down the steady state for the FP equation and numerically compute the flux, J. This is the FI curve.

6. First passage time. Show that

$$< T^n >= \int_0^\infty t^{n-1} G(x,t)\ dt.$$

Use the fact that $G(x,t)$ satisfies

$$G_t(x,t) = f(x)G_x(x,t) + (\sigma^2/2)G_{xx}(x,t)$$

when f is independent of time, to show that the moments, $T_n \equiv< T^n >$ satisfy

$$-nT_{n-1} = f(x)T_n' + (\sigma^2)/2T_n''.$$

Suppose that the domain is $(-\infty, b)$ and the condition at $x = b$ is absorbing ($T(b) = 0$.) Show that,$T(x)$, the first moment is given by

$$T(x) = \frac{2}{\sigma^2}\int_x^b\ dy \int_{-\infty}^y\ dz e^{(2/\sigma^2)\int_y^z f(s)\ ds}.$$

7. Provide a complete analysis of the firing rate for the piece-wise linear ring model:

$$dV = (I + abs(V - \pi))dt + \sigma dW.$$

Start with a Monte-Carlo simulation on the circle $[0, 2\pi)$ and compute the firing rate as a function of I for several values of σ. Fix the noise and the current I and compute the ISI histogram. Write a closed for expression for the firing rate. Numerically solve the first-passage time equation and use this to compute the ISI histogram. Compare it to the Monte-Carlo simulation.

8. Show that ν^{-1} from equation (11.21) is the same as $T(V_{reset})$ in equation (11.26). From this, derive the simple expression for the firing rate of the integrate-and-fire model (11.22).

9. For large negative arguments

$$\sqrt{\pi}e^{s^2}(1 + \mathrm{erf}(x)) \sim \frac{1}{s} + O(s^{-3}).$$

Use this to obtain the firing rate for the LIF model when I is large. Is this the same as the noiseless value?

10. Provide an approximation to the firing rate of the LIF (equation (11.22)) when $1 \ll \sigma$, the large noise case. The approximation should be valid up to order 1 in σ^{-1}. (Hint: use Taylor's theorem since both of the limits of the integral will be small.)

11. Do the necessary rescaling to obtain (11.23).

12. Starting with equation (11.25) with $f(V) = |V|^p + I$ where $p > 1$ find a rescaling analogous to that done (11.22) in (11.23) to reduce the dependence of the firing rate on noise and current to one parameter and two equations for $I > 0$ and $I < 0$. When $I = 0$ show:

$$\nu = K\sigma^{2\frac{p-1}{p+1}},$$

where K is some $p-$dependent constant. Note that for $p = 2$ you recover Sigeti and Horsthemke's result without doing much of anything!

13. (Estimating conductances.) Rudolph and Destexhe (several papers) describe a method for estimating the conductances of excitatory and inhibitory inputs into a neuron by measuring the distribution of the subthreshold voltages. They derive a system of stochastic differential equations and then reduce this to a Fokker-Planck equations for which they can find the stationary distribution. Their method has some flaws (see Lindner and Longtin), but some of the basic ideas still hold. In this exercise, we will use some very simple approximations to perform the estimates. Consider the following SDE:

$$CdV/dt = I - g_L(V - E_L) + g_e(t)(V_e - V(t)) + g_i(t)(V_i - V(t))$$

where $g_{e,i}(t)$ are stochastic conductances of the excitatory and inhibitory neurons. Rudolph et al, assume that these conductances obey a first order stochastic differential equation. Here, instead, we assume that they are of the form:

$$g_{e,i}(t) = \bar{g}_{e,i} + \sigma_{e,i}\frac{dW_{e,i}}{dt}$$

where $W_{e,i}(t)$ are wiener processes. The problem, now is that that the noise appears multiplicatively in the voltage equation. Let us avoid this by making a rather crude approximation. Replace $V(t)$ in the conductance terms by $\bar{V}$, the mean voltage in absence of the fluctuations. Then we obtain

$$CdV = [I - g_L(V - E_L) - \bar{g}_e(V - V_e) - \bar{g}_i(V - V_t)]dt + \sigma_e[\bar{V} - V_e]dW_e(t) + \sigma_i[\bar{V} - V_i].$$

Now, the noise terms are constant; however, $\bar{V}$ depends on $\bar{g}_{e,i}$. Proceed as follows: (i) Compute $\bar{V}$, the mean potential as a function of $\bar{g}_{e,i}$ and I. (ii) Using two different values of I, find $\bar{g}_{e,i}$ in terms of the mean voltage (experimentally observed) and the other known parameters, $V_L, g_L, I, V_{e,i}$. (iii) Use the fact that the sum of two independent wiener processes with amplitude a, b is a wiener process with amplitude $\sqrt{a^2 + b^2}$ to find the stationary distribution of the voltages at the two different currents. This will be a Gaussian with mean $\bar{V}$ and variance σ^2. Express σ^2 in terms of the known parameters, the already determined $\bar{g}_{e,i}$ and the unknowns, $\sigma_{e,i}$. Since σ is experimentally observable for each applied current, I, solve for $\sigma_{e,i}$ in terms of known and experimentally observable quantities using 2 applied currents.

14. Colored noise. Consider the rescaled voltage driven by colored noise:

$$\frac{dv}{dt} = -\beta v + y, \tau dy = -ydt + \sqrt{2D}dW.$$

Verify that the Fokker-Planck equation for this is:

$$P_t = [(\beta v - y)P]_v + [yP/\tau + DP_y/\tau^2]_y$$

where the domain is the plane. Amazingly enough, a steady state for this equation can be found exactly! Show that

$$P(v, y) = N \exp(Av^2 + Bvy + Cy^2)$$

where N is a normalization constant and A, B, C are unknown constants. Find these constants in terms of β, τ, D. (It will help a great deal to use a symbolic package like Maple.)

15. (Analysis of moment equations.) In this exercise, we will examine certain aspects of the moment equations.

    (a) As you will show next in this exercise, the only situation in which there is a bounded solution to the moment equations is near a stable fixed point, we will first explore the effects of noise near a fold bifurcation. Consider the following system:

    $$x' = x^2 + a + v$$
    $$v' = 2xv + \sigma^2$$

    Find all the stable fixed points and the curve of fold points in the two parameters a, σ^2. In particular, show that the effect of noise is to make the bifurcation occur at lower values of a. Turn this into an integrate and fire model by assuming that when x reaches some large number, say,10, it is reset to a large negative number, say, -10 and the variance is reset to 0. Numerically find the FI curve for different values of σ. Show that it is always concave down so that it does not look like the FI curve computed from the Fokker-Plank equation. Finally, prove that $v(t)$ is always nonnegative in this model.

    (b) We now consider the general moment equations (11.34) and (11.35) when the noise is zero, that is $g_{ij} = 0$. The covariance equations are redundant since $C_{ij} = C_{ji}$ is enforced. However, it is much more convenient to work with the full n^2 equations rather than the $n(n+1)/2$ independent ones. Clearly, $C_{ij} = 0$ is invariant and the first moments obey the deterministic dynamics. We now look at the stability of these equations around some deterministic solution, $(m, C) = (m_0(t), 0)$. Let $A(t) = a_{ij}(t)$ be the linearization of the deterministic system about $m_0(t)$. That is

    $$a_{ij}(t) = \frac{\partial f_i}{\partial x_j}$$

    evaluated along the solution $m_0(t)$. The linearization of the full (m, C) system about $(m_0, 0)$ is an $n + n^2-$dimensional square matrix. However, the lower left $n^2 \times n^2$ block is all zeros, so that the linearized system

is block triangular. Stability is determined solely by looking at the two blocks: the $n \times n$ upper block which is the matrix $A(t)$ and the lower right $n^2 \times n^2$ block which is formed from equation (11.35). Note that the coefficients multiplying C_{ij} are entries of the matrix $A(t)$, so that the lower block is very closely related to the upper block. The linearization of equation (11.35) can be rewritten as

$$C'_{ij} = \sum_{l=1}^{n} \left(a_{il}(t) C_{lj} + a_{jl}(t) C_{il} \right). \tag{11.44}$$

Suppose that $u(t), v(t)$ are two solutions to $y' = A(t)y$. $u(t), v(t)$ are vectors with components, $u_i(t), v_i(t)$, $i = 1, \ldots, n$. **Prove that** $C_{ij} = u_i(t)v_j(t)$ **solves equation (11.44).** Thus, if A is constant, then the solutions, $u(t), v(t)$ are exponentials, say $\bar{u}e^{\lambda t}, \bar{v}e^{\nu t}$ where $\bar{u}, \bar{v}$ are constant vectors. This means that the solutions to (11.44) are also exponentials with exponet, $\lambda + \nu$, Thus, the eigenvalues associated with (11.44) are just sums of the eigenvalues associated with A. From this, you can conclude that the full moment expansion near an asymptotically stable fixed point of the deterministic system is also asymptotically stable.

What about periodic orbits? Suppose that the deterministic system has a stable periodic solution, $m_0(t)$. Then the system $y' = A(t)y$ has a periodic solution, $m'_0(t)$. This means that the equation (11.44) also has a periodic solution where we take $u(t) = v(t) = m_0(t)$. All other solutions to $y' = A(t)y$ decay and similarly do those of (11.44). But the existence of a periodic solution to (11.44) is bad since as soon as g_{ij} is non-zero, the solutions to (11.44) will grow. Prove this. That is suppose we have the system $Z' = B(t)Z$ where $B(t)$ is a periodic matrix. Suppose that there is a unique periodic solution, $Z_0(t)$ and all of the other linearly independent solutions to $Z' = A(t)Z$ exponentially decay as $t \to \infty$. Let P be a constant vector. Show that solutions to

$$Z' = B(t)Z + P$$

will grow in time unless P is chosen very carefully. (This is a tricky problem related to the Fredholm alternative).

16. Solve the functional equation $G(0) = 1$ and $G(t + s) = G(t)G(s)$ for all t, s. Assume that $G(t)$ is continuously differentiable. (Hint: take s small and derive a differential equation for $G(t)$.)

17. Compute the CV for spike production in the ML model with Class I and Class II excitability parameters in both the sub and supra-threshold regimes of current with a fixed strength of additive white noise.

18. Simulate a Poisson process with an absolute refractory period. That is, let r_{max} be the maximal rate. Each time a spike occurs, the rate is set to 0 and after τ msec it returns to r_{max}. Compute the CV for this process. Write

down the ISI histogram using equation (11.42) and use this to ompute the CV exactly.

19. Create a function $h(t)$ such that the density function $f(t)$ has power law behavior for large t, that is $f(t) \sim 1/t^m$ as $t \to \infty$. Compute the CV for this. Note that m must be larger than 2 in order to compute the CV. Show that the CV is always larger than 1 for this process.

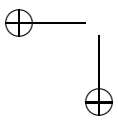
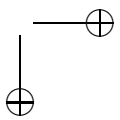

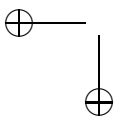

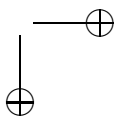

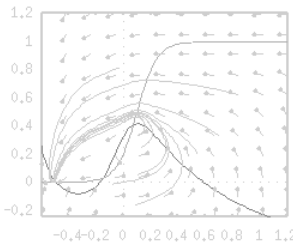

Chapter 12

Firing rate models.

One of the most common ways to model large networks of neurons is to use a simplification called a firing rate model. Rather than track the spiking of every neuron, instead, one tracks the averaged behavior of the spike rates of groups of neurons within the circuit. These models are also called population models since they can represent whole populations of neurons rather than single cells. In this book, we will call them rate models although their physical meaning may not be the actual firing rate of a neuron. In general, there will be some invertible relationship between the firing rate of the neuron and the variable at hand. We derive the individual model equation in several different ways, some of the derivations are rigorous and are directly related to some biophysical model and other derivations are *ad hoc.* After deriving the rate models, we apply them to a number of interesting phenomena including working memory, hallucinations, binocular rivalry, optical illusions, and traveling waves. We also describe a number of theorems about asymptotic states as well as some of the now classical work on attractor networks. Much of this chapter is based on a lengthy review article by one of the authors (GBE), but some new material is also included related to recent work by Omurtag, Knight, and Cai.

There are many reasons to use firing rate models. First of all, there is the obvious issue of computational efficiency. Modeling a network of thousands of individual conductance based neurons can tax even the fastest computers. For this reason, many large scale simulations use simple spiking models like the integrate-and-fire model. Alternatively, firing rate models are used. In many experimental preparations, what is measured is not the intracellular potential of neurons but instead the probability of firing. This type of recording is done with an extracellular electrode and thus spikes can be detected but the other aspects of the cell are unknown. Hence, to better compare with experiments, it makes sense to consider the firing rate instead of the potential. Field potential recordings, electroencephalograms (EEGs) and functional magnetic resonance imaging (FMRI) presumably represent large populations of neurons. Thus, a model at this scale may be better posed in terms of population equations.

Rate models are among the oldest forms of modeling of the brain and the

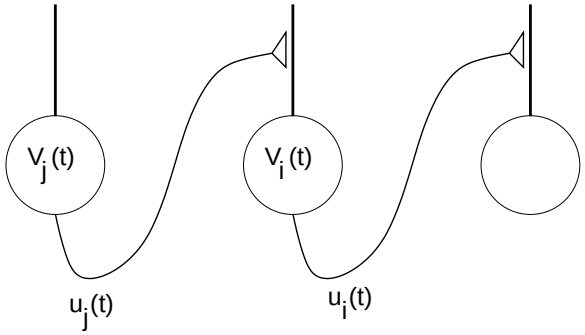

Figure 12.1. *Schematic of a pair of neurons synaptically coupled.*

nervous system going back to Rashevsky in the late 1930's. Jack Cowan has written a very comprehensive history of the early days of neural network research and the reader is advised to look some of this up.

Rate models are essentially the underlying "biology" in the very popular and useful theory of neural networks. For example, the "connectionist" models developed under the Parallel Distributed Processing (PDP) program by McClelland and Rumelhart and the "back propagation" models are all connected to the wet nervous system (albeit, occasionally rather tenuously) via rate models. Massively recurrent attractor networks, perceptrons, hidden layer models, Adaptive Resonance Theory (and its descendents) are all essentially rate models. We will spend little time in this chapter on the more machine-like and abstract ideas of neural network theory and instead focus on the connection of rate models to biophysics and the usefulness of these networks in modeling biological phenomena.

12.1 A number of derivations.

12.1.1 Heuristic derivation.

We start with a very simple somewhat abstract derivation that was advocated in early work of Cowan and later Ermentrout and Cowan. Figure 12.1 shows a schematic for a pair of neurons with a synapse from one to the other. The measurable output is the firing rate, $u_i(t)$, which depends in a nonlinear way on the somatic potential, $V_i(t)$:

$$u_i(t) = F_i(V_i(t)).$$

Now, the reader might recall that most of our biophysical models produced firing rates as a function of the applied current, so she may be puzzled at the use of voltage as a driver for the output of the cell. We justify this by assuming that the current flowing into the axon hillock (which is the site of action potentials) is proportional to the voltage drop between the soma and the resting potential of the hillock compartment. Thus, the somatic potential is passively converted to an axon hillock current via Ohm's law that $I = V/R_m$ where R_m is the membrane

resistance. Each time that a presynaptic cell fires a spike, a postsynaptic potential (PSP) appears at the soma. The size of this potential, as well as the sign, depends on the nature of the synapse, the position on the dendrite and so on. We define $\Phi_{ij}(t)$ to be the PSP appearing on postsynaptic cell i due to a single spike from presynaptic cell j. Let $t_1, t_2, \ldots, t_m$ be the firing times of the presynaptic cell. By assuming linear summation of the PSPs, the total potential received at the soma is

$$G_{ij}(t) = \sum_l \Phi_{ij}(t - t_l).$$

The firing rate $u_j(t)$ determines the instantaneous number of spikes that a neuron fires in an infinitesimal time interval. That is, we can think of $u_j(t)dt$ as the probability of a spike occurring in the time interval $(t, t + dt)$. Thus the above sum can be rewritten as

$$G_{ij}(t) = \int_{t_0}^{t} \Phi_{ij}(t - s)u_j(s - \tau_{ij})\, ds$$

where τ_{ij} is the possible axonal delay in the spike arising at j arriving at i. If the effects of each cell linearly sum, then we can close this model resulting in an integral equation for either V_i or u_i

$$V_i(t) = \sum_j G_{ij}(t) = \sum_j \int_{t_0}^{t} \Phi_{ij}(t - s)F_j(V_j(s - \tau_{ij})) \tag{12.1}$$

$$u_i(t) = F_i\left(\sum_j \int_{t_0}^{t} \Phi_{ij}(t - s)u_j(s - \tau_{ij})\ ds\right). \tag{12.2}$$

Both of these rather formidable equations can be greatly simplified once we discuss the PSP function $\Phi_{ij}(t)$. To do this, let us consider a passive membrane with a time constant τ_m and into which a presynaptic current is injected:

$$\tau_m \frac{d\Phi}{dt} + \Phi = R_m I(t).$$

For simplicity, suppose that $I(t)$ is an alpha function of the form:

$$I(t) = \exp(-t/\tau_d) - \exp(-t/\tau_r).$$

Here τ_d is the decay of the synaptic current and τ_r is the rise time of the current. Assuming that $\Phi(0) = 0$, we can solve this simple differential equation to obtain the postsynaptic voltage response:

$$\Phi(t) = \frac{\tau_d}{\tau_d - \tau_m}\left(e^{-t/\tau_d} - e^{-t/\tau_m}\right) - \frac{\tau_r}{\tau_r - \tau_m}\left(e^{-t/\tau_r} - e^{-t/\tau_m}\right). \tag{12.3}$$

This response depends on three parameters, the postsynaptic time constant and the presynaptic rise and decay times. One could make this response function far more complex by including dendritic filtering properties and so on as long as it remains

linear. (If the response is nonlinear then we cannot simply sum the inputs from different neurons, nor can we even sum the individual PSPs to form the integral.)

The Volterra integral equations (12.1,12.2) are not simple to analyze so that one generally attempts to convert them into differential or differential-delay equations. For $\Phi(t)$ represented as a finite sum of exponentials, we can always invert the integral equation to form a set of differential equations. To see this, consider first the simple integral equation:

$$x(t) = \int_{t_0}^{t} e^{-(t-s)/\tau} y(s-r)\ ds$$

where r is the possible delay. Differentiate x with respect to t to obtain:

$$\frac{dx}{dt} = y(t-r) - \frac{1}{\tau}\int_{t_0}^{t} e^{-(t-s)/\tau} y(s-r)\ ds = y(t-r) - x(t)/\tau.$$

Thus, we see that $x(t)$ satisfies:

$$\frac{dx}{dt} + x/\tau = y(t-r).$$

If $\Phi(t)$ is the sum of several exponentials, then we can break the Volterra integral equation into a set of differential equations using the above identity.

This approach is not entirely satisfactory since for each connection $\Phi_{ij}(t)$ we need (in the present case) three differential equations. If the network of interest consists of a homogeneous population of neurons, that is, their synaptic time constants are the same and they have the same membrane time constant, then we can write $\Phi_{ij}(t) = w_{ij}\Phi(t)$ where w_{ij} represent the magnitudes of the connections. Suppose the delays, τ_{ij} are the same for all cells, say, $\tau_{ij} = r$. Then the voltage equation (12.1) now becomes:

$$(LV_i)(t) = \sum_j w_{ij} F_j(V_j(t-r)) \tag{12.4}$$

where L is a linear homogeneous differential operator. Equation (12.4) is essentially the classical model for a neural network. We can similarly reduce equation (12.2) to a set of differential equations. Let

$$z_i(t) = \int_{t_0}^{t} \Phi(t-s) u_i(s-r)\ ds.$$

Thus

$$(Lz_i)(t) = u_i(t-r) = F_i(\sum_j w_{ij} z_j(t-r)). \tag{12.5}$$

This is not quite the same as an equation for the firing rate, $u_i(t)$, but this variable is obtained easily from $z_i(t)$ by differentiation. Pinto et al call $z_i(t)$ the *synaptic drive.*

This drastically simplifies the simulation and analysis of single populations of differential equations but we are still stuck with difficulties when we have, say, an

excitatory and an inhibitory population. Key to the reduction was the idea that $\Phi_{ij}(t) = w_{ij}\Phi(t)$. However, if we examine equation (12.1) carefully, we see that we can make a less restrictive assumption that $\Phi_{ij}(t) = w_{ij}\Phi_i(t)$ for then we obtain:

$$(L_i V_i)(t) = \sum_j w_{ij} F_j(V_j(t-r)).$$

Similarly, examining equation (12.2), if we assume that $\Phi_{ij}(t) = w_{ij}\Phi_j(t)$, then we obtain

$$(L_i z_i)(t) = F_i(\sum_j w_{ij} z_j(t-r)).$$

Rather than a system of N^2 differential equations for a network of N neurons, we just have N differential equations. Thus, we now want to examine more closely what these two assumptions entail.

Suppose that $\Phi_{ij} = w_{ij}\Phi_i(t)$. This means that the response of neuron i to any inputs depends (up to a scalar constant which could be negative or positive) only on the properties of the *postsynaptic* cell. This assumption is valid if the shape and temporal properties of the presynaptic currents are the same no matter what type is the presynaptic cell. This kind of model would fail to distinguish between, say, a slow NMDA current and a fast AMPA current or even between the fast AMPA and somewhat slower GABA currents. However, looking at equation (12.3), we see that if $\tau_m \gg \{\tau_d, \tau_r\}$ then $\Phi(t) \approx \exp(-t/\tau_m)/\tau_m$ which is independent of the presynaptic time scales. That being the case, our system of differential equations is first order:

$$\tau_{m,i}\frac{dV_i(t)}{dt} + V_i(t) = \sum_j w_{ij} F_j(V_j(t-r)). \tag{12.6}$$

Equation (12.6) is commonly used as a model neural network and within the scope of our derivation, the time scale associated with each element in the network is that of the *membrane time constant.*

Now, suppose that $\Phi_{ij} = w_{ij}\Phi_j(t)$. This means that the shape of the PSP depends only on the *presynaptic* cell. To us, this is a more reasonable assumption since we can distinguish different types of synapses (and, below, allow us to incorporate synaptic depression and potentiation). Suppose that the rise time of the synapse and the membrane time constant of the postsynaptic cell are small compared to the decay of the synapse. Then $\Phi_j(t) \approx \exp(-t/\tau_d)/\tau_d$ and, as above, we derive the following equation for the *synaptic drive:*

$$\tau_d\frac{dz_i(t)}{dt} + z_i(t) = F_i(\sum_j w_{ij} z_j(t-r)). \tag{12.7}$$

This model is also a very popular version for neural networks. In this case, the temporal dynamics are dominated by the synaptic decay, τ_d.

Equations (12.6,12.7) are often regarded as equivalent, but in the present derivation, they are not. Rather, they represent two distinct assumptions about the dominant time scales.

Before discussing the forms of the firing rate functions, F_i, we turn to a derivation based on the theory of averaging and some assumptions about the types of bifurcation in the conductance-based models.

12.1.2 Derivation from averaging.

(**This section is somewhat rough-going; the reader may want to skip to the end.**) Consider the following conductance-based network:

$$C\frac{dV_i}{dt} + I_i(V_i, \ldots) = -\sum_j g_{ij} s_j (V_i - V_{syn,j}) \tag{12.8}$$

$$\tau_{syn}\frac{ds_i}{dt} + s_i = R_i(V_i, s_i). \tag{12.9}$$

Here, I_i represents all the nonlinear conductances which lead to action potentials. To simplify the derivation, we have assumed that a synapse from cell j produces the same conductance change regardless of the post-synaptic target. This is not an unreasonable assumption. Weakening this assumption results in more differential equations just as the more general assumptions in the previous section. Suppose that $\tau_{syn} \gg 1$. This means that the synapses are slow. (Synapses which rise rapidly but decay slowly provide a different limit which we explore later in this book.) If the synapses are slow, then $s_i(t)$ will change very slowly relative to the dynamics of the membrane thus we can treat s_i as constant. For ease in exposition, we will suppose that all the neurons are excitatory which means that $V_{syn,j} = V_e$. Let $G_i = \sum_j g_{ij} s_j$. Since s_j are roughly constant, so is G_i so we can treat it as a parameter. Equation (12.8) is now isolated from the rest of the population because G_i is just a constant. We can compute the bifurcation diagram of the membrane potential obtaining:

$$V_i(t) = \bar{V}_i(t; G_i).$$

We will assume only two types of behavior: stable fixed points or limit cycles. In the latter case, we assume that the period is $T_i(G_i)$. We now return to the synaptic equations (12.9) but substitute $\bar{V}_i(t; G_i)$ for V_i since the potential changes at a faster time scale than the synapses. Thus (12.9) becomes:

$$\frac{ds_i}{dt} = \frac{1}{\tau_{syn}}(-s_i + R_i(\bar{V}_i(t; G_i), s_i)).$$

If $\bar{V}_i$ is a stable fixed point, then the s_i equation is straightforward since the right-hand side is independent of t. However, if $\bar{V}_i$ is periodic, then we are still safe since we can apply the averaging theorem and obtain:

$$\frac{ds_i}{dt} = \frac{1}{\tau_{syn}}(-s_i + \left\langle R_i(\bar{V}_i(t; G_i), s_i)) \right\rangle$$

where

$$\left\langle R_i(\bar{V}_i(t; G_i), s_i)) \right\rangle = \frac{1}{T_i(G_i)} \int_0^{T_i(G_i)} R_i(\bar{V}_i(t; G_i), s_i)\ dt \equiv Q_i(G_i, s_i).$$

Thus, since all the quantities involved depend on G_i, we have reduced this conductance based model to a system of first order equations for the synaptic gates, s_i:

$$\tau_{syn}\frac{ds_i}{dt} + s_i = Q_i(\sum_j g_{ij}s_j, s_i). \tag{12.10}$$

We now explore (12.10), specifically $Q(G,s)$, in more detail. In chapter **, we modeled synapses as:

$$\frac{ds}{dt} = \alpha(V)(1-s) - \beta s$$

in much the same way as we model channels. Factoring out the $\beta = 1/\tau_{syn}$, we see that $R(V,s) = \alpha(V)\tau_{syn}(1-s)$. The function $\alpha(V)$ is zero except when the neuron spikes. Let us suppose that the width of a spike is independent of the firing rate of the neuron so that

$$\int_0^T \alpha(\bar{V}(t))\tau_{syn}\ dt = \gamma,$$

where γ is a constant essentially independent of T, the period. Let us define

$$F(G) \equiv \frac{1}{T(G)}$$

as the firing rate of the conductance based model given synaptic conductance G. Then, with these approximations

$$Q_i(G_i, s_i) \equiv \frac{1}{T_i(G_i)}\int_0^{T_i(G_i)} R_i(\bar{V}_i(t;G_i), s_i)\ dt = \mu_i F_i(G_i)(1-s_i).$$

Putting all these terms together, equation (12.10) can now be written as

$$\tau_i\frac{ds_i}{dt} = \mu_i F_i(\sum_j g_{ij}s_j)(1-s_i) - s_i. \tag{12.11}$$

With the exception of the $1-s$ term, equation (12.11) is the same as equation (12.7). This makes sense, for in both cases, the time scale is the synaptic decay. Here, the variable $s_i(t)$ is the fraction of open synaptic channels, while in equation (12.7), $z_i(t)$ was called the synaptic drive.

If there are different types of synapses, say, excitatory and inhibitory, the synaptic current is

$$I_{syn} = G_{ex}(V - V_{ex}) + G_{in}(V - V_{in})$$

and the period, T is a function of two variables, G_{ex}, G_{in}. This may seem to be a problem since it is not clear how T should depend on the two conductances; we'd like it to be additive or some simple functional. If the conductance based neuron is operating near a saddle-node bifurcation, then we know that

$$F(I_{syn}) \approx K\sqrt{I_{syn} - I^*}$$

where I^* is the critical current at which the saddle-node appears. Let V^* be the potential at the saddle-node. Then (at least near the saddle-node)

$$I_{syn} = G_{ex}(V^* - V_{ex}) + G_{in}(V * -V_{in})$$

so that the firing rate is an *additive* function of the inhibitory and excitatory conductances.

The big advantage of deriving firing rate models from conductance-based models using averaging is that it is simple to incorporate slow currents such as spike-frequency adaptation and also short-term synaptic plasticity. We will introduce some of these models later and others will be provided as exercises.

12.1.3 Populations of neurons.

The derivations above were motivated by considering a single conductance-based neuron and then from this deriving a model for the firing rate. However, the main role of firing rate models is not to mimic single cells, but rather, to examine large numbers of neurons in some "average" fashion. We can draw the analogy between intra- and extracellular recordings in physiology. Intracellular recording enables one to track the membrane potential of a single neuron. Extracellular recordings, such as the local field potential represent the responses of many neurons. Sharp electrodes (also extracellular) can resolve spikes of individual neurons. However, these spiking events are probabilistic, so that experimentalists repeat the same stimulus over many trials to obtain a poststimulus time histogram (PSTH). The PSTH has units in spikes per unit time (often millisecond) so that it is effectively a rate. The intuition behind the PSTH is that it is *assumed to be true* that if we were able to record simultaneously from 100 nearby locations, we would get the same result as from recording from one location 100 times. In order for this to be reasonable, we have to assume that the neurons fire largely independently of each other. Once this assumption is made, then we see that the firing rate of the population is exactly the same as that of an individual neuron and the equations derived in the above section can thus be interpreted as the population firing rate. However, in the derivation from averaging, the firing rate function is deterministic. Thus, if every cell were identical, then they would all fire in perfect concert. Thus, we need to account for differences between neurons when we treat populations. One way to do this is to include the effects of noise. In chapter NOISE, we saw that extrinsic noise can smooth the firing rate as a function of the input current. Thus, for example, we could replace a firing rate function $F = \sqrt{I}$ by a smoothed version of this which has a nonzero firing rate even for subthreshold inputs ($I < 0$). Another way to smooth the firing rate function is to assume heterogeneity. For example, suppose that the firing rate is $F(I - I^*)$ for $I > I^*$ and zero otherwise as would be the case for a SNIC bifurcation. If the threshold values I^* are taken from some distribution, $Q(I)$, then we can write an "average" firing rate function:

$$F_Q(I) = \int Q(I^*)F(I - I^*)\, dI^*. \tag{12.12}$$

We will leave it as an exercise to the reader to explore specific forms for the averaged firing rate.

Let us give a quick derivation of a typical firing rate or population model. Consider N identical neurons which receive (possibly random inputs) and between which there are recurrent connections. We will assume, for simplicity, that all the neurons are excitatory (multiple types of neurons are easily generalizable) and the the connections are all identical as are the inputs, the strengths of which are scaled by $1/N$. Each neuron undergoes dynamics:

$$C\frac{dV_i}{dt} = -I_{ion,i} + \bar{g}s_i(V_i - E_{syn})$$

where $\bar{g}s_i$ is the conductance felt by each neuron. Since all inputs are excitatory and we assume that the recurrent synapses have dynamics similar to the input synapses, we have:

$$(Ls_i)(t) = J_T \sum_k \delta(t - t_k^T) + \sum_{j,k} J_{ij}\delta(t - t_k^j)$$

where L is a linear differential operator which governs the synapse. Alternatively, we could generalize this and write:

$$s_i(t) = \int_{t_0}^{t} \alpha(t - t') \left(J_T \sum_k \delta(t' - t_k^T) + \sum_{j,k} J_{ij}\delta(t' - t_k^j) \right) \, dt'. \tag{12.13}$$

Here t_k^T are the spike times from the inputs and t_k^j are the spike times of the j^{th} cell in the network.

Key to the notion of population models is the fact that we assume that the neurons are firing independently of each other within the network. Is this a good assumption? If there is a great deal of extrinsic independent noise, then it is likely that there are few correlations between neighboring neurons. A given population of interest often receives inputs from an earlier processing stage. (For example, layer 4 in the cortex receives inputs from the thalamus.) If the incoming action potentials come from randomly chosen subsets of the input layer, then we expect that spiking within the output layer would be uncorrelated. However, it turns out that this seemingly obvious assumption is not true. In recent experiments, Reyes et al examined the following scenario. Starting with N independent Poisson trains of spikes, a subset of $m \ll N$ was selected and injected into a neuron. The spike times of this neuron were recorded. A different set of m spikes was selected and the experiment was repeated until there were N new spike trains. These formed the basis for a repeat of the first set of experiments; N new spike trains were collected from these spike trains and so on. By layer 10 (ten iterations), there was considerable synchrony between the spike trains so that it was no longer reasonable to assume independence. The reason for this is that even though each trial shared only a few inputs, this was enough to become amplified over multiple layers leading to synchrony. Thus, the assumption of independence is at best an approximation and, at worst, wrong. In the Reyes experiment, there was no recurrent coupling between cells within a layer. Recurrent connections can either increase or decrease

the synchrony, depending on the nature of the coupling. Indeed, we say in chapter OSCILLATOR that synaptic time scales, intrinsic currents, and the sign of the coupling can all have dramatic effects on the synchronization between coupled neurons. Since the only theory that has been done on the issue of asynchrony is for very simple models (leaky integrate and fire, quadratic integrate and fire), little more can be said about the assumption of independence for recurrently connected neurons.

There is one last issue that we want to discuss before moving on to applications of firing rate models. This is the issue of time constants. Figure * in chapter NOISE showed that a noisy integrate and fire model with high noise could follow a stimulus rather robustly if we added a small time constant to the dynamics. Specifically, let $I(t)$ be a time varying input and let $F(I)$ be the noisy firing rate as a function of the constant input (cf equations (12.19) or (12.20)). Then the firing rate for a time varying stimulus is

$$\tau_f \frac{df}{dt} = -f + F(I(t)).$$

The parameter τ_f is ad hoc and chosen to be small. It is not related an membrane or synaptic time constants but depends on all of these as well as the characteristics of the noise (see Fourcaud & Brunell, 2002). With low noise, then the instantaneous firing rate can be very complicated. In project (*) below, we suggest a way to look at these dynamics.

12.2 Population density methods.

Gerstner and Kistler provide a quick derivation for firing rate models of whole populations of neurons. McLaughlin, Shelley, and others at NYU have also derived such models. The equations which result are similar to those that we derived for globally coupled oscillators in chapter [OSCIL] Basically in all the derivations, the authors start with simple models for neurons such as the leaky integrate and fire model and from these derive an equation for the distribution of the potential. The flux of the potential across threshold is the firing rate of the cells. In general, the equations which result from these derivations are difficult to solve and often require special numerical methods. That said, there are still much faster to solve than the full network of spiking neurons. We will eschew a detailed study of the differences between the various derivations and sketch a fairly general equation based on the work of Gerstner and Kistler which to us is the most transparent derivation. Thus, this section is closely related to Chapter 6.2 in Gertner and Kistler. We will approach it slightly more generally so that the resulting model is not tied to the specific form of the LIF. The idea is to consider a one-dimensional neural model with some reset conditions.

We will write:

$$\frac{dv_i}{dt} = f(v_i) + g(v_i)I_i(t)$$

where f is the spiking dynamics and g is the response to inputs. I_i is all the synaptic currents coming into the cell. If the model requires reset, then we have a conditions that when $v_i = \theta$, then v_i is reset to $v_r < \theta$. For example, the LIF model has

$f(v) = -v/\tau$ and $g(v) = R/\tau$ where R is the membrane resistance. We define

$$\int_u^{u+\Delta u} p(u,t)\, du = \lim_{N\to\infty} \left(\frac{\#\text{cells with } u < v_i(t) \le u + \Delta u}{N} \right).$$

The function $p(u,t)$ is the membrane potential density. We have the following normalization:

$$\int_{-\infty}^{\theta} p(u,t)\, du = 1.$$

This says that the probability is conserved. The firing rate or population activity, $A(t)$ is defined as the flux of cells across threshold:

$$A(t) = J(\theta, t).$$

We will define this flux shortly. Neurons which cross the threshold reappear at the reset value, v_r so that this must be added to the evolution equations in the form of a source terms $A(t)\delta(v - v_r)$. We remark that these discontinuities will disappear if we use a model such as the theta model instead of the LIF since the "threshold" at π is just part of the full cycle. We assume that all neurons receive the same external input, $I_{ext}(t)$ and that there is random background input. Excitatory and inhibitory synaptic inputs are allowed as well. Synapses of type k occur at a rate $\nu_k(t)$. These could be from external sources or from within the network if it is recurrent. In order to avoid adding an additional equation, we will assume that the synaptic inputs are in the form of delta functions. Consider the single cell:

$$\frac{dv}{dt} = f(v) + g(v)w\delta(t - t^*)$$

where t^* is the time of the input and w is the amplitude. If v is the value right before t^*, then $v + wg(v) \equiv G(v,w)$ is the value of the potential right after the input. In order for the derivation we provide below to be valid, we will assume that the function $G(v,w)$ is invertible with respect to v. In exercise *, below, you are invited to show that for small w the inverse of G is:

$$H(v,w) \equiv G^{-1}(v,w) = v - g(v)w + g'(v)g(v)w^2 + O(w^3). \tag{12.14}$$

We note that if $g(v)$ is constant then the inverse is exact. For the theta model, $g(v) = 1 + \cos v$ where $v = \pi$ is the spike. Cai et al consider $g(v) = (v_s - v)$ where v_s is the synaptic reversal potential. An exact inverse can be found in this case.

With these asides out of the way, we continue the derivation. Each synapse of type k has an amplitude of w_k and occurs at a rate $\nu_k(t)$. The dynamics satisfy

$$\begin{aligned} \frac{\partial p(v,t)}{\partial t} &= -\frac{\partial}{\partial v}\left((f(v) + g(v)I_{ext}(t))p(v,t)\right) \\ &\quad + \sum_k \nu_k(t)[p(H(v,w_k),t)H_v(v,w_k) - p(v,t)] + A(t)\delta(v - v_r). \end{aligned} \tag{12.15}$$

The first term in the right-hand-side is just the drift due to the uncoupled dynamics of each neuron. The last term is the reinjection of cells which cross through the

threshold for spiking. The middle term is the gain of cells which were at $H(v, w_k)$ and jumped to v due to the synaptic input as well as the loss of those which jump from v to $G(v, w_k)$. The strange term H_v multiplying the probability arises because we want to conserve total probability. Note that it is bounded because G is invertible and thus monotone. We remark that $p(v, t) = 0$ for $v > \theta$. Right away, we can see that there is troub (??) lurking about if you are interested in simulation. Equation (12.15) is a functional partial differential equation because of the term H appearing *as an argument* of the density p. The firing rate is determined from the flux across threshold. To determine this, we rewrite (12.15) as a continuity equation. Note that

$$\nu_k[p(H(v, w_k), t)H_v(v, w_k) - p(v, t)] = -\frac{\partial}{\partial v}\nu_k \int_{H(v,w_k)}^{v} p(u, t)\ du.$$

Thus for any v, equation (12.15) can be written as

$$\frac{\partial p}{\partial t} = -\frac{\partial J}{\partial v} + A(t)\delta(v - v_r)$$

where

$$J(v, t) = [f(v) + g(v)I_{ext}(t)]p(v, t) + \sum_k \int_{H(v,w_k)}^{v} p(u, t)\ du.$$

Note that $J(v, t) = 0$ for $v > \theta$. If w_k is small, then we can expand this equation in a Taylor series to obtain the diffusion approximation. From equation (12.14),

$$\int_{H(v,w_k)}^{v} p(u, t)\ du \approx \int_{v-w_k g(v)+w_k^2 g'(v)g(v)}^{v} p(u, t)\ du.$$

Applying the fundamental theorem of calculus, this integral is approximately:

$$w_k g(v)p(v, t) - \frac{1}{2}[w_k^2 g(v)^2 p(v, t)]_v.$$

With this approximation the diffusive approximation for the population density equation is

$$\frac{\partial p(v, t)}{\partial t} = A(t)\delta(v - v_r) - \frac{\partial J_D(v, t)}{\partial v} \tag{12.16}$$

where

$$J_D(v, t) = [f(v) + g(v)(I_{ext}(t) + \sum_k w_k \nu_k(t))]p(v, t) \tag{12.17}$$
$$- \frac{1}{2}\frac{\partial}{\partial v}\left(\sum_k \nu_k(t) w_k^2 g(v)^2 p(v, t)\right).$$

Since these are just PDEs, they are amenable to numerical solution. If the inputs $\nu_k(t)$ are external, then we can define

$$\sigma^2(t) = \sum_k \nu_k(t) w_k^2$$

and

$$r(t) = I_{ext}(t) + \sum_k \nu_k(t) w_k.$$

If everything is stationary, then

$$J_D(v,t) = [f(v) + g(v)r]p(v,t) - \frac{\sigma^2}{2}\frac{\partial g^(v)p(v,t)}{\partial v}$$

where r and σ^2 are constant. Solving the steady state equations is identical to the single noisy integrate and fire model we studied in chapter [NOISE].

If we are using a discontinuous neural model, such as the LIF, then we have $p(\theta,t) = 0$ and firing rate, $A(t)$ is given by:

$$A(t) = J_D(\theta,t) = -\frac{1}{2}\frac{\partial}{\partial v}\left(\sum_k \nu_k(t) w_k^2 g(v)^2 p(v,t)\right)|_{v=\theta}.$$

However, if we instead use a continuous model on the circle such as the theta model, then the equations are considerably simpler. The term $A(t)\delta(v - v_r)$ no longer appears since the natural flow of the dynamics takes v through π and the domain of the model is $[0, 2\pi)$. In this case, we get

$$A(t) = J_D(\pi,t) = f(\pi)p(\pi,t)$$

since, for the theta model, $g(\pi) = 0$. For time dependent inputs to the theta model (or other ring models), we can solve the full equations by writing $p(x,t)$ in a finite Fourier series and then writing differential equations for the coefficients. See project 6 in the oscillator chapter.

Because the PDEs that result from these models can be quite difficult to solve (when the noise is low), we will generally use simple ODE forms of population models.

12.3 The Wilson Cowan equations.

One of the most influential models in the neural network literature is the one developed by Hugh Wilson and Jack Cowan in the early '70s. The original equations have the following form:

$$\begin{aligned} \tau_e \frac{dE}{dt} &= -E + (1 - r_e E)F_e(\alpha_{ee}E - \alpha_{ie}I + T_e(t)) \\ \tau_i \frac{dI}{dt} &= -I + (1 - r_i I)F_i(\alpha_{ei}E - \alpha_{ii}I + T_i(t)) \end{aligned} \tag{12.18}$$

where T_j is the input from the thalamus and r_e, r_i represent the refractory fraction of the neurons available to fire. The term $(1 - r_e E)$ is an approximation of

$$1 - \int_{t-r_e}^{t} E(s)\, ds$$

which represents the fraction of neurons available to fire given that they have an absolute refractory period of r_e. In a recent paper, Curtu and Ermentrout analyzed the behavior of the original integro-differential equations for a single excitatory population. The extra pro-multiplicative factor $(1 - r_e E)$ does not make too much of a difference in the analysis of the equations so we will generally set $r_e = r_i = 0$. We first consider a single scalar model for one recurrent population of neurons. Then we turn to the pair and we will look at mutually excitatory, inhibitory, and mixed populations. The last case is the WC equations.

A note on the gain functions.

What should one use for a gain function, $F(u)$? The traditional form for this is the logistic function, $F(u) = 1/(1 + \exp(-\beta(u - u_T)))$, which we have also encountered in our study of voltage-gated conductances. With the use of a logistic function, we interpret the function F as a probability of firing rather that an actual firing rate. Another similar choice for F is $F(u) = 1 + \mathrm{erf}(u)$ where erf(u) is the error function (integral of a Gaussian). Pinto et al use this model to study the mean field approximation for a model of cortex.

If we regard F as an actual firing rate of a single cell, then we could use an approximation for a neuron which undergoes a saddle-node bifurcation to periodic firing; namely:

$$F(u) = A\sqrt{\max(u - u_T)}$$

where u_T is the minimal current needed to induce firing. This gain function is continuous, but not differentiable and so will lead to problems when it comes time to numerically analyze models. In the presence of noise, we saw in Chapter $NOISE$ that the function is smoothed out. The following two variants of the above are good approximations to the noisy firing rate:

$$F(u) = A\sqrt{(u - u_T)/(1 - exp(-(u - u_T)/\beta))} \tag{12.19}$$

$$F(u) = A\sqrt{\beta \log[1 + \exp((u - u_T)/\beta)]}. \tag{12.20}$$

Here, β is a measure of the "noise"; as $\beta \to 0$, both these functions approach a pure square-root model. There are two more functions which are commonly encountered:

(i) the step function for which the neuron either is not firing at all or is firing at the maximal rate. This turns out to be the easiest to analyze and we will return to it when we get to networks.

(ii) the piecewise linear function

$$F(u) = \max(u - u_T, 0).$$

Linearity makes it possible to also analyze this function.

For the most part, there is little to recommend for the piecewise linear function other than it can be analyzed. The main objection we have for this function is that the firing rate can become infinite in recurrent networks. The step function and the logistic function which both saturate do not suffer from this problem. The square-root model is sublinear for large inputs so that it, too, does not "run away."

12.3.1 Scalar recurrent model.

As a warmup problem, we consider the simple recurrent neural network model:

$$\frac{du}{dt} = -u + F(\alpha u + \beta)$$

where β is the input and α is the strength of the connections. We leave as an exercise the analysis of this scalar model. We will assume that $F(u) \geq 0$, $F'(u) > 0$ so that the firing rate is a monotonic function. If the connections are inhibitory, $\alpha < 0$, then there is a unique asymptotically stable equilibrium point. If the connections are excitatory, then the situation is more interesting. In many firing rate functions, the derivative $F'(u)$ has a single maximum (that is F has a single inflection point). If this is the case, then you should be able to show that there are at most three fixed points to the scalar neural network. In general, if the nonlinear gain function $F(u)$ has $2m+1$ inflection points and aside from these $F''(u)$ is nonzero, then it is possible for the recurrent excitatory neural network to have $2m+3$ fixed points of which $m+1$ are stable.

To analyze bifurcations in a scalar firing rate model, we consider the current to be a parameter and ask when there is a saddle-node bifurcation. The condition is straightforward:

$$-1 + \alpha F'(\alpha u + \beta) = 0. \tag{12.21}$$

Since $F'(u)$ has a single maximum, if α is sufficiently large, we can choose u so that equation (12.21) has two roots. Given such a u, say, $\bar{u}$, we plug this into the equilibrium condition and solve for β:

$$\bar{u} = F(\alpha\bar{u} + \beta).$$

Since F is invertible we can solve for β. If α is chosen to be precisely the reciprocal of the maximum of F', then the two saddle-node roots of equation (12.21) merge at a codimension two cusp point. For more complex functions F with multiple inflection points, is is possible to have even higher codimension bifurcations such as the "butterfly catastrophe" (see Cowan & Ermentrout, 1978).

12.3.2 Two neuron networks.

We dispense with networks for which the interactions between the cells are the same, excitatory or inhibitory. The following theorem allows us to concentrate on fixed points alone:

Theorem. Consider the planar system:

$$\begin{aligned} x' &= f(x,y) \\ y' &= g(x,y) \end{aligned}$$

such that $f_y g_x > 0$ for all (x,y). Then there are no limit cycles.

With some hints, we leave the proof of this to the reader. We note that this bears a resemblance to Bendixon's negative criterion which states that if $f_x + g_y$ is

of fixed sign in a region, R, then there will be no limit cycles contained wholly in R.

An obvious consequence of this is that for the two population neural model

$$\begin{aligned} \tau_1 u_1' &= -u_1 + F_1(w_{11}u_1 + w_{12}u_2) \\ \tau_2 u_2' &= -u_2 + F_2(w_{21}u_1 + w_{22}u_2) \end{aligned} \tag{12.22}$$

if $F_j'(u) > 0$ and $w_{12}w_{21} > 0$, then there are no limit cycles and just fixed points. Thus, the entire phase portrait can be worked out by looking at the intersections of the nullclines. We will suppose that F_j are saturating nonlinearities with a maximum of 1 and minimum of 0 without loss of generality. We also assume that they are monotonic and have a single inflection point. Let G_j be the inverse of F_j. $G_j(x)$ have vertical asymptotes at $x = 0$ and $x = 1$ and are monotonically increasing. The u_1 nullcline has the form:

$$u_2 = (G_1(u_1) - w_{11}u_1)/w_{12} \equiv H_1(u_1).$$

If $w_{11} < 0$, then H_1 is a monotonic function much like G_1. However, if $w_{11} > 0$, then if the self-connection is large enough, the function H_1 has a cubic shape. Similar considerations hold for the u_2 nullcline: if $w_{22} > 0$, it can have a "cubic" shape. Figure 12.2A,B shows several different possibilities. We can freely shift the u_1 nullcline up and down by varying the inputs and the u_2 nullcline left and right as well. Up to nine fixed points are possible or as few as one. Bifurcations are generically saddle-nodes (although below, we consider an important symmetric situation which results in a pitchfork). Consider the case when both nullclines are "cubic." Thus, we can define the outer and middle branches of the cubic. Any fixed point which occurs on the intersection of two outer branches is a stable node. Any occurring on two inner branches is an unstable node. The rest are saddle points. We leave this as an exercise to the interested reader. Saddle points are important since their stable manifolds form separatrices dividing the plane into the domains of attraction for multiple stable fixed points. Figure 12.2C shows such an example. There are two states to this mutually excitatory network, one where both populations are firing at a low rate and one at a high rate.

Before turning to the excitatory-inhibitory networks which show the richest dynamics, we consider an important example that will appear throughout this chapter and plays a fundamental role in later sections. Many cognitive and other processes require making a choice between two or more competing sensory inputs. Suppose you have a trusty musket and on your left is a charging lion and on your right a charging pug. To which do you attend? There, the choice is rather obvious. However, suppose instead of the lion, you are confronted by another pug. Then, most likely, unless you like dogs or are afraid of them, you will ignore them. Instead, if you are being charged by two lions, it is likely you will select one of them at random (if one is a bit closer, then there will be a strong bias) and stick with it.

Figure 12.3A shows a model for competition between two neural pools, labeled 1 and 2. Each receives an input and inhibits the other pool. Since this example illustrates many of the mathematical concepts we will encounter later, we will sketch most of the details. We write $I_1 = I(1+a)$ and $I_2 = I(1-a)$ where a is an asymmetry

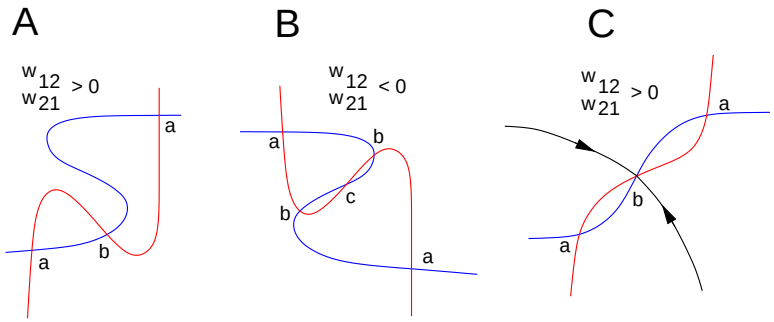

Figure 12.2. *Nullcline configurations for mutually excitatory/inhibitory networks (A) mutual excitation, (B) mutual inhibition, (C) mutual excitation with weak self-connections.*

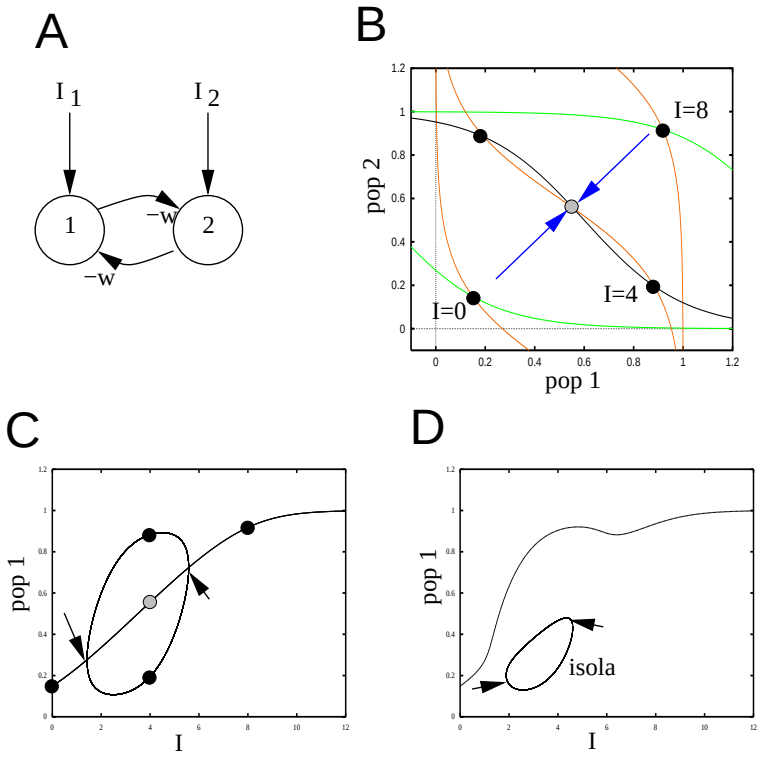

Figure 12.3. *The simplest model for competition between two populations. (A) the circuit (B) nullclines for identical inputs at 3 different strengths (C) bifurcation diagram when the inputs are identical (D) same as (C) but there is a small bias to population 1*

parameter and I is the total input. When $a = 0$, the input is unbiased and does not favor either unit (think of the two charging pugs). The extreme asymmetry case (lion versus pug) would have $a = \pm 1$. We will restrict our analysis to $a = 0$ and leave the $a \neq 0$ case for numerical analysis. The equations for this figure are

$$\begin{aligned} u_1' &= -u_1 + F(I - wu_2) \\ u_2' &= -u_2 + F(I - wu_1). \end{aligned} \tag{12.23}$$

We will assume that F is a monotone increasing positive function with $F'(x) \to 0$ as $x \to \infty$ and we assume that F is bounded as well. The weight $w \geq 0$. *Because of the symmetry*, one solution to this equation is homogeneous, $u_1 = u_2 = \bar{u}$ and

$$\bar{u} = F(I - w\bar{u}).$$

We leave as an exercise, the proof that there is a unique homogeneous equilibrium point, that it is positive, and that it is a monotonically increasing function of I and decreasing function of w. Let $c = F'(I - w\bar{u}) > 0$ be the derivative of F at the equilibrium value. The linearization of equation (12.23) is

$$\begin{aligned} v_1' &= -v_1 - cwv_2 \\ v_2' &= -v_2 - cwv_1. \end{aligned}$$

This is a simple 2×2 matrix, A, but rather than immediately writing down the eigenvalues, we step aside for a moment to discuss matrices of a special form, so-called circulant matrices.

ASIDE. Let $a_0, \ldots, a_{n-1}$ be fixed numbers (real or complex) and consider the matrix, A formed as follows:

$$A = \begin{pmatrix} a_0 & a_1 & \ldots & a_{n-1} \\ a_{n-1} & a_0 & \ldots & a_{n-2} \\ \vdots & \vdots & \ddots & \vdots \\ a_1 & a_1 & \ldots & a_0 \end{pmatrix}.$$

Such a matrix is called a *circulant* matrix and the eigenvectors and eigenvalues are easy to write down. Let $z_k = \exp(2\pi ik/n)$ for $k = 0, \ldots, n-1$. Let $\vec{v}_k$ be the column vector whose j^{th} entry is z_k^{j-1}. Then $\vec{v}_k$ is an eigenvector for A and the eigenvalue is

$$\lambda_k = \sum_{j=0}^{n-1} a_j z_k^j.$$

For example, if $n = 2$, then the eigenvectors are $(1, 1)^T$ and $(1, -1)^T$ with eigenvalues $a_0 + a_1$ and $a_0 - a_1$ respectively. **END ASIDE**

Since the linearization, A is a circulant matrix, the eigenvectors and eigenvalues are $\{(1, 1), -1 - cw\}$ and $\{(1, -1), -1 + cw\}$. The first of these eigenvalues is always negative; thus any *homogeneous* perturbation (along the eigenvector, $(1, 1)$)

decay to zero. However, if w is large enough, then $-1+cw$ can become positive for a range of inputs I which means that asymmetric perturbations (along the eigenvector, $(1,-1)$) will grow in time. At a critical value of the input, say, I_0, the asymmetric eigenvalue will be zero and we expect a bifurcation to occur. Since this problem has symmetry, the bifurcation at a zero eigenvalue will not be the generic fold, but rather a pitchfork bifurcation. This is typical in systems in which there is a circulant matrix involved (that is there is a symmetry.) Since the growth will be along the asymmetric eigenvector, the bifurcation solutions will have a form:

$$(u_1, u_2) = (\bar{u} + r, \bar{u} - r)$$

where $|r|$ is the amplitude of the solution. r can be either positive or negative corresponding to u_1 "winning" or u_2 "winning." Figure 12.3B shows the phase-plane and nullclines for equation (12.23) where $F(u) = 1/(1+\exp(-(u-1)))$, $w = 5$, and I is a parameter. At low inputs, both units fire equally at the same value. For intermediate values of the inputs, the homogeneous fixed point is unstable and there are two stable fixed points corresponding to one of the two units "winning." The saddle point (grey circle) has a stable manifold (blue arrows) which separates the phase-plane into two regions; those in the upper left tend to the u_2-dominant fixed point and those in the lower right to the u_1-dominant fixed point. Thus, without any input bias, the final outcome of the competition depends on any initial activity of the two units. At high inputs, then once again, the homogeneous solution is the only solution and both units fire at high rates. Figure 12.3C shows the bifurcation diagram for the symmetric input case. For I between the two arrows, one or the other population of neurons is dominant. If there is a slight bias in the inputs, then as the input increases, the favored population will always win (Figure 12.3D) but with a strong enough perturbation, it is possible to switch to the less favored population for a limited range of inputs. This figure shows what is called an *isola*, a small island of solutions. The arrows denote a pair of fold bifurcations. As the bias disappears, the isola grows and merges with the main branch of solutions to become figure 12.3C. As the bias, a increases, the isola shrinks to a point and disappears.

This example illustrates the basic concept underlying *symmetry-breaking* instabilities and bifurcations and pattern formation. The symmetric solution loses stability due to the negative interactions and results in new solutions which are no longer so symmetric.

12.3.3 Excitatory-inhibitory pairs.

We turn our attention to two population models in which one population is excitatory and the other inhibitory:

$$\tau_1 u_1' = -u_1 + F(w_{11}u_1 - w_{12}u_2 + I_1) \tag{12.24}$$

$$\tau_2 u_2' = -u_2 + F(w_{21}u_1 - w_{22}u_2 + I_2). \tag{12.25}$$

u_1 (u_2) is the excitatory (inhibitory) population. It is possible to do a fairly comprehensive local bifurcation analysis of this system if the inputs are the main parameters. Borisyuk and Kirillov (1992) provide such an analysis when $F(u) =$

$1/(1+\exp(-u))$; Hoppensteadt and Izhikevich perform a similar analysis. Choosing this F has the advantage of allowing us to note that

$$\frac{dF}{du} = F(1-F).$$

Let

$$G(y) = \ln \frac{y}{1-y}$$

be the inverse of $F(u)$. At an equilibrium point, we can solve for I_j:

$$I_j = G(u_j) - w_{j1}u_1 + w_{j2}u_2. \tag{12.26}$$

Let $B_j = w_{j1}u_1 - w_{j2}u_2 + I_j$ be the total input into each population. The linearization matrix has the form

$$A = \begin{pmatrix} -1 + w_{11}F'(B_1) & -w_{21}F'(B_1) \\ w_{12}F'(B_2)/\tau & (-1 - w_{22}F'(B_2))/\tau \end{pmatrix}.$$

We can rewrite $F'(B_j) = u_j(1-u_j)$ using the fact that at equilibrium, $F(B_j) = u_j$ and that $F' = F(1-F)$. There are two types of bifurcations of interest for this model: Hopf and saddle-node bifurcations. Saddle-nodes can be visualized by examining intersections of the nullclines. For the WC network, there can be up to 5 different fixed points. Hopf bifurcations can be easily found using the identities above. Recall that a necessary condition for there to be imaginary eigenvalues for A is that the trace of A vanishes:

$$\mathrm{Tr} \equiv -1 + w_{11}u_1(1-u_1) - 1/\tau - w_{22}u_2(1-u_2)/\tau = 0.$$

Clearly, since $0 < u_j < 1$, the trace is always negative unless $w_{11} > 4$, so that there must be sufficient recurrent excitation. We solve the above equation for $u_1 = U_1^{\pm}(u_2)$; there are two roots since it is quadratic. Plugging u_1 as a function of u_2 into equations (12.26), we can parameterize I_1, I_2 by the single number, u_2. Letting u_2 range between 0 and 1 for each of the two branches, $U_1^{\pm}(u_2)$, we get curves of Hopf points. This same method is not useful for the curve of folds (where the determinant vanishes) since the determinant is a quartic function of u_1, u_2 and so not readily solvable.

The easiest way to compute diagrams is through numerical methods. Figure 12.4 shows the behavior of this network for a fixed set of weights and time constant. As the excitatory input increases, the rest state increases until it loses stability at a Hopf bifurcation. Since increasing I_1 lifts the u_1-nullcline up, we can see the effect by looking at Figure 12.4C. At negative inputs, the excitatory nullcline intersects at a point where the slope of the nullcline is negative and thus the fixed point is stable. As input increases, the intersection moves to the middle branch and for sufficient input, becomes unstable. This leads to a Hopf bifurcation and limit cycle. Note that as the input increases, the excitatory nullcline gets closer and closer to the upper part of the inhibitory nullcline so that the period of the limit cycle increases. For sufficient input, there is an intersection of the nullclines at high values of excitation and inhibition

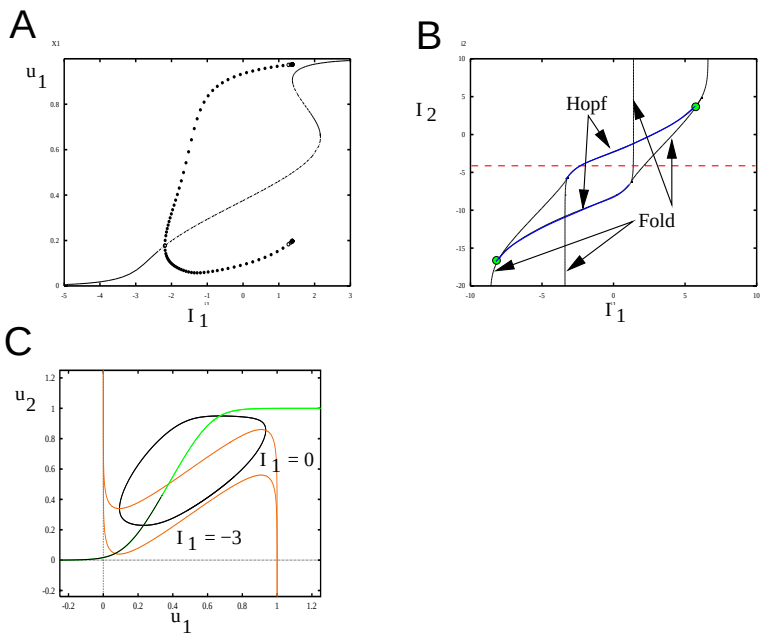

Figure 12.4. *Sample bifurcation diagram for an excitatory and inhibitory population. Parameters are* $w_{11} = 12, w_{12} = 10, w_{21} = 16, w_{22} = 4, \tau = 2$. *(A) Behavior of* u_1 *as* I_1 *increases,* $I_2 = -4$. *(B) Two parameter diagram as a function of the inputs,* I_1, I_2. *Green circle indicate Takens-Bogdanov points. (C) Phaseplane for* $I_2 = -4, I_1 = 0$.

Up-down states.

Recent experiments (Shu et al 2003) in prefrontal cortical slices show that local recurrent networks of excitatory and inhibitory neurons are able to produce epochs of sustained firing both spontaneously and through stimulation. These two states (firing and quiescent) are observed in extracellular and intracellular recordings of neurons. Figure 12.5A shows an example of a recording from a cortical slice preparation with inhibition and excitation intact. The network undergoes bouts of sustained activity lasting up to 4 seconds followed by quiescence. Intracellular recordings of a pyramidal cell in the network show that during the bouts of activity, the membrane potential is depolarized ("up state") compared to that during the quiescent period ("down state"). Stimuli allow one to switch from the down to the up state and vice versa. Importantly, depolarizing stimuli can switch the network from the up to the down. Furthermore, when the network is in the down state, very strong stimuli cause a brief bout of activity immediately followed by a return to the down state. These two properties allow us to make some good guesses as to what the local dynamics must be. Figure 12.5B shows a simulation of equations (12.24,12.25) when there is colored noise added to the inputs. The noise is needed to effect spontaneous switching between states. Holcman and Tsodyks (2006) have recently proposed a

model for this phenomena using recurrent excitation and synaptic depression and no inhibition. Here we suggest a very simple explanation for the properties of up and down states using a combination of excitation and inhibition. Figure 12.5C shows the phase-plane in the absence of noise for the simulation shown in B. As one would expect, there are two stable fixed points corresponding to the up and down states in the network. Separating these states is a saddle-point whose stable manifold acts as a threshold. In bistable systems such as that shown in figure 12.3B, the stable manifold is such that only negative perturbations of the state (1,0) can take it to state (0,1). Thus, in the up-down model, the stable manifold must be curved since strong depolarizing inputs can also cause a switch from up to down. Figure 12.5C shows that the stable manifold of the saddle point curves around so that if a stimulus takes the excitatory population beyond about 0.4, then there will be an immediate return to the down state. Modest stimuli will take the system from the down to the up and vice versa. Other properties of the up/down states follow immediately. For example, a depolarizing shock in the up state can take the system to the down state. Shu et al observe that there is a delay before going to the down state which is dependent on the amplitude of the stimulus. As can be seen in the figure, a stimulus which is close to the stable manifold but slightly beyond the right-hand branch will take much longer to go to the down state than will a stronger stimulus. Strong stimuli during the down state can induce a brief period of activation followed by a return to the down state as well. Adding a small amount of noise to the model equations can cause spontaneous transitions between up and down states much as is seen in figure 12.5A. Because the upper state is closer to instability and has complex eigenvalues, this could explain the fact that the upper state is much noisier than the lower state. Indeed, in a recent paper (Volgushev et al 2006), the authors use the large standard deviation of the "up state" as a means of automatically determining when neurons are in the up state.

2: Volgushev M, Chauvette S, Mukovski M, Timofeev I. Related Articles, Links Abstract Precise long-range synchronization of activity and silence in neocortical neurons during slow-wave sleep. J Neurosci. 2006 May 24;26(21):5665-72.

Holcman D, Tsodyks The emergence of Up and Down states in cortical networks. PLoS Comput Biol. 2006 Mar;2(3):e23. Epub 2006 Mar 24.

Whisker barrels.

Everyone who has ever had the pleasure of playing with a rat knows that the rat has several rows of whiskers which it uses to feel the world around it. Indeed, the usual white lab rats, that are popular with neuroscientists, are virtually blind and use their whiskers to navigate in their environment. Rats' whiskers are almost as sensitive as human fingers in discriminating textures. Each whisker projects (through the brainstem and then the thalamus) to a well defined aggregate of neurons in layer 4 of the cortex in the somatosensory area. These discrete areas are called barrels (see Figure 12.6A,B) and consist of a mixture of excitatory (70%) and inhibitory (30%) neurons which are recurrently connected. Thus, the local circuitry of the barrel is a perfect example of an excitatory-inhibitory network. Inputs to the barrel come from other layers of cortex and from the thalamus. In this example, we

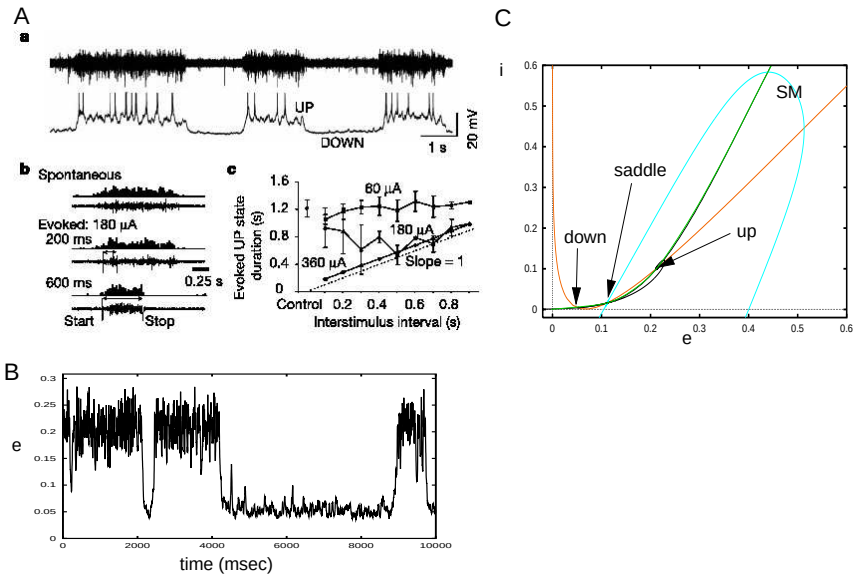

Figure 12.5. *Modeling up and down states in cortex. (A) Experimental data from Shu et al showing (a) extracellular (upper curve) and intracellular (lower curve) recordings over about 10 seconds; (b) shows evoked states via external stimuli, (B) Simulation of up/down states in a noisy Wilson-Cowan model showing spontaneous switching. (C) Phaseplane explanation of the balanced bistable state. (Parameters are* $\tau_1 = 5, \tau_2 = 3$, $w_{11} = 16, w_{21} = 24$, $w_{12} = 10, w_{22} = 6$, $I_1 = -3.7, I_2 = -6.7$. *Colored noise is added to the inputs.)*

restrict our attention to the local recurrent interactions and the thalamic inputs as shown in Figure 12.6C. Dan Simons and his collaborators have shown that the barrel circuit is exquisitely sensitive to the timing of the inputs from the thalamus. That is, the barrels respond strongly to rapidly increasing inputs and weakly to slow inputs. Figure 12.6D shows a typical example. The left hand response is very large compared to the right-hand one and the corresponding thalamic inputs show a rapid onset versus a more gradual onset. Pinto et al reduced a large scale spiking model due to Kyriazi & Simons to a network which should be familiar to the reader by now:

$$\tau_e \frac{du}{dt} = -u + F_e(w_{ee}u - w_{ie}v + w_{te}T(t))$$
$$\tau_i \frac{dv}{dt} = -v + F_i(w_{ei}u - w_{ii}v + w_{ti}T(t)).$$

The thalamic input, $T(t)$ consists of a constant background activity plus a triangle lasting 15 msec. The height of the triangle is constant, but the onset slope can be varied. The question is whether the network responds differently to different slopes of input. The input drives both the inhibition and the excitation which is

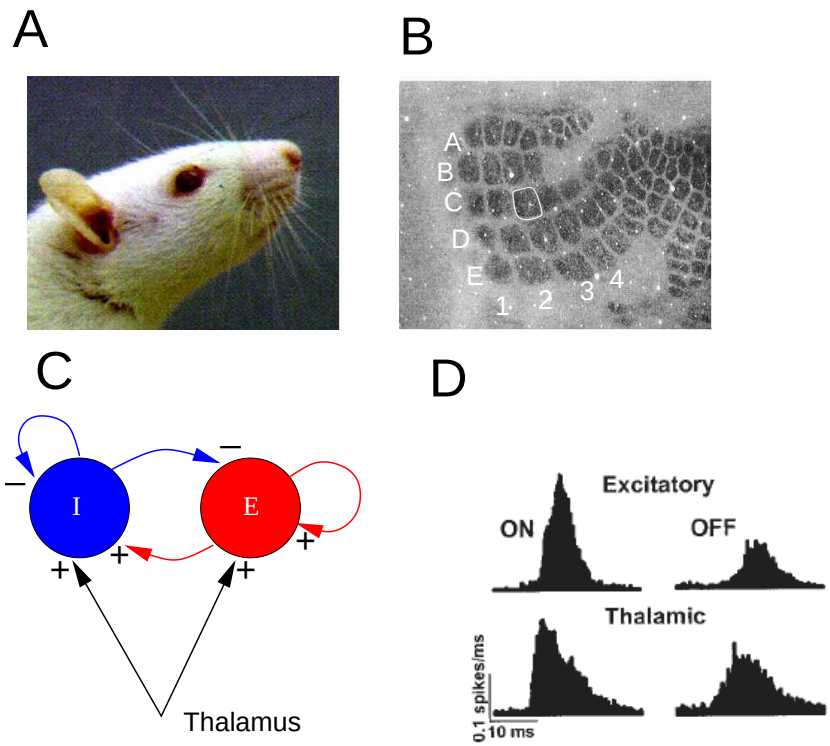

Figure 12.6. *Whisker barrel system of the rat. (A) Rat face (B) layer 4 cortex in the whisker area of the rat showing discrete barrels corresponding to individual whiskers. The C3 barrel is circled. (C) Local circuitry within a barrel showing strongly recurrent excitatory and inhibitory network along with thalamic input. (D) Population response of excitatory cells to experimental movement of a whisker. Thalamic response is also shown.*

crucial. Intuitively, if the slope is too small, then the inhibition can catch up and suppress the excitation. This provides what the experimentalists call a "window of opportunity" for the barrel cells to produce a response.

Figure 12.7A shows that in absence of inputs, the barrel network has a stable rest state. A perturbation in the excitatory direction past the right (middle) branch of the excitatory nullcline will be greatly amplified before returning to rest (an example of an excitable system). However, in the barrels, inputs come into both the excitatory and the inhibitory cells so that it is not clear what type of response occurs. Two responses are shown in the phase-plane and in the accompanying plot in Figure 12.7B corresponding to triangle inputs which have a width of 15 milliseconds and identical amplitude, The only difference is that they reach the peak amplitude at 1.6 and 3.2 milliseconds, respectively. By rising more quickly, the excitatory cells have a chance to react before the inhibition is engaged. The result is a significantly larger response for the fast rising inputs compared to the slower ones.

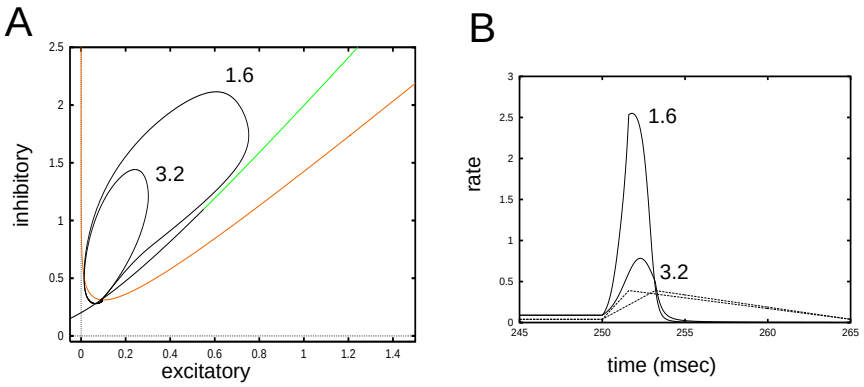

Figure 12.7. *Simulation of the barrel network. (A) Phaseplane for the barrel network at rest with two responses superimposed corresponding to input peaks at 1.6 and 3.2 msecs. (B) Firing rate of the excitatory population for the two inputs in (A) along with the inputs themselves (dashed).* ($F_e(x) = 5.12/(1+\exp(-(x-15)/4.16))$, $F_i(x) = 11.61/(1+\exp(-(x-15)/3.94)$, $w_{ee} = 42, w_{ie} = 24.6$, $w_{ei} = 42, w_{ii} = 18$, $\tau_e = 5, \tau_i = 15$, $w_{te} = 53.43, w_{ti} = 68.4$.*)*

12.3.4 Generalizations of firing rate models.

Various bells and whistles can be added to firing rate models in order to match their architecture with a more biologically realistic one. For example, many cortical neurons are endowed with spike-frequency adaptation which occurs at a much slower time scale than inhibition and is dependent only on the local neuron rather than on other neurons. Another example is short-term synaptic plasticity such as the depression or facilitation of synapses. Adaptation can be introduced as an activity dependent negative feedback. For example, a single excitatory population with adaptation can be written as:

$$\tau \frac{du}{dt} = F(au - cz) \tag{12.27}$$
$$\tau_z \frac{dz}{dt} = R(u,z) - z$$

where $R(u,z)$ is the activation of adaptation by excitation. There are several different possible models of this. The simplest is that $R(u,z) = u$. This linear adaptation allows for various interesting dynamics. If we recall that F is actually the firing rate, then a more realistic model would be $R(u,z) = \alpha F$ and if there was saturation (as would be the case if the adaptation was based on the conductance of some channel) then,

$$R(u,z) = \alpha F(1-z).$$

This assures that the adaptation can never exceed 1. The reader should explore this model on her own choosing, for example, $\tau_z \gg \tau$.

Synaptic depression (or facilitation) is more interesting as its effects are multiplicative. Let us recall the model for short-term depression of a synapse (8.13)

from the chapter on synapses:

$$\frac{dd}{dt} = \frac{1-d}{\tau_d} - \left(\sum_j \delta(t - t_j) \right) a_d d.$$

where t_j are the spike times of the presynaptic neuron. a_d is the degree of depression and τ_d is the recovery rate back to full strength. If we average this model over many repetitions of the same process, then the spike times are replaced by the firing rate of the presynaptic cell; thus, in terms of the firing rate, the model for synaptic depression is:

$$\frac{dd}{dt} = \frac{1-d}{\tau_d} - a_d F d.$$

We remark that several authors replace F in the above equation by u which is often also called the firing rate. Depending on the interpretation and derivation of the firing rate, either can be correct. If the firing rate models are derived from synaptic dynamics, then F is the firing rate, but if we are approximating a noisy model neurons response to inputs, then u is the approximation of the firing rate.

We illustrate extended firing rate models by looking at two examples.

Binocular rivalry.

When a person looks at two different objects in each of his eyes, such as vertical stripes in the left and horizontal in the right, then he does not perceive a mixture, but rather, he sees only one or the other. After a second or two the dominant percept disappears and the other object becomes dominant. Then there is another switch and so on. The switching is random, but there is a peak in the switching time histogram so that many models assume that the switching is governed by oscillatory dynamics. We will start with the competitive model, equation (12.23), but add the additional adaptation:

$$\begin{aligned} u_1' &= -u_1 + F(I - wu_2 - gz_1) \\ z_1' &= (u_1 - z_1)/\tau \\ u_2' &= -u_2 + F(I - wu_1 - gz_2) \\ z_2' &= (u_2 - z_2)/\tau. \end{aligned} \tag{12.28}$$

Here u_1 represents the right eye pattern and u_2 the left eye pattern. If the degree of adaptation, g is small enough, then we expect that the behavior should be like that of equation (12.23); for large enough w; as I increases there will be a pitchfork bifurcation from the homogeneous state to a state when one or the other "wins." Because of symmetry, either left or right can win. As in the competitive model, there will be a homogeneous rest state, $(u_1, z_1, u_2, z_2) = (\bar{u}, \bar{u}, \bar{u}, \bar{u})$. The stability of this state is found by studying the eigenvalues of a 4×4 matrix:

$$M = \begin{pmatrix} -1 & -cg & -cw & 0 \\ 1/\tau & -1/\tau & 0 & 0 \\ -cw & 0 & -1 & -cg \\ 0 & 0 & 1/\tau & -1/\tau \end{pmatrix} = \begin{pmatrix} A & B \\ B & A \end{pmatrix}$$

where A, B are 2×2 matrices and $c = F'(I - (w + g)\bar{u})$. Just like the competition model, the structure of M has symmetry so that we can reduce the computation of the eigenvalues to those of two 2×2 matrices, $C^+ = A + B$ and $C^- = A - B$. These two correspond to eigenvectors of the form, (x, y, x, y) and $(x, y, -x, -y)$. The former represents symmetric perturbations of the steady state and the latter, asymmetric. Consider, first, symmetric perturbations:

$$C^+ = \begin{pmatrix} -1 - cw & -cg \\ 1/\tau & -1/\tau \end{pmatrix}.$$

Since C^+ has a negative trace (recall that $F' > 0$ so that c is positive and w, g are non-negative) and a positive determinant all eigenvalues of C^+ have negative real parts. The asymmetric perturbations are more interesting:

$$C^- = \begin{pmatrix} -1 + cw & -cg \\ 1/\tau & -1/\tau \end{pmatrix}.$$

If we treat c as a parameter (this is related to the intensity of the stimulus and, of course, the shape of F), then the determinant vanishes when $w > g$ and $c = c_0 \equiv 1/(w - g)$ and the trace vanishes when $c = c_H \equiv 1/w(1 + 1/\tau)$. Thus, if g is close to w and τ is large, the trace will become positive at smaller inputs than it takes to make the determinant negative. That is, there will be a Hopf bifurcation as the input increases when the time constant of adaptation is large and the strength of adaptation is also sufficiently large. In contrast, with weak or very fast adaptation, the network will maintain its winner-take-all behavior. This simple mechanism provides a means by which there will be periodic switching of the dominance of the two percepts. While this is a somewhat naive model, it is able to explain some aspects of rivalry and, in fact, make some testable predictions (Wilson et al, 2001). We will leave the full numerical exploration of this model as an exercise to the reader.

Wilson HR, Blake R, Lee SH. Dynamics of traveling waves in visual perception. Nature. 2001 Aug 30;412(6850):907-10.

Synaptic depression and oscillations.

Many neuronal networks show spontaneous oscillations during development; it is believed that the activity may help strengthen connections between neurons which are important later in the animals life. A striking example of this is spontaneous episodes of activity in the spinal cord of embryonic chickens. Isolated spinal cord preparations produce bursts of activity every 2-30 minutes and within these bouts of activity, produce 0.1-2 Hz oscillations. Tabak et al (2000) suggest that the mechanism underlying this is recurrent excitatory connections coupled to synaptic depression with two different time scales. The slow scale depression accounts for the long inter-burst interval and the faster depression for the oscillations within a burst. Here, we will be concerned only with the higher frequency oscillations. Let $u(t)$ denote the firing rate of the population and $d(t)$ the efficacy of the synapse.

Then the equations are:

$$u' = -u + f(wdu) \qquad (12.29)$$
$$\tau d' = 1 - d - \alpha u d.$$

Our model for d is slightly different from the one in Tabak et al, but the nullclines are qualitatively similar. In the Tabak et al paper, they use:

$$f(x) = 1/(1 + \exp(-(x - \theta)/k))$$

with $k = 0.05$ and $\theta = 0.18$. By choosing $w = 1, \alpha = 5$, and $\tau = 5$, it is possible to get sustained oscillations. We leave a complete analysis of this to the reader. A related model and phenomena is found in a paper of Tsodyks et al

Tabak J, Senn W, O'Donovan MJ, Rinzel J. Modeling of spontaneous activity in developing spinal cord using activity-dependent depression in an excitatory network. J Neurosci. 2000 Apr 15;20(8):3041-56.

12.4 Projects.

1. Consider a pair of neurons (excitatory and inhibitory) coupled as:

$$u_e(t) = F_e(w_{ee}\Phi_{ee} * u_e(t) - w_{ei}\Phi_{ei}(t) * u_i(t))$$
$$u_i(t) = F_i(w_{ie}\Phi_{ie} * u_e(t) - w_{ii}\Phi_{ii}(t) * u_i(t))$$

   where $\Phi_{jk}(t) = \exp(-t/\tau_{ij})/\tau_{ij}$ and $U(t) * V(t) = \int_0^t U(t-s)V(s)ds$. If τ_{ij} is independent of i or independent of j, then these can be converted to a apir of first order differential equations. However, if all τ_{ij} are different, then these integral equations can be converted into 4 first order differential equations. Write down these four equations. Is there any behavior (eg limit cycles) that occurs for the four equation model which would not occur for the two-equation model when τ_{ij} is independent of i or j? For example, can you prove that a fixed point for the four variable model is asymptotically stable if it is stable for the two variable model?

2. Consider a noisy integrate and fire model, $V' = -V + I$, for which the current makes a step from I_1 to I_2. Using the Fokker-Planck equation, examine the temporal dynamics on the firing rate for this transition in the low and high noise regimes ($\sigma = 0.4, 1$). In the low noise case, the approach to the steady state rate f is a damped oscillation. For different steps in the current estimate both the damping and the oscillation rate. The figure below illustrates an example of a step and a fit to a damped oscillation. Use this to suggest a linear model for the firing rate:

$$u'' + 2au' + (a^2 + f^2)(u - f) = 0$$

   where f is the instantaneous firing rate. It may be necessary to also include the derivative of f in the calculation. You will find that for slowly varying

stimuli, this does not do any better than the simple ad hoc first order equation, $\tau_f u' = f - u$.

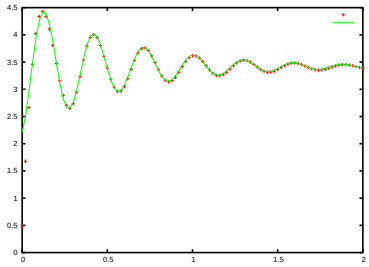

3. Based on the previous exercise, the temporal dynamics of the response of a neuron depends on the steady state firing rate. Consider the same equation as in the previous exercise, but f now depends on u as:

$$f = F(wu - u_{th})$$

where F is a nonlinear function as explored in this chapter. Do the dynamics of the scalar recurrent network exhibit anything new? Show that even this second order model cannot produce limit cycle oscillations.

4. Explore the effects of changing the temporal dynamics of inhibition on the barrel network. For example, quantify how that "window of opportunity" depends on the time constant of the inhibitory response.

5. In Volgushev et al (2006), the authors look at the propagation of down to up and up to down transitions in cortex by recording over a 12 mm spatial area in the cat cortex during sleep. Adapt the population model for up-down states to an array of, say, nearest neighbor coupled populations and add independent noise to each population sufficient to induce spontaneous switching. Do you see any evidence for propagation of states, eg, if one group of cells switches from down to up, does this switch propagate across the network. Explore different levels of noise and different degrees of coupling. In order to couple two networks, you should look at a model of the form:

$$\tau_e u_j' + u_j = F_e(w_{ee}\bar{u}_j - w_{ie}\bar{v}_j)$$

where

$$\bar{u}_j = (1-c)u_j + (c/2)[u_{j+1} + u_{j-1}]$$

and $c \geq 0$ is the degree of coupling. Similar equations for the inhibitory population, v_j should be written as well with a possibly different coupling strength. Use parameters as in figure 12.5.

12.5 Exercises.

1. Derive equation (12.3).

2. We can write (12.3) as

$$\Phi(t) = Ae^{-at} + Be^{-bt} + Ce^{-ct}$$

where a, b, c are positive numbers. Show that A, B, C are such that $\Phi(0) = \Phi'(0) = 0$. (Note the first part is by definition. Use the definition of $\Phi(t)$ to prove the second part.) Now that you have done that, suppose:

$$x(t) = \int_0^t \Phi(t-s)y(s)\ ds.$$

What third order differential equation does $x(t)$ satisfy?

3. Consider the scalar neural network:

$$u'' + (a+b)u' + abu = F(u)$$

where a, b are positive. Prove that there can be no limit cycle solutions. Suppose $F(0) = 0$. What types of bifurcations are possible?

4. In exercise 2 you show that the general $\Phi(t)$ leads to a third order differential equation. Consider the scalar neural network:

$$[(d/dt + a)(d/dt + b)(d/dt + c)]u = F(\alpha u).$$

Suppose that $F' > 0$ and a, b, c are positive. For $\alpha < 0$ show that there exists a unique fixed point and show that a Hopf bifurcation is possible as one of the parameters varies. (Hint: Think about the Routh-Hurwitz criteria.) If $\alpha > 0$ show there cannot be a Hopf bifurcation. We conjecture that there can be no periodic solutions if $\alpha > 0$, but have no proof.

5. Derive equation (12.14)

6. Consider the delayed excitatory network:

$$u_t + u = F(\alpha u(t-\tau))$$

where we have set $\tau_m = 1$ without loss of generality. Assume that $F'(u) > 0$ and $\alpha > 0$. Prove that there exists at least one fixed point and prove that there can never be a Hopf bifurcation no matter what the delay.

7. Consider the delayed inhibitory network:

$$u_t + u = F(-\alpha u(t-\tau))$$

where $F(u) \geq 0$, $F'(u) > 0$ and $\alpha > 0$. Prove that there is a unique fixed point (see the next exercise) and that there can be a Hopf bifurcation. Simulate this network using $F(u) = 1/(1 + \exp(-(u + I))$ where I is input to the network. Use $\alpha = 8$ and $I = 1$ and treat τ as a parameter.

8. Suppose that $G(u) \geq 0$ and $G'(u) < 0$ for all u. Prove that there is a unique root fixed point to
$$u_t + u = G(u)$$
and that it is asymptotically stable.

9. Consider equation (12.12). (a) If $F(I) = \sqrt{I - I^*}$ for $I > I^*$ and is zero otherwise, compute $F_Q(I)$ when $I*$ is taken from a uniform distribution $I_{min} \leq I^* \leq I_{max}$. (b) If $F(I - I^*) = \max(I - I^*, 0)$ and I^* is taken from a Gaussian distribution with mean $\bar{I}$ and standard deviation σ, compute $F_Q(I)$. (c) Repeat (b) for $F(I - I^*) = 1$ for $I > I^*$ and 0 otherwise.

10. Compute the firing rate function for the integrate and fire model based on the conductance of the synapse. That is, suppose that V satisfies:
$$C\frac{dV}{dt} = -g_L(V - E_L) - g(V - E_{syn})$$
where $E_L < V_T < E_{syn}$ is the threshold to spike and upon spiking, V is reset to $E_r < V_T$. Compute the firing rate as a function of the synaptic conductance, g. What happens as $g \to \infty$? Can you do some asymptotics of this to get a simple formula for large conductances? Plot the $F - g$ curve for $C = 1$, $g_L = .05$, $E_L = -65$, $E_r = -70$, $E_T = -50$ and $E_{syn} = 0$.

11. Consider a recurrent scalar network with the threshold linear firing rate:
$$\frac{du}{dt} = -u + [au - u_T]_+.$$
Show that is $a > 1$, then sufficiently large initial conditions grow exponentially. For a fixed positive value of u_T and $a > 1$, find the critical value of u_0 such that if $u(0) > u_0$, $u(t)$ grows exponentially without bound.

12. Suppose that $F(u) \geq 0$, $F'(u) > 0$ and $F''(u)$ has a single zero. Assume that F and its derivatives are continuous on R. Prove that there are at most three fixed points to the neural network equation $u' = -u + F(u)$.

13. (Hard.) Suppose that $F'(u) \geq 0$ and $F(u)$ has k inflection points. Show that there can be up to $k + 2$ fixed points to $u = F(u)$. (Hint: use the previous exercise and proceed inductively.)

14. Find the saddle nodes and the cusp bifurcation for the scalar model with $F(u) = 1/(1 + \exp(-u))$. (Note that $F' = F(1 - F)$.)

15. Prove that if $f_y g_x > 0$ in the plane, there are no limit cycles to $x' = f(x, y)$, $y' = g(x, y)$. Here is a brief hint to get you started. In order for there to be a limit cycle, $x'(t)$ must change sign. Suppose, first that $f_y > 0$ and $g_x > 0$. (The other case follows similarly.) Suppose that $x'(t)$ is positive and then vanishes at $t = t_1$. We cannot have $y'(t_1) = 0$ since then we would be at a fixed point. Thus either $y'(t_1) > 0$ or $y'(t_1) < 0$. Suppose the first case. Then

$x''(t_1) = f_y y'(t_1) > 0$ so that for $t > t_1$ $x'(t) > 0$ so that x' does not change sign. Continue to argue in this manner for all the other cases. You will need to use the fact that $g_y > 0$ for this.

16. Prove that if $F'(u) > 0$, $F(u) > 0$, $F(-\infty) = 0$, then there is a unique solution to

$$u = F(I - wu)$$

for all I and $w > 0$. Prove that u is a monotonically increasing function of I and that $u > 0$. Prove that u is a monotonically decreasing function of w.

17. In the mutual interaction model (12.23), what happens if the interaction is positive (that is, $-w$ is positive)? Show that asymmetric perturbations are always stable.

18. (Disinhibition and epilepsy). One model for epilepsy is that it arises when the inhibition is partially blocked. Consider the WC model:

$$u_1' = -u_1 + F(12u_1 - 12u_2 - 3)$$
$$3u_2' = -u_3 + F(18u_1 - 4u_2 - 5)$$

Show through simulation that there is a unique stable equilibrium. Now, suppose that a drug such as bicuculline is applied which has the effect of reducing the inhibitory strength. Incorporate a parameter p to the model multiplying the strength of inhibition (don't forget the inhibitory-inhibitory connection) such that when $p = 1$ the inhibition is at full strength and at $p = 0$ it is completely blocked. Compute the bifurcation diagram for the model as p decreases and show that there can be a Hopf bifurcation and for severely reduced inhibition a completely active state.

19. Consider the binocular rivalry model described by equation (12.28) with $w = 5, g = 1, \tau = 20$ and $F(x) = 1/(1 + \exp(-(x - 2)))$. Compute the bifurcation diagram of this model as a function of the parameter I. Now set $g = 0.25$ and compute the diagram again. Note that there is no Hopf bifurcation and there is only the pitchfork. Set $g = 0.5$ and compute as much as you can of the bifurcation diagram. Find the curve of branch points and Hopf points as a function of the two parameters, g and I.

12.6 Some methods for delay equations.

Delay equations do not commonly appear in the curricula of most dynamics courses so that we review a number of well-known results mostly from the classic text by Bellman and Cooke. Here we focus on systems with only one delay and only consider the linear stability theory around equilibria for delay equations. We start with a simple scalar example:

$$\frac{dx}{dt} = f(x(t), x(t - \tau))$$

and let $\bar{x}$ be a fixed point, $f(\bar{x}, \bar{x}) = 0$. The linearized equation has the form:

$$\frac{dy}{dt} = ay(t) + by(t - \tau).$$

Here a, b are the derivatives of f with respect to the first and second arguments evaluated at the fixed point. As with ordinary differential equations, we look for solutions of the form $y(t) = \exp(\lambda t)$ leading to:

$$\lambda = a + be^{-\lambda\tau}.$$

There are infinitely many roots to this equation; if any of them has a positive real part, then we say the fixed point is unstable. If all roots have negative real parts, then the fixed point is linearly asymptotically stable. For general systems with one delay, if the delay appears only in one variable, then, the characteristic equation will take the form:

$$M(\lambda) \equiv P(\lambda) + Q(\lambda)e^{-\lambda\tau} = 0.$$

Thus, for many commonly encountered problems, the stability of fixed points relies on solving the polynomial-exponential characteristic equation. Before state some theorems about stability, we consider a more general question; can a delay destabilize a fixed point which, in absence of delay, was stable? Stability can be lost via a zero eigenvalue or through complex conjugate eigenvalues. In the former case, one must have $P(0) + Q(0) = 0$ which is clearly independent of the delay. Thus, we focus on determining if it is possible for a delay to cause $M(\lambda)$ to have imaginary eigenvalues. If this happens, then:

$$\Gamma(\omega) \equiv \frac{P(i\omega)}{Q(i\omega)} = e^{-i\omega\tau}.$$

The left hand side of this expression traces out a curve in the complex plane (see figure 12.8) and the right hand side traces out the unit circle. Suppose that when $\Gamma(0)$ lies outside the unit circle and as ω varies it never crosses the circle (case 1). Then, there will be no delay τ which can change the stability, since the two curves never intersect. If $\Gamma(0)$ is inside the unit circle and never leaves it, then, again, no stability change can occur. However, if the two curves intersect (case 2), then we can always choose τ so that they intersect at the same value of ω. Thus, we can destabilize the equilibrium by changing the delay. Since the critical eigenvalue is $i\omega$, we expect to get a bifurcation to periodic orbits, although the proof of this is much more difficult than that of the ODE case. As an example, consider the above scalar problem.

$$\Gamma(\omega) = \frac{i\omega - a}{b}.$$

This traces a vertical line in the complex plane. If $|a/b| < 1$, then $\Gamma(\omega)$ will cross the unit circle and there will be delay-induced instability. Note that in order for the fixed point to be stable in absence of a delay, we have, $a + b < 0$. For delay-induced instability, the magnitude of b must be larger than a, so these two inequalities imply

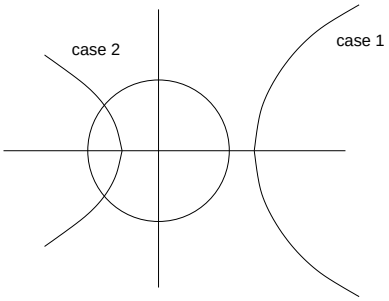

Figure 12.8. *Stability plots for delay equations.*

that b is negative and sufficiently large. We have thus shown a classic result that delayed negative feedback can induce oscillations.

We conclude with a theorem from Bellman and Cooke giving general results for scalar delay equations. We rewrite the characteristic equation as

$$e^{\lambda\tau}P(\lambda) + Q(\lambda) = 0$$

and let $z = \lambda\tau$. Since $\tau > 0$, if z has a positive real part, then so does λ. The following theorem provides necessary and sufficient conditions for stability of the scalar delay equations, which can be written as $H(z) = \tau a e^z + b\tau - ze^z = 0$.

Theorem (Bellman & Cooke, p444). All roots of $pe^z + q - ze^z$ have negative real parts if and only if

(a). $p < 1$, and

(b). $p < -q < \sqrt{r_1^2 + p^2}$

where r_1 is a root of $r = p\tan r$ such that $0 < r < \pi$. If $p = 0$, we take $r_1 = \pi/2$.

Using this theorem as well as the easy graphical method above, you should have no trouble solving the problems for delay equations.

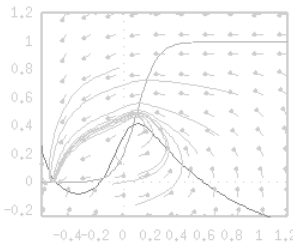

Chapter 13

Spatially distributed networks.

13.1 Introduction.

In the previous chapters, we have focused generally on single neurons, small populations of neurons and the occasional array of neurons. With the advent of multi-electrode recording, intrinsic imaging, calcium imaging, and even functional magnetic resonance imaging (FMRI), it is becoming possible to explore spatio-temporal patterns of neural activity. This leads to a wealth of interesting fodder for the mathematically inclined and it is the goal of this chapter to provide some examples of this type of analysis. In Chapter *, we looked at the propagation of action potentials down an axon; this is modeled as a partial differential equation. By looking for traveling waves, we were able to reduce the equations to a set of ODEs. When neurons are coupled together with chemical synapses, the natural form of coupling is not through partial derivatives with respect to space, but rather through nonlocal spatial interactions such as integral equations. As with the PDEs, it is possible to look for specific forms of solution (such as traveling waves or stationary patterns), but the resulting simplified equations do not reduce to ODEs. Thus, new techniques must be developed for solving these equations and (if desired) proving their existence and stability.

This chapter begins with a few words on unstructured networks such as random networks and Hopfield networks. Such networks are amenable to various types of analysis and are popular among theoretical physicists due to their similarity to spin glasses. On the other hand, it is difficult to access their behavior experimentally since they do not produce coherent activity that is easily visualized, measured, or quantified.

We then turn to models for spatially structured networks where the connectivity between neurons depends on their distance from each other. We focus our attention on populations of firing rate models for which the theory is much more developed. We discuss an important existence theorem for traveling fronts and then use this to analyze traveling pulses in networks. We discuss the classic work of Shunichi Amari and the relationship between localized stationary activity and working

memory. The Amari model sets the stage for stability analysis when there are delays and other sorts of temporal dynamics. We then turn to so-called ring models for the emergence of tuning curves in the visual system. Finally, we conclude with a bifurcation theory analysis of pattern formation applied to visual hallucinations.

13.2 Unstructured networks.

In this section, we review some general results on "neural networks" or artificial networks. These include some feed-forward models such as those used in the so-called back propagation literature and Hopfield and related attractor networks. We also state and prove the very general Cohen-Grossberg theorem. Specifically, we are interested in networks of the two general forms:

$$\tau_j \frac{du_j}{dt} + u_j = F_j \left(\sum_k w_{jk} u_k \right) \tag{13.1}$$

$$\tau_j \frac{dV_j}{dt} + V_j = \sum_k w_{jk} F_k(V_k). \tag{13.2}$$

The first of these is the so-called "firing rate " formulation, while the second is the voltage formulation. Cowan & Sharp review the history of neural networks and provide a guide to the main results.

13.2.1 McCulloch-Pitts.

McCulloch-Pitts (MC) models consist of "neurons" which have two states, 0 and 1. The next state of neuron i is determined by the quantity:

$$\mu_i = H \left(\sum_j w_{ij} N_j - \theta_i \right)$$

where H is the step function and w_{ij}, θ_i are real numbers. It is important that $w_{ii} = 0$ for otherwise, there may be ambiguity in the value of μ_i. Updating can be done either synchronously (like a discrete dynamical system) or it could be done asynchronously. In the latter case, an index, k is randomly chosen and the neuron, k is assigned the value μ_k according to the above quantity. In order for this network to do something useful, it is necessary to make appropriate choices for the weights. There are a number of learning algorithms which set the weights in such a way as to produce a desired output for a given input. We point the reader to, for example, Parallel Distributed Processes (McLelland and Rumelhart) as a classic text on learning algorithms for feed-forward networks.

13.2.2 Hopfield's model.

As with the McCulloch-Pitts model, we will consider now a network of asynchronously updated two-state neurons. It is convenient to set their states to be

$-1, 1$ instead of $0, 1$. Thus, consider a network of the form:

$$S_i(t+1) = \text{sgn}\left(\sum_j w_{ij} S_j - \theta_j\right),$$

where $\text{sgn}(x)$ is $+1$ for non-negative x and -1 for $x < 0$. If we update asynchronously, then w_{ii} should be zero. To see why, suppose we want to figure out S given:

$$S = \text{sgn}(S - 1/2).$$

Clearly, we could choose $S = 1$ or $S = -1$ and satisfy this constraint. Thus, we will assume that $w_{ii} = 0$. Furthermore, for simplicity, let us assume that $\theta_i = 0$. Hopfield noticed that if $w_{ij} = w_{ji}$ then this dynamical system has an energy function:

$$U = -\frac{1}{2}\sum_{ij} w_{ij} S_i S_j.$$

To see that this is an energy function, let S'_k be a new state of the system. The change in energy, $U' - U$ is

$$-\frac{1}{2}(S'_k - S_k)\left[\sum_j S_j w_{kj} + \sum_i S_i w_{ik}\right].$$

However, since $w_{ij} = w_{ji}$, the energy difference is:

$$\Delta U = -(S'_k - S_k)\sum_j w_{kj} S_j = -(S'_k - S_k)S'_k.$$

The last equality comes from the fact that $S'_k = \sum_j w_{kj} S_j$. If $S'_k = 1$, then $\Delta U \leq 0$ (with equality only if $S'_k = S_k$) and if $S'_k = -1$, then ΔU is also less than or equal to 0. Thus, the energy U will decrease until a minimum is reached and the dynamics always converges to an equilibrium. Note the importance of the symmetry assumption. If $w_{ij} \neq w_{ji}$, then there is no guarantee that there will be convergence to steady state.

The ideas of Hopfield can be extended to continuous neural networks as long as there are symmetric connections between the weights. Hopfield proved such a result shortly after his discrete model came out (1984). At roughly the same time, Michael Cohen and Steve Grossberg proved a more general result. We now discuss the two different models. First consider the continuous network in the "voltage" formulation:

$$C_i \frac{dV_i}{dt} = \sum_j w_{ij} f_j(V_j) - V_i/R_i + I_i \tag{13.3}$$

where the functions $f_j(V_j) \equiv U_j$ represent the firing rate at the axon hillock of a neuron with somatic potential V_j (see previous chapter). We assume that $w_{ij} = w_{ji}$ and that f_j is monotone increasing function. Hopfield forms the following function:

$$E = -\frac{1}{2}\sum_{i,j} w_{ij} U_i U_j + \sum_i \frac{1}{R_i}\int_0^{U_i} f_i^{-1}(U)dU + \sum_i I_i U_i. \tag{13.4}$$

In exercise ** below, you are asked to show the following:

$$\frac{dE}{dt} = -\sum_i \frac{dU_i}{dt}\left(\sum_j w_{ij}U_j - \frac{V_i}{R_i} + I_i\right). \tag{13.5}$$

Note that the term in the parenthesis is just the dynamics of the individual neuron, that is, $C_i dV_i/dt$. Thus,

$$\begin{aligned}\frac{dE}{dt} &= -\sum_i C_i \frac{dU_i}{dt}\frac{dV_i}{dt} \\ &= -\sum_i C_i (f_i^{-1})'(V_i)(dV_i/dt)^2.\end{aligned}$$

As long as f_i are monotone increasing, then $dE/dt \leq 0$. Thus, solutions to (13.3) will converge to an equilibrium point.

Cohen and Grossberg (1983) studied the following class of models:

$$\frac{dx_i}{dt} = a_i(x_i)\left(b_i(x_i) - \sum_{j=1}^{N} c_{ij} d_j(x_j)\right) \tag{13.6}$$

where

1. $c_{ji} = c_{ij}$;
2. $a_i(x_i) \geq 0$;
3. $d_i'(x_i) \geq 0$.

Suppose, for example, that $a_i = 1/\tau_i$, $b_i = I_i - x_i$, and $c_{ij} = -w_{ij}$. Then (13.6) becomes

$$\tau_i \frac{dx_i}{dt} = I_i - x_i + \sum_{j=1}^{N} w_{ij} d_j(x_j).$$

which is identical to (13.3) after multiplication by R_i. Thus, the Cohen-Grossberg equations cover the Hopfield model. Consider the following function:

$$E = -\sum_i \int^{x_i} b_i(y) d_i'(y)\, dy + \frac{1}{2}\sum_{j,k} c_{jk} d_j(x_j) d_k(x_k). \tag{13.7}$$

Then,

$$\frac{dE}{dt} = -\sum_i a_i(x_i) d_i'(x_i)\left(b_i(x_i) - \sum_j c_{ij} d_j(x_j)\right)^2. \tag{13.8}$$

From the assumptions (2,3), this is non-positive. This derivative vanishes only when $a_i = 0$, $d_i' = 0$ or the terms in the parentheses vanish.

13.2.3 Designing memories.

Given that the unstructured networks we have described so far all converge to fixed points, we can ask some questions about how to design the weights of the network in such a way that they converge to a desired pattern. Many theoreticians (and experimentalists) think of Hopfield networks as a kind of association cortex where memories are stored in the weights and the resulting steady state patterns are the activities which are retrieved from the memory. That is, a memory is a vector of activities or potentials which should be one of the stable fixed points of the network (13.1) or (13.2). If initial data are close to this vector, then the network dynamics should converge to it. Thus, the network is able to perform *pattern completion* from partial information. Suppose the network has "stored" two memories. Then we want it to be able to retrieve these when initial conditions or inputs are biased towards one or the other. Our question in this section is: "How do we choose the weights to get a series of specified vectors as stable equilibria for the neural network?"

Consider an N-neuron network which should converge to a single memory specified by a vector ξ. We take as the weight matrix, the outer product:

$$w_{ij} = \xi_i \xi_j / N.$$

Clearly, $w_{ij} = w_{ji}$. The dynamics satisfy:

$$\frac{dV_i}{dt} = -V_i + \xi_i (1/N) \sum_{j=1}^{N} \xi_j F(V_j).$$

Let $U = (1/N) \sum_j \xi_j F(V_j)$. Then

$$V_i' = -V_i + \xi_i U.$$

The steady state for this is just $V_i = U\xi_i$. Finally, we see that U must satisfy:

$$U = (1/N) \sum_{j=1}^{N} \xi_j F(\xi_j U).$$

Thus, if this nonlinear equation for U has a solution, then there will be a steady state which is just proportional to the memory, ξ, where the constant of proportionality is U. Exercise ** asks you to explore the emergence of a stable memory when $F(V) = \tanh(bV)$ and ξ is a vector of -1 and 1.

Now consider the case of 2 memories, $\xi^{1,2}$ and weights,

$$w_{ij} = (\xi_i^1 \xi_j^1 + \xi_i^2 \xi_j^2)/N.$$

Let

$$U_m = (1/N) \sum_j \xi_j^m F(V_j)$$

for $m = 1, 2$. Notice that the vector V must satisfy:

$$V' = -V + \xi^1 U_1 + \xi^2 U_2.$$

Suppose the memory vectors are linear independent (a reasonable assumption). Any component of the vector V orthogonal to $\xi^{1,2}$ decays exponentially, so that all the dynamics is along the directions corresponding to $\xi^{1,2}$. Thus, we can write

$$V(t) = r_1(t)\xi^1 + r_2(t)\xi^2$$

and study the dynamics of $r_{1,2}(t)$. Clearly, we must have:

$$\xi^1(r_1' + r_1 - U_1) + \xi^2(r_2' + r_2 - U_2) = 0.$$

Since $\xi^{1,2}$ are linearly independent, we must have

$$\begin{aligned} r_1' &= -r_1 + (1/N)\sum_j \xi_j^1 F(r_1\xi_j^1 + r_2\xi_j^2) \\ r_2' &= -r_2 + (1/N)\sum_j \xi_j^2 F(r_1\xi_j^1 + r_2\xi_j^2) \end{aligned} \tag{13.9}$$

With this choice of weights, we have reduced this $N-$dimensional dynamical system to a two-dimensional system. If there is a fixed point for this system where $r_1 \gg r_2$, then $V(t)$ will be dominated by ξ^1, so that the first memory is recalled. In the perfect case, equilibria should be proportional to $(1, 0)$ or $(0, 1)$ implying that there is no mixing of the memories. Exercise ** explores the dynamics of a two-memory model. In in addition, we choose an odd function for F and take the ξ's from the set $\{-1, 1\}$, then it is possible to show that the recall will be perfect if the two memories are orthogonal. In general the "contamination" is related to the dot product of the two memories. If the elements in the memories are ± 1, then $< \xi^m, \xi^m >= N$. Consider $< \xi^1, \xi^2 >$. If the two memories are independent and randomly chosen from ± 1, then this dot product is just the result of a random walk of N steps of size ± 1. The expected value is 0 and the standard deviation is $\sqrt{N}$. Thus, the relative contamination between the memories scales like $\sqrt{N}/N = 1/\sqrt{N}$. For large N the contamination is small.

13.3 Waves

We saw in chapter * that a brain slice preparation is able to generate traveling waves of activity in experiments as well as in networks of biophysically-based and simple spiking neurons. In this section, we return to model for neural waves in the context of firing rate models. The mathematical theory developed in chapter ** presumed that the wave of activity consisted of but a single spike traveling wave. In figure 13.1 we show two examples of traveling waves in brain slices. Figure 13.1e shows that typically there are multiple spikes per wave. Other preparations show similar behavior – the single spike assumption was to make the mathematical analysis of the spiking models easier and to make a closed form solution possible for

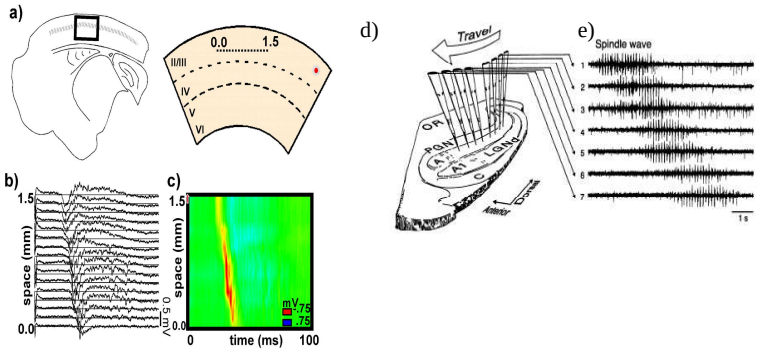

Figure 13.1. *Two examples of propagation in slices (a-c) a cortical layer 2/3 slice. A multiple electrode array is placed into the slice in which inhibition is blocked. Local shocking produces an event which propagates along the slice with a characteristic speed. (d,e) Similar experiment in the ferret thalamus showing the propagation of sleep spindles.(a-c from Pinto et al 2006; d,e from Kim et al, 1995.)*

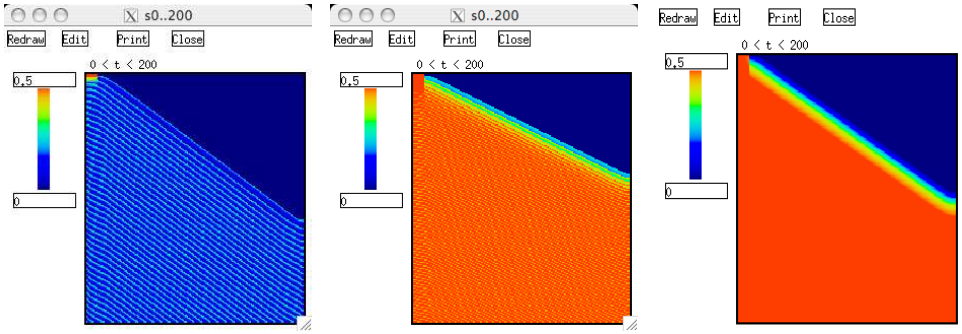

Figure 13.2. *Space-time plots for the simulation of a network of 200 neurons coupled with an exponentially decaying weight function. Time goes down and spatial position is across. Colored according to the synaptic gate, s. (A) Traub model with synaptic decay of 3 msec; (B) Traub model with synaptic decay of 10 msec; (C) Firing rate model derived from the biophysical model.*

the integrate-and-fire model. In many of the brain slice experiments, the inhibition is blocked so that all that remains is an excitatory population of cells. It should be clear to the reader that the existence of propagation of activity across a slice is not surprising given the large amount of recurrent excitation. Thus, a natural question is how does the activity terminate? In all experimental preparations, the propagating burst of activity stops after a few spikes. Pinto et al recently addressed this question experimentally and suggested several plausible mechanism for the termination of spiking in recurrent networks when the inhibition is blocked. Before turning to the modeling of wave termination, we begin with a simulation and analysis of the propagation of a front of activity.

13.3.1 Wavefronts

In chapter (oscillators) we saw that it was possible to produce a single-spike traveling wave by "preventing" the cell from producing a spike after it has already spiked. In practice, this is very hard to do without a very strong negative feedback term which prevents the neuron from spiking again. Indeed, if we consider a biophysical model like the Traub model with excitatory synapses which are (i) strong enough to excite neighboring cells and (ii) have realistic decay times (2-3 msec), then the recurrent excitation causes the neurons to fire again after they spike due to neighboring cells firing.

We thus connect a network of biophysically based neurons with synaptic coupling. The synaptic current is given by

$$I_{syn}(x,t) = \left(g_{syn} \int_{-\infty}^{\infty} J(x-y) s(y,t)\ dt \right) (V(x,t) - V_{syn}). \tag{13.10}$$

$s(x,t)$ satisfies a differential equation of the form:

$$\tau_{syn} \frac{\partial s}{\partial t} = -s + f(V) h(s). \tag{13.11}$$

The function $f(V)$ is zero unless the voltage is above some threshold (see Chapter *synapse*). If the synapses are saturating, then $h(s) = 1 - s$ (e.g. for NMDA synapses, cf chapt synapse), otherwise, $h(s) = 1$. Figure 13.2A shows a simulation of 200 neurons which in then absence of synaptic inputs have a unique stable rest state when the synaptic time constant, $\tau_{syn} = 3$msec. Figure 13.2B shows the same simulation with a time constant of 10 msec. Shown is the synaptic gating variable, $s(x,t)$ for saturating synapses. There appears to be a wave front with a constant velocity initiated by the first spike (more evident in A) with a series of spikes occurring in the wake of the wave apparently persisting forever. This kind of persistence is not biologically realistic; activity eventually terminates and the slice returns to rest as is seen in Figure 13.1. In the next section, we discuss various slow processes which act to terminate the wave front activity. We remark that, at the slower time scale, $s(x,t)$ is nearly constant while at the fast time scale the large variations of s can clearly be seen. The slower time scale simulation suggests that we use the reduction techniques of Chapter *firing rate* to consider a simpler scalar firing rate model.

Consider

$$\tau_{syn} \frac{\partial s(x,t)}{\partial t} = -s(x,t) + F(I_{rev} \int_{-\infty}^{\infty} J(x-y) s(y,t)) h(s(x,t)). \tag{13.12}$$

The function $F(I)$ is the average of $f(V(t))$ when the single neuron is provided with a constant current I. For example, at low currents, when the neuron is not firing, $F(I) = 0$. Figure 13.2C shows a simulation of equation (13.12) when F is chosen to match the Traub model simulated in the other two panels and $\tau_{syn} = 10$msec. What is apparent in this picture is that there is a constant velocity wave front joining two stable rest states. Without loss of generality, we assume that the integral of $J(x)$

is 1 and, since this is an excitatory network, we suppose that $J(x) \geq 0$. As in the simulations, we suppose that $J(x)$ is symmetric and monotonically decreasing for $x > 0$. Let

$$g(s) = -s + F(I_{rev}s)h(s).$$

We suppose that $g(s)$ has three roots, $a < b < c$ with $g'(a) < 0$, $g'(c) < 0$, and $g'(b) > 0$. That is, $g(s)$ is our favorite: cubic-shaped. (The reader may ask if everything in biology is cubic shaped – the short answer is pretty much, yes!) The simulation of the scalar network suggests that there is a traveling wave solution to equation (13.12) with constant velocity, ν, that is a function, $s(x,t) = S(\xi)$ where $\xi = x - \nu t$, $S(-\infty) = c$ and $S(\infty) = a$. Since any wave is translation invariant, we set the origin so that $S(0) = b$. With this assumption, we find that $S(\xi)$ must satisfy the integro-differential equation:

$$-\nu\tau_{syn}\frac{dS}{d\xi} = -S + h(S)F(I_{rev}J(\xi) * S(\xi)) \tag{13.13}$$

Here $J(x) * s(x)$ is the spatial convolution over the real line of the function $J(x)$ with $s(x)$. Ermentrout and McLeod proved the existence of such a traveling wave when $h(s) = 1$. Chen generalized this proof to cover the case $h(s) = 1 - s$, a fact which was exploited in a paper by Chen et al for a related model. We briefly sketch the idea of the proof as the method has been used by many other authors to prove existence theorems for nonlocal equations.

Parameterize the functions $J(x)$ and $F(s)$ by functions $J_p(x)$ and $F_p(s)$ where $0 \leq p \leq 1$, $F_1(s) = F(s)$ and $J_1(x) = J(x)$. Each F_p has a corresponding g_p that has three roots with the properties above. Each $J_p(x)$ has the same properties as $J_1(x)$, that is, it is symmetric, integrates to 1, non-negative, and monotone decreasing for $x > 0$. Choose $J_0(x) = (1/2)\exp(-|x|)$ and $F_0(x)$ so that

$$\int_{a_0}^{c_0} g_0(u)\, du = 0.$$

Then, it turns out (see exercise **), that there is a function $S_0(\xi)$ satisfying equation (13.13) with $\nu = 0$ and satisfying the conditions at $\pm\infty$. Using this basic solution, Ermentrout & McLeod apply the implicit function theorem by Linearizing equation (13.13) about $S_0(\xi)$. They obtain a linear operator, L_0, and prove that this operator has a simple zero eigenvalue (corresponding to the translation invariance of the traveling wave). Thus, for small values of the parameter p, they have to solve:

$$L_0\phi(\xi) = r_0(\xi;\nu_0).$$

In general, since L has a one-dimensional nullspace, there is no hope for solving this. However, the velocity ν is not likely to remain at 0 as the function F_p changes, so that a judicious choice of ν will put $r_0(\xi;\nu)$ in the range of L_0 so that it is possible to find a traveling wave solution for p sufficiently close to 0. The solution can be continued, say up to $p = p^*$. If $p^* = 1$, then the desired wave front has been found. Otherwise, repeat the method using $S_{p^*}(\xi)$ as the base solution. There are, of course, many technical details, but this is the essence of the proof. If $F(I)$ in

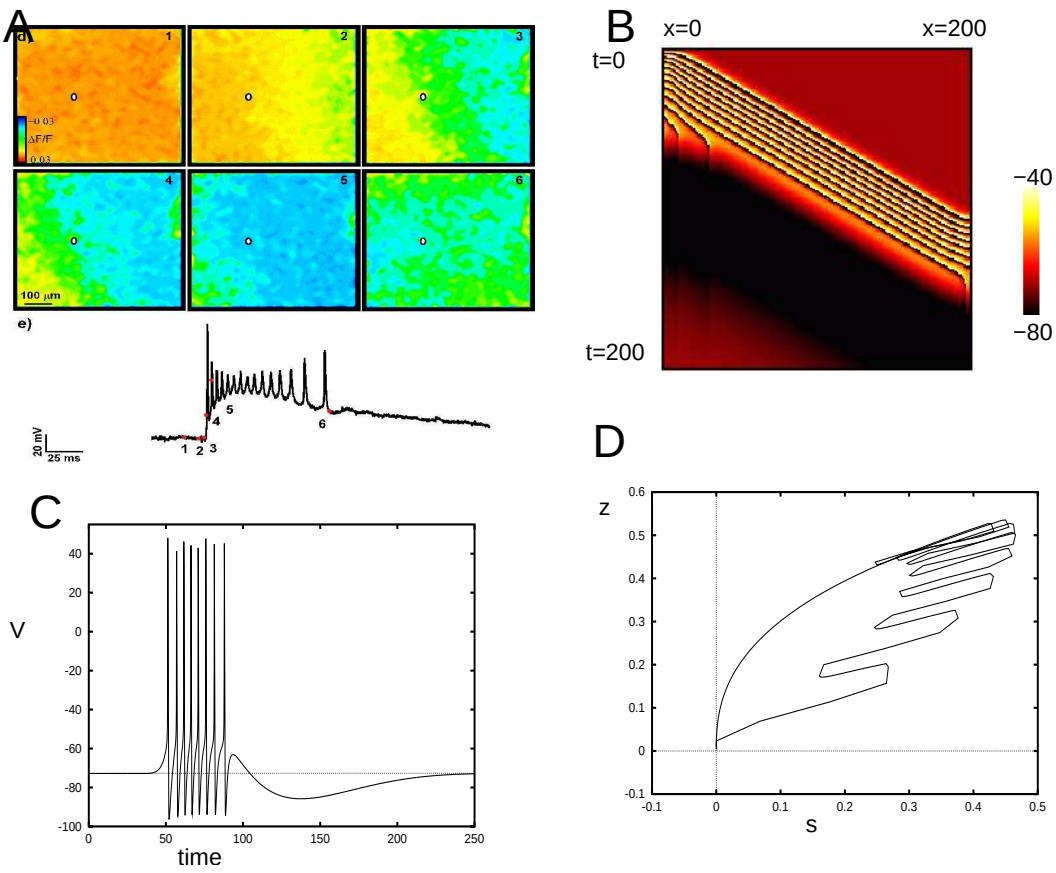

Figure 13.3. *Waves in a slice preparation and simulations. (A) Experimental waves show spatial distribution of potential in an evoked wave. Inset shows the intracellular potential of a single cell as the wave passes through. (B) Simulation of the Traub model with an additional slow potassium current which terminates spikes. (C) Single cell potential as the wave passes through. (D) Plot of the synaptic gate against the slow potassium gate.*

equation (13.12) is chosen to be the Heaviside step function, then an exact expression can be found for the traveling wave solution. (This is exercise ***.) We remark that the velocity of the waves is an increasing function of the parameter I_{rev} if the function F is monotone increasing.

13.3.2 Pulses.

Wavefronts are almost never seen in experiments. Instead, pulses are commonly observed in which each neuron involved in the activity produces a number of spikes before returning to rest. Figure 13.3 shows an example of an experiment in which

the slice is imaged simultaneously with an intracellular recording of a neuron. The neuron produces a finite number of spikes before returning to rest. What terminates the activity remains an active area of research (Pinto et al 2006). In Figure 13.3B-D, we depict a simulation of the same model which produced Figure 13.2 but with the addition of a slow outward current which becomes active only when the neuron is firing. (It is much like the high-threshold adaptation described in Chapter ???). This slow current gradually builds up enough to terminate the firing and thus the wavefront is turned into a wave pulse. Here eight spikes are produced in each neuron as the wave progresses through the one-dimensional domain. Figure 13.3D shows a phase-plane of the synapse at a particular location versus the slow outward gate. Other mechanisms could also be responsible for the termination of the wave. For example, synaptic depression of the excitatory synapses, or inactivation of the sodium channels (depolarization block). Figure 13.3A is suggestive of either spike adaptation (the interspike interval increases over the duration of the pulse) or depolarization block (the size of the spikes is smallest at the peak of the underlying depolarization). In the subsequent analysis, here, we will assume that the mechanism is adaptation; the slow accumulation of an outward current.

We now describe a simple model for the pulse and sketch how it can be analyzed. We first note that the recovery process, the slow potassium current, is slow compared to the other currents in the model. In absence of this recovery variable, the model produces a front. If we turn off the slow outward current, the velocity of the front is faster than with the adaptation, but only by about 25%. This suggests an approach like we used to construct action-potentials in Chapter * where we exploited the time-scale differences between the upstroke of the action potential and the recovery variables. We start with a general model for a network with slow processes. As in our firing rate model for the fronts, we start with two "slow" currents added to the voltage equations: synaptic and adaptation:

$$I_{slow}(x,t) = -g_{syn}s_{total}(x,t)(V_{syn} - V(x,t)) - g_z z(x,t)(V_z - V(x,t))$$

where the synapses satisfy equation (13.11) and z satisfies

$$\tau_z \frac{dz}{dt} = -z + f_z(V)(1-z).$$

Here, $f_z(V)$ is zero unless the neuron is depolarized sufficiently and τ_z is the time constant of the slow recovery process. As in the previous section, we will treat the synapses as if they were slow enough to be considered constant and, in addition, suppose that the slow recovery variable, z, is also slow. The total current into a cell is approximated by

$$I_{slow}(x,t) \approx I_{rev}s_{total}(x,t) + I_z z(x,t)$$

where $I_{rev} = g_{syn}(V_{rest} - V_{syn}) > 0$ and $I_z = g_z(V_{rest} - V_z) < 0$. As in the previous section, s_{total} is the total input at x from other cells. We now have a simplified network model identical to equation (13.12) but with the additional slow recovery process.

$$\tau_{syn}\frac{\partial s(x,t)}{\partial t} = -s(x,t) + \alpha_s \nu(x,t)h(s(x,t)) \tag{13.14}$$

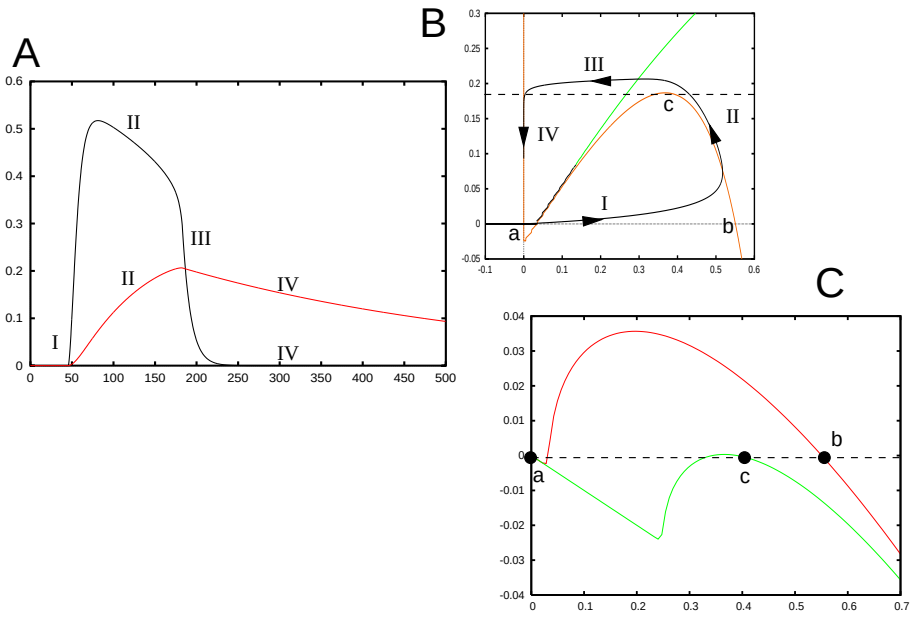

Figure 13.4. *Singular construction of th traveling pulse. (A) Simulation of the network in equation (13.14- 13.15) showing four stages in the evolution of the wave. Synaptic activity and adaptation are shown. (B) Phase plane of (A). (C) "Fast" local dynamics showing bistability.*

$$\tau_z \frac{\partial z(x,t)}{\partial t} = -z(x,t) + \alpha_z \nu(x,t)(1-z) \tag{13.15}$$

$$\nu(x,t) = F[I_{rev} J(x) * s(x,t) + I_z z(x,t)]. \tag{13.16}$$

The firing rate of a neuron at position x is now a function of both the synaptic activity and the degree of spike adaptation. We define $\epsilon = \tau_{syn}/\tau_z \ll 1$ to be our small parameter and use singular perturbation to find a traveling pulse solution, $(s(x,t), z(x,t)) = (S(\xi), Z(\xi)$ where $\xi = x - ct$ and c is the velocity of the traveling wave. Without loss of generality, we can set $\tau_{syn} = 1$. Letting U' denote the derivative of U with respect to the moving coordinate ξ, we must solve:

$$\begin{aligned} -cS' &= -S + \alpha_s \nu(S,Z)(1-S) \equiv f(S,Z) \\ -cZ' &= \epsilon[-Z + \alpha_z \nu(S,Z)(1-Z)] \equiv g(S,Z) - \\ \nu(S,Z) &= F(I_{rev} J(\xi) * S(\xi) + I_z Z(\xi)). \end{aligned} \tag{13.17}$$

That is, we need to find $(S(\xi), Z(\xi))$ such that as $\xi \to \pm\infty$, (S,Z) tend to the rest state of the network. Notice that $\xi < 0$ corresponds to events which occur *after* the pulse has passed through and $\xi > 0$ to those before the pulse.

Figure 13.4A shows the time course of the synaptic dynamics and the adaptation at a spatial location in the middle of the one-dimensional medium. Since this

plot shows the *time course* and ξ, the moving coordinate is proportional to $-ct$, the dependent variables (S, z) increase to the left and decrease to the right in this picture. The behavior can be broken into four segments: (I) starting from rest, there is an upstroke to the excited state; (II) there is a slow growth of the adaptation as the excited neuron fires; (III) adaptation reaches a value which forces the synaptic activity to make a fast downstroke to rest; (IV) a slow recovery of adaptation back to rest. Since we assume ϵ is small on the upstroke and downstroke of the pulse, we suppose that the adaptation is constant. On the initial upstroke, since the neuron starts from rest, $Z = z_{rest}$, the resting state of the adaptation. In this example, z_{rest} is essentially 0. At $Z = z_{rest}$ the $S-$dynamics is bistable. Figure 13.4C shows the fast dynamics, $F(S, Z)$ for $Z = z_{rest}$, has three zeros with those labeled a,b corresponding to the stable roots. The Ermentrout-McLeod theory for the scalar neural network (or more precisely, the generalization by Chen) implies that there is a unique traveling wavefront joining the two points a, b. This traveling front travels at the velocity, $c = c_0$ which is therefore the same velocity as the pulse. Once the upjump has been made, the slow dynamics take over and we introduce a new space-time scale: $\xi = \epsilon\eta$. In these coordinates equations (13.17) become:

$$\begin{aligned} \epsilon S_\eta &= f(S, Z) \\ Z_\eta &= g(S, Z) \end{aligned}$$

and the convolution $J(\xi) * S(\xi)$ becomes:

$$R(\eta) = \frac{1}{\epsilon} \int_{-\infty}^{\infty} J[(\eta - \eta')/\epsilon] S(\eta') \, d\eta'.$$

We have assumed that $J(x)$ is symmetric, peaked at $x = 0$, non-negative, and has an integral of 1. Thus, the function $J(x/\epsilon)/\epsilon$ tends to a Dirac delta function as $\epsilon \to 0^+$. Our equations become:

$$\begin{aligned} 0 &= -S + \alpha_S F(I_{rec} S + I_z Z)(1 - S) \equiv f(S, Z) \\ Z_\eta &= -Z + \alpha_Z F(I_{rec} S + I_z Z)(1 - Z). \end{aligned}$$

Figure 13.4B shows the phase-plane for the local S, Z excitable system. The $S-$nullcline is exactly the points where $f(S, Z) = 0$. For a range of Z (here, between 0.025 and 0.2) there are three roots, S to $f(S, Z) = 0$. Since the solution has jumped to region II which corresponds to the large value of S, we take the largest root, call it $S^+(Z)$, and plug this into the Z equation:

$$-c_0 \frac{dZ}{d\eta} = g(S^+(Z), Z).$$

The phaseplane in figure 13.4B shows that along this curve $dZ/d\eta > 0$ so that $Z(\eta)$ grows for η decreasing. This is more easily seen in figure 13.4A in the region II. At what point is there a jump made back to the left? In the case of the singular action potential (chapt *) this jump occurred at a value of the recovery variable (the equivalent of Z, here) such that the traveling "back" has the same velocity

as the front. For the reaction-diffusion equations, such as the FitzHugh-Nagumo equations, the existence of this jump point is guaranteed. However, there is no guarantee that there will be a similar jump point for the integral equations. Indeed, it appears that for our present wave model, the jump occurs when the recovery Z reaches the maximum of the nullcline. Returning to the ξ coordinates, we have to solve:

$$-cS' = f(S, Z_{max})$$

where $f(S, Z_{max})$ has only two fixed points: one corresponding to the point a in figure 13.4C and the other, a degenerate point corresponding to the point c in the same figure. The existence of a wave front for this problem was proven by Diekmann (?) who showed that there are infinitely many velocities, c. Assuming that one of these wave velocities is the same as c_0, we can complete the down jump. The last part of the construction is the return to rest along the left branch of the nullcline. For our problem, $S \approx 0$ so that Z satisfies

$$c_0 Z_\eta = Z$$

so that

$$Z = Z_{max} e^{\epsilon \xi / c_0}.$$

Thus, as intuitively expected, once the wave passes by and there is no more neural firing, the recovery variable, Z decays with a time course of $1/\epsilon$. An explicit solution for a simplified version of this model can be found when the firing rate is a step function. Exercise * takes you through the necessary steps.

13.4 Bumps.

Working memory refers to the short-term memory that is used for simple tasks such as remembering a phone number as you walk from the phone-directory to the telephone. It is memory which you do not need to permanently store and is analogous to the storage in the RAM of a computer during some task as opposed to keeping it on the disk drive. One of several theories of the mechanism for working memory is that it represents a transient but metastable state of neuronal activity. This theory is based on experiments first done over three decades ago by Joachim Fuster. In these experiments, neurons in the prefrontal cortex of the monkey are recorded while the monkey does a simple memory task. The monkey stares at a fixation point on a video monitor. A brief spot of light (*the stimulus*) appears somewhere in the surrounding area of the screen. Typically the stimulus lasts at most a second and is then turned off. The monkey waits (for a period called the *delay period*). A signal is given and the monkey must make an eye movement (*saccade*) to the location of the stimulus. Thus, the monkey has to remember the position of the stimulus for up to several seconds after it has been turned off. What Fuster (and many subsequent experimentalists) found is that certain neurons would begin to fire at a rate above background during the delay period and then return to background levels after the monkey makes the saccade. This increased firing, which occurs in a restricted spatial region, is believed to be the neuronal correlate of working memory.

There are many other examples of this type of activity in the brain. Brody and his colleagues found neurons in the prefrontal cortex of monkey which fired at a rate that was proportional to the vibration frequency of a brief stimulus to the fingertip during the delay period. That is, not only did the neurons firing during the memory period, but they also coded for one of the stimulus properties.

Theoretically, these local regions of higher neural activity are regarded as stationary spatial patterns in a recurrent neural network. Wilson and Cowan (1973) were among the first to try to define working memory in terms of the behavior of firing rate models, mainly through simulations of a two layer neural network. In an influential paper Amari (1977) created a simplified neural network that was analytically tractable and allowed him to find explicit solutions for stationary patterns as well as to ascertain their stability. Since these papers, there have been hundreds of theoretical and computational models for working memory. Most of the recent work has focused on obtaining local increases in firing in spiking models such as integrate and fire and more biophysical models. While the details differ, the principal for the patterns remains identical to that of the Amari paper.

13.4.1 The Wilson-Cowan equations.

Unlike traveling waves, inhibition plays a major role in the production of spatially localized stationary patterns. We will start our analysis with the following "synaptically" based neural network equations:

$$\tau_e \frac{\partial u_e(x,t)}{\partial t} = -u_e(x,t) + F_e(\int_\Omega J_{ee}(x-y)u_e(y,t) - J_{ie}(x-y)u_i(y,t)\ dy + I_e(x,t)) \tag{13.18}$$

$$\tau_i \frac{\partial u_i(x,t)}{\partial t} = -u_i(x,t) + F_i(\int_\Omega J_{ei}(x-y)u_e(y,t) - J_{ii}(x-y)u_i(y,t)\ dy + I_i(x,t)). \tag{13.19}$$

This is a two-layer network model where $u_{e,i}(x,t)$ represents the synaptic activity of a population of excitatory and inhibitory neurons. The functions $J(x)$ represent the connectivity between the two populations; these are non-negative functions which, in general, depend only on $|x-y|$, the distance between two areas. The domain of the model, Ω, can be one or two-dimensional. While not strictly true, we will call these the Wilson-Cowan equations. (The published Wilson-Cowan equations have a term $(1-r_e u_e)$ multiplying S_e and a similar term for u_i representing the refractory period.) If we pick $r_{e,i}=1$ then the WC equations are the same as those that we derived from averaging, eg equation (13.14) in this chapter.

The Wilson-Cowan equations can be transformed into equations similar to those analyzed by Amari in which the nonlinearities are placed inside the spatial integration. We, instead, first make some simple assumptions about the inhibition to reduce equations (13.18-13.19) to a scalar equation and then make the transformation. Suppose that $\tau_i \ll \tau_e$, that F_i is linear, and that $J_{ii}=0$. The most unreasonable of these assumptions is that inhibition is faster than excitation. (If we suppose that the excitation is dominated by the slow NMDA types of recep-

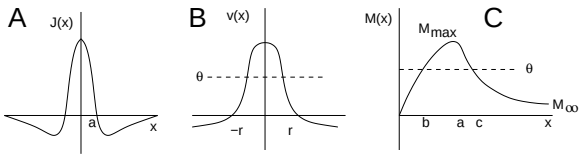

Figure 13.5. *(A) Composite interaction function; (B) "bump" solution; (C) integral of $J(x)$ showing allowable widths of the "bump".*

tors, then this is not a bad assumption.) The assumption on J_{ii} is unnecessary but simplifies the algebra. We set $\tau_i = 0$ and solve for $u_i(x,t)$:

$$u_i(x,t) = F_i(\int_\Omega J_{ei}(x-y)u_e(y,t)\ dy + I_i(x,t)).$$

The linearity assumption on F_i means that we can absorb the slope the intercept of F_i into J_{ei} and I_i. We substitute $u_i(x,t)$ into equation (13.18) to obtain:

$$\tau_e \frac{\partial u_e(x,t)}{\partial t} = -u_e(x,t) + F_e(\int_\Omega J(x-y)u_e(y,t) + I(x,t))$$

where

$$J(x) = J_{ee}(x) - \int_\Omega J_{ei}(x-y)J_{ie}(y)\ dy$$

and

$$I(x,t) = I_e(x,t) - \int_\Omega J_{ei}(x-y)I_i(y,y)\ dy.$$

The spatial kernel, $J(x)$, is a composite of the excitatory and the inhibitory interactions. If we suppose, for example, that the connectivity is a Gaussian and that the space constant (the decay of connectivity) for excitatory (inhibitory) connections is σ_e (σ_i), then $J(x)$ is comprised of the difference of two Gaussians, one with a space constant of σ_e and the other with a space constant of $\sigma = \sqrt{\sigma_e^2 + \sigma_i^2}$. If recurrent excitation is strong, then $J(x)$ will be positive near $x = 0$ and negative for larger values of x since $\sigma > \sigma_e$. Figure 13.5A shows a typical shape for $J(x)$. Interactions like this are called "Mexican hat interactions" since, in two spatial dimensions, the shape of the interactions resembles a sombrero. We let $v(x,t) = J(x) * u_e(x,t) + I(x,t)$ so that $v(x,t)$ satisfies:

$$\tau_e v_t + v = J(x) * F(v(x,t)) + \hat{I}(x,t) \tag{13.20}$$

where

$$\hat{I} = \tau I_t + I.$$

Equation (13.20) is the model that Amari analyzed in his famous 1977 paper when F is the Heaviside step function.

We now suppose that $F(v) = H(v-\theta)$ is a step function and that there is no input, $I = \hat{I} = 0$. The spatial domain, Ω, will be the real line. A "bump"

is defined as a stationary solution to (13.20) which has a spatially localized peak (Figure 13.5B. Such a solution satisfies:

$$v(x) = \int_{-\infty}^{\infty} J(x-y)H(v(y)-\theta)\ dy.$$

We construct a bump solution by supposing that $v(x) > \theta$ on an interval $-r < x < r$ and $v(x) < \theta$ outside this interval. (See Figure 13.5B.) From the definition of the step function,

$$v(x) = \int_{-r}^{r} J(x-y)\ dy = \int_{x-r}^{x+r} J(y)\ dy = M(x+r) - M(x-r)$$

where $M(x) = \int_0^x J(y)\ dy$. Continuity of $v(x)$ at $x = \pm r$ implies that $v(\pm r) = \theta$ so that we must have

$$\theta = M(2r) = -M(-2r).$$

If $J(y)$ is not symmetric, then we cannot satisfy both of these equations simultaneously and there will be no stationary bump. Instead, there will be motion of the bump much like motion is induced with a transport term in diffusion equations.(See exercise *) However, if $J(y)$ is an even function, then $M(y)$ is odd and both of these equations reduce to the same equation, $M(2r) = \theta$. We remind the reader that $2r$ is exactly the width of the bump. Figure 13.5C shows that for a Mexican hat interaction as in figure 13.5A, there will be either one, two or no roots to this equation. If the threshold, θ is larger than the maximum of $M(x)$, M_{max} then there are no roots and no bumps. If the threshold lies between (M_∞, M_{max}), then there are two roots and two different bumps. If $M_\infty > 0$, then for $0 < \theta < M_\infty$, there is a single root. Laing et al (2002) consider more general functions $J(x)$ which have multiple "wiggles" so that $M(x)$ will oscillate; for example, $J(x) = \exp(-|x|)\cos\omega x$. This means that there can many (even infinitely many) roots to $M(2r) = \theta$ and thus, many different bump widths. We explore the stability below.

13.4.2 Stability

We derived the Amari model from the full Wilson-Cowan equations by assuming that the inhibition was fast so that we could eliminate its dynamics from the equations. Thus, to properly analyze stability of the bump, we should consider the bump with respect to the full set of equations (13.18-13.19). We will leave a variant of this analysis as an exercise. For ease in exposition, we only examine stability with respect to (13.20). Thus, we suppose that

$$v_0(x) = \int_{x-r}^{x+r} J(y)\ dy$$

is a stationary solution and that r satisfies, $M(2r) = \theta$. We formally linearize about this solution resulting in the linear equation:

$$\tau_e w_t + w = \int_{-\infty}^{\infty} J(x-y)\delta(v_0(y)-\theta)\ w(y,t)dy.$$

Here, we use the fact that the derivative of the step function is the delta function. Since the linear equation is autonomous, we can look for exponentially decaying solutions, $w(x,t) = \exp(\lambda t)\phi(x)$ where $\phi(x)$ obeys the eigenvalue problem:

$$\tau_e \lambda \phi(x) = \int_{-\infty}^{\infty} J(x-y)\delta(v_0(y)-\theta)\phi(y)\ dy. \tag{13.21}$$

Recall that the delta function satisfies:

$$\int_{-\infty}^{\infty} \delta(x-a)\phi(x)\ dx = \phi(a)$$

for any smooth functions $\phi(x)$. Furthermore, any standard text (see eg Keener) provides the following identity. Suppose $f(0) = 0$ and $f'(0) \neq 0$. Then

$$\int_{-\infty}^{\infty} \delta(f(x))\phi(x)\ dx = \frac{\phi(0)}{|f'(0)|}.$$

The argument inside the delta function in equation (13.21) vanishes at $y = \pm r$ so that $\phi(x)$ must satisfy:

$$(\tau_e\lambda + 1)\phi(x) = \frac{J(x+r)}{|v_0'(-r)|}\phi(-r) + \frac{J(x-r)}{|v_0'(r)|}.$$

Using the definition of $v_0(x)$, it is easy to compute that

$$v_0'(x) = J(x+r) - J(x-r),$$

so that $|v_0'(\pm r)| = |J(2r) - J(0)|$. For the case illustrated in Figure 13.5, $|v_0'(\pm r)| = J(0) - J(2r)$. We let $z^{\pm} = \phi(\pm r)$ and setting $x = \pm r$ in the eigenvalue equation, we must satisfy:

$$\begin{aligned}(\tau_e\lambda + 1)z^- &= \frac{J(0)}{J(0)-J(2r)}z^- + \frac{J(2r)}{J(0)-J(2r)}z^+ \\ (\tau_e\lambda + 1)z^+ &= \frac{J(2r)}{J(0)-J(2r)}z^- + \frac{J(0)}{J(0)-J(2r)}z^+.\end{aligned}$$

Miraculously, the stability reduces to the analysis of a 2×2 symmetric matrix. Because the matrix has the form

$$A = \begin{pmatrix} a & b \\ b & a \end{pmatrix}$$

the eigenvalues are $a + b$ and $a - b$ which, for our system translates to $\lambda = 0$ and

$$\lambda = \frac{1}{\tau_e} - 1 + \frac{J(0) + J(2r}{J(0) - J(2r)}.$$

This eigenvalue is negative if and only if $J(2r) < 0$. Consulting Figure 13.5A,C, we see that only the wider bump (corresponding to $2r = c$) falls in the region where $J(2r) < 0$. In conclusion, if θ is between M_∞ and M_{max}, then there are two bumps and the wider one is stable. The narrow bump is unstable and for $0 < \theta < M_\infty$, where there is only one bump; this bump is also unstable.

13.4.3 More general stability.

We transformed the Wilson-Cowan equations and assumed that the inhibition was fast and linear to derive the Amari model, (13.20). If we take a step back and consider the dynamics of inhibition, then we can obtain some more interesting types of instabilities. Consider the "dynamic" inhibition version of the Amari model where we set the time constant of excitation to 1 and let τ_i be a parameter:

$$u_e'(x,t) = -u_e(x,t) + J_{ee}(x) * H(u_e - \theta) - J_{ie}(x) * u_i \tag{13.22}$$

$$\tau_i u_i'(x,t) = -u_i(x,t) + J_{ei}(x) * H(u_e - \theta). \tag{13.23}$$

Here the inhibition is linear and there is no inhibitory-inhibitory interaction. A time-independent solution to these equations satisfies $u_e(x) = U(x)$, $u_i(x) = J_{ei}(x) * H(U(x) - \theta)$ where

$$U(x) = J(x) * H(U(x) - \theta)$$

with

$$J(x) = J_{ee}(x) - J_{ei}(x) * J_{ie}(x).$$

Thus, stationary solutions to equations (13.22-13.23) satisfy the same equations as the simple Amari model, so that there will be a bump. We will leave the analysis of the stability of these bumps with respect to the full equations to the reader.

13.4.4 More general firing rates.

The construction of solutions to the Amari model (13.20) depended on the fact that the nonlinearity was a Heaviside step function. Kishimoto & Amari used a fixed point theorem to prove that there were bump solutions to a smooth version of the equations. Specifically, consider

$$u(x) = \int_{-\infty}^{\infty} J(x-y)F(u(y))\ dy. \tag{13.24}$$

Suppose that $F(u) = 0$ for $u < \theta_1$, $F(u) = 1$ for $u > \theta_2$ and $F(u) = \phi(u)$ for $\theta_1 < u < \theta_2$ with $\phi(u)$ differentiable, monotonic and satisfying, $\phi(\theta_1) = 0$, $\phi(\theta_2) = 1$. This implies that $H(u - \theta_1) \geq F(0) \geq H(u - \theta_2)$. Assume that there are bump solutions for $H(u - \theta_j), j = 1, 2$. Then under fairly reasonable conditions on the interaction functions, $J(x)$, there is a bump solution for $F(u)$.

Laing & Troy take a somewhat different approach. They choose interaction functions, $J(x)$, whose Fourier transforms are rational functions:

$$\hat{J}(k) \equiv \int_{-\infty}^{\infty} J(x)e^{-ikx}\ dx = \frac{N(k^2)}{D(k^2)},$$

where N, D are polynomials. For example, the Fourier transform of

$$J(x) = (1+b^2)\exp(-|x|)(b\cos(bx) + sin(x))/(4b)$$

is

$$\hat{J}(k) = \frac{(b^2+1)^2}{(1+(k-b)^2)(1+(k+b)^2)}.$$

Formally taking the Fourier transform of equation (13.24), we get

$$\hat{u}(k) = \hat{J}(k)\hat{F(u)}(k).$$

Since $\hat{J}$ is a rational function, we unwrap it obtaining:

$$D(k^2)\hat{u}(k) = N(k^2)\hat{F(u)}(k).$$

Since N, D are polynomials in k (in fact, even polynomials), we inverse transform the equation to obtain an ordinary differential equation:

$$L_1 u(x) = L_2 F(u(x))$$

where L_j are linear differential operators. For example, in the example above, u formally satisfies:

$$u_{xxxx} + 2(b^2-1)u_{xx} + (1+b^2)^2 u = (1+b^2)^2 F(u). \tag{13.25}$$

This is a 4^{th} order differential equation. Suppose that $F(0) = 0$ and so $u = 0$ is a rest state. Then a bump would be a solution to this PDE which is homoclinic to $u = 0$. Ed Krisner proves the existence of homoclinic solutions to (13.25) using a shooting argument. (See exercise ***).

13.4.5 Applications of bumps.

We have thus far regarded bumps as the neural equivalent of working memory and the delayed response task. But, stationary patterns of neural might be relevant in many other neural phenomena. Suppose that the "x" variable in our model represents some other feature of the sensory world other than spatial location, for example, angular preference. Cortical neurons associated with many sensory and motor systems show increased firing rates when presented with oriented stimuli. For example, neurons in the visual cortex show specificity for line segments that depends on their angular orientation. Other visual cells are selective for the direction of motion of a moving grating. In rats, cells in layer IV of the cortex respond to movements of the whiskers; some of these cells are very specific about the direction of movement. Figure 13.6 shows a cartoon of orientation preference for a visual cortical neuron and directional preference for a neuron in the rat somatosensory cortex. A number of researchers believe that the strength of these preferences for certain features is a consequence of recurrent excitatory connections coupled with strong inhibition.

When an oriented stimulus is presented, neurons show a *tuning curve* in which their activity depends on the angle of the stimulus with a peak at the preferred angle. Figure 13.6B,C shows two different ways to plot the degree of tuning. An untuned neuron could produce a flat curve instead of B and a perfect circle instead of C. The mechanism for this tuning sensitivity controversial, at least in the case of orientation tuning in the visual cortex. The arguments are as to whether this localized activity occurs due to feedforward wiring from the thalamus or that recurrent connections

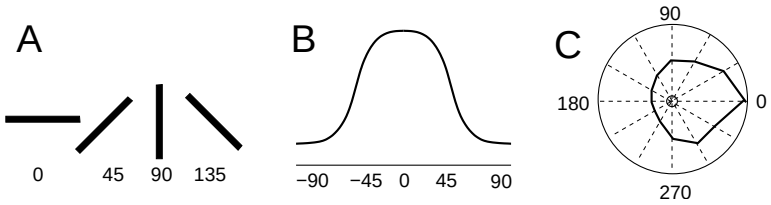

Figure 13.6. *Orientation tuning in neurons. (A) Sample stimuli to the visual system consist of oriented bars; (B) Firing rate of a visual cortex neuron as a function of the stimulus angle; (C) "Polar plot" for a neuron in the somatosensory cortex of the rat showing the strength (radial coordinates) of the response as a function of the direction of the whisker.*

and lateral inhibition lead to the amplification with the feedforward behavior only biasing the results.

Consider a periodic version of the Amari model:

$$\frac{\partial u(\theta,t)}{\partial t} = -u(\theta,t) + \int_0^{2\pi} J(\theta-\theta')F(u(\theta',t)) + S(\theta,t) \tag{13.26}$$

Here, $u(\theta,t)$ represents the activity of neurons responding to a stimulus moving in the direction θ. (If we wish to consider orientated bars, then the domain is $[0,\pi)$, since there is no difference between a bar which is at 0 degrees and one which is at 180 degrees.) $S(\theta,t)$ is the possible bias due to the inputs to the cortex from the thalamus. In the pure feedforward model, the recurrent connections $J*F$ play very little role and the activity is dominated by the inputs, S. In the recurrent model, S is small and broadly tuned; the recurrent interactions amplify and sharpen the tuning. Both arguments have experimental evidence to back them up. The Amari-type analysis can be applied to the case where there is a step function nonlinearity with no inputs. A time-independent input, $S(\theta)$, makes the analysis more difficult, but is quite "doable", particularly if there is a single local peak. (See Amari 1977 for the analysis on the real line.)

For a general nonlinearity, we can exploit the fact that the domain is periodic an thus the function J is also periodic. Suppose, for example, that $J(\theta) = A + B\cos\theta$. If $B > |A|$ then $J(\theta)$ has a Mexican-hat like shape. By approximating $J(\theta)$ by only a few terms of its Fourier series (here only two), then we can reduce the infinite-dimensional equation (13.26) to a finite dimensional one, since

$$K(\theta,t) = \int_0^{2\pi} (A + B\cos(\theta-\theta'))F(u(\theta',t))\ d\theta'$$

can be expressed as

$$K(\theta,t) = C_0(t) + \cos\theta C_1(t) + \sin\theta D_1(t)$$

where

$$C_0(t) = A\int_0^{2\pi} F(u(\theta',t)\ d\theta'$$

$$C_1(t) = B\int_0^{2\pi} \cos(\theta')F(u(\theta',t)\ d\theta'$$
$$D_1(t) = B\int_0^{2\pi} \sin(\theta')F(u(\theta',t)\ d\theta'.$$

From this, equation (13.26) becomes

$$u_t = -u + C_0(t) + C_1(t)\cos\theta + D_1(t)\sin\theta.$$

Thus, only the constant and first Fourier modes of $u(x,t)$ are nontrivial; all other modes decay to zero. This allows one to write

$$u(x,t) = c_0(t) + c_1(t)\cos\theta + d_1(t)\sin\theta$$

and finally, to write:

$$c_0' = -c_0 + C_0$$
$$c_1' = -c_1 + C_1$$
$$d_1' = -d_1 + D_1.$$

This is a **third order ODE**. Furthermore, $d_1 = 0$ is invariant (see exercises) since we can always look for even solutions to this homogeneous translation-invariant set of equations. Thus, equation (13.26), with a simple choice for a kernel, reduces to a planar differential equation. Finally, if we include an inhomogeneity for the equations, $S(\theta,t)$, and write

$$S(\theta,t) = p_0(t) + p_1(t)\cos\theta + q_1(t)\sin\theta + \ldots$$

then we replace the three autonomous ODEs by

$$\begin{aligned} c_0' &= -c_0 + C_0 + p_0 \\ c_1' &= -c_1 + C_1 + p_1 \\ d_1' &= -d_1 + D_1 + q_1. \end{aligned} \tag{13.27}$$

In the exercises, you explore various aspects of this model using the computer.

As a final example of models using bumps, we consider Zhang's (1996) model for head direction cells in the hippocampus. Head direction cells signal the head direction of moving animals regardless of the location of the animal in the environment. They have tuning curves very much like those in Figure 13.6A. That is, they show a strong preference for particular angles and are therefore often considered as exemplars of bump attractors. Thus, the head direction system is often modeled as a network of recurrently connected neurons and the peaked attractor represents the current angle of the animals head. As the animal moves around in its environment, its head angle will change relative to its body angle so that we expect the peak of of the neural representation to move as well. As you perhaps explored in the exercises on equation (13.27) it is possible to move a bump with external inputs, but the analytic solution to this problem is not generally possible. An alternative

method of shifting the bump is to vary the connection weights by biasing them in one direction or the other. Specifically, Zhang supposes that the bump satisfies the equation:

$$\frac{\partial u(\theta,t)}{\partial t} = -u(\theta,t) + \int_0^{2\pi} J(\theta-\theta',t)F(u(\theta',t))\ d\theta' \tag{13.28}$$

where the weights, $J(\theta,t)$, are not constant in time and most importantly, not symmetric. The reader may recall that in the Amari model, if the weights are not symmetric, then it was impossible to find a stationary bump solution and instead there is a moving solution. In exercise *, we created an asymmetric weight matrix by shifting a symmetric matrix. Zhang finds a much easier way to make the weights time-dependent and asymmetric. He supposes that

$$J(\theta,t) = K(\theta) + \gamma(t)K'(\theta) \tag{13.29}$$

where $K(\theta)$ is a symmetric weight function that leads to stationary bumps and $\gamma(t)$ is an external signal which will serve to shift the bump. When $\gamma(t)$ is nonzero, the interaction, J, is not symmetric so we expect movement of the bump. Suppose that $U(\theta)$ is a stationary solution to

$$U(\theta) = \int_0^{2\pi} K(\theta-\theta')F(U(\theta'))\ d\theta'.$$

Consider the time-dependent problem (13.28) with $J(\theta,t)$ as in (13.29). Let

$$\phi(t) = \int_0^t \gamma(s)\ ds$$

be the integrated signal and let $u_0(\theta,t) = U(\theta+\phi(t))$. Then it is easy to see (exercise **) that u_0 exactly satisfies equation (13.28) with J as in (13.29). $\phi(t)$ is the *integrated* phase shift of the bump due to the inputs. Thus, a brief negative input will shift the bump counterclockwise, while a brief positive input will shift it clockwise. No matter how fast the inputs vary, the bump will follow them exactly (or at least there is a solution which can follow them – stability has not yet been determined). We remark that models like this are called neural integrators since they integrate the inputs and maintain them. Integrators are found in a variety of neural systems ranging from the oculomotor plant in the goldfish (Tank Seung) to the brain of an ant (Muller & Wehner,1988).

13.5 Spatial patterns - Hallucinations

Press on your eyeballs with the palms of your hands. After a few seconds, the random light flashes that you see will become organized into faint flickering geometric patterns. Better yet, stare a diffused strobe light flickering at roughly 20 Hz and your visual field will break up into similar geometric patterns. Even more intense patterns arise upon the ingestion of various hallucinogenic drugs such as lysergic acid diethylamide or mescaline. These simple geometric visual patterns

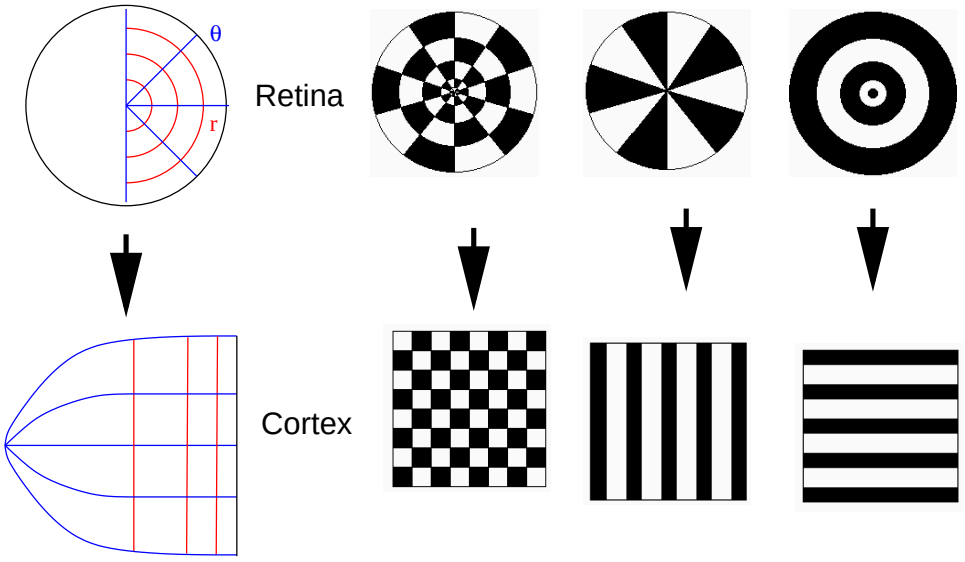

Figure 13.7. *The transformation from retinal to cortical coordinates (left) and its effect on three of Kluver's form constants. Most notably, bullseyes (starbursts) are transformed into horizontal (vertical) stripes.*

(called *phosphenes*) are ubiquitous in their appearance and their forms seem to be independent of any cultural influences. Kluver (1966) noted the relatively few such patterns that subjects report during the early stages of drug intoxication and classified the patterns into four types of *form constants*:

1. grating, lattice, fretwork, filigree, honeycomb, or chessboard;
2. cobwebs;
3. funnel, tunnel, cone, or vessel;
4. spiral.

Typically, during stroboscopic stimulation, human subjects report bullseyes (tunnel) and starbursts (funnel/cone) which are examples of the third type of form constant, whereas hallucinogens lead to more varied patterns such as honeycombs and spirals.

In 1979 Ermentrout and Cowan noticed that many of the form constants can be transformed to periodic patterns on the plane through the mapping from the retina to the visual cortex. Figure 13.7 shows the transformation. If we let r denote the distance from the center of the fovea (in visual science, this is called the eccentricity) and θ denote the angle around the retina, the transformation to the cortex is well-approximated by the formula:

$$(r, \theta) \to \lambda(\log(1 + r/r_0), -\frac{r\theta}{r + r_0}).$$

The parameter, λ is called the magnification factor and r_0 is an empirically defined constant. For $r \gg r_0$, this mapping is just the complex logarithm, $z = r\exp(i\theta) \to (\log r, \theta)$ with the angle reversed. Figure 13.7 shows that the form constants are transformed into even simpler forms under this mapping. Spirals, for example, become diagonal lines away from the fovea.

Ermentrout and Cowan suggested that the spatially periodic patterns arose spontaneously in the visual cortex due to an instability of the resting activity. For example, the hallucinogens are known to enhance cortical excitability by causing the release of glutamate via activation of specific serotonin receptors. Flickering light could interact resonantly with intrinsic oscillatory activity in cortex to increase overall excitability. Thus, we will explore a simple spatial neural network as some parameter is varied leading to a loss of stability of a uniform state. In order to simplify the mathematical analysis, we will regard the visual cortex as a two-dimensional sheet with periodic boundary conditions (in order to avoid boundary effects and to make it possible to compute eigenfunctions as well as to avoid mathematical difficulties arising in the infinite plane). The general idea is that we will start with a spatially homogeneous system and study the stability of the spatially uniform state. As we change some parameters, the uniform state loses stability to certain spatially varying modes which grow until the nonlinearities cause them to saturate. We will not go through the complete analysis, but we will touch on the main points which are (i) linear stability analysis and (ii) pattern selection. For simplicity of exposition, we will analyze a scalar neural network with lateral inhibitory connections much like figure 13.5A in two-spatial dimensions and with a smooth nonlinearity. Let $u(x, y, t)$ be the activity of a local region of cortex and suppose that it satisfies

$$\tau \frac{\partial u(x,y,t)}{\partial t} = -u(x,y,t) + J(x,y) * F(u(x,y,t)) \tag{13.30}$$

where

$$J(x,y) * v(x,y) = \int_0^L \int_0^L J((x-x', y-y')v(x',y')\ dx'\ dy'.$$

Here, we will exploit two assumptions; the connections between cells are: (i) rotationally symmetric and (ii) translationally invariant. Since our domain is periodic, we assume that $J(x \pm L, y) = J(x, y \pm L) = J(x, y)$ for all $x, y \in [0, L)$. Rotational symmetry means that interactions depend only on distance between neurons. To construct such a $J(x, y)$, we start with a function, $w(x)$ which is even and satisfies

$$\int_{-\infty}^{\infty} w(x)\ dx = C < \infty.$$

For example, $w(x)$ could be like the lateral inhibitory kernel used in the Amari model. Let

$$J(x,y) = \sum_{n=-\infty}^{\infty} \sum_{m=-\infty}^{\infty} w(\sqrt{((x+nL)^2 + (y+mL)^2)}).$$

It is clear that $J(x,y)$ is $L-$periodic in x,y. Furthermore, J depends only on the distance from the origin of (x,y) so that it is rotationally invariant. The reader can verify that $J(x,y)$ is integrable on the square, $\Lambda = [0,L)\times[0,L)$. Henceforth, we assume that $L = 2\pi$, since we can always rescale the spatial dimensions so that the "cortex" is the unit square. The periodicity of $J(x,y)$, as well as the translation invariance, implies that

$$\int_0^{2\pi}\int_0^{2\pi} J(x-x',y-y')\exp[i(kx'+jy')]\ dx'\ dy' = \hat{J}(k^2+j^2)\exp[i(kx+jy)]$$

for any integers (k,j) and

$$\hat{J}(l^2) = \int_{-\infty}^{\infty} w(x')e^{-ilx'}\ dx'.$$

This last equality is due to the rotational invariance of the function $w(x)$ and the definition of J. With these necessary preliminaries we turn to the analysis of equation (13.30). We suppose that $F(0) = 0$ and $F'(0) = \alpha > 0$ is a parameter. Think of this as the excitability of the network. For larger α, the network is more excited. We also assume that $F(u)$ is at least C^3. Since $F(0) = 0$, then $u(x,y,t) = 0$ is a solution to (13.30) and represents the background state of the cortex. To determine stability, we linearize about $u = 0$ and obtain the linearized equation:

$$\tau\frac{\partial v}{\partial t} = -v + \alpha J(x,y) * v(x,y,t).$$

Since J preserves sine and cosines, the general solution to the linear problem is

$$v(x,y,t) = e^{\lambda t}e^{i(kx+jy)}$$

where the eigenvalue λ satisfies:

$$\lambda = -1 + \alpha J(k^2\hat{}+j^2).$$

Note that λ depends only on α and $l^2 = j^2+k^2$. If α is small enough, then $\lambda < 0$ for all (k,j). If we suppose that the interactions are like those in the Amari model (that is, lateral-inhibitory or "Mexican hat") such as shown in Figure 13.8A, the function $\hat{J}(l)$ will look like Figure 13.8B. In the figure, we have plotted l as a continuous variable, but in our square domain it takes on discrete values of the form $\sqrt{k^2+j^2}$ where (k,j) are integers. The important point is that if the interactions are like a Mexican hat, then the function $\hat{J}$ has a maximum value at some $l = l^*$ that is bounded away from 0.

Suppose that we increase the excitability parameter, α. Then as soon as α exceeds, $1/\hat{J}(l^*) \equiv \alpha^*$, the rest state will be unstable and spatial perturbations of the form $\exp i(kx+jy)$ with $k^2+j^2 = (l^*)^2$ will grow at an exponential rate. Since actual values of l are discrete, then there will generically be a small range of values of α such that only modes exactly equal to l^* will grow and all other modes will decay. This phenomenon when a few spatial modes grow and the remainder decay

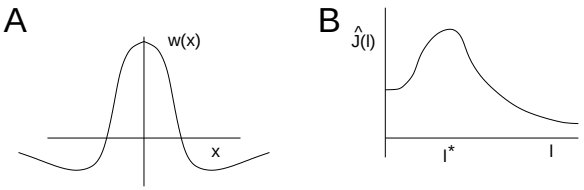

Figure 13.8. *(A) The lateral inhibitory kernel, $w(x)$ and the corresponding Fourier transform (B)*

is the essence of what is called the *Turing instability* after Alan Turing's ground breaking paper on pattern formation in 1952. This simple mechanism underlies the formation of spatial patterns in hundreds of other biological and physical examples. (See Murray for dozens of applications in biology.) Of course, this simple analysis is only the beginning. It is also necessary that we analyze what happens to the full nonlinear problem when α is larger than α^*. The resulting nonlinear analysis (called the *normal form* by mathematicians and *mode* or *amplitude expansion* by physicists) tells us exactly what actual patterns arise. We will sketch this out in the next few paragraphs.

The complexity of the patterns which arise as α increases beyond α^* depends on the value of l^* since this determines how many values of (k, j) satisfy $k^2 + j^2 = (l^*)^2$. For example, suppose that $l^* = 7$. The only pairs are $(\pm 7, 0)$ and $(0, \pm 7)$; there are 4 of them. If $l^* = 5$, then there are many more: $(\pm 5, 0)$, $(0, \pm 5)$,$(\pm 4, \pm 3)$, $(\pm 4, \mp 3)$, $(\pm 3, \pm 4)$, and $(\pm 3, \mp 4)$. If $l^* = \sqrt{2}$, then $\pm(1, -1)$ and $\pm(1, 1)$ are the only four. For larger values of l^* there can be arbitrarily many. For any given l^*, we enumerate all the values of (j_n, k_n) such that $j_n^2 + k_n^2 = l^{*2}$ and write the corresponding functions of x, y as:

$$\Phi_n(x, y) = e^{i(j_n x + k_n y)}.$$

The idea of normal form methods is that we seek solutions to (13.30) when the parameter, α is close to α^* and thus the solutions are expected to lie close to the homogeneous resting state. Hence, we suppose that $\alpha - \alpha^* = \epsilon^2 p$ where ϵ is a small positive amplitude parameter and p is a scaling factor. We seek solutions to (13.30) of the form:

$$u(x, y, t) = \sum_n \epsilon z_n(\eta)\Phi_n(x, y) + \epsilon^2 w_2 + \dots$$

where $\eta = \epsilon^2 t$ is a slow time scale and $w_2, w - 3, \dots$ are orthogonal to $\Phi_n(x, y)$. The complex functions z_n are the so-called amplitude variables and describe the behavior near the resting state in a subspace spanned by the nullspace of the linearized equations. There is a straightforward, but somewhat tedious procedure to go trough in order to get the equations for the z_n, and the interested reader should consult **??? In general, the resulting equations take the following form:

$$\frac{dz_n}{d\eta} = z_n(bp + \sum_m a_{nm} z_m \bar{z_m}) \tag{13.31}$$

where a_{nm}, b are real coefficients whose values depend strongly on the details of the model. We remark that in our example system, the loss of stability is at a zero eigenvalue (which is the only possibility for a *scalar* model). However, in more complex models, such as the full Wilson-Cowan equations, it is possible to lose stability at an imaginary pair of eigenvalues. In this case, the coefficients in the normal form equation (13.31) are complex. Here, for simplicity, we study only the emergence of solutions at a zero eigenvalue. We can write $z_n = r_n \exp(i\theta_n)$ and then let $R_n = r_n^2$ to reduce equation (13.31) to a Lotka-Volterra model:

$$R_n' = 2R_n(bp + \sum_m a_{nm} R_m)$$

and use this to determine the dynamics of the normal form. There is a great deal of redundancy in the equations (13.31) since the pairs, (k_n, j_n) and $(-k_n, -j_n)$ are complex conjugates so that the corresponding z's have the same values of r and R. Thus, the conversion to r or R has the desirable effect of reducing the dimension by half. Furthermore, the parameters, a_{nm} are not independent and are generally related to each other. In particular, $a_{nm} = a_{mn}$. This last condition precludes any complex dynamics such as oscillations and chaos.

Consider, for example, the case when there are just 4 elements in the nullspace, say, $(\pm 7, 0)$ and $(0, \pm 7)$ which we identify as $n = 1, 2, 3, 4$. Then $z_2 = \bar{z_1}$ and $z_4 = \bar{z_3}$. The amplitude equations are determined solely by R_1 and R_3:

$$\begin{aligned} R_1' &= 2R_1(bp - aR_1 - cR_3) \\ R_3' &= 2R_3(bp - aR_3 - cR_1) \end{aligned} \tag{13.32}$$

Note that in this case, $a_{nn} = a_{mm}$. We are only interested in solutions for which $R_n = r_n^2 \geq 0$. We absorb b into p (so we set $b = 1$ without loss of generality). There are four solutions: $(0, 0)$, $(p/a, 0)$, $(0, p/a)$, and $(p/(a+c), p/(a+c))$. Before continuing, we first interpret these solutions within the context of the patterns for the full model, (13.30). Consider, the last solution. Recall that to lowest order $u(x, y, t)$ is a sum of the $z_n = \sqrt{R_n} e^{i\theta_n}$ so that for our particular choice of l^* we have

$$u(x, y) = 2\sqrt{R_1} \cos 7x + \theta_1 + 2\sqrt{R_3} \cos 7y + \theta_3$$

where the θ's are arbitrary phase-shifts (since we have periodic boundary conditions). The four solutions to the normal form correspond respectively to (i) no pattern, (ii) vertical stripes, (iii) horizontal stripes, (iv) checkerboards. Thus, in one simple example, we can explain several of Kluver's form constants for hallucinations: bullseyes, pinwheels, and checkerboards. If instead, we had, eg, $(6, 6), (6, -6), (-6, 6), (-6, -6)$ as our unstable modes, then the three nonzero patterns for $u(x, y)$ would be two diagonal striped patterns (corresponding to spiral form constants) and checkerboards.

We leave the analysis of the stability as an exercise for the reader, but we do summarize it here. The solutions $(p/a, 0), (0, p/a)$ are stable if and only if $c > a > 0$ while the solution $(p/(a+c), p/(a+c))$ is stable if and only if $a > c > 0$. Finally, $(0, 0)$ is stable if and only if $p < 0$.

13.6 Exercises

1. Consider the two cell network:

$$S_1(n+1) = \text{sgn}(-S_2(n))$$
$$S_2(n+1) = \text{sgn}(S_1(n))$$

   Does this ever settle down? This shows that the symmetry of weights is absolutely necessary for convergence.

2. Given the energy function (13.4), derive the derivative (13.5).

3. Consider equation (13.3), for 2 neurons. Let $R_i = 1, C_i = 1, I_i = 0$, $f_i(v) = 1/(1 + exp(-(v-3))$, and $w_{21} = w_{12} = 6$. Draw the phaseplane for this and compute the energy function, E. Superimpose this on the phaseplane.

4. Derive equation (13.8) from equations (13.6) and (13.7).

5. Prove that the Destexhe (1994) shunting model:

$$\frac{dx_i}{dt} = -A_i x_i + (B_i - x_i)[I_i + f_i(x_i)] - (x_i + C_i)\left[J_i + \sum_{j=1}^{N} D_{ij} g_j(x_j)\right]$$

   converges to equilibria under the assumptions that $D_{ij} = D_{ji} \geq 0$, A_i, B_i, C_i are non-negative and $g_j'(x_j) \geq 0$. (Hint, let $y_i = x_i - C_i$ be a simple change of variables and use the Cohen-Grossberg theorem.) Suppose, additionally, that I_i, J_i, f_i, g_i are all positive. Prove that if $x_i(0) \in (-C_i, B_i)$ then $x_i(t)$ remains in this interval.

6. Explore the following three variable model based on (13.6):

$$x_1' = x_1(1 - x_1 - 2x_2 - x_3/2)$$
$$x_2' = x_2(1 - x_2 - 2x_3 - x_1/2)$$
$$x_3' = x_3(1 - x_3 - 2x_1 - x_2/2).$$

   This is of the form of the Cohen-Grossberg model but violates the symmetry of interactions. Numerically solve this system and describe the behavior.

7. Consider the single memory network

$$V_i' = -V_i + \xi_i(1/N)\sum_{j=1}^{N} \xi_j \tanh(bV_j)$$

   where ξ_j is either -1 or 1. Show that if $b > 0$ is too small, the only solution to this is that V_i converge to 0. Prove that as b increases, there is a pitchfork bifurcation and that V_i will converge to a fixed point proportional to the vector ξ. Show that the "anti memory", proportional to $-\xi$ is also a stable fixed point.

8. Let $F(V) = \tanh(bV)$. Create two random memories of length 100 consisting of -1 and 1. Numerically study the bifurcation as the gain, b increases for equation (13.9). In the perfect recall case of memory 1, $r_2 = 0$. For your simulated example, how small is r_2 as b increases? Suppose that the two memories are orthogonal. Can you prove that the recall is perfect in this case? (Exploit the fact that F is an odd function and that all the ξ components are ± 1.)

9. Consider the equation:

$$S(x) = f(\frac{1}{2}\int_{-\infty}^{\infty} e^{-|x-y|}S(y)\ dy).$$

Suppose that $g(u) - u + f(u)$ has three zeros, $a < b < c$, $g'(a) < 0$, $g'(b) > 0$, $g'(c) < 0$ and that

$$\int_a^c g(u)du = 0.$$

Prove that there is a bounded solution to this equation satisfying

$$S(-\infty) = c \qquad S(+\infty) = a.$$

Hint: Let

$$z(x) = (1/2)\int_{-\infty}^{\infty} e^{-|x-y|}S(y)\ dy.$$

Show that

$$z - z_{xx} = S$$

by either using Fourier transforms or directly differentiating. Thus, transform the integral equation to

$$z - z_{xx} = f(z)$$

which is a second order integrable differential equation which has a solution, $z(-\infty) = c$ and $z(+\infty) = a$. Conclude that S also satisfies these conditions.

10. Consider:

$$-\nu\tau S' = -S + \alpha H[J(\xi) * S(\xi) - \theta](1 - S)$$

where $H(u)$ is the step function. Suppose that

$$0 < \theta < \frac{\alpha}{2(1+\alpha)}.$$

Find the unique traveling wave solution joining the states $S = 0$ with $S = \alpha/(1+\alpha)$.

11. Devise a model similar to equations (13.14) and (13.15) which use synaptic depression as the slow recovery instead of adaptation. You should consult chapter SYNAPSES in order to model the depression. Note that the degree of depression should depend on the firing rate of the neuron, act as a multiplicative factor on the synaptic strength, and have its own dynamics. Draw

some representative (s, d) phaseplanes for the local (spatially homogeneous) case where d is the depression variable. Find conditions in which the local dynamics admits oscillations. Compare your model and simulations with Tsodyks et al (2000) See also Loebel & Tsodyks (2002).

12. Consider the traveling pulse equations for the analogue of equation (13.17) with step function nonlinearities and no saturation of the synapse and adaptation variables:

$$\begin{aligned} -cS' &= -S + \nu \\ -c\tau Z' &= -Z + k\nu \\ \nu &= \text{Heav}(\int_{-\infty}^{\infty} J(\xi - \xi')S(\xi')\ d\xi' - -bZ - \theta) \end{aligned}$$

Construct a traveling pulse for this equation using $J(x) = \exp(-|x|)/2$. Here is how to proceed. Let

$$U(\xi) = \int_{-\infty}^{\infty} J(\xi - \xi')S(\xi')\ d\xi' - -bZ - \theta.$$

Suppose that $U(\xi) > 0$ for $0 < \xi < a$ where a is the width of the pulse. Then for $\xi < 0$ or $\xi > a$, we have

$$-cS' = -S \quad -c\tau Z' = -Z.$$

As $\xi \to \pm\infty$, these must be bounded so the reader should verify that $(S, Z) = (0, 0)$ for $\xi > a$. For $\xi < 0$, the solutions are exponentials with unknown constants. For $0 < \xi < a$, $U > 0$ so that the step function is 1 in this region and

$$-cS' = -S + 1 \quad -c\tau Z' = -Z + k.$$

Solutions should be continuous, so that at $\xi = a$, $S(a) = Z(a) = 0$ since (S, Z) vanish for $\xi > a$. This gives a unique solution to (S, Z) in the region $0 < \xi < a$. Furthermore by continuity, this also provides values for the unknown constants in the region $\xi < 0$. Now, you should have a solution for all of ξ which contains two unknown constants, the velocity, c and the width, a. Since $U(\xi) > 0$ for $0 < \xi < a$ and $U(\xi) < 0$ for $\xi < 0$ and $\xi > a$, it must be the case (by continuity) that $U(0) = U(a) = 0$. These two equations will yield the unknown constants, a, c Unfortunately, you will probably not be able to solve for a, c explicitly and must resort to a numerical solution. However, the problem has now been reduced to two algebraic equations!

13. Construct spatially periodic solutions to the Amari model, equation (13.20) satisfying $v(x+b) = v(x)$ and $v(x) > \theta$ for $0 < x < a < b$. Can you determine their stability?

14. In this exercise, you will create a numerical model for equations (13.22- (13.23) and compare the bump with the solution you construct analytically. After

this, do the next exercise to determine the stability of your bump solution. For the simulations, choose $J_{ee}(x) = a\exp(-(x/\sigma_e)^2)/(\sigma_e sqrt\pi)$, $J_{ei}(x) = exp(-(x/\sigma_e)^2)/(\sigma_e sqrt\pi)$, and $J_{ie}(x) = exp(-(x/\sigma_i)^2)/(\sigma_i sqrt\pi)$. Choose $\sigma_e = 8$, $\sigma_i = 6$ and $a = 1.05, \theta = .05, \tau_i = .1$. First, compute the width of the bump by computing the composite interaction function, $J(x) = J_{ee}(x) - J_{ie}(x) * J_{ei}(x)$. (Note that $*$ means the convolution.) Next, simulate the model by choosing a big enough domain and a suitable discretization. Show that there is a bump that has the same width as the theory predicts. Proceed to the next exercise!

15. Determine the stability of the stationary solution

$$(u_e(x), u_i(x)) = (U(x), J_{ei}(x) * H(U(x) - \theta))$$

with

$$U(x) = J(x) * H(U(x) - \theta), \quad J(x) = J_{ee}(x) - J_{ei}(x) * J_{ie}(x)$$

as a function of the time constant of inhibition in equations (13.22-13.23). Linearize about the steady solution and use the properties of the Dirac delta function to reduce the stability question to that of a four-dimensional matrix.

16. Suppose that $J(x)$ is a Mexican-hat type interaction. That is:

    (a) $J(-x) = J(x)$;

    (b) $J(x) > 0$ on $(-a, a)$ with $a > 0$ and $J(\pm a) = 0$;

    (c) $J(x)$ is decreasing on $(0, a]$;

    (d) $J(x) < 0$ on $(-\infty, -a) \cup (a, \infty)$;

    (e) $J(x)$ is continuous with a finite integral;

    (f) $J(x)$ has a unique minimum on $(0, \infty)$ at a point, $d > a$ and $J(x)$ is strictly increasing on (d, ∞).

    Can you construct a double "bump" solution for equation (13.20)? That is, $v(x) > \theta$ in the union of two intervals, $(r_1, r_2) \cup (r_3, r_4)$? The answer to this may be: no - you have to figure it out. (Hint: consult SIAM J. Appl math 63:62-97,2002).

17. More fun with the Amari model Consider linear differential operator,

$$Lu \equiv a_m d^m u/dt^m + a_{m-1} d^{m-1} u/dt^{m-1} + \ldots + a_1 du/dt + u$$

and suppose that all the roots to the characteristic polynomial have negative real parts (that is, $p(x) = a_m x^m + \ldots a_1 x + 1$ has roots with negative real parts.) Consider the generalized Amari model:

$$Lu(x,t) = J(x) * H(u(x,t) - \theta).$$

A time-independent solution satisfies:

$$U(x) = J(x) * H(U(x) - \theta);$$

identical to the Amari model. Analyze the stability of the bump. For example, if $m = 1$, this is the case we have done. In particular, for $m = 2$, show that there is still a stable bump solution for all $a_1, a_2 > 0$. What happens when $m = 3$? Can there be a loss of stability?

18. There are many variants to the Amari model incorporating adaptation and dendritic interactions. Coombes and his collaborators have written many papers on the analysis of these variants. In the spirit of Serge Lang's book on homology, pick any of Coombes' papers and obtain the same stability criteria without looking at his calculations. A good place to start is the review by Coombes (2005)

19. Asymmetric weights.) Consider the Amari model:

$$u_t = -u + W(x) * H(u(x,t) - \theta)$$

where $W(x) = J(x + \alpha)$ with $J(x)$, the usual "Mexican hat" function. When α is nonzero, $W(x)$ is not symmetric so that there will be no stationary bump. However, there may be a traveling bump. Let $u(x,t) = U(x - ct)$ where c is the velocity of the moving bump. Try to construct a moving bump where you try to find c as a function of α. (Hint: Let a be the width of the bump. Then you will have to solve:

$$-cU'(y) = -U(y) + int_0^a W(y - y')dy'$$

where $y = x - ct$ is the moving coordinate. This linear equation has two parameters, (c, a) plus a constant of integration. The condition that $U(y) \to 0$ as $y \to \pm\infty$ will determine the integration constant. The other two parameters are determined by the conditions that $U(0) = \theta$ and $U(a) = \theta$.)

20. The bump equation (13.25) contains only even derivatives so that there will be even solutions to it. Thus, to prove the existence of a homoclinic, we need to find a solution $u(x)$ such that $u(0) = \alpha, u''(0) = \beta$, $u'(0) = u'''(0) = 0$ and u and its derivatives vanish as $x \to \infty$. This problems is a two-dimensional shooting problem since we have to find the two parameters (α, β) so that the condition at ∞ holds. Two-dimensional shooting is very much more difficult, both numerically and analytically than one-dimensional (one parameter) shooting. Thus, the proof would be much simpler if we could somehow reduce it to a one-dimensional shooting problem. Show that if $u(x)$ is a solution to (13.25), then

$$(u'''u' - (u'')^2/2 + (b^2 - 1)u'^2 + (1 + b^2)^2 Q(u) = E$$

where E is a constant and

$$Q(u) = \int_0^u v - F(v)\ dv.$$

Use the boundary conditions at $x = \infty$ to compute E for the homoclinic and then use this to find an expression for β in terms of α, thus effectively reducing the existence to a one-dimensional shooting problem.

21. (Ring model). (A) Suppose that $q_1 = 0$ in equation (13.27). Prove that $d_1 = 0$ is invariant so that if you start with an even initial condition, the solution will continue to be even. (B) Prove that a stable fixed point to (13.27) corresponds to a stable solution to the full integral equation (13.26) for $J(\theta) = A + B\cos\theta$. (C) Use the computer to explore (13.27) when

$$J(\theta) = A + B\cos\theta$$

and $F(u) = \sqrt{\max(u-k, 0)}$ choosing, $A = 2$ and $B = 6$. Vary the threshold k and assume that the solutions are even functions of θ so that the model reduces to a planar system. How many fixed points are there and what is their stability when $k = 1$, $k = 0.5$? (D) One point of interest in these models is the contrast dependence of the output relative to the inputs. Consider (13.26) with $S(\theta, t) = a_0 + a_1\cos\theta$. The ratio of a_1/a_0 is called the contrast. The output contrast is c_1/c_0 where the c_j satisfy equation (13.27). Explore the bifurcations and nature of the fixed points as the contrast of the inputs varies. (E) Follow the moving bump. Suppose that a stimulus runs through feature space in a periodic manner. That is, in the ring model, we drive (13.26) with a stimulus $S(\theta, t) = a_1\cos(\theta - \omega t)$. Derive the appropriate version of (13.27) and then numerically study the behavior for $A = 2$, $B = 6$ $k = 1$ (with the same nonlinearity as in the other parts of this exercise) $a_1 = 0.1$ and $\omega \in [0.02, 0.05]$. Use two different initial conditions, $c_0 = 6$ and $c_0 = 0$ with the other variables set to 0. What is the behavior if you try to drive it too fast.

22. (Zhang's head direction model. Suppose that $K(\theta)$ is a symmetric weight function and $U(\theta)$ is a stationary bump solution to

$$U(\theta) = \int_0^{2\pi} K(\theta - \theta')F(U(\theta'))\, d\theta'.$$

Show that

$$u(\theta, t) = U(\theta + \int_0^t \gamma(s)\, ds)$$

is a solution to

$$\frac{\partial u(\theta, t)}{\partial t} = -u(\theta, t) + \int_0^{2\pi} J(\theta - \theta', t)F(u(\theta', t))\, d\theta'$$

where

$$J(\theta) = K(\theta) + \gamma(t)K'(\theta).$$

Simulate the Zhang model using the ring model of exercise * and your choice of inputs $\gamma(t)$.

23. Prove the stability results for equation (13.32).

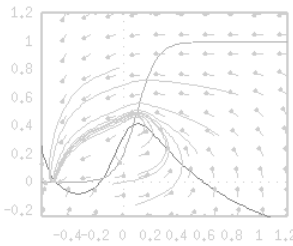

Chapter 14

Models

The models used in this book are presented below in the syntax of the authors software.

14.1 Channels

Hodgkin-Huxley

```
#  Hodgkin huxley equations
init v=-65  m=.05  h=0.6  n=.317
par i0=0
par vna=50  vk=-77  vl=-54.4  gna=120  gk=36  gl=0.3  c=1  phi=1
par ip=0 pon=50 poff=150
is(t)=ip*heav(t-pon)*heav(poff-t)
am(v)=phi*.1*(v+40)/(1-exp(-(v+40)/10))
bm(v)=phi*4*exp(-(v+65)/18)
ah(v)=phi*.07*exp(-(v+65)/20)
bh(v)=phi*1/(1+exp(-(v+35)/10))
an(v)=phi*.01*(v+55)/(1-exp(-(v+55)/10))
bn(v)=phi*.125*exp(-(v+65)/80)
v'=(I0+is(t) - gna*h*(v-vna)*m^3-gk*(v-vk)*n^4-gl*(v-vl)-gsyn*s*(v-vsyn))/c
m'=am(v)*(1-m)-bm(v)*m
h'=ah(v)*(1-h)-bh(v)*h
n'=an(v)*(1-n)-bn(v)*n
s'=sinf(v)*(1-s)-s/tausyn
# track the currents
sinf(v)=alpha/(1+exp(-v/vshp))
par alpha=2,vshp=5,tausyn=20,gsyn=0,vsyn=0
aux ina=gna*(v-vna)*h*m^3
aux ik=gk*(v-vk)*n^4
aux il=gl*(v-vl)
# track the stimulus
```

```
aux stim=is(t)
@ bound=10000
done
```

HH equiv potentials

```
#  hh.ode equivalent potentials
init v=-65  vm=-65,vn=-65,vh=-65
par i0, vna=50  vk=-77  vl=-54.4  gna=120  gk=36  gl=0.3  c=1  phi=1
par eps=.1
am(v)=phi*.1*(v+40)/(1-exp(-(v+40)/10))
bm(v)=phi*4*exp(-(v+65)/18)
ah(v)=phi*.07*exp(-(v+65)/20)
bh(v)=phi*1/(1+exp(-(v+35)/10))
an(v)=phi*.01*(v+55)/(1-exp(-(v+55)/10))
bn(v)=phi*.125*exp(-(v+65)/80)
minf(v)=am(v)/(am(v)+bm(v))
ninf(v)=an(v)/(an(v)+bn(v))
hinf(v)=ah(v)/(ah(v)+bh(v))
km(v)=am(v)+bm(v)
kn(v)=an(v)+bn(v)
kh(v)=ah(v)+bh(v)
mp(v)=(minf(v+eps)-minf(v-eps))/(2*eps)
np(v)=(ninf(v+eps)-ninf(v-eps))/(2*eps)
hp(v)=(hinf(v+eps)-hinf(v-eps))/(2*eps)
v'=(I0 - gna*hinf(vh)*(v-vna)*minf(vm)^3-gk*(v-vk)*ninf(vn)^4-gl*(v-vl))/c
vm'=km(v)*(minf(v)-minf(vm))/mp(vm)
vn'=kn(v)*(ninf(v)-ninf(vn))/np(vn)
vh'=kh(v)*(hinf(v)-hinf(vh))/hp(vh)
aux n=ninf(vn)
aux h=hinf(vh)
done
```

HH rinzel reduction

```
#  reduced HH equations using the rinzel reduction and n
#  as the variable
init v=-65 n=.4
par i0=0
par vna=50  vk=-77  vl=-54.4  gna=120  gk=36  gl=0.3  c=1  phi=1
par ip=0 pon=50 poff=150
is(t)=ip*heav(t-pon)*heav(poff-t)
am(v)=phi*.1*(v+40)/(1-exp(-(v+40)/10))
bm(v)=phi*4*exp(-(v+65)/18)
ah(v)=phi*.07*exp(-(v+65)/20)
bh(v)=phi*1/(1+exp(-(v+35)/10))
an(v)=phi*.01*(v+55)/(1-exp(-(v+55)/10))
bn(v)=phi*.125*exp(-(v+65)/80)
```

```
v'=(I0+is(t) - gna*h*(v-vna)*m^3-gk*(v-vk)*n^4-gl*(v-vl))/c
m=am(v)/(am(v)+bm(v))
#h'=ah(v)*(1-h)-bh(v)*h
n'=an(v)*(1-n)-bn(v)*n
h=h0-n
par h0=.8
@ bound=10000
done
```

Morris-Lecar

```
# Morris-Lecar model Methods Chapter
dv/dt = ( I - gca*minf(V)*(V-Vca)-gk*w*(V-VK)-gl*(V-Vl)+s(t))/c
dw/dt = phi*(winf(V)-w)/tauw(V)
v(0)=-16
w(0)=0.014915
minf(v)=.5*(1+tanh((v-v1)/v2))
winf(v)=.5*(1+tanh((v-v3)/v4))
tauw(v)=1/cosh((v-v3)/(2*v4))
param vk=-84,vl=-60,vca=120
param i=0,gk=8,gl=2,c=20
param v1=-1.2,v2=18
# Uncomment the ones you like!!
par1-3 v3=2,v4=30,phi=.04,gca=4.4
set hopf {v3=2,v4=30,phi=.04,gca=4.4}
set snic  {v3=12,v4=17.4,phi=.06666667,gca=4}
set homo {v3=12,v4=17.4,phi=.23,gca=4}
#par4-6 v3=12,v4=17.4,phi=.06666667,gca=4
#par7-8 v3=12,v4=17.4,phi=.23,gca=4
param s1=0,s2=0,t1=50,t2=55,t3=500,t4=550
# double pulse stimulus
s(t)=s1*heav(t-t1)*heav(t2-t)+s2*heav(t-t3)*heav(t4-t)
@ total=150,dt=.25,xlo=-75,xhi=75,ylo=-.25,yhi=.5,xp=v,yp=w
done
```

Butera-Smith

```
# butera and smith model using NaP
par cm=21,i=0
xinf(v,vt,sig)=1/(1+exp((v-vt)/sig))
taux(v,vt,sig,tau)=tau/cosh((v-vt)/(2*sig))
# leak
il=gl*(v-el)
par gl=2.8,el=-65
# fast sodium --  h=1-n
minf(v)=xinf(v,-34,-5)
ina=gna*minf(v)^3*(1-n)*(v-ena)
```

```
par gna=28,ena=50
# delayed rectifier
ninf(v)=xinf(v,-29,-4)
taun(v)=taux(v,-29,-4,10)
ik=gk*n^4*(v-ek)
par gk=11.2,ek=-85
# NaP
mninf(v)=xinf(v,-40,-6)
hinf(v)=xinf(v,-48,6)
tauh(v)=taux(v,-48,6,taubar)
par gnap=2.8,taubar=10000
inap=gnap*mninf(v)*h*(v-ena)
v' = (i-il-ina-ik-inap)/cm
n'=(ninf(v)-n)/taun(v)
h'=(hinf(v)-h)/tauh(v)
@ total=40000,dt=1,meth=cvode,maxstor=100000
@ tol=1e-8,atol=1e-8
@ xlo=0,xhi=40000,ylo=-80,yhi=20
done
```

Calcium-dependent inactivation

```
# L-type calcium current with calcium-dependent inactivation
# Poirazi P, Brannon T, Mel BW (2003a)
# Arithmetic of subthreshold synaptic summation in a model CA1 pyramidal cell.
# Neuron 37:977-987
# adjusted beta slightly from .028 to .01
# from ModelDB
!faraday=96520
!rgas=8.3134
!temp=273.15+celsius
h=ki/(ki+ca)
xi=v*faraday*2/(rgas*1000*temp)
cfedrive=.002*faraday*xi*(ca-cao*exp(-xi))/(1-exp(-xi))
m=alpm(v)/(alpm(v)+betm(v))
ical=pcal*m*h*cfedrive
par ki=.001,celsius=25,cao=2,pcal=2,cainf=1e-4,taur=200
init ca=1e-4,v=-65
alpm(v) = 0.055*(-27.01 - v)/(exp((-27.01-v)/3.8) - 1)
betm(v) =0.94*exp((-63.01-v)/17)
# migliore model:
# alpm(v) = 15.69*(-1.0*v+81.5)/(exp((-1.0*v+81.5)/10.0)-1.0)
# betm(v) = 0.29*exp(-v/10.86)
v'=-gl*(v-el)-ical+i0
ca'=-ical*beta-(ca-cainf)/taur
par beta=.01,i0=0,el=-70,gl=.05
```

```
aux ica=ical
@ total=1000,meth=qualrk,tol=1e-8,atol=1e-8,dt=.25
@ xp=v,yp=ca,xlo=-80,xhi=-10,ylo=0,yhi=2
done
```

T-type current with rebound

```
# cat-spike.ode
# i=+/-.25 for 25 msec or -2 for rebound + depolarized
# Huguenard and Mccormick T-type calcium kinetics
# using CFE with calcium fixed in concentration
# sodium and potassium channels added for spiking
#
i(t)=i0+i1*heav(t-ton)*heav(ton+tdur-t)
!faraday=96520
!rgas=8.3134
!temp=273.15+celsius
xi=v*faraday*2/(rgas*1000*temp)
cfedrive=.002*faraday*xi*(cai-cao*exp(-xi))/(1-exp(-xi))
m=minf(v)
par el=-65,celsius=25,cao=2,pcat=.15,cai=1e-4
par gna=8,gk=4,ena=55,ek=-90
minf(v)=1/(1+exp(-(v+59)/6.2))
hinf(v)=1/(1+exp((v+83)/4))
# tauh(v)=if(v<(-82))then(exp((v+469)/66.6))else(28 + exp(-(v+24)/10.5))
tauh(v)=22.7+.27/(exp((v+48)/4)+exp(-(v+407)/50))
i_cat=pcat*m*m*h*cfedrive
amna=.091*(v+38)/(1-exp(-(v+38)/5))
bmna=-.062*(v+38)/(1-exp((v+38)/5))
ahna=.016*exp((-55-v)/15)
bhna=2.07/(1+exp((17-v)/21))
mna=amna/(amna+bmna)
ank=.01*(-45-v)/(exp((-45-v)/5)-1)
bnk=.17*exp((-50-v)/40)
v'=-gl*(v-el)-i_cat+i(t)-gna*mna^3*hna*(v-ena)-gk*n^4*(v-ek)
h'=(hinf(v)-h)/tauh(v)
hna'=ahna*(1-hna)-bhna*hna
n'=ank*(1-n)-bnk*n
init h=.16,v=-76
par gl=.05,i0=0,i1=0,ton=100,tdur=25
aux icat=i_cat
@ meth=qualrk,dt=.25,total=500,atol=1e-8,rtol=1e-8
@ nmesh=100,xp=v,yp=h,xlo=-90,ylo=-.1,xhi=20,yhi=.8,bound=1000
done
```

Connor stevens

```
# constev.ode
```

```
i(t)=i0+i1*heav(t-ton)
par i0,ga=47.7
par gtotal=67.7
!gk=gtotal-ga
init v=-65
par ek=-72  ena=55  ea=-75  el=-17
par gna=120   gl=0.3
par ms=-5.3  hs=-12  ns=-4.3
par ap=2  ton=100  i1=0
# Hodgkin-Huxley with shifts - 3.8 is temperature factor
am(V)=-.1*(V+35+ms)/(exp(-(V+35+ms)/10)-1)
bm(V)=4*exp(-(V+60+ms)/18)
minf(V)=am(V)/(am(V)+bm(V))
taum(V)=1/(3.8*(am(V)+bm(V)))
ah(V)=.07*exp(-(V+60+hs)/20)
bh(V)=1/(1+exp(-(V+30+hs)/10))
hinf(V)=ah(V)/(ah(V)+bh(V))
tauh(V)=1/(3.8*(ah(V)+bh(V)))
an(V)=-.01*(V+50+ns)/(exp(-(V+50+ns)/10)-1)
bn(V)=.125*exp(-(V+60+ns)/80)
ninf(V)=an(V)/(an(V)+bn(V))
# Taun is doubled
taun(V)=2/(3.8*(an(V)+bn(V)))
# now the A current
ainf(V)=(.0761*exp((V+94.22)/31.84)/(1+exp((V+1.17)/28.93)))^(.3333)
taua(V)=.3632+1.158/(1+exp((V+55.96)/20.12))
binf(V)=1/(1+exp((V+53.3)/14.54))^4
taub(V)=1.24+2.678/(1+exp((V+50)/16.027))
# Finally the equations...
v'=-gl*(v-el)-gna*(v-ena)*h*m*m*m-gk*(v-ek)*n*n*n*n-ga*(v-ea)*b*a*a*a+i(t)
M'=(minf(v)-m)/taum(v)
H'=(hinf(v)-h)/tauh(v)
N'=(ninf(v)-n)/taun(v)
A'=(ainf(v)-a)/taua(v)
B'=(binf(v)-b)/taub(v)
@ total=200,xhi=200,ylo=-70,yhi=20
done
```

Inward rectifier + potassium pump

```
# inward rectifier with potassium pump
v'=-gl*(v-el)-ikir
ek=90*log10(kout)
ikir=gk/(1+exp((v-vth)/vs))*(v-ek)
par gk=.8
par vth=-85,vs=5,el=-60,gl=0.05
```

```
init v=-63
par beta=0.04,tau=1000
init kout=.1
kout'=(ikir*beta-(kout-.1))/tau
aux vk=ek
@ total=2000,meth=qualrk,dt=.5,tol=1e-8,atol=1e-8
done
```

Destexe & Pare model

```
# currents from destexhe and pare
# J. Neurophys 1999
# sodium
am(v)=-.32*(v-vt-13)/(exp(-(v-vt-13)/4)-1)
par i=0,gkm=2
# shifted to acct for threshold
num vt=-58,vs=-10
bm(v)=.28*(v-vt-40)/(exp((v-vt-40)/5)-1)
ah(v)=.128*exp(-(v-vt-vs-17)/18)
bh(v)=4/(1+exp(-(v-vt-vs-40)/5))
ina(v,m,h)=gna*m^3*h*(v-ena)
par gna=120,ena=55
# delayed rectifier
an(v)=-.032*(v-vt-15)/(exp(-(v-vt-15)/5)-1)
bn(v)=.5*exp(-(v-vt-10)/40)
ikdr(v,n)=gk*n^4*(v-ek)
par gk=100,ek=-85
# slow potassium current
akm(v)=.0001*(v+30)/(1-exp(-(v+30)/9))
bkm(v)=-.0001*(v+30)/(1-exp((v+30)/9))
ikm(v,m)=gkm*m*(v-ek)
#
v'=(I-gl*(v-el)-ikdr(v,n)-ina(v,m,h)-ikm(v,mk))/cm
m'=am(v)*(1-m)-bm(v)*m
h'=ah(v)*(1-h)-bh(v)*h
n'=an(v)*(1-n)-bn(v)*n
mk'=akm(v)*(1-mk)-bkm(v)*mk
init v=-73.87,m=0,h=1,n=.002,mk=.0075
# passive stuff
par gl=.019,el=-65,cm=1
# numerics stuff
@ total=1000,dt=.25,meth=qualrk,xhi=1000,maxstor=10000
@ bound=1000,ylo=-85,yhi=-50
done
```

Sag and inward rectifier

```
# sag + inward rectifier

par i=0
par gl=.025,el=-70
# sag
# migliore tau0=46,vm=-80,b=23
# migliore vt=-81,k=8
# mccormick tau0=1000,vm=-80,b=13.5
#
ih=gh*(V-eh)*y
par gh=0.25,eh=-43
yinf(v)=1/(1+exp((v-vt)/k))
ty(v)=tau0/cosh((v-vm)/b)
par k=5.5,vt=-75
par tau0=1000,vm=-80,b=13.5
#
# kir
par ek=-85,gk=1
ikir=gk*minf(v)*(v-ek)
minf(v)=1/(1+exp((v-va)/vb))
par va=-80,vb=5
v'=i-gl*(v-el)-ih-ikir
y'=(yinf(v)-y)/ty(v)
init v=-68
init y=.24
@ total=1000,meth=qualrk,dt=.25
@ xp=v,yp=y,xlo=-90,xhi=-40,ylo=0,yhi=0.6
@ nmesh=100
done
```

CAN current

```
# can.ode
# spiking model plus CAN current

# sodium
am(v)=-.32*(v-vt-13)/(exp(-(v-vt-13)/4)-1)
num vt=-58,vs=-10
bm(v)=.28*(v-vt-40)/(exp((v-vt-40)/5)-1)
ah(v)=.128*exp(-(v-vt-vs-17)/18)
bh(v)=4/(1+exp(-(v-vt-vs-40)/5))
ina(v,m,h)=gna*m^3*h*(v-ena)
par gna=120,ena=55
# delayed rectifier
an(v)=-.032*(v-vt-15)/(exp(-(v-vt-15)/5)-1)
bn(v)=.5*exp(-(v-vt-10)/40)
```

```
ikdr(v,n)=gk*n^4*(v-ek)
par gk=100,ek=-85
# voltage
v'=(I-gl*(v-el)-ikdr(v,n)-ina(v,m,h)-ican)/cm
m'=am(v)*(1-m)-bm(v)*m
h'=ah(v)*(1-h)-bh(v)*h
n'=an(v)*(1-n)-bn(v)*n
# can dynamics
par taumc=4000
ican=gcan*mc*(v-ecan)
par ecan=-20
par gcan=.05,alpha=.005
mc'=alpha*ca^2*(1-mc)-mc/taumc
# pulse function for calcium entry
puls(t)=heav(t)*heav(wid-t)
# here is the calcium
ca=puls(t-t1)+puls(t-t2)+puls(t-t3)
par t1=200,t2=700,t3=1200
par wid=50
# initial data
init v=-64.97,m=0.003,h=.991,n=.01,mc=0
# passive
par gl=.019,el=-65,cm=1,i=0
# keep track of calcium
aux stim=10*ca-100
# XPP stuff
@ total=2000,dt=.05,meth=rk4,xhi=2000,maxstor=100000
@ bound=1000,ylo=-100,yhi=20
@ nplot=2,yp2=stim
done
```

Calcium-dependent AHP

```
# ahp.ode
# uses very simple model of AHP with ca dynamics
# and high threshold Calc
# sodium
am(v)=-.32*(v-vt-13)/(exp(-(v-vt-13)/4)-1)
par i=0,gkm=2
# shifted to acct for threshold
num vt=-58,vs=-10
bm(v)=.28*(v-vt-40)/(exp((v-vt-40)/5)-1)
ah(v)=.128*exp(-(v-vt-vs-17)/18)
bh(v)=4/(1+exp(-(v-vt-vs-40)/5))
ina(v,m,h)=gna*m^3*h*(v-ena)
par gna=120,ena=55
```

```
# delayed rectifier
an(v)=-.032*(v-vt-15)/(exp(-(v-vt-15)/5)-1)
bn(v)=.5*exp(-(v-vt-10)/40)
ikdr(v,n)=gk*n^4*(v-ek)
par gk=100,ek=-85
#
# l-type calcium
ica(v)=gca*(v-eca)/(1+exp(-(v-vlth)/kl))
par vlth=-5,kl=5,gca=.5,eca=120
mahp(ca)=ca^2/(kca^2+ca^2)
iahp(ca)=gahp*mahp(ca)*(v-ek)
par gam=1,tauca=300,kca=2,gahp=1
v'=(I-gl*(v-el)-ikdr(v,n)-ina(v,m,h)-ica(v)-iahp(ca))/cm
m'=am(v)*(1-m)-bm(v)*m
h'=ah(v)*(1-h)-bh(v)*h
n'=an(v)*(1-n)-bn(v)*n
ca'=-(gam*ica(v)+ca)/tauca
#
init v=-73.87,m=0,h=1,n=.002
# passive stuff
par gl=.019,el=-65,cm=1
aux mahpx=mahp(ca)
# numerics stuff
@ total=1000,dt=.25,meth=qualrk,xhi=1000,maxstor=10000
@ bound=1000,ylo=-85,yhi=-50
done
```

HH cable

```
#  hhhcable.ode
init v[1..150]=-65  m[j]=.05  h[j]=0.6  n[j]=.317
par L=10,ri=100,d=.1
par vna=50  vk=-77  vl=-54.4  gna=120  gk=36  gl=0.3  c=1  phi=1
# two stimulus protocol
par ip1=0,ip2=0
par wid=2,t1=10,t2=50
# smooth step function
sheav(z)=1/(1+exp(-b*z))
par b=5
# local pulse
par xwid=5
lpul(t,x)=sheav(xwid-x)*sheav(t)*sheav(wid-t)
is(t,x)=ip1*lpul(t-t1,x)+ip2*lpul(t-t2,x)
am(v)=phi*.1*(v+40)/(1-exp(-(v+40)/10))
bm(v)=phi*4*exp(-(v+65)/18)
ah(v)=phi*.07*exp(-(v+65)/20)
```

```
bh(v)=phi*1/(1+exp(-(v+35)/10))
an(v)=phi*.01*(v+55)/(1-exp(-(v+55)/10))
bn(v)=phi*.125*exp(-(v+65)/80)
# boundaries are zero flux
!dd=4*d*150*150/(ri*L*L)
v0=v1
v151=v150
%[1..150]
v[j]'=(is(t,[j]) - gna*h[j]*(v[j]-vna)*m[j]^3-gk*(v[j]-vk)*n[j]^4\
     -gl*(v[j]-vl)+(dd)*(v[j+1]-2*v[j]+v[j-1]))/c
m[j]'=am(v[j])*(1-m[j])-bm(v[j])*m[j]
h[j]'=ah(v[j])*(1-h[j])-bh(v[j])*h[j]
n[j]'=an(v[j])*(1-n[j])-bn(v[j])*n[j]
%
aux stim1=is(t,1)
aux vp50=(is(t,50) - gna*h50*(v50-vna)*m50^3-gk*(v50-vk)*n50^4\
     -gl*(v50-vl)+DD*(v51-2*v50 +v49))/c
@ bound=10000
@ meth=cvode,bandlo=4,bandup=4
@ tol=1e-10,atol=1e-10,dt=.05,total=80
done
```

noisy LIF without reset

```
# noisy LIF without reset
f(v)=I-V
wiener w
V'=f(V)+sig*w
init V=0
par I=0,sig=1
@ meth=euler,total=200
done
```

First passage BVP

```
# first passage set up to compute the firing times
# this is defined on an interval [0,1]
# and split up to get the interior value
#
par I=-1,sig=1,vreset=-1,vspike=10,a=10
b=(vreset+a)
c=(vspike-vreset)
# ok - here it is
# u is lower and w is upper interval
# s lies between 0 and 1
# u(s=0) = T(-A)
# u(s=1) = w(s=0)=T(V_reset)
```

```
# w(s=1) = T(V_spike)
# gotta write it as a system
du/dt=up
dup/dt=-2*b*b/sig-2*f(-a+b*s)*up*b/sig
dw/dt=wp
dwp/dt=-2*c*c/sig-2*f(vreset+c*s)*wp*c/sig
ds/dt=1
# 5 equations - 5 boundary conds
# du/ds=0 at s=0
bndry up
# w=0 at s=1
bndry w'
# du/ds(1)=dw/ds(0)
bndry up'-wp
# u(1)=w(0)
bndry u'-w
# s=t
bndry s
# set up some numerics
@ total=1,dt=.005
# here is f, dont want to forget  f
f(x)=x^2+I
done
```

QIFA period as BVP

```
# boundary value problem
# to find period of the QIFA model
v'=p*(v^2+i-u)
u'=p*a*(b*v-u)
p'=0
b v'-1
b v-c
b u-(u'+d)
par I=1
par c=-.25,a=.1,b=1,d=.5
init p=5.6488
init v=-.25,u=1.211
@ total=1,dt=.005
done
```

Golomb amitai

```
# Golomb amitai
# ionic currents
i_ion(v,h,n,z)=gl*(v-vl)+(gna*minf(v)^3*h+gnap*pinf(v))*(v-vna)+(gk*n^4+gz*z)*(v-vk)
minf(v)=1/(1+exp(-(v-thetam)/sigmam))
```

```
pinf(v)=1/(1+exp(-(v-thetap)/sigmap))
GAMMAF(VV,theta,sigma)=1.0/(1.0+exp(-(VV-theta)/sigma))
v'=I-i_ion(v,h,n,z)-gsyn*s*(v-vsyn)
h'=phi*(GAMMAF(V,thetah,sigmah)-h)/(1.0+7.5*GAMMAF(V,t_tauh,-6.0))
n'=phi*(GAMMAF(V,thetan,sigman)-n)/(1.0+5.0*GAMMAF(V,t_taun,-15.0))
z'=(GAMMAF(V,thetaz,sigmaz)-z)/tauZs
s'=alpha*(1-s)/(1+exp(-(v-vsth)/vshp))-beta*s

# synaptic parameters
p gsyn=0.2
p vsth=-10,vshp=5,alpha=.6,beta=.015,vsyn=0

# kinetic parameters/shapes
p phi=2.7
p thetam=-30.0,sigmam=9.5,thetah=-53.0,sigmah=-7.0
p thetan=-30.0,sigman=10.0,thetap=-40.0,sigmap=5.0
p thetaz=-39.0,sigmaz=5.0,tauZs=75.0
# ionic parameters
p VNa=55.0,VK=-90.0,VL=-70.0,t_tauh=-40.5,t_taun=-27.0
p gNa=24.0,gK=3.0,gL=0.02,I=0.0
p gNaP=0.07,gZ=.1
# set gz=0 and gl=.09,vl=-85.5 to compensate
done
```

McCormick Huguenard - many channels

```
# the McCormick-Huguenard channel models -- Mix and match as you like
#
# UNITS: millivolts, milliseconds, nanofarads, nanoamps, microsiemens
# moles
# cell is 29000 micron^2 in area so capacitance is in nanofarads
# all conductances are in microsiemens and current is in nanofarads.
#
par I=0,c=.29
v'=(I -ina-ik-ileak-ik2-inap-it-iahp-im-ia-ic-il-ih+istep(t))/c
# the current is a step function with amplitude ip
istep(t)=ip*heav(t-t_on)*heav(t_off-t)
par ip=0.0,t_on=100,t_off=200
# passive leaks
par gkleak=.007,gnaleak=.0022
Ileak=gkleak*(v-ek)+gnaleak*(v-ena)
#
aux i_leak=ileak
#  INA
par gna=0,Ena=45
Ina=gna*(v-ena)*mna^3*hna
```

```
amna=.091*(v+38)/(1-exp(-(v+38)/5))
bmna=-.062*(v+38)/(1-exp((v+38)/5))
ahna=.016*exp((-55-v)/15)
bhna=2.07/(1+exp((17-v)/21))
mna'=amna*(1-mna)-bmna*mna
hna'=ahna*(1-hna)-bhna*hna
#
aux i_na=ina
# Delayed rectifier IK
par gk=0,Ek=-105
Ik=gk*(v-ek)*nk^4
ank=.01*(-45-v)/(exp((-45-v)/5)-1)
bnk=.17*exp((-50-v)/40)
nk'=ank*(1-nk)-bnk*nk
#
aux i_k=ik
# INap  same tau as Na but diff activation
par gnap=0
inap=gnap*map^3*(v-ena)
map'=(1/(1+exp((-49-v)/5))-map)/(amna+bmna)
#
aux i_nap=inap
# ia  A-type inactivating potassium current
#
ia=ga*(v-ek)*(.6*ha1*ma1^4+.4*ha2*ma2^4)
mainf1=1/(1+exp(-(v+60)/8.5))
mainf2=1/(1+exp(-(v+36)/20))
tma=(1/(exp((v+35.82)/19.69)+exp(-(v+79.69)/12.7))+.37)
ma1'=(mainf1-ma1)/tma
ma2'=(mainf2-ma2)/tma
hainf=1/(1+exp((v+78)/6))
tadef=1/(exp((v+46.05)/5)+exp(-(v+238.4)/37.45))
tah1=if(v<(-63))then(tadef)else(19)
tah2=if(v<(-73))then(tadef)else(60)
ha1'=(hainf-ha1)/tah1
ha2'=(hainf-ha2)/tah2
par ga=0
aux i_a=ia
#
# Ik2  slow potassium current
par gk2=0,fa=.4,fb=.6
Ik2=gk2*(v-ek)*mk2*(fa*hk2a+fb*hk2b)
minfk2=1/(1+exp(-(v+43)/17))^4
taumk2=1/(exp((v-80.98)/25.64)+exp(-(v+132)/17.953))+9.9
mk2'=(minfk2-mk2)/taumk2
hinfk2=1/(1+exp((v+58)/10.6))
```

```
tauhk2a=1/(exp((v-1329)/200)+exp(-(v+129.7)/7.143))+120
tauhk2b=if((v+70)<0)then(8930)else(tauhk2a)
hk2a'=(hinfk2-hk2a)/tauhk2a
hk2b'=(hinfk2-hk2b)/tauhk2b
aux i_k2=ik2
#
# IT and calcium dynamics -- transient low threshold
# permeabilites in 10-6 cm^3/sec
#
par Cao=2e-3,temp=23.5,pt=0,camin=50e-9
number faraday=96485,rgas=8.3147,tabs0=273.15
# CFE stuff
xi=v*faraday*2/(rgas*(tabs0+temp)*1000)
# factor of 1000 for millivolts
cfestuff=2e-3*faraday*xi*(ca-cao*exp(-xi))/(1-exp(-xi))
IT=pt*ht*mt^2*cfestuff
mtinf=1/(1+exp(-(v+52)/7.4))
taumt=.44+.15/(exp((v+27)/10)+exp(-(v+102)/15))
htinf=1/(1+exp((v+80)/5))
tauht=22.7+.27/(exp((v+48)/4)+exp(-(v+407)/50))
mt'=(mtinf-mt)/taumt
ht'=(htinf-ht)/tauht
# il   L-type noninactivating calcium current -- high threshold
par pl=0
il=pl*ml^2*cfestuff
aml=1.6/(1+exp(-.072*(V+5)))
bml=.02*(v-1.31)/(exp((v-1.31)/5.36)-1)
ml'=aml*(1-ml)-bml*ml
aux i_l=il
# calcium concentration
par depth=.1,beta=1,area=29000
ca'=-.00518*(it+il)/(area*depth)-beta*(ca-camin)
ca(0)=50e-9
aux i_t=it
# ic  calcium and voltage dependent fast potassium current
ic=gc*(v-ek)*mc
ac=250000*ca*exp(v/24)
bc=.1*exp(-v/24)
mc'=ac*(1-mc)-bc*mc
par gc=0
aux i_c=ic
# ih  Sag current -- voltage inactivated inward current
ih=gh*(V-eh)*y
yinf=1/(1+exp((v+75)/5.5))
ty=3900/(exp(-7.68-.086*v)+exp(5.04+.0701*v))
y'=(yinf-y)/ty
```

```
par gh=0,eh=-43
# im   Muscarinic slow voltage gated potassium current
im=gm*(v-ek)*mm
mminf=1/(1+exp(-(v+35)/10))
taumm=taumm_max/(3.3*(exp((v+35)/20)+exp(-(v+35)/20)))
mm'=(mminf-mm)/taumm
par gm=0,taumm_max=1000
aux i_m=im
# Iahp  Calcium dependent potassium current
Iahp=gahp*(v-ek)*mahp^2
par gahp=0,bet_ahp=.001,al_ahp=1.2e9
mahp'=al_ahp*ca*ca*(1-mahp)-bet_ahp*mahp
aux i_ahp=iahp
aux cfe=cfestuff
#  set up for 1/2 sec simulation in .5 msec increments
@ total=500,dt=.5,meth=qualrk,atoler=1e-4,toler=1e-5,bound=1000
@ xhi=500,ylo=-100,yhi=50
init v=-70,hna=0.5
done
```

Traub fast dynamics with two types of SFA

```
itrb(v,m,h,n)=gna*h*m^3*(v-ena)+(gk*n^4)*(v-ek)+gl*(v-el)
v'=-(itrb(v,m,h,n) -i+i_ca+i_ahp+i_m)/c
m'=am(v)*(1-m)-bm(v)*m
n'=an(v)*(1-n)-bn(v)*n
h'=ah(v)*(1-h)-bh(v)*h
w'=(winf(v)-w)/tw(v)
s'=alphas*(1-s)/(1+exp(-(v-vthr)/vsshp))-betas*s
# calcium
mlinf=1/(1+exp(-(v-vlth)/vshp))
i_ca=gca*mlinf*(v-eca)
ca'=(-alpha*i_ca-ca/tauca)
# k-ca
i_ahp=gahp*(ca/(ca+kd))*(v-ek)
i_m=gm*w*(v-ek)
#
#
am(v)=.32*(54+v)/(1-exp(-(v+54)/4))
bm(v)=.28*(v+27)/(exp((v+27)/5)-1)
ah(v)=.128*exp(-(50+v)/18)
bh(v)=4/(1+exp(-(v+27)/5))
an(v)=.032*(v+52)/(1-exp(-(v+52)/5))
bn(v)=.5*exp(-(57+v)/40)
#
TW(vs)=tauw/(3.3*EXP((vs-vwt)/20.0)+EXP(-(vs-vwt)/20.0))
```

```
WINF(vs)=1.0/(1.0+EXP(-(vs-vwt)/10.0))
#
init v=42.68904,m=.9935,n=.4645,h=.47785,w=.268,s=.2917,ca=.294
par ek=-100,ena=50,el=-67,eca=120
par gl=.2,gk=80,gna=100,gm=0
par c=1,i=0
par gahp=0,gca=1,kd=1,alpha=.002,tauca=80,phi=4
par vshp=2.5,vlth=-25,vsshp=2,vthr=-10
# reyes set  vlth=-5,vsshp=10
par betas=.1,alphas=2
par vwt=-35,tauw=100
aux iahp=i_ahp
aux im=i_m
@ meth=qualrk,dt=.1,tol=1e-5,total=25.01,xlo=0,xhi=25,ylo=-85,yhi=50
@ bounds=1000000
done
```

Wang-Buszaki nearest neighbor chain

```
# wang buszaki fsu
p i0=0.5,ip=0,ton=20,toff=60
p phi=5.0
p gL=0.1
p EL=-65.0
p gNa=35.0
p ENa=55.0
p gK=9.0
p EK=-90.0
p gsyn=0.02,esyn=-80
#
table wr wbfreq.tab
i(x)=i0+i1*wr(x)
par i1=0.0035
v0=v1
v51=v50
s0=s1
s51=s50
V[1..50]'=-gL*(V[j]-EL)-gNa*(Minf(v[j])^3)*h[j]*(V[j]-ENa)-\
gK*(n[j]^4)*(V[j]-EK)+i([j])+gsyn*(esyn-v[j])*(s[j-1]+s[j+1])
h[1..50]'=phi*(alphah(v[j])*(1-h[j])-betah(v[j])*h[j])
n[1..50]'=phi*(alphan(v[j])*(1-n[j])-betan(v[j])*n[j])

s[1..50]'=ai(v[j])*(1-s[j])-s[j]/taui
#
ai(v)=ai0/(1+exp(-(v-vst)/vss))
par ai0=4,taui=6,vst=0,vss=5
#
```

```
alpham(v) = 0.1*(V+35.0)/(1.0-exp(-(V+35.0)/10.0))
betam(v)  = 4.0*exp(-(V+60.0)/18.0)
Minf(v) = alpham(v)/(alpham(v)+betam(v))
#
alphah(v) = 0.07*exp(-(V+58.0)/20.0)
betah(v)  = 1.0/(1.0+exp(-(V+28.0)/10.0))
#
alphan(v) = 0.01*(V+34.0)/(1.0-exp(-(V+34.0)/10.00))
betan(v)  = 0.125*exp(-(V+44.0)/80.0)

#
#
V[1..50](0)=-64
h[1..50](0)=0.78
n[1..50](0)=0.09
#
@ XP=T
@ YP=V
@ TOTAL=200
@ DT=0.2,bound=10000
@ METH=qualrk
@ TOLER=0.00001
@ XLO=0.0, XHI=30.0, YLO=-90.0, YHI=30.0
done
```

Amari model - with inhibition

```
# Amari model with dynamic inhibition
# play with taui
par sige=8,sigi=6
table je % 51 -25 25 exp(-(t/sige)^2)/(sige*sqrt(pi))
table ji % 51 -25 25 exp(-(t/sigi)^2)/(sigi*sqrt(pi))
hue[0..150]=heav(ue[j]-thr)
special ke=conv(even,151,25,je,hue0)
special ki=conv(even,151,25,ji,ui0)
ue[0..150]'=-ue[j]+ae*ke([j])-ki([j])
ui[0..150]'=(-ui[j]+ke([j]))/taui
par taui=.1
par thr=.05,ae=1.05
ue[50..75](0)=1
ui[50..75](0)=1
@ dt=.005,nout=20,total=50
done
```

Hansel-Sompolinski model

```
# simple ring model dynamics
# u' = -u + J* F(u)
```

```
#  J = A + B cos(x-y)
#
par a=2,b=6
table cs % 100 0 99 cos(2*pi*t/100)
table sn % 100 0 99 sin(2*pi*t/100)
f(u)=sqrt(max(u-thr,0))
fu[0..99]=f(c0+c1*cs([j])+d1*sn([j]))
c0'=-c0+a*sum(0,99)of(shift(fu0,i'))*.01+p0
c1'=-c1+b*sum(0,99)of(shift(fu0,i')*cs(i'))*.01+p1*cos(w*t)
d1'=-d1+b*sum(0,99)of(shift(fu0,i')*sn(i'))*.01+p1*sin(w*t)
par thr=1
par p0=0,p1=0,w=0
done
```

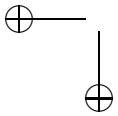
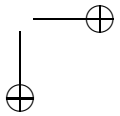

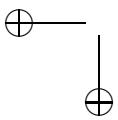

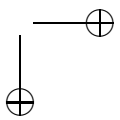

Bibliography

[1]

[2]

[3]

[4] D. G. Aronson and H. F. Weinberger. Nonlinear diffusion in population genetics, combustion and nerve pulse propagation. In J. Goldstein, editor, *Partial Differential Equations and Related Topics, Lecture Notes in Math*, pages 5–49. Springer, 1975.

[5] R. Bertram, M. J. Butte, T. Kiemel, and A. Sherman. Topological and phenomenological classification of bursting oscillations. *Bulletin of Mathematical Biology*, **57**:413–439, 1995.

[6] M. D. Bevan, P. J. Magill, D. Terman, J. P. Bolam, and C. J. Wilson. Move to the rhythm: oscillations in the subthalamic nucleus-external globus pallidus network. *Trends in Neuroscience*, **25**:523–531, 2002.

[7] T. G. Brown. The intrinsic factors in the act of progression in the mammal. *Proceedings of Royal Society London B*, **84**:308–319, 1911.

[8] C. Conley. *Isolated invariant sets and the Morse index. CBMS Lecture Notes in math.*, volume **38. AMS Press, Providence, R. I.**

[9] S. Coombes and P. C. Bressloff. *Bursting: The genesis of rhythm in the nervous system.* World Scientific, 2005.

[10] P. Dayan and L. F. Abbott. *Theoretical Neuroscience*. MIT Press, Cambridge, MA; London, England, 2001.

[11] A. Destexhe, D. Contreras, T. J. Sejnowski, and M. Steriade. A model of spindle rhythmicity in the isolated thalamic reticular nucleus. *Journal of Neurophysiology*, 72:803–818, 1994.

[12] G. B. Ermentrout and N. Kopell. Parabolic bursting in an excitable system coupled with a slow oscillation. *SIAM Journal on Applied Mathematics*, 46:223–253, 1986.

[13] J. W. Evans. Nerve axon equations. iv. *Indiana Univ. Math. J.*, 24:1169–1190, 1975.

[14] C. P. Fall, E. Marland, J. M. Wagner, and J. J. Tyson. *Computational Cell Biology*. Springer Verlag, New York, 2002.

[15] N. Fenichel. Geometric singular perturbation theory. *J. Diff. Eq.*, 31:53–91, 1979.

[16] P. C. Fife and J. B. McLeod. The approach of solutions of nonlinear diffusion equations to traveling wave solutions. *Arch. Rational Mechanics and Analysis*, 65:355–361, 1977.

[17] R. A. FitzHugh. Impulses and physiological states in theoretical models of nerve membrane. *Biophysical Journal*, 1:445–466, 1961.

[18] W. Gerstner, J. L. van Hemmen, and J. Cowan. What matters in neuronal locking? *Neural Comput.*, 8:1653–1676, 1996.

[19] D. Golomb, X.-J. Wang, and J. Rinzel. Synchronization properties of spindle oscillations in a thalamic reticular nucleus model. *J. Neurophysiology*, 72:1109–1126, 1994.

[20] J. Guckenheimer and P. Holmes. *Nonlinear Oscillations, Dynamical systems, and Bifurcations of Vector Fields*. Springer-Verlag, New York, 1983.

[21] S. P. Hastings. On the existence of homoclinic and paeriodic orbits for the fitzhugh-naguo equations. *Quart. J. Math. Oxford*, 27:123–124, 1976.

[22] B. Hille. *Ion Channels of Excitable Membranes. (2nd ed.)*. Sunderland, Mass: Sinauer, 2001.

[23] E. M. Izhikevich. Neural excitability, spiking, and bursting. *International journal of bifurcation and chaos*, 10:1171–1266, 2000.

[24] E. M. Izhikevich. *Dynamical Systems in Neuroscience*. MIT Press, Cambridge, Mass., 2007.

[25] J. J. B. Jack, D. Noble, and R. W. Tsien. *Electrical Current Flow in Excitable Cells*. Clarendon Press, Oxford, 1975.

[26] D. Johnston and S. M. Wu. *Foundations of Cellular Neurophysiology*. MIT Press, Cambridge, Mass., 1995.

[27] C. K. R. T. Jones. Stability of the traveling wave solution of the fitzhugh-nagumo equations. *Transactions of the A.M.S.*, 286:431–469, 1984.

[28] E.R. Kandel, J.H. Schwartz, and T.M. Jessell. *Principles of Neural Science*. Appleton & Lange, Norwalk, Conn., 1991.

[29] J. Keener and J. Sneyd. *Mathematical Physiology*. Springer-Verlag, New York, 1998.

[30] C. Koch. *Biophysics of Computation*. Oxford University Press, London and New York, 1999.

[31] C. Koch and eds. I. Segev. *Methods in Neuronal Modeling: from Synapses to Networks*. MIT Press, Cambridge, MA, 1998.

[32] N. Kopell and B. Ermentrout. Mechanisms of phase-locking and frequency control in pairs of coupled neural oscillators. In B. Fiedler, G. Iooss, and N. Kopell, editors, *Handbook of Dynamical Systems II: Towards Applications*. Elsevier, Amsterdam, 2002.

[33] N. Kopell and D. Somers. Anti-phase solutions in relaxation oscillators coupled through excitatory interactions. *Journal of mathematical Biology*, 33:261–280, 1995.

[34] G. Laurent. Olfactory network dynamics and the coding of multidimensional signals. *Nature Rev. Neurosci.*, 3:884–895, 2002.

[35] E. Lee and D. Terman. Uniqueness and stability of periodic bursting solutions. *J. Diff. Eq.*, 158:48–78, 1999.

[36] A. R. Martin, B. G. Wallace, P. A. Fuchs, and J. G. Nicholls. *From Neuron to Brain: A Cellular and Molecular Approach to the Function of the Nervous System*. Sinauer Associates, 2001.

[37] D. H. Perkel and B. Mulloney. Motor pattern production in reciprocally inhibitory neurons exhibiting postsynaptic rebound. *Science*, 145:61–63, 1974.

[38] L. Perko. *Differential Equations and Dynamical Systems*. Springer-Verlag, New York, 1996.

[39] W. Rall. Core conductor theory and cable properties of neurons. In E. R. Kandel, editor, *Handbook of Physiology*, volume 1, pages 39–97. American Physiology Society, 1977.

[40] J. Rinzel. Bursting oscillations in an excitable membrane model. In B. D. Sleeman and R. J. Jarvis, editors, *Ordinary and Partial Differential Equations; Proceedings of the 8th Dundee Conference, Lecture Notes in Mathematics 1151*. Springer, 1985.

[41] J. Rinzel. A formal classification of bursting mechanisms in excitable systems. In E. Teramoto and M. Yamaguti, editors, *Mathematical Topics in Population Biology, Morphogenesis and Neurosciences, vol. 71 of Lecture Notes in Biomathematics*. Springer-Verlag, 1987.

[42] J. Rinzel. Electrical excitability of cells, theory and experiment: Review of the hodgkin-huxley foundation and an update. *Bulletin of Mathematical Biology*, 52:3–23, 1990.

[43] J. Rinzel and G. B. Ermentrout. Analysis of neural excitability and oscillations. In C. Koch and I. Segev, editors, *Methods in Neuronal Modeling*. MIT Press, 1989.

[44] J. Rinzel, D. Terman, X.-J. Wang, and B. Ermentrout. Propagating activity patterns in large-scale inhiitory neuronal networks. *Science*, 279:1351–1355, 1998.

[45] I. Segev, J. Rinzel, and G. Shepherd. *The Theoretical Foundation of Dendritic Function: Selected Paper of Wilfrid Rall with Commentaries*. MIT Press, Canbridge, Ma., 1994.

[46] A L. Shilnikov and G. Cymbalyuk. Trnsition between tonic spiking and bursting in a neuron model via the blue-sky catastrophe. *Physical Review Letters*, 94:048101, 2005.

[47] M. Steriade. *Neuronal Substrates of Sleep and Epilepsy*. Cambridge University Press, Cambridge, 2003.

[48] S. H. Strogatz. *Nonlinear Dynamics and Chaos*. Addison-Wesley, Readings, Mass., 1984.

[49] D. Terman. Chaotic spikes arising from a model of bursting in excitable membranes. *SIAM Journal on Applied Mathematics*, 51:1418–1450, 1991.

[50] D. Terman. The transition from bursting to continuous spiking in an excitable membrane model. *J. Nonlinear Sci.*, 2:133–182, 1992.

[51] D. Terman and D. L. Wang. Global competition and local cooperation in a network of neural oscillators. *Physica D*, 81:148–176, 1995.

[52] H. C. Tuckwell. *Introduction to Theoretical Neurobiology*. Cambridge University Press, Cambridge, 1988.

[53] C. van Vreeswijk, L. F. Abbott, and G. B. Ermentrout. When inhibition not excitation synchronizes neural firing. *Journal of Computational Neuroscience*, 1:313–321, 1994.

[54] X.-J. Wang and J. Rinzel. Alternating and synchronous rhythms in reciprocally inhibitory model neurons. *Neural Computation*, 4:84–97, 1992.

[55] L. Zhang. On stability of traveling wave solutions in synaptically coupled neuronal networks. *Differential and Integral Equations*, 16:513–536, 2003.